

JHU/APL
SES 025
(QM-78-231)
JUNE 1980



III

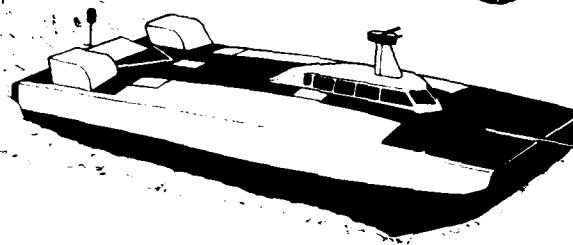
12

SES Program Reports

DOCUMENTATION OF DESIGN, PERFORMANCE, AND QUALIFICATION OF THE SES WAVE PROFILING SYSTEM

T. M. RANKIN
R. L. KONIGSBERG

DTIC
SERIES 1000
A



THE JOHNS HOPKINS UNIVERSITY ■ APPLIED PHYSICS LABORATORY

Approved for public release; distribution unlimited.

DDC FILE COPY

AD A088593

80 9 2 170

(SHU/APL/QM-78-231)

Unclassified

PLEASE FOLD BACK IF NOT NEEDED
FOR BIBLIOGRAPHIC PURPOSES

SECURITY CLASSIFICATION OF THIS PAGE

REPORT DOCUMENTATION PAGE		
1. REPORT NUMBER JHU/APL/SES-025	2. GOVT ACCESSION NO AD-A088 593	3. RECIPIENT'S CATALOG NUMBER
4. TITLE (and Subtitle) DOCUMENTATION OF DESIGN, PERFORMANCE, AND QUALIFICATION OF THE SES WAVE PROFILING SYSTEM		5. TYPE OF REPORT & PERIOD COVERED SES Program Reports
		6. PERFORMING ORG. REPORT NUMBER
7. AUTHOR(s) T. M. Rankin and R. L. Konigsberg		8. CONTRACT OR GRANT NUMBER(s) N00024-78-C-5384
9. PERFORMING ORGANIZATION NAME & ADDRESS The Johns Hopkins University Applied Physics Laboratory Johns Hopkins Rd. Laurel, MD 20810		10. PROGRAM ELEMENT, PROJECT, TASK AREA & WORK UNIT NUMBERS Task 269D
11. CONTROLLING OFFICE NAME & ADDRESS Naval Sea Systems Command Code PMS-304-24 Washington, DC		12. REPORT DATE June 1980
14. MONITORING AGENCY NAME & ADDRESS Naval Plant Representative Office Johns Hopkins Rd. Laurel, MD 20810		13. NUMBER OF PAGES 417
16. DISTRIBUTION STATEMENT (of this Report) Approved for public release; distribution unlimited.		15. SECURITY CLASS. (of this report) Unclassified
17. DISTRIBUTION STATEMENT (of the abstract entered in Block 20, if different from Report)		15a. DECLASSIFICATION/DOWNGRADING SCHEDULE
18. SUPPLEMENTARY NOTES		
19. KEY WORDS (Continue on reverse side if necessary and identify by block number) Vertical reference system Wave profiling system Radar altimeters Coordinate converter Strapdown inertial system Motion compensation Maneuver compensation Accelerometers		
20. ABSTRACT (Continue on reverse side if necessary and identify by block number) This report describes the design, calibration, and laboratory qualification testing of the complete motion-compensated wave profiling system (except for the altimeter) as installed on the high-speed surface effect ship, the SEA-100A. It also describes the detailed design and analysis of the strapdown inertial motion compensation system used to remove vehicle motion from the altimeter signal. The system is necessary to achieve real-time on-board wave profiling.		

DD FORM 1 JAN 73 1473

Unclassified

SECURITY CLASSIFICATION OF THIS PAGE

JHU/APL
SES 025
(QM-78-231)
JUNE 1980

SES Program Reports

**DOCUMENTATION OF DESIGN,
PERFORMANCE, AND QUALIFICATION
OF THE SES WAVE PROFILING SYSTEM**

T. M. RANKIN
R. L. KONIGSBERG

THE JOHNS HOPKINS UNIVERSITY ■ APPLIED PHYSICS LABORATORY
Johns Hopkins Road, Laurel, Maryland 20810
Operating under Contract N00024-78-C-5384 with the Department of the Navy

Approved for public release; distribution unlimited.

PREFACE

The Applied Physics Laboratory (APL) is engaged under contract with the Surface Effect Ship Project Office (PMS-304), Naval Sea Systems Command, in the development of an on-board, real-time wave profiling system for use on the SES-100A.

This report describes the design, calibration, and laboratory qualification testing of the complete wave profiling system except for the altimeter. Results of testing two microwave altimeters are contained in Refs. 1 and 2. Reference 3 is an operator's manual for the wave profiling system. The detailed analysis of the vertical gyro is contained in Ref. 4.

APL acknowledges that without the full cooperation of and technical assistance from PMS-304, including the Surface Effect Ship Test Facility (SESTF), successful completion of this phase of the wave profiling system development would not have been possible.

CONTENTS

	List of Illustrations	9
	List of Tables	18
1	Introduction	19
2	The Wave Profiling System Design Approach	21
3	Profiler Requirements	22
4	Development of the Theoretical Model	24
5	Error Analysis	29
	Accelerometer Error Model Analysis	29
	Gyro Error Model Analysis	36
	Discussion of System Errors	37
6	System Alignment, Calibration, and Testing in the Laboratory	40
	MCU Alignment and Calibration	42
	GCU Alignment and Calibration	51
7	System Mechanical Design Details	56
	BAU	56
	Wave Profiling System Electronics Rack	58
8	Detailed Electronic Design	59
	Error Considerations	59
	Description of the Instrumentation Diagram for the Motion-Compensated Wave Profiler	70
	Channel Gain Calculations and Assignment of Block Gains	75
	Circuit Descriptions	88
	Determination of the System Filter Time Constants τ_a and τ_b	137

9	Vertical Gyro Maneuver Compensation Electronics . . .	147
	Instrumentation Diagram Description . . .	150
	Channel Gain Calculations and Assignment of Block Gains	156
	Description of Γ_p and Γ_R Correction Circuits . . .	172
	References	189
	Appendix A: Wave Profiling System Electronics Schematics, Assembly Drawings, and Photographs	217
	Appendix B: Wave Profiling System Electronic Unit Chassis Wiring Diagrams and Photographs . .	312
	Appendix C: Bow Accelerometer Unit Wiring Diagram, Photographs, and Mechanical Design Drawings	337
	Appendix D: Cockpit Display Unit	362
	Appendix E: Results of Computer Simulation Study Relating to the Fifth-Order Filter Response to Vehicle Height Changes . . .	376

ILLUSTRATIONS

1	Encounter frequency versus ship speed assuming $\lambda = 13 h$ and a two-dimensional sea	191
2	Geometrical relationship of a vehicle boom altimeter profiling waves	192
3	Exact coordinate converter implementation	193
4	Simplified coordinate converter	194
5	Vertical gyro tilt (steady-state error) due to ship's maneuvers	195
6	Special test circuit to set gain potentiometer P1 on board #7	196
7	Special test circuit for setting gain potentiometer P2 on card #7	197
8	Fractional error (ϵ_3) in calculation of h_v , as a function of θ and ϕ channel gain A for $ \theta =$ $ \phi = 0.175$ rad, assuming surge and sway accelerations are insignificant compared to vertical acceleration ($k = 0$)	198
9	Rss fractional error due to surge and sway accelerations, as a function of θ and ϕ channel A for $ \theta = \phi = 0.25$ rad and $ \theta = \phi =$ 0.175 rad, and for $k = 0.01$ and $k = 0.10$	199
10	Simplified block diagram of motion-compensated wave profiler	200
11	Five-stage filter configuration required for double integration function	201
12	Electronic instrumentation diagram for motion- compensated wave profiler	203
13	Complete schematic of offset adjustment amplifier shown in Fig. A9-1	205

THE JOHNS HOPKINS UNIVERSITY
APPLIED PHYSICS LABORATORY
LAUREL MARYLAND

14	Block diagram for error analysis of MCU system . . .	206
15	Power spectral density of ship's vertical acceleration	207
16	Power spectral density of encountered wave height . . .	208
17	Power spectral density of encountered wave height . . .	209
18	Simplified block diagram of vertical gyro maneuver compensation electronics	211
19	Instrumentation diagram for vertical gyro maneuver compensation electronics	213
20	Input-output characteristic for nonlinear gain amplifier K_4	215
21	Outputs of VGMCE ($-E_g$) and SN193 vertical gyro roll pendulum transducer (E_{OR}) as functions of pendulum tilt angle	216
A1-1	Schematic, Card No. 1, MCU \ddot{Z} accelerometer scaling, 1 g bias and summing amplifier	219
A1-2	Component layout, Card No. 1, MCU \ddot{Z} accelerometer scaling, 1 g bias summing amplifier	221
A1-3	MCU \ddot{Z} accelerometer scaling, 1g bias and summing amplifier	223
A2-1	Schematic, Card No. 2, MCU synchro-to-DC converter (normalized)	225
A2-2	Component layout, Card No. 2, MCU synchro-to-DC converter (normalized)	227
A2-3	MCU synchro-to-DC converter (normalized)	229
A3-1	Schematic Card No. 3, MCU 400 Hz square wave reference generator and normalizing DC reference signal	231
A3-2	Component layout, Card No. 3, MCU square wave reference generator 400 Hz	233
A3-3	MCU 400 Hz reference	235

THE JOHNS HOPKINS UNIVERSITY
APPLIED PHYSICS LABORATORY
LAUREL, MARYLAND

A4-1	Schematic, Card No. 4, MCU altimeter filter circuits	237
A4-2	Component layout, Card No. 4, MCU altimeter filter circuits	239
A4-3	MCU altimeter filter circuits	240
A5-1	Schematic, Card No. 5, MCU high-pass filter	241
A5-2	Component layout, Card No. 5, MCU high-pass filter	242
A5-3	MCU high-pass filter	243
A6-1	Schematic, Card No. 6, MCU low-pass filter	245
A6-2	Component layout, Card No. 6, MCU low-pass filter	247
A6-3	MCU low-pass filter	248
A7-1	Schematic, Card No. 7, MCU system output signal conditioning	249
A7-2	Component layout, Card No. 7, MCU system output signal conditioning and rms converter	251
A7-3	MCU system output conditioner and rms converter	253
A8-1	Schematic, Card No. 8, \ddot{X} , \ddot{Y} accelerometer scaling coordinate conversion and DAS buffer	255
A8-2	Component layout, Card No. 8, MCU \ddot{X} , \ddot{Y} accelerometer scaling, coordinate conversion and DAS buffer	257
A8-3	MCU \ddot{x} , \ddot{y} , accelerometer scaling, coordinate conversion, and DAS buffer	259
A9-1	Schematic, Card No. 9, MCU altimeter signal conditioning	261
A9-2	Component layout, Card No. 9, MCU altimeter signal conditioning	263
A9-3	MCU altimeter signal conditioning	265

THE JOHNS HOPKINS UNIVERSITY
APPLIED PHYSICS LABORATORY
LAUREL MARYLAND

A10-1	Schematic, Card No. 10, MCU reset timing and control	267
A10-2	Component layout, Card No. 10, MCU reset timing and control	269
A10-3	MCU reset timing and control	271
A11-1	Schematic, Card No. 11, MCU ship's angular motion meter drive	273
A11-2	Component layout, Card No. 11, MCU ship's angular motion meter drive	275
A11-3	MCU angular motion meter drive	276
A12-1	Schematic, Card No. 12, GCU 400 Hz reference	277
A12-2	Component layout, Card No. 12, GCU 400 Hz reference	279
A12-3	GCU 400 Hz reference	281
A13-1	Schematic, Card No. 13, GCU V_S and $\dot{\psi}$ signal conditioner	283
A13-2	Component layout, Card No. 13, GCU V_S and $\dot{\psi}$ signal conditioner	285
A13-3	GCU V_S and $\dot{\psi}$ signal conditioner	287
A14-1	Schematic, Card No. 14, GCU gyro pendulum simulator roll channel	289
A14-2	Component layout, Card No. 14, GCU gyro pendulum simulator roll channel	291
A14-3	GCU gyro pendulum simulator roll channel	293
A15-1	Schematic, Card No. 15, GCU gyro pendulum simulator pitch channel	295
A15-2	Component layout, Card No. 15, GCU gyro pendulum simulator pitch channel	297
A15-3	GCU gyro pendulum simulator pitch channel	299

THE JOHNS HOPKINS UNIVERSITY
APPLIED PHYSICS LABORATORY
LAUREL, MARYLAND

A16-1	Schematic, Card No. 16, simulator pendulum, 400 Hz model, maneuver compensation amplifier	301
A16-2	Component layout, Card No. 16, GCU simulator pendulum - 400 Hz modulator maneuver compensation amplifier	303
A16-3	GCU simulated pendulum, 400 Hz modulator maneuver compensation amplifier	305
A17-1	Schematic, Card No. 17, MCU system test reference generator	307
A17-2	Component layout, Card No. 17, GCU MCU system test reference generator	309
A17-3	GCU MCU system test reference generator	311
B1-1	Block diagram of wave profiling system	313
B1-2	Interface diagram of motion compensated wave profiling system for the SES-100A	314
B1-3	Wave profiling system	315
B1-4	Cabling diagram for SES-100A motion compensation rack	316
B1-5	MCU/DAS cable diagram	317
B1-6	GCU/DAS cable diagram	318
B1-7	MCU/GCU cable diagram	319
B1-8	MCU/GCU cable diagram	319
B1-9	GCU/CDU cable wiring diagram	319
B1-10	MCU/BAU cable wiring diagram	319
B2-1	Wiring diagram, MCU	321
B2-2	Front panel of MCU	323
B2-3	Top view of MCU, cover removed	324
B2-4	Bottom view of MCU	325
B2-5	Rear view of MCU showing connectors	326

B3-1	Vertical gyro maneuver compensation, block diagram	327
B3-2	Chassis wiring diagram, gyro compensation unit	329
B3-3	Front panel of GCU	331
B3-4	Top view of GCU, cover removed	332
B3-5	Bottom view of GCU	333
B3-6	Rear view of GCU	334
B4-1	Wave profiling system mounted on Ling shaker for vertical axis vibration qualification testing	335
B4-2	Input vibration spectrum as per Mil Spec 167	336
C1-1	BAU wiring diagram	338
C1-2	BAU (a) with cover removed; (b) unit with cover	339
C1-3	Resistance-temperature curve for BAU temperature sensor	340
C1-4	BAU installation details	341
C1-5	Bow boom accelerometer unit	342
D1-1	Cockpit control and display unit (CDU)	372
D1-2	Cockpit control display unit, wiring diagram	373
D1-3	Cockpit display unit, mechanical design	374
D1-4	Cockpit display unit, front panel details	375
E1-1	Acceleration input (a)	379
E1-2	Acceleration input (b)	380
E1-3	Acceleration input (c)	381
E1-4	Acceleration input (d)	382
E1-5	Block diagram of the fifth-order filter	383

E2-1	First-stage filter output in response to a 5 ft vehicle height change in a 15 s period for $\tau_a = 20$	384
E2-2	Second-stage filter output in response to a 5 ft vehicle height change in a 15 s period for $\tau_a = 20$	385
E2-3	Third-stage filter output in response to a 5 ft vehicle height change in a 15 s period for $\tau_a = 20$	386
E2-4	Fourth-stage filter output in response to a 5 ft vehicle height change in a 15 s period for $\tau_a = 20$	387
E2-5	Fifth-order filter output in response to a 5 ft vehicle height change in a 15 s period for $\tau_a = 20$	388
E2-6	First-stage filter output in response to a 0.5 ft vehicle height change in a 0.5 s period for $\tau_a = 20$	389
E2-7	Second-stage filter output in response to a 0.5 ft vehicle height change in a 0.5 s period for $\tau_a = 20$	390
E2-8	Third-stage filter output in response to a 0.5 ft vehicle height change in a 0.5 s period for $\tau_a = 20$	391
E2-9	Fourth-stage filter output in response to a 0.5 ft vehicle height change in a 0.5 s period for $\tau_a = 20$	392
E2-10	Fifth-order filter output in response to a 0.5 ft vehicle height change in a 0.5 s period for $\tau_a = 20$	393
E2-11	First-stage filter output in response to a 5 ft vehicle height change in a 15 s period for $\tau_a = 20$	394
E2-12	Second-stage filter output in response to a 5 ft vehicle height change in a 15 s period for $\tau_a = 20$	395

E2-13	Second-stage filter output in response to a 5 ft vehicle height change in a 15 s period for $\tau_a = 20$	396
E2-14	Fourth-stage filter output in response to a 5 ft vehicle height change in a 15 s period for $\tau_a = 20$	397
E2-15	Fifth-order filter output in response to a 5 ft vehicle height change in a 15 s period for $\tau_a = 20$	398
E2-16	First-stage filter output in response to a 2 ft vehicle height change in a 0.5 s period for $\tau_a = 20$	399
E2-17	Second-stage filter output in response to a 2 ft vehicle height change in a 0.5 s period for $\tau_a = 20$	400
E2-18	Third-stage filter output in response to a 2 ft vehicle height change in a 0.5 s period for $\tau_a = 20$	401
E2-19	Fourth-stage filter output in response to a 2 ft vehicle height change in a 0.5 s period for $\tau_a = 20$	402
E2-20	Fifth-order filter output in response to a 2 ft vehicle height change in a 0.5 s period for $\tau_a = 20$	403
E2-21	Fifth-order filter output in response to a 5 ft vehicle height change in a 15 s period for $\tau_a = 30$	404
E2-22	Fifth-order filter output in response to a 0.5 ft vehicle height change in a 0.5 s period for $\tau_a = 30$	405
E2-23	Fifth-order filter output in response to a 5 ft vehicle height change in a 15 s period for $\tau_a = 30$	406
E2-24	Fifth-order filter output in response to a 2 ft vehicle height change in a 0.5 s period for $\tau_a = 30$	407

THE JOHNS HOPKINS UNIVERSITY
APPLIED PHYSICS LABORATORY
LAUREL, MARYLAND

E2-25	Fifth-order filter output in response to a 5 ft vehicle height change in a 15 s period for $\tau_a = 40$ 408
E2-26	Fifth-order filter output in response to a 0.5 ft vehicle height change in a 0.5 s period for $\tau_a = 40$ 409
E2-27	Fifth-order filter output in response to a 5 ft vehicle height change in a 15 s period for $\tau_a = 40$ 410
E2-28	Fifth-order filter output in response to a 2 ft vehicle height change in a 0.5 s period for $\tau_a = 40$ 411
E2-29	Fifth-order filter output in response to a 5 ft vehicle height change in a 15 s period for $\tau_a = 4.0$ 412
E2-30	Fifth-order filter output in response to a 0.5 ft vehicle height change in a 0.5 s period for $\tau_a = 4.0$ 413
E2-31	Fifth-order filter output in response to a 5 ft vehicle height change in a 15 s period for $\tau_a = 4.0$ 414
E2-32	Fifth-order filter output in response to a 2 ft vehicle height change in a 0.5 s period for $\tau_a = 4.0$ 415

TABLES

1	Tumble test data, Sundstrand Q Flex accelerometer, model QA1200 AA08 SN210	34
2	Conventions for MCU	41
3	System coordinate transformation test data	46
E2-1	Fifth-order filter, summary of response data	378

E2-25	Fifth-order filter output in response to a 5 ft vehicle height change in a 15 s period for $\tau_a = 40$. 408
E2-26	Fifth-order filter output in response to a 0.5 ft vehicle height change in a 0.5 s period for $\tau_a = 40$. 409
E2-27	Fifth-order filter output in response to a 5 ft vehicle height change in a 15 s period for $\tau_a = 40$. 410
E2-28	Fifth-order filter output in response to a 2 ft vehicle height change in a 0.5 s period for $\tau_a = 40$. 411
E2-29	Fifth-order filter output in response to a 5 ft vehicle height change in a 15 s period for $\tau_a = 4.0$. 412
E2-30	Fifth-order filter output in response to a 0.5 ft vehicle height change in a 0.5 s period for $\tau_a = 4.0$. 413
E2-31	Fifth-order filter output in response to a 5 ft vehicle height change in a 15 s period for $\tau_a = 4.0$. 414
E2-32	Fifth-order filter output in response to a 2 ft vehicle height change in a 0.5 s period for $\tau_a = 4.0$. 415

1. INTRODUCTION

Early in 1977, the Surface Effect Ship Project Office (PMS-304), Naval Sea Systems Command, requested that APL support the development of instrumentation for use on board a 100-ton surface effect ship (SES), the SES-100A, which was operating in the Chesapeake Bay. The instrumentation was needed to provide a real-time description of the encountered water surface. The envisioned system would provide inertial sensors and the necessary signal processing to remove the base motion from a vehicle-to-surface height sensor yielding the wave profile.

In the Chesapeake Bay, the water surface conditions can vary significantly. This on-board instrumentation is needed in lieu of the fixed-site wave measurements to provide a continuous, real-time, local description of the encountered sea state. These data would be used in the post-test analysis and correlation studies relating the measured vehicle responses to the input sea conditions encountered during the long high-speed test runs of the SES. Additionally, a real-time output of the wave conditions encountered during the test run would enable the test conductor to judge whether or not the desired test conditions were met. This capability could significantly improve testing efficiency and eliminate unnecessary data reduction and analysis.

The instrumentation to be developed should use existing on-board equipment where applicable.

APL, while conducting a preliminary study of the problem, consulted with concerned individuals at the Surface Effect Ship Test Facility (SESTF), PMS-304, and the David Taylor Naval Ship Research and Development Center. In April 1977, APL submitted a proposal (Ref. 5) to the Sensors and Controls Branch of PMS-304 for the development of a wave profiler for the SES. The proposal was for an inertially compensated laser altimeter wave profiling instrument. It was APL's opinion that the available microwave altimeters would not meet the on-board wave profiler requirements for the SES; hence the development included improving the existing microwave altimeters if possible or developing alternatively a new laser altimeter.

The instrumentation development program proceeded as two semiparallel efforts. One effort was to define the capability of two microwave radar altimeters (the available Collins ALT 50 and

the to-be-purchased TRT AHV 20) used as wave height sensors when mounted in a forward location on the SES bow boom. The other effort was to develop the inertial sensor suite and associated electronic signal processor to remove base motion from the altimeter signal.

This report contains the details of the second effort wherein the hardware for the vehicle motion determination was designed, tested, qualified, delivered, and installed on the SES-100A.

2. THE WAVE PROFILING SYSTEM DESIGN APPROACH

The following approach was used to develop the system design:

1. Consider the SES operational requirements and available sensors,
2. Develop the theoretical model of the system,
3. Analyze and simplify the model to optimize the design for practical use, and
4. Develop the basic systems hardware to fit the model and conduct tradeoffs where necessary to achieve the simplest system that would still meet the design requirements.

To accomplish 1 above, APL received the SES-100A operational envelope and some of the existing vehicle response data that had been gathered while operating in the Chesapeake Bay (Refs. 6 and 7 are typical) together with the system requirements and specifications documented by PMS-304 in Ref. 8. The Surface Effect Ship Test Facility was visited for discussions of their needs and how they would use such a system on the SES-100A. APL reviewed with SESTF personnel the sensors now on the SES-100A and discussed in general terms the SES-100A operational constraints and performance envelopes.

The theoretical model of the system was derived from basic physics where the motion of the altimeter transducer mounting site was described exactly.

The exact model, which includes six degrees of freedom (three linear and three angular), was simplified by (a) sensor consideration, (b) making error studies to show how some terms were not significant for the operational range and could be neglected, and (c) considering the impact of the operational usage of the equipment.

The final system hardware configuration was developed to fit the analytical model by generating analytic models of the sensors and electronics and then combining each in an optimal way by tradeoffs, again considering operational usage and accuracy constraints.

3. PROFILER REQUIREMENTS

The SES, supported by a captured air cushion, can skim the water's surface at speeds greater than 60 kt. The forces that keep the vehicle on the water's surface are provided by a pressurized air chamber (plenum). This is formed by the vehicle's fixed structure on top and on two sides (port and starboard), by the flexible (movable) seals on the bow and stern, and on the bottom by the surface of the water itself. The steady-state pressure within the plenum must be adequate to support the weight of the SES. The air is supplied by axial fans that run at a relatively fixed rpm supplying a volume rate of flow into the plenum. The input rate of flow depends on the ratio of plenum pressure to the outside ambient pressure. The pressure (p) increases inside the plenum until enough force ($F = pA$, where A = planform of the plenum) is generated to cause the vehicle to rise to the surface. At this point, the air escapes from the plenum, reaching equilibrium when the input volume flow rate equals the output volume flow rate. If the vehicle is moving over a water surface containing waves, the plenum volume changes, causing an increase in pressure proportional (to first order) to the decrease in volume. The pressure increase results in a vertical force proportional to the pressure increase, hence a vertical acceleration of the SES.

Analytical predictions of the motions of larger SES (up to 3000 tons) indicate that the heave resonance at certain combinations of sea state and ship heading may be sufficient to induce crew seasickness. For this reason, a ship ride control system is being designed to attenuate the heave motions and to improve crew habitability. The SES-100A design for ride control is to vent dynamically the plenum to maintain a constant pressure under the vehicle. This is done by sensing plenum pressure and hence commanding the opening of vents to maintain the pressure constant. The SES-100A test data show that the pressure fluctuation and the resulting vertical acceleration are reduced by an active ride control system.

The evaluation of a ride control system requires correlating the vehicle vertical response to the water surface conditions (sea state) as they are encountered. In particular, a precise measure of the wave profile must be available if a model of the system is to be generated for simulation work. Also, to improve the ride further, one could sense volume change rather than the resulting pressure change as the ride control sensor. One could conceive a system where a wave profiler could be used to compute the volume change

about to occur and eliminate the effect. Hence there is the present need for an on-board wave profiler and a suggestion of the possibility of not only using the device as an R&D instrumentation tool but also as a part of the active control system for ride control and for vehicle stabilization and control.

How does one profile a wave? Apparently there are many approaches to wave profiling (sea-state definition), but most appear inadequate in the SES application because of the short measurement distance and because the surface to be measured is rough water. The profiler accuracy requirement is based on the vehicle's response to changing volumes within the plenum due to wave encounters. The vehicle acceleration is proportional to $1/[1-(\Delta V/V)]$ (to first order the ratio of the change in plenum volume (ΔV) to the steady-state plenum volume (V)). For the fixed planform area, this converts to $1/[1-(\Delta h/h)]$ (the ratio of the change in height (Δh) to the steady-state height (h)). Hence for a plenum height of 10 ft, for example, a 1.0 ft change in height at 1 Hz will produce a 0.1 g input at 1 Hz. To be useful a wave profiler must be able to profile the waves to better than 0.1 ft at the encounter frequencies of interest.

The frequencies of waves encountered are determined by the encountered sea state and the vehicle speed. Using the Pierson-Moskowitz sea spectrum definition where $\lambda = 13.14 h$, Fig. 1 results, which relates wave encounter frequency as a function of vehicle speed for different wave heights. This also assumes head seas and that the waves have no speed of their own. The effect of wave speed is to shift the spectrum but not to change it significantly. The lower amplitude waves have the higher encounter frequencies. However, the high frequency-low amplitude waves have less effect on the vehicle due to effects such as wave pumping and vehicle natural response to pressure fluctuations. Referring to data from tests of the SES-100A in the Chesapeake Bay, the center of gravity vertical acceleration power spectral density and the cushion pressure power spectrum each peak around 1.5 Hz with the energy spread from 0.5 to 5 Hz. It is obvious that the smaller waves ($h < 1$ ft) that have wave lengths of ≈ 13 ft have very small effects on the vehicle. Hence the system response should be accurate to at least 5 Hz. These wave profiler system requirements are documented in part in Refs. 8 and 9.

4. DEVELOPMENT OF THE THEORETICAL MODEL

The output from a vehicle-mounted altimeter that is being used as a surface profiler is corrupted by the vehicle motions.

In Fig. 2, the altimeter output (E_0) is the sum of the output due to the mean height (h_0), the vehicle motion (h_v), and the surface fluctuation (h_w). For a surface vehicle traversing the water, the mean height (h_0) is assumed to be relatively fixed and not a strong function of time. Both h_v and h_w are functions of time and are highly dependent on vehicle speed over the water. The altimeter output is given by

$$E_0(t) = h_0 + h_v(t) + h_w(t) . \quad (1)$$

If $h_v(t)$ can be determined accurately by an independent measurement, the altimeter output signal can be corrected by a simple subtraction to yield the mean altitude plus the profile of the wave surface. This corrected altimeter signal can be analyzed to yield the encountered wave profile, and if the ship's speed was also recorded the sea state can be determined.

The vehicle vertical motion for this sample model can be obtained, for example, from a single vehicle-mounted vertical acceleration sensing accelerometer whose output (\ddot{h}_v) is ideally integrated twice as shown in Eq. 2 to yield a continuous signal, if scaled correctly, representing vehicle vertical height,

$$h_v(t) = \iint \ddot{h}_v dt dt . \quad (2)$$

Basically, this is what we want to implement but for a more complex situation where the vehicle has three angular motions and three linear motions. The problem is to measure the total acceleration using a triad of vehicle-mounted accelerometers and to transform this measurement to the local vertical reference axis for double integration. The exact equation for the coordinate transformation of accelerations sensed in body coordinates to the acceleration of the body in local level reference coordinates is given in Eq. 3:

$$[A] = [M] [a] , \quad (3)$$

where

$$[A] = \begin{bmatrix} \ddot{X} \\ \ddot{Y} \\ \ddot{Z} \end{bmatrix} \quad \begin{array}{l} \text{local horizontal components} \\ \text{of acceleration} \\ \\ \text{vertical component of acceleration} \end{array}$$

$$[a] = \begin{bmatrix} \ddot{x} \\ \ddot{y} \\ \ddot{z} \end{bmatrix} \quad \begin{array}{l} \text{deck-mounted accelerator triad, when} \\ \ddot{x} \text{ is the component along vehicle } C_L, \\ \ddot{y} \text{ is the component athwartship, and} \\ \ddot{z} \text{ is perpendicular to the deck plane,} \end{array}$$

and $[M]$ is the 3×3 coordinate transformation matrix for ordered angular motions (Ref. 10). Assuming the order of motions is heading (ψ), then pitch (θ), and finally roll (ϕ), the $[M]$ matrix in Eq. 4 results:

$$[M] = \begin{bmatrix} C\theta C\psi & -S\psi C\phi + C\psi S\theta S\phi & S\psi S\phi + C\psi S\theta C\phi \\ S\psi C\theta & C\psi C\phi + S\psi S\theta S\phi & -C\psi S\phi + S\psi S\theta C\phi \\ -S\theta & C\theta S\phi & C\theta C\phi \end{bmatrix} , \quad (4)$$

where $C = \text{cosine}$ and $S = \text{sine}$.

Substituting and solving Eq. 3 for the vertical acceleration \ddot{Z} in terms of the body angles and body accelerations, Eq. 5 results:

$$\ddot{Z} = -\ddot{x} \sin\theta + \ddot{y} \cos\theta \sin\phi + \ddot{z} \cos\theta \cos\phi . \quad (5)$$

This is an exact equation for the vertical acceleration in terms of the body-sensed acceleration components (\ddot{x} , \ddot{y} , and \ddot{z}) and the associated body attitudes (roll ϕ , pitch θ).

Now that we have developed the basic system model for determining vehicle vertical motion, the sensor models and electronic models are exercised in the system model to determine error sensitivities. These error sensitivities when in conjunction with the operational requirements provide requirements for sensor and electronics performance. Performance tradeoffs are then conducted to obtain a final simplified system design that is more easily implemented in the hardware.

Since the heading attitude does not appear in the exact transformation Eq. 5, the roll and pitch attitudes with the correct order of motion can be obtained from a single sensor called a vertical gyro. With the accelerometer triad mounted at the altimeter site and aligned relative to the axes of the vertical gyro and Eq. 5 implemented electronically as shown in Fig. 3, the system output will ideally yield the local vertical component of vehicle acceleration at the altimeter measurement site. Double integration of Eq. 5 with the appropriate scaling will ideally yield the vehicle vertical motion as a function of time. Subtracting this signal from the altimeter output signal ideally produces the desired wave profile. However, when we consider a realistic but simple model of an accelerometer as shown in Eq. 6,

$$A_0 = a_0 + a_1 \ddot{h} = \ddot{z} , \quad (6)$$

and consider the case where both the angles θ and ϕ are zero exactly, then Eq. 5 becomes simply

$$\ddot{Z} = \ddot{z} .$$

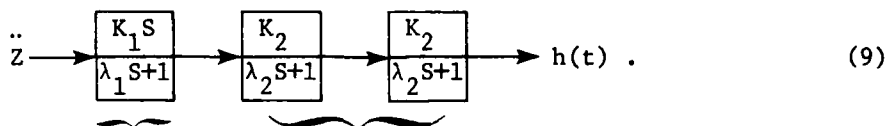
Substituting Eq. 6 for \ddot{Z} , the equation becomes

$$\ddot{Z} = a_0 + a_1 \ddot{h} . \quad (7)$$

Double integrating, Eq. 7 becomes Eq. 8:

$$\begin{aligned}\iint \ddot{z} dt dt &= \iint (a_0 + a_1 \ddot{h}) dt dt \\ &= a_0 \frac{t^2}{2} + a_1 \iint \ddot{h} dt dt \\ &= \frac{a_0 t^2}{2} + a_1 h(t) .\end{aligned}\quad (8)$$

Realistically $a_0 \neq 0$; hence the desired height function $h(t)$ is corrupted by the error $a_0 t^2/2$, which will saturate the system in 15 s if $a_0 \approx 1$ mg. The same problem of "DC offset" can be caused by tilt, misalignment, other transducer errors, and electronic errors. The double integrator can be designed to reject these DC offset-type errors and still yield accurate height $h(t)$ over the frequency range of interest. To accomplish DC rejection and still accomplish double integration ($1/S^2$) at higher frequencies, a special filter is required. To achieve DC isolation, a high-pass filter ($S/\lambda S+1$) is required prior to the integration. Also a low-pass filter ($1/\lambda S+1$) becomes an integrator for signal frequencies well above the filter corner frequency ω ($\omega = 1/\lambda$). Hence the minimum signal processor required to achieve the double integration is shown in Eq. 9.



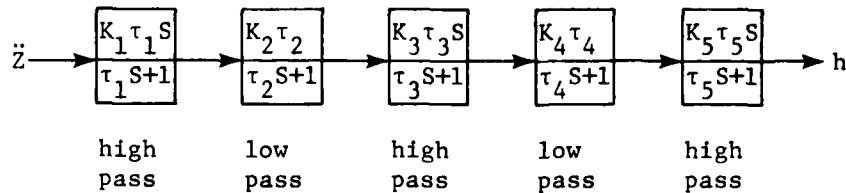
high-pass filter low-pass filters

At higher frequencies ($\omega > \omega_1, \omega_2, \omega_3$), Eq. 9 reduces to

$$\ddot{z} \rightarrow \left[\frac{K}{S^2} \right] \rightarrow h ; \quad K = \frac{K_1 K_2^2}{\lambda_1 \lambda_2^2} . \quad (10)$$

Further consideration of both actual electronic implementations is discussed in the detailed electronic design section of this report. Achieving the required accuracy over the frequency range from 0.05 Hz and up requires that each low-pass filter be isolated by high-pass filters to achieve the accuracy and bandwidth desired.

The resulting filter is fifth order as shown in the following diagram.



This fifth-order filter $\frac{K \tau^5 S^3}{(\tau S + 1)^5}$ (for $\tau_1 = \tau_2 = \dots = \tau_5$ and with

$K = K_1 K_2 K_3 K_4 K_5$) reduces to a double integration (K/S^2) for sufficiently high angular signal frequencies ω compared to $1/\tau$. The selection of the τ_i to be used in the filter is discussed in the detailed electronic design section and in Appendix E.

5. ERROR ANALYSIS

Equation 5 represents the exact coordinate transformation from body to reference coordinates. Since the SES-100A roll and pitch altitude excursions are small (typically less than $\pm 10^\circ$), the maximum error in assuming $\cos \theta = \cos \phi = 1$ in the system is shown in the detailed electronic design section to be about 3% in height. For a height excursion of, for example, ± 5 ft, this simplification results in an error of ± 0.15 ft. Also, if we consider the case where the x and y axis accelerometers are excluded (i.e., a single vertical accelerometer) and implement the following equation,

$$\ddot{Z} = \ddot{z} \cos \theta \cos \phi,$$

the resulting errors for angles of $\pm 10^\circ$ are 3% of h. For this extreme case of $\pm 10^\circ$ combined with height excursions of 5 ft, there is an error of 0.15 ft, which is not tolerable. Another algorithm was found by the authors experimentally when the cosine terms were not included but, by simple gain changes ($\sin \theta \rightarrow [\sin \theta]/2$, $\sin \phi \rightarrow [\sin \phi]/2$, the accuracy of the system was greatly improved. This simplified coordinate correction is shown in Fig. 4. For example, with the new algorithm the system maximum errors for $\pm 10^\circ$ excursion of θ or ϕ are shown to be less than 0.03%, which is an improvement of 135 over the other case. Now the maximum error in height attributable to the coordinate transformation simplification for a vehicle height excursion of ± 5 ft is only 0.0015 ft, which is acceptable.

ACCELEROMETER ERROR MODEL ANALYSIS

Typically, an accelerometer model is given by

$$E_0 = a_0 + a_1 \ddot{x}_1 + a_2 \ddot{x}_2 + a_3 \ddot{x}_3 + a_4 \Delta T + a_5 \ddot{x}_1^2 + a_6 \ddot{x}_1 \ddot{y}_1 + \dots, \quad (11)$$

where the a_i 's are the sensitivity coefficients as follows:

- a_0 = zero output (volts),
- a_1 = scale factor (volts/input unit of acceleration),

5. ERROR ANALYSIS

Equation 5 represents the exact coordinate transformation from body to reference coordinates. Since the SES-100A roll and pitch altitude excursions are small (typically less than $\pm 10^\circ$), the maximum error in assuming $\cos \theta = \cos \phi = 1$ in the system is shown in the detailed electronic design section to be about 3% in height. For a height excursion of, for example, ± 5 ft, this simplification results in an error of ± 0.15 ft. Also, if we consider the case where the x and y axis accelerometers are excluded (i.e., a single vertical accelerometer) and implement the following equation,

$$\ddot{Z} = \ddot{z} \cos \theta \cos \phi,$$

the resulting errors for angles of $\pm 10^\circ$ are 3% of h. For this extreme case of $\pm 10^\circ$ combined with height excursions of 5 ft, there is an error of 0.15 ft, which is not tolerable. Another algorithm was found by the authors experimentally when the cosine terms were not included but, by simple gain changes ($\sin \theta \rightarrow [\sin \theta]/2$, $\sin \phi \rightarrow [\sin \phi]/2$, the accuracy of the system was greatly improved. This simplified coordinate correction is shown in Fig. 4. For example, with the new algorithm the system maximum errors for $\pm 10^\circ$ excursion of θ or ϕ are shown to be less than 0.03%, which is an improvement of 135 over the other case. Now the maximum error in height attributable to the coordinate transformation simplification for a vehicle height excursion of ± 5 ft is only 0.0015 ft, which is acceptable.

ACCELEROMETER ERROR MODEL ANALYSIS

Typically, an accelerometer model is given by

$$E_0 = a_0 + a_1 \ddot{x}_1 + a_2 \ddot{x}_2 + a_3 \ddot{x}_3 + a_4 \Delta T + a_5 \ddot{x}_1^2 + a_6 \ddot{x}_1 \ddot{y}_1 + \dots, \quad (11)$$

where the a_i 's are the sensitivity coefficients as follows:

a_0 = zero output (volts),

a_1 = scale factor (volts/input unit of acceleration),

a_2, a_3 = cross-coupling scale factor,
 a_4 = zero output temperature sensitivity,
 x_i 's = three-body acceleration components, and
 E_0 = accelerometer output.

There are many other terms in the accelerometer error model, but our past experience with accelerometers has shown that the other terms are insignificant when operating in a shipboard environment.

Typically, the a_0 term is called the accelerometer bias. In this system, the three accelerometers will be aligned so that their input axes are orthogonal and their outputs are summed with the -1 g bias so that the \ddot{Z} result will be exactly zero. The a_0 term is determined for a particular unit by tumble-testing the accelerometer in the laboratory. This test is described in the following.

The accelerometer scale factor, a_1 , relates the output in volts in response to acceleration inputs along the input reference axis, x_1 . x_1 is usually defined mechanically (to some accuracy specification) to several case reference locations. a_1 is found by tumble-testing the accelerometer in the laboratory. The tumble test consists of tumbling in a precisely known manner the accelerometer input axis through a 1 g field and recording the response to the acceleration inputs at discrete levels of the + and -1 g acceleration input. A least-squares polynomial fit to the data then determines the desired coefficients of the accelerometer model. For the inertial grade accelerometer such as the Sundstrand Q Flex Model QA 1200, the higher order terms are negligible as will be shown from the analysis of the residuals for the first-order linear least-squares fit. The tumble test is also used to determine the exact location of the input reference axis. Usually a computer regression analysis is applied to the tumble test data using at least 36 data points to determine the polynomial coefficients and the axis definition. A simpler solution in determining the coefficients and input axes alignments is possible for precision accelerometers. The simpler technique is easily done using desk calculations. The data outputs to be used in the calculations are from the tumble test. These are inputs = x_1 and output of acceleration = y_1 . Linear fit to the data using first-order least-squares fit to get a_1 and b_1 ($y = a_1 + b_1x$) is possible as follows:

$$x_1 = g \sin \theta_1,$$

θ_1 = tumble angle measured from some reference starting position (usually the accelerometer mounting reference surface),

$$y_1 = \text{accelerometer output in volts} = b g \sin \theta_1,$$

g = gravity,

b = volts/g (scale factor), and

a = bias (volts).

The accelerometer output tumble data

$$y_1 = a + b g \sin \theta_1 + \text{other unknowns}$$

is actually a periodical function in θ . The first step is to "linearize" the data by substituting x_1 for $g \sin \theta_1$.

The second step is to compute by the method of least squares the first-order coefficients a_1 and b_1 from the tumble data and then compute

$$y_{c1} = a_1 + b_1 x_1$$

where $x_1 = g \sin \theta_1$.

Now compute the residuals to get

$$y_{R1} = y_1 - y_{c1}.$$

Now, assuming that the error (residuals) is due to misalignment of the accelerometer input reference axis to the case reference, again compute the coefficients of the linear fit to the residual data. Now these coefficients are a_2 and b_2 for the fit

$$y_{c1}' = a_2 + b_2 x_1'$$

where $x_1' = g \cos \theta_1 (= x_2)$.

Now from

$$Y = a_1 + b_1 x_1 + a_2 + b_2 x_2$$

and substituting for x_1 and x_2 , we get

$$\begin{aligned} Y &= a_1 + a_2 + b_1 g \sin \theta + b_2 g \cos \theta \\ &= (a_1 + a_2) + g \sqrt{b_1^2 + b_2^2} \sin (\theta + \phi) \end{aligned}$$

where

$$\phi = \tan^{-1} \frac{b_2}{b_1} \text{ is the misalignment angle,}$$

$$(a_1 + a_2) = \text{bias, and}$$

$$\sqrt{b_1^2 + b_2^2} \text{ is the scale factor.}$$

Finally, to ensure that the accelerometer error model has no significant higher order terms, the residuals from the second fit that determined the quadrature error are further analyzed to ensure that the higher order (x_i^2) terms are small; i.e.,

$$\begin{aligned} Y &= a_1 + b_1 x_1 + a_2 + b_2 x_2 \\ &+ C_1 x_1^2 + C_2 x_2^2 + \dots, \text{ etc.,} \end{aligned}$$

We want C_1, C_2 , etc. to be small ($\frac{C_i}{b} < 0.001 \text{ g/g}^2$). Now if the higher order coefficients are small, further data simplification is possible. Note that from the data linear model equation

$$Y_1 = a_1 + b_1 g \sin \theta_1 + a_2 + b_2 g \cos \theta_1$$

for angles $\theta_1 = 0^\circ, 90^\circ, 180^\circ$, and 270° , and for $g = 1$, yielding the output data:

$$Y_0 = a_1 + a_2 + b_2, \quad \theta = 0$$

$$Y_{180} = a_1 + a_2 - b_2, \quad \theta = 180$$

$$Y_{90} = a_1 + a_2 + b_1, \quad \theta = 90$$

$$Y_{270} = a_1 + a_2 - b_1, \quad \theta = 270$$

can be manipulated as follows to yield the coefficients without using a least-squares fit.

$$Y_0 + Y_{180} = 2(a_1 + a_2) = \text{twice bias} = 2a$$

$$Y_{90} + Y_{270} = 2(a_1 + a_2) = \text{twice bias} = 2a$$

$$Y_0 - Y_{180} = 2(b_2)$$

$$Y_{90} - Y_{270} = 2(b_1)$$

Hence

$$a = \frac{Y_0 + Y_{180} + Y_{90} + Y_{270}}{4}$$

$$b_1 = \frac{Y_{90} - Y_{270}}{2}$$

$$b_2 = \frac{Y_0 - Y_{180}}{2}$$

$$b = \sqrt{b_1^2 + b_2^2}$$

$$\theta = \tan^{-1} \frac{b_2}{b_1}$$

to get $Y = a + b x$, for $x = g \sin(\theta + \phi)$.

Tumble test data (36 points) are shown in Table 1 for one of the three Sundstrand accelerometers tested to show the values of the sensitivity coefficients of the accelerometer model. The

Table 1
Tumble test data, Sundstrand Q Flex accelerometer,
model QA1200 AA08 SN210.

θ_1 (deg)	x_1 (g)	y_1 (V)
0	0	+0.0077
10	0.173648	+0.4419
20	0.342020	+0.8629
30	0.5	+1.2577
40	0.64278	+1.6145
50	0.76604	+1.9224
60	0.866025	+2.1721
70	0.93969	+2.3559
80	0.9848	+2.4683
90	1.00	+2.5060
100	0.9848	+2.4677
110	0.93969	2.3544
120	0.866025	2.1966
130	0.76604	1.9196
140	0.64278	1.611
150	0.5	1.2538
160	0.34202	0.8586
170	0.173648	0.4374
180	0.0	0.0032
190	-0.173648	-0.4308
200	-0.34202	-0.8517
210	-0.5	-1.2467
220	-0.64278	-1.6036
230	-0.76604	-1.9116
240	-0.866025	-2.1613
250	-0.93969	-2.3450
260	-0.9848	-2.4573
270	-1.00	-2.4947
280	-0.9848	-2.4565
290	-0.93969	-2.3434
300	-0.866025	-2.1590
310	-0.76604	-1.9086
320	-0.64278	-1.6000
330	-0.5	-1.2428
340	-0.34202	-0.8475
350	-0.173648	-0.4263
360	0	+0.0076

Results:

First linear fit

$$Y_1 = a_1 + b_1 x_1 = a_1 + b_1 g \sin \theta_1$$

$$a_1 = -0.005783 \text{ V}$$

$$b_1 = 2.50084 \text{ V/g}$$

Second linear fit on residuals of first fit

$$Y_2 = a_2 + b_2 x_2 = a_2 + b_2 g \cos \theta_1$$

$$a_2 = 0.0001785 \text{ V}$$

$$b_2 = 0.0019045 \text{ V/g}$$

Combined fit

$$Y = a + b x$$

$$a = -0.0010347 \text{ V} = 40 \text{ } \mu\text{g}$$

$$b = 2.5001861 \text{ V/g}$$

$$\text{rms of residuals} = 0.000095 \text{ V} = 3.2 \text{ } \mu\text{g}$$

$$\phi = 2.5 \text{ arc min} \pm \left(\tan^{-1} \frac{b_2}{b_1} \right)$$

results show that the first-order least-squares fit gives $a_1 = -0.005783$ V for the bias and $b_1 = 2.50084$ V/g for the scale factor. The second-order least-squares fit to the residuals remaining from the first fit yields $a_2 = 0.0001785$ V and $b_2 = 0.0019045$ V/g.

Hence the accelerometer misalignment to its reference surface is 2.6 arc min. The second-order coefficients, if computed, could be a maximum of 0.000285 V/g², which is extremely small and cannot have any effect on the system. The maximum equivalent acceleration squared error coefficient would be ≈ 0.0001 g/g². The tumble test data were taken over a period of 3 h operation. If only the four position data were used for the coefficient determination, the following will result compared to Table 1 results from the least-squares fit (in parentheses).

$$b_1 = \frac{Y_{90} - Y_{270}}{2} = 2.50035 \quad (2.50084)$$

$$(a_1 + a_2) = \frac{Y_{90} + Y_{270}}{4} = 0.00565 \quad (0.00560)$$

$$b_2 = \frac{Y_0 - Y_{180}}{2} = 0.00225 \quad (0.0019)$$

$$\theta = \tan^{-1}\left(\frac{b_2}{b_1}\right) = \tan^{-1} \frac{0.00225}{2.50035} = 3.09 \text{ arc/min} \quad (2.6)$$

The errors in the simple technique compared to the more exact method of least-squares fit are as follows:

$$\text{SF error} = 0.00049 \text{ V/g} = 0.02\%$$

$$\text{Bias error} = 0.00005 \text{ V} = 0.00012 \text{ g}$$

$$\text{Alignment error} = 0.5 \text{ arc min} \approx 0.01^\circ$$

Hence for the typical Sundstrand QA 1200 accelerometer the errors in calibration and alignment using the four-position data are quite insignificant.

GYRO ERROR MODEL ANALYSIS

Reference 4 describes the development of the vertical gyro model. As a result of the study, the vertical gyro erection control electronics used on the SES-100A required modifications to provide for the ship's maneuver compensation. This compensation was necessary to increase the operational usage of the wave profiling system on the SES-100A.

Systematically, a vertical gyro erects to the total acceleration vector. This vector is assumed to be the gravity vector (local vertical). However, on ships, etc., the vector tilts away from the local vertical by an amount proportional to the lateral acceleration resulting from maneuvering. The tilt angle of the local vertical is given to first order in Eq. 12:

$$\theta_T = \tan^{-1} \frac{a}{g}, \quad (12)$$

where

θ_T = tilt angle,

a = magnitude of the lateral acceleration component perpendicular to the g vector, and

g = magnitude of the local gravity vector.

Figure 5 shows tilt angles as functions of the ship's speed and turning rates. Typically, for the SES-100A at 50 kt and for a $1.5^\circ/\text{s}$ turning rate, the tilt error is 4° . The vertical gyro is designed to filter the effects of those lateral accelerations that occur at the higher frequencies due to the ship's natural response to the sea. However, the ship's maneuvers are sustained for very long periods (very low frequencies) and hence are not filtered. To ensure alignment of the accelerometers and the vertical gyro necessary for precise vertical motion determination in the wave profiling system, the uncompensated system could not be used during maneuvers, and long delays would have been required after maneuvers to allow the vertical gyro to reerect to the undisturbed g vector.

The ship's maneuver compensation signals for the vertical gyro are derived from two ship reference sensors: the ship's speed log (v_s) and the ship's yaw rate ($\dot{\psi}$) gyro. The two acceleration terms \dot{v}_s and $v_s \dot{\psi}$, are computed in the Maneuver Compensation Unit (MCU)

electronics from the two inputs. The computed signals are used as inputs to the simulated gyro two-axis, vertical sensor (two-axis electromagnetic pendulum). These simulated pendulum responses to the maneuver accelerations are subtracted from the actual pendulum response signals to ideally cancel the maneuver acceleration influence at its source. Hence the vertical gyro is no longer sensitive to maneuver-induced accelerations. This addition of the ship's maneuver compensation to the vertical reference system provides for accurate gyro performance for all the ship's users.

The maneuver acceleration errors now have been reduced to the effect of the error in the ship's speed source, the error in the yaw rate, and the error in the compensation electronics. With a goal of $<0.1^\circ$ of error in the roll and pitch axis alignment, the steady-state error in the ship's speed can be as large as $\pm 5\%$. Doubling these errors only doubles the error in the height error from 0.05 to 0.1 ft.

DISCUSSION OF SYSTEM ERRORS

The vertical motion model is given by

$$h(t) = \iint \ddot{h} dt dt . \quad (13)$$

The errors then are errors in integration or error in \ddot{h} . The errors in the integration are discussed in the detailed electronics design section. The exact equation for \ddot{h} is as shown in Eq. 14 when \ddot{h} is replaced by \ddot{Z} from Eq. 5.

$$\ddot{Z} = -\ddot{x} \sin \theta + \ddot{y} \sin \phi \cos \theta + \ddot{z} \cos \theta \cos \phi . \quad (14)$$

The error sources then are in the mechanization of Eq. (14), where

\ddot{x} is the x body axis accelerometer output in response to the ship's total inputs,

\ddot{y} is the y body axis accelerometer output in response to the ship's total inputs,

\ddot{z} is the z body axis accelerometer output in response to the ship's total inputs,

$\sin \theta$ is the vertical gyro output about the pitch gimbal in response to the ship's inputs,

$\sin \phi$ is the vertical gyro output about the roll gimbal in response to the ship's inputs, and

$\cos \theta$ and $\cos \phi$ must be derived from $\sin \theta$, $\sin \phi$, respectively.

However, the mechanization used in the system as given in Eq. 15 from Fig. 4 does not require computation of $\cos \theta$, $\cos \phi$ or the associated multiplications.

$$\ddot{z} = -\ddot{x} \frac{\sin \theta}{2} + \ddot{y} \frac{\sin \phi}{2} + \ddot{z} . \quad (15)$$

The accelerometers and the vertical gyro have bandwidths well in excess of the ship's natural frequencies or the resonance frequencies; hence phase delays are not a problem. Height errors due to phase delay in the electronics are considered in the detailed electronic design section.

The sources for error are in the generation of these five terms

$$\ddot{x} , \frac{\sin \theta}{2} , \ddot{y} , \frac{\sin \phi}{2} , \text{ and } \ddot{z} ,$$

i.e., the four sensors used as a measure of \ddot{x} , \ddot{y} , \ddot{z} , θ , and ϕ . Actually the problem is simply the error in the three terms,

$$\ddot{x} \frac{\sin \theta}{2} , \ddot{y} \sin \phi , \ddot{z} .$$

The accelerometer model is shown later to be simply

$$\ddot{x} = E_x = a_1 + b_1 \ddot{x} + \text{misalignment term},$$

$$\ddot{y} = E_y = a_2 + b_2 \ddot{y} + \text{misalignment term},$$

$$\ddot{z} = E_z = a_3 + b_3 \ddot{z} + \text{misalignment term}.$$

The a_1 terms are bias terms and have been shown by actual accelerometer testing to be very stable and are not functions of time. Hence, the fifth-order filter that does the double integration rejects these terms. The b terms are the accelerometer scale factor

terms that relate the accelerometer output signal to the input acceleration along its input axis. The scale factor accuracy and stability are determined by testing. However, the accelerometer scale factor error tolerance is determined from the integral equation:

$$h(t) = \iint \ddot{z}(t) dt dt .$$

If

$$\ddot{z}(t) = (b + \epsilon) \ddot{z}(t) ,$$

where b (the exact scale factor) and ϵ (scale factor error) are constants, the maximum error in h is directly proportional to the product of the maximum excursion in h and the error ϵ . The maximum height excursion for consideration is 5 ft. Hence, the maximum error in the scale factor is the ratio of the maximum allowed height error divided by the height excursion or $0.05/5 = 1\%$. The stability and linearity of the accelerometer chosen for this system are better than 0.1%. The only mechanization problem is to ensure that b is set to better than 1% and remains stable. This is true for the vertical axis. For the other two axes where the outputs are attenuated by the roll and pitch angles and the maximum input accelerations are about 10 times lower, the scale factor error can be 10 times larger or greater than 10%.

6. SYSTEM ALIGNMENT, CALIBRATION, AND TESTING IN THE LABORATORY

This section discusses the calibration procedures and test sequences used during the system test and calibration. Also discussed is the self-test feature of the electronics system. The reader should refer to Ref. 3 for a detailed description of the hardware and its operation. The vertical gyro testing was documented in Ref. 4, and the accelerometer triad assembly and detailed testing are discussed in several other sections of this report. The accelerometer scaling is part of the MCU electronics since the accelerometer output scaling resistor is located on cards #1 and #8 approximately 150 ft (cable) from the accelerometer. The microwave radar altimeter is discussed in Refs. 1, 2, and 11. For this system design and testing, the altimeter interface is assumed to be a gain (200 MV/ft) with electronic provisions for offset and gain adjustments. No attempts were made in the electronic design to accommodate altimeter transfer function time constants and other peculiarities since very little was known about the altimeters at the time of the electronic system design. The sign conventions for all system interfaces are shown in Table 2. The system is designed to accommodate two independent altimeter inputs at the same time. A front panel selector switch is provided for selecting which of the two units signals will be used by the wave profiling system. A discussion of the altimeter selector switch and altitude offset adjustment procedure is contained in Ref. 3.

The electronics in both the MCU and the Gyro Compensation Unit (GCU) are built as 22 cards, of which 17 are different designs (5 being duplicates). There are two each of card #2, two each of card #8, two each of card #6, and three each of card #5. Each of the 17 cards is also spared for a total of 39 cards delivered with the system. The schematics, assembly drawing, and photographs for the 17 card designs are contained in Appendix A (Figs. A1-1 through A17-3). The design details for the electronics are contained in the detailed electronic design section of this report. The chassis drawings show the card-to-card wiring connections and the system interconnections with the external sensors and user equipment.

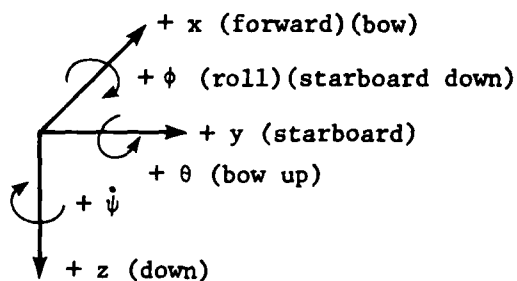
It is assumed that all the following tests are conducted with the system completely interconnected (except for disconnecting the DAS cables J2 and J8) unless noted otherwise, and that the gyro and accelerometer unit are aligned and mounted on an indexing table. All cards must be removed except for card #1 and two #8 cards. The cards are inserted into the system (and remain in)

Table 2
Conventions for MCU.

V_s = Ship's speed (+ forward)
 $\dot{\psi}$ = Yaw rate (+ turn to starboard)
 \dot{V}_s = Forward acceleration (+ for increasing speed)

x, \dot{x}, \ddot{x} = Ship's (+ forward) }
 y, \dot{y}, \ddot{y} = Starboard positive } ship's deck coordinates
 z, \dot{z}, \ddot{z} = Down positive }

X } = Local horizontal (+ forward)
 Y } (+ starboard) } reference coordinates
 Z = Vertical (+ down)



only as they are sequentially tested in the following steps. Refer to the chassis layout and assembly drawing for card locations, etc. Turn on the MCU and GCU and check the voltage using the front panel selector switches and meters.

MCU ALIGNMENT AND CALIBRATION

1. Card #3 - 400 Hz Reference for MCU (A3-1, A3-2, A3-3)
Set input (ship's supply to 115 V rms - 400 Hz and ensure that the output E_{R1} is +8 VDC ± 0.08 VDC. If not, adjust P1 on card #3 until the E_{R1} voltage is correct. Also ensure that E_{R2} is as specified on Fig. A3-1 (i.e., in square wave at 400 Hz, +4.1 V to -0.6 V). The 8 VDC signal is used to isolate the system from the ship's 400 Hz power fluctuations.
2. Card #2 - Normalized Synchro to DC Converters (Figs. A2-1, A2-2, A2-3)
This card provides the DC output signal that represents the sine of the pitch angle (θ_p), also represented as θ in the theory, for the coordinate converter input. This circuit, as shown in Fig. A2-1, first demodulates the gyro pitch synchro signal (S_1/S_3), then normalizes with respect to the ship's power in the divider circuit and puts out a buffered DC signal. Using a scope with the gyro case pitched up exactly $5^\circ \pm 0.05^\circ$, adjust the phase of E_{02} via P1 on card #2 (pitch) to be exactly in phase with the reference 400 Hz supplied at the ship's input, which is pin 6 of the ship's isolation transformer (TI) in the MCU. Now the signals at E_{03} can be checked. Read E_{03} at a pitch forward up of 5° ($E_{03} \cong 2.69$ V) and then move the gyro case through 10° to forward down 5° to read $E_{03} \cong -2.69$. The difference should be 5.38 VDC ± 0.005 VDC. Rotate the gyro case toward zero angle (level) by monitoring the synchro signal (S_1/S_3) at T_2 on a scope or rms voltmeter. When the signal reaches a minimum,

the gyro is considered level. If the case level reference is not level to $<0.1^\circ$, there is a gyro problem. E_{03} , E_{04} , and E_{05} should each be zero at this case attitude. If E_{05} is not zero, adjust P2 on card #2 (pitch) until E_{05} goes to zero. Now swing the gyro case through $+5^\circ$ to -5° reading E_{06} at the peaks. The difference should be $1.745 \text{ VDC} \pm 0.005 \text{ VDC}$ for 10° . Adjust P3 until the scaling requirement is satisfied. Repeat this step for the roll axis of the gyro, which is roll card #2, marked θ_R or ϕ .

3. Card #8 (Figs. A8-1, A8-2, A8-3)

The two cards #8 provide the \ddot{x} accelerometer and \ddot{y} accelerometer scale factor control, buffered accelerometer outputs to DAS, and the multiplication of the accelerometer signal and the associated gyro angle as part of the coordinate transformation mechanization as follows:

$$\theta \text{ channel} \quad \ddot{y} \frac{\sin \theta}{2}$$

$$\phi \text{ channel} \quad \ddot{x} \frac{\sin \phi}{2}$$

The scaling of the accelerometer is checked for each channel by a $\pm 1 \text{ g}$ two-position tumble about each axis where the difference in the measured values at pin 1 on card #8 must be $5.000 \text{ VDC} \pm 0.0025 \text{ VDC}$. The DAS-buffered output will be saturated for these $\pm 1 \text{ g}$ inputs. To check the DAS outputs, set the input by repositioning the accelerometer until the value of pin 1 is, for example, 1 VDC . The DAS output should be $8X1$ or $8 \text{ VDC} \pm 1\%$. Ensure that only the five cards (one each #2, two each #3, and two each #8) are inserted into the MCU. Jumper pins 6 to 7 on card #8 allow the signal to flow through the system. Position the accelerometer until the input to the multiplier is, for example, 0.2179 VDC (for a 5° angle). The signal input for that card at the Y input on the

multiplier will be 0.3112 VDC for a 5° angle. The output will be the product of these two values divided by 10 or 0.0678 VDC $\pm 1\%$. Repeat for both cards #8. Temporarily allow the jumpers to remain on the cards until instructed to remove them later in the following sequence of procedures.

Card #11 -- Ship's Angular Motion Meter Drive (Figs. A11-1, A11-2, A11-3)

This card is inserted and tested here in the sequence to allow for accurate positioning of the gyro case while it is mounted on an indexing table. This card provides the drive signal to the gyro angle display meters. Since these display meters are used as instruments in gyro testing for the vertical gyro compensation system, they should be accurate. The two input signals to card #11 are DC voltages proportional to the sine of the associated gyro angle (roll or pitch) scaled at 10 V/rad or 0.1745 V/deg. The meters are full scale for $\pm 2^\circ$. The meter drive amplifier (LM101AH) saturates at ± 13 V or $\pm 2.6^\circ$, hence it self-protects the meters from excessive overdrive. To set the angle meters to read accurately, move the gyro through the range from $+2^\circ$ to -2° and adjust P1 (P2) until the meter reads accurately (i.e., $4^\circ \pm 0.04^\circ$) for each axis separately.

4. Card #1 (Figs. A1-1, A1-2, A1-3)

This card provides the electronics as shown in Fig. A1-1 necessary to provide the proper scaling for the \ddot{z} accelerometer, the DAS buffering, and the remainder of the coordinate conversion including the $1g$ bias electronics. The \ddot{z} accelerometer scale factor test is conducted in the same manner as for cards #8 in step 3, except that the DAS scale factor is 0.5 V/g for the \ddot{z} channel instead of 20 V/g on cards #8. Now provide a jumper from pin 1 to pin 11 and a jumper from pin 8 to pin 9 on board #1. With the system level and aligned (i.e., the accelerometer triad aligned to the vertical gyro), the output of this coordinate conversion at E_a on pin 17 of card #1 should be zero if the system is sitting on a nonaccelerating base. If E_a is not zero, either the

system is not level or aligned or something has changed and adjustment is necessary. Pot P1 is provided to null output over a small range. The pot resolution is approximately 0.5 mV DC. Hence the null at E_a is 0 ± 0.5 mV. Signal E_a is the ve-

hicle vertical acceleration that results from the coordinate transformation of the three-body axis acceleration signals to the local vertical axis as defined by the vertical gyro. Included here for reference purposes are the data obtained during a precision laboratory test of this portion of the system. The vertical gyro and Bow Accelerometer Unit (BAU) were aligned and leveled on a precision two-axis Leitz indexing table that provided for static positioning of roll and pitch attitudes independently and combined. The output E_a (\ddot{h}) was recorded using a Data Precision digital voltmeter for each attitude up to the maximum attitude for which the system electronics was designed ($\pm 13^\circ$).

The sensor signals \ddot{x} , \ddot{y} , \ddot{z} , $\sin \phi$, $\sin \phi$, $\frac{\ddot{y} \sin \phi}{2}$, $\frac{\ddot{x} \sin \theta}{2}$ were also recorded to ensure each was representative of its theoretical equivalent. Table 3 contains the measured data. A simple, quick analysis of the table is achieved by knowing that for all static attitudes E_a must be zero. The error in E_a for all combinations of angles up to $\pm 13^\circ$ was a maximum of 1 mV DC (0.016 ft/s^2 or 1 part in 2000). This table presents the actual measured data that demonstrate that this simplified coordinate transformation algorithm, when used on the SES (in maximum attitude of $\pm 6^\circ$), is almost exact; i.e., the static error in determining \ddot{h} is less than 0.01%. Hence the vehicle vertical acceleration as output by this system could be used as a very accurate measure of vehicle bow vertical acceleration response to the sea. A simple check of the coordinate conversion system can be made if one aligns the gyro and accelerometer to each other in a block in the

Table 3
System coordinate transformation test data.

Input Attitude (deg)		Accelerometer Outputs			Gyro Output		Products		Σ Output**
		\ddot{x}	\ddot{y}	\ddot{z}	$\sin \theta$	$\sin \psi$	$\frac{\ddot{x} \sin \theta}{2}$	$\frac{\ddot{y} \sin \psi}{2}$	\ddot{h}
Pitch	Roll	(V)	(V)	(V)	(V)	(V)	(V)	(V)	(V)
0	0	-0.00079	0.0056	-2.5057	-0.002	-0.006	-0.00038	-0.0007	-0.00015
-1 (forward down)	0	-0.0443	0.00557	-2.5052	0.0834	-0.0053	-0.00067	0.0008	± 0.00001
-2 (forward down)	0	-0.0881	0.0056	-2.5043	0.1707	-0.0049	-0.00190	-0.00082	± 0.00001
-4 (forward down)	0	-0.17509	0.0055	-2.4995	0.3483	-0.0072	-0.0065	-0.00088	± 0.00001
-6 (forward down)	0	-0.26199	0.0055	-2.4918	0.5251	-0.01	-0.0142	-0.00091	0.00008
1 (forward up)	0	0.04275	0.00578	-2.5053	-0.08895	-0.0077	-0.0008	-0.0009	0.00005
2 (forward up)	0	0.08635	0.00578	-2.5042	-0.179	-0.0071	-0.00205	-0.00091	0.0001
4 (forward up)	0	0.17349	0.00578	-2.4995	-0.3546	-0.0044	-0.00683	-0.00091	0.00027
6 (forward up)	0	0.2603	0.00590	-2.4919	-0.5312	-0.00185	-0.01462	-0.00085	0.0004
0	-1 (starboard up)	-0.00082	0.0479	-2.5052	0.004	-0.0886	-0.00036	-0.0014	0.0001
0	-2 (starboard up)	-0.00082	0.0917	-2.5042	0.0033	-0.17717	-0.0004	-0.0028	0.00015
0	-4 (starboard up)	-0.00082	0.17921	-2.4995	0.0033	-0.357	-0.0004	-0.0076	0.00043
0	-6 (starboard up)	-0.00289	0.2666	-2.4919	-0.003	-0.529	-	-	0.00059
0	≈ 1 (starboard down)*	-0.00086	+0.0058	-	-0.0016	0.001	-	-	0.00001
0	≈ 4 (starboard down)*	-0.00085	-0.1653	-2.4999	-	0.33991	-	-	0.00001
-4	≈ 4 (starboard down)*	-0.1749	0.1805	-2.4934	0.3488	-0.3592	-0.0065	-0.0078	0.00055
+4	≈ 4 (starboard down)*	-0.17295	0.1808	-2.4934	-0.3556	-0.3573	-0.0068	-0.0077	0.00079
+4	≈ 4 (starboard down)*	0.1730	-0.1647	-2.4937	-0.3570	0.3392	-0.0069	-0.0067	0.00039
-4	≈ 4 (starboard down)*	-0.1748	-0.1649	-2.4939	0.3407	0.3365	-0.0064	-0.0065	± 0.00005
-6	≈ 6 (starboard down)*	-	-	-	-	-	-	-	0.00086
-13	≈ 6 (starboard down)*	-	-	-	-	-	-	-	-0.00092
0	≈ 13 (starboard down)*	-	-	-	-	-	-	-	-0.001
14	≈ 6 (starboard down)*	-	-	-	-	-	-	-	-0.002
-14	≈ 6 (starboard down)*	-	-	-	-	-	-	-	-0.002

* Large roll attitudes not input accurately due to Leitz head readout accuracy ($\approx \pm 0.05^\circ$)

** 1 g bias set to +2.507 VDC

laboratory and monitors \ddot{h} for gross attitudes ($<13^\circ$) of the system without actually measuring the input angles. The \ddot{h} output should be well within ± 0.015 V ($\approx 1\%$ error). If something has changed significantly in the system, a closer look would be necessary.

5. Insert cards #4 and #9 and ensure that J2 and J8 cables are disconnected

Refer to Figs. A9-1 and A4-1 for card #9 and card #4, respectively. The two independent altimeter signal input conditioning circuits are on card #9, and the selected altimeter signal filtering is done via card #4. Card #9 has been set up for a 0.00 VDC offset from each altimeter and a scale factor of 200 mV/ft. The offset adjust is provided as a switch on the back panel of the MCU in 5 ft equivalent height steps to 25 ft of height and a continuous adjustment on the chassis from 0 to 5 ft. The two channels' 25 ft offset adjustments are not independently switched. If this height offset switch is used to set in an offset greater than 5 ft but not the same for both channels, the switch must be repositioned to the correct value each time you reselect an altimeter channel. Also, if the altimeter gain is different from 200 mV/ft by 75%, the resistor R_1 (R_1') must be changed to accommodate the scale factor change. E_{03} (E_{03}') on card #9 is $1.25 \times E_1$ (E_1'); hence a 10 ft equivalent altitude input change (Δ of 2 V) yields a change at E_{03} (E_{03}') of 2.5 VDC. If not, adjust P_1 (P_1') for the respective channel until a 10 ft change yields a 2.5 V change at E_{03} (E_{03}'). Note that this system does not allow for negative inputs from the altimeter without circuit modifications. Card #4 is the low-pass filter to output the mean height h_0 and a high-pass filter to remove h_0 from the altimeter signal (h_0 and h_v and h_w) to yield the $h_v - h_w$ output into the ship's motion compensation summing amplifier. The "reset" relays will not be energized, so to check the DC gain of the two filters

apply a 250 mVDC input at the common point (junction of the 5.11 M Ω , 1K, and 2.49 M Ω resistor) and observe that the outputs E_{01} and E_{02} settle to 340 mV \pm 6 mV and 500 mV \pm 10 mV, respectively. Remove card #9 and apply an oscillatory input at pin 1 on card #4 at 20 Hz and check the gains E_{01}/E_1 to be -1.359 ± 0.002 to ensure the dynamic response of the filter. The signal at E_{02} should be zero steady state during this test. Remove the signal and reinsert card #9.

6. Card #10 - MCU Reset Timing and Control

Card #10 gives the timing circuits that provide for a delayed power-on reset of the system or for a command reset function either activated by the operator in DAS via the MCU front panel or via the CDU reset button in the cockpit. Also provided for test convenience are two reset defeat buttons inside the MCU chassis to allow switching back to normal operation without waiting for the usual reset delay. The reset function is actually two timed sequences. First, it removes all signals from the input to the integrators, provides shorts for discharging the integrators, disconnects the outputs, and provides zero outputs for 30 s. After 30 s, the reset function removes the integrator shorts and allows signals into the integrators but does not connect the output until ≈ 150 s have elapsed. Then the system switches back to normal operation. The reset signal affects relays on boards Nos. 10, 5, 6, 7, and 4 and display lamps on the MCU and CDU. There are no adjustments on the card. To change the timing, refer to the detailed electronics design section.

7. Card #5 - MCU High-Pass Filter

Card #6 - MCU Low-Pass Filter

The electronic schematics for cards #5 and #6 are shown in Figs. A5-1 and A6-1, respectively. Card #5 is a high-pass filter and card #6 is a low-pass filter. Three each of card #5 and two each of card #6, staggered, make up the fifth-order filter, which does the double integration of the vehicle vertical

acceleration signal to yield vehicle height. There are no adjustments on these cards since each of the parts that affect the time constant of the filter is selected and matched and the system dynamic gains are adjusted on card #7. An operational check of the Philbrick model 1701 operational amplifier can be made by selecting reset, removing the BAU cable at J1, and removing card #1 to allow inputting a signal at pin 1 on card 5. In reset, the OA DC gain is unity; hence the output on pin 16 will be the negative of the input value. The output of the second stage of the filter card #6 on pin 16 will be $\approx 1/80$ of the input value. To check the next two stages for functional operation, remove card #6 (second-stage filter) and input a signal on pin 1 of the third filter (card #5) and repeat the above. However, observe that the output of the fifth filter is the negative of the fourth stage when in reset. This completes the functional check of the five #5 and #6 cards. Now ensure that all cables are connected and all cards are inserted except card #7.

8. Card #7 - MCU System Output Signal Conditioner and rms Converter

Card #7 (Figs. A7-1, A7-2, A7-3) contains the summing amplifier that sums the vehicle motion $-h_v$ with the filtered altimeter signal $(h_v + h_w)$ to yield h_w , the wave profile. It also contains output buffer amplifiers for outputting h_v and h_0 and the h_w rms. The summing amplifier on card #7 is used to adjust the system gain from h through the five-stage filter to the output h_v since no variable gain adjustments were possible at each stage of the five-stage filter. Setting up card #7 is accomplished by first adjusting Pot P1 to yield equal weighting of the vehicle motion signal h_v and the altimeter channel signal $(h_v + h_w)$ so that, when h_w is zero (no wave motion), the output of the summing amplifier is zero when $-h_v + (h_v + h_w) = 0$ over the frequency range of interest. Then the gains are adjusted by P2 and P3 to yield the correct output scaling. Since these signals are AC and not

DC, several special test circuits, as shown in Figs. 6 and 7, are required to aid in setting these gains. To begin, remove the BAU cable at J1 on MCU. Remove the two #8 cards. Set up according to Fig. 6. Ground the terminals shown grounded in Fig. 6. Set up the test circuit as shown and apply the 1 Hz (± 0.001 Hz) input signal. The input amplitude is not that important; however, set it to at least 0.2 V and observe the system output on a sensitive scope. After all settles out to steady state (several minutes), adjust P1 until the amplitude of the 1 Hz output signal reaches a minimum (not necessarily zero). This completes the P1 adjustment. Now ground pin 1 on card #9 and set up according to Fig. 7. With $E(z)$ set to zero, observe that $H_{w rms}$ at CDU display goes to zero. If not, adjust P4 (on card #7) until the digit display reads zero. Now apply $E(z) = 3.065$ V peak at 1 Hz and observe E_0 on a sensitive oscilloscope. After E_0 settles to a steady-state amplitude, adjust P2 until E_0 reaches a minimum amplitude at 1 Hz. Now observe that the CDU digital display reads 0.707 ± 0.01 steady state. Now remove the special connection from pin 22 on card #7 and connect to pin 20; with $E(z)$ set to at least 3.065 V peak at 1 Hz adjust P3 until E_0 reaches a minimum amplitude at 1 Hz. Next ground $E(z)$ input and remove the ground at card #9 pin 1 and apply a known DC voltage. After several minutes, observe that E_{03} on card #7 settles to $2.5 \pm 0.1\%$ times the DC input level. This completes the final system adjustments with the exception of the self-test.

9. Self-Test

The signal source for the self-test circuitry is contained on card #17 in the GCU-MCU system test reference generator. The schematic for this circuitry is shown in Fig. A17-1. E_{01} is a 4 V amplitude signal at 2 Hz. E_{05} is -6.045 VDC reference voltage. E_{04} is 0.82 V peak-to-peak at 2 Hz. E_{01} is input to

simulate the two gyro sine θ , ϕ inputs at the multipliers. E_{03} is the DC input at \ddot{x} , \ddot{y} input points at the multipliers simulating accelerometer inputs.

E_{04} is the equivalent altimeter input signal. The system output at the CDU digital display for E_{01} and E_{03} inputs is 0.138. The output for E_{04} is 1.138. Combined, the CDU digital display reads 1.000. If the system has just been calibrated, the self-test circuitry may need adjustment if the CDU on self-test does not read 1.000 ± 0.05 . Adjust P1 for E_{01} to read 0.0 V peak-to-peak of 2 Hz. Adjust P2 for E_{04} to read 0.82 V peak-to-peak at 2 Hz.

There is no variable adjustment for E_{03} . Operate self-test and then make the final adjustment to get 1.000 on the CDU using P2 on card #17.

GCU ALIGNMENT AND CALIBRATION

This section discusses the sequence of operations necessary to align and calibrate the GCU. It is assumed that the personnel are familiar with the system and are expert at testing electronics; the procedural details for each operation are not included here. A detailed discussion of the theory and operation of the vertical gyro is contained in Ref. 4. Figure B3-1 shows the gyro compensation system signal flow, and Figs. B3-2 through B3-4 are the photographs of the system as delivered. The electronics for the GCU are contained on cards #12, #13, #14, #15, and #16. The associated schematics, assembly drawings, and card photographs are contained in Figs. A12-1 through A16-3. The system should be completely interconnected and the GCU cards should be inserted. Place the system in normal operation.

1. Card #12 - GCU 400 Hz Reference (Fig. A12-1, A12-2, A12-3)

Card #12 contains the phase shift electronics for the 400 Hz signals that are used in the simulated pendulum circuits. The phase difference is determined by comparing the actual pendulum signal when

tilted at about 0.5° with the 400 Hz reference signal on an oscilloscope and is adjusted to zero by potentiometer P1. The pendulum is tilted by using the special test switches on the front of the GCU. After the reference phase is correct, ensure that the ship's input is exactly 115 V rms and adjust P2 until the output E_{R2} at pin 17 on card #12 is 7.07 V rms $\pm 1\%$.

2. Card #13 - GCU V_s and $\dot{\psi}$ Signal Conditioner

Card #13 contains the buffers for accepting the ship's speed (V_s) and yaw rate ($\dot{\psi}$) from DAS and generates the roll channel equivalent acceleration signal $V_s \dot{\psi}$. Disconnect the DAS cable J8 from the system and ground pins 1 and 6 on card #13. Adjust P1 until E_{01} is zero. Adjust P3 until E_{03} is zero. Now adjust P5 until P5 is zero ± 0.005 VDC. Input a 2 VDC ± 0.002 VDC signal at pins 1 and 6. Adjust P2 until E_{02} is -2 VDC ± 0.002 VDC. Adjust P4 until E_{03} is 2 VDC ± 0.002 VDC. Now E_{04} should be -0.4 VDC ± 0.004 VDC. Reverse the polarity of the 2 VDC input and ensure that the voltage is -2 VDC ± 0.002 VDC and observe that the output E_{04} is -0.4 VDC ± 0.004 VDC. Remove the input signal and ground pins 1 and 6 on card #13.

3. Card #14 - GCU Gyro Pendulum Simulator

This roll channel card accepts simulated acceleration input signals representing lateral acceleration ($V_s \dot{\psi}$). The card provides the selection of the simulated gyro pendulum time constant and provides the nonlinear gain characteristics of the simulated pendulum electromagnetic pickoff. The time constant select switch is mounted inside the chassis and must be manually switched to the time corresponding to the gyro in use on the SES. Two time constants are available, 8 s and 27 s, as determined by the 0.8 μ F and 2.7 μ F capacitors on the card. For any other gyro pendulum time constant, these values must be changed accordingly.

This card variable gain adjustment (P_1) is accomplished on a system basis later in step 5. The nonlinear characteristics of the card #14 output amplifier should be tested over a range of input voltages in an attempt to match the gyro pendulum nonlinear characteristics. The system test push-buttons on the front panel in conjunction with P_1 test and adjust for one point on the curve (i.e., $\pm 0.5^\circ$). The gyro pendulum was tested in the laboratory to determine the nonlinear gain characteristics using electronics similar to the GCU. The data from those laboratory tests are contained in Ref. 4.

4. Card #15 - GCU Gyro Pendulum Simulator, Pitch Channel (Figs. A15-1, A15-2, A15-3)

Card #15 accepts inputs of the ship's speed (V_s) and generates (\dot{V}_s) by differentiating. $A(+)\dot{V}_s$ represents forward acceleration of the vehicle. The circuitry (other than the differentiation) on card #15 achieves the same function as that on card #14 except that it is the pitch channel rather than the roll channel. The same general discussion applies except for the signal levels, etc. The simulated pendulum time constants were selected by the chassis mounted switch in step 3.

5. Card #16 - GCU Simulated Pendulum 400 Hz Modulator and Maneuver Compensation Amplifier (Figs. A16-1, A16-2, A16-3)

Card #16 provides the electronics that converts the roll and pitch channel simulated pendulum response signals to 400 Hz AC signals and then appropriately sums them with the actual pendulum 400 Hz signals to provide for the ship's maneuver compensation. The card also contains a 400 Hz demodulator that, via the front panel selector switch, demodulates selected signals from each channel for display on the GCU front panel meter (tilt angle meter). The signals displayed from each of the roll and pitch

channels are actual pendulum angle, computed pendulum response, and the sum of these (error signal). The card also provides for the gyro compensation bypass mode of operation. This is accomplished by a set of normally closed relay contacts that, when unenergized, return the gyro pendulum signals to the gyro erection amplifier unaltered. This bypass relay can be controlled from the GCU front panel or from the CDU in the cockpit. To test and calibrate card #16, its electrical zero must be set. Remove cards #14 and #15 and select gyro bypass mode of operation. Ground pins 1 and 2 on card #16. Observe E_{03} and E_{04} on an oscilloscope and adjust P3 and P2, respectively, until E_{03} and E_{04} reach a minimum level. Now select the roll channel on the tilt angle meter select switch and observe that for the computed pendulum the position of the function select switch results in the meter reading zero. If not, adjust P3 until the meter reads zero. Repeat for pitch channel and potentiometer P2. P1 on card #16 sets the display meter sensitivity. However, this is set in combination with the variable gain adjustments on cards 14 and 15. The test input signals at pin 8 and each card #14 and #15 exactly represent an equivalent acceleration tilt angle (0.5°) voltage at each summing amplifier. Hence by inserting the test voltage when the system is operating correctly, the gyro will precess to 0.5° as indicated on the front panel of the ship's angle indicator and the pendulum angle will be 0.5° . To set the system gain, remove all grounds from the GCU cards except V_g and ψ input signal grounds on card #13 and assure that the DAS cable J8 is still not connected. Press the test switch for the roll channel on the GCU front panel and hold. The gyro angle should read about $+0.5^\circ$. Switch to the opposite polarity and the final gyro angle should go to about -0.5° . The difference in the two positions should be 1.0° . If not, then the variable gain adjust potentiometer P1 on card #14 must be changed until the condition of 1° is satisfied to $\pm 0.05^\circ$. Now check that the actual pendulum angle indicated is correct ($0.5 \pm 0.05^\circ$) on the GCU front panel by

pressing to test and holding until steady state and observing the actual pendulum output indicated on tilt angle meter when the tilt angle selector switch is in the "roll pendulum" position. If not, adjust potentiometer P1 on card #16 until the condition is satisfied. Repeat this procedure for the pitch channel. The calibration of the actual gyro pendulum can be done with equivalent static inputs at pin 1 representing yaw rate ($\dot{\psi}$) and dynamic inputs at pin 6 representing the ship's speed (V_s) to yield V_s and $V_s \dot{\psi}$ over the range of interest. Compute the equivalent angle \dot{V}_s/g and $V_s \dot{\psi}/g$. Observe the steady-state gyro angle response on the ship's angle readout meter on the MCU. The angle response should agree to the equivalent input to better than 0.05° . The gyro angle meters are good to 2° maximum. The example is as follows:

Acceleration of the gyro case forward causes the gyro pendulum meter to indicate a positive pendulum angle. Insert the ship's speed, V_s , so that \dot{V}_s is $+10$ kt/min, accelerating forward. In steady state, the gyro pitch angle indicated is -0.49° , the pitch pendulum indicated is positive 0.49° , and the computed (simulated) pendulum signal indicated is -0.49° . With no compensation, the response to forward acceleration is for the pendulum to tilt back from down, which, due to the closed erection loop, torques the gyro spin axis to follow. Thus the gyro response to forward acceleration is for a pitch angle readout of positive pitch angle as if the ship had pitched forward up. The opposite case with no real acceleration input, a forward acceleration (\dot{V}_s) input to the compensation system, will cause the opposite effect; i.e., the indicated gyro pitch angle will be negative as if the ship had pitched forward point down. Hence, for the maneuver compensated gyro, response to actual acceleration is to remain vertical. One must remember that the actual pendulum is moving, but there is no gyro torquing (no gyro error) since the simulated signal cancels the pendulum signal, steady state and dynamically.

7. SYSTEM MECHANICAL DESIGN DETAILS

The wave profiling system consists of the MCU/GCU, the BAU, the cockpit CDU, the vertical gyro system, and the altimeter. The altimeter antennas and the BAU are mounted on a retractable boom that extends forward of the SES to provide a clear view of the water surface for the altimeter antenna system.

The system interface and operation are contained in Ref. 3. This section discusses the accuracy and reliability of the mechanical details of the design of the system.

BAU

The BAU must operate on the bow boom that protrudes forward of the SES approximately 8 ft when extended for normal operation. The unit (Fig. C1-2) is completely environmentally sealed to operate submersed in water. The cable (Fig. B1-10) and connector are waterproof. The top cover is sealed via a large O ring. The three accelerometers are the Sundstrand model QA-1200-AA08. The units are described generally in Appendix C. The accelerometers' sensitive axes (input axes) are aligned orthogonally to each other to better than 0.5 arc min in the triad mount. This is accomplished by the detailed test technique described in the error analysis section of this document. The accelerometers are mounted to the triad using nonmetallic spacers and a special isolated bolt system shown in Fig. C1-6 to electrically isolate the accelerometer case from the mount. This allows control of the case grounds, providing for better long-term stability of the system.

The base of the triad mount has had all its surfaces machined and checked to be accurate to better than 0.5 arc min; when the case cover is installed and bolted down, the top surface is parallel to the mounting reference surface to better than 0.5 arc min. Hence the top of the cover is a good reference surface for two axes (roll and pitch). The third axis (heading) is provided by reference scribe lines on the forward and aft vertical surfaces of the mount, as well as by the sides of the base of the mount. Each accelerometer has been shimmed to be aligned to these reference surfaces to better than 0.5 arc min of angle.

The package is then mounted by a set of alignment bolts to the bow boom mounting plate as shown in Fig. C1-5. The three adjustment (alignment) bolts provide a means for leveling the two level axes to the vertical gyro reference level surface. As shown in the figure, the heading reference axis is transferred to the bow boom mounting plate via the three alignment bolts and the center alignment post. These scribe lines on the bow boom mounting plate provide a 10 in. lever arm necessary to transfer the heading reference of the gyro mount forward to the BAU via an optical alignment (heading transfer). The sequence of alignment would be to first establish heading at the BAU and secure the four bow boom mounting plate bolts, then transfer the level alignment from the gyro mount to the BAU via an accurate clinometer or equivalent instrument. All axes should be accurately aligned to the gyro and remain stable to better than 0.1° to ensure precision operation of the wave profiling system.

The altimeter antenna system is mounted below the BAU and must be centered 5 in. forward of the boom bulkhead as shown in Fig. C1-5. This forward location is the location of the η accelerometer.

The Sundstrand accelerometer contains its own electronics. Yaw provides ± 15 VDC and the accelerometer provides an output DC current signal proportional to input acceleration. To guarantee scaling accuracy, etc., the accelerometer scaling resistor that changes the current to a voltage proportional to acceleration is contained in the system electronics rack, 150 ft distant from the accelerometers. The technique minimizes pickup noise, zero offset, etc.

A temperature monitor thermistor is mounted inside the BAU to provide a sensor for mounting the BAU temperature if needed at any time. The temperature-resistance curve is contained in Fig. C1-3. The test points for this sensor are located on the front panel of the MCU, designated "Therm."

The Sundstrand Q-flex accelerometer model QA-1200-AA08 is very stable relative to temperature. The AA08 version is better than $10 \mu\text{g}/^\circ\text{C}$; hence there is no requirement for heaters, etc., in the BAU to control temperature. As shown in the detailed design section of this report, it is not the offset that generated problems but the offset rate, and, since the BAU is sealed, we do not expect that the temperature rate at the accelerometer during normal operation will exceed $2.4^\circ\text{C}/\text{min}$.

The accelerometers have an extremely high bandwidth. The boom vibratory motions are sensed and integrated by the system and removed appropriately from the ideal altimeter measurement. Higher

frequency motions obviously are very small motions (less than 0.5 in.) and do not cause direct errors. The accelerometers are scaled to 5 g and will survive 100 g of shock. Boom retraction and extension must be done with caution to assure that high g (greater than 100 g) are not imparted to the accelerometers.

WAVE PROFILING SYSTEM ELECTRONICS RACK

The rack houses the MCU and GCU electronics. Each unit (MCU and GCU) is mounted on slides that provide access to the electronics cards, etc.

The complete rack including the electronics and cards has been successfully vibration-tested to MIL SPEC 167. However the unit must be secured at both the top and bottom. Figures B4-1 is a photograph of the system mounted on the Ling shaker for the vertical axis shake. Figure B4-2 is the record of the vibration levels and frequencies. The unit was exposed to more than 6 h of vibration and more than 200 h of powered-up operation without any electronic parts failures.

8. DETAILED ELECTRONIC DESIGN

ERROR CONSIDERATIONS

One of the equations that requires electronic implementation to effect ship's motion compensation is (from Eq. 5, Section 4):

$$\ddot{h}_z = -\ddot{x} \sin \theta + \ddot{y} \cos \theta \sin \theta + \ddot{z} \cos \theta \cos \phi = \ddot{h}_v, \quad (16)$$

where

$\ddot{h}_z = \ddot{h}_v$ = desired local vertical component of acceleration of the vehicle (ship) in inertial space,

$\ddot{x}, \ddot{y}, \ddot{z}$ = the ship body accelerations measured by the accelerometer triad, and

θ, ϕ = the ship pitch and roll angles, respectively.

The accelerometers sense the following signals, where the matrix in Eq. 17 below is the inverse of the M matrix in Eq. 4 of Section 4 with $\psi = 0$:

$$\begin{bmatrix} \ddot{x} \\ \ddot{y} \\ \ddot{z} \end{bmatrix} = \begin{bmatrix} \cos \theta & 0 & -\sin \theta \\ \sin \theta \sin \phi & \cos \phi & \cos \theta \sin \phi \\ \sin \theta \cos \phi & -\sin \phi & \cos \theta \cos \phi \end{bmatrix} \begin{bmatrix} \ddot{h}_x \\ \ddot{h}_y \\ \ddot{h}_z \end{bmatrix}$$

Note: Matrix multiplication is assumed here, (17)

where $\ddot{h}_x, \ddot{h}_y, \ddot{h}_z$ are components of acceleration in inertial space with the local vertical denoted by $\ddot{h}_z (= \ddot{h}_v)$, and with \ddot{h}_x and \ddot{h}_y denoting two directions, located in the local horizontal plane, that are orthogonal to each other and orthogonal to the local vertical with \ddot{h}_x along the forward direction of the ship.

If Eq. 17 is substituted in Eq. 16, it will be seen that what is being calculated in Eq. 16 is indeed \ddot{h}_z , since an identity results; the terms involving \ddot{h}_x and \ddot{h}_y cancel out and do not therefore appear in Eq. 16 after the substitution.

The electronic implementation of Eq. 16 is complicated and can be considerably simplified if certain assumptions are made. If both θ and ϕ are confined to the range $|\theta|, |\phi| \leq 0.25$ rad (14.3°) and if we make the assumption that $\cos \theta \approx 1.00$, $\cos \phi \approx 1.00$ over the confined ranges for $|\theta|$ and $|\phi|$, Eq. 16 may be simplified to the following form, where \ddot{h}_a is now the value calculated, and where \ddot{h}_a now differs from \ddot{h}_v because of the approximations made:

$$\ddot{h}_a = -\ddot{x} \sin \theta + \ddot{y} \sin \phi + \ddot{z} \quad \text{with } |\theta|, |\phi| \leq 0.25 \text{ rad}$$

$$\cos \theta \approx 1.00, \cos \phi \approx 1.00.$$

(18)

The fractional error, ϵ_1 , in using \ddot{h}_a as a measure of \ddot{h}_v ($= \ddot{h}_z$) is defined as

$$\epsilon_1 = \frac{\ddot{h}_a - \ddot{h}_v}{\ddot{h}_v} = \frac{\ddot{h}_a - \ddot{h}_z}{\ddot{h}_z}.$$

(19)

If we substitute the expressions for \ddot{x} , \ddot{y} , and \ddot{z} obtained from Eq. 17 into Eq. 18 and find ϵ_1 in accordance with Eq. 19, using the power series approximations for $\sin \theta$, $\cos \theta$, $\sin \phi$, $\cos \phi$, we obtain the following expression for ϵ_1 (again assuming $|\theta|, |\phi| \leq 0.25$ rad):

$$\epsilon_1 \approx \theta \left(\frac{\theta^2 + \phi^2}{2} \right) \left(\frac{\ddot{h}_x}{\ddot{h}_z} \right) - \frac{\phi^3}{2} \left(\frac{\ddot{h}_y}{\ddot{h}_z} \right) + \left(\frac{\theta^2 + \phi^2}{2} \right).$$

(20)

\ddot{h}_x and \ddot{h}_y in Eq. 20 represent the ship's surge and sway accelerations, respectively, relative to an earth horizontal plane and are likely not to exceed $(\ddot{h}_z/20)$. Additionally, if $|\theta|, |\phi| \leq 0.25$ rad, the largest contribution to the error ϵ_1 in Eq. 20

is the last term on the right side; by comparison, the errors contributed by the first two terms on the right side of Eq. 20 may be neglected. Hence, subject to the approximations that $|\theta|, |\phi| \leq 0.25$ rad, $(\ddot{h}_x/\ddot{h}_z) \leq \frac{1}{20}$, $(\ddot{h}_y/\ddot{h}_z) \leq \frac{1}{20}$, Eq. 20 may be approximated by

$$\epsilon_1 \approx \left(\frac{\theta^2 + \phi^2}{2} \right). \quad (20a)$$

If $|\theta|, |\phi| \leq 0.25$ rad (14.3°), $\epsilon_1 \leq 0.063$ or less than 7%; if $|\theta|, |\phi| \leq 0.175$ rad (10.0°), $\epsilon_1 \leq 0.031$ or about 3%.

Equation 18 was initially implemented electronically and the errors observed were about those expected. However, we determined experimentally, when \ddot{h}_x and \ddot{h}_y were both zero, that by a simple change in the gains in the θ and ϕ synchro channels and without changing the form of the electronic circuit block diagram, much improved accuracy could be obtained. To achieve the improved accuracy in the measurement of \ddot{h}_v ($=\ddot{h}_z$) via the accelerometer triad, the following equation was implemented:

$$\ddot{h}_b = -\ddot{x} \sin \theta + \ddot{y} \sin \phi + \ddot{z}. \quad (21)$$

Again, a fractional error in using \ddot{h}_b as a measure of \ddot{h}_v may be defined as

$$\epsilon_2 = \frac{\ddot{h}_b - \ddot{h}_v}{\ddot{h}_v} = \frac{\ddot{h}_b - \ddot{h}_z}{\ddot{h}_z}. \quad (22)$$

If we substitute the expressions for \ddot{x} , \ddot{y} , and \ddot{z} obtained from Eq. 17 into Eq. 21 and find ϵ_2 in accordance with Eq. 22, using the power series approximations for $\sin \theta$, $\cos \theta$, $\sin \phi$, $\cos \phi$, we obtain the following expression for ϵ_2 (again assuming $|\theta|, |\phi| \leq 0.25$ rad):

$$\epsilon_2 \approx \frac{\theta}{2} \left(\frac{\ddot{h}_x}{\ddot{h}_z} \right) - \frac{\phi}{2} \left(\frac{\ddot{h}_y}{\ddot{h}_z} \right) - \left(\frac{\theta^4 + \phi^4}{8} \right) . \quad (23)$$

We note now that the error term on the extreme right of Eq. 23 is much smaller than the corresponding error term given in Eq. 20, confirming our experimental observations. However, the surge and sway error terms (involving \ddot{h}_x and \ddot{h}_y , respectively) are now larger. Nevertheless, by this simple change in the synchro channel gain, improved accuracy in the measurement of \ddot{h}_v can be obtained when surge and sway accelerations are small compared to \ddot{h}_v . Assuming the surge and sway terms on the right side of Eq. 23 are equal in magnitude and root sum squared, their combined error would be equal to the last term on the right side of Eq. 23 when

$$\left| \frac{\ddot{h}_x}{\ddot{h}_z} \right| = \left| \frac{\ddot{h}_y}{\ddot{h}_z} \right| = \frac{\sqrt{2}}{4} |\theta|^3 ,$$

assuming $|\theta| = |\phi|$. If $|\theta| = |\phi| = \frac{1}{4}$ rad,

$$\left| \frac{\ddot{h}_x}{\ddot{h}_z} \right| = \left| \frac{\ddot{h}_y}{\ddot{h}_z} \right| = 0.00552$$

and the combined error term due to surge and sway is

$$\frac{0.250}{2} (0.00552) \sqrt{2} = 0.00098 .$$

This is also the error contributed by the last term on the right side of Eq. 8. If $|\theta| = |\phi| = 0.175$ rad,

$$\left| \frac{\ddot{h}_x}{\ddot{h}_z} \right| = \left| \frac{\ddot{h}_y}{\ddot{h}_z} \right| = 0.00189,$$

the combined error term now becomes 0.00023, which is the same as the error contributed by the last term of Eq. 23.

By inspection of Eq. 23, as $|\theta|$ and $|\phi|$ become smaller, assuming the surge and sway acceleration ratios remain constant, the error terms due to surge and sway become more dominant.

At this time it is appropriate to ask if there might be a better choice of the θ and ϕ synchro channel gains, rather than $1/2$ for each. To answer this question, assume the equation to be implemented electronically is of the form

$$\ddot{h}_c = -A\ddot{x} \sin \theta + A\ddot{y} \sin \phi + \ddot{z}, \quad (24)$$

where the constant A is to be chosen to minimize the magnitude of the fractional error ϵ_3 defined as follows:

$$\epsilon_3 = \frac{\ddot{h}_c - \ddot{h}_v}{\ddot{h}_v} = \frac{\ddot{h}_c - \ddot{h}_z}{\ddot{h}_z}. \quad (25)$$

Again, if we substitute the expressions for \ddot{x} , \ddot{y} , and \ddot{z} obtained from Eq. 17 into Eq. 24 and find ϵ_3 in accordance with Eq. 25, using the power series approximations for $\sin \theta$, $\cos \theta$, $\sin \phi$, $\cos \phi$, we obtain the following expression for ϵ_3 (again assuming $|\theta|, |\phi| \leq 0.25$ rad):

$$\epsilon_3 \approx \theta \left[(1-A) + \left(\frac{4A-1}{6} \right) \theta^2 + (A-\frac{1}{2}) \phi^2 \right] \left(\frac{\ddot{h}_x}{\ddot{h}_z} \right) + \theta \left[(A-1) + \left(\frac{1-4A}{6} \right) \theta^2 \right] \left(\frac{\ddot{h}_y}{\ddot{h}_z} \right) + \left[\left(\frac{2A-1}{2} \right) (\theta^2 + \phi^2) + \left(\frac{1-8A}{24} \right) (\theta^4 + \phi^4) + \left(\frac{1-2A}{4} \right) \theta^2 \phi^2 \right]. \quad (26)$$

The contributions to ϵ_3 due to surge and sway accelerations are the first two terms on the right of Eq. 26. The value of A that minimizes each of these contributions is very close to unity. This may be verified by setting the respective terms equal to 0 and solving each for A and making the approximation that $|\theta|, |\phi| \leq 0.25$ rad. With A = 1, Eq. 24 becomes identical to Eq. 18, the equation originally implemented electronically, while the fractional error given by Eq. 26 reduces to ϵ_1 given by Eq. 20 where $|\theta|, |\phi| \leq 0.25$ rad is assumed.

If we disregard the error contributions due to surge and sway accelerations, the value of A that minimizes the error in the last term on the right of Eq. 26 is very close to 1/2. This may be verified by setting this term equal to 0 and solving for A as a function of θ and ϕ . Performing the latter operation, we obtain the following expression for A:

$$A = \frac{1}{2} \left[\frac{1 - \frac{\theta^4 + \phi^4}{12(\theta^2 + \phi^2)} - \frac{\theta^2 \phi^2}{2(\theta^2 + \phi^2)}}{1 - \frac{\theta^4 + \phi^4}{3(\theta^2 + \phi^2)} - \frac{\theta^2 \phi^2}{2(\theta^2 + \phi^2)}} \right] \quad (27)$$

If it is again assumed that $|\theta|, |\phi| \leq 0.25$ rad, the bracketed term in Eq. 27 is very close to unity and hence $A \approx \frac{1}{2}$ to a good approximation. With A = $\frac{1}{2}$, Eq. 24 becomes identical to Eq. 21, the equation finally implemented electronically, while the fractional effort ϵ_3 given by Eq. 26 reduces to ϵ_2 given by Eq. 23.

Thus, if the surge and sway acceleration ratios $\left(\frac{\ddot{h}_x}{\ddot{h}_z}\right)$ and $\left(\frac{\ddot{h}_y}{\ddot{h}_z}\right)$ are insignificant, choose $A \approx \frac{1}{2}$ to minimize ϵ_3 . If the acceleration ratios are not insignificant, a value of A between $\frac{1}{2}$ and 1 should be chosen, depending on how large these ratios are. To see how these ratios influence the choice of A, assume the following:

$$\left| \frac{\ddot{h}_x}{\ddot{h}_z} \right| = \left| \frac{\ddot{h}_y}{\ddot{h}_z} \right| = k, \quad k \geq 0. \quad (28)$$

With $k = 0$, the acceleration ratios are 0 and the fractional error ϵ_3 in Eq. 26 may be plotted as a function of A , as in Fig. 8, for two different assumed values of $|\theta| = |\phi|$. For $|\theta| = |\phi| = 0.175$ rad (10.0°), the magnitude of the maximum fractional error ϵ_3 becomes about 0.030 (or 3.0%) when $A = 0$ or $A = 1$; $|\epsilon_3|$ becomes a minimum near $A = \frac{1}{2}$. For $|\theta| = |\phi| = 0.025$ rad (14.3°), $|\epsilon_3|$ maximum occurs again at $A = 0$ or $A = 1$ and is as high as 0.062, or about 6.2%; again, $|\epsilon_3|$ becomes a minimum near $A = \frac{1}{2}$.

The effect of $k > 0$ may be seen by referring to Fig. 9. In this figure, the RSS value of the first two terms on the right of Eq. 26 is plotted as a function of A for two different assumed values of $|\theta| = |\phi|$ and two different values of k . For $|\theta| = |\phi| = 0.175$ rad (10.0°) and $k = 0.01$, the RSS fractional error is a maximum of 0.0024 at $A = 0$ and is essentially 0 at $A = 1$. For $k = 0.10$, the RSS fractional error is much larger, having the value of 0.0242 at $A = 0$; at $A = 1$, the fractional error is again close to 0. At $A = \frac{1}{2}$, the fractional error is 0.0125, which is significant compared to the fractional error at $A = \frac{1}{2}$ when $k = 0$ (from Fig. 8). If k is of the order of 0.10, a value of A somewhere between $\frac{1}{2}$ and 1 may be desirable in order to minimize the magnitude of the total error $|\epsilon_3|$.

It is of interest to note that if $A = 0$, Eq. 24 degenerates into that which is simplest to implement electronically,

$$\ddot{h}_c = \ddot{z} \quad (29)$$

For this case, only one accelerometer instead of three is required, and the synchro channel circuitry may be removed. However, the price paid for this simplicity is higher system errors as may be seen by referring to Figs. 8 and 9 with $A = 0$. For this case, all three error terms on the right side of Eq. 26 are at their maximum values. Thus, for $k = 0$, $|\theta| = |\phi| = 0.175$ rad (10.0°), the fractional error $|\epsilon_3|$ becomes 0.030, or 3.0%, (see Fig. 8). If k ranges between 0.01 and 0.10, an RSS fractional error contribution ranging between 0.00224 and 0.0243 in addition to the Fig. 8 fractional error, manifests itself (see Fig. 9).

Figure 10 is a simplified block diagram showing how the generated signal for \ddot{h}_b , which is a measure of \ddot{h}_v , is processed and combined with the altimeter signal to produce the desired wave height signal, h_w . The altimeter measures ship motion in

addition to wave height variations, h_w , at an average wave height of h_0 . h_0 is filtered out by means of a high-pass filter, the output of which then becomes proportional to $(h_w - h_v)$.

In the accelerometer path, \ddot{h}_v ($\approx \ddot{h}_b$) is integrated twice to yield a signal proportioned to h_v . h_v in this path is then summed with $(h_w - h_v)$ in the altimeter path to yield the desired wave height variations, h_w .

In Fig. 10, the +1g bias source is required to null the gravitational acceleration sensed by the accelerometer triad.

In performing two electronic integrations on \ddot{h}_v to yield h_v , problems evolve because of accelerometer and amplifier offsets; these offsets would also be integrated and create, ultimately, amplifier saturation and an unusable system. Hence the double integration must be replaced by at least two cascaded first-order low-pass filters that together represent a good approximation to a double integration for all wave height frequencies equal to and above some prescribed frequency. This prescribed frequency should be the lowest significant wave height frequency expected. To be a good approximation to an integrator (and thereby minimize the error in the integration process), the filter cutoff frequency should be well below the lowest significant wave height frequency.

If two cascaded first-order low-pass filters are used as integrators, the offsets created by the amplifiers used to generate these filters still become a problem because of the relatively large DC gain required for each filter. Each gain is proportional to the inverse of the filter angular cutoff frequency, ω_a , and hence proportional to the filter time constant $\tau_a (= \frac{1}{\omega_a})$.

Information concerning wave height frequencies indicates that τ_a should be in the neighborhood of 4 s and possibly larger. Calculations show that the required DC gain of each filter stage will be about 10 for $\tau_a = 4$ s, yielding a cascaded DC gain of approximately 2500. Small amplifier and accelerometer offsets will be amplified by this gain and may become equivalently large wave height errors. To overcome this deficiency, it is necessary to

block the DC offsets from the output by means of at least one first-order high-pass filter, having a cutoff angular frequency of about ω_a , placed at the output of the cascaded low-pass filters. However, even this solution is not satisfactory, because small offsets may tend to use up a sizable portion of the dynamic range of the individual amplifiers in the cascaded low-pass filters. For example, 1 MVDC offset at the output of the summing amplifier, which combines the accelerometer signals in the x, y, and z channels and drives the cascaded filter stages, can become approximately 2.5 VDC at the output of the second-stage low-pass filter, assuming $\tau_a = 4$ s. If τ_a is higher, the offset at the output of the second-stage low-pass filter is higher.

By carrying this offset argument further in order to keep the effects of offsets within reasonable bounds, we are led to a five-stage filter configuration that uses three first-order high-pass filters with two first-order low-pass filters arranged as shown in Fig. 11. In this configuration, the output offset of each filter stage can be held to a reasonably small value. Furthermore, the output offset of the last stage, which represents an error in the measurement of h_v , can be held to insignificance in terms of the error in h_v by using a DC operational amplifier with reasonably low DC offset to generate the high-pass filter function.

If an analysis is made of the effect on the measurement of h_v due to the rate of change of DC offset of the amplifiers in the filter stage, particularly in the first two stages, and in the x, y, z summation amplifier driving the five-stage filter, we are led to the conclusion that very low DC offset amplifiers are required. Each critical amplifier requires an offset in the microvolt region in order to guarantee that its time rate of change due to environmental changes will be correspondingly small, preferably of the order of 1.0 $\mu\text{V/s}$ or less. This implies that chopper-stabilized amplifiers should be used since these are known to have very low DC offsets. For this purpose, the Philbrick model 1701 chopper-stabilized amplifier was chosen. This amplifier has an initial DC voltage offset of 15 μV maximum with a temperature coefficient of voltage offset of 0.25 $\mu\text{V}/^\circ\text{C}$ maximum. Its initial bias current is 50 pA maximum with a temperature coefficient of 1 pA/ $^\circ\text{C}$. The expected impedance level to be used in each amplifier is of the order of 5 M Ω so that the latter temperature coefficient translates into an equivalent temperature coefficient of voltage offset of 5 $\mu\text{V}/^\circ\text{C}$.

This is over an order of magnitude higher than the temperature coefficient of voltage offset ($0.25 \mu\text{V}/^\circ\text{C}$) and can be tolerated if the rate of change of ambient temperature about the amplifier unit is less than approximately $(1.0 \mu\text{V/s})/(5 \mu\text{V}/^\circ\text{C}) = 0.2^\circ\text{C/s}$. The latter does not appear to be a severe requirement after initial warm-up of the amplifiers. However, the amplifiers should be protected against rapid ambient temperature changes that might take place in the environment in which they are to be used.

The Philbrick model 1701 amplifier operates on $\pm 15 \text{ V}$ supplies and has voltage and current offset changes due to power and supply voltage changes. Typical offsets are $\pm 0.2 \mu\text{V/V}$ of power supply change, and $\pm 2 \text{ pA/V}$ of power supply change. If the power supplies are stable to within $\pm 1\%$ (corresponding to a maximum change of 0.3 V = worst case difference change between the two supplies), the change in voltage offset is about $0.06 \mu\text{V}$ (insignificant) while the change in equivalent voltage offset due to current offset at the $5 \text{ M}\Omega$ impedance level is $0.60 \mu\text{V}$. The latter offset change is acceptable if the power supply change does not occur in less than 0.6 s .

Calculations indicate that the internal noise generated by the Philbrick amplifiers should not introduce significant errors in the measurement of h_v .

Since all three high-pass filter sections are identical and both low-pass filter sections are identical in the five-stage filter, it was decided to use the same type amplifiers for all the stages — namely, the Philbrick model 1701, even though the DC offset requirements on the third, fourth, and fifth stages are not as severe as those for the first two stages. This permits interchangeability of stages for the respective filter types.

Since the outputs of the multipliers in the \ddot{x} and \ddot{y} channels in Fig. 10 drive the input of the summing amplifier, the multipliers must have correspondingly low output DC offset in order that the rate of change of DC offset does not create large errors in the measurement of h_v . For this purpose, the Intronic model M311 multiplier was chosen. This is a high-precision ultrastable pulse height/pulse width type of multiplier with an output offset of 10 MV maximum but with a temperature coefficient of output offset of only $20 \mu\text{V}/^\circ\text{C}$. This temperature coefficient can be tolerated if the rate of change of ambient temperature about the multiplier unit is less than $(1.0 \mu\text{V/s})/(20 \mu\text{V}/^\circ\text{C}) = 0.05^\circ\text{C/s}$ (or 3.0°C/min). The latter requirement points up the fact that the multipliers should be protected against rapid environmentally induced temperature changes and should have adequate time for warm-up prior to use — perhaps 10 min at least.

No data are given for the Intronic multipliers with respect to the output offset voltage sensitivity to supply voltage changes and with respect to its time stability. However, measurements were made on one model M311 multiplier with the result that the output offset changes less than 25 μV for a 1% change in either the +15 V or -15 V supply. If the multiplier output drift rate is to be held to less than, for example, 1.0 $\mu\text{V/s}$, the power supply drift rate should not exceed $(1.0 \mu\text{V/s}) / (25 \mu\text{V}/\%) = 0.04\%/s$ or 6.0 MV/s for both the +15 V and -15 V supplies. This is not a severe requirement once the power supplies are allowed to warm up and stabilize. Time stability measurements indicate that the multiplier is stable to well within 0.4 $\mu\text{V/min}$ (after a suitable warm-up period). It is likely that any changes observed were due to temperature changes. After a 5 min warm-up the drift rate did not exceed 20 $\mu\text{V/min}$, which is satisfactory for our application.

Calculations show that the internal noise generated by the M311 multipliers should not introduce significant errors in the measurement of h_v .

For small angles θ and ϕ (assuming $|\theta|, |\phi| < \frac{1}{4}$ rad (14.3°), the z accelerometer senses the major portion of the h_v motion. The output DC voltage offset of this accelerometer drives the x, y, z summing amplifier input directly (see Fig. 9) and hence its rate of change of offset is of concern. Any DC offset appearing at the output of the x or y accelerometer is effectively multiplied by $-\frac{\sin \theta}{2}$ or $\frac{\sin \phi}{2}$ respectively, and hence is reduced by at least a factor of 8 (since $\sin 14.3^\circ \approx 0.25$) before the offset reaches the summing amplifier input where it is added to the z accelerometer signal. Hence, the rate of change of DC offset for each of these accelerometers is not as critical as for the z accelerometer. Design information on the Sondstrand QA 1200 - AA08 linear forced feedback accelerometer (used on the z axis as well as on the x and y axes) indicates that offset stability, due to temperature changes, of the accelerometer is of the order of 5.5 $\mu\text{g}/^\circ\text{F}$ ($= 10 \mu\text{g}/^\circ\text{C}$). For a scale factor of 2.50 V/g, this is equivalent to 2.5×10^{-6} V/ $^\circ\text{C}$. In order not to exceed a drift rate of the order of 1.0 $\mu\text{V/s}$, the temperature of the accelerometer should not change at a rate greater than $(1.0 \mu\text{V/s}) / (25 \mu\text{V}/^\circ\text{C}) = 0.040^\circ\text{C/s}$ or 2.4 $^\circ\text{C/min}$. This is a requirement that should be achievable on the SES. Power supply changes of $\pm 1\%$ do not produce any significant output offset changes for this accelerometer.

The +15 V and -15 VDC power supplies used in the system are contained in a single module, the Analog Devices model 925 modular power supply. It operates from 50 to 400 Hz prime power and has a 350 MA rating for each supply. The line and load regulation values are 0.02 and 0.02%, respectively; these values are more than satisfactory for this application. Each supply has a temperature coefficient of voltage of 0.015%/°C or 2.25 MV/°C. To satisfy the M311 multiplier drift rate requirement due to power supply drift rate, it was indicated that the latter should not exceed 0.04%/s. For these power supplies, we require that the module case temperature not change by more than $(0.04\%/s)/(0.015\%/^{\circ}\text{C}) = 2.7^{\circ}\text{C/s}$. This value should not be difficult to achieve even during power supply warm-up.

DESCRIPTION OF THE INSTRUMENTATION DIAGRAM FOR THE MOTION-COMPENSATED WAVE PROFILER

Figure 12 is an electronic instrumentation diagram for the motion-compensated wave profiler. The outputs of the accelerometer channels x, y, z are combined at the input to summation amplifier K_{13} along with a stable +1 g bias source. The latter is required to cancel the static -1 g acceleration sensed by the accelerometers (mainly the z accelerometer) due to gravitational attraction.

As can be seen, the x and y accelerometer signals are first passed through isolating unity gain buffer amplifiers and then through multipliers via the M_1 and M_2 inputs, in order to implement Eq. 24 with $A = 0.500$. The other inputs to the multipliers represent the $\sin \theta$ and $\sin \phi$ channel signals that appear at multiplier inputs N_2 and N_1 , respectively. Signals proportional to $\sin \theta$ (in pitch channel) and $\sin \phi$ (in roll channel) are derived from the $S_1 - S_3$ outputs of three-wire synchros. Each signal is a 400 Hz suppressed carrier signal, the amplitude of which is proportional to the sine of the angular deviation from the null position. The null position in each channel corresponds to $\theta = 0$ and $\phi = 0$. The phase of the signal is either in phase (ideally) or 180° out of phase (ideally) with the 400 Hz carrier reference depending on the direction of rotation of the synchro from the null position. The signal phase therefore carries the information concerning the sign of the deviation of the synchro rotor from the null position. In order to derive the DC signal in each channel whose amplitude is proportional to the sine of the angular deviation from the null position and whose sign indicates the direction

of rotation from the null position, it is necessary to use phase sensitive demodulation. Each synchro signal is first passed through an isolation transformer (IT in Fig. 12) so that the electronics ground may be isolated from the synchro wires. The signal is then passed through a fixed gain, fixed phase shift amplifier stage (K_1 and K_7) having a limiter to prevent unduly large AC signals from reaching and overloading succeeding stages. The limit level is set near 12° in each of the θ and ϕ channels, which is well above the maximum expected pitch and roll angles. The fixed phase shift, which is about -135° , is combined with an adjustable phase shift in the succeeding amplifier (K_2 and K_8) to produce either a signal exactly in phase or 180° out of phase (depending on synchro rotor direction of rotation) with the 400 Hz reference at the demodulator (K_3 and K_9) input. The output of the adjustable phase shift amplifier, the amplitude of which is proportional to $\sin \theta$ or $\sin \phi$, and the phase of which contains the information on the direction of rotation and therefore the signal sign, is then fed to the demodulator (K_3 and K_9) where in combination with the 400 Hz carrier reference signal it is demodulated.

The 400 Hz carrier reference signal for the demodulator should be a square wave signal whose zero crossovers should coincide with the zero crossovers of the input signal (to the demodulator) that is to be demodulated. As indicated previously, phase corrections of the synchro signals to permit coincidence between signal and reference zero crossovers are accomplished via the adjustable phase shift amplifiers (K_2 and K_8). The square wave reference is generated from the 115 Vrms, 400 Hz sine wave reference supply (used to supply the synchros) by first passing it through a stepdown transformer and then squaring the wave via a hysteresis switch and limiter. The hysteresis switch prevents noise from affecting the switching of the waveform around zero crossover of the sinewave. The output of the hysteresis switch is then passed to a square wave reference generator that adjusts the levels of the positive and negative portions of the square wave to be compatible with the T^2L electronic switch contained in each demodulator.

The output of the demodulator therefore contains a DC signal with amplitude proportional to the sine of the synchro rotation angle (from the null position) and sign denoting synchro rotation direction, and harmonics of the 400 Hz carrier frequency, particularly even harmonics. These harmonics are effectively removed subsequently

by the following stage (K_4 and K_{10}), which is a second-order low-pass filter having a cutoff frequency set at about 80 Hz. This cutoff frequency is well above maximum expected signal frequencies in the roll and pitch channels and is sufficiently low to attenuate the carrier harmonics to insignificance.

The output of the second-order low-pass filter is then passed to a divider stage input (M_3 and M_4) where the signal amplitude is normalized to the 400 Hz reference signal amplitude. If the 115 Vrms, 400 Hz reference should change in amplitude, the Θ and ϕ synchro outputs will change proportionally. Since the signals proportional to $\sin \Theta$ and ϕ supplied to the N_2 and N_1 multiplier inputs should be independent of reference amplitude, a means for removing the dependence on reference amplitude must be provided. Each divider stage, in conjunction with a DC signal proportional to reference amplitude applied at the divisor input (N_3 and N_4), provides the means for removing the dependence. For this purpose the amplitude of the 115 Vrms, 400 Hz reference (E_R) is measured by an adjustable gain absolute value detector (K_{17}) that full-wave rectifies the 400 Hz wave and generates a DC voltage proportional to the average value of the rectified wave. An isolation transformer (IT) is used to isolate the 400 Hz reference signal from the detector signal ground. The detector also generates harmonics of the 400 Hz reference frequency that are subsequently filtered by the following second-order low-pass filter (K_{18}) having a cutoff frequency at 10 Hz. The detector gain is made adjustable to permit the proper DC level to be set at the divider input (N_3 and N_4).

The output of the divider in each synchro channel is then passed through an adjustable gain amplifier (K_5 and K_{11}) to ensure that the proper signal level reaches the multiplier input (N_1 and N_2). This adjustment permits absorption of circuit tolerances. The gains K_6 and K_{12} actually represent attenuators inserted in the signal lines to multiplier inputs N_1 and N_2 . Each attenuator has its gain set to $1/2$, which represents the adjustment of the gain A in the basic equation used to calculate \ddot{h}_s in Eq. 24, which is equivalent to \ddot{h}_b in Eq. 21; \ddot{h}_c for $A = \frac{1}{2}$ (or \ddot{h}_b) is a measure of \ddot{h}_v .

Since the sign of the x accelerometer signal when multiplied by a signal proportional to $\sin \theta$ must be opposite to the corresponding sign of the multiplied signal in the y accelerometer channel (see Eq. 24), a signal reversal must be produced at the output of the x multiplier. The sign reversal may be conveniently produced by interchanging the output leads of the isolation transformer used to isolate the electronics ground from the pitch synchro S1-S3 wires.

At the summation amplifier K_{13} , the accelerometer channel signals are combined along with the stable +1 g bias voltage to produce a signal proportional to \ddot{h}_b at K_{13} output, where \ddot{h}_b is an approximation to \ddot{h}_v and is given by Eq. 21. The output of amplifier K_{13} is then passed through the five-stage high-pass filter where double integration of signal frequencies appreciably above the filter cutoff frequency is performed. The filter cutoff frequency is given by $f_a = \frac{\omega_a}{2\pi} = \frac{1}{2\pi\tau_a}$, where τ_a is the time constant set in each of the five filter stages. In this system, τ_a has been set to 20 s, corresponding to $f_a = 0.00796$ Hz.

The output of the five-stage filter now represents a signal proportional to h_b (which is an approximation to h_v) and is sent through adjustable gain scaling amplifier K_{15} to produce the desired ship's vertical motion scale factor of 1.00 ft/V. The gain adjustment on K_{15} permits absorption of circuit tolerances in the stages producing signal (h_b) ($\approx h_v$) at the output of the five-stage filter.

The output of the five-stage filter is also passed to the input of adjustable gain summing amplifier F_{16} , which has two gain adjustments. The other input to K_{16} comes from the altimeter channel that produces a signal proportional to $(h_w - h_v)$. The summing amplifier therefore is to combine a signal proportional to $[h_v]$ ($\approx h_b$), from the five-stage filter output, with that proportional to $(h_w - h_v)$ to yield an output proportional to (h_w) only. Thus, one gain adjustment on K_{16} amplifier permits normalization of the signals proportional to (h_v) and $(h_w - h_v)$ so that

they add properly to produce a signal proportional to just (h_w) . The other K_{16} gain adjustment permits setting the output scale factor to the desired 1.00 ft/V for wave height.

For the purpose of providing a readout of the rms value of the wave height variations, the output of K_{16} summing amplifier is passed to an rms-to-DC converter (K_{26}).

The altimeter channel signal $(h_w - h_v)$ is generated directly from one of two supplied altimeters that are to be used with the motion compensation system. These altimeters are the Collins model Alt 50 and the TRT model AllV20. Each altimeter measures $(h_0 + h_w - h_v)$, and its output is amplified by a three-stage amplifier (K_{21} and K_{22}) that has a gain adjustment for the purpose of normalizing the output to a prescribed scale factor at the altimeter select switch. This permits selection of either altimeter output at the same scale factor for subsequent signal processing. The output of each altimeter has such a wide range for its scale factor (100 MV/ft to 250 MV/ft) that it is necessary to provide some means for normalizing the scale factor to 250 MV/ft. Provision is also made to permit adjustment of the initial height to compensate for altimeter height offset and permit direct readings of h_0 . Thus, in the three-stage amplifier in each channel, the first stage serves as a high input impedance buffer amplifier that prevents significant loading of the altimeter output signal. This stage also contains a limiter that is activated for total altimeter signals exceeding heights in the range of 33.6 to 84 ft, depending on the altimeter scale factor. The second stage of the three-stage amplifier has an adjustable gain for normalizing the output scale factor. The third stage has the bias offset adjustment that can range between 0 and 31 ft.

The altimeter signal selected by the altimeter select switch is then fed into a singlestage high-pass filter where the DC and very low frequency altitude variations are removed, allowing only the ship's motion and wave height variations $(h_w - h_v)$ above the filter cutoff frequency to pass through relatively unattenuated. The cutoff frequency is approximately 0.0064 Hz corresponding to $\tau_b \approx 25$ s.

The output of the altimeter select switch is also fed to the input of a single-stage low-pass filter with the intent of passing primarily the mean value of the height, (h_0) , while attenuating the (h_v) and (h_w) variations above the filter cutoff

frequency. The filter cutoff frequency has also been set at approximately 0.0064 Hz corresponding to $\tau_c \approx 25$ s. K_{25} in Fig. 12 is a buffer amplifier that provides isolation between the load and the output of the low-pass filter.

DC power to operate the various amplifiers in the wave profiler is obtained from a dual ± 15 VDC module, Analog Devices model 925. Each output has a 350 MA rating with 0.02% line regulation, 0.02% load regulation.

The demodulators make use of +5 VDC power as well as ± 15 VDC, and so require a +5 VDC supply, Analog Devices model 905. This supply is rated at 1 A output current with 0.02% line regulation, 0.05% load regulation. Not shown on Fig. 12 are various relays used for function switching and discharging (or resetting to zero) long time constant filter capacitors (particularly in the five-stage filter and in the high- and low-pass filters in the altimeter channel). These relays also operate on +5 VDC power and hence the current rating of the model 905 power supply was chosen to satisfy both the relay and demodulator requirements. Prime power to all DC power supplies is derived from a 115 Vrms, 400 Hz source.

CHANNEL GAIN CALCULATIONS AND ASSIGNMENT OF BLOCK GAINS

With reference to Fig. 12, this section will concern itself with the calculation of channel gains and the assignment of block gains.

Consider the signals being summed at the input to summing amplifier K_{13} ; assume each signal is summed with equal weight at the input to K_{13} . Excluding the (+1 g) bias source which is also summed at K_{13} input, we obtain the following equation by considering the signal paths from the \ddot{x} , \ddot{y} , and \ddot{z} accelerometers to the input of K_{13} , where S_1 is the sum of the signals at K_{13} input:

$$S_1 = \ddot{x} \left(K_c \frac{N_2}{10} \right) + \ddot{y} \left(K_b \frac{N_1}{10} \right) + \ddot{z} (K_a) , \quad (30)$$

where

$$N_2 = K_{20} E_R (\sin \theta) (-n_2) K_7 K_8 K_9 K_{10} \left(\frac{10}{N_4} \right) K_{11} K_{12} . \quad (31)$$

$$N_1 = K_{19} E_R (\sin \phi) n_1 K_1 K_2 K_3 K_4 \left(\frac{10}{N_3}\right) K_5 K_6, \text{ and} \quad (32)$$

$$N_4 = E_R n_3 K_{17} K_{18} = N_3 = E_{R_N}. \quad (33)$$

Substituting Eqs. 31, 32, and 33 into Eq. 30 and noting that $K_{12} = K_6 = \frac{1}{2}$,

$$S_1 = -\left(\frac{\ddot{x} \sin \theta}{2}\right) \left(\frac{n_2 K_c K_{20} K_7 K_8 K_9 K_{10} K_{11}}{n_3 K_{17} K_{18}}\right) + \left(\frac{\ddot{y} \sin \phi}{2}\right) \left(\frac{n_1 K_b K_{19} K_1 K_2 K_3 K_4 K_5}{n_3 K_{17} K_{18}}\right) + \ddot{z}(K_a). \quad (34)$$

We desire, from Eq. 21, that the sum yields a signal proportional to \ddot{h}_b , which is to be a measure of \ddot{h}_v . Thus we require in Eq. 34 that by comparing with the terms in Eq. 21

$$\frac{n_2 K_c K_{20} K_7 K_8 K_9 K_{10} K_{11}}{(n_3 K_{17} K_{18}) K_a} = 1, \quad (35)$$

$$\frac{n_1 K_b K_{19} K_1 K_2 K_3 K_4 K_5}{(n_3 K_{17} K_{18}) K_a} = 1 \quad (36)$$

The gain factor $(n_3 K_{17} K_{18})$ is chosen such that when $E_R = 115.0$ Vrms, the normalizing reference signal E_{R_N} will be 8.00 ± 0.08 VDC. This permits the dividers $\left(\frac{10M_3}{N_3} \text{ and } \frac{10M_4}{N_4} \text{ blocks}\right)$ to

operate at signal levels yielding nearly the best accuracy by making N_3 and N_4 near their upper limit (10.0 VDC). Also, the second-order low-pass filter (K_{18}) operates near its maximum output capability without overload at the 8.00 VDC level. Moreover, the dividers and K_{18} can handle a 10% increase in E_R without overload to these blocks. Thus:

$$E_R(n_3 K_{17} K_{18}) = 8.00 \text{ VDC nominally with } E_R = 115.0 \text{ Vrms, or}$$

$$K_{17} K_{18} = \frac{8.00}{115.0 n_3} = \frac{0.06957}{n_3} \text{ VDC/Vrms .} \quad (37)$$

The IT's chosen were the UTC H-5 type. This transformer has a primary-to-secondary-impedance ratio of nominally 15 000 Ω to 95 000 Ω when used to isolate the pitch and roll synchro S1-S3 outputs from the MCU electronics ground. When used to isolate the 115 Vrms, 400 Hz reference E_R , the primary and secondary winding connections are interchanged. The turns ratio n_1 , n_2 , n_3 for each of the respective transformers is therefore

$$n_1 = -n_2 \sqrt{\frac{95K}{15K}} = 2.517 , \quad (38)$$

$$n_3 = \frac{1}{n_1} = 0.3974 . \quad (39)$$

The gain product $K_{17} K_{18}$ in Eq. 37 then becomes

$$K_{17} K_{18} = \frac{0.06957}{0.3974} = 0.1751 \text{ VDC/Vrms .} \quad (37a)$$

The gains K_{17} and K_{18} were distributed as follows:

$$K_{17} = 0.0875 \text{ VDC/Vrms} , \quad (37b)$$

$$K_{18} = 2.000 \text{ VDC/VDC} . \quad (37c)$$

It should be noted here that the minus sign associated with $(-n_2)$ implies that the connections to the primary (or secondary) of that transformer are interchanged in order to produce the proper sign of the \ddot{x} contribution at the K_{13} input.

The accelerometers \ddot{x} , \ddot{y} , \ddot{z} are torque-rebalance types and their associated metering resistances are to be adjusted to yield a common scale factor of (2.500 V/g) where $g = 32.2 \text{ ft/s}^2$

Thus

$$K_a = K_b = K_c = 2.500 \text{ V/g or } 0.07764 \text{ V/(ft/s}^2) . \quad (40)$$

The constants K_{19} and K_{20} (roll and pitch synchro gains) in Eqs. 36 and 35, respectively, may be evaluated by noting that $(K_{19}E_R)$ and $(K_{20}E_R)$ each must be 11.8 Vrms (nominal) when $E_R = 115.0 \text{ Vrms}$; hence

$$K_{19} = K_{20} = \frac{11.8 \text{ Vrms}}{115.0 \text{ Vrms}} = 0.1026 \text{ Vrms/Vrms} . \quad (41)$$

The limiter and fixed phase shift amplifiers (K_1 and K_7) in the roll and pitch signal channels, in addition to adjustable phase shift amplifiers (K_2 and K_8), provide corresponding signals to the demodulator inputs (K_3 and K_9) that do not overload the demodulators at maximum expected pitch and roll angles (θ and ϕ , respectively) up to approximately $\pm 12^\circ$. In addition, the adjustable phase shift feature permits correction of any phase shift in the synchro signals, with respect to the demodulator reference

signal, at the demodulator inputs. K_1 and K_7 each have an assigned gain of 1.038 Vrms/Vrms (nominally) and a fixed phase shift of -135° (nominally) at the 400 Hz carrier frequency. K_2 and K_8 each has a fixed gain of 1.000 (nominally) and an adjustable phase shift ranging between 0 and -90° at the 400 Hz carrier frequency. The gain products (K_1K_2) and (K_7K_8) then are

$$K_1K_2 = K_7K_8 = 1.038 \text{ } \underline{-135^\circ \text{ to } -225^\circ} \text{ Vrms/Vrms at 400 Hz .} \quad (42)$$

The normal roll and pitch channel synchro signals appearing at the inputs of K_1 and K_7 , respectively, may therefore deviate in phase from their respective correct phases with respect to the 400 Hz carrier reference signal by up to $\pm 45^\circ$. These phases are still correctable at the demodulator inputs, where the phases must be correct with respect to the 400 Hz reference signal, via the phase adjustments on K_2 and K_8 amplifiers. This range of phase adjustment should be more than adequate.

The demodulator gain magnitudes, K_3 and K_9 , were assigned the following values for signals either in phase or 180° out of phase with the 400 Hz reference signal:

$$K_3 = K_9 = 1.000 \text{ VDC/Vrms (nominally) .} \quad (43)$$

The second-order low-pass filters (K_4 and K_{10}) were designed to filter out the demodulator carrier noise, have a cutoff frequency of 80 Hz, and were assigned the following DC gains:

$$K_4 = K_{10} = 1.000 \text{ VDC/VDC (nominally) .} \quad (44)$$

In Eqs. 35 and 36, the values for the following constants and gains have been defined or assigned above: $n_1, n_2, n_3, K_a, K_b, K_c, K_1, K_2, K_3, K_4, K_7, K_8, K_9, K_{10}, K_{17}, K_{18}, K_{19}$, and K_{20} .

If these values are substituted in Eqs. 35 and 36, the nominal gain settings for the adjustable gain amplifiers K_{11} and K_5 may be found as follows after noting that $K_a = K_b = K_c$, nominally:

$$K_{11} = \frac{n_3 K_{17} K_{18}}{n_2 K_{20} K_7 K_8 K_9 K_{10}} = \frac{0.3974(0.0875)(2.000)}{2.517(0.1026)(1.038)(1.000)(1.000)(1.000)}$$

$$= 0.2594 \text{ VDC/VDC, nominally,} \quad (45)$$

$$K_5 = \frac{n_3 K_{17} K_{18}}{n_1 K_{19} K_1 K_2 K_3 K_4} = \frac{0.3974(0.0875)(2.000)}{2.517(0.1026)(1.038)(1.000)(1.000)(1.000)}$$

$$= 0.2594 \text{ VDC/VDC, nominally.} \quad (46)$$

The adjustments for gains K_{11} and K_5 permit tolerances in the various gain blocks to be absorbed so that Eqs. 35 and 36 may be satisfied. The largest gain tolerances are likely to be in the values of K_{19} and K_{20} , the synchro gains and provision is made to allow an adjustment of K_5 and K_{11} each with at least a tolerance of $\pm 25\%$ about the nominal value of 0.2594. Regardless of the actual values of the various constants in Eqs. 35 and 36, excluding K_5 and K_{11} , Eqs. 35 and 36 should be satisfied within $\pm 0.5\%$ by appropriately adjusting K_5 and K_{11} . It will be noted that misadjustments of θ and φ channel gains, which are contained in Eqs. 35 and 36, respectively, and appear in Eq. 34, are equivalent to a misadjustment of the value of A in Eq. 24 around the nominal value of $A=1/2$. From Fig. 8, we note that around $A=1/2$, a change in A of less than $\pm 0.5\%$ ($\rightarrow A=0.500 \pm 0.0025$) causes the fractional error ϵ_3 to change less than $\pm 0.05\%$ in the worst case when $\theta=\varphi=0.25 \text{ rad } (14.3^\circ)$. Hence, an error in the adjustment of the θ and φ channel gains of less than $\pm 0.5\%$ causes a negligible error in ϵ_3 , the fractional error in the measurement of h_v .

For the nominal values of the constants above, the signals at nodes N_1 and N_2 become

$$N_1 = \sin \phi \left(\frac{10n_1 K_1 K_2 K_3 K_4 K_5 K_6 K_{19}}{n_3 K_{17} K_{18}} \right) = 5.00 \sin \phi \text{ VDC}, \quad (47)$$

$$N_2 = -\sin \theta \left(\frac{10n_2 K_7 K_8 K_9 K_{10} K_{11} K_{12} K_{20}}{n_3 K_{17} K_{18}} \right) = -5.00 \sin \theta \text{ VDC}. \quad (48)$$

If ϕ and θ are small, $\sin \phi \approx \phi$, and $\sin \theta \approx \theta$ and the ratios (N_1/ϕ) and (N_2/θ) , for small rotation angles of the synchros from the null positions become

$$\frac{N_1}{\phi} = 5.00 \text{ VDC/rad} = 0.0873 \text{ VDC/deg}, \quad (49)$$

$$\frac{N_2}{\theta} = -5.00 \text{ VDC/rad} = -0.0873 \text{ VDC/deg}. \quad (50)$$

Assuming the gains K_5 and K_{11} have been properly adjusted, the signals appearing at the input of the K_{13} summing amplifier are now in the correct proportions. These signals are now summed at K_{13} input via equal valued, precision resistors; these resistors along with an identical resistance for the +1 g bias source appear as the input resistors to a fixed gain operational amplifier, the gain of which has been set, arbitrarily, to -0.700 nominally ($= K_{13}$). The individual summing resistors are matched to within 0.2% so that the relative gains in the z, y, and x channels are maintained overall within $\pm 1\%$ (this includes the path gains in the y and x channels).

Since the accelerometer triad signals, when summed at the input to K_{13} , sense the acceleration of gravity, a -1 g signal appears at the input of K_{13} . This signal is effectively cancelled by a positive signal (equivalent to +1 g bias) generated by a very stable

bias source. The latter should be stable within $\pm 0.05\%$ due to all environments, including a temperature environment of $\pm 10^\circ\text{C}$ about nominal (taken as 25°C), and its rate of change due to environmental changes should preferably not exceed about $1.0 \mu\text{V/s}$, the same requirement for the \ddot{z} accelerometer offset and for the offsets at the output of the multipliers in the \ddot{x} and \ddot{y} channels. With a slight readjustment of the $+1 \text{ g}$ bias source, all offset sources generated by the multipliers in the \ddot{x} and \ddot{y} channels, by the \ddot{z} , \ddot{x} , \ddot{y} accelerometers, and by the summation amplifier K_{13} can be nulled to within $\pm 0.5 \text{ MV}$ at the output of the K_{13} amplifier, which is the input to the five-stage filter. This prevents a large offset from appearing at the input to the five-stage filter; a large offset will cause a correspondingly long settling time due to the turn-on transient generated in the filter by the offset.

To establish the values of the gain constants K_{14} , K_{16} , K_{15} , and K_{26} , the following analysis applies. Since the gains in the \ddot{x} and \ddot{y} channels have been properly proportioned with respect to the \ddot{z} channel, we need only consider the \ddot{z} channel by setting $\theta = 0$, $\varphi = 0$. If a vertical acceleration signal of amplitude \ddot{z}_1 and angular frequency ω_1 (due to ship's motion) is sensed by the \ddot{z} accelerometer, it will produce an output h_w at block K_e output, in the absence of an altimeter signal at the input to block K_{16} , as follows:

$$h_w = \ddot{z} K_a K_{13} \frac{K_{14} (\tau_a)^5 s^3}{(\tau_a s + 1)^5} K_{16} K_e, \quad (51)$$

where

$$s = j \omega_1, \quad j = \sqrt{-1}, \quad \ddot{z} = \ddot{z}_1,$$

and where

$$\ddot{z} = \ddot{z}_1 \sin \omega_1 t. \quad (52)$$

Assume that the angular frequency (ω_1) of the ship's vertical motion is sufficiently high with respect to the five-stage filter cut-off angular frequency ($\frac{1}{\tau_a}$) so that the filter effectively becomes a double integrator producing a signal proportional to vertical height h_v , where

$$h_v = h_{v1} \sin \omega_1 t, \quad (53)$$

where: h_{v1} = amplitude of vertical height, and where, by integrating Eq. 52 twice

$$h_{v1} = - \frac{\ddot{z}_1}{\omega_1^2}. \quad (54)$$

However, the amplitude of the h_w output should be just h_{v1} at angular frequency ω_1 , in the absence of an altimeter signal. Thus, if we let $s = j\omega_1$, $j = \sqrt{-1}$, \ddot{z} = amplitude of vertical acceleration = \ddot{z}_1 , $\omega_1 \tau_a \gg 1$, Eq. 51 reduces to

$$h_w = h_{v1} = - \left[\frac{\ddot{z}_1}{(\omega_1)^2} \right] K_a K_{13} K_{14} K_{16} K_e. \quad (55)$$

Comparing Eqs. 55 and 54, we see that for the h_w output at the output of block K_e to be the true vertical height motion of amplitude h_{v1} , in the absence of an altimeter path signal, we require

$$K_a K_{13} K_{14} K_{16} K_e = 1. \quad (56)$$

K_a , K_{13} , K_e in Eq. 56 have been previously assigned so that K_{14} and K_{16} are to be assigned values consistent with Eq. 56. Thus

$$K_a = 2.500 \text{ VDC/g} = 0.07764 \text{ VDC}/(\text{ft/s}^2) \text{ with } g = 32.2 \text{ ft/s}^2$$

$$K_{13} = -0.700 \text{ VDC/VDC}; K_e = 1.000 \text{ ft/VDC}$$

$$K_{14}K_{16} = \frac{1}{0.07764(-0.700)(1.000)} = -18.40 \text{ (VDC rad}^2\text{)/(VDC s}^2\text{)}.$$

(57)

The five-stage filter consists of three high-pass and two low-pass cascaded first-order filters, each with a cut-off angular frequency $(\frac{1}{\tau_a})$. This filter $G_1(s)$ is constructed with five operational amplifiers having transfer functions cascaded as follows:

$$G = \left(\underbrace{\text{HP Filter}}_{-\frac{\tau_a s}{\tau_a s+1}} \right) \cdot \left(\underbrace{\text{LP Filter}}_{-\frac{K_m \tau_a}{\tau_a s+1}} \right) \cdot \left(\underbrace{\text{HP Filter}}_{-\frac{\tau_a s}{\tau_a s+1}} \right) \cdot \left(\underbrace{\text{LP Filter}}_{-\frac{K_m \tau_a}{\tau_a s+1}} \right)$$

$$\cdot \left(\underbrace{\text{HP Filter}}_{-\frac{\tau_a s}{\tau_a s+1}} \right) = \frac{K_{14} \tau_a^5 s^3}{(\tau_a s+1)^5} \quad (58)$$

It will be noted in Eq. 58 that the high-frequency gain (i.e., when $\omega\tau_a \gg 1$ with $s=j\omega$) of each high-pass filter is -1.000 VDC/VDC nominally, while the low-frequency gain (i.e., when $\omega\tau_a \ll 1$) of each low-pass filter is $(-K_m \tau_a)$. τ_a has been assigned the value of 4 s nominally. To keep the low-frequency gain of each low-pass filter within reasonable bounds $(-K_m \tau_a)$ was assigned the value of -50.0 VDC/VDC, so that $K_m = \frac{10.0}{4} = 2.50 \text{ (VDC rad/VDC s)}$, $K_{14} = -K_m^2 = -6.25 \text{ (VDC rad}^2\text{/VDC s}^2\text{)}$. With $K_{14} = -6.25 \text{ (VDC rad}^2\text{/VDC s}^2\text{)}$ we can now find K_{16} in Eq. 57:

$$K_{16} = \frac{-18.40}{-6.25} = 2.944 \text{ VDC/VDC} . \quad (59)$$

Since the five-stage filter has component tolerances, τ_a in each stage will not be exactly 20 s and may deviate by as much as 6% from the desired 4 s value. Also, the high-frequency gain of the high-pass filters each will not be exactly -1.000 VDC/VDC. Furthermore, there is a tolerance on K_m in each low-pass filter. Thus K_{14} is subjected to rather wide tolerances, and, as a consequence, K_{16} must be made adjustable to absorb these tolerances so that Eq. 56 may be satisfied to within $\pm 0.5\%$.

The values of gain constants K_{15} and K_{26} may now be established. Since the scale factor at the output of K_{16} is 1.00 VDC/ft, the equivalent scale factor at K_{16} input is $1.00 \text{ (VDC/ft)}/K_{16}$ or $1.00 \text{ (VDC/ft)}/2.944 = 0.3397 \text{ VDC/ft}$ (nominally). But at the output of K_{15} the scale factor desired is 1.00 VDC/ft. Consequently, $(0.3397 \text{ VDC/ft}) K_{15} = 1.00 \text{ VDC/ft}$, and therefore $K_{15} = 2.944 \text{ VDC/VDC}$ nominally. Since K_{14} has wide tolerances, the scale factor at the input to blocks K_{15} and K_{16} is also subject to wide tolerances. Hence K_{15} must be made adjustable to absorb these tolerances so that the scale factor at K_{15} output is the desired value within $\pm 0.5\%$.

K_{26} represents an rms-to-DC converter. It is an Analog Devices model AD536J integrated circuit true rms-to-DC converter. Its function is to determine the rms value of the instantaneous wave height, which, by definition, is

$$h_w(\text{rms}) = \left[\left(\frac{1}{T_2 - T_1} \right) \int_{T_1}^{T_2} h_w^2(t) dt \right]^{1/2} , \quad (60)$$

where $h_w(t)$ is the instantaneous value of wave height and $(T_2 - T_1)$ is the averaging time interval. This equation is essentially solved by the true rms-to-DC converter if the internal time constant of the low-pass filter contained in the converter is much greater than the longest period of the input signal. That is, the filter cutoff frequency should be much lower than the lowest wave frequency encountered. The output of the converter is a DC voltage that represents

the rms value of the wave height. The converter gain is K_{26} and $K_{26} = 1.00 \text{ VDC/Vrms}$. Since the scale factor at K_{16} output has been set to 1.00 VDC/ft , this is equivalent to 1.00 Vrms/ft rms , and it follows that the scale factor at the output of K_{26} is 1.00 VDC/ft rms .

The remaining gains to be determined or assigned are related to the altimeter paths in Fig. 12. The altimeters, either of which may be selected by the altimeter select switch, have scale factors that may range between 0.100 and 0.250 VDC/ft . Consequently, a means for normalizing the gain to the switch select point is required. The three-stage amplifier following each altimeter output is designed for this purpose and has other features as well. The three-stage amplifier consists of a buffer amplifier, scale adjustment amplifier, and an offset adjustment amplifier. The buffer amplifier nominally has a gain of -1.000 VDC/VDC and has a high input impedance ($1 \text{ M}\Omega$) so that the loading on each altimeter is insignificant. The second stage or scale adjustment amplifier has a gain adjustment that permits normalization of the scale at the output of the third stage to -0.250 VDC/ft . The third stage has a height offset adjustment that permits compensation for any altimeter positive height offset in the range 0 to 31 ft .

Including any altimeter height offset, the minimum linear range of the three-stage amplifier is 0 to 40.0 ft if the altimeter scale factor ranges between 0.100 and 0.210 VDC/ft ; if the scale factor ranges between 0.210 and 0.250 VDC/ft , the minimum linear range decreases linearly from 0 to 40.0 ft to 0 to 33.6 ft . The first stage has a limit level that becomes activated before the second stage reaches its dynamic range limitation, whenever the altimeter scale factor ranges between 0.210 and 0.250 VDC/ft . For scale factors below 0.210 VDC/ft , the dynamic range limitation of the second stage becomes effective before the limit level is reached in the first stage.

The output of the single-stage high-pass filter in the altimeter signal path, which is the input to amplifier K_{16} , must have the proper scale factor so that the ship's motion ($-h_v$) sensed by the altimeter may cancel exactly the signal due to the ship's motion sensed by the accelerometer triad and appearing at the input to K_{16} . The nominal scale factor at the K_{16} input has previously been shown to be 0.3397 VDC/ft . Hence at high frequencies where $\omega \gg (1/\tau_b)$, $1/\tau_b$ being the cutoff angular frequency of the high-pass filter, K_{23} must satisfy the following requirement:

$$K_{23} = \frac{0.3397 \text{ (VDC/ft)}}{-0.250 \text{ (VDC/ft)}} = 1.359 \text{ VDC/VDC (nominally)} . \quad (61)$$

τ_b was chosen to be approximately 25.5 s, corresponding to a high-pass filter cutoff frequency of 0.0062 Hz (approximately).

The widest tolerance of K_{23} is approximately $\pm 2\%$. As noted previously, K_{14} , the gain constant associated with the five-stage filter in the accelerometer path has a wide tolerance. Consequently, in order to obtain precise cancellation of the ship's motion when the signal from the altimeter path is summed with the signal from the accelerometer path at the input of K_{16} amplifier (which is an operational amplifier), it is necessary to alter the ratio of the summing resistors at K_{16} input. For this purpose, the K_{16} input summing resistor ratio is made adjustable. As noted previously, the K_{16} amplifier also has a scale factor adjustment so that the desired scale factor at the K_{16} amplifier output can be obtained.

The remaining path in which gain constants are to be established is the altimeter-ship's mean height ($+h_0$) path. At the buffer amplifier K_{25} output, a scale factor of +0.500 VDC/ft is required. Since the scale factor at the single-stage low-pass filter input is -0.250 VDC/ft, it follows that the product of the DC gain constants K_{24} and K_{25} must be

$$K_{24}K_{25} = \frac{+0.500 \text{ VDC/ft}}{-0.250 \text{ VDC/ft}} = -2.00 \text{ VDC/VDC} . \quad (62)$$

Buffer amplifier K_{25} is a unity gain (+1.00 VDC/VDC) amplifier driving the load. Consequently K_{24} has been assigned a gain of -2.00 VDC/VDC. This gain has been made adjustable via a trim resistor to absorb component tolerances. The time constant τ_c of the low-pass filter has been chosen to be approximately 25.5 s corresponding to a filter cutoff frequency of 0.0062 Hz (approximately).

CIRCUIT DESCRIPTIONS

This section will deal with the circuit descriptions of the various blocks shown on Fig. 12.

Card # 8, Fig. A8-1, Schematic of \ddot{x} , \ddot{y} Accelerometer Scaling Coordinate Conversion and DAS Buffer

The outputs of the Sundstrand accelerometer triad, \ddot{x} , \ddot{y} , and \ddot{z} shown in Fig. 12 are combined after multiplication in the x and y channels in the K_{13} summing amplifier along with the $+1$ g bias source. Figure A8-1 is a schematic of the unity gain buffer amplifier and Intronic M311 multiplier used in the x and y channels (Note: the x and y channel blocks are identical and hence only one schematic covering either channel is shown). Also shown in Fig. 12 and Fig. A8-1 is a buffer amplifier having a gain of $+8.00$ VDC/VDC, the output of which is sent to DAS. The scale factor at its input is that of the accelerometer (K_b or K_c), which is 2.500 V/g. The scale factor of the signal sent to DAS is therefore 20.0 V/g.

In Fig. A8-1, the scale factor of the \ddot{x} or \ddot{y} accelerometer is set by means of the net loading resistance across the accelerometer output. This resistance consists of the series combination of the $1.50K \Omega$ and $R_a(R_b)$ resistors (where R_a applies to y channel and R_b applies to x channel). The nominal scale factor of each accelerometer is 1.33 MA/g and hence a nominal net loading resistance of 1875Ω is required to yield the desired scale factor of 2.500 V/g. Since the accelerometer scale factors have a $\pm 10\%$ tolerance, the net loading resistance could range between 1705 and 2083Ω . $R_a(R_b)$ is thus a trim resistor to be selected to yield the 2.500 V/g scale factor to within $\pm 3\%$. A $\pm 3\%$ tolerance will yield an error in the measurement of h_w of less than 0.01 ft in the worst case when $\theta = \varphi = \frac{1}{4}$ radian and when $h_v = 5$ ft. The $1.5K \Omega$ fixed resistor and $R_a(R_b)$ can each have a temperature coefficient of better than ± 100 ppm/ $^{\circ}C$ (a normal tolerance). If we assume a $\pm 10^{\circ}C$ ambient temperature environment, the maximum scale factor change would be $\pm 0.1\%$, which is small compared to the initial adjustment tolerance.

The gain of 8.00 VDC/VDC amplifier yielding the 20 V/g signal to DAS uses an LM108AH, which is a low offset IC (integrated circuit) DC operational amplifier (DCOA). Including a $\pm 10^\circ\text{C}$ change in ambient temperature, the output offset should be within 0.000 ± 0.007 V corresponding to an offset of ± 350 μg maximum, which is negligible. The gain of 8.00 VDC/VDC is obtained within $\pm 0.5\%$ by properly selecting R_E (having a nominal value of $200\text{K } \Omega$) as indicated in Note 4 of Fig. A8-1. The $5.11\text{K } \Omega$ resistor at the LM108AH output is to protect the amplifier in the event that the output lead to DAS is inadvertently shorted to ground. The input impedance of the DAS load is assumed to be $\geq 1\text{ M}\Omega$, so that the loading error will not exceed about 0.5% . At the input of the amplifier is a first-order low-pass filter, formed by the $909\text{K } \Omega$ resistor and 180 pF capacitor, which has a cutoff frequency of about 97 Hz . At 20 Hz , the input impedance of the filter, which loads the $[1.5\text{K } \Omega + R_a(R_b)]$ resistance tending to change the scale factor of the accelerometer output, is approximately $4500\text{K } \Omega$ reactive. This produces a scale factor change of less than 0.01% , which is negligible.

The LM108AH buffer amplifier driving the multiplier in Fig. A8-1 has a very high input impedance at low frequencies and hence does not load the loading resistance $[1.5\text{K } \Omega + R_c(R_d)]$ across the accelerometer output. The amplifier is connected as a voltage follower and has unity gain ($+1.00\text{ VDC/VDC}$). Its output drives the M311 multiplier "X" input, which has a $10\text{ M}\Omega$ input impedance. The output offset of this amplifier is less than 6 MV , which includes a $\pm 10^\circ\text{C}$ ambient temperature change. The output offset drift rate at the multiplier output, due to the multiplier and any offset drift rate at its X and Y inputs, should be less than $1.4\text{ } \mu\text{V/s}$ ($\rightarrow 1.0\text{ } \mu\text{V/s}$ at input to five-stage filter) in order not to incur errors in the measurement of h_w exceeding 0.05 ft . Since $E_0 = \frac{XY}{10}$, correspondingly the X input drift rate should not exceed $\frac{10E_0}{Y}$ with the Y input at its maximum value, and the Y input drift rate should not exceed $\frac{10E_0}{X}$ with the X input drift rate at its maximum value. Since $\ddot{y} = \ddot{h} \sin \phi$ with $\ddot{h} = 1\text{ g (DC)}$, $\phi = \frac{1}{4}\text{ rad maximum}$, $\ddot{y}(\text{max}) = 0.247\text{ g}$. Likewise, $\ddot{x} = \ddot{h} \sin \theta$ with $\ddot{h} = 1\text{ g (DC)}$, $\theta = \frac{1}{4}\text{ rad maximum}$, so that $\ddot{x}(\text{max}) = 0.247\text{ g}$. For the scale factor 2.5 V/g , $\ddot{y}(\text{max}) = \ddot{x}(\text{max}) = 0.618\text{ V maximum}$ appearing at the X input of the M311 multiplier. The voltage signal appearing at the Y input is $5 \sin \theta\text{ V}$ for the

pitch channel and $5 \sin \varphi$ V for the roll channel (the signals at Pin 5 in Fig. A8-1 are respectively $10 \sin \varphi$ V and $10 \sin \varphi$ V). Hence the maximum signal appearing at the Y input for $\theta = \varphi = \frac{1}{2}$ rad maximum is just $5 \sin (\frac{1}{2} \text{ rad}) = 1.24$ V. Using these values, we conclude that the X input drift rate should not exceed $\frac{10(1.4 \mu\text{V/s})}{0.618} = 22.7 \mu\text{V/s}$. Also, the Y input drift rate should not exceed $\frac{10(1.4 \mu\text{V/s})}{1.24} = 11.3 \mu\text{V/s}$. At Pin 5 input this drift rate should not exceed $2(11.3) = 22.6 \mu\text{V/s}$ since the two 14.7K resistors form an attenuator with gain (1/2). This attenuator represents the gain K_6 (K_{12}) in Fig. 12. Thus, the output offset drift rate of the LM108AH buffer amplifier driving the multiplier X input should not exceed $22.7 \mu\text{V/s}$. With temperature changes, the output offset drift rate of the LM108AH DCOA should not exceed $5.2 \mu\text{V}/^\circ\text{C}$, so that ambient temperature changes should be held to less than $(22.7 \mu\text{V/s})/(5.2 \mu\text{V}/^\circ\text{C}) = 4.4^\circ\text{C/s}$. This is not a severe requirement at all; however, the equipment should be insulated to preclude rapid ambient temperature changes. For the LM108AH, the output offset changes by less than 2.4 μV for a 1% change in either supply voltage. For a maximum of $22.7 \mu\text{V/s}$ change, either supply should not change by more than $(22.7 \mu\text{V/s})/(2.4 \mu\text{V}/1\%) = 9.5\%/s$. Since the supplies are well regulated and have a maximum temperature coefficient of $0.015\%/^\circ\text{C}$, the output offset changes of the LM108AH buffer amplifier driving the multiplier, due to sensitivity to power supply changes, are negligible.

The output offset drift rate of the multiplier itself should not exceed $1.4 \mu\text{V/s}$. As previously indicated the Intronic M311 multiplier has a maximum output offset temperature coefficient of $20 \mu\text{V}/^\circ\text{C}$, so that the ambient temperature should not be allowed to change faster than $(1.4 \mu\text{V/s})/(20 \mu\text{V}/^\circ\text{C}) = 0.07^\circ\text{C/s}$ or 4.2°C/min . As previously indicated (see p. 69) the output offset drift rate of the multiplier due to power supply changes (i.e., changes in the +15 V and -15 V supplies) can be held to less than $1.0 \mu\text{V/s}$ if the drift rate of the supplies does not exceed 6 MV/s . This is not a severe requirement. If all equipment (power supplies, DCOA's, multipliers, etc.) are given sufficient warm-up time (such as a minimum of 15 min) the drift rate should be under $1.4 \mu\text{V/s}$ at the output of the multiplier due to all causes.

Card # 1, Fig. A1-1, MCU \ddot{z} Accelerometer Scaling, 1g Bias and Summing Amplifier

Figure A1-1 is a schematic of the \ddot{z} channel buffer amplifier that provides a signal to DAS. Also shown are the summing amplifier

K_{13} of Fig. 12 and the +1 g stable bias source. The outputs of the multipliers of Fig. A8-1 drive inputs at Pins 4 and 6 in Fig. A1-1.

The buffer amplifier driving DAS has a gain of 0.2 VDC/VDC. The scale factor at its input, which is that for the z accelerometer input (K_a in Fig. 12), is 2.5 VDC/g. Consequently the scale factor at the output of the buffer amplifier is 0.500 VDC/g.

In Fig. A1-1 the scale factor for the z accelerometer is set by the net loading resistance across the accelerometer output. This net resistance consists of the parallel combination of ($1.5K \Omega + R_a$), ($R_b + R_c$), and R_d . The nominal scale factor of the z accelerometer is 1.33 MA/g with a $\pm 10\%$ tolerance. The net loading resistance should range between 1705 and 2083 Ω , with a mean value of 1875 Ω , for the desired scale factor of 2.500 V/g. R_a is a trim resistor to be selected to yield the 2.500 V/g scale factor with $\pm 0.2\%$. A $\pm 0.2\%$ tolerance will yield an error in the measurement of h_w of less than 0.01 ft when $h_v = 5$ ft maximum. The combined temperature coefficient of the 1.5K Ω and R_a resistances in series should be chosen with care. Assuming a $\pm 10^\circ\text{C}$ ambient temperature change, if these resistances change by $\pm 0.2\%$ due to temperature changes, the corresponding error in the measurement of h_w would be 0.01 ft when $h_v = 5$ ft maximum. This would call for a combined temperature coefficient not exceeding ± 200 ppm/ $^\circ\text{C}$. However, this is not the only criterion by which the temperature coefficient should be selected. As indicated earlier, the rate of change of any DC offset appearing at the five-stage filter input should preferably be of the order of 1.0 $\mu\text{V/s}$ or less so that h_w measurement errors of less than 0.05 ft are incurred. Since the summing amplifier in Fig. A1-1 drives the five-stage filter and has a nominal gain of magnitude of 0.700 to the z accelerometer output signal, the corresponding allowable rate of change of DC offset referred to the accelerometer output signal is $(1.0 \mu\text{V/s}) / 0.700 = 1.4 \mu\text{V/s}$. The rate of change of DC offset at the accelerometer terminals (excluding that due to the accelerometer itself) is due to three sources:

1. The presence of an initial (approximately) 1 g DC bias at the z accelerometer output. The actual output will in general be slightly lower than 1 g depending on θ and ϕ angles but for $\theta = \psi \leq \frac{1}{4}$ rad, the DC bias will be within 7% of 1 g and hence is essentially 1 g ($\rightarrow 2.50$ V).

2. The presence of DC bias current at the (+) input of the LM108AH buffer amplifier; and
3. The presence of DC bias current at the input to the Philbrick model 1701 DCOA.

With respect to the 1 g DC bias at the output of the z accelerometer, this develops approximately (depending on θ and ϕ angles) 2.50 V across the $(1.5K \Omega + R_a)$ resistors. If we desire that the rate of change of DC offset not exceed 1.4 $\mu\text{V/s}$, then these resistors should not change by more than $(1.4 \mu\text{V/s})/2.50 \text{ V} = 0.56 \text{ ppm/s}$ due to ambient temperature changes. This calls for precision resistors with low temperature coefficients. If the temperature coefficient is better than $\pm 5 \text{ ppm/}^\circ\text{C}$ for the combined resistance $(1.5K \Omega + R_a)$, then the maximum allowable rate of change of ambient temperature would be $(0.56 \text{ ppm/s})/(\pm 5 \text{ ppm/}^\circ\text{C}) = \pm 0.11^\circ\text{C/s}$ or $\pm 6.7^\circ\text{C/min}$, a value that should be achievable assuming the equipment is suitably insulated from the external environment. The 1.5K fixed resistor should be selected to meet the $\pm 5 \text{ ppm/}^\circ\text{C}$ temperature coefficient requirement. R_a , which is much smaller than 1.5K Ω (not exceeding $2083 - 1500 = 583 \Omega$, where 2083 Ω is the upper limit for the net loading resistance when the accelerometer is on the -10% limit of its tolerance), may have a temperature coefficient proportionally higher and hence may be as high as $(1500/583)(\pm 5 \text{ ppm/}^\circ\text{C}) = \pm 12.9 \text{ ppm/}^\circ\text{C}$. If R_a were 205 Ω , corresponding to the +10% limit of the accelerometer tolerance, its temperature coefficient would need only be $\pm 36.5 \text{ ppm/}^\circ\text{C}$.

In Fig. A1-1 it will be noted that the accelerometer output drives resistance R_d (nominally 1 M Ω). This resistance must also have a low temperature coefficient of resistance for the same reason given for $(1.5K \Omega + R_a)$ resistance. A change in current through R_d caused by a change in R_d causes a change of DC offset because approximately 2.50 V bias (\rightarrow 1 g bias) is applied to this resistor. The effect is identical to that caused by a change in the $(1.5K \Omega + R_a)$ resistance and hence the temperature coefficient of R_d should be better than $\pm 5 \text{ ppm/}^\circ\text{C}$. Likewise, the +1 g bias voltage developed by the stable bias voltage source is applied through R_g (1 M Ω nominally) to the summing amplifier (Philbrick model 1701). Changes in R_g have an effect identical to changes in R_d and the $(1.5K \Omega + R_a)$ resistance. Hence R_g should have a temperature coefficient better than $\pm 5 \text{ ppm/}^\circ\text{C}$.

With respect to the presence of DC bias current at the (+) input of the LM108AH buffer amplifier, this current produces a voltage across the $(1.5K \Omega + R_a)$ resistance. If this bias current is I_{b1} , the voltage produced, E_{b1} , is to a good approximation

$$E_{b1} = I_{b1} \left(\frac{R_c}{R_b + R_c} \right) (1.5K + R_a) . \quad (63)$$

For the values given in Fig. A1-1, this becomes (with $R_a = 583 \Omega$)

$$E_{b1} = 417 I_{b1} . \quad (63a)$$

The bias current I_{b1} has a maximum temperature coefficient of about $17(10^{-12}) A/^{\circ}C$. Consequently E_{b1} can change due to temperature changes by: $E_{b1} = 417(17)10^{-12} = 7.1(10^{-9}) V/^{\circ}C$. E_{b1} is allowed to change by no more than $1.4 \mu V/s$, so that the maximum rate of change of ambient temperature for the LM108AH becomes $(1.4 \mu V/s) / [7.1(10^{-9}) V/^{\circ}C] = 197^{\circ}C/s$. Since temperature changes this rapid would never occur, we conclude that bias current changes in the LM108AH are of no significance with respect to the rate of change of offset allowable at the z accelerometer terminals.

With respect to DC bias current changes at the input to the Philbrick DCOA, this current (I_{b2}) produces an equivalent bias voltage E_{b2} across the $(1.5 \Omega + R_a)$ resistance. This voltage can be shown to be

$$E_{b2} = I_{b2} R_d . \quad (64)$$

The bias current I_{b2} has a maximum temperature coefficient of $1(10^{-12}) A/^{\circ}C$. Consequently E_{b2} can change due to temperature changes by: $E_{b2} = 1(10^{-12})(1)10^{-6} = 1.0 (10^{-6}) V/^{\circ}C$. If E_{b2} is

allowed to change by no more than $1.4 \mu\text{V/s}$, the maximum rate of ambient temperature for the Philbrick DCOA becomes $(1.4 \mu\text{V/s})/[1.0(10^{-6}) \text{ V/}^\circ\text{C}] = 1.4^\circ\text{C/s}$. This is not a severe requirement at all but the DCOA should be insulated from the external environment to preclude it from seeing rapid ambient temperature changes.

As shown in Fig. A1-1 the buffer amplifier driving the DAS load has a gain of 0.200 VDC/VDC by virtue of the input attenuator network consisting of R_c and R_b . This attenuator has a gain of 0.200 VDC/VDC while the amplifier itself from its (+) input to its output has a gain of +1.000 VDC/VDC, yielding an overall gain of +0.200 VDC/VDC. The $5.11\text{K } \Omega$ resistance between the amplifier output and the DAS load protects the amplifier against inadvertent DAS load shorts. It is assumed that the DAS load normally is $\geq 1 \text{ M}\Omega$ so that the loading error on the signal does not exceed about 0.5%.

The Philbrick model 1701 summing amplifier has a nominal closed loop gain of (-0.700) to each input signal; this gain is set by the ratio of the feedback resistor ($700\text{K } \Omega$) to each input resistor ($1 \text{ M}\Omega$). This amplifier was chosen for this application because of its low DC offset voltage and current. Its temperature coefficients are $0.25 \mu\text{V/}^\circ\text{C}$ for offset voltage and $1 \text{ pA/}^\circ\text{C}$ for offset (bias) current. The effect of bias current has been explained above where it was shown that, for this bias current temperature coefficient, the ambient temperature could change up to a rate of 1.4°C/s without exceeding the maximum desired $1.0 \mu\text{V/s}$ drift rate at the input to the five-stage filter. With regard to the offset (bias) voltage, a $0.25 \mu\text{V/}^\circ\text{C}$ temperature coefficient at the amplifier input ("IN") node is equivalent to $\left[1 + \left(\frac{700\text{K}}{1000\text{K}/4}\right)\right] (0.25) = 0.95 \mu\text{V/}^\circ\text{C}$ at the amplifier output (= input to five-stage filter). For a $1.0 \mu\text{V/s}$ maximum drift rate at the five-stage filter input, the ambient temperature of the amplifier could change at a maximum rate of $(1.0 \mu\text{V/s})/(0.95 \mu\text{V/}^\circ\text{C}) = 1.1^\circ\text{C/s}$. Again, this is a rather fast temperature change that will not exist in practice and should present no problem if the DCOA is insulated properly from the external environment.

The temperature coefficients on the nominally $1 \text{ M}\Omega$ resistors connected to inputs E_d and E_e in Fig. A1-1 at the summing amplifier input may be established as follows. The maximum signal that could appear at either E_e or E_d input is $(5 \sin \theta) \text{ V}$ or $(5 \sin \phi) \text{ V}$, respectively. For $\theta = \phi = \frac{1}{2} \text{ rad}$ maximum, this signal would be 1.24 V .

Since the maximum allowable drift rate at E_d or E_e input is $1.4 \mu\text{V/s}$, the resistance change should not exceed $(1.4 \mu\text{V/s})/(1.24 \text{ V}) = 1.1 \text{ ppm/s}$. If R_e and R_f each have temperature coefficients of $\pm 10 \text{ ppm/}^\circ\text{C}$, then the rate of change of ambient temperature could be as high as $(1.1 \text{ ppm/s})/(\pm 10 \text{ ppm/}^\circ\text{C}) = \pm 0.11^\circ\text{C/s}$ or $\pm 6.7^\circ\text{C/min}$; this is the same ambient temperature rate calculated for R_d and R_g cases and should be achievable assuming the equipment is suitably insulated from the external environment.

The stable bias voltage source in Fig. A1-1 must be capable of generating a voltage that can cancel the nominal (-1 g) bias voltage sensed by the accelerometer triad and any DC offsets generated by the \ddot{z} accelerometer and the signals from the roll and pitch channels that are applied to nodes E_d and E_e , respectively. In addition, this voltage must cancel any DC offset generated by the summing amplifier. In practice, the bias source should be adjustable so that the output voltage at node E_g can be adjusted to $0.0 \pm 0.5 \text{ MV}$. A zero or at most a small DC output offset at node E_g is desired in order to limit the transient voltage excursions at the output of the five-stage filter, which is driven by voltage E_g , when the equipment is first turned on.

The 1N938B and 1N4579 zener diodes are low temperature coefficient zener diodes and are used to control the voltage excursions at node E_{z2} to within the tolerances required such that voltage E_f does not vary by more than $1.4 \mu\text{V/s}$ due to ambient temperature changes. The 1N938B diode has the following characteristics:

$$E_{z1} = 9.0 \text{ V} \pm 5\%; R_{z1} \leq 30 \Omega @ I_{z1} = 7.5 \text{ MA};$$

$$\text{Temperature coefficient of voltage: } \pm 0.001\%/^\circ\text{C}.$$

The 1N4579 diode has the following characteristics:

$$E_{z2} = 6.4 \text{ V} \pm 5\%; R_{z2} \leq 50 \Omega @ I_{z2} = 2.0 \text{ MA};$$

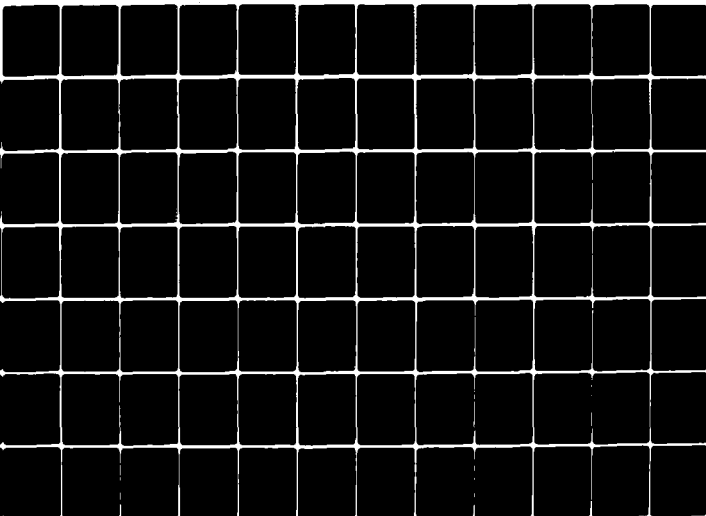
$$\text{Temperature coefficient of voltage: } \pm 0.0005\%/^\circ\text{C}.$$

AD-A088 593

JOHNS HOPKINS UNIV LAUREL MD APPLIED PHYSICS LAB F/G 13/10
DOCUMENTATION OF DESIGN, PERFORMANCE, AND QUALIFICATION OF THE --ETC(U)
JUN 80 T M RANKIN, R L KONIGSBERG N00024-78-C-5384
JHU/APL/SES-025 NL

UNCLASSIFIED

2 of 5
AD-A
100193



The bias voltage source network resistances are chosen such that +1 g bias voltage, $\rightarrow +2.50$ V nominally, is developed at node E_f with the ability to adjust E_f via potentiometer P_1 such that all amplifier offsets and summing amplifier circuit tolerances may be trimmed out with respect to DC offset. This trimming would permit E_g to be set to 0.0 MV within ± 0.5 MV. Close to 0.5 MA is passed through R_w , R_x , R_y , and P_1 to develop the required 2.50 V. Assuming nominal values, $E_{z2} = 6.400$ V, $R_w = 7.80K \Omega$, $R_x = 4.42K \Omega$, $P_1 = 50 \Omega$ (i.e., with P_1 at midposition), then for $E_f = 2.500$ V, R_y nominally must be 529Ω . For the actual component values used in this system, R_y was adjusted to 357Ω as indicated in Fig. A1-1. R_y is trimmed so that the null at node E_g occurs with P_1 set in midposition. Final trimming is performed with P_1 ; P_1 has a resolution in the adjustment of E_g of about 0.13 MV with an approximate range of adjustment of ± 6.5 MV about midposition. R_v is chosen such that for the actual measured values of E_{z1} and E_{z2} , the zener current for the 1N4579 diode is close to its 2.0 MA rated operating current in order to avail ourselves of its very low temperature coefficient of voltage. R_t is chosen such that for the actual measured value of E_{z1} , assuming the +15 V DC supply to the network is within $\pm 1\%$ of +15 V, the zener current for the 1N938B diode is close to its 7.5 MA rated operating current in order to avail ourselves of its low temperature coefficient of voltage.

If we assume E_f bias voltage was allowed to vary a maximum of $1.4 \mu V/s$, in order not to introduce an error greater than 0.05 ft in the measurement of h_w , we can find the required tolerances and temperature coefficients for the various components in the bias voltage network as follows:

$$E_f = \left(\frac{R_x + R_y + P_1}{R_w + R_x + R_y + P_1} \right) E_{z2} \quad (65)$$

The time rate of change of E_f due to each component variation is then

a. Due to R_x :

$$\frac{dE_f}{dt} = \left[E_{z2} \frac{R_x R_w}{(R_w + R_x + R_y + P_1)^2} \right] \left(\frac{dR_x}{R_x} \right) \frac{1}{dt},$$

where

$\frac{dR_x}{R_x}$ = fractional change in R_x , and $\left(\frac{dR_x}{R_x} \right) / dt$ is
time rate of fractional change in R_x .

Assume the following nominal component values: $E_{z2} = 6.4$ V, $R_x = 4.42K \Omega$, $R_z = 529 \Omega$, $R_w = 7.80K \Omega$, $P_1 = 50 \Omega$ (set at midposition), $R_w + R_x + R_y + P_1 = 12.799K \Omega$,

$$\frac{dE_f}{dt} \leq 1.4 \mu V/s, \left(\frac{dR_x}{R_x} \right) \frac{1}{dt} \leq 1.04(10^{-6})/s \text{ or } 1.04 \text{ ppm/s.}$$

If R_x has a temperature coefficient of ± 25 ppm/ $^{\circ}C$ or better, then the maximum time rate of temperature change for R_x becomes $(1.04 \text{ ppm/s})/(\pm 25 \text{ ppm}/^{\circ}C) = \pm 0.042^{\circ}C/s$ or $\pm 2.5^{\circ}C/min$. This value can be achieved if we insulate the components against rapid environmental temperature changes. Further improvement by a factor of 2.5 can be obtained by changing to a ± 10 ppm/ $^{\circ}C$ temperature coefficient.

b. Due to R_y :

$$\frac{dE_f}{dt} = \left[E_{z2} \frac{R_y R_w}{(R_w + R_x + R_y + P_1)^2} \right] \left(\frac{dR_y}{R_y} \right) \frac{1}{dt},$$

where

$\frac{dR_y}{R_y}$ = fractional change in R_y , and $\left(\frac{dR_y}{R_y}\right)/dt$ is the time rate of fractional change in R_y .

Again, assuming nominal component values with $\frac{dE_f}{dt} \leq 1.4 \mu\text{V/s}$:

$$\left(\frac{dR_y}{R_y}\right)/dt \leq 8.7 (10^{-6})/\text{s} \text{ or } 8.7 \text{ ppm/s.}$$

If R_y has a temperature coefficient of $\pm 100 \text{ ppm}/^\circ\text{C}$ or better, then the maximum time rate of temperature change for R_y becomes $(8.7 \text{ ppm/s})/(\pm 100 \text{ ppm}/^\circ\text{C}) = \pm 0.087^\circ\text{C/s}$ or $\pm 5.2^\circ\text{C/min}$. This value should be achieved without difficulty.

c. Due to P_1 :

$$\frac{dE_f}{dt} = \left[E_{z2} \frac{P_1 R_w}{(R_w + R_x + R_y + P_1)^2} \right] \left(\frac{dP_1}{P_1}\right)/dt,$$

where $\frac{dP_1}{P_1}$ = fractional change in P_1 and $\left(\frac{dP_1}{P_1}\right)/dt$ is the time rate of fractional change in P_1 . Again, assuming nominal component values with $\frac{dE_f}{dt} \leq 1.4 \mu\text{V/s}$.

$$\left(\frac{dP_1}{P_1}\right)/dt \leq 92 (10^{-6})/\text{s} \text{ or } 92 \text{ ppm/s.}$$

If P_1 has a temperature coefficient of ± 100 ppm/ $^{\circ}\text{C}$ or better, then the maximum time rate of temperature change for P_1 becomes $(92 \text{ ppm/s})/(\pm 100 \text{ ppm}/^{\circ}\text{C}) = \pm 0.92^{\circ}\text{C/s}$ or 55°C/min , a value easily achieved.

d. Due to R_w :

$$\frac{dE_f}{dt} = \left[-E_{z2} \frac{(R_x + R_y + P_1) R_w}{(R_w + R_x + R_y + P_1)^2} \right] \left(\frac{dR_w}{R_w} \right) \frac{1}{dt},$$

where $\frac{dR_w}{R_w}$ = fractional change in R_w , and $\left(\frac{dR_w}{R_w} \right) / dt$ is the time rate of fractional change in R_w . Again, assuming nominal component values with $\frac{dE_f}{dt} \leq 1.4 \text{ } \mu\text{V/s}$.

$$\left(\frac{dR_w}{R_w} \right) \frac{1}{dt} \leq 0.92 (10^{-6})/\text{s} \text{ or } 0.92 \text{ ppm/s}.$$

If R_w has a temperature coefficient of ± 25 ppm/ $^{\circ}\text{C}$ or better, then the maximum time rate temperature change of R_w becomes $(0.92 \text{ ppm/s})/(\pm 25 \text{ ppm}/^{\circ}\text{C}) = \pm 0.037^{\circ}\text{C/s}$ or $\pm 2.2^{\circ}\text{C/min}$. Again, this value can be achieved if we insulate the components against rapid environmental temperature changes. Further improvement by a factor of 2.5 can be obtained by changing to a ± 10 ppm temperature coefficient.

e. Due to E_{z2} :

$$\frac{dE_f}{dt} = \left[\frac{(R_x + R_y + P_1) E_{z2}}{R_w + R_x + R_y + P_1} \right] \left(\frac{dE_{z2}}{E_{z2}} \right) \frac{1}{dt},$$

where $\left(\frac{dE_{z2}}{E_{z2}}\right)$ = fractional change in E_{z2} and $\left(\frac{dE_{z2}}{E_{z2}}\right)/dt$ is the time rate of fractional change in E_{z2} . Assuming nominal component values with $\frac{dE_f}{dt} \leq 1.4 \mu\text{V/s}$:

$$\left(\frac{dE_{z2}}{E_{z2}}\right) \frac{dt}{dt} \leq 0.56 (10^{-6})/\text{s} \text{ or } 0.56 \text{ ppm/s.}$$

If E_{z2} has a temperature coefficient of $\pm 5 \text{ ppm}/^\circ\text{C}$ ($\rightarrow \pm 0.0005\%/^\circ\text{C}$ rating for 1N4579), then the maximum time rate of temperature change of E_{z2} becomes:
 $(0.56 \text{ ppm/s})/(\pm 5 \text{ ppm}/^\circ\text{C}) = 0.11^\circ\text{C/s}$ or 6.7°C/min .
 This value should be achievable if the diode is insulated from rapid environmental temperature changes and if we allow a suitable warm-up period for the diode (for example, 15 min).

It should be emphasized here that each of the various time derivative values was calculated on the basis that $\frac{dE_f}{dt}$ will be less than $1.4 \mu\text{V/s}$. If all error sources happen to add at any time, the actual $\frac{dE_f}{dt}$ value will be much greater than the desired $1.4 \mu\text{V/s}$ and errors in the measurement of h_w will be much greater than 0.05 ft . However, we can assume that errors will add statistically on an rss basis so that if there are n error sources, each capable of producing a $\frac{dE_f}{dt}$ value of $1.4 \mu\text{V/s}$, the actual error will be $1.4 \sqrt{n} \mu\text{V/s}$. This points to the fact that the individual error sources should be held to values lower by a factor of \sqrt{n} in order to ensure statistically that the overall value for $\frac{dE_f}{dt}$ is less than $1.4 \mu\text{V/s}$. If $n=10$, then each error source should be reduced by a factor of 3.16, which either makes the temperature coefficient requirements more stringent or insulation against rapid temperature environment changes more important.

It was determined that $\left(\frac{dE_{z2}}{E_{z2}}\right)/dt$ should not exceed 0.56 ppm/s.

E_{z2} can change due to temperature as well as due to current changes in the diode due to changes in E_{z1} or due to changes in the series current setting resistance R_v . If R_{z2} is the dynamic impedance of the 1N4579 diode, it can be shown that the fractional change in E_{z2} due to changes in E_{z1} and R_v are as follows:

a. Due to R_v :
$$\left(\frac{dE_{z2}}{E_{z2}}\right) = \left(\frac{E_{z1} - E_{z2}}{E_{z2}}\right) \left(\frac{R_{z2}}{R_v}\right) \left(\frac{dR_v}{R_v}\right)$$

b. Due to E_{z1} :
$$\left(\frac{dE_{z2}}{E_{z2}}\right) = \left(\frac{E_{z1}}{E_{z2}}\right) \left(\frac{R_{z2}}{R_v + R_{z2}}\right) \left(\frac{dE_{z1}}{E_{z1}}\right)$$

If we assume nominal component values, $E_{z1} = 9.0$ V, $E_{z2} = 6.4$ V, $R_t = 604 \Omega$, $R_v = 1.05K \Omega$, $R_{z2} \leq 50 \Omega$, then

$$\left(\frac{dE_{z2}}{E_{z2}}\right) = -0.0193 \left(\frac{dR_v}{R_v}\right) \text{ due to } R_v$$

$$\left(\frac{dE_{z2}}{E_{z2}}\right) = 0.0639 \left(\frac{dE_{z1}}{E_{z1}}\right) \text{ due to } E_{z1}$$

If now in each case we assume $\left(\frac{dE_{z2}}{E_{z2}}\right)/dt \leq 0.56$ ppm/s, then

$$\left|\left(\frac{dR_v}{R_v}\right)\right| \leq 29.0 \text{ ppm/s due to } R_v$$

$$\left(\frac{dE_{z1}}{E_{z1}} \right) \frac{dt}{dt} \leq 8.8 \text{ ppm/s due to } E_{z1} .$$

If R_v has a temperature coefficient of $\pm 100 \text{ ppm}/^\circ\text{C}$, then the maximum time rate of temperature change of R_v becomes

$$(29.0 \text{ ppm/s}) / \pm 100 \text{ ppm}/^\circ\text{C} = \pm 0.29^\circ\text{C/s or } \pm 17.4^\circ\text{C/min} .$$

There should be no problem in achieving this value with proper insulation.

If $\frac{dE_{z1}}{E_{z1}}$ has a temperature coefficient of $\pm 10 \text{ ppm}/^\circ\text{C}$

($\rightarrow \pm 0.001\%/^\circ\text{C}$) for 1N938B diode, then the maximum time rate of temperature change of E_{z1} becomes $(8.8 \text{ ppm/s}) / \pm 10 \text{ ppm}/^\circ\text{C} = \pm 0.99^\circ\text{C/s or } \pm 53^\circ\text{C/min}$, a value easily achieved.

E_{z1} may also change due to power supply changes and due to changes in R_t . To assess the changes in E_{z1} due to these causes, and the corresponding effects on E_{z2} , we can find the changes in E_{z1} , due to changes in $+15 \text{ V}$ power supply (E_h) and due to R_t , assuming the dynamic impedance of the 1N938B diode is R_{z1} . These changes are

a. Due to E_h :

$$\frac{dE_{z1}}{E_{z1}} = \left(\frac{R_{z1}}{R_{z1} + R_t} \right) \left(\frac{dE_h}{E_h} \right)$$

b. Due to R_t :

$$\frac{dE_{z1}}{E_{z1}} = - \left(\frac{E_h - E_{z1}}{E_{z1}} \right) \left(\frac{R_{z1}}{R_t} \right) \left(\frac{dR_t}{R_t} \right) .$$

It was shown previously that if $\left(\frac{dE_{z2}}{E_{z2}}\right) dt \leq 0.56 \text{ ppm/s}$, corresponding to $\frac{dE_f}{dt} \leq 1.4 \text{ } \mu\text{V/s}$, then we require $\left(\frac{dE_{z1}}{E_{z1}}\right)/dt \leq 8.8 \text{ ppm/s}$. If we restrict $\left(\frac{dE_{z1}}{E_{z1}}\right)/dt$ to the latter value, then $\left(\frac{dE_h}{E_h}\right)/dt$ and $\left(\frac{dR_t}{R_t}\right)/dt$ must satisfy the following requirements, assuming $R_{z1} \leq 30 \text{ } \Omega$, $R_t = 604 \text{ } \Omega$, $E_h = 15.0 \text{ V}$, $E_{z1} = 9.0 \text{ V}$:

$$\left(\frac{dE_h}{E_h}\right)/dt \leq 186 (10^{-6})/\text{s} \text{ or } 186 \text{ ppm/s}$$

$$\left|\left(\frac{dR_t}{R_t}\right)/dt\right| \leq 266 (10^{-6})/\text{s} \text{ or } 266 \text{ ppm/s} .$$

The model 925 Analog Devices $\pm 15 \text{ V}$ supply that provides E_h (+ 15 V) has a maximum temperature coefficient of voltage of $0.015\%/^{\circ}\text{C}$. Consequently the maximum allowable time rate of change of ambient temperature becomes

$$(186 \text{ ppm/s})/(150 \text{ ppm}/^{\circ}\text{C}) = 1.24^{\circ}\text{C/s} \text{ or } 74.4^{\circ}\text{C/min} .$$

This value should be easily achieved with proper insulation against rapid environmental temperature changes, assuming the power supply is allowed sufficient warm-up time (such as 15 min) before the equipment is used.

If we assume R_t has a temperature coefficient of $\leq \pm 100 \text{ ppm}/^{\circ}\text{C}$, then the maximum allowable time rate of change of ambient temperature becomes $(266 \text{ ppm/s})/\pm 100 \text{ ppm}/^{\circ}\text{C} = 2.66^{\circ}\text{C/s}$. This value should be easily achieved with proper insulation.

Changes in the $700\text{K } \Omega$ feedback resistor in the Philbrick model 1701 DCOA circuit of Fig. A1-1 can affect the gain and therefore scale factor in the measurement of h_v . It should have sufficient temperature stability so that not more than 0.01 ft error in the measurement of h_w occurs if $h_v \leq 5 \text{ ft}$. The maximum allowable temperature coefficient of this resistor, assuming a $\pm 10^{\circ}\text{C}$ temperature environment, becomes

$$\leq \frac{0.01 \text{ ft}}{5 \text{ ft } (\pm 10^\circ\text{C})} = \pm 200 \text{ ppm}/^\circ\text{C}.$$

A resistor with a temperature coefficient of $\pm 100 \text{ ppm}/^\circ\text{C}$ (easily obtained) should be adequate.

Since any change in R_d also affects the gain in the same way that the $700\text{K } \Omega$ feedback resistor does, it should also have a temperature coefficient $\leq \pm 200 \text{ ppm}/^\circ\text{C}$ assuming a $\pm 10^\circ\text{C}$ temperature environment. However, it was pointed out previously that R_d required a much greater temperature stability because of the effect it can have on the rate of change of DC offset with temperature changes due to the approximate lg bias voltage (depending on θ and φ) of 2.50 V applied to R_d . Because of this, it was shown previously that R_d should have a temperature stability of $\leq \pm 5 \text{ ppm}/^\circ\text{C}$ assuming ambient temperatures do not change at a rate greater than $\pm 0.11^\circ\text{C/s}$ or $\pm 6.7^\circ\text{C/min}$.

Card # 2, Fig. A2-1, Schematic of MCU Synchro-to-DC Converter (Normalized)

Figure A2-1 is a schematic of synchro channel blocks representing either blocks K_1, K_2, K_3, K_4 ($10 \frac{M_3}{N_3}$) divider, K_5 in the roll channel, or blocks K_7, K_8, K_9, K_{10} ($10 \frac{M_4}{N_4}$) divider, K_{11} in the pitch channel as shown on Fig. 12. The associated isolation transformers, UTC H-5, having a primary to secondary impedance ratio of $15\text{K } \Omega$ to $95\text{K } \Omega$, are connected between the synchro outputs and the inputs of blocks K_1 and K_7 and are not shown on this schematic. Instead, the transformers appear in Fig. B2-1. In that diagram, the roll synchro output is connected to primary winding 1-2 on T3 transformer, which is the low impedance side ($15\text{K } \Omega$), while the $95\text{K } \Omega$ secondary winding connects to block K_1 input through the No. 2 card connector. Pins 8 of the roll and pitch H-5 transformers are common and are connected to signal ground. The pitch synchro output is connected to primary winding 1-2 on T2 transformer, which is the $15\text{K } \Omega$ side while T2 secondary ($95\text{K } \Omega$) winding connects to block K_7 input through the other No. 2 card connector. In Fig. B2-1, it is not obvious that

the connections from the pitch synchro to transformer T2 pins 1-2 have been reversed when compared to the like roll-synchro-to-transformer connections. As discussed previously, however, the transformer connection reversal in the pitch channel is necessary in order to ensure proper summation of signals in the z, x, and y channels at block K₁₃ (Fig. 12).

The limiter and fixed phase shift amplifier in Fig. A2-1 serves two functions. At 400 Hz, it produces a fixed -135° phase shift. When combined with the adjustable phase shift amplifier following this stage, the phase of the 400 Hz synchro signal, which is not necessarily exactly in phase or 180° out of phase with the 400 Hz reference signal, may be shifted between -135 and -225° in order to bring the synchro signal phase relationship into exact correspondence with the 400 Hz reference phase for proper demodulation at the demodulator. The limiter portion of the amplifier serves to limit the peak output voltage swing to about 8.79 V at node E₀₁, in Fig. A2-1. The roll or pitch synchro S1-S3 winding output driving the H-5 transformer is given by $11.8 \sin \varphi$ (Vrms) or $11.8 \sin \theta$ (Vrms) (nominal). The H-5 transformer has a primary to secondary turns ratio of $1/n$ with $n = \sqrt{95K/15K} = 2.517$, so that the corresponding secondary voltage driving node E₁ in Fig. A2-1 is $11.8 (2.517) \sin \varphi = 29.7 \sin \varphi$ (Vrms) or $29.7 \sin \theta$ (Vrms). Since the gain of the limiter and fixed phase shift amplifier is 1.038 Vrms/Vrms (nominally), it follows that output node E₀₁ = $29.7 (1.038) \sin \varphi = 30.8 \sin \varphi$ (Vrms) or $30.8 \sin \theta$ (Vrms), or E₀₁ = $30.8 (1.414) \sin \varphi = 43.6 \sin \varphi$ V peak (VPK) or $43.6 \sin \theta$ (VPK). Consequently, when φ (or θ) = 11.6°, the 8.79 V peak output limit at node E₀₁ is reached. Above 11.6°, the output at node E₀₁ limits and the waveform changes gradually from a sine wave to a square wave as E₀₁ increases. The system therefore effectively limits for roll or pitch angles above about 11.6° (about 0.20 rad).

The adjustable phase shift amplifier in Fig. A2-1 has nominally unity gain independent of the setting of potentiometer P₁. By adjusting potentiometer P₁ the phase of output signal E₀₂ may be conveniently shifted with respect to input signal E₀₁ over a 90° range. P₁ is adjusted so that the phase of the roll or pitch synchro signal, as it appears at node E₀₂, is shifted to be in correspondence with the phase of the 400 Hz reference signal appearing at

node E_{R2} (at the DG191BP switch input, pin 15). This stage therefore permits the compensation for phase shift (relative to the 400 Hz reference) in the S_1-S_3 synchro output. The resistor R_a (100 Ω) in this stage isolates the preceding stage (limiter and fixed phase shift amplifier) from the loading effects of capacitor C_a , especially if P_1 were set to 0 Ω . In this case the large loading capacitance of C_a might cause instability in the preceding stage if R_a were 0 Ω instead of 100 Ω .

The 400 Hz demodulator in Fig. A2-1 is a switching type, the switches of which are operated by a 400 Hz square wave T^2L compatible signal, derived from the 400 Hz sine wave reference (the same reference used for the synchros) applied to the DG191BP analog electronic switch. During the first half cycle of the 400 Hz reference wave, the switches D3-S3 and D1-S1 are in the positions shown and the demodulator has a gain, to the corresponding half cycle of the wave appearing at node E_{02} , of $-R_F/(R_d + R_e) = (-51.1K)/46.0K = -1.111$. The waveform at node E_{03} is therefore that at node E_{02} but inverted and larger by a factor of 1.111. Since the waveform at node E_{02} is a half sine wave during the first half cycle of the reference switching waveform, the output at node E_{03} is also a half sine wave (but inverted and larger in amplitude). During the second half cycle of the reference waveform, switch D3-S3 closes while D1-S1 opens; the gain of the demodulator, it can be shown, then becomes +1.111 V/V. However, the phase of the sine wave at node E_{02} has reversed during the second half cycle of the reference waveform so that the output at node E_{03} is another half sine wave of the same phase as the first half cycle sine wave but larger by a factor of 1.111 compared to the input E_{02} . Thus the signal E_{02} as it appears at node E_{03} has been full wave rectified and a DC voltage has been generated proportional to the signal E_{02} . The signal of the DC voltage depends on the phase of E_{02} waveform relative to the 400 Hz reference waveform (i.e., whether it is either exactly in phase or 180° out of phase). Since the gain of the demodulator is 1.111 V/V, or 1.111 Vrms/Vrms, it follows that the gain to the DC component of the rectified sine wave is $[(2/\pi)/(1/\sqrt{2})] 1.111$, or $\left(\frac{0.637}{0.707}\right) (1.111) = 1.000$ VDC/Vrms. That is, every 1.000 Vrms at node E_{02} produces 1.111 Vrms (rectified) at node E_{03} , which

has a DC component of $1.111 \text{ Vrms} \times \left(\frac{0.637 \text{ VDC}}{0.707 \text{ Vrms}} \right) = 1.000 \text{ VDC}$. The waveform at node E_{03} consists of the desired DC component plus the undesired AC half cycle ripple with harmonics of the fundamental frequency of 800 Hz (which is twice the reference and signal frequencies of 400 Hz). The AC ripple may be filtered conveniently by the following stage second-order low-pass filter.

The second-order low-pass filter circuit is the well-known Sallen and Key design using a DCOA as an active device having a DC gain of +1.000. Its transfer function is given by

$$\frac{E_{04}}{E_{03}} = \frac{1}{\tau_1^2 s^2 + 2\zeta_1 \tau_1 s + 1} \quad (66)$$

where

$$\begin{aligned} s &= j\omega; \\ j &= \sqrt{-1}; \\ \omega &= 2\pi f; \\ f &= \text{frequency}; \\ \tau_1^2 &= R_1 R_2 C_1 C_2; \\ 2\zeta_1 \tau_1 &= (R_1 + R_2) C_2; \\ \zeta_1 &= \text{damping factor}; \\ \omega_1 &= \frac{1}{\tau_1} = 2\pi f_1; \text{ and} \\ f_1 &= \text{filter cutoff frequency.} \end{aligned}$$

f_1 and ζ_1 were chosen at 80.0 Hz and 0.500, respectively. The components R_1 , R_2 , C_1 , C_2 were assigned values to yield these values of f_1 and ζ_1 . Since the fundamental ripple frequency at the demodulator output is 800 Hz, this component will be attenuated by a factor of close to 100 by the filter. The ratio of fundamental ripple frequency amplitude to DC for a full wave rectified sine

wave is 2 to 3. Hence, relative to the DC value, the 800 Hz ripple amplitude will be a factor of $100 \left(\frac{3}{2}\right) = 150$ below the DC level. The next higher harmonic of 800 Hz is 1600 Hz and this will be attenuated by a factor of 400 by the filter. The amplitude of the harmonic is only $\frac{2}{15}$ of the DC value; hence at the filter output the 1600 Hz ripple amplitude will be a factor of $\frac{15}{2} (400) = 3000$ below the DC level. Higher harmonics of 800 Hz will therefore produce insignificant levels at the filter output compared to the DC level.

The analog divider in Fig. A2-1 corresponds to the $\left(10 \frac{M_3}{N_3}\right)$ or $\left(\frac{10M_4}{N_4}\right)$ divider block in Fig. 12. Its purpose is to make output voltage E_{05} insensitive to changes in the 115 V, 400 Hz reference voltage for a given roll or pitch angle. If for a given roll or pitch angle, the 115 V reference voltage increases by a factor p , the synchro signal output voltage at S_1 - S_3 terminals will also increase by the same factor p . If we trace this signal through the various circuits, starting at transformer H5 primary, we eventually arrive at signal E_{04} , which is a DC voltage proportional to S_1 - S_3 AC terminal voltage. E_{04} therefore increases by a factor p . E_{04} is the Z_2 input of the AD534J analog divider and the other input to the divider at node X1 is E_{R1} , a DC signal proportional to the 115 V, 400 Hz reference voltage; consequently, E_{R1} also increases by a factor p . As a result, the output E_{05} does not change at all as the 115 V, 400 Hz reference voltage changes since $E_{05} = 10 \frac{E_{04} (1 + p)}{E_{R1} (1 + p)} = 10 \left(\frac{E_{04}}{E_{R1}}\right)$. Thus E_{05} is made insensitive to 115 V, 400 Hz reference voltage changes, as desired. The generation of signal E_{R1} is described below. A DC offset null adjustment at node E_{05} is provided by the network containing potentiometer P_2 . Any DC offset represents an equivalent angle offset in pitch and roll and may be reduced to insignificance by adjusting P_2 so that E_{05} is nulled within ± 10 MV when the roll or pitch angle is set exactly to 0° . For the nominal scale factor shown at node E_{05} , 10 MV represents only about 0.015° , an insignificant error.

The scale factor at K_{11} (or K_{12}) block input node in Fig. 12 is 10.0 V/rad for small pitch or roll angles (i.e., $\leq 5^\circ$). This node is identical to E_{06} in Fig. A2-1. The LM108A adjustable gain buffer amplifier is provided to absorb synchro scale factor tolerances and circuit tolerances. The scale factor at node E_{06} may be adjusted by potentiometer P_3 with a range of $\pm 25\%$ about the nominal scale factor of 10.0 V/rad. The adjustment may be accomplished by changing the pitch or roll angle from the null (0°) position, for example, 5° , and adjusting P_3 so that E_{06} changes by 0.1745 V/deg ($\rightarrow 10.0$ V/rad), which would be 0.873 VDC for a 5° change.

As pointed out in the discussion on DC offset drift rates at the M311 multiplier Y input (Fig. A8-1), a drift rate of 11.3 $\mu\text{V/s}$ could be tolerated. At node E_{06} in Fig. A2-1, the allowable drift rate becomes twice this value, or 22.6 $\mu\text{V/s}$ since an attenuator with a gain of 1/2 separates node E_{06} with the multiplier Y input. Assuming a nominal gain of 0.260 VDC/VDC for the adjustable gain buffer amplifier in Fig. A2-1, the allowable drift rate at node E_{05} becomes $(22.6/0.260) = 87 \mu\text{V/s}$. The DC offset at node E_{05} is due to the AD534J divider itself and any DC offset generated at nodes E_{04} and E_{R1} . The divider output at Node E_{05} has a temperature drift of 100 $\mu\text{V}/^\circ\text{C}$ and hence its temperature drift rate should be held to within $(87 \mu\text{V/s})/(100 \mu\text{V}/^\circ\text{C}) = 0.87^\circ\text{C/s}$, a value which should be achievable without difficulty if it is suitably insulated from the external environment. No data are given for the sensitivity of the divider output versus supply voltage variations. Since the ± 15 VDC supplies for the divider are well regulated and not likely to change temperature rapidly after a suitable warm-up period, the divider output drift rate due to power supply changes is not expected to exceed the desired 87 $\mu\text{V/s}$ value and will likely be less.

With respect to DC offset drift rates at the divider output due to changes in DC offset at the divider input nodes E_{04} and E_{R1} (Fig. A2-1), the following approximate relations can be shown to hold between the drift ΔE_{05} at node E_{05} and the drift ΔE_{04} and ΔE_{R1} :

(a) Due to drift ΔE_{04} at node E_{04} :

$$\Delta E_{05} = 10 \frac{\Delta E_{04}}{E_{R1}}$$

(b) Due to drift ΔE_{R1} at node E_{R1} :

$$|\Delta E_{05}| = 10 \left(\frac{E_{04}}{E_{R1}^2} \right) \Delta E_{R1} .$$

If E_{05} is allowed to change at a maximum rate of 87 $\mu\text{V/s}$ (see above), then $\Delta E_{04} \leq \frac{E_{R1}}{10} \Delta E_{05} = \frac{8.00}{10} (87) 10^{-6} = 70 \mu\text{V/s}$, where $E_{R1} = 8.00 \text{ V}$ nominally. Due to all DC offset sources that make up E_{04} , E_{04} is not expected to change by more than 50 $\mu\text{V/}^\circ\text{C}$ due to temperature changes acting on the demodulator and second-order low-pass filter. Hence, the maximum rate of change of temperature becomes $(70 \mu\text{V/s}) / (50 \mu\text{V/}^\circ\text{C}) = 1.4^\circ\text{C/s}$, a value that should not be difficult to achieve. Due to power supply drift rates acting on the demodulator and second-order low-pass filter, the DC offset drift rate at node E_{04} should be negligible because the LM108AH DCOA has an excellent power supply rejection ratio (96 dB minimum) and the $\pm 15 \text{ V}$ power supplies are well regulated with a reasonably low temperature coefficient of voltage.

Again, if E_{05} is allowed to change at a maximum rate of 87 $\mu\text{V/s}$, then

$$\Delta E_{R1} \leq \frac{E_{R1}^2}{10 E_{04}} |\Delta E_{05}| \text{ with } |\Delta E_{05}| = 87 \mu \text{ V/s} .$$

E_{04} maximum occurs when the pitch or roll angle reaches 11.6° , the limit level set by the limiter stage at the output of the H-5 transformer. Since the nominal scale factor at node E_{04} in Fig. A2-1 is 0.538 VDC/deg, it follows that E_{04} maximum is 11.6 deg $(0.538 \text{ VDC/deg}) = 6.24 \text{ VDC}$. Assuming $E_{R1} = 8.00 \text{ V}$, ΔE_{R1} then becomes

$$\Delta E_{R1} \leq \frac{(8.00)^2}{(10(6.24))} (87)10^{-6} = 89.2(10^{-6}) \mu\text{V/s};$$

this is the maximum allowable drift rate for E_{R1} .

Card # 3, Fig. A3-1, Schematic of MCU 400 Hz Square Wave Reference Generator and Normalized DC Reference Signal

E_{R1} in Fig. A2-1 is derived from the 115 V, 400 Hz reference voltage E_R as shown in Fig. 12. In this diagram E_{R1} is the normalizing reference signal (DC) E_{RN} . E_R is first passed through a UTC H-5 T1, which has a primary to secondary turns ratio of 0.3974 and is shown in Fig. B2-1. The transformer secondary voltage is nominally 115 (0.3974) = 45.7 Vrms. The transformer secondary drives pin 1 in Fig. A3-1, which is the schematic of the square wave reference generator (generating E_{R2}) and of the normalizing signal E_{R1} ($= E_{RN}$ of Fig. 12).

In Fig. A3-1, the H-5 transformer output drives an absolute value detector with signal E_1 ($= 45.7$ Vrms nominally), which yields positive going full wave rectified sine waves at an 800 Hz frequency at node E_{01} . The average value of this waveform is a DC voltage that is proportional to the actual voltage of the 115 V, 400 Hz reference source. Nominally it is 4.00 VDC at node E_{01} . To remove the 800 Hz ripple and higher harmonics, the output at node E_{01} is followed by a second-order low-pass filter (again a Sallen and Key filter type) having the following transfer function:

$$\frac{E_{R1}}{E_{01}} = \frac{K_2}{\tau_2^2 s^2 + 2\zeta_2 \tau_2 s + 1}$$

where

$$s = j\omega;$$

$$j = \sqrt{-1};$$

$$\omega = 2\pi f;$$

f = frequency;

$$\tau_2^2 = R_1 R_2 C_1 C_2;$$

$$2\zeta_2 \tau_2 = R_2 C_2 + R_1 (C_1 + C_2 - K_2 C_1);$$

$$K_2 = \left(1 + \frac{R_4}{R_3}\right);$$

ζ_2 = damping factor;

$$\omega_2 = \frac{1}{\tau_2} = 2\pi f_2; \text{ and}$$

f_2 = filter cutoff frequency.

f_2 , ζ_2 and K_2 were chosen at 4.00 Hz, 0.500, and 2.00 VDC/VDC, respectively. The components R_1 , R_2 , C_1 , C_2 , R_3 , and R_4 were assigned values to yield these values of f_2 , ζ_2 and K_2 . The attenuation to the fundamental 800 Hz component is close to a factor of 40 000 so that the signal appearing at node E_{R1} is essentially DC of value twice E_{01} DC and with an insignificant amount of ripple. E_{R1} is therefore nominally 8.00 VDC. The

nominal gain of the absolute value detector is given by $\frac{|E_{01}|}{|E_1|} =$

$\left(\frac{R_b}{R_a}\right) \left(\frac{R_d}{R_c}\right) \frac{V_{rms}}{V_{rms}}$. To produce 4.00 VDC at node E_{01} , the rms voltage at this node must be $\frac{\pi\sqrt{2}}{4} (4.00) = 4.44$ Vrms. Consequently $\frac{|E_{01}|}{|E_1|} = \frac{4.44 \text{ Vrms}}{45.7 \text{ Vrms}} = 0.0972 \text{ Vrms/Vrms}$, or $\frac{4.00 \text{ VDC}}{45.7 \text{ Vrms}} = 0.0875 \text{ VDC/Vrms}$, nominally. Since $R_c = R_d$ and $R_b = 10K \Omega$, it follows that $R_a = \frac{10K}{0.0972} = 102.9K \Omega$. R_a consists of potentiometer P_1 (20K Ω) and a 90.9K Ω resistance in series. Nominally potentiometer P_1 would be set at 12.0K Ω . To absorb circuit tolerances, potentiometer P_1 is adjusted such that $E_{R1} = 8.00 \text{ VDC} \pm 0.080 \text{ VDC}$ with the reference voltage E_R set at exactly 115 Vrms.

It was indicated previously that the allowable DC drift rate for E_{R1} should be less than $89.2 (10^{-6}) \mu\text{V/s}$. In Fig. A3-1, the DC drift in E_{R1} is due to DC drift in the second-order low-pass filter and in the absolute value detector stages. An estimate of the drift due to temperature at node E_{R1} due to both of these stages is a maximum of $150 \mu\text{V}/^\circ\text{C}$. The maximum rate of temperature change is therefore $[89.2(10^{-6}) \text{ V/s}]/(150 \mu\text{V}/^\circ\text{C}) = 0.59^\circ\text{C/s}$, which is easily achieved, assuming the stages are suitably insulated from the external environment. The LM101AH DCOA used in these stages has a fairly good power supply rejection ratio (80 dB min) and considering the fact that the $\pm 15 \text{ VDC}$ power supplies themselves are well regulated and have a low temperature coefficient of voltage, the drift rate at node E_{R1} , due to power supply voltage drift rates, should be negligible.

In Fig. A2-1 it will be noted that a T^2L compatible square wave reference voltage E_{R2} is required to drive the DG191BP electronic switch for demodulation of the signal appearing at node E_{02} . E_{R2} is derived from the 115 Vrms, 400 Hz reference source as shown in Fig. 12. The circuits used to derive E_{R2} are shown in Fig. A3-1. The signal E_1 , which is the output of the H-5 reference transformer, is first attenuated by the resistance network R_e and R_f , which yields an output of about 5.38 Vrms, nominally, across R_f . This signal is then applied to the hysteresis switch and limiter stage, the output of which switches back and forth between about +13 and -13 V near the zero crossover of the input 400 Hz waveform. A square waveform is thus generated at node E_{02} . Positive feedback is added to the switch via resistor R_g so that switching occurs when the input (across R_f) crosses about +0.4 V for the positive-going portion of the sine wave, and -0.4 V for the negative-going portion of the sine wave. This hysteresis window of 0.8 V prevents noise of amplitude less than 0.8 V (across R_f) from affecting switch operation when the input signal is near the zero crossover region. The final stage, called the square wave reference generator, converts E_{02} to signal E_{R2} . E_{R2} is a 400 Hz square wave ranging between -0.6 and about +4.1 V (a T^2L compatible drive signal for DG191BP switch in Fig. A2-1). When E_{02} is approximately +13 V, E_{R2} is limited to about -0.6 V by the feedback diode D_1 , which has a forward voltage

drop of about 0.6 V. When E_{O2} is approximately -13 V, D_1 is back biased and the gain to signal E_{O2} becomes $(-\frac{R_h}{R_j})$ or $-\left(\frac{31.6K}{100K}\right) = -0.316$; in this case $E_{R2} = -0.316 (-13) = +4.1$ V. Hence, E_{R2} switches between the levels of -0.6 and +4.1 V at the 400 Hz rate.

Cards # 5, and # 6, Figs. A5-1 and A6-1, Schematics of MCU High-Pass Filter and MCU Low-Pass Filter

Figures A5-1 and A6-1 are schematics of one high-pass and one low-pass section, respectively, of the five-stage high-pass filter block shown in Fig. 12. Figure 11 shows how the high-pass and low-pass filter sections are cascaded to form the five-stage filter. It was indicated in Section 8 under "Error Considerations" that the first two stages of the five-stage high-pass filter are critical with respect to rate of change of DC offset. For this reason, Philbrick model 1701 chopper-stabilized amplifiers were chosen for this application. To permit interchangeability, all three high-pass sections of the five-stage filter were made identical, using the same type of DCOA and same component values. Likewise, both low-pass sections were made identical for interchangeability. The DC offset characteristics of the Philbrick model 1701 DCOA were discussed above with respect to Fig. A1-1 for the summing amplifier.

With regard to voltage offset of the DCOA for the first high-pass filter stage (Fig. A5-1), a $0.25 \mu V/^{\circ}C$ temperature coefficient translates into $0.5 \mu V/^{\circ}C$ equivalent input to the five-stage filter. For a maximum allowable drift rate of $1.0 \mu V/s$ at the input to the five-stage filter, the maximum allowable rate of change of temperature for the DCOA becomes: $(1.0 \mu V/s)/(0.5 \mu V/^{\circ}C) = 2^{\circ}C/s$, a value that should be achievable without much difficulty. With regard to the current offset of the DCOA for the first high-pass filter stage, a $1 pA/^{\circ}C$ temperature coefficient translates into a voltage of $(1 pA/^{\circ}C) \times R_1$ (Fig. A5-1) where $R_1 = 4 M\Omega$ at the input to the five-stage filter. For a maximum allowable drift rate of $1.0 \mu V/s$ at the input to the five-stage filter, the maximum allowable rate of change of temperature for the DCOA becomes: $(1.0 \mu V/s)/[1(10^{-12})(4) 10^6 V/^{\circ}C] = 0.25^{\circ}C/s$, a value that can be achieved without difficulty if the DCOA is insulated from the external temperature environment.

For the first low-pass filter stage (Fig. A6-1), a $0.25 \mu V/^{\circ}C$ temperature coefficient for voltage offset for the DCOA translates into $0.25 \mu V/^{\circ}C$ equivalent input to the five-stage filter. This is

a factor of two better (i.e., lower) than that for the first high-pass filter stage and hence the temperature drift requirement for the DCOA becomes 4°C/s maximum for a maximum allowable drift rate of $1.0 \mu\text{V/s}$ at the input to the five-stage filter, a value that should present no problem. A $1 \text{ pA}/^{\circ}\text{C}$ temperature coefficient for current offset for the DCOA translates into $(1 \text{ pA}/^{\circ}\text{C}) \times R_1$ (Fig.

A6-1) where $R_1 = 80.6 \text{ K } \Omega$, at the input to the five-stage filter.

For a maximum allowable drift rate of $1.0 \mu\text{V/s}$ at the input to the five-stage filter, the maximum allowable rate of change of temperature for the DCOA becomes: $(1.0 \mu\text{V/s})/[1(10^{-12})(80.6)10^3 \text{ V}/^{\circ}\text{C}] = 12.4^{\circ}\text{C/s}$, a value easily achieved.

The effects of DC offset changes in the last three stages of the five-stage filter become much less than those listed above for the first two stages. Hence these effects need not be considered inasmuch as the same DCOA type (Philbrick model 1701) is also used in the last three stages.

With regard to the high-pass filter, Fig. A5-1, the transfer function is given by

$$\frac{E_{01}}{E_1} = - \frac{R_2 C_1 s}{(R_1 C_1 s + 1)(R_2 C_3 s + 1)} = - \frac{\tau_a s}{(\tau_a s + 1)(\tau_d s + 1)}, \quad (68)$$

where

$$R_1 = R_2, \tau_a = R_2 C_1 = R_1 C_1, \tau_d = R_2 C_3.$$

C_3 in Fig. A5-1 is used to ensure high-frequency stability of the DCOA in the closed loop and is responsible for the real pole whose time constant is $\tau_d = R_2 C_3 = 200 (10^{-6}) \text{ s}$, corresponding to a cutoff frequency of close to 800 Hz. At signal frequencies at or below 20 Hz, this pole may be neglected. Assuming signal frequencies $\gg \frac{1}{2\pi\tau_a}$ (where $\tau_a = 4 \text{ s}$) but not exceeding 20 Hz, Eq. 68 becomes

$$\frac{E_{01}}{E_1} \approx - 1.000. \quad (68a)$$

In Fig. A5-1, the Teledyne model 431D-5 relay is placed in the reset position during power turn-on time for the DCOA. This prevents a large charge from accumulating across C_1 during power turn-on. For a large charge, C_1 would require a relatively long time to discharge because of the 4 s time constant formed by $R_1 C_1$. After the DCOA has stabilized, which should take no longer than 10 s, the relay contacts may be placed in the normal position. The 1K Ω resistance in series with the relay contacts prevents damage to the contacts, if the relay is placed in the reset position while C_1 has a large charge across it, by limiting the current flow in the contact.

With regard to the low-pass filter, Fig. A6-1, the transfer function is given by

$$\frac{E_{01}}{E_1} = - \left(\frac{R_2}{R_1} \right) \left(\frac{1}{R_2 C_1 s + 1} \right) = - \sqrt{K_{14}} \left(\frac{\tau_a}{\tau_a s + 1} \right), \quad (69)$$

where

$$\sqrt{K_{14}} \tau_a = \frac{R_2}{R_1}; \tau_a = R_2 C_1.$$

K_{14} is the overall gain constant for the five-stage filter given in Fig. 12. For the values shown in Fig. A6-1, $R_2/R_1 = 9.92$, $\tau_a = 4$ s. Hence $\sqrt{K_{14}} = 2.48$ nominally, which is close to the desired nominal value of 2.50. At signal frequencies $\gg \frac{1}{2\pi\tau_a}$. Eq. 69 becomes

$$\frac{E_{01}}{E_1} = - \frac{\sqrt{K_{14}}}{s}. \quad (69a)$$

This transfer function corresponds to pure integration in the time domain. Two such stages in the five-stage filter yield the desired double integration, which converts a measure of acceleration into a measure of height. As in the case for the high-pass

filter section, the Teledyne model 431D-5 relay is used in the reset position to prevent a large charge from accumulating across C_1 during power turn-on. After the DCOA has stabilized (in less than 10 s), the relay contacts may be placed in the normal position.

The nominal scale factor at the input summing node of the adjustable gain summing amplifier, K_{16} in Fig. 12, is 0.3944 VDC/ft. To incur an error of less than 0.01 ft in the measurement of h_w and h_v , the output offset of the last stage of the five-stage high-pass filter, must therefore be $<0.3944 (0.01) = 3.944$ MV. The last stage is a high-pass filter section shown in Fig. A5-1. Its output DC offset for all environments (which includes temperature, power supply, and time changes) can be shown to be ≤ 300 μ V. Hence the error in the measurement of h_w and h_v will be much less than 0.01 ft due to DC output offset in the last stage of the five-stage high-pass filter.

The internal noise generated by the DCOA's used in the five-stage high-pass filter is not expected to contribute a significant error in the measurement of h_w and h_v . Measurements made on the system outputs (h_w and h_v) confirm the latter statement when the filter time constant $\tau_a = 4$ s.

Card # 9, Fig. A9-1, Schematic of MCU Altimeter Signal Conditioning

Figure A9-1 is a schematic of the altimeter signal conditioning circuit. As indicated in Fig. 12, there are two identical (except for gain adjustment) three-stage amplifiers, one for the Collins model ALT50 altimeter, and the other for the TRT model AllV20 altimeter. A front panel switch permits selection of either altimeter channel. Since the channel circuitry is identical, only the Collins altimeter channel will be discussed.

It is assumed that for each altimeter channel the signal source impedance of the altimeter is less than 100 Ω and that the scale factor may range between 100 to 250 MV/ft. It is also assumed that the altimeter signal is always positive. The input stage in Fig. A9-1 is a fixed gain buffer amplifier that has a high input impedance (1 M Ω) and hence does not significantly load the altimeter signal. Its gain is set by the negative ratio of feedback resistance (1 M Ω) to input resistance (1 M Ω) and is

therefore -1.000 nominally. The 10 pF feedback capacitance provides high frequency stability in the closed loop; it has an insignificant effect on the stage transfer function for signal frequencies up to 20 Hz. The network involving the diode D_1 causes the output of the buffer amplifier to limit at -8.4 V. Hence, linear amplification occurs for outputs E_{01} down to -8.4 V and correspondingly for inputs E_1 up to +8.4 V. This corresponds to height signals ranging between 0 and 84 ft and between 0 and 33.6 ft, depending on the altimeter scale factor (assumed, as noted above, to range between 100 and 250 MV/ft).

The second stage is a scale adjustment amplifier that permits the output scale factor at node E_{03} to be adjusted to -250 MV/ft. This adjustment therefore permits absorption of the altimeter scale factor tolerance and first- and third-stage amplifier gain tolerances. The stage gain is given by the negative ratio of feedback resistance ($R_a + P_1$) to R_1 . For a specified altimeter scale factor in the 100 to 250 MV/ft range, P_1 is first set to 0 Ω and R_1 is then selected to yield a scale factor, at node E_{03} , of -245 ± 5 MV/ft. Then P_1 is adjusted to bring the scale factor to the desired -250 MV/ft $\pm 0.1\%$. The 10 pF feedback capacitance provides high frequency stability in the closed loop without affecting the signal frequency transfer function up to 20 Hz.

The third and last stage is the offset adjustment amplifier that may be used to compensate for any altimeter bias ranging between 0 and +31 ft. The stage gain to the altimeter signal is set by the negative ratio of the feedback resistance (R_b) and input resistance (R_c) and is therefore -1.000 nominally. Before discussing the offset adjustment, it should be noted that the maximum linear signal range at node E_{02} is +10.0 V and is -10.0 V at node E_{03} . If the altimeter scale factor is 100 MV/ft, the scale adjustment amplifier gain must be -2.50 VDC/VDC and nodes E_{02} and E_{03} are then limited to altimeter signals not exceeding 40 ft. For an altimeter scale factor ranging between 100 and 210 MV/ft, node E_{01} is above or equal to the -8.4 V limit level and nodes E_{02} and E_{03} are limited to altimeter signals not exceeding 40 ft based on the linear signal range of the third amplifier stage. For an

altimeter scale factor ranging between 210 and 250 MV/ft, nodes E_{02} and E_{03} are limited to altimeter signals ranging between 40 and 33.6 ft, based on the -8.4 V limit level of the buffer amplifier (first amplifier stage).

The effects of changes in DC offset in all three amplifier stages can be shown to be negligible when measured at node E_{03} . For all environments (temperature: $25^{\circ}\text{C} \pm 10^{\circ}\text{C}$; power supply: $\pm 15\text{V} \pm 1\%$), node E_{03} should not change by more than 1 MVDC due to the DC offset changes in all three stages; this is equivalent to an altimeter error not exceeding 0.004 ft.

The offset adjustment in the third stage is best described using Fig. 13, which shows the complete circuit of this stage. The circuit is used in the third stage of each altimeter channel. The switch SW1 and potentiometer P2 are not mounted on the card and hence are not shown in Fig. A9-1. The correspondence between the resistors in the circuits of Fig. 13 and Fig. A9-1 may be checked by observing the labelling of the resistors. The scale factor at node E_{02} is +250 MV/ft. If the altimeter has a bias anywhere in the range 0 to +31 ft, it may be nulled out by adjusting the voltage E_b via SW1 and voltage E_a via potentiometer P2. The equivalent scale factor at each of the nodes E_a and E_b is -250 MV/ft because the summing resistances R_c , R_d , and R_e are all equal in value. At node E_b the voltage may be changed in steps of -1.25 V, which is equivalent to -5.0 ft steps (nominally). At node E_a the voltage may be continuously changed from 0 to -1.5 V, which is equivalent to 0 to -6 ft. Taken together, E_a and E_b may be adjusted to null out any altimeter bias at node E_{02} from 0 to +31 ft. Once adjusted, the bias voltages E_a and E_b should not drift significantly since any drift results in an altimeter error. Consequently, R_2 , P_2 , the 3K Ω resistors, R_c , R_d , R_e , and R_f , in addition to the 1N938B zener diode potential, each require stability against temperature changes so that E_{03} does not change by more than 0.15% (\rightarrow <0.05 ft in worst case). Assuming a $25^{\circ}\text{C} \pm 10^{\circ}\text{C}$ temperature environment and a power supply ($\pm 15\text{V}$) change of less than $\pm 1\%$ due to all environments, these limits should be met using the specified components.

The 10 pF feedback capacitance in Fig. 13 provides high frequency stability in the closed loop without affecting the signal frequency transfer function up to 20 Hz.

Card # 4, Fig. A4-1, Schematic of MCU Altimeter Filter Circuits

Figure A4-1 is a schematic of the altimeter filter circuits. This schematic includes the single stage high-pass filter and single stage low-pass filter shown in the altimeter signal path in Fig. 12. The transfer function for the high-pass filter stage is given by

$$\frac{E_{01}}{E_1} = \left(-\frac{R_2}{R_1} \right) \frac{(R_1 C_1 s)}{(R_1 C_1 s + 1)(R_2 C_2 s + 1)} = K_{23} \frac{(\tau_b s)}{(\tau_b s + 1)(\tau_e s + 1)} \quad (70)$$

where

$$K_{23} = -\left(\frac{R_2}{R_1} \right),$$

$$\tau_b = R_1 C_1, \text{ and}$$

$$\tau_e = R_2 C_2.$$

K_{23} is the high frequency gain in the single stage high-pass filter block in Fig. 12. C_2 in Fig. A4-1 is used to ensure high frequency stability of the DCOA in the closed loop and is responsible for the real pole whose time constant is $\tau_e = R_2 C_2 = 69.4 (10^{-6})$ s, corresponding to a cutoff frequency of close to 2.3 kHz. At signal frequencies at or below 20 Hz, this pole may be neglected. Assuming signal frequencies $\gg \left(\frac{1}{2\pi\tau_b} \right)$, where $\tau_b \approx 25.5$ s, but not exceeding 20 Hz, Eq. 70 becomes

$$\frac{E_{01}}{E_1} = K_{23} = -\frac{R_2}{R_1} = -1.359 \text{ (nominally)}. \quad (70a)$$

To minimize errors in the summation at summation amplifier, block K_{16} in Fig. 12, τ_b was chosen at approximately 25 s. Test data indicate that most signal frequencies are $\gg \left(\frac{1}{2\pi\tau_b} \right)$.

The relay K_1 is for the purpose of keeping C_1 from attaining a large charge during equipment turn-on when the relay is in the reset position. The high frequency gain may be trimmed to yield the desired output scale factor (0.3397 V/ft) by appropriately selecting resistance R_3 .

The transfer function of the low-pass filter stage is given by

$$\frac{E_{02}}{E_1} = \left(-\frac{R_6}{R_4} \right) \left(\frac{1}{R_6 C_3 s + 1} \right) = \frac{K_{24}}{(\tau_c s + 1)}, \quad (71)$$

where

$$K_{24} = -\left(\frac{R_6}{R_4} \right) \text{ and}$$

$$\tau_c = R_6 C_3.$$

K_{24} is the low frequency gain in the single stage high-pass filter block in Fig. 12. At signal frequencies $\ll \left(\frac{1}{2\pi\tau_c} \right)$, where $\tau_c \approx 25.5$ s, Eq. 71 becomes

$$\frac{E_{02}}{E_1} = K_{24} = -\left(\frac{R_6}{R_4} \right) = -2.000 \text{ (nominally)}. \quad (71a)$$

The relay K_2 is for the purpose of keeping C_3 from attaining a large charge during equipment turn-on when the relay is in the reset position. The low frequency gain may be trimmed to yield the desired output scale factor (500 MV/ft) by appropriately selecting resistance R_5 .

The effect of DC offset in the high-pass filter DCOA would merely add a DC component to the h_v and h_w values. However, it can be shown that the equivalent height due to this offset is negligible. At node E_{01} in Fig. A4-1, the maximum DC offset due to all environments should not exceed 3 MV, which translates into a height error of less than 0.01 ft for a scale factor of 0.3397 V/ft at node E_{01} .

With respect to DCOA DC offset in the low-pass filter, this would produce an insignificant error in the measurement of average height h_0 . At node E_{02} the maximum DC offset due to all environments should not exceed 3 MV, which translates into a height error of less than 0.01 ft for a scale factor of 500 MV/ft at node E_{02} .

Card # 7, Fig. A7-1, Schematic of MCU System Output Signal Conditioner

Figure A7-1 is a schematic of the MCU output signal conditioner, which consists of four sections:

1. Adjustable gain summing amplifier. This is block K_{16} in Fig. 12. The inputs to this block are signals proportional to $(+h_v)$ and $+(h_w - h_v)$. These signals are summed in the correct proportions to produce a signal proportional to $[(+h_v) + (h_w - h_v)] = h_w$; this is the desired wave height independent of ship's motion with a scale factor of 1.000 ft/V.
2. Adjustable gain scaling amplifier. This is block K_{15} in Fig. 12. The input to this block is a signal proportional to $(+h_v)$; the output is a signal properly scaled to yield a scale factor of 1.000 ft/V.
3. Buffer amplifier. This is block K_{25} in Fig. 12. The input to this block is a signal proportional to $(+h_0)$ at the scale factor 2.000 ft/V. The output has an identical scale factor. The amplifier is used to isolate the load from the preceding single-stage low-pass filter stage (see Fig. 12).
4. True rms-to-DC converter. This is block K_{26} in Fig. 12. This block converts the rms value of the input h_w waveform into an equivalent DC voltage.

The adjustable gain summing amplifier in Fig. A7-1 has two input signals: one proportional to $(+h_v)$, the ship's vertical motion that has been processed in the accelerometer channels; the other proportional to $+(h_w - h_v)$, which is the difference between the wave height we desire to measure and the ship's vertical motion and has been processed in the altimeter channel. This amplifier

is required to properly sum the signals so that its output at node E_{01} is proportional only to h_w (i.e., the h_v contribution is nulled out) and also so that the desired scale factor of 1.000 ft/V is attained. Nominally, the scale factor at input node E_b is 0.3397 V/ft. Consequently the effective nominal scale factor at node E_a must also be 0.3397 V/ft for the signals to sum properly. The nominal scale factor at node E_a may be verified by referring to Fig. 12 and noting that the constants K_a , K_{13} , and K_{14} have been assigned the following nominal values:

$$K_a = 2.50 \text{ V/g}; K_{13} = -0.700 \text{ VDC/VDC}; K_{14} = -6.25 \text{ rad}^2/\text{s}^2.$$

The transfer function from \ddot{z} to node E_a , the output of the five-stage high-pass filter, in Fig. 12 is given by

$$\frac{E_a}{\ddot{z}} = K_a K_{13} K_{14} \frac{\tau_a^5 s^3}{(\tau_a s + 1)^5} \quad (72)$$

At signal frequencies $\gg \frac{1}{2\pi\tau_a}$, Eq. 72 becomes to a good approximation

$$\frac{E_a}{\ddot{z}} \approx \frac{K_a K_{13} K_{14}}{s^2} \quad (73)$$

Noting that $\ddot{z}/s^2 = z \triangleq h_v$ (assuming $\varphi = \theta = 0^\circ$), then

$$\begin{aligned} \frac{E_a}{h_v} &\approx K_a K_{13} K_{14} = \frac{2.50 \text{ V}}{\text{g}} \times \left(-0.700 \frac{\text{VDC}}{\text{VDC}} \right) \times \left(-6.25 \frac{\text{rad}^2}{\text{s}^2} \right) \\ &\times \frac{1 \text{ g s}^2}{32.2 \text{ ft}} = 0.3397 \text{ V/ft} \quad (74) \end{aligned}$$

Since the desired amplifier output scale factor is 1.000 V/ft, it should have a nominal gain of $(1.000 \text{ V/ft}) / (0.3397 \text{ V/ft}) = 2.944$ volts/volt. This is the nominal gain that has been assigned to block K_{16} in Fig. 12.

The actual scale factor at node E_b in Fig. A7-1 has been established at the desired value of 0.3397 V/ft within a tolerance of $\pm 0.25\%$ by prior adjustment of the gain constants K_{21} (and K_{22}) and K_{23} in the blocks shown in Fig. 12 (see also Figs. A9-1 and A4-1).

Because of component tolerance, mainly in the five-stage high-pass filter block in Fig. 12, the scale factor at node E_a in Fig. A7-1 may deviate significantly from the desired value of 0.3397 V/ft. Two adjustments have been provided on the adjustable gain summing amplifier:

1. Adjustment potentiometer P_1 , which is adjusted so that signals at nodes E_a and E_b sum in the correct proportions, and
2. Adjustment potentiometer P_2 , which is adjusted so that the scale factor at the output node E_{01} is the desired value of 1.000 V/ft.

The transfer functions from node E_a to node E_{01} and from node E_b to node E_{01} are (see nomenclature in Fig. A7-1):

For Node E_a to Node E_{01}

$$E_{01} = \left(\frac{R_b}{R_a + R_b} \right) \left(1 + \frac{R_c}{R_d} \right) E_a . \quad (75)$$

From Node E_b to Node E_{01}

$$E_{01} = \left(\frac{R_a}{R_a + R_b} \right) \left(1 + \frac{R_c}{R_d} \right) E_b . \quad (76)$$

These transfer functions neglect the negative real pole (i.e., low-pass filtering) introduced by the 0.01 MFD feedback capacitor in the adjustable gain summing amplifier. The maximum time constant corresponding to this pole is $[0.01 (10^{-6})] \times [46.4K + 25K] = 714 (10^{-6})$ s corresponding to a cutoff frequency of about

220 Hz. Since signal frequencies are $\ll 220$ Hz, the above transfer functions become very good approximations to the actual transfer functions. For the scale factors at node E_{01} due to signals E_a and E_b to be identical we require that R_a be adjusted as follows:

$$R_a = R_b \left(\frac{E_a}{E_b} \right). \quad (77)$$

Eq. 77 was obtained by equating Eq. 75 to Eq. 76. Hence potentiometer P_1 should be adjusted so that Eq. 77 is satisfied. In practice, the adjustment may be made by injecting a signal equivalent to $h_v = h_{v1} \sin [2\pi(1.0)t]$ into the altimeter channel (in place of the altimeter) at the input to, for example, block K_{21} (Fig. 12) and injecting a suitably proportioned, precisely known signal into the z accelerometer channel (in place of the z accelerometer) at the input to block K_{13} (Fig. 12). This signal represents a vehicle oscillating in the vertical direction at a 1.00 Hz rate with an h_{v1} ft amplitude. The proper amplitude of the z signal is derived from the h_v signal, assuming gain K_{21} has been established for a known altimeter scale factor K_g (Fig. 12), thereby yielding a precisely known scale factor of -0.250 V/ft at the input to the single-stage high-pass filter block in the altimeter channel (Fig. 12). Thus, if K_g is 0.200 V/ft, K_{21} would have been adjusted to be -1.25 V/V. The proper sign of the z signal relative to the h_v signal is established by noting that a positive acceleration \ddot{z} ($= \ddot{h}_v$) is in the downward direction and requires a positive voltage at the input to z channel. However a positive acceleration of the vehicle would cause the altimeter to register a positive output voltage and hence the signs of both signals should be identical. Having established the proper amplitudes and signs of both the h_v and z signals, we seek a null at E_{01} output node in Fig. A7-1 by adjusting potentiometer P_1 . This is the desired mode of operation of the system since E_{01} should not respond to signal h_v representing vehicle motion.

The amplitude of the z signal voltage is determined as follows:

$$E_{h_v} = K_g h_{v1} = \text{equivalent amplitude of output voltage of altimeter for given amplitude of vehicle motion } h_{v1}; \quad (78)$$

$$\ddot{h}_{v1} = h_{v1} \omega^2 = \text{amplitude of vehicle acceleration, where } \omega = 2\pi f \text{ and } f = 1.00 \text{ Hz; and} \quad (79)$$

$$E_{h_v}'' = k_a \ddot{h}_{v1} = K_a h_{v1} \omega^2 = \text{Equivalent output voltage of accelerometer for given amplitude of motion } h_{v1}, \text{ with } h_{v1} \text{ given in terms of } E_{h_v} \text{ and } K_g \text{ by Eq. 78.} \quad (80)$$

Solving these equations for E_{h_v}'' in terms of E_{h_v} :

$$E_{h_v}'' = K_a \omega^2 \left(\frac{E_{h_v}}{K_g} \right). \quad (81)$$

If $K_a = 2.50 \frac{V}{g} \times \frac{1 g s^2}{32.2 ft} = 0.07764 V/(ft/s^2)$ and $K_g = 0.200 V/ft$, $\omega = 2\pi f = 2\pi \text{ rad/s}$ for $f = 1.000 \text{ Hz}$, then

$$\frac{E_{h_v}''}{E_{h_v}} = \frac{0.07764 V/s^2}{ft} \times \frac{4\pi^2 \text{ rad}^2}{s^2} \times \frac{ft}{0.200 V} = 15.32 V/V. \quad (82)$$

In this case the signal applied to the \ddot{z} channel input should be 15.32 times the amplitude of the signal applied to the h_v channel. This gain can be obtained with good accuracy ($\pm 0.05\%$) by using precision resistors to establish the closed loop gain for a high open loop gain DCOA external to the MCU system. Assuming the DCOA is connected for a gain of -15.32, another DCOA is required to yield a gain of -1.000 for an overall gain of +15.32. This is necessary because the sign of the E_{h_v} and E_{h_v}'' signals should be identical. For good accuracy, the frequency must also be known precisely and a precision counter capable of measuring the period of a 1 Hz wave (1.000 s) is required.

If E_a and E_b node scale factors (Fig. A7-1) were identical, R_a would equal R_b and the gain from either node to E_{01} node would be identical for both signals and would be $(1.000 \text{ V/ft})/(0.3397 \text{ V/ft})$ or 2.944 V/V nominally. In general these scale factors are not equal and to adjust node E_{01} to the required value of 1.000 V/ft, an adjustment of potentiometer P_2 is made. This adjustment would be made after potentiometer P_1 has been adjusted. In practice the adjustment may be made by injecting a precisely known signal into the \ddot{z} channel input (in place of the \ddot{z} accelerometer) and noting the output at node E_{01} . A 1.000 Hz signal source may again be used for the \ddot{z} input. The equations that now apply are the following:

Let the injected signal be equivalent to $\ddot{z} = \ddot{z}_1 \sin \omega t$,
where $\omega = 2\pi f$, $f = 1.000 \text{ Hz}$, \ddot{z}_1 amplitude of acceleration.

Then

$$E_z'' = K_a \ddot{z}_1 = \text{equivalent amplitude of output voltage of accelerometer for given acceleration amplitude } \ddot{z}_1. \quad (83)$$

Also

$$z = h_v = \iint \ddot{z} \, dt \, dt = -\left(\frac{\ddot{z}_1}{\omega^2}\right) \sin \omega t = -h_{v1} \sin \omega t, \quad (84)$$

where the amplitude of the equivalent vehicle motion is

$$h_{v1} = \frac{\ddot{z}_1}{\omega^2}. \quad (85)$$

The equivalent amplitude of the output voltage at node E_{01} of Fig. A7-1 should be for a scale factor of $(1/K_e)$ where K_e is the wave height scale factor (1.000 ft/V desired) in Fig. 12:

$$E_{h_v} = \frac{\ddot{z}_1}{K_e \omega^2}, \quad (86)$$

where \ddot{z}_1 is given in terms of E_z and K_a by Eq. 83.

Solving Eqs. 86 and 83 for E_{h_v} in terms of E_z ,

$$E_{h_v} = \frac{E_z}{K_a K_e \omega^2} = E_{01} \text{ of Fig. A7-1.} \quad (87)$$

If $K_a = 0.07764 \text{ V/(ft/s}^2\text{)} = 2.50 \text{ V/g}$ and $K_e = 1.000 \text{ ft/V}$, $\omega = 2\pi f$
 $= 2\pi \text{ rad/s}$ for $f = 1.000 \text{ Hz}$, then

$$\frac{E_{h_v}}{E_z} = \frac{\text{ft}}{0.07764 \text{ V/s}^2} \times \frac{\text{V}}{1.000 \text{ ft}} \times \frac{\text{s}^2}{4\pi^2 \text{ rad}^2} = 0.3263 \text{ V/V.} \quad (87a)$$

In this case, the output at node E_{01} should be 0.3263 times the signal applied to the \ddot{z} channel input. The sign of the E_{01} signal should be opposite to that of the \ddot{z} signal. Assume now that the E_{01} signal is amplified precisely by a gain of $-\left(\frac{1}{0.3263}\right) = -3.065$ using an external precision DCOA with precision gain setting resistors. Also assume that the signal applied to the \ddot{z} input is amplified by a gain of precisely -1.000 using another external precision DCOA with precision gain setting resistors. Then the sum of the two output signals from the DCOA should be exactly zero if the gain of block K_{16} (Fig. 12), the adjustable gain summing amplifier, has been properly set. Hence, the procedure is to sum the two output signals at the input of another external precision DCOA having -1.000 gain to both signals and to adjust potentiometer P_2 in Fig. A7-1 until a null is observed at the DCOA summing amplifier output. For good accuracy, a precision counter should be used to measure the 1.000 Hz test frequency.

Any DC offset in the DCOA used for the adjustable gain summing amplifier of Fig A7-1 will result in an equivalent output DC height error at node E_{01} . The output DC offset at node E_{01} should not exceed 4.0 MV for all environments; hence the equivalent height error should be less than 0.01 ft, which is negligible for a E_{01} node scale factor of 1.000 ft/V.

The true rms-to-DC converter (Fig. A7-1) is an Analog Devices model AD536KD IC device that converts the rms value of the wave height h_w , at node E_{01} of the adjustable gain summing amplifier, to an equivalent DC voltage. Its scale factor is 1.000 VDC/Vrms; since node E_{01} scale factor is 1.000 V/ft for instantaneous height quantities and is correspondingly 1.000 Vrms/(ft rms), the equivalent scale factor at the output of the true rms-to-DC converter is 1.000 VDC/(ft rms). According to the manufacturer, the AD536KD computes the true rms level of a complex AC (or AC plus DC) input signal and gives an equivalent DC output level. It has a crest factor compensation scheme that allows measurements within 1% error at crest factors up to 6. Note: crest factor is the ratio of the peak signal to the rms value. The 300 MFD capacitor connected between its pins 4 and 14 sets the averaging period. For this value capacitance, the reading error (in addition to its normal error) should not exceed 1% for signals concentrated at 0.04 Hz. At signal frequencies above 0.04 Hz the error decreases, and at 0.14 Hz the reading error should not exceed 0.1%. Assuming all error sources add on an rss basis, the overall accuracy for signal frequencies above 0.04 Hz should be better than $\pm 1\%$. Any output DC offset may be nulled by means of potentiometer P_4 in Fig. A7-1.

Changes caused by environment should not exceed 2 MV so that for a scale factor of 1.000 ft rms/VDC, the equivalent rms height error should not exceed 0.002 ft, which is negligible.

The adjustable gain scaling amplifier in Fig. A7-1 corresponds to block K_{15} in Fig. 12. Its output is a measure of ship's vertical motion h_v . The nominal scale factor at its input node E_a is 0.3397 V/ft. The desired output scale factor at node E_{02} is 1.000 V/ft; hence the nominal amplifier gain is $(1.000 \text{ V/ft}) / (0.3397 \text{ V/ft}) = 2.944 \text{ V/V}$. Since the scale factor at node E_a has a wide tolerance, the gain of this amplifier must be set via potentiometer P_3 to compensate for this tolerance. This adjustment may be made at the same time that potentiometer P_2 is adjusted, using the same technique with external DCOA's and precision resistors as

explained above. The only difference is that the output voltage is now measured at node E_{02} instead of node E_{01} . Since the output scale factor at node E_{02} is identical to that at node E_{01} , the closed loop gains of the external DCOA's do not change for this measurement. The transfer function for the adjustable gain scaling amplifier is given by (see Fig. A7-1)

$$\frac{E_{02}}{E_a} = \left(1 + \frac{R_e}{R_f} \right) . \quad (88)$$

The effect of the 0.015 MFD feedback capacitor in Fig. A7-1 has been neglected in Eq. 88. Its effect is to introduce lag-lead factors in the transfer function with the worst case lag time constant being $20.5K [(0.015)10^{-6}] = 308 (10^{-6})$ s corresponding to a lag cutoff frequency of about 520 Hz. The corresponding lead time constant is $82.5 (10^{-6})$ s corresponding to a lead cutoff frequency of about 1.93 kHz. The effect of this capacitor, therefore, at signal frequencies below 20 Hz may be neglected.

Any DC offset of the DCOA used for the adjustable gain scaling amplifier of Fig. A7-1 will result in an equivalent output DC height error at node E_{02} . The output DC offset at node E_{02} should not exceed 3 MV for all environments; hence the equivalent height error should be less than 0.01 ft, which is negligible for a E_{02} node scale factor of 1.000 ft/V.

The buffer amplifier in Fig. A7-1 is block K_{25} in Fig. 12 and is used to isolate the load from the single-stage low-pass filter block preceding it. It has unity gain and negligible DC offset. Since the input scale factor has been set at 0.500 V/ft, the output scale factor is the same. The 0.33 MFD feedback capacitor ensures high frequency stability for the closed loop.

It will be noted in Fig. A7-1 that all amplifier outputs are isolated from DAS inputs by 5.11K resistors. If the DAS inputs are inadvertently shorted to ground, the resistors prevent damage to the amplifier output circuits. All DAS inputs are assumed to have input impedances ≥ 1 M Ω . The signal loading at the 5.11K resistor outputs is therefore about 0.5% or less.

In Fig. A7-1, the relays K_1 and K_2 provide means for disconnecting the MCU outputs from DAS inputs.

Card # 10, Fig. A10-1, Schematic of MCU Reset Timing and Control

Figure A10-1 is a schematic of the timing and control circuitry for activating the relays on the various cards.

When power is first turned on, the +5 V supply is applied instantly to the NE555A dual timer unit at its V_{cc} pin 14. Timers Nos. 1 and 2 are both operated as one-shot multi-vibrators and require trigger signals to initiate the timing cycles. Also applied is +5 V to the trigger pin 6 of timer No. 1 through resistance R_1 (147K). Capacitor C_1 , which is connected to trigger pin 6, however, is initially discharged so that the trigger potential with respect to ground rises exponentially at power turn-on from zero toward 5 V with time constant $R_1 C_1$ ($= 0.323$ s). If the trigger potential is below the threshold level of about $V_{cc}/3 = \frac{5V}{3} = 1.67$ V, the timing of timer No. 1 will begin. Since the trigger potential initially starts at 0 V (which is < 1.67 V), timer No. 1 has effectively been reset by the trigger potential at power turn-on and begins its timing. This timing is set by components $R_2 C_2$. C_2 charges from initially 0 V exponentially through R_2 from the +5 V supply. When its potential reaches $2 V_{cc}/3 = 3.33$ V, the capacitor charge reaches the reset potential at the threshold pin 2 and C_2 rapidly discharges and the circuit awaits the initiation of the next timing cycle from the trigger source at pin 6. The time for C_2 to reach the 3.33 V threshold potential is about $1.1 R_2 C_2 = 27$ s and this is the nominal duration of the timing interval. Before this timing cycle ends, the trigger potential at pin 6 rises above its threshold level (in about 130 ms after power turn-on) so that it is no longer capable of restarting the timing cycle.

During timer No. 1 cycle time (27 s) after power turn-on, the output potential at pin 5 is high at close to +5 V and hence transistor Q_1 receives base current, which switches it into its saturated state. All relay coils connected to the collector of Q_1 are then activated. The contacts associated with these relays act to short all large value capacitors in the various filter circuits

of Figs. A4-1, A5-1, and A6-1 while allowing sufficient warm-up time for the DCOA's with which they operate. At the end of the 27 s timing cycle, the output potential at pin 5 drops below 0.25 V and Q_1 then turns off; all associated relays are then deactivated. This connects the capacitor in the various filter circuits for normal operation.

During power turn-on, timer No. 2 also receives its trigger potential (at pin 8) from the charge across capacitor C_1 so that its timing cycle is also started at power turn-on. The cycle time in this case is set by the timing components R_3C_3 and the cycle ends when the C_3 capacitor potential reaches 3.33 V. This time is about $1.1 R_3C_3 = 150$ s. At the end of the cycle time the threshold potential (3.33 V) is reached at pin 12 and the capacitor C_3 rapidly discharges. The circuit then awaits initiation of the next timing cycle from the trigger source. Since the potential across C_1 has risen above the trigger threshold level (in about 130 ms after power turn-on) before the timer No. 2 cycle has ended, it is no longer capable of restarting the timing cycle.

During timer No. 2 cycle time (150 s) after power turn-on, the output potential at pin 9 is high at close to +5 V and hence transistor Q_2 receives base current, which switches it into its saturated state. All relay coils connected to the collector of Q_2 are then activated. The contacts associated with these relays act to disconnect all MCU output signals from DAS (see Fig. A7-1) for 150 s and ground the DAS inputs. This action permits the MCU sufficient time to warm up and allows all system transients to die down immediately after power turn-on before the MCU output signals are routed to the DAS inputs.

After power is turned on and the system is in normal operation, it is possible to retrigger both timers and restart the timing cycles and reactivate the respective relays, if desired, by depressing either the pushbutton (PB) reset switch on the front panel or the PB reset switch on the cockpit display. The timing cycle of each timer may be interrupted, if so desired, by depressing the DCOA reset defeat switch PB for timer No. 1, or the DAS output disconnect defeat switch PB for timer No. 2. Depressing either PB switch grounds the respective reset input node (pin 4 or pin 10 on the NE556A) and causes the output (pin 5 or pin 9 on NE556A) to go low and deactivate all associated relays. Releasing the PB switch removes the ground, but the output still remains low unless the timers are retriggered by depressing the PB reset switch on the front panel or the PB reset switch on the cockpit display.

Relay K_1 on Fig. A10-1 is also activated by timer No. 2 when the other relays are activated. The contacts of this relay supply power to the cockpit display lamps and front panel lamps. When the relay is activated, the 150 s timer No. 2 is in its timing cycle and all MCU outputs are disconnected from the DAS inputs. During this time interval, all red lamps will glow indicating that the MCU is not ready for signal readout. After the timing cycle ends, the MCU outputs are connected to the DAS inputs and the green lamps will glow indicating that the MCU is ready for signal readout.

Cockpit Display Unit, Fig. D1-2, Cockpit Control Display Unit Wiring Diagram

Figure D1-2 is a schematic of the Cockpit Control Display Unit (CDU) with the green and red lamps for indicating whether the MCU outputs are connected to the DAS. As indicated in the discussion of timing and control schematic, Fig. A10-1, the red lamp glow indicates no connections are made and the green lamp glow indicates connections are made and the system is ready for signal readout.

Also shown in Fig. D1-2 is the Cockpit Display reset PB switch, which is also shown for reference purposes on Fig. A10-1. If this switch is depressed, it retriggers both the 27 s and 150 s timers into their respective timing cycles. The cockpit display red lamp will then glow indicating that the MCU system outputs have been disconnected from the DAS inputs. At the end of the 150 s timing interval, the green lamp will glow on the cockpit display indicating that the MCU outputs are ready to deliver signals to the DAS inputs.

The gyro compensation bypass switch shown in Fig. D1-2 when in the GCU position, applies power to a relay coil, the contacts of which connect to the GCU signals. In the bypass position, the relay coil is deactivated and the GCU is bypassed and its signals are not used. In the latter case the vertical gyro is being used in its normal mode without gyro compensation for ship maneuvers.

Figure D1-2 shows the cockpit display digital panel meter manufactured by Datel (model 3100L). It has been connected for a full-scale capability of 1.999 V and its input is connected to the rms wave height output signal, h_w (rms) in Fig. A7-1. The display scale factor is 1 ft rms/V; hence readings are directly in feet rms. The input impedance of the device (between pins 4 and 2, with pin 2 being the analog low side of the signal) is 100 M Ω minimum.

Card # 11, Fig. A11-1, Schematic of MCU Ship's Angular Motion Meter Drive

Figure A11-1 is a schematic of the roll and pitch angle read-out meter circuits. The input scale factors are each 0.1745 V/deg. The gain of each amplifier is

$$\text{Roll channel: Gain} = -\frac{R_2}{R_1} = -\frac{1000K}{34.8K} = -28.7 \text{ (nominal)}$$

$$\text{Pitch channel: Gain} = -\frac{R_4}{R_3} = -\frac{1000K}{34.8K} = -28.7 \text{ (nominal) .}$$

The nominal scale factors at the output nodes E_{01} and E_{02} are $0.1745 \times 28.7 = 5.01$ V/deg. For $\pm 2^\circ$ full-scale meter readings, the LM101AN DCOA output voltage must have a capability of 10.02 V. These DCOA's actually have a guaranteed output voltage capability of ± 12 V into a 10K Ω load. Output limiting occurs around ± 13 V so that should the roll and pitch angles exceed 2° in magnitude, the meters will be overloaded by a factor of $13/10.02 = 1.3$. This overload will not damage the meters. Calibration of the nominal 100 μ A meters is accomplished by applying a known synchro angle of, for example, 2° and adjusting the respective potentiometers P_1 and P_2 for a full-scale deflection of the meter. These potentiometers are capable of adjusting the full-scale meter current within a $\pm 5\%$ range and should absorb all circuit and meter tolerances.

The 0.01 MFD feedback capacitor across each DCOA serves to provide high-frequency stability in the closed loop while providing a low-pass filter to signal frequencies with a cutoff frequency of about 16 Hz.

Card # 17, Fig. A-17-1, Schematic of MCU System Test Reference Generator

Figure A17-1 is a schematic of the MCU system test reference generator. This is a two-stage feedback sine wave oscillator with automatic adjustment of the loop gain to unity at the frequency at which the total loop phase shift is exactly -360° .

The loop gain adjusts itself to unity through the limiting action of the paralleled IN459 diodes that limit the potential at node E_d to approximately 0.45 V. The transfer function of each stage is as follows:

First Stage:

$$\frac{E_{01}}{E_{02}} = \frac{1}{\tau_1^2 s^2 + 2\zeta_1 \tau_1 s + 1}, \quad (89)$$

where

$$\tau_1^2 = R_1 R_2 C_1 C_2 \text{ and}$$

$$2\zeta_1 \tau_1 = (R_1 + R_2) C_2.$$

Second Stage:

$$\frac{E_{02}}{E_d} = - \left(\frac{1}{R_3 C_3 S} \right). \quad (90)$$

The first stage is therefore a second-order low-pass filter. The second stage is a pure integrator with -180° phase shift due to the phase reversal of the DCOA and an additional -90° due to the integration, where $S = j\omega$, $j = \sqrt{-1}$, $\omega = 2\pi f$, and f = signal frequency. If the signal frequency is the desired test frequency f_0 , i.e., $f = f_0$ (with $\omega = 2\pi f_0 = \omega_0$), then at the desired test frequency the second stage has a total phase shift of -270° . For oscillations to take place, therefore, the first stage must produce a phase shift of -90° , making the total loop phase shift exactly -360° . This assumes that the phase shift in the diode network transfer function (E_d/E_{01}) is negligible.

To obtain -90° phase shift in the first stage, we require $\tau_1^2 s^2 + 1 = 0$ in Eq. 89, for $S = j\omega_0 = j2\pi f_0$, at the desired test frequency f_0 . The desired test frequency f_0 was chosen to be 2.00 Hz nominally.

Arbitrarily we chose $\zeta_1 = 0.500$ and the signal level at frequency f_0 at node E_{01} to be 8.00 V peak-to-peak sine wave (or 2.828 Vrms). The magnitude of the first stage gain at frequency f_0 is as follows:

$$\left| \frac{E_{01}}{E_{02}} \right| = \frac{1}{2\zeta_1} = 1.000 \quad (\text{from Eq. 89, with } \tau_1^2 s^2 + 1 = 0) . \quad (91)$$

Hence, it follows that $E_{02} = 8.00$ V peak-to-peak sine wave, or 2.828 Vrms, at frequency f_0 . The sine wave signal E_{01} becomes limited at node E_d due to the limiting action of the IN459 diodes. The signal limits at about ± 0.45 V peak-to-peak at node E_d and it therefore looks essentially like a square wave at fundamental frequency f_0 . The fundamental component of the square wave, obtained by a Fourier analysis of the square wave, is given by

$$E_d (\text{rms}) = \frac{2\sqrt{2}}{\pi} E_d ,$$

where

$$E_d = 0.45 \text{ V} . \quad (92)$$

The magnitude of the gain of the second stage at frequency f_0 from Eq. 90 is

$$\frac{E_{02} (\text{rms})}{E_d (\text{rms})} = \frac{1}{2\pi f_0 R_3 C_3} , \text{ with } S = j\omega_0, j = \sqrt{-1}, \omega_0 = 2\pi f_0 \quad (93)$$

with $E_d (\text{rms})$ given by Eq. 92, and $E_{02} (\text{rms}) = 2.828$ vrms.

Hence we require that $R_3 C_3$ be chosen such that, from Eqs. 92 and 93,

$$R_3 C_3 = \left(\frac{1}{2\pi f_0} \right) \left[\frac{E_d \text{ (rms)}}{E_{02} \text{ (rms)}} \right] = \frac{\sqrt{2}}{\pi^2 f_0} \left[\frac{E_d}{E_{02} \text{ (rms)}} \right]$$

With $E_d = 0.45$ V, $E_{02} \text{ (rms)} = 2.828$ Vrms, $f_0 = 1.965$ Hz (for nominal values of R_1 , R_2 , C_1 , C_2 in Fig. A17-1), $R_3 C_3 = 0.01160$ s. C_3 was chosen to be $0.775 (10^{-6})$, so that $R_3 = 0.01160 / [0.775(10^{-6})] = 15.0K \Omega$ nominally. The actual value of R_3 (which absorbed circuit component tolerances), shown in Fig. A17-1, was $14.7K \Omega$ and was chosen to make $E_{01} = 2.828$ Vrms.

In the MCU system tests, output E_{03} was set to 8.00 VPTP (potentiometer P_1 was therefore set at full-scale value) with the load connected, and E_{04} was set via potentiometer P_2 to 0.82 VPTP with the load connected.

The zener diode network shown in Fig. A17-1 using the IN4577 diode was added to supply a regulated source at -6.4 V $\pm 5\%$. In the MCU system tests, node E_{05} potential was measured to be -6.045 V with the load connected.

The 1000 pF feedback capacitance in the first stage is used to provide high-frequency stability of the DCOA in the closed loop. Its effect on the first stage transfer function is negligible.

In order to hold the net DC offset at node E_{01} to a minimum, the forward conduction characteristics of the IN459 diodes should be reasonably matched.

DETERMINATION OF THE SYSTEM FILTER TIME CONSTANTS τ_a AND τ_b

Figure 14 is a block diagram of the MCU system, which may be used for error analysis. It is desired to determine the acceptable values of τ_a and τ_b time constants for a given maximum error in the measurement of wave height h_w . In Fig. 14, the signal proportional to mean height h_0 cannot pass through the high-pass filter in the altimeter channel and so does not appear in Eqs. 1 through 5 in the figures. In this figure, h_{wa} is a measure of the actual wave height, h_w . Also, the three accelerometers are combined and shown

as one effective accelerometer capable of measuring only the vertical component of ship's motion. Any error in the combination signal can be grouped into the fractional error ϵ_1 . ϵ_1 also includes any errors in the gain constants K_a (accelerometer scale factor), K_{13} , and K_{14} ; these errors may be caused by changes due to environmental influences.

For the error analysis, we start with Eq. 5 in Fig. 14.

$$h_{wa} = K_n \left[\frac{(1+\epsilon_1)(\tau_a S)^5}{(\tau_a S+1)^5} - \frac{(\tau_b S)}{(\tau_b S+1)} \right] h_v + K_n \left[\frac{\tau_b S}{\tau_b S+1} \right] h_w, \quad (94)$$

where h_{wa} is the measured value of h_w .

The desired value of the wave height at the system output is h_w , and if the system were perfect the contribution due to h_v would be nil and the net signal from the altimeter path to the output would be

$$h_{wa} = h_w = K_g K_{21} K_{23} K_{16} K_e h_w = K_n h_w \text{ for the perfect system.} \quad (95)$$

Consequently, from Eq. 95 it follows that K_n must satisfy the following equation:

$$K_n = K_g K_{21} K_{23} K_{16} K_e = 1. \quad (96)$$

The error in using h_{wa} in the imperfect system as a measure of h_w is then

$$\epsilon_h = h_{wa} - h_w. \quad (97)$$

Substituting Eq. 94 into Eq. 97 and making use of Eq. 96,

$$\begin{aligned} \epsilon_h = & \left[\frac{(1+\epsilon_1)(\tau_a S)^5}{(\tau_a S+1)^5} - \frac{(\tau_b S)}{(\tau_b S+1)} \right] h_v \\ & + \left[\frac{\tau_b S}{\tau_b S+1} - 1 \right] h_w = \epsilon_{h_v} + \epsilon_{h_w}. \end{aligned} \quad (98)$$

ϵ_h is composed of two parts: an error term involving h_v and another term involving h_w ; calling these error terms ϵ_{h_v} and ϵ_{h_w} , respectively, we have

$$\begin{aligned} \epsilon_{h_v} = & \left[\frac{(1+\epsilon_1)(\tau_a S)^5}{(\tau_a S+1)^5} - \frac{(\tau_b S)}{(\tau_b S+1)} \right] h_v = \text{error in measurement of} \\ & h_w \text{ due to } h_v \text{ and filter} \\ & \text{time constants } \tau_a, \tau_b; \\ & \text{and} \end{aligned} \quad (99)$$

$$\epsilon_{h_w} = - \left[\frac{h_w}{\tau_b S+1} \right] = \text{error in measurement of } h_w \text{ due to filter} \\ \text{time constant } \tau_b. \quad (100)$$

Now consider the error term ϵ_{h_v} given by Eq. 99. The two terms may be algebraically combined to yield a common denominator as follows:

$$\epsilon_{h_v} = \frac{N_1(S)}{D_1(S)} h_v. \quad (101)$$

where

$$N_1(S) = (1+\epsilon_1)(\tau_a S)^5 (\tau_b S+1) - \tau_b S(\tau_a S+1)^5 \quad \text{and} \quad (102)$$

$$D_1(S) = (\tau_a S+1)^5 (\tau_b S+1) , \quad (103)$$

if we let

$$\tau_b = k\tau_a , \quad (104)$$

where k is some constant yet to be determined. Now substitute τ_b from Eq. 104 into Eqs. 102 and 103 and expand the $(\tau_a S+1)^5$ term using the binomial expansion theorem and retain only the two higher power terms involving the variable S :

$$N_1(S) \approx (\tau_a S)^5 \left[\epsilon_1(k\tau_a S+1) + (1-5k) \right] \quad (105)$$

$$D_1(S) \approx (\tau_a S)^5 \left[k\tau_a S+1 \right] . \quad (106)$$

These equations are subject to the following approximations:

$$|(\tau_a S)^4(1-5k)| \gg k |10(\tau_a S)^3 + 10(\tau_a S)^2 + 5(\tau_a S) + 1| \quad (107)$$

and

$$|(\tau_a S)^5| \gg |5(\tau_a S)^4 + 10(\tau_a S)^3 + 10(\tau_a S)^2 + 5(\tau_a S) + 1| , \quad (108)$$

with $S = j\omega$, $\omega = 2\pi f$, f = signal frequency, and $j = \sqrt{-1}$.

Substituting Eqs. 105 and 106 into Eq. 101 we have

$$\epsilon_{h_v} = \left[\frac{\epsilon_1(k\tau_a S+1) + (1-5k)}{(k\tau_a S+1)} \right] h_v = \epsilon_1 h_v + \left[\frac{1-5k}{k\tau_a S+1} \right] h_v . \quad (109)$$

Let $S = j\omega$ in Eq. 109 and assume

$$k\omega\tau_a \gg 1 ; \quad (110)$$

then Eq. 109 becomes

$$\epsilon_{h_v} \approx \epsilon_1 h_v + \left[\frac{1-5k}{k\omega\tau_a} \right] h_v . \quad (111)$$

Eq. 111 indicates that there are two sources of error that make up ϵ_{h_v} :

1. ϵ_1 , the fractional error in adjusting the acceleration channel gain to equal the altimeter channel gain, and
2. An error source inversely proportional to frequency.

If $\epsilon_1 \leq 0.01$, i.e., the channel gains are within 1% of each other, then if the ship's vertical height $h_v < 5$ ft, it follows that ϵ_{h_v} due to ϵ_1 will be < 0.05 ft, an error bordering on insignificance.

To determine the error ϵ_{h_v} due to the frequency-dependent term, we need to know the power spectrum density for h_v . Figure 15 is a typical power spectrum density (PSD) for the vertical acceleration of the ship. To be able to use this information, the frequency dependent term in Eq. 111 must be placed in a form showing the acceleration variable \ddot{h}_v instead of h_v itself. To do this, we note

$$h_v = \frac{\ddot{h}_v(S)}{S^2} = - \frac{\ddot{h}_v(j\omega)}{\omega^2} , \quad (112)$$

where $S = j\omega$, and $j = \sqrt{-1}$.

If we denote the frequency-dependent error term in Eq. 111 by $\epsilon_a(\omega)$ and substitute Eq. 112 into Eq. 111 we have

$$\epsilon_a(\omega) = \left(\frac{1-5k}{k\omega\tau_a} \right) \left(-\frac{\ddot{h}_v}{\omega^2} \right) = \left(\frac{5k-1}{k\tau_a} \right) \left(\frac{\ddot{h}_v}{\omega^3} \right). \quad (113)$$

To be able to use Eq. 113 we must keep in mind that relations 107, 108, and 110 must hold. In the MCU system design we chose $\tau_a = 20$ s, and $\tau_b = 25$ s, and therefore, from Eq. 104, $k = 1.25$. In Fig. 15, the lowest significant frequency for vertical acceleration is about 1 Hz. The minimum value of ω is therefore about 6.28 rad/s. If we substitute these values of τ_a , k , and ω in relations 107, 108, and 110, with $S = j\omega$, $j = \sqrt{-1}$, we see that each of these relations is satisfied and hence $\epsilon_a(\omega)$ in Eq. 113 is a good approximation to Eq. 101 with $N_1(S)$ given by Eq. 102 and $D_1(S)$ given by Eq. 103.

If we denote the PSD for \ddot{h}_v by $a_v^2(\omega)$, then the error in Eq. 113 may be transformed to the following expression yielding the mean squared error over the frequency range of $a_v^2(\omega)$:

$$\begin{aligned} \epsilon_a(\omega)^2 &= \left[\frac{5k-1}{k\tau_a} \right]^2 \int_0^\infty \frac{a_v^2(\omega)}{\omega^6} d\omega \\ &= \left[\frac{5k-1}{k\tau_a} \right]^2 \sum_{n=1}^\infty \left(\frac{a_v^2[(n-\frac{1}{2})\Delta\omega]}{[n-\frac{1}{2})\Delta\omega]^6} \Delta\omega \right). \end{aligned} \quad (114)$$

Because of the irregularity of the PSD curve in Fig. 15, the integration indicated in Eq. 114 will be performed approximately as indicated on the extreme right side of Eq. 114. The calculation requires that the curve be broken up into small strips each of width $\Delta\omega$. Then a_v^2 is read off the curve at the midpoint of each strip, multiplied by the strip width $\Delta\omega$, and then divided by the sixth power of ω at the midpoint of the strip. All the contributions thus calculated, as the number of the strip (n) varies between 1 and ∞ , are then summed to arrive at the approximation to the integral. Beyond $f = 5$ Hz, the contributions are negligible as may

be seen in Fig. 15, since the PSD amplitude for all frequencies above 5 Hz are zero. Hence if the strip width is made 0.1 Hz ($\rightarrow \Delta\omega = 0.628$ rad/s), (n) need run only between 1 and 50.

This calculation was carried out with the result that, for $\tau_a = 20$ s, $\tau_b = 25$ s, $k = \tau_b/\tau_a = 1.25$ (the values used in the MCU system design), $[\epsilon_a(\omega)]^2 = 69.0 (10^{-6}) \text{ ft}^2$, or $\epsilon_a(\omega) = 8.30 (10^{-3})$ ft rms. This may be considered a negligible error.

Now consider the error term ϵ_{h_w} given by Eq. 100. The square of the magnitude of ϵ_{h_w} is given by

$$|\epsilon_{h_w}|^2 = \frac{h_w^2}{[1+(\omega_e \tau_b)^2]}, \quad (115)$$

where $S - j\omega$, $j = \sqrt{-1}$, and $\omega = \omega_e =$ encountered wave angular frequency seen by the altimeter.

To determine the error magnitude $|\epsilon_{h_w}|$, we need to know the encountered PSD, $S_e(\omega_e)$, for h_w . This is obtained from the Pierson-Moskowitz spectral form (Ref. 12):

$$S(\omega) = \alpha \left(\frac{g^2}{\omega^5} \right) e^{-\beta \left(\frac{\omega_\mu}{\omega} \right)^4}, \quad (116)$$

where

$$\omega_\mu = \frac{g}{U};$$

$$U^2 = 2g \sigma \sqrt{\frac{\beta}{\alpha}};$$

$$\sigma = \frac{h_{1/3}}{4};$$

$\alpha, \beta = \text{constants};$

U = wind velocity;

g = gravitational acceleration;

$$\sigma = \text{rms height of PSD} = \int_0^{\infty} S(\omega) d\omega = \int_0^{\infty} S(\omega_e) d\omega_e; \text{ and}$$

$h_{1/3}$ = significant wave height.

For a moving ship the encountered PSD, $S_e(\omega_e)$, is related to the PSD of Eq. 116 as follows:

$$S_e(\omega_e) = \frac{S(\omega)}{1 - \left(\frac{2V \cos \psi}{g} \right) \omega^2}, \quad (117)$$

where ω is given implicitly in terms of the encountered wave angular frequency ω_e as

$$\omega_e = \omega - \left(\frac{V \cos \psi}{g} \right) \omega^2. \quad (118)$$

In Eqs. 117 and 118,

V = ship velocity;

ψ = heading angle;

$\psi = 180^\circ \rightarrow$ heading sea; and

$\psi = 0^\circ \rightarrow$ following sea.

The following values were assumed (assuming $h_{1/3}$ for sea state 3):

$$V = 40 \text{ kt (67.5 ft/s)}; h_{1/3} = 5 \text{ ft}; \alpha = 0.0081; \beta = 0.74.$$

Two values of ψ were chosen: (a) $\psi = 180^\circ$ (\rightarrow heading sea), and (b) $\psi = 90^\circ$. For these values of ψ the encountered PSD's become

$$S_e(\omega_e) = \frac{8.398 e^{-0.74 \left(\frac{1.161}{\omega} \right)^4}}{\omega^5 (1+4.194\omega)}, \quad \psi = 180^\circ, \quad (119)$$

with $\omega_e = \omega + 2.097 \omega^2$.

$$S_e(\omega_e) = S(\omega) = \frac{8.398 e^{-0.74 \left(\frac{1.161}{\omega} \right)^4}}{\omega^5}, \quad \psi = 90^\circ, \quad (120)$$

with $\omega_e = \omega$.

$S_e(\omega_e)$ for $\psi = 180^\circ$ (Eq. 119) is plotted in Fig. 16 as a function of ω_e . Figure 17 is another plot for $S_e(\omega_e)$ except for $\psi = 90^\circ$ (Eq. 120).

Using the curves of $S_e(\omega_e)$ we can find $|\epsilon_{h_w}|^2$ from Eq. 115 by replacing h_w^2 by the following integral:

$$|\epsilon_{h_w}|^2 = \int_0^\infty \frac{S(\omega_e) d\omega_e}{[1+(\omega_e \tau_b)^2]} = \sum_{n=1}^\infty \frac{S_e[(n-\frac{1}{2})\Delta\omega_e]}{1+[\tau_b(n-\frac{1}{2})\Delta\omega_e]^2} \Delta\omega_e \quad (\text{ft}^2). \quad (121)$$

Equation 121 will be integrated approximately, as indicated on the extreme right side of the equation, by breaking up the $S_e(\omega_e)$ curve into small vertical strips, each of width $\Delta\omega_e$. The S_e value is then read off the curve at the midpoint of each strip, multiplied by the strip width $\Delta\omega_e$, and then divided by the $[1+(\omega_e \tau_b)^2]$ factor

evaluated at the midpoint of the strip. All the strip contributions thus calculated, as the number of the strip takes on values between 1 and ∞ , are then summed to arrive at the approximation to the integral. From the form of the $S_e(\omega_e)$ curves in Figs. 16 and 17, it will be seen that the number of strips required will be finite since $S_e(\omega_e)$ is essentially 0 beyond $\omega_e = 40$ rad/s in Fig. 16 and beyond $\omega_e = 6.0$ rad/s in Fig. 17.

These calculations were carried out for two values of τ_b :
(a) $\tau_b = 25$ s (value used in MCU system), and (b) $\tau_b = 12.5$ s.
The following results were obtained:

$$\underline{\psi = 180^\circ}: \quad \tau_b = 25 \text{ s}, \quad |\epsilon_{h_w}| = 0.0138 \text{ ft rms},$$

$$\tau_b = 12.5 \text{ s}, \quad |\epsilon_{h_w}| = 0.0276 \text{ ft rms}.$$

$$\underline{\psi = 90^\circ}: \quad \tau_b = 25 \text{ s}, \quad |\epsilon_{h_w}| = 0.0436 \text{ ft rms},$$

$$\tau_b = 12.5 \text{ s}, \quad |\epsilon_{h_w}| = 0.0870 \text{ ft rms}.$$

The worst value occurs for $\psi = 90^\circ$ with $\tau_b = 12.5$ s, with $|\epsilon_{h_w}|$ not being insignificant. It is therefore wiser to use the higher value of τ_b ($= 25$ s) to reduce the $|\epsilon_{h_w}|$ error by a factor of about two.

9. VERTICAL GYRO MANEUVER COMPENSATION ELECTRONICS

The Vertical Gyro Maneuver Compensation Electronics (VGMCE) is designed to maintain the vertical gyro spin axis parallel to the local vertical in the presence of ship's maneuvers.

Figure 18 is a simplified block diagram of the VGMCE. Since the Γ_R (vertical gyro roll pendulum angle) and Γ_P (vertical gyro pitch pendulum angle) signals are in the form of 400 Hz suppressed carrier signals, the VGMCE (the pendulum simulator) must generate signals in the same form. This is the reason for the use of the 400 Hz modulators and the 400 Hz reference signal.

If the ship is moving at a constant velocity V_s and is turning at rate $\dot{\psi}$, these quantities are measured by ship sensors and presented to the VGMCE as DC analog voltages. These voltages are the outputs of blocks K_L (for velocity V_s) and K_G (for yaw rate $\dot{\psi}$). After amplification, the signals proportional to V_s and $\dot{\psi}$ are multiplied to develop a signal proportional to $V_s \dot{\psi}$. The latter signal is then passed through a first-order low-pass (LP) filter, a non-linear gain stage, and then to the 400 Hz modulator. At the output of the modulator, a 400 Hz suppressed carrier signal proportional to $(V_s \dot{\psi}/g) = \Gamma_{RC}$, and properly scaled, is then subtracted (at the input of a unity gain summation amplifier) from the signal appearing at the output of the vertical gyro (VG) roll pendulum angle sensor (i.e., at block K_R output). The latter signal is proportional to Γ_R where $\Gamma_R = \tan^{-1}\left(\frac{V_s \dot{\psi}}{g}\right)$. For $|\Gamma_R| \leq 10^\circ$, $\Gamma_R \approx \frac{V_s \dot{\psi}}{g}$ with an error of about 1% or less; hence, for Γ_R angles up to 10° in magnitude the error in the subtraction process will be 1% or less. The output of the unity gain summation amplifier is then used to drive the VG roll erection amplifier.

If the ship is turning at rate $\dot{\psi}$ and moving with velocity V_s , the output of the unity gain summation amplifier will be a perfect null (ideally), and the VG will not be torqued about the pitch axis. This is the desired mode of action, and the gyro will

maintain its spin axis along the local vertical in the presence of the turning maneuver. On the other hand, during normal ship operation, the signal proportional to spin axis tilt will pass through the unity gain summation amplifier without change in amplitude or phase (since θ_{RC} signal = 0). If $\Gamma_R \neq 0$ for some reason other than

$V_s \dot{\psi}/g \neq 0$, the implication is that the gyro spin axis is not vertical.

In this case, the Γ_R signal will drive the VG roll erection amplifier and torque the VG about the pitch axis. This action will move the gyro spin axis until it lines up with the VG roll pendulum along the local vertical and the signal Γ_R itself will tend to a null condition (ideally).

The first-order LP filter shown in the Γ_{RC} signal patch attempts to simulate the time response of the Γ_R signal so that the signals Γ_{RC} and Γ_R will sum to zero at the summation amplifier at all times when the ship is moving at velocity V_s and turning at rate $\dot{\psi}$.

The nonlinear gain block shown in the Γ_{RC} signal path is required to ensure that the Γ_{RC} signal does not exceed in amplitude the Γ_R signal during large turning maneuvers. Measurements on the Γ_R output signal indicate that the latter is linear with Γ_R up to about the equivalent of 1° of roll motion; for $\Gamma_R > 1^\circ$, the output starts to limit. If similar limiting were not performed on the Γ_{RC} signal, Γ_{RC} could exceed Γ_R at the summation amplifier input when $\Gamma_R > 1^\circ$ with the result that the VG roll loop will have, in effect, positive feedback with consequent instability.

If the ship is accelerating in the forward direction (Fig. 18), the instantaneous velocity V_s will be measured by the ship velocity sensor and presented to the VGMCE as a varying DC analog voltage. This voltage appears at the output of block K_L . After amplification, the signal proportional to V_s is passed through a differentiator, amplifier, and LP filter where a signal proportional to (\dot{V}_s/g) is developed. The signal proportional to (\dot{V}_s/g) is then passed through the nonlinear gain stage and then to the 400 Hz modulator. At the output of the modulator, a 400 Hz suppressed carrier

signal proportional to (\dot{V}_s/g) ($= \Gamma_{PC}$), and properly scaled, is then subtracted at the input of a unity gain summation amplifier from the signal appearing at the output of the VG pitch pendulum angle sensor (i.e., at block K_p output). The latter signal is proportional to Γ_p where $\Gamma_p = \tan^{-1} (\dot{V}_s/g)$. For $|\Gamma_p| \leq 10^\circ$, $\Gamma_p \approx \dot{V}_s/g$ with an error of about 1% or less; hence, for Γ_p angles up to 10° in magnitude the error in the subtraction process will be 1% or less. The output of the unity gain summation amplifier is then used to drive the VG pitch erection amplifier.

If the ship is accelerating in the forward direction at rate \dot{V}_s , the output of the unity gain summation amplifier will be a perfect null (ideally), and the VG will not be torqued about the roll axis. This is the desired mode of action, and the gyro will maintain its spin axis along the local vertical in the presence of the accelerating motion. On the other hand, during normal ship pitch motion with the ship moving at constant velocity (i.e., with $\dot{V}_s = 0$), the signal proportional to Γ_p will pass through the unity gain summation amplifier without change in amplitude or phase (since Γ_{PC} signal = 0). If $\Gamma_p \neq 0$ for some reason other than $\dot{V}_s/g \neq 0$, the implication is that the gyro spin axis is not vertical. In this case, the Γ_p signal will drive the VG pitch erection amplifier and torque the VG about the roll axis. This action will move the gyro spin axis until it lines up with the VG pitch pendulum axis along the local vertical and the signal Γ_p itself will tend to a null condition (ideally).

The first-order LP filter shown in the \dot{V}_s/g signal path attempts to simulate the time response of the Γ_p signal so that the signals Γ_{PC} and Γ_p will sum to zero at the summation amplifier at all times when the ship is accelerating at rate \dot{V}_s .

The nonlinear gain block shown in the Γ_{PC} signal is required to ensure that the Γ_{PC} signal does not exceed in amplitude the Γ_p signal during large accelerations \dot{V}_s . The nonlinearity is required for the same reason given for the Γ_R signal as explained above. As noted for the Γ_R signal, the Γ_p signal output is linear up to about 1° of pitch motion; beyond 1° the output starts to limit.

INSTRUMENTATION DIAGRAM DESCRIPTION

Figure 19 shows the VGMCE instrumentation diagram. Considering the $(V_s \dot{\psi}/g)$ correction signal path, the ship's yaw rate signal, at block K_G output, is passed through amplifiers K_a and K_1 and then to the x_{11} input of multiplier M1. Ship's velocity signal at block K_L output is passed through buffer amp block K_b to the y_{11} input of multiplier M1. The output of multiplier M1, E_3 , is then proportional to $(V_s \dot{\psi}/g)$ and is passed through the LP filter block so that this signal, which will ultimately be used to null the VG roll pendulum angle signal E_{OR} at the output of block K_R , will have approximately the same response time as E_{OR} . The output of the LP filter, E_4 , then drives adjustable gain amplifier K_3 . This amplifier allows the signal to be scaled properly and permits the injection of a self-test roll signal E_{TR} when testing the VGMCE system for proper operation. The output of block K_3 , E_5 , then drives the nonlinear gain amp, block K_4 , which prevents the roll pendulum correction signal E_8 from exceeding the roll pendulum angle signal E_{OR} when E_{OR} exceeds about 1° in magnitude. As indicated earlier in this section, $E_8 \leq E_{OR}$ at all times to ensure that the VG roll loop remains stable. The output of block K_4 , E_6 , then drives the 400 Hz modulator M2, which develops a suppressed carrier signal of the same form as the VG roll pendulum angle signal E_{OR} . The output of the modulator, E_7 , is then attenuated in block K_5 and the output of the latter, E_8 , is then summed with the roll pendulum angle signal, E_{OR} , at the input of the summation and unity gain buffer amp block K_6 . The output of the latter, E_9 , then represents the roll pendulum error signal that drives the VG to produce torque about the pitch axis.

The attenuator block K_5 is required because the signal level of E_{OR} is relatively small even for a VG roll pendulum angle (Γ_R) of 3° . The correction signal at node E_8 will correspondingly be small. If the attenuator were omitted, node E_7 signal level would

be the same as that at node E_8 and hence the output signal level of multiplier M2 will be small. Unfortunately the errors due to the use of a multiplier become more significant for low signal output (and input) levels. Hence, it is desirable to operate the multiplier at the highest output level without causing saturation in the unit. Therefore, to reduce the multiplier errors, the signal level at node E_6 is forced to be higher by proper adjustment of the path gain between nodes E_3 and E_6 by the inverse of the attenuation factor of block K_5 . Attenuation factor K_5 is about $(1/30)$ so that node E_6 and E_7 levels are forced to be higher by a factor of 30; this reduces the multiplier errors significantly. Increasing the signal level in this manner also forces the nonlinear gain stage, block K_4 , to operate at a higher output level and makes the errors introduced by this stage look smaller.

Considering the \dot{V}_s/g correction signal path, the ship's velocity signal at block K_L output is passed through the buffer amp block K_b and then to the input of the differentiator and LP filter block, node E_2 . The output of this block, E_{10} , is then proportional to \dot{V}_s/g with the proper time response because of the action of the LP filter. E_{10} then drives adjustable gain amplifier K_{11} . This amplifier allows the signal to be scaled properly and permits the injection of a self-test pitch signal E_{TP} when testing the VGMCE system for proper operation. The output of block K_{11} , E_{11} , then drives the nonlinear gain amp, block K_{12} , which prevents the pitch pendulum correction signal E_{14} from exceeding the pitch pendulum angle signal E_{OP} when E_{OP} exceeds about 1° in magnitude. As indicated earlier in this section, $E_{14} \leq E_{OP}$ at all times to ensure that the VG pitch loop remains stable. The output of block K_{12} , E_{12} , then drives the 400 Hz modulator that develops a suppressed carrier signal of the same form as the VG pitch pendulum angle signal, E_{OP} . The output of the modulator, E_{13} , is then attenuated in block K_{13} and the output of the latter, E_{14} , is then summed with the pitch pendulum angle signal, E_{OP} , at

the input of the summation and unity gain buffer amp block K_{14} . The output of the latter, E_{15} , then represents the pitch pendulum error signal that drives the VG to produce torque about the roll axis.

The attenuator block K_{13} serves the same purpose for the \dot{V}_S/g correction signal path with respect to errors in the multiplier M3 and limiter amp K_{12} , as attenuator block K_5 does for the $V\dot{\psi}/g$ correction signal path, as explained above.

The modulators M2 and M3 and demodulator M4 require a 400 Hz reference signal that is "phase matched" with the signals appearing at nodes E_{OR} and E_{OP} . "Phase matched" here means that the zero crossover times of the sine wave reference signal waveform should be coincident with the zero crossover of the E_{OR} and E_{OP} sine wave signals. Practically, it is not necessary to have exact matching. With respect to the modulated signals E_8 and E_{14} , ideally each signal should match in amplitude the signals E_{OR} and E_{OP} , respectively; in addition, the phases of signals E_8 and E_{14} should be 180° out of phase with signals E_{OR} and E_{OP} , respectively. If, for example, the amplitudes of E_8 and E_{OR} are identical, i.e., $|E_8| = |E_{OR}|$ but the phase of E_8 relative to E_{OR} deviates from 180° by a small angle, a nonzero error signal will be generated at node E_9 in Fig. 19. This error signal will consist of the sum of two terms at the 400 Hz carrier frequency:

- (1) A component in phase with the signal E_{OR} , and
- (2) A component in quadrature with the signal E_{OR} .

The gyro torquer will only recognize the in-phase component and hence cause the platform containing the gyro spin axis and accelerometers in the VG to move to a new angle about the roll axis such that E_{OR} changes to an amplitude that exactly cancels the in-phase component of error signal. This causes the gyro spin axis to deviate from the vertical. The magnitude of this deviation is a function of the phase shift ϕ and an estimate of the magnitude may be calculated as follows.

Let

$$E_{OR} = E_a \sin \omega t = \text{roll pend. angle signal}, \quad (122)$$

$$E_8 = E_a \sin (\omega t - \phi) = \text{roll correct. signal}, \quad (123)$$

$$\omega = 2\pi f, f = 400 \text{ Hz carrier frequency}, \quad (124)$$

$$\phi = \text{phase shift in signal } E_8, \text{ and}$$

$$E_9 = E_{OR} - E_8 = \text{error signal driving gyro torquer amplifier.} \quad (125)$$

Then

$$E_9 = E_a [\sin \omega t - \sin (\omega t - \phi)] = E_a (1 - \cos \phi) \sin \omega t + E_a \sin \phi \cos \omega t. \quad (126)$$

The in-phase component of Eq. 126 is $[E_a (1 - \cos \phi) \sin \omega t]$, and it is this component that will torque the gyro and cause E_{OR} to change by ΔE_{OR} in such a way as to null this component. If ΔE_a is the change in amplitude of E_{OR} ,

$$\Delta E_{OR} = \Delta E_a \sin \omega t = E_a (1 - \cos \phi) \sin \omega t, \quad (127)$$

$$\therefore \Delta E_a = E_a (1 - \cos \phi), \quad (128)$$

$$\text{or } \left(\frac{\Delta E_a}{E_a} \right) = 1 - \cos \phi = 2 \sin^2 \left(\frac{\phi}{2} \right) \approx \frac{\phi^2}{2}, \text{ for } \phi^2 \ll 12. \quad (129)$$

Equation 129 states that the fractional change in E_a , which is equivalent to the fractional change in the VG platform position (or gyro spin axis position) relative to the roll pendulum position, is approximately given by $\phi^2/2$ where ϕ is measured in radians. If we allow a maximum change in platform position of 0.1° around the roll axis and assume the maximum angular deviation of the roll pendulum position from the gyro spin axis, due to ship's maneuver ($V_s \dot{\psi}/g$) is 3° , then, equivalently

$$\frac{\Delta E_a}{E_a} = \frac{0.1^\circ}{3^\circ} \approx \frac{\phi^2}{2}; \text{ solving for } \phi,$$

$$\phi = 0.258 \text{ rad or } 14.8^\circ.$$

Thus, a phase shift of approximately 15° can be tolerated without incurring a movement of the gyro spin axis from the local vertical of more than 0.1° , assuming the ship's maneuver does not cause the roll pendulum angle to be more than 3° from the local vertical. A similar statement may be made concerning the phase shift of E_{14} relative to E_{OP} in Fig. 19 for the pitch pendulum angle signal.

If we assume a maximum ship's acceleration \dot{V}_s of 15 kt/min ($= 0.422 \text{ ft/s}^2 = 0.0131 \text{ g}$), the maximum pitch pendulum angle due to \dot{V}_s becomes $\approx \frac{\dot{V}_s}{g} = 0.0131 \text{ rad or } 0.75^\circ$. Again, allowing for a maximum platform error around the pitch axis of 0.10° maximum, $\frac{\psi^2}{2} \approx \frac{0.10}{0.75}$, and $\psi = 0.52 \text{ rad or } 29.6^\circ$. In this case we can tolerate a much larger phase shift in E_{14} relative to E_{OP} without creating a movement of the gyro spin axis around the pitch axis from the local vertical in excess of 0.10° . Hence the phase shift requirement for the pitch pendulum signal channel is not as severe as that for the roll pendulum signal channel.

Since the phases of signals E_8 and E_{14} are controlled by the phase of 400 Hz reference signal E_{R2} driving the multipliers M2 and M3 in Fig. 19, E_{R2} is provided with a phase adjustment. E_{R2} is developed from the 115 V, 400 Hz reference power, the same power source for the roll and pitch pendulum angle transducers. Isolation transformer K_T permits isolation of 115 V, 400 Hz power ground from the VGMCE system ground. The isolation transformer output then drives a fixed phase shift network, block K_7 , with a phase shift of approximately -45° . The output of the latter then drives an adjustable phase shift, constant gain amplifier block K_8 with a phase shift adjustment capable of ranging between 0 and -180° (the actual adjustment range is less). The latter, when

added to the -45° fixed phase shift, yields an overall phase adjustment capability of between -45° and -225° . The nominal phase setting at the output of the adjustable phase shift amplifier should be -90° so that block K_8 should be set for approximately -45° nominally. The output of K_8 then drives an adjustable gain amplifier block K_9 . The gain of the latter is adjusted to yield the design level for E_{R2} , which is 7.07 Vrms when the line voltage is 115 Vrms.

It is possible that the phase difference between signals E_{OR} and E_{OP} is not zero in general so that the phase setting of the reference E_{R2} must be chosen as a compromise. It is not likely that the phase difference will exceed 30° so that in the worst case the phase of E_{R2} can be set either midway between the actual phases of E_{OR} and E_{OP} or slightly closer to E_R than to E_{OP} without causing a VG platform error exceeding 0.1° around either the roll or pitch axes. Actual gyro test data shows that the two pendulum phases are matched to better than 5° .

Multiplier M_4 is used as a demodulator for signal readout on a panel meter. The demodulator output is proportional to $\cos \varphi$, where φ is the phase shift between the reference signal E_{R2} and the particular signal being read out. If the phase correction in E_{R2} is such that the phase of E_{R2} is midway between the phases of signals E_{OR} and E_{OP} then φ will be identical in magnitude for both E_{OR} and E_{OP} measurements and the error in the measurement of either will be identical, assuming the meter is calibrated to read correctly for $\varphi = 0^\circ$. Signals E_8 and E_{14} will be read correctly on the meter since these signals are always exactly in phase (or exactly 180° out of phase) with the reference. If $|\varphi| \leq 15^\circ$, the maximum error in reading E_{OR} or E_{OP} will be $\leq 3.4\%$ ($= 1 - \cos \varphi$). The errors in reading the pitch and roll error signals E_9 and E_{15} will be much larger on a percentage basis of the error signal since the error signals (if any) during transient conditions are much less than the signals E_{OR} and E_{OP} . However, the magnitude of the error in degrees will be small since the error signal itself is small. In the worst case, the magnitude of the error in the measurement of the error signal will not exceed 0.12° when measuring an error signal caused by a roll pendulum angle of 3° when that angle deviates from the roll correction angle by 0.3° during a transient condition for a reference phase shift angle of 15° ($\approx \varphi$).

The output of the signal readout demodulator drives a passive low pass (LP) filter containing a meter scaling network (block K_{15}). The LP filter removes the carrier frequency ripple components at the output of the demodulator and allows the DC component to pass through to the readout meter. The scaling network in the filter circuit permits adjustment of the full-scale meter reading.

The entire system is run on the 115 V, 400 Hz prime power that is also used to supply the multiplier reference voltages. Power for all amplifiers and multipliers is derived from ± 15 VDC supplies driven by the 115 V, 400 Hz line.

CHANNEL GAIN CALCULATIONS AND ASSIGNMENT OF BLOCK GAINS

With reference to the instrumentation diagram shown in Fig. 19, this section will concern itself with the calculation of channel gains and the assignment of block gains.

Generation of Γ_{RC} Compensation Signal

Consider the $\dot{\psi}$ and V_s path gains to node E_8 where the signal at node E_8 is combined with E_{OR} , the signal from the VG roll pendulum angle transducer. In evaluating these path gains, the filter time constant τ_1 need not be considered, it being assumed that the response time for the Γ_R signal is matched by the generated $V_s \dot{\psi}/g$ signal via the filter time constant τ_1 . Also block K_4 is assumed to operate in the small signal region where the gain is linear. Thus

$$E_1 = x_{11} = \dot{\psi} K_G K_a K_1, \quad (130)$$

$$E_2 = y_{11} = V_s K_L K_b, \quad (131)$$

$$E_3 = K_{M1} x_{11} y_{11} = K_{M1} (\dot{\psi} K_G K_a K_1) (V_s K_L K_b), \quad (132)$$

$$E_6 = x_{12} = K_2 K_3 K_4 K_3 = (K_2 K_3 K_4) K_{M1} (K_G K_a K_1) (K_L K_b) (V_s \dot{\psi}), \quad (133)$$

$$E_{R1} = E_b \sin \omega t \quad (134)$$

where

$$E_b = \text{amplitude of 115 Vrms reference sine wave} \\ = 115 \sqrt{2} V, \text{ nominally,}$$

$$E_{R2} = y_{12} = K_T K_7 K_8 K_9 E_{R1} \angle \alpha = K_T K_7 K_8 K_9 E_b \sin (\omega t + \alpha) \quad (135)$$

where

α = phase shift due to phase shift networks in blocks K_7 and K_8 ,

$$\alpha = \alpha_1 + \alpha_2; \alpha_1 \approx -45^\circ; 0 \leq \alpha_2 \leq -180^\circ; -45^\circ \leq \alpha \leq -225^\circ,$$

$$E_7 = K_{M2} x_{12} y_{12} \\ = K_{M2} (K_2 K_3 K_4) K_{M1} (K_G K_{a1}) (K_L K_b) (K_T K_7 K_8 K_9) E_b (V_s \dot{\psi}) \sin (\omega t + \alpha), \quad (136)$$

$$E_8 = K_5 E_7 \\ = K_5 K_{M2} (K_2 K_3 K_4) K_{M1} (K_G K_{a1}) (K_L K_b) (K_T K_7 K_8 K_9) E_b (V_s \dot{\psi}) \sin (\omega t + \alpha), \quad (137)$$

$$E_{OR} = K_R \Gamma_R E_{R1} \angle \beta = K_R \Gamma_R E_b \sin (\omega t + \beta) \\ = K_R \left(\frac{V_s \dot{\psi}}{g} \right) E_b \sin (\omega t + \beta), \quad (138)$$

where

β = phase shift in VG roll pendulum angle transducer

$$\Gamma_R = \tan^{-1} \left(\frac{V_s \dot{\psi}}{g} \right) \approx \frac{V_s \dot{\psi}}{g}.$$

We require for compensation during a turning maneuver

$$E_{OR} - E_8 = 0 \quad (139)$$

Substituting Eqs. 137 and 138 into 139, we obtain

$$\begin{aligned} & K_R \left(\frac{V_s \dot{\psi}}{g} \right) E_b \sin(\omega t + \beta) \\ & - K_5 K_{M2} (K_2 K_3 K_4) K_{M1} (K_G K_a K_1) (K_L K_b) (K_T K_7 K_8 K_9) E_b (V_s \dot{\psi}) \sin(\omega t + \alpha) = 0. \end{aligned} \quad (140)$$

To produce the desired cancellation of signals, the phase shift α in the reference channel should be adjusted to equal phase shift β . For this condition, Eq. 140 reduces to

$$(K_R/g) = (K_G K_a K_1) (K_L K_b) (K_T K_7 K_8 K_9) (K_2 K_3 K_4 K_5) (K_{M1} K_{M2}) . \quad (141)$$

The factor $(K_T K_7 K_8 K_9)$ is chosen such that $|E_{R2}| = 7.07$ Vrms when $|E_{R1}| = 115$ Vrms so that

$$(K_T K_7 K_8 K_9) = (7.07/115) = 0.0615 \text{ Vrms/Vrms}. \quad (142)$$

This choice permits the multipliers M1, M2, M3, and M4 to operate at optimum conditions (by making the y_{11} , y_{12} , y_{13} , and y_{14} inputs as large as feasible without overload). Note that the compensation system is independent of the amplitude of the reference voltage, E_b .

The isolation transformer K_T (Fig. 19) is a UTC H-5 having a stepdown turns ratio of 0.397. The output of this transformer drives block K_7 , which further attenuates the signal while shifting its phase approximately -45° . The attenuation factor of block

K_7 has been set at 0.0692 so that the signal reaching the input of block K_8 is 115 Vrms $(0.397)(0.0692) = 3.16$ Vrms. This signal level is conveniently handled by block K_8 , which merely shifts the phase of the signal in the 0 to -180° range without affecting the amplitude. Hence, the output of block K_8 is also 3.16 Vrms. To develop 7.07 Vrms at the output of adjustable gain amplifier block K_9 , the latter should be adjusted for a nominal gain of

$$K_9 = \frac{7.07 \text{ Vrms}}{3.16 \text{ Vrms}} = 2.24 \text{ Vrms/Vrms} . \quad (143)$$

The following signal scale factors were given:

$$K_G = 57.3 \text{ V/(rad/s)} = 1.00 \text{ VDC/(deg/s)} \text{ (nominally)} , \quad (144)$$

$$K_L = 0.100 \text{ V/kt} = 0.0592 \text{ VDC/(ft/s)} \text{ (nominally)} , \quad (145)$$

$$K_R = 10.0 \text{ Vrms/rad} = 0.1745 \text{ Vrms/deg} \text{ (nominally)} . \quad (146)$$

Also, the multiplier gains K_{M1} and K_{M2} taken from the manufacturer's data are

$$K_{M1} = 0.100 \text{ VDC/(VDC}\times\text{VDC)} , \quad (147)$$

$$K_{M2} = 0.100 \text{ Vrms/(VDC}\times\text{Vrms)} . \quad (148)$$

Gain K_b is chosen such that at maximum ship's speed of 100 kt, E_2 in Fig. 19 will be 10 VDC. This ensures that the y_1 input of multiplier M1 does not exceed the maximum allowable input while providing the maximum possible input to the multiplier to improve its accuracy. Since the output of block K_L is 10.0 VDC for $V_s = 100$ kt, it follows that

$$K_b = 1.00 \text{ VDC/VDC} . \quad (149)$$

Gain ($K_a K_1$) is chosen such that at maximum ship's yaw rate of 10 deg/s, E_1 in Fig. 19 will be 10 VDC. This ensures that the x_{11} input of multiplier M1 does not exceed the maximum allowable input while providing the maximum possible input to the multiplier to improve its accuracy. Since the output of block K_G is 10.0 VDC nominally for $\dot{\psi} = 10$ deg/s, it follows that

$$K_a K_1 = 1.00 \text{ VDC/VDC nominally (where the sign of } K_a K_1, \text{ which is negative, is not considered here).} \quad (150)$$

In the actual circuitry, $K_a = 1.00$ VDC/VDC nominally, while $K_1 = 1.00$ VDC/VDC (again, not considering the sign of K_1 , which is negative). However, K_a is made adjustable to absorb the tolerances in K_G and K_L scale factors and in the other blocks in the $\dot{\psi}$ and V_s paths to node E_4 in Fig. 19. It is desired to make the voltage at node E_4 equal to the roll test signal voltage corresponding to $\frac{V_s \dot{\psi}}{g} = 0.50^\circ$ for system calibration purposes. Since the roll test signal will be standardized at a voltage corresponding to $\theta_R = 0.50^\circ$, assuming K_R has its nominal scale factor, K_a must be adjusted to yield this standardized voltage at node E_4 when $\frac{V_s \dot{\psi}}{g} = 0.50^\circ$. To absorb the tolerance in scale factor K_R itself, K_3 is provided with an adjustable gain as explained below.

K_3 , the adjustable gain amplifier in Fig. 19, is made adjustable to compensate for tolerances in K_R (the Γ_R scale factor) and in the gain constants K_4 , K_{M2} , and K_5 . However, the most significant tolerance is that for K_R . For a given ship's yaw rate $\dot{\psi}$ and velocity V_s , the VG roll pendulum angle Γ_R will be $\tan^{-1} \left(\frac{V_s \dot{\psi}}{g} \right) \approx \frac{V_s \dot{\psi}}{g}$ for $|\Gamma_R| \leq 10^\circ$. However, because of the scale factor tolerances, the output of block K_R may be in the range of 10.0 ± 2.5 Vrms/rad; i.e., the scale factor may have a tolerance as much as $\pm 25\%$.

For a nominal K_R scale factor of 10.0 Vrms/rad or 0.1745 Vrms/deg, a VG roll pendulum angle of 0.50° would yield a transducer output 0.08725 Vrms at node E_{OR} , Fig. 19. To achieve a null at the input of block K_6 , node E_8 must also be 0.08725 Vrms and in phase opposition to E_{OR} . If $K_5 = 1.00$ Vrms/Vrms, node E_7 voltage would also be 0.08725 Vrms, a value that is too low since the errors caused by the multiplier M2 would be significant. Hence it is desirable to raise the level of node E_7 voltage to reduce the importance of multiplier M2 errors. For this purpose, precision resistive attenuator K_5 is inserted between nodes E_7 and E_8 , forcing node voltage E_7 to be higher by the inverse of the attenuation factor. This attenuation factor was chosen to be (nominally)

$$K_5 = 0.03213 \text{ Vrms/Vrms} . \quad (151)$$

Hence node E_7 voltage becomes $\left(\frac{0.08725}{0.03213} \right) = 2.715$ Vrms when $\Gamma_R = 0.50^\circ$, with K_R at its nominal scale factor (0.1745 Vrms/deg). Since $E_{R2} = 7.07$ Vrms (see above) and $K_{M2} = 0.100$ Vrms/(VDC-Vrms), it follows that node E_6 voltage must be nominally $\frac{2.715 \text{ Vrms (VDC-Vrms)}}{0.100 \text{ Vrms (7.07 Vrms)}} = 3.840$ VDC. This voltage is large enough to permit operation of the multiplier M2 with reasonably small errors and small enough to allow the limiter amplifier, K_4 , to operate at nominal equivalent

output angles as high as $(10.0 \text{ VDC}/3.840 \text{ VDC}) \times 0.50^\circ = 1.30^\circ$, if K_4 were linear out to its maximum output voltage capability of 10.0 VDC in magnitude. However, K_4 will be designed to limit before 10.0 VDC output so that its output voltage capability will never be exceeded. K_4 linear gain was nominally chosen as follows:

$$K_4 = \frac{1}{K_5} = 31.12 \text{ VDC/VDC (nominally and not considering the sign of } K_4, \text{ which is negative).} \quad (152)$$

Note that K_4 was chosen to be the inverse of the attenuation factor. For $\Gamma_R = 0.50^\circ$, K_R at its nominal scale factor, the signal level at node E_5 is then $\frac{3.840 \text{ VDC}}{31.12} = 0.1234 \text{ VDC}$.

Adjustable gain amplifier K_3 was designed to sum the roll test signal voltage E_{TR} and node E_4 voltage with equal weight. Nominally, its gain to both signals was adjusted to be

$$K_3 = 1.00 \text{ VDC/VDC (nominally and not considering the sign of } K_3, \text{ which is negative).} \quad (153)$$

For K_3 at its nominal value corresponding to K_R being at its nominal value, it follows that node E_4 voltage and the roll test signal voltage E_{TR} should each be 0.1234 VDC. Since the nominal values of K_G , K_L , K_a , K_b , K_1 , K_{M1} are known (see above), the nominal value of K_2 may be evaluated as follows:

$$(K_G K_a K_1)(K_L K_b) K_{M1} K_2 (V_s \dot{\psi}) = E_4, \quad (154)$$

where it is known that, when $\Gamma_R = 0.50^\circ$ with K_R , K_5 , K_{M2} , E_{R2} , K_4 , and K_3 at their nominal values, $E_4 = 0.1234 \text{ VDC}$. Also note that

$$\text{when } \Gamma_R = \left(\frac{V_s \dot{\psi}}{g} \right) = 0.50^\circ, \left(V_s \dot{\psi} \right) \text{ must be, with } g = 32.2 \text{ ft/s}^2:$$

$$(V_s \dot{\psi}) = \Gamma_R g = \frac{0.50^\circ \text{ rad}(32.2 \text{ ft})}{57.3^\circ \text{ s}^2} = 0.2810 \text{ ft/s}^2. \quad (155)$$

Substituting the value of $(V_s \dot{\psi})$ from Eq. 155 and the known nominal gain constants and the value of E_4 for $\Gamma_R = 0.50^\circ$ into Eq. 154 and solving for K_2 we obtain

$$K_2 = \frac{0.1234 \text{ VDC} \times \text{rad} \times \text{VDC} \times \text{ft} \times \text{VDC} \times \text{VDC} \times \text{VDC} \times \text{s}^2}{57.3 \text{ VDC/s}(1.00 \text{ VDC})(0.0592 \text{ VDC/s}) \times 1.00 \text{ VDC} \times 0.100 \text{ VDC}(0.2810 \text{ ft})} =$$

$$1.295 \text{ VDC/VDC (nominally)}. \quad (156)$$

Any tolerances on constants K_G , K_a , K_L , K_b , K_{M1} , and K_2 may be absorbed by adjusting K_a to yield $E_4 = 0.1234 \text{ VDC} = E_{TR}$ when the $(V_s \dot{\psi})$ product, for a known ship's speed and turning rate, equals 0.2810 ft/s^2 in accordance with Eq. 155. If K_G and K_L are known for a particular ship, a more convenient way of setting the gain K_a would be to simulate the voltage outputs of K_G and K_L for assumed V_s and $\dot{\psi}$ values, subject to the condition that the particular values chosen for V_s and $\dot{\psi}$ satisfy Eq. 155. Then, these voltages could be injected into the respective amplifiers K_a and K_b , and K_a would then be adjusted to yield $E_4 = 0.1234 \text{ VDC}$.

Summarizing the design thus far we have the following constants including their correct signs:

$$K_G = 1.00 \text{ V/(deg/s)}; K_L = 0.0592 \text{ VDC/(ft/s)};$$

$$K_R = 0.1745 \text{ Vrms/deg};$$

$$K_a = 1.00 \text{ VDC/VDC}; K_1 = -1.00 \text{ VDC/VDC}; K_b = 1.00 \text{ VDC/VDC};$$

$$K_{M1} = 0.100 \text{ VDC/(VDC-VDC)}; K_2 = -1.295 \text{ VDC/VDC};$$

$$K_3 = -1.00 \text{ VDC/VDC};$$

$$K_4 = -31.12 \text{ VDC/VDC}; K_{M2} = 0.100 \text{ Vrms/(VDC-Vrms)};$$

$$K_5 = 0.03213 \text{ Vrms/Vrms}$$

$$K_T = 0.397 \angle 0^\circ \text{ Vrms/Vrms}; K_7 = 0.0692 \angle -45^\circ \text{ Vrms/Vrms};$$

$$K_8 = 1.00 \angle \alpha_2 \text{ Vrms/Vrms}, 0 \leq \alpha_2 \leq -180^\circ; \text{ and}$$

$$K_9 = 2.24 \angle 0^\circ \text{ Vrms/Vrms}.$$

The time constant τ_1 in the LP filter in Fig. 19 should be chosen to match the open loop response time of the VG Γ_R output for the particular VG chosen. At the time of this report, two gyros were available having equivalent first-order time constants of 8 and 27 s. To permit use of either gyro, a selector switch is provided within the equipment for choosing either time constant.

The signs of the gains of the various blocks were established in the following manner for the roll pendulum correction circuitry. From measurements of one of the vertical gyros, it was determined that the roll pendulum signal E_{OR} leads the 400 Hz reference E_{R1} by approximately 90° when V_s signal voltage is positive (\rightarrow ship forward velocity) and $\dot{\psi}$ signal voltage is positive (\rightarrow the ship turning to the right). Hence, if we assume that the signals E_8 and E_{OR} in Fig. 19 are resistively added at the same K_6 amplifier input node, then E_8 must have a phase 180° from E_{OR} in order to null E_{OR} . Therefore E_8 should lag the 400 Hz reference E_{R1} by approximately 90° . Since K_5 is a resistive attenuator, E_7 must be in phase with E_8 and should lag E_{R1} by 90° . If input E_6 to multiplier M2 is positive, E_7 will be in phase with E_{R2} and E_{R2} should therefore lag E_{R1} by approximately 90° . The amplifier blocks in the $\dot{\psi}$ and V_s channels were designed such that positive output signals from blocks K_L and K_G (\rightarrow ship forward velocity V_s and ship turning to the right at rate $\dot{\psi}$, respectively) would yield a positive signal for E_6 . Hence the design of the reference channel blocks from K_T input (E_{R1}) to K_9 output (E_{R2}) must be such that E_{R2} lags E_{R1} by approximately 90° . As noted previously, the reference channel is provided with an adjustable phase shift capability so that E_{R2} phase may be adjusted about the 90° lag angle, relative to E_{R1} , to make the phase of E_8 exactly 180° relative to E_{OR} phase for proper cancellation of signals.

To establish that E_6 will be positive when K_G and K_L outputs are both positive, note that K_a and K_b are both positive gains. However, K_1 is a negative gain so that E_1 is negative while E_2 is positive. K_{M1} is a positive gain so that E_3 must be negative for negative input E_1 and positive input E_2 to multiplier M1. Since K_2 is a negative gain, E_4 must be positive for a negative input E_3 . K_3 is a negative gain so that E_5 must be negative for a positive input E_4 . Finally, K_4 is a negative gain so that E_6 must be positive as required for a negative input E_5 .

Generation of Γ_{PC} Compensation Signal

Now consider the V_s path gain to node E_{14} where the signal at node E_{14} is combined with E_{OP} , the signal from the VG pitch pendulum angle transducer. Again, as in the case for Γ_{RC} compensation signal, the time constant τ_2 need not be considered when evaluating the path gain since it is assumed that the response time for the Γ_p signal is matched by the generated \dot{V}_s/g signal via the filter time constant τ_2 . Also, block K_{12} is assumed to operate in the small signal region where the gain is linear. Thus:

$$\begin{aligned} E_{12} = x_{13} &= V_s (K_L K_b) (K_{10} s) (K_{11} K_{12}) = (V_s s) (K_L K_b) (K_{10} K_{11} K_{12}) \\ &= \dot{V}_s (K_L K_b) (K_{10} K_{11} K_{12}) \end{aligned} \quad (157)$$

where

$$V_s s = \dot{V}_s ;$$

$$E_{R2} = y_{13} = (K_T K_7 K_8 K_9) E_b \sin (\omega t + \alpha) \quad (\text{see Eq. 135}) \quad (158)$$

where

$$\alpha = \alpha_1 + \alpha_2; \alpha_1 \approx -45^\circ; 0 \leq \alpha_2 \leq -180^\circ; -45^\circ \leq \alpha \leq -225^\circ;$$

$$E_{13} = K_{M3} x_{13} y_{13} = K_{M3} \dot{V}_s (K_L K_b) (K_{10} K_{11} K_{12}) (K_T K_7 K_8 K_9) E_b \sin (\omega t + \alpha); \quad (159)$$

$$\begin{aligned} E_{14} &= K_{13} E_{13} \\ &= K_{13} K_{M3} (K_L K_b) (K_{10} K_{11} K_{12}) (K_T K_7 K_8 K_9) E_b (\dot{V}_s) \sin (\omega t + \alpha); \text{ and} \end{aligned} \quad (160)$$

$$\begin{aligned} E_{OP} &= K_P \Gamma_P E_{R1} \angle \gamma = K_P \Gamma_P E_b \sin (\omega t + \gamma) \\ &= K_P \left(\frac{\dot{V}_s}{g} \right) E_b \sin (\omega t + \gamma) \end{aligned} \quad (161)$$

where

γ = phase shift in VG pitch pendulum angle transducer

$$\Gamma_P = \tan^{-1} \left(\frac{\dot{V}_s}{g} \right) \approx \frac{\dot{V}_s}{g} \text{ for } |\Gamma_P| \leq 10^\circ$$

$$E_{R1} = E_b (\sin (\omega t + \gamma) \text{ from Eq. 134.})$$

For compensation during a forward ship acceleration we require

$$E_{OP} - E_{14} = 0 \quad (162)$$

Substituting Eqs. 160 and 161 into 162 we obtain

$$K_P \left(\frac{\dot{V}_s}{g} \right) E_b \sin(\omega t + \gamma) - (K_L K_b)(K_T K_7 K_8 K_9)(K_{10} K_{11} K_{12} K_{13}) K_{M3} E_b \dot{V}_s \sin(\omega t + \alpha) = 0 \quad (163)$$

To produce the desired cancellation of signals, the phase shift α in the reference channel should be adjusted to equal the phase shift γ . Ideally, phase shift γ in the VG pitch pendulum transducer and phase shift β in the VG roll pendulum transducer would be identical so that one adjustment of phase shift α ($=\beta$) in the reference channel will be correct for both pitch and roll compensation signals. Practically, however, this will not be so and measurement errors (discussed above) will be introduced. If we assume, nevertheless, that $\alpha=\gamma$, then Eq. 163 reduces to

$$(K_P/g) = (K_L K_b)(K_T K_7 K_8 K_9)(K_{10} K_{11} K_{12} K_{13}) K_{M3} \quad (164)$$

The factor $(K_T K_7 K_8 K_9)$ has been chosen and is given by Eq. 142. This choice permits optimum operation of multiplier M3. Note that the compensation system is independent of the reference voltage amplitude E_b . The Γ_P signal scale factor, K_P , is given as follows:

$$K_P = 10.0 \text{ Vrms/rad} = 0.1745 \text{ Vrms/deg (nominally)} \quad (165)$$

The multiplier gain K_{M3} taken from the manufacturer's data is

$$K_{M3} = 0.100 \text{ Vrms/(VDC-Vrms)} \quad (166)$$

K_L and K_b are given by Eqs. 145 and 149, respectively.

K_{11} , the adjustable gain amplifier in Fig. 19, is made adjustable to compensate for tolerances in K_P (the Γ_P scale factor) and in the gain constants K_{12} , K_{M3} , and K_{13} . The most significant

tolerance however is that for K_p . For a given ship's forward acceleration \dot{V}_s , the VG pitch pendulum angle Γ_p will be $\tan^{-1}\left(\frac{\dot{V}_s}{g}\right) \approx \frac{\dot{V}_s}{g}$ for $|\Gamma_p| \leq 10^\circ$. Because of the scale factor tolerance, the output of block K_p may be in the range 10.0 ± 2.5 Vrms/rad corresponding to a $\pm 25\%$ tolerance about the nominal value.

For a nominal K_p scale factor of 10.0 Vrms/rad or 0.1745 Vrms/deg, a VG pitch pendulum angle of 0.50° would yield a transducer output of 0.08725 Vrms at node E_{OP} , Fig. 19. To achieve a null at the input of block K_{14} , node E_{14} voltage must also be 0.08725 Vrms and in phase opposition to E_{OP} . If $K_{13} = 1.00$ Vrms/Vrms, node E_{13} voltage would also be 0.08725 Vrms, a value that is too low for the output of multiplier M3 relative to the latter's error. Hence, just as in the case for the roll pendulum correction channel, it is desirable to raise the level of E_{13} voltage to reduce the importance of the multiplier errors. For this purpose precision resistive attenuator K_{13} is inserted between nodes E_{13} and E_{14} , forcing node voltage E_{13} to be higher by the inverse of the attenuation factor. This attenuation factor was chosen to be

$$K_{13} = 0.03213 \text{ Vrms/Vrms} . \quad (167)$$

For this value of K_{13} , node E_{13} voltage becomes $\left(\frac{0.08725}{0.03213}\right) = 2.715$ Vrms when $\Gamma_p = 0.50^\circ$, with K_p at its nominal value of 0.1745 Vrms/deg. Since $E_{R2} = 7.07$ Vrms as discussed in the section for the Γ_R compensation signal and $K_{M3} = 0.100$ Vrms/(VDC-Vrms), it follows that node E_{12} voltage must be nominally $\frac{2.715 \text{ Vrms}(\text{VDC-Vrms})}{0.100 \text{ Vrms}(7.07 \text{ Vrms})} = 3.840$ VDC. This voltage is sufficiently large to permit multiplier M3 operation with reasonably small errors and sufficiently small to allow the limiter amplifier, K_{12} , to operate at nominal equivalent output angles as high as $(10.0 \text{ VDC}/3.840 \text{ VDC}) \times 0.50^\circ = 1.30^\circ$, if

K_{12} were linear out to its maximum output voltage capability of 10.0 VDC in magnitude. However, K_{12} will be designed to limit before 10.0 VDC output so that its output voltage capability will never be exceeded. K_{12} linear gain was nominally chosen as follows:

$$K_{12} = \frac{1}{K_{13}} = 31.12 \text{ VDC/VDC (nominally and disregarding the sign of } K_{12}, \text{ which is negative).} \quad (168)$$

Note that K_{12} value was chosen to be the inverse of the attenuation factor. For $\Gamma_p = 0.50^\circ$, K_p at its nominal scale factor, the signal level at node E_{11} is then $\frac{3.840 \text{ VDC}}{31.12} = 0.1234 \text{ VDC}$.

Adjustable gain amplifier K_{11} was designed to sum the pitch test signal voltage E_{TP} and node E_{10} voltage with equal weight. Nominally its gain to both signals was adjusted to be

$$K_{11} = 1.00 \text{ VDC/VDC (nominally and not considering the sign of } K_{11}, \text{ which is negative).} \quad (169)$$

For K_{11} at its nominal value, corresponding to K_p being at its nominal value, it follows that node E_{10} voltage and the pitch test signal voltage E_{TP} should each be 0.1234 VDC. Since the nominal values of K_L and K_b are known (see Eqs. 145 and 149, respectively), the nominal value of K_{10} may be evaluated as follows:

$$K_L K_b K_{10} [sV_s] = K_L K_b K_{10} \dot{V}_s = E_{10}, \quad (170)$$

where it is known that when $\Gamma_p = 0.50^\circ$ with K_L and K_b at their nominal values, $E_{10} = 0.1234 \text{ VDC}$. Also, $\frac{\dot{V}_s}{g} = \Gamma_p = 0.50^\circ$, so that \dot{V}_s must be with $g = 32.2 \text{ ft/s}^2$:

$$\dot{V}_s = \Gamma_P g = \frac{0.50^\circ \text{ rad } (32.2 \text{ ft})}{57.3^\circ \text{ s}^2} = 0.2810 \text{ ft/s}^2. \quad (171)$$

Substituting the known values into Eq. 170 and solving for K_{10} , we have

$$K_{10} = \frac{0.1234 \text{ VDC ft} \times \text{VDC} \times \text{s}^2}{0.0592 \text{ VDC s} \times 1.00 \text{ VDC} \times 0.2810 \text{ ft}} = 7.42 \text{ VDC}/(\text{VDC} \times (\text{rad/s})). \quad (172)$$

Any tolerances on constants K_L , K_b , and K_{10} may be absorbed by adjusting K_b to yield $E_{10} = 0.1234 \text{ VDC} = E_{TP}$ when $\dot{V}_s/g = 0.2810 \text{ ft/s}^2$. If K_L is known for a particular ship, a more convenient way of setting the gain K_b would be to simulate the voltage output of K_L for an assumed \dot{V}_s value of 0.2810 ft/s^2 . This voltage could be injected into amplifier K_b and K_b would then be adjusted to yield $E_{10} = 0.1234 \text{ VDC}$.

Note that the adjustment of gain K_b affects both of the $V_s \dot{\psi}/g (= \Gamma_P)$ and $\dot{V}_s/g (= \Gamma_P)$ path gains. Since K_a may be adjusted to compensate for the $V_s \dot{\psi}/g$ path gain tolerance, K_b should be adjusted first to compensate for \dot{V}_s/g path gain tolerances. Then, K_a may be adjusted to compensate for $V_s \dot{\psi}/g$ path gain tolerances after K_b has been set.

Summarizing the design thus far, we have the following constants including their correct signs:

$$K_L = 0.0592 \text{ VDC}/(\text{ft/s}); K_P = 0.1745 \text{ Vrms/deg};$$

$$K_b = 1.00 \text{ VDC/VDC};$$

$$K_{10} = -7.42 \text{ VDC}/[\text{VDC} \times (\text{rad/s})]; K_{11} = -1.00 \text{ VDC/VDC};$$

$$K_{12} = -31.12 \text{ VDC/VDC};$$

$$K_{M3} = 0.100 \text{ Vrms}/(\text{VDC-Vrms}); K_{13} = 0.03213 \text{ Vrms/Vrms}.$$

The time constant τ_2 in the LP filter in Fig. 19 should be chosen to match the open loop response time of the VG Γ_p output for the particular VG chosen. As indicated in the Γ_R section of this report, the two gyros available have equivalent first-order time constants of 8 and 27 s. To permit use of either gyro, a selector switch is provided for choosing either time constant.

The signs of the gains of the various blocks were established in the following manner for the pitch pendulum correction circuitry. The sign of K_b has been established to satisfy the requirements in the Γ_R correction circuitry. Hence, the signs of the other blocks in the Γ_p correction circuitry must be consistent with this choice of sign for K_b . From measurements on one of the vertical gyros, it was determined that the pitch pendulum signal E_{OP} lags the 400 Hz reference E_{R1} by approximately 90° when V_s signal voltage is positive and increasing (\rightarrow ship's forward acceleration). Hence if we assume that the signals E_{14} and E_{OP} in Fig. 19 are resistively added at the same K_{14} amplifier input node, then E_{14} must have a phase 180° from E_{OP} in order to null E_{OP} . Therefore E_{14} should lead the 400 Hz reference E_{R1} by approximately 90° . Since K_{13} is a resistive attenuator, E_{13} must be in phase with E_{14} and should lead E_{R1} by approximately 90° . If input E_{12} to multiplier M3 is positive, E_{13} will be in phase with E_{R2} . E_{R2} however lags E_{R1} by approximately 90° , as noted in the Γ_R correction circuitry design; hence E_{13} must lag E_{R1} by approximately 90° , for E_{12} positive. Since E_{13} must lead E_{R1} by approximately 90° , it follows that E_{12} must be negative. The amplifier blocks in the Γ_p correction circuitry from K_L output to K_{12} output were designed to yield a negative signal for E_{12} when the ship accelerates in the forward direction. For a ship acceleration in the forward direction, K_L output is positive and increasing. K_b is a positive gain and hence its output is positive and increasing. The differentiator block $K_{10}s/(\tau_2s+1)$ has an output sign reversal so that its output would be negative for a positive increasing input signal from K_b output.

K_{11} has a negative gain so that its output is positive for a negative input from the differentiator block output. Finally, K_{12} has a negative gain so that its output, which is E_{12} , is negative for a positive input from K_{11} output. Hence E_{12} is negative as required for E_{14} to null E_{OP} at the input of block K_{14} .

DESCRIPTION OF Γ_P AND Γ_R CORRECTION CIRCUITS

Reference Channel Blocks K_T , K_7 , K_8 , K_9 in Fig. 19

Figure A12-1 is a schematic of the GCU 400 Hz reference generator. This figure shows the circuit diagrams for the blocks K_T , K_7 , K_8 , and K_9 of Fig. 19, the instrumentation diagram. The transformer block shown in Fig. 19 is the UTC H-5 transformer shown on Fig. A12-1; however, this transformer is actually shown on "Chassis Wiring Diagram, Gyro Compensation Unit", Fig. B-2-1, and is redrawn on Fig. A12-1 for reference purposes only.

The UTC H-5 transformer in Fig. A12-1 is block K_T in Fig. 19. It has a primary-to-secondary impedance ratio of $95K \Omega / 15K \Omega$, or a corresponding voltage or turns ratio of $\sqrt{\frac{95K}{15K}} = 2.517 \text{ Vrms/Vrms}$. The secondary voltage is therefore $\frac{1}{2.517} = 0.397$ times the primary voltage; i.e., gain $K_T = 0.397 \text{ Vrms/Vrms}$ with 0° phase shift. The voltage E_a in Fig. A12-1 is then attenuated and phase shifted by the $15K-1.62K-0.27 \text{ MFG}$ network. For the indicated transfer function, node E_1 voltage becomes for 115 Vrms, 400 Hz reference supply voltage E_{R1} : $E_1 = 115 (0.397 \angle 0^\circ) (0.0692 \angle -44.8^\circ) = 3.16 \angle -44.8^\circ \text{ Vrms}$; i.e., $K_7 = 0.0692 \angle -44.8^\circ \text{ Vrms/Vrms}$ at 400 Hz.

The adjustable phase shift amplifier (Fig. A12-1) has unity gain but has a phase adjustment (α_2) ranging between 0 and -127° . Hence, the output signal E_{01} will have the same magnitude as the input E_1 but of different phase. If P_1 were made infinite or very high in value, the phase shift could be adjusted out to -180° . However, since only approximately -45° phase shift is required for this

stage, P_1 is limited to $100K \Omega$ to yield reasonable resolution in the adjustment of α_2 . The 30 pF capacitors connected to the LM108AH amplifier are required for high-frequency stabilization of the amplifier. They do not affect the 400 Hz transfer function significantly.

The adjustable gain amplifier (Fig. A12-1) is required to absorb the tolerance of components in the circuits for K_T , K_7 , and K_8 , such that when $E_{R1} = 115 \text{ Vrms}$, $E_{R2} = 7.07 \text{ Vrms}$ $\angle \alpha_2 - 44.8^\circ$ with $0 \leq \alpha_2 \leq -127^\circ$. Since E_{01} , the input to this amplifier, is nominally 3.16 Vrms, to obtain an output of 7.07 Vrms, the amplifier should have a gain of $\frac{7.07}{3.16} = 2.24 \text{ Vrms/Vrms}$. For this nominal gain, the potentiometer P_2 would be set at $25.9K \Omega$. The gain may be set anywhere in the range 1.67 to 2.77 Vrms/Vrms to compensate for any circuit component tolerances, so that $E_{R2} = 7.07 \text{ Vrms}$ when $E_{R1} = 115 \text{ Vrms}$. Again, the 30 pF capacitors used in this amplifier are for high-frequency stabilization of the amplifier and in no way affect the transfer function at 400 Hz.

$\dot{\psi}$ and V_s Channel Blocks K_G , K_a , K_1 , $M1$, K_L , and K_b in Fig. 19

Figure A13-1 is a schematic of the GCU V_s and $\dot{\psi}$ signal condition blocks K_G , K_a , K_1 , $M1$, K_L , and K_b of Fig. 19.

Considering the $\dot{\psi}$ channel in Fig. A13-1, the input scale factor K_G is given as $1.00 \text{ VDC}/(\text{deg/s})$. The adjustable gain amplifier, K_a , is to have a nominal DC and low-frequency gain of 1.00 VDC/VDC ; for this gain, the potentiometer P_2 should be set to $262K$. The gain may be set anywhere in the range 0.84 to 1.53 VDC/VDC to compensate for any scale factor tolerance on K_G and any circuit component tolerances. Potentiometer P_2 will also compensate for the gain tolerances on amplifier K_1 , the multiplier $M1$, and low-pass filter $\left(\frac{K_2}{\tau_1 s + 1}\right)$ blocks in Fig. 19, so that the DC signal reaching node E_4 in Fig. 19 equals the calibrated value of roll test signal E_{TR} when $(V_s \dot{\psi}/g) = 0.50^\circ$. This adjustment is explained in Note 6 for Fig. A13-1.

Potentiometer P_1 is a DC offset control for setting the net offset voltage at node E_{04} , the output of multiplier M1, to 0.000 ± 0.005 VDC with V_s at its maximum value of 100 kt and $\dot{\psi} = 0.0$ deg/s after potentiometer P_5 has been adjusted, as noted in multiplier M1 description below. At node E_{04} , a 0.005 VDC offset amounts to a Γ_R measurement error of approximately 0.026° when the ship is moving at maximum forward velocity of 100 kt. At a slower forward velocity the Γ_R measurement error will be proportionately less due to offset in the $\dot{\psi}$ path.

The 0.01 MFD capacitor connected between pins 2 and 6 of the LM108AH DCOA ensures high-frequency stability of the DCOA without significantly affecting the DC and low-frequency response in the $\dot{\psi}$ signal path.

The K_1 amplifier stage has a fixed gain of -1.00 VDC/VDC at DC and low frequencies, and this gain is determined by the R_5 - R_6 resistor network. The tolerance in this gain is better than $\pm 2\%$ and may be absorbed by adjusting potentiometer P_2 in the K_a adjustable gain amplifier stage. The 0.47 MFD capacitor connected between pins 2 and 6 of the LM108AH DCOA ensures high-frequency stability of the DCOA without significantly affecting the DC and low-frequency response in the $\dot{\psi}$ signal path. Any output DC offset at node E_{02} due to the amplifier in this stage and in the previous stage may be nulled by potentiometer P_1 as explained above. The changes in DC offset at node E_{02} caused by the K_a and K_1 amplifier stages due to temperature changes of $\pm 10^\circ\text{C}$ are negligible.

Considering the V_s channel in Fig. A13-1, the input scale factor K_L is given as 0.100 VDC/kt or 0.0592 VDC/(ft/s). The adjustable gain amplifier K_b is to have a nominal DC and low-frequency gain of 1.00 VDC/VDC; for this gain, the potentiometer P_4 should be set to 125K. The gain may be set anywhere in the range 0.75 to 1.25 VDC/VDC to compensate for any scale factor tolerance on K_L and any circuit component tolerances. Assuming the gain potentiometer P_4 has been properly adjusted to yield the equivalent of 0.0592 VDC/(ft/s) at node E_{03} , gain potentiometer P_2 in the $\dot{\psi}$ channel will

be used to compensate for its own circuit tolerances and gain tolerances of blocks in the $\dot{\psi}$ path leading to node E_4 in Fig. 19 as explained above.

Potentiometer P_3 in Fig. A13-1 is a DC offset control for setting the net offset voltage at node E_{04} , the output of multiplier M1, to 0.000 ± 0.005 VDC with $\dot{\psi}$ at its maximum value of $10^\circ/\text{s}$ and $V_s = 0.0$ kt, after potentiometer P_5 has been adjusted, as noted in the multiplier M1 description below. At node E_{04} , a 0.005 VDC offset amounts to a Γ_R measurement error of approximately 0.026° when the ship is turning at a maximum rate of $10.0^\circ/\text{s}$. At a slower turning rate, the Γ_R measurement error will be proportionately less due to offset in the V_s path. Changes in the output DC offset in stage K_b due to $\pm 10^\circ\text{C}$ temperature changes are negligible.

The 0.027 MFD capacitor connected between pins 2 and 6 of the LM108AH DCOA ensures high-frequency stability of the DCOA without significantly affecting the DC and low-frequency response in the V_s signal path.

The multiplier M1 is an Analog Devices model AD534J that has a nominal transfer function given by $E_{04} = 0.100 (E_{02} \times E_{03})$. The scale factor 0.100 VDC/(VDC-VDC) has a tolerance of $\pm 0.25\%$ that introduces negligible error. This tolerance along with other gain tolerances in the $\dot{\psi}$ path, however, may be absorbed by gain potentiometer P_2 adjustment, as noted above. The scale factor temperature coefficient is $\pm 0.02\%/^\circ\text{C}$, and, for a $\pm 10^\circ\text{C}$ environment, this error source may be neglected.

The feedthrough errors for the x and y channels of multiplier M1 are given as $\pm 0.3\%$ and $\pm 0.01\%$, respectively. For this reason, the V_s path signal should be applied to the y channel. In the absence of a turning rate $\dot{\psi}$ but for a ship speed of maximum 100 kt, the signal level at the x channel input would be 0.0 VDC while the signal level at the y input would be 10.0 VDC. The multiplier output at node E_{04} could then be in error by ± 0.001 VDC ($= \pm 0.01\% \times 10.0$ VDC) due to feedthrough. This translates into an error in Γ_R generation of $\pm 0.0052^\circ$, which is very small and may be neglected. This error would be 30 times larger if the V_s path signal were applied to the x channel input instead of the y channel input.

If the ship is moving at maximum velocity ($V_s = 100$ kt) and is turning at maximum rate ($\dot{\psi} = 10^\circ/\text{s}$) (assuming it were possible to achieve this rate at $V_s = 100$ kt), an error is introduced at the output of the multiplier M1 due to its nonlinearity of $\pm 0.4\%$. The multiplier output would ideally be 10.0 VDC, which corresponds to $\Gamma_R = 52.5^\circ$; due to nonlinearity the error in Γ_R would be $\pm 0.21^\circ$ ($= \pm 0.4\% \times 52.5^\circ$). The nonlinearity error however will be much smaller in general since, if $V_s = 100$ kt and $\dot{\psi} = 10^\circ/\text{s}$, the ship would be asked to produce a 0.92 g maneuver, an acceleration that is not likely. For $V_s = 100$ kt, $\dot{\psi}$ will more likely not exceed $1.09^\circ/\text{s}$ ($\rightarrow 0.10$ g maneuver) and the nonlinearity error in Γ_R generation is not likely to exceed $\pm 0.023^\circ$, which is small.

The input offsets of the x and y multiplier channels may be effectively nulled by means of potentiometers P_1 and P_3 , using the procedures outlined in Notes 5 and 7 in Fig. A13-1, while the output offset of the multiplier M1 may be nulled by potentiometer P_5 . Changes in the input offsets due to temperature are a maximum of $100 \mu\text{V}/^\circ\text{C}$ and for a $\pm 10^\circ\text{C}$ environment would yield a maximum change of ± 1 MV. In the $\dot{\psi}$ channel this would be equivalent to a maximum error in the generation of Γ_R of $\pm 0.0052^\circ$, assuming V_s is at its maximum of 100 kt; this is a negligible error. In the V_s channel a ± 1 MV multiplier input offset change is equivalent to a maximum error in the generation of Γ_R of $\pm 0.0052^\circ$, assuming $\dot{\psi}$ is at its maximum of $10^\circ/\text{s}$; this is a negligible error. Changes in the multiplier output offset due to temperature are a maximum of $200 \mu\text{V}/^\circ\text{C}$: for a $\pm 10^\circ\text{C}$ environment, the output offset could be a maximum of ± 2 MV (at node E_{04} in Fig. A13-1). This is equivalent to an error in Γ_R generation of $\pm 0.010^\circ$, a negligible error.

Potentiometer P_5 may be used to null any significant net offsets at the output of the LP filter block, $(K_2/(\tau_1 s + 1))$ in Fig. 19. If the null at this point is within ± 2.5 MV, the equivalent Γ_R error is only 0.01° . This adjustment should take precedence over the multiplier output null adjustment.

$V_s \dot{\psi}$ Channel Blocks $K_2/(\tau_1 s + 1)$, K_3 , and K_4 in Fig. 19

Figure A14-1 is a schematic of the GCU ($V_s \dot{\psi}$) blocks $K_2/(\tau_1 s + 1)$, K_3 , and K_4 of Fig. 19.

The multiplied signal E_3 of Fig. 19 becomes the input to the $K_2/(\tau_1 s + 1)$ LP filter block and is signal E_1 in Fig. A14-1. The filter time constant τ_1 is determined by the $R_2 C_1$ product and C_1 is selected by means of a chassis mounted switch, i.e., either node 5 or 6 will be connected to node 4 by means of the switch. The time constants that may be selected are 8 and 27 s, which match those of the two vertical gyros available for tests. Note that the capacitors C_1 also guarantee high-frequency stability of the LM108AH DCOA.

K_2 DC gain should be nominally -1.295 and is actually -1.296 in Fig. A14-1. The adjustable gain amplifier, K_a in Fig. 19, is capable of absorbing any tolerance in K_2 DC gain as noted above. The DC offset at the output node E_{01} of the LM108AH DCOA (Fig. A14-1) is nominally 0.0 MV at 25°C. However it may take on any value between +3.2 and -3.2 MV; this is equivalent to a Γ_R error of $\pm 0.013^\circ$, which is negligible. This offset, however, may be nulled to within ± 2.5 MV ($\rightarrow \Gamma_R$ error of $\pm 0.01^\circ$) if desired by adjusting potentiometer P_5 in the multiplier M1 circuit of Fig. A13-1. For $\pm 10^\circ\text{C}$ temperature changes, the DC offset at node E_{01} in Fig. A14-1 should not change by more than ± 0.4 MV, which corresponds to a Γ_R error of less than 0.002° — a negligible error.

Adjustable gain amplifier K_3 (Fig. A14-1) has a DC and low-frequency gain set by the $-(R_4/R_{3a})$ resistance ratio. For a nominal gain of -1.00, potentiometer P_1 would be set to 25K Ω . Potentiometer P_1 however will be set to compensate for the tolerance in the small signal gain of the succeeding nonlinear gain amplifier, K_4 in Fig. 19 and Fig. A14-1, and for any gain tolerances in the multiplier M2, attenuator K_5 , and scale factor K_R for the VG roll pendulum angle transducer in Fig. 19.

The output DC offset of K_3 stage in Fig. A14-1 should not exceed 1 MV at 25°C, and this corresponds to a negligible Γ_R error ($< 0.005^\circ$). Changes in the output DC offset for $\pm 10^\circ\text{C}$ temperature changes are less than 1 MV and hence are negligible.

The roll VG channel may be conveniently checked by injecting a DC signal into the K_3 amplifier, which represents the equivalent of $+0.50^\circ$ or -0.50° of roll pendulum angle deflection. The circuit for doing this is shown in Fig. A14-1 and is shown for reference purposes only since it is not contained on Card No. 14. In Fig. A14-1, if the roll/pitch select switch is in the "roll" position and if the PB switch is pressed and held, either a -123 MVDC or +123 MVDC signal is applied to R_{3b} as an input to the K_3 adjustable gain amplifier. These signals represent either -0.50° or $+0.50^\circ$, respectively, in Γ_R units. This signal will pass through blocks K_3 , K_4 , M_2 , K_5 , and K_6 of Fig. 19 to the input of the roll erection amplifier, which will torque the gyro about its pitch axis. The gyro then torques the platform about the roll axis causing the platform to tilt about the roll axis in accordance with the roll axis closed-loop dynamics. Ultimately the roll angle pendulum will reach an angle of 0.50° in a direction such as to generate a signal E_{OR} (Fig. 19), which nulls the signal E_g caused by the test signal E_{TR} injected into Block K_3 . When this occurs, the torquing of the gyro and the platform will cease. Thus a +123 MVDC test signal (E_{TR} in Fig. 19) will cause the VG platform to tilt in a direction equivalent to the tilt that the pendulum would undergo if there was a positive turning rate $\dot{\psi}$ (i.e., turning to the right) when the ship is going at forward velocity V_s . The amount of the latter pendulum tilt would be $+0.50^\circ$.

The stability of the ± 123 MVDC source, which is mainly a function of the temperature coefficient of the 1N704A zener diodes (Fig. A14-1), should be better than 0.5% for a $\pm 10^\circ\text{C}$ temperature environment and $\pm 1\%$ regulated supplies ($\pm 15\text{V}$).

The 0.1 MFD capacitor connected between pins 2 and 6 of the K_3 amplifier (Fig. A14-1) is used for high-frequency stability of the LM108AH DCOA. It does not affect the DC and low-frequency response of K_3 amplifier.

In Fig. A14-1, the nonlinear gain amplifier (limiter) stage K_4 has a linear DC and low-frequency small signal nominal gain of -30.1 given by the $-(R_6/R_5)$ resistance ratio. Nominal gain for this stage should be -31.12; the deviation from the desired gain may be compensated for by adjustment of potentiometer P_1 of K_3 stage.

When the output signal level magnitude increases and reaches 5.8 VDC, soft limiting via the FD300 feedback diodes D_1 and D_2 in the output starts. This is equivalent to $(\pm 5.8 \text{ V}/30.1) = \pm 0.193 \text{ VDC}$ at K_4 input, which is equivalent to $\pm 0.78^\circ$ of Γ_R nominally. As the signal output magnitude increases and reaches about 7.0 VDC, hard limiting sets in via the FD300 feedback diodes D_3 and D_4 . This is equivalent to K_4 input of $\pm 0.35 \text{ VDC}$, which is equivalent to $\pm 1.4^\circ$ of Γ_R . Figure 20 is a plot of E_{03} versus E_{02} where E_{03} and E_{02} refer to Fig. A14-1. This plot has been translated into equivalent $(-E_g)$ signal in Fig. 19 as a function of the input tilt angle generated by the VGMCS and is shown in Fig. 21. Also shown in Fig. 21 for comparison purposes is a plot of the vertical gyro roll pendulum transducer output, E_{OR} , versus tilt angle for SN193 vertical gyro, which was tested in the laboratory. From 0° up to about $\pm 0.6^\circ$ of tilt angle, the match between $-E_g$ and E_{OR} is fairly good, and we would expect almost perfect cancellation of E_{OR} by E_g at block K_6 (Fig. 19) assuming the phase of signal E_g has been properly corrected and the system time constants are matched. Above about $\pm 0.9^\circ$, the E_g output magnitude is generally less than E_{OR} , which is the desired mode of operation. For tilt angles between about ± 0.6 and $\pm 0.9^\circ$, the VGMCE overcompensates undesirably. However, by reducing block K_3 gain slightly, much of the overcompensation may be eliminated at a slight sacrifice in the accuracy of compensation in the 0 to $\pm 0.6^\circ$ tilt angle range.

In Fig. A14-1, the FD300 diodes are a very low leakage type, and are required because of the high impedance level ($10 \text{ M}\Omega = R_6$) at which the amplifier operates when not in the limiting region. The output DC offset at node E_{03} due to the diode leakage current ($< 2(10^{-9})$ amperes for each diode for a $\pm 10^\circ$ environment and the LM108AH DCOA should not exceed 75 MVDC. This is equivalent to a Γ_R angle error of not more than 0.01° , which is negligible.

The actual stage transfer function contains a low-pass filter with a 0.010 s time constant; this filter has an insignificant effect on the system since the latter time constant is insignificant compared to the system time constant set by R_2 and C_1 in the LP filter stage of Fig. A14-1.

As in previous stages, the 30 pF capacitor in the nonlinear gain stage (Fig. A13-1) is required for high-frequency stability of the LM108AH DCOA.

$V_s \psi$ Channel Blocks M_2 , K_5 , K_6 , and K_R in Fig. 19

Figure A16-1 is a schematic of GCU ($V_s \psi$) blocks M_2 , K_5 , K_6 in Fig. 19. Block K_R in Fig. 19 represents the roll pendulum angle transducer scale factor with a nominal value of 10.0 Vrms/rad. The output of this transducer appears at pin 6 of the connector in Fig. A16-1.

The output of the nonlinear gain amplifier K_4 , E_6 in Fig. 19, appears as E_1 at pin 1 of the connector in Fig. A16-1 and drives the multiplier M2 X_1 input. The other input to the multiplier is E_{R2} at Y_1 input and is the 7.07 Vrms 400 Hz reference. The multiplier is an Analog Devices model AD534J and is used as a modulator that produces a suppressed carrier output waveform at node E_{01} , Fig. A16-1. It has a nominal transfer function given by $E_{01} = 0.100 (E_1 E_{R2})$. The scale factor 0.100 Vrms/(Vdc \times Vrms) has a tolerance of $\pm 0.25\%$, which introduces negligible error; however, if desired, this tolerance may be absorbed by adjustment of gain K_3 in the adjustable gain amplifier of Fig. 19. The scale factor temperature coefficient of $\pm 0.02\%/^{\circ}\text{C}$ for a $\pm 10^{\circ}\text{C}$ environment yields negligible error.

The feedthrough errors for the x and y channels of multiplier M2 are given as $\pm 0.3\%$ and $\pm 0.01\%$, respectively. To minimize feedthrough errors the 7.07 Vrms, 400 Hz reference signal (E_{R2}) should be fed to the y input of M2. In the absence of a roll pendulum signal (E_1 , Fig. A16-1), the output E_{01} will not exceed $\pm 0.01\%$ (7.07 Vrms) = 0.7 MVRms. At node E_{01} the scaling is $\approx 0.19^{\circ}/\text{Vrms}$ so that the 0.7 MVRms feedthrough signal represents a negligible error of 0.00013 $^{\circ}$.

The equivalent input offset of multiplier M2 x channel should not exceed 6 MV in magnitude including a $\pm 10^\circ\text{C}$ temperature environment. This translates into an equivalent Γ_R measurement error of 0.00081° for a node E_1 (Fig. A16-1) scaling of $\approx 0.135^\circ/\text{VDC}$; this is a negligible error.

The signal at node E_{01} (Fig. A16-1) is a suppressed carrier 400 Hz type, the amplitude of which is proportional to signal E_1 at multiplier M2 input. It contains a small DC offset due to the multiplier output circuit. The offset may be nulled via adjustment of potentiometer P_3 ; however, since the offset does not affect the modulated signal per se, it should be unnecessary to null it. The only reason for performing the null operation would be to ensure that the DC offset reaching node E_{03} (Fig. A16-1) that connects to the VG roll erection amplifier input via the relay K_1 contacts is small. Depending on relay K_1 contact position, the roll erection amplifier normally receives a low-level 400 Hz signal either from the roll pendulum transducer output (output of Block K_R in Fig. 19) or from the output of the summation and unity gain buffer amplifier (block K_6 in Fig. 19), which is node E_{03} in Fig. A16-1. It is not known whether this amplifier can tolerate a comparatively large DC level at node E_{03} so it is wise to reduce this level to a value much lower than the maximum AC input signal level handled by the roll erection amplifier. It is likely that this amplifier can handle signal levels corresponding to $\Gamma_R \approx 0.50^\circ$ or about 87 MVrms; hence the DC offset at node E_{03} should probably be held below 10 MV. At node E_a (Fig. A16-1) the DC offset due to the multiplier output should preferably not exceed 5 MV (which would yield a 5 MV output offset at node E_{03} - half the maximum preferred of 10 MV). At node E_{01} the corresponding multiplier DC offset output could therefore be as high as $(5 \text{ MV}/0.03113) = 161 \text{ MVDC}$, where 0.03113 is the attenuation factor of the $R_1 - R_2$ attenuator network. Since the multiplier output DC offset is not expected to exceed 40 MV due to all environments (including $\pm 10^\circ\text{C}$ temperature changes), it is hardly necessary to adjust potentiometer P_3 at all (pin 6 of multiplier M2 could be grounded without any detrimental effect).

The attenuator K_5 shown in Fig. A16-1 is a resistive network consisting of R_1 and R_2 and has an attenuation factor of $K_5 = 0.03113$. This network is then followed by the summation and unity gain buffer amplifier. This is a unity gain differential amplifier with positive gain to both signals E_a (which is E_8 in Fig. 19) and E_{OR} (which is the VG roll pendulum angle signal). The contacts on relay K_1 (Fig. A16-1) connect the output of the VG roll pendulum transducer (E_{OR}) to this amplifier through the summing resistor R_4 . Signal E_a connects to the other summing resistor R_3 . The net DC and low-frequency gain is unity to each signal. The 75 and 30 pF capacitors are required for high-frequency stability of the LM108AH DCOA and do not significantly affect the amplitude and phase response to 400 Hz signals E_a and E_{OR} .

Relay K_1 is used to route the roll pendulum pickoff signal either directly to the roll erection amplifier (when the VGMCU is not in use) or to the summation and unity gain buffer amplifier (when the VGMCU is in use) via a front panel switch (not shown in Fig. A16-1).

(\dot{V}_s/g) Channel Blocks ($K_{10}s/(\tau_2 s + 1)$, K_{11} , and K_{12} in Fig. 19)

Figure A15-1 is a schematic of the GCU (\dot{V}_s/g) path blocks $K_{10}s/(\tau_2 s + 1)$, K_{11} , and K_{12} of Fig. 19.

The ship's velocity signal E_2 of Fig. 19 becomes the input to the $K_{10}s/(\tau_2 s + 1)$ differentiator and LP filter block and is signal E_1 in Fig. A15-1. The differentiation is accomplished via capacitance C_1 ($= C_{1a}$ or C_{1b}) and resistance R_2 ($= R_{2a}$ or R_{2b}) in Fig. A15-1. The LP filter time constant is established by the $R_1 C_1$ ($= R_1 C_{1a}$ or $R_1 C_{1b}$) product. R_2 and C_1 are selected by means of a chassis-mounted switch. R_2 must be changed whenever C_1 is changed in order to keep gain K_a constant ($= K_{10}$ in Fig. 19). The LP filter time constants that may be selected are 8 and 27 s, the latter time constants match those of the two vertical gyros available for tests. Capacitance C_2 (Fig. A15-1) ensures high-frequency stability of the LM108AH DCOA.

K_a gain (Fig. A15-1) should be $-7.42 \text{ VDC}/(\text{VDC} \times \text{rad/s})$ and is very close to the desired value. The DC offset at the output node E_{01} of the LM108AH DCOA is nominally 0.0 MV at 25°C . However it may take on any value between +20 MV and -20 MV (worst case limits); this is equivalent to a Γ_p error of $\pm 0.08^\circ$, which may be considered negligible. These offset values include a $\pm 10^\circ\text{C}$ temperature environment.

Adjustable gain amplifier K_{11} (Fig. A15-1) is similar to adjustable gain amplifier K_3 , which was discussed above and the same comments made with respect to K_3 apply to K_{11} . Testing of the pitch VG channel may be conveniently checked in the same way that the roll VG channel was tested as discussed above except that the roll/pitch test switch would be placed in the "pitch" position. In this case, the test signal passes through blocks K_{11} , K_{12} , M_3 , K_{13} , and K_{14} of Fig. 19 to the input of the pitch erection amplifier, which will torque the gyro about its roll axis. The gyro then torques the platform about the pitch axis causing the platform to tilt about the pitch axis in accordance with the pitch axis closed loop dynamics. Ultimately, the pitch pendulum angle will reach an angle of 0.50° in a direction such as to generate a signal E_{OP} (Fig. 19), which nulls the signal E_{14} caused by the test signal E_{TP} injected into Block K_{11} . When this occurs, the torquing of the gyro and the platform will cease.

In Fig. A15-1 the nonlinear gain amplifier (limiter) stage K_{12} is identical in design to block K_4 in Fig. 19, which has been discussed above. The comments with respect to the design for block K_4 apply to block K_{12} .

\dot{V}_s/g Channel Blocks M_3 , K_{13} , K_{14} , and K_p in Fig. 19

Figure A16-1 is a schematic of GCU (\dot{V}_s/g) blocks M_3 , K_{13} , K_{14} in Fig. 19. Block K_p in Fig. 19 represents the pitch pendulum angle transducer scale factor with a nominal value of 10.0 Vrms/rad . The output of this transducer appears at pin 9 of the connector in Fig. A16-1.

The output of the nonlinear gain amplifier K_{12} , E_{12} in Fig. 19, appears as E_2 at pin 2 of the connector in Fig. A16-1 and drives the multiplier M3 X_1 input. The other input to the multiplier is E_{R2} at Y_1 input and is the 7.07 Vrms 400 Hz reference. The multiplier is an Analog Devices model AD534J and is used as a modulator that produces a suppressed carrier output waveform at node E_{02} , Fig. A16-1. It has a nominal transfer function given by $E_{02} = 0.100 (E_2 E_{R2})$. The scale factor 0.100 Vrms/(VDC \times Vrms) has a tolerance of $\pm 0.25\%$, which introduces negligible error; however, if desired, this tolerance may be absorbed by adjustment of gain K_{11} in the adjustable gain amplifier of Fig. 19. The scale factor temperature coefficient of $\pm 0.02\%/^{\circ}\text{C}$ for a $\pm 10^{\circ}\text{C}$ environment yields negligible error. The other errors in this multiplier are similar to those for multiplier M2 in Fig. A16-1 and have been discussed above.

The offset null potentiometer P_2 in Fig. A16-1 is similar in function to potentiometer P_3 in Fig. A16-1, which has been discussed above.

The attenuator K_{13} in Fig. 19 is the resistive network consisting of R_7 and R_8 in Fig. A16-1 and has an attenuation factor of $K_{13} = 0.03113$. This network is followed by the summation and unity gain buffer amplifier. This is a unity gain differential amplifier with positive gain to both signals E_b (which is E_{14} in Fig. 19) and E_{OP} (which is the VG pitch pendulum angle signal). The contacts on relay K_2 (Fig. A16-1) connect the output of the VG pitch pendulum transducer (E_{OP}) to this amplifier through the summing resistor R_{10} . Signal E_b connects to the other summing resistor R_9 . The net DC and low-frequency gain is unity to each signal. The 75 pF and 30 pF capacitors are required for high-frequency stability of the LM108AH DCOA and do not significantly affect the amplitude and phase response to 400 Hz signals E_b and E_{OP} .

As in the case for relay K_1 with respect to the roll pendulum pickoff signal discussed above, relay K_2 routes the pitch pendulum pickoff signal either directly to the pitch erection amplifier (when the VGCU is not in use) or to the summation and unity gain buffer amplifier (when the VGCU is in use) via a front panel switch (not shown in Fig. A16-1).

Signal Readout Meter Channel Blocks M4, K₁₅, and M in Fig. 19

Figure A16-1 is a schematic of the GCU meter channel blocks M4 and K₁₅ in Fig. 19. The readout meter M in Fig. 19 is not shown in Fig. A16-1 since it is mounted on the front panel. Meter M is a zero centered 100-0-100 μ A meter calibrated to read $\pm 2.0^\circ$ full scale. A front panel tilt angle switch not shown in Fig. A16-1 selects any of the following seven signals for meter readout (the switch wiper is connected to pin 17 of the connector shown in Fig. A16-1):

1. Pitch pendulum error (connector pin 13, Fig. A16-1),
2. Pitch pendulum correction (connector pin 12, Fig. A16-1),
3. Pitch pendulum angle (connector pin 9, Fig. A16-1),
4. Roll pendulum error (connector pin 11, Fig. A16-1),
5. Roll pendulum correction (connector pin 8, Fig. A16-1),
6. Roll pendulum angle (connector pin 6, Fig. A16-1), and
7. OFF (connector pin 3, Fig. A16-1). In this position the multiplier M4 input X₁ is grounded.

Multiplier M4 is operated as a demodulator (Fig. A16-1) that uses E_{R2}, the 7.07 Vrms 400 Hz reference, for demodulation of any of the pitch and roll signals selected by the tilt angle selector switch. For proper operation of the VGMCE, the phase of each of the selected signals should be either in phase or 180° out of phase with the 400 Hz reference signal E_{R2} as explained in the Instrumentation Diagram Description.

The output of the demodulator, E_{O5}, is as follows:

Let:

$$E_s = E_{sM} \sin (\omega_c t + \varphi)$$

$$E_{R2} = E_{R2M} \sin \omega_c t$$

$$K_{M4} = \text{multiplier scale factor}$$

where

$$\varphi = 0^\circ \text{ or } 180^\circ$$

$$\omega_c = \text{reference angular frequency}$$

$$= 2\pi f_c, f_c = 400 \text{ Hz}$$

E_{sM} and E_{R2M} are peak values or amplitudes of respective sine waves.

Then

$$E_{05} = K_{M4} E_s E_{R2} = K_{M4} E_{sM} E_{R2M} \sin(\omega_c t + \varphi) \sin \omega_c t \quad (173)$$

or

$$E_{05} = \frac{K_{M4} E_{sM} E_{R2M}}{2} [\cos \phi - \cos(2\omega_c t + \varphi)], \quad (174)$$

= DC component + second harmonic component.

The DC component of E_{05} , denoted by $E_{05}(\text{DC})$, will be read by the DC meter M in Fig. 19. The other component of E_{05} is the second harmonic of the reference frequency, which will be 800 Hz. The latter will be filtered by the capacitor C_1 in Fig. A16-1. Thus

$$E_{05}(\text{DC}) = \frac{K_{M4} E_{sM} E_{R2M}}{2} \cos \varphi, \text{ with } \varphi = 0^\circ \text{ or } 180^\circ. \quad (175)$$

If $\phi = 0^\circ$, $E_{05}(\text{DC})$ will be positive; if $\varphi = 180^\circ$, $E_{05}(\text{DC})$ becomes negative. Hence the phase of the signal relative to the reference determines the sign of the DC output. The scale factor of the output is then (where I_M is the meter DC current)

$$K_{15} = \frac{I_M}{E_{sM}} = \frac{[E_{05}(\text{DC})/R_{13}]}{E_{sM}} = \frac{K_{M4} E_{R2M}}{2R_{13}} \text{ A/VPk} \quad (176)$$

where R_{13} is the total meter circuit resistance (Fig. A16-1). If we desire $I_0 = 100 (10^{-6})$ A full scale for Γ_p or Γ_R angle of 2° , we note that the Γ_p or Γ_R pendulum pickoff has a nominal scale factor of 10.0 Vrms/rad or 0.1745 Vrms/deg so that the pickoff signal amplitude corresponding to 2° would be 0.349 Vrms. Thus, the value of R_{13} in Eq. 176 may be computed as follows:

$$R_{13} = \frac{K_{M4} E_{sM} E_{R2M}}{2 I_M} \quad (177)$$

where

$$K_{M4} = 0.100 \text{ VPk}/(\text{VPk} \times \text{VPk}) \quad (\text{VPk} = \text{peak voltage}),$$

$$E_{sM} = 0.3490 \times \sqrt{2} = 0.494 \text{ VPk} = \text{peak value of signal corresponding to } 2^\circ \text{ of pickoff deflection},$$

$$E_{R2M} = 7.07 \times \sqrt{2} = 10.0 \text{ VPk} = \text{peak value of 400 Hz reference signal } E_{R2},$$

$$I_M = 100 (10^{-6}) \text{ A} = \text{desired full scale meter reading for } 2^\circ \text{ of pickoff deflection, and}$$

$$R_{13} = \frac{0.100 \text{ VPk} (0.494 \text{ VPk}) (10.0 \text{ VPk})}{\text{VPk} \times \text{VPk} (2) (100) 10^{-6} \text{ A}} = 2.47 \text{K } \Omega .$$

Nominally, therefore, the potentiometer P_1 should be set to $2470 - (750 + 750 + 465) = 505 \Omega$ (Fig. A16-1), where 465 Ω is the approximate DCR of the readout meter M, so that the total resistance R_{13} would be 2.47K Ω . For a particular VG, however, the roll or pitch pendulum scale factor may be 0.1745 Vrms/deg $\pm 25\%$; hence P_1 should be adjusted to compensate for the actual tolerance on the scale factor.

Filtering of the second harmonic current from the meter M is accomplished with the capacitor C_1 . The actual meter current is given by

$$I_M = \left(\frac{E_{05}}{R_{13}} \right) \left(\frac{1}{\tau_a s + 1} \right) \text{ in Fig. A16-1}$$

where

$$\tau_a = \left(\frac{R_{14} R_{15}}{R_{14} + R_{15}} \right) C_1 .$$

For the nominal values of R_{14} , R_{15} , and C_1 , $\tau_a = \left(\frac{750(1720)}{750 + 1720} \right) \times (10)10^{-6} = 5.22 (10^{-3})$ s. Thus at 800 Hz the second harmonic currents in the meter will be attenuated by a factor of $\approx 2\pi(2f_c)\tau_a = 2\pi(800)(5.22)10^{-3} = 26.2$.

The DC output offset of the multiplier M4 typically should not exceed 10 MV including the effects of a $\pm 10^\circ\text{C}$ temperature environment. Hence the equivalent meter error due to this offset typically should not exceed 0.04° , which is negligible. If desired a DC offset null control circuit similar to that for multiplier M2 may be connected to the Z_2 node of multiplier M4 so that the offset may be nulled.

REFERENCES

1. E. Robinson, "Radar Altimeters for Surface Effect Ships," APL/JHU F1B78U-006A, Jan 1978.
2. E. Robinson, "Performance of Radio Altimeters for Point Source Reflectors," APL/JHU F1B78U-060, May 1978.
3. T. M. Rankin, "Operator's Manual, Surface Effect Ship Wave Profiling System," APL/JHU SES 023, Jul 1978.
4. T. M. Rankin, "Vertical Gyro Performance on a High-Speed Surface Effect Ship," APL/JHU SES 024, Nov 1978.
5. "Development Program Proposal, Wave Profiler for the Surface Effect Ship," APL/JHU Lett. CQO-1959, 22 Apr 1977.
6. "Group Analysis Report for SES-100A, Group XI Test Series," Maritime Dynamics, Inc., MDR Report No. 1048-46, Oct 1976.
7. "Group Analysis Report for SES-100A Group X Test Series," Maritime Dynamics, Inc., MDR Report No. 1044-21, Dec 1975, and Ref. 6 above.
8. "Wave Height Sensor Requirement/Specification," PMS 304-20A.1/FNS, Ser. 4064, 14 Jun 1977.
9. "SES-100A Wave Height Sensor Performance Requirements," Maritime Dynamics Inc., MDR Report No. 1049-53, Mar 1977.
10. H. Goldstein, Classical Mechanics, Addison-Wesley, 1950.
11. J. B. L. Rao and S. K. Meads, "Analysis of Attitude Errors Arising from Area Target Returns in FM Altimeters," NRL Report No. 3714, Feb. 1978.
12. H. L. Donnelly and J. F. George, "The Surface Effect Ship Operational Environment and Its Effect on Installed Weapons and Supporting Equipment, Phase I, Final Report," APL/JHU SES 004, Jun 1973.

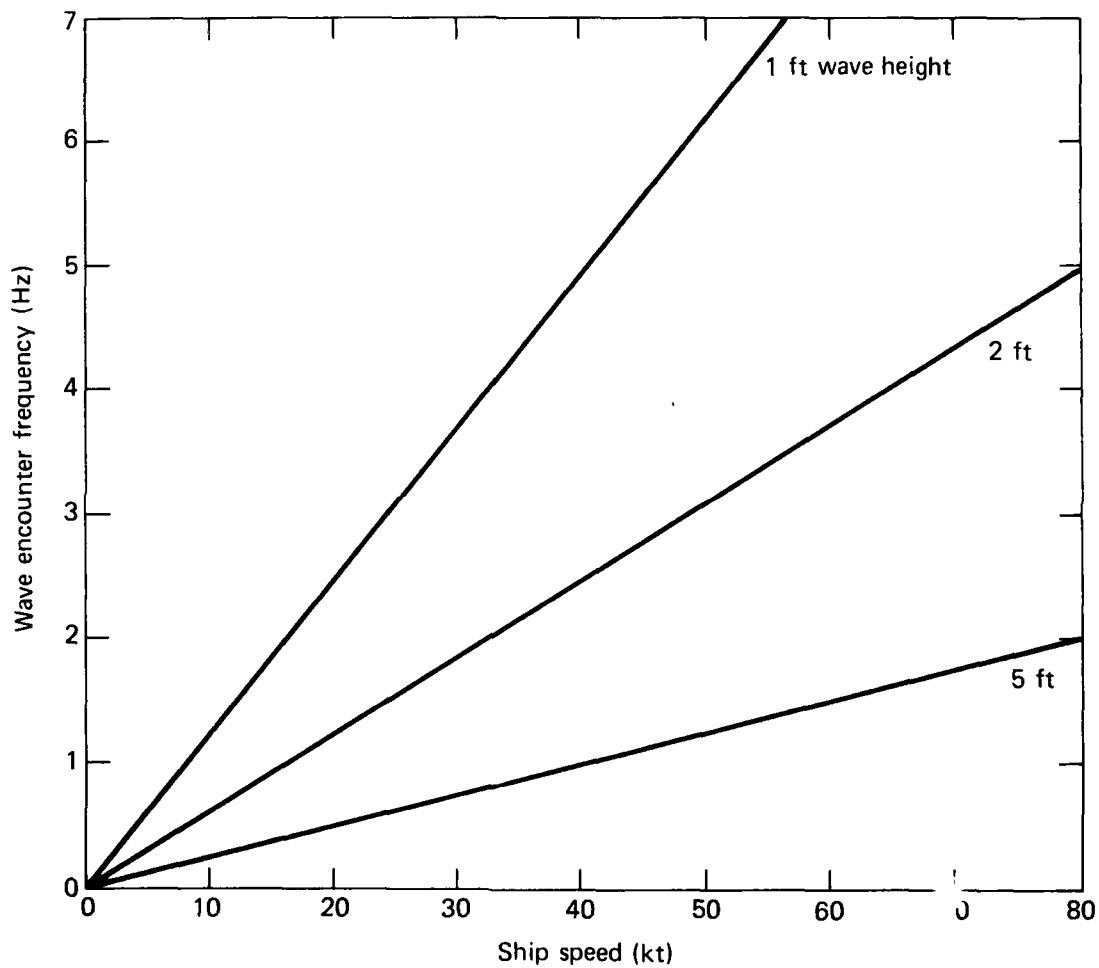


Fig. 1 Encounter frequency versus ship speed assuming $\lambda = 13$ h and a two-dimensional sea.

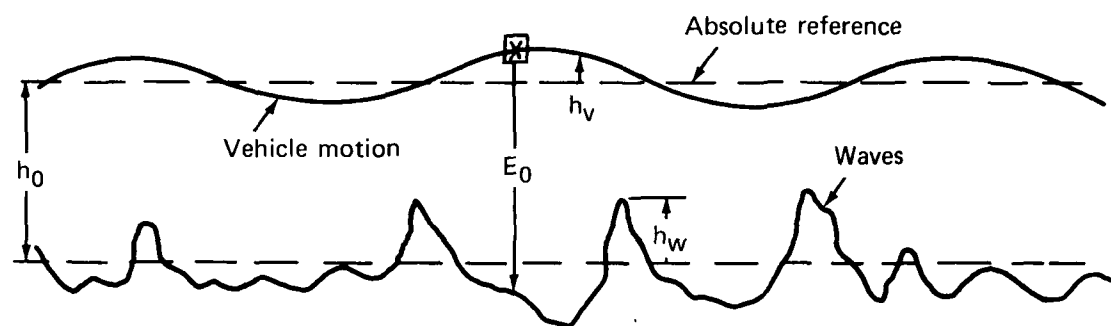


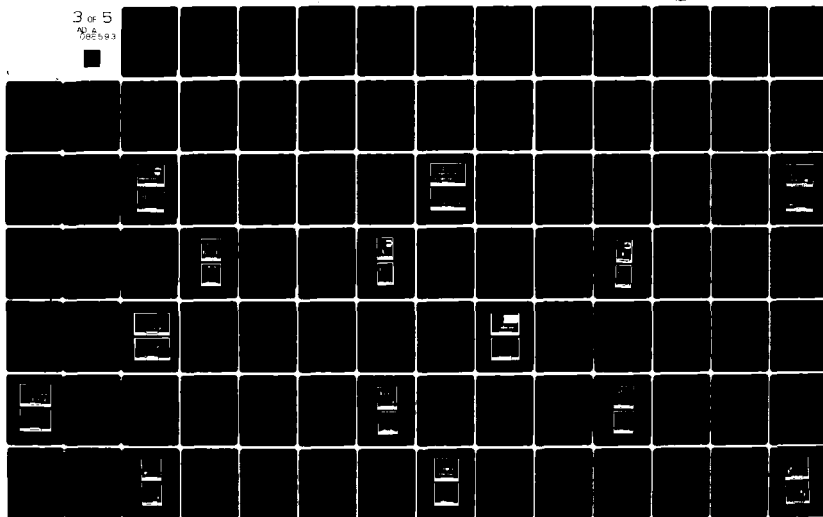
Fig. 2 Geometrical relationship of a vehicle boom altimeter profiling waves.

AD-A088 593

JOHNS HOPKINS UNIV LAUREL MD APPLIED PHYSICS LAB F/G 13/10
DOCUMENTATION OF DESIGN, PERFORMANCE, AND QUALIFICATION OF THE --ETC(U)
JUN 80 T M RANKIN, R L KONIGSBERG N00024-78-C-5384
JHU/APL/SES-025 NL

UNCLASSIFIED

3 of 5
AD-A
706593



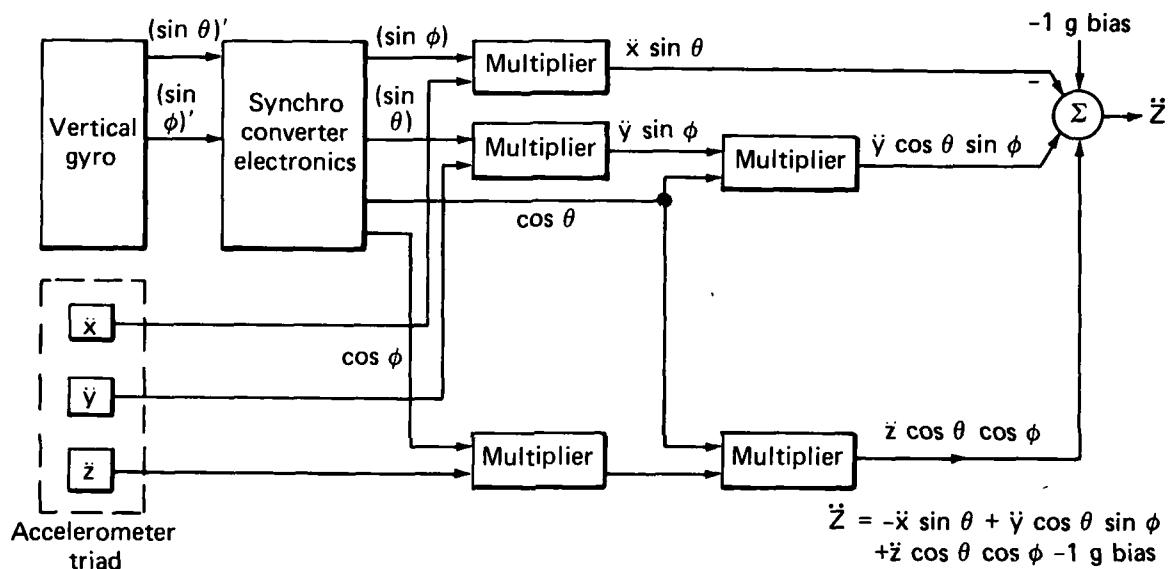


Fig. 3 Exact coordinate converter implementation.

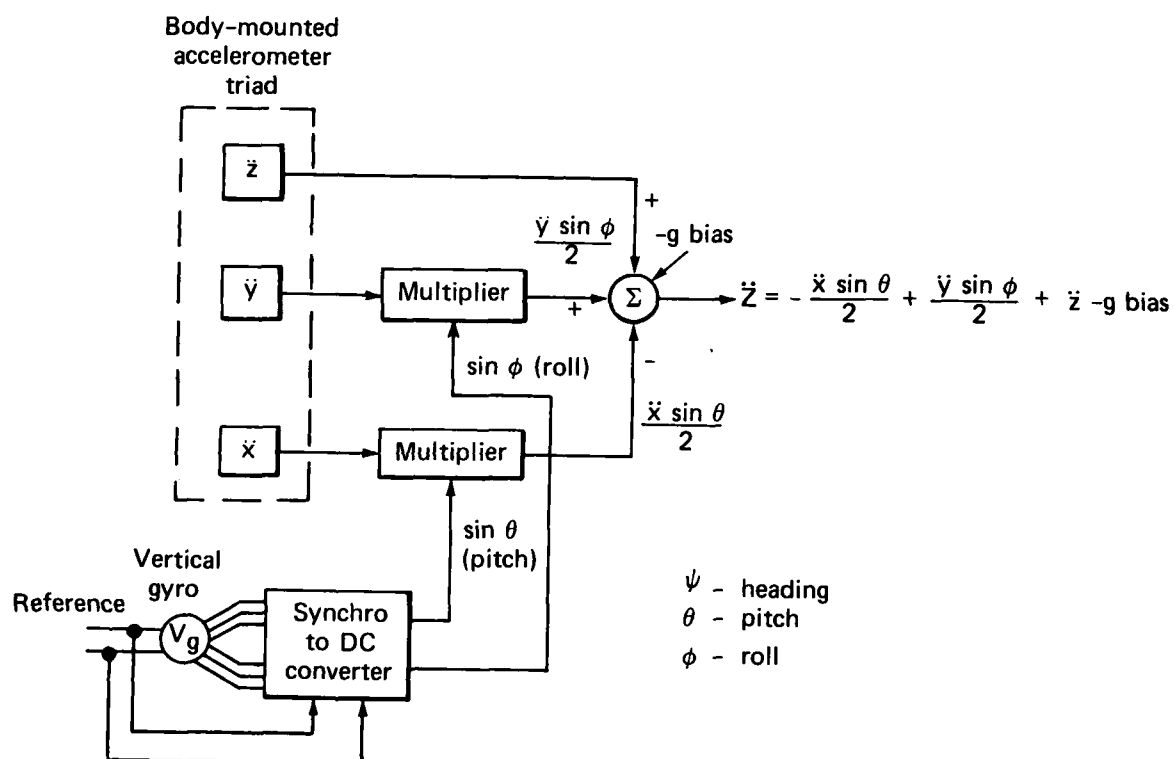
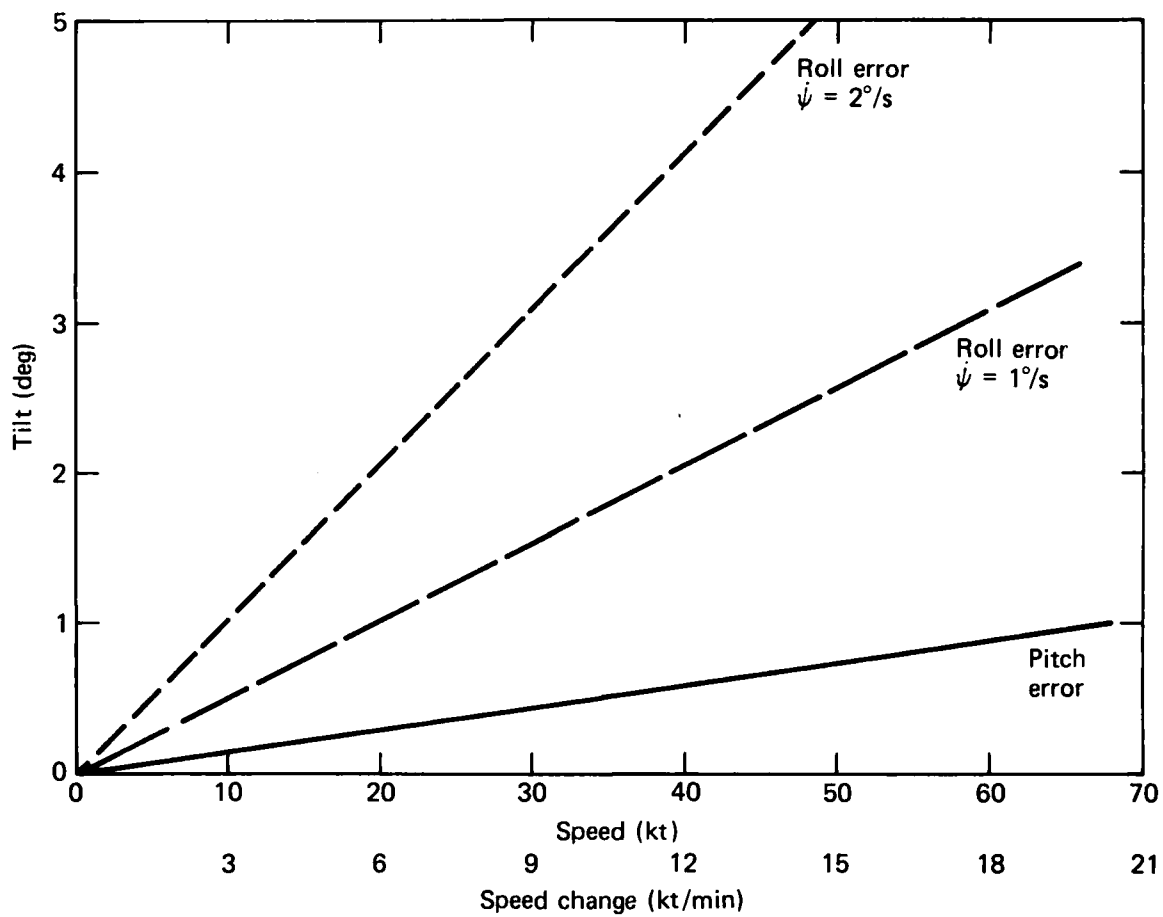


Fig. 4 Simplified coordinate converter.



$$\text{Roll error angle} = \frac{V\dot{\psi}}{g}$$

$$\text{Pitch error angle} = \dot{V}/g$$

Fig. 5 Vertical gyro tilt (steady-state error) due to ship's maneuvers.

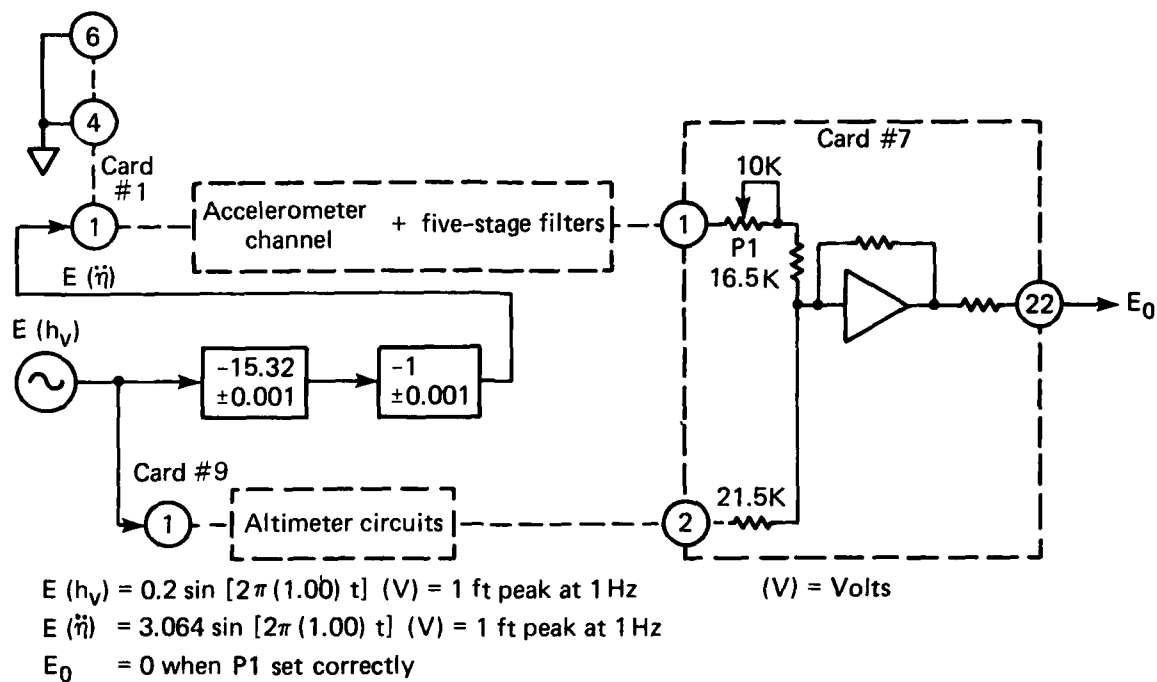
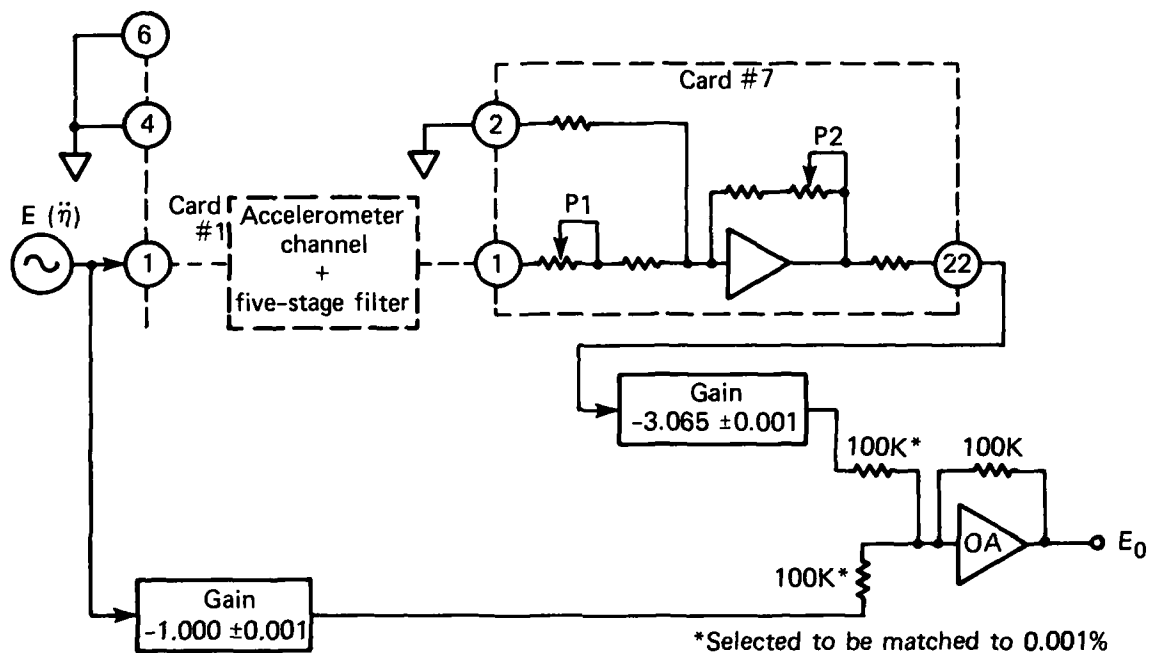


Fig. 6 Special test circuit to set gain potentiometer P1 on board #7.



$$E(\eta) = 3.065 \sin [2\pi (1.00) t] \text{ (V)}$$

(V) = Volts

$E_0 = 0$ when P2 is adjusted correctly

Note: P1 must be set correctly before P2 can be set.

Fig. 7 Special test circuit for setting gain potentiometer P2 on card #7.

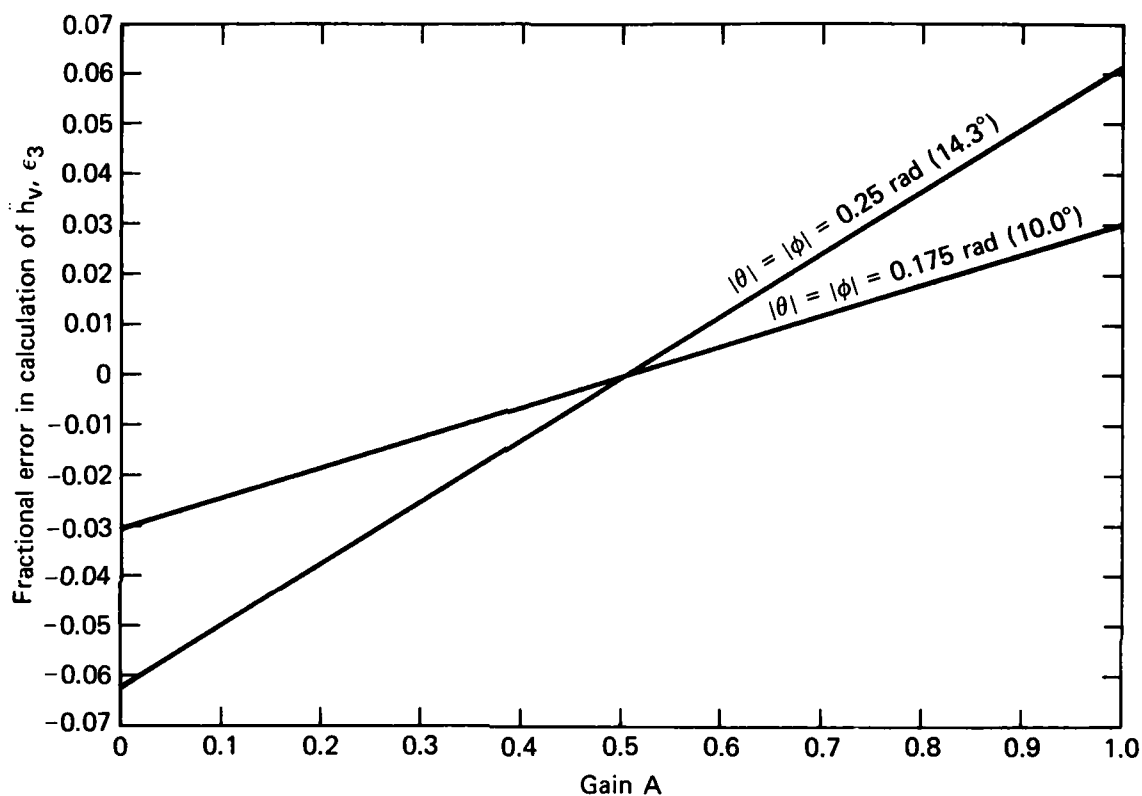


Fig. 8 Fractional error (ϵ_3) in calculation of \ddot{h}_v , as a function of θ and ϕ channel gain A for $|\theta| = |\phi| = 0.25$ rad and $|\theta| = |\phi| = 0.175$ rad, assuming surge and sway accelerations are insignificant compared to vertical acceleration ($k = 0$).

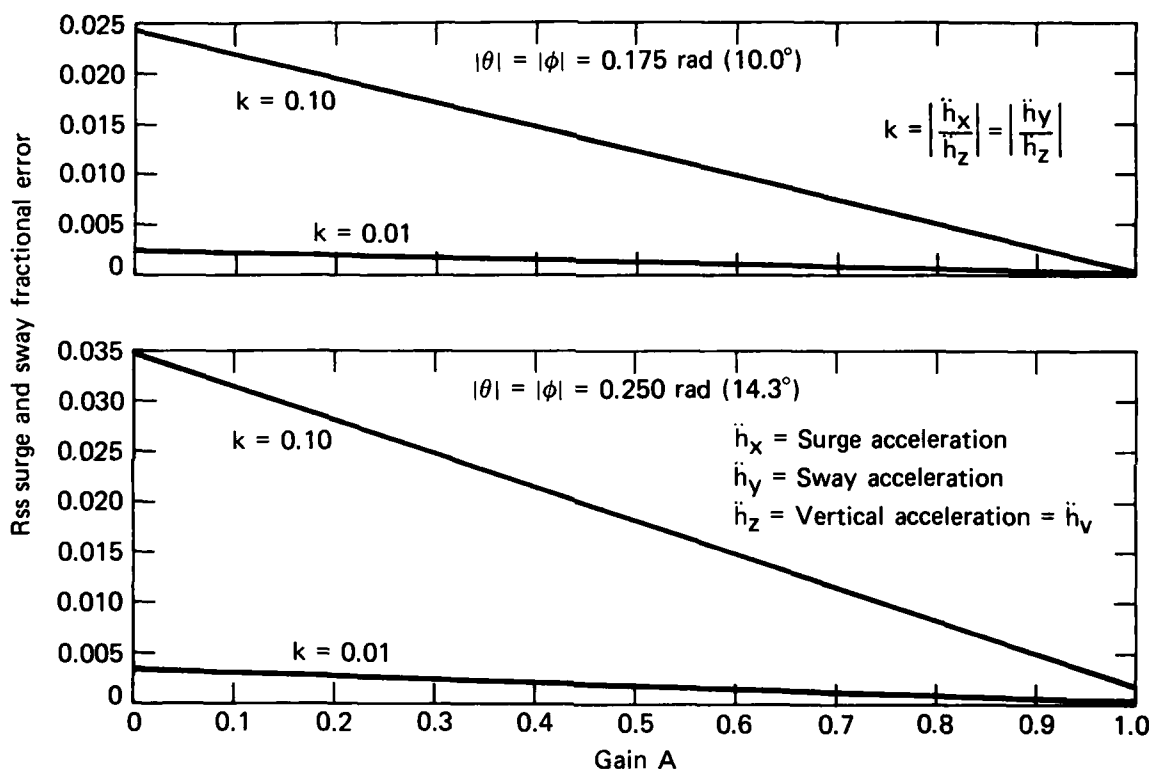


Fig. 9 Rss fractional error due to surge and sway accelerations, as a function of θ and ϕ channel gain A for $|\theta| = |\phi| = 0.25 \text{ rad}$ and $|\theta| = |\phi| = 0.175 \text{ rad}$, and for $k = 0.01$ and $k = 0.10$.

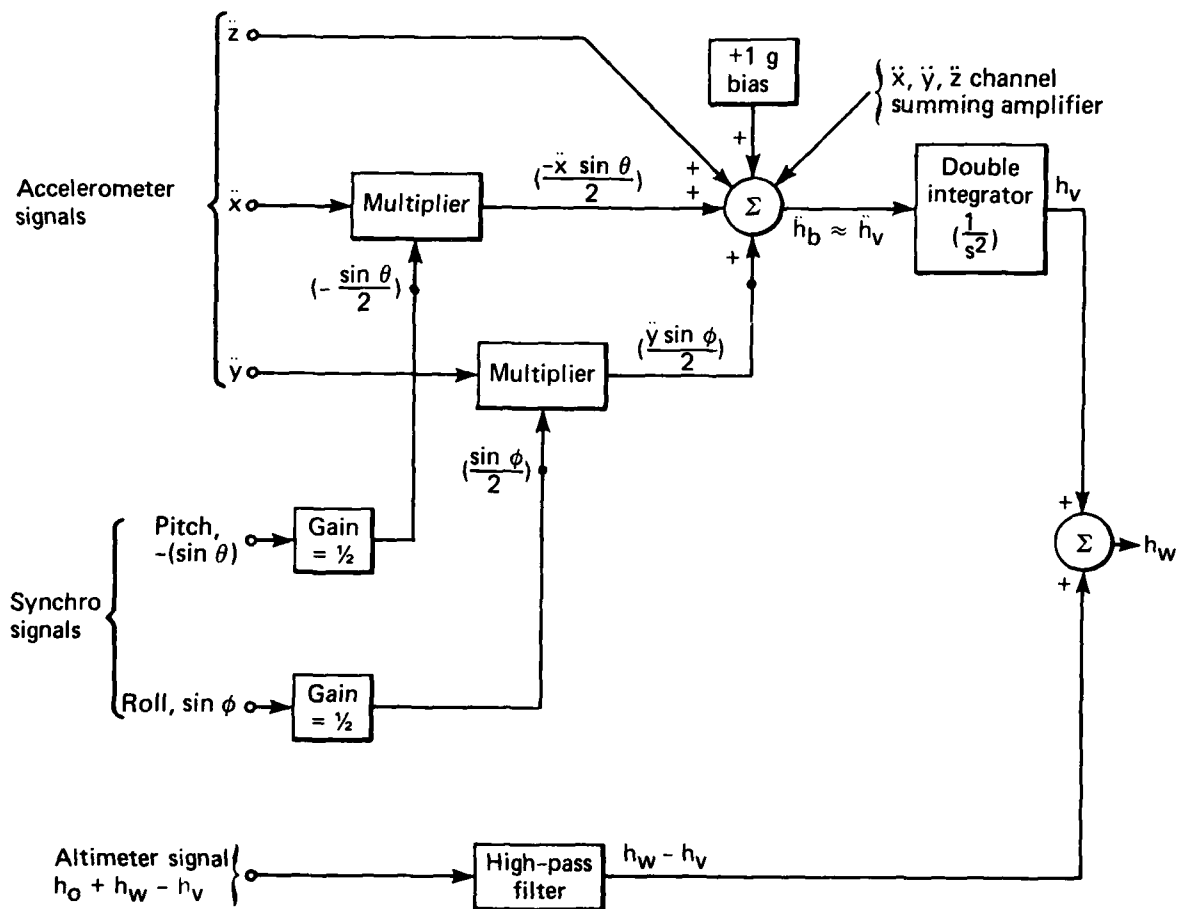
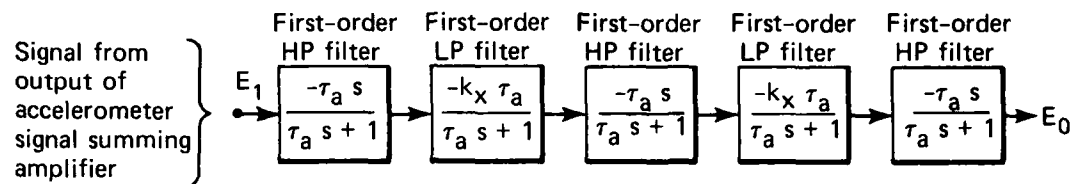


Fig. 10 Simplified block diagram of motion-compensated wave profiler.



$$\text{Transfer function: } \frac{E_0}{E_1} = - \frac{(k_x)^2 (\tau_a)^5 s^3}{(\tau_a s + 1)^5}$$

where ω_a = cutoff angular frequency of each filter = $\frac{1}{\tau_a}$; $s = j\omega$, $j = \sqrt{-1}$

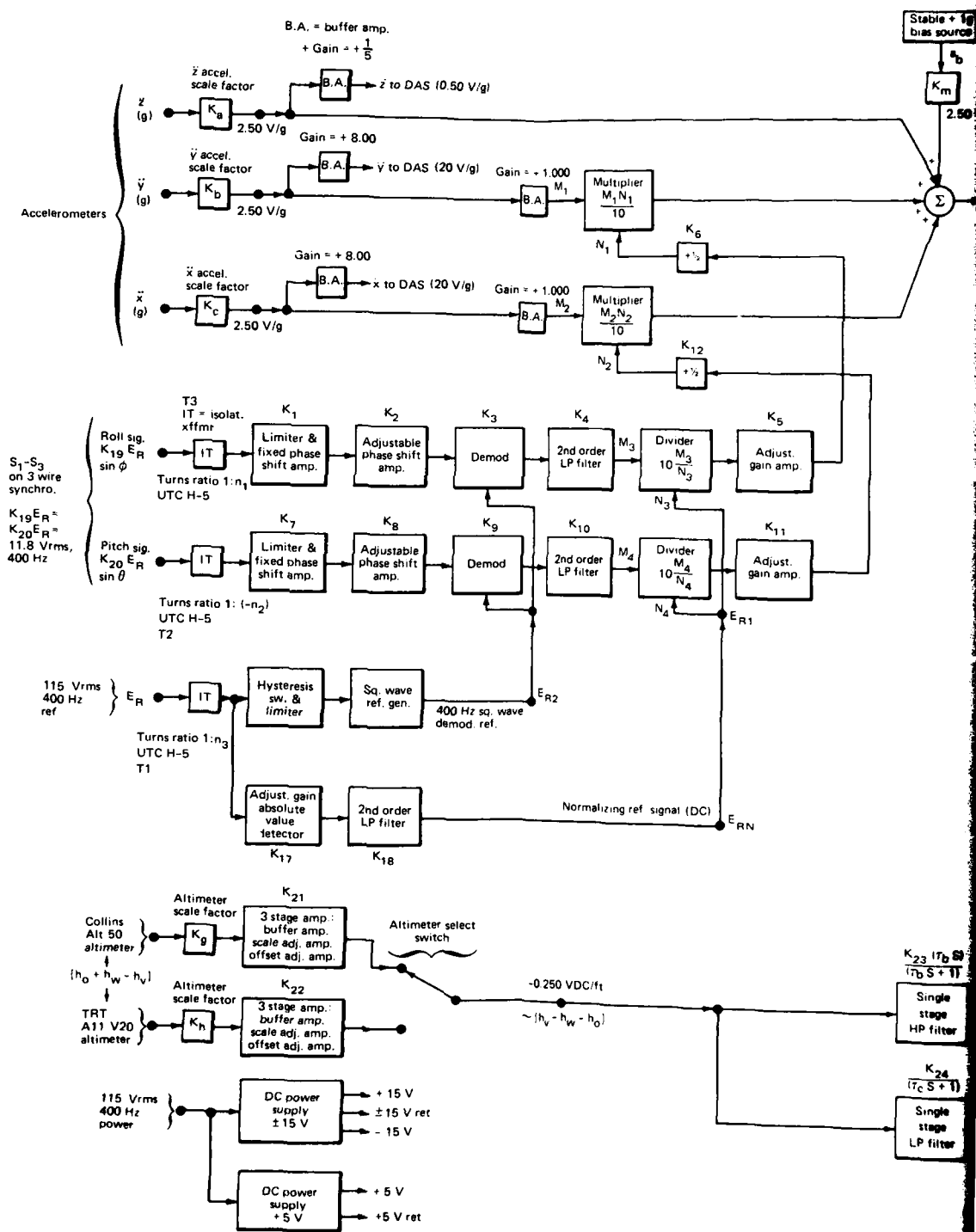
if ω_1 = lowest significant wave height angular frequency,

and $\omega_1 \gg \omega_a$, then

$$\frac{E_0}{E_1} \approx - \left(\frac{(k_x)^2}{s^2} \right).$$

This is the double integration function required of the filter for angular frequencies $\omega_1 \gg \omega_a$.

Fig. 11 Five-stage filter configuration required for double integration function.



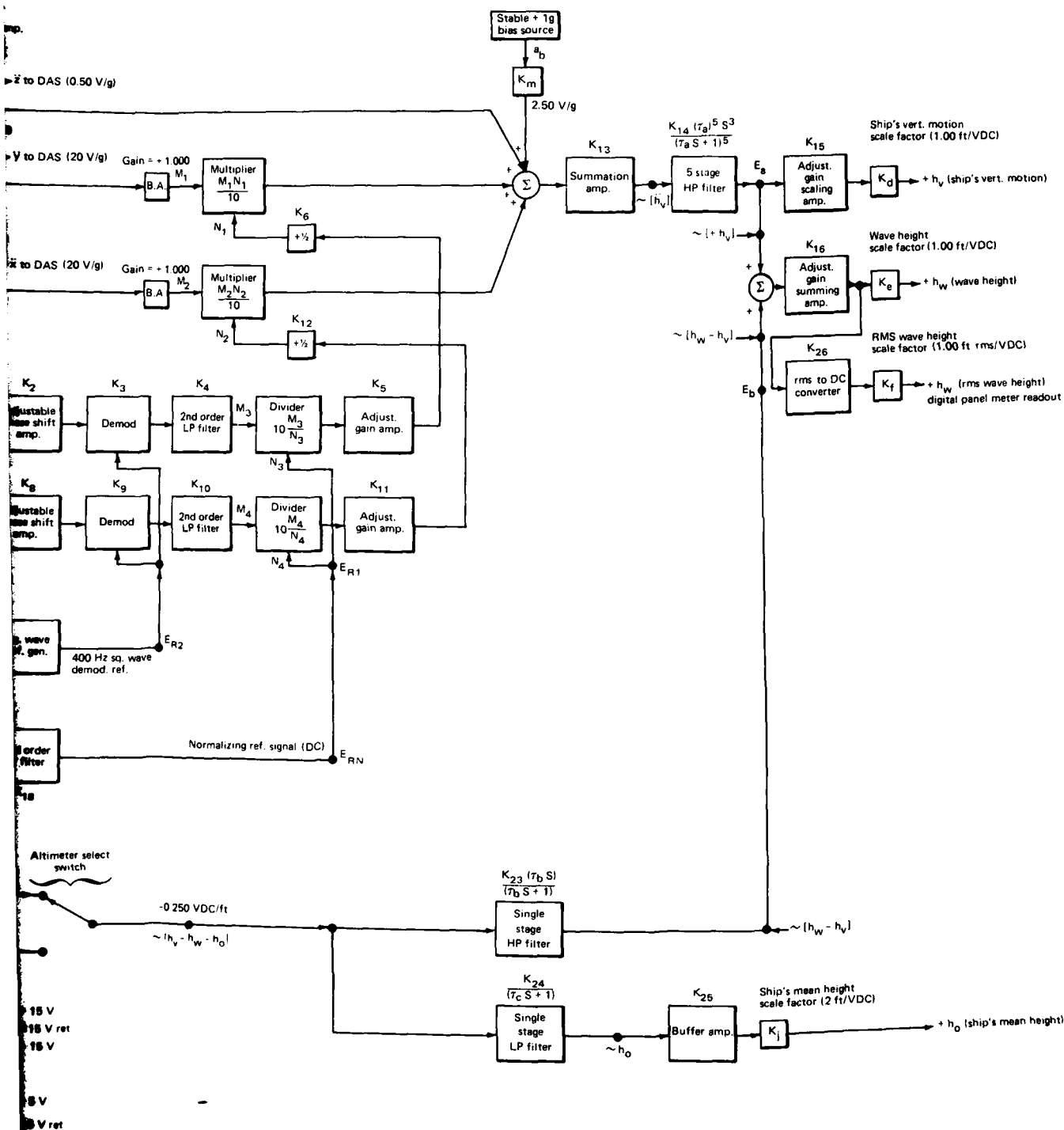


Fig. 12 Electronic instrumentation diagram for motion-compensated wave profiler.

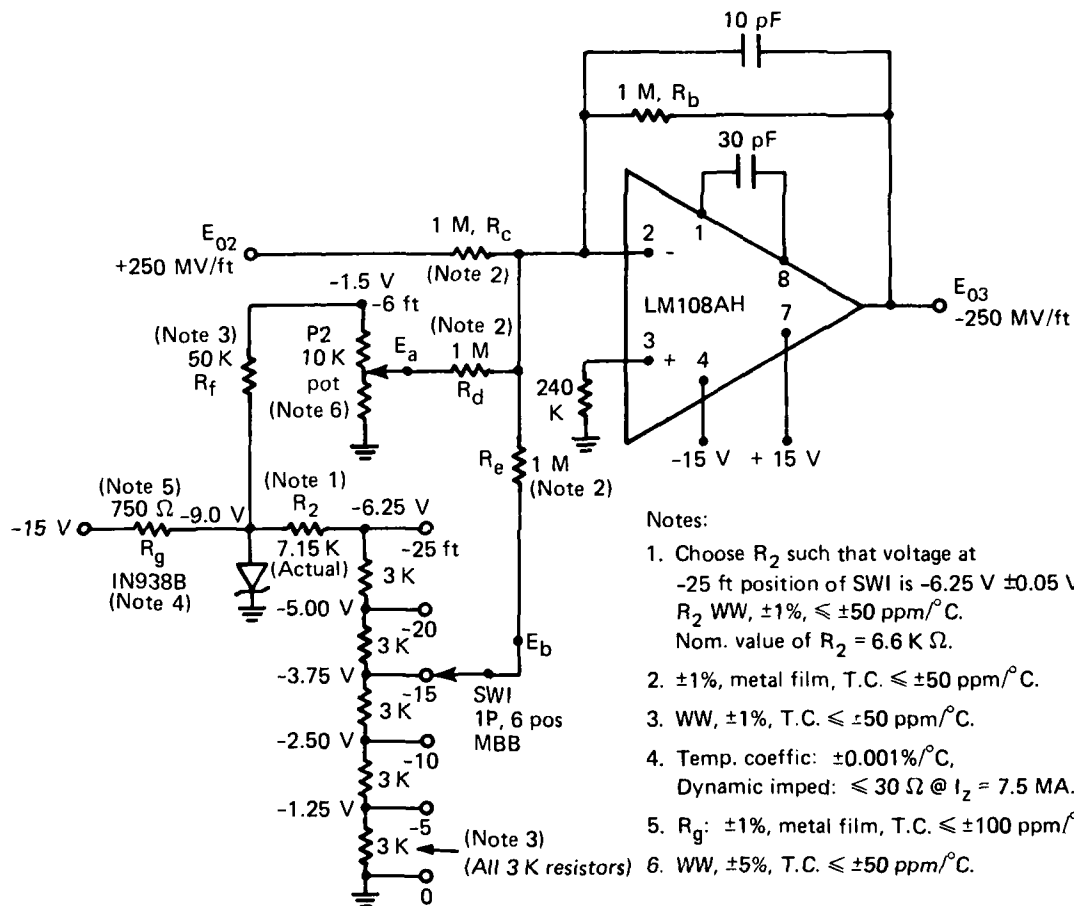
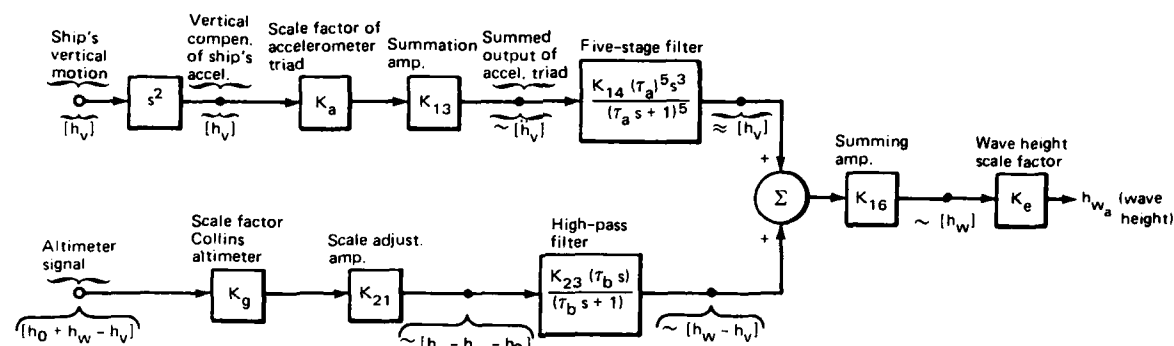


Fig. 13 Complete schematic of offset adjustment amplifier shown in Fig. A9-1.



$$(1) h_{wa} = \left[\frac{K_a K_{13} K_{14} (\tau_a s)^5 s^5}{(\tau_a s + 1)^5} h_v + \frac{K_g K_{21} K_{23} (\tau_b s)}{(\tau_b s + 1)} (h_w - h_v) \right] K_{16} K_e$$

or

$$(2) h_{wa} = \frac{K_m (\tau_a s)^5}{(\tau_a s + 1)^5} h_v + \frac{K_n (\tau_b s)}{(\tau_b s + 1)} (h_w - h_v)$$

Neglecting h_0

h_{wa} = measured value of h_w

h_w = wave height

h_0 = mean height

h_v = ship's vertical motion

(3) where $K_m = K_a K_{13} K_{14} K_{16} K_e$; $K_n = K_g K_{21} K_{23} K_{16} K_e$;

(4) let $[K_a K_{13} K_{14}] (K_{16} K_e) = [(K_g K_{21} K_{23}) (1 + \epsilon_1)] (K_{16} K_e)$, or $K_m = K_n (1 + \epsilon_1)$

where ϵ_1 = fractional error in adjusting the accelerometer channel gain to equal the altimeter channel gain.

(5) $\therefore h_{wa} = K_n \left[\frac{(1 + \epsilon_1) (\tau_a s)^5}{(\tau_a s + 1)^5} - \frac{\tau_b s}{(\tau_b s + 1)} \right] h_v + K_n \left[\frac{\tau_b s}{\tau_b s + 1} \right] h_w$

Note: Notation used herein corresponds to that used in Fig. 12.

Fig. 14 Block diagram for error analysis of MCU system.

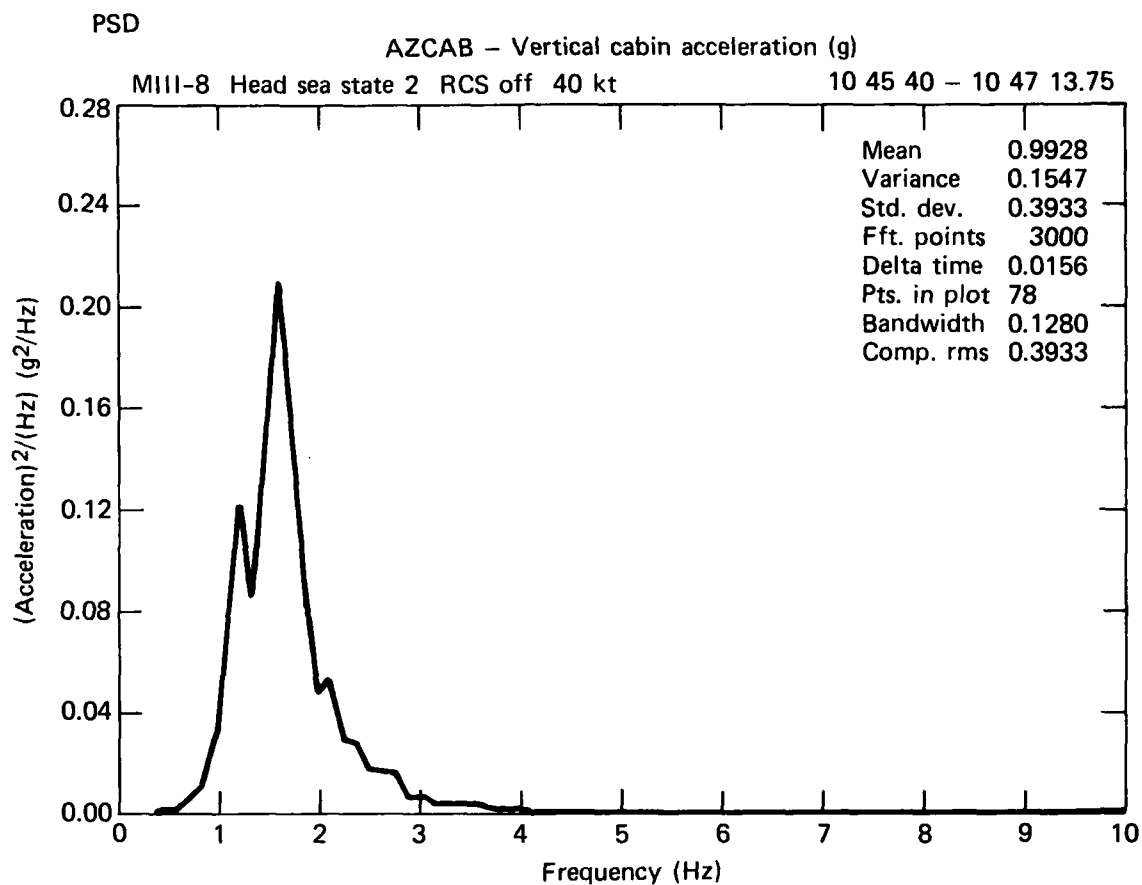


Fig. 15 Power spectral density of ship's vertical acceleration.

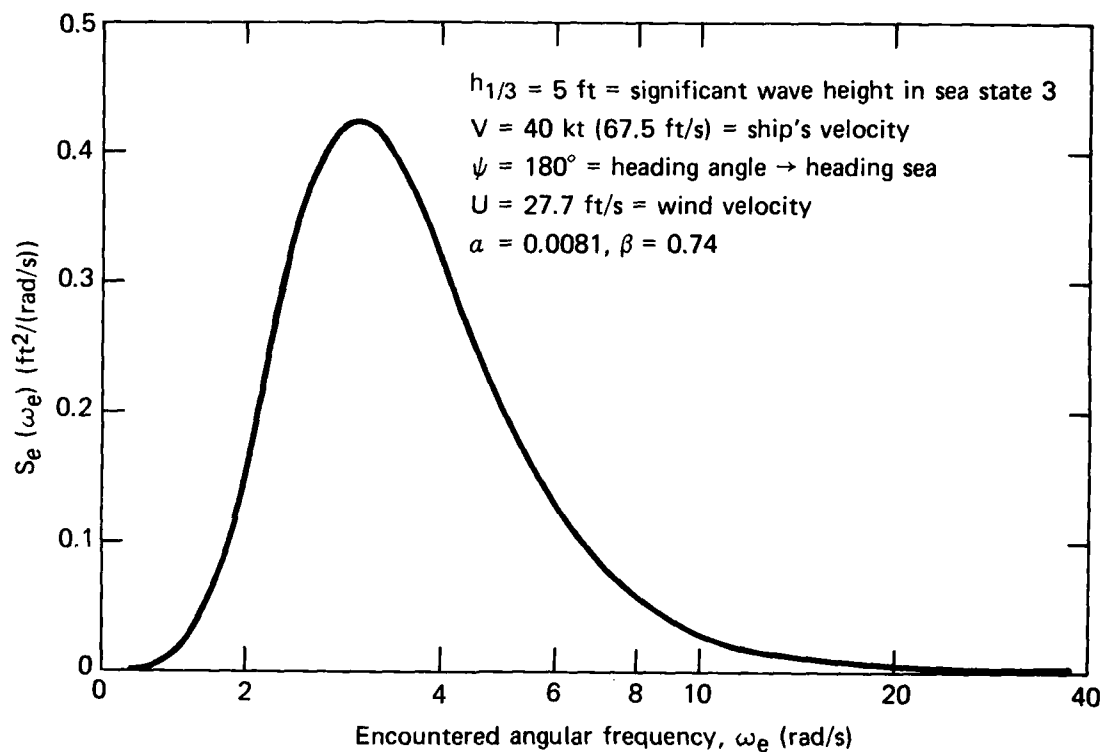


Fig. 16 Power spectral density of encountered wave height.

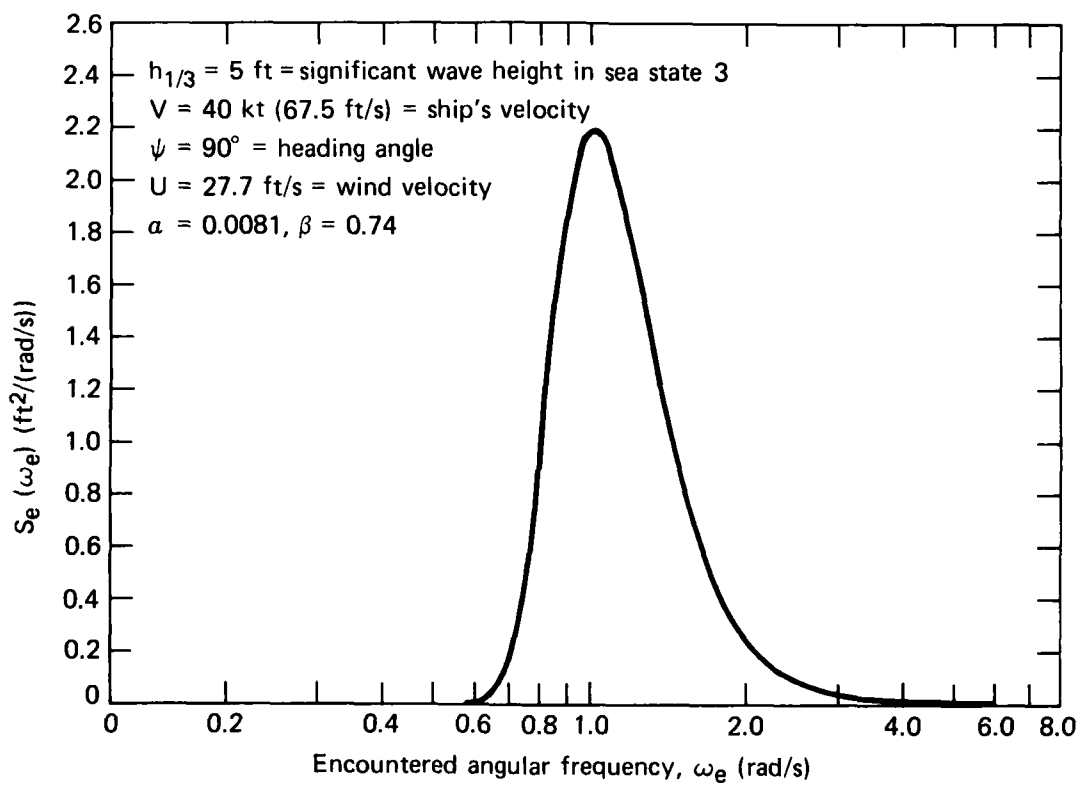
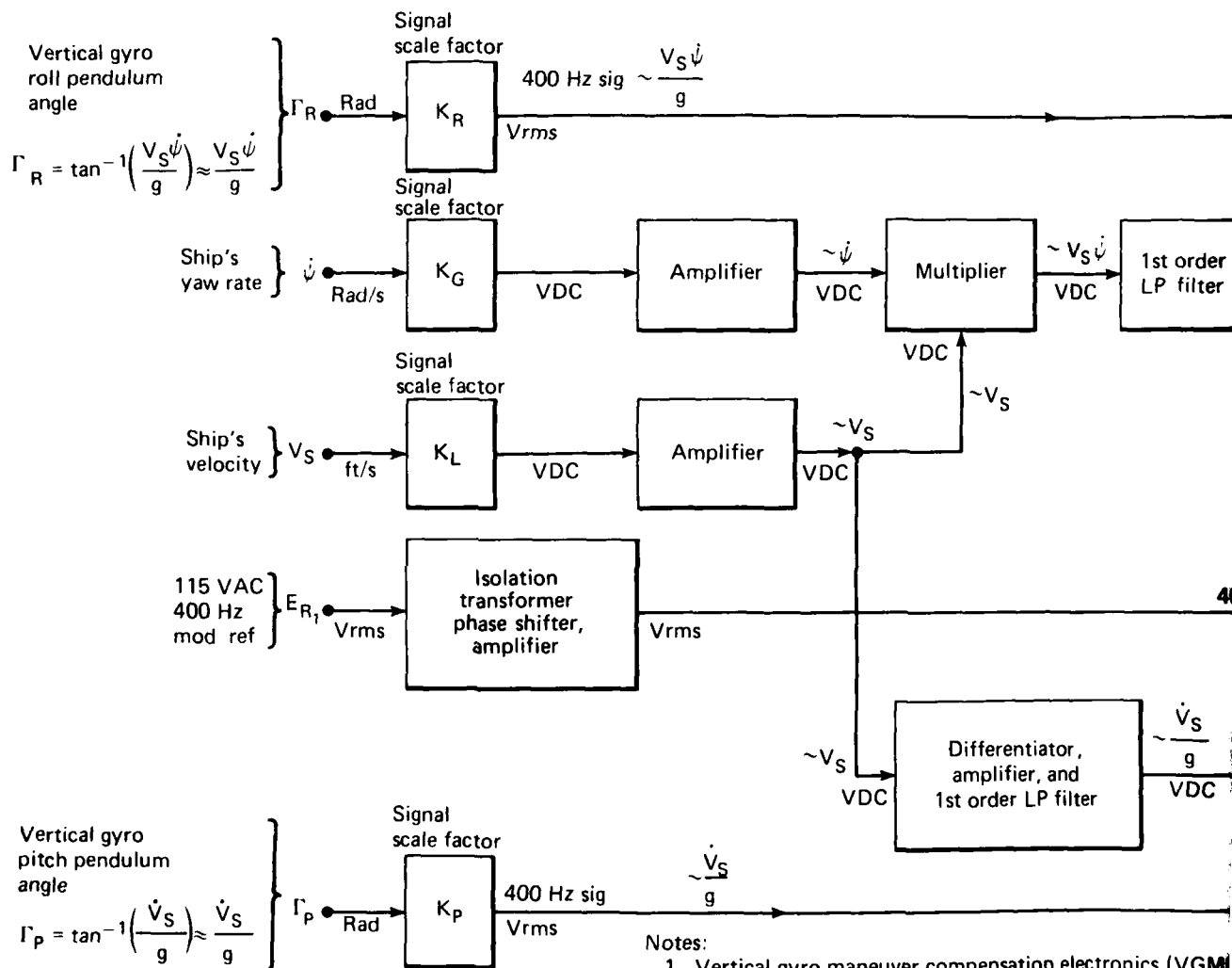


Fig. 17 Power spectral density of encountered wave height.



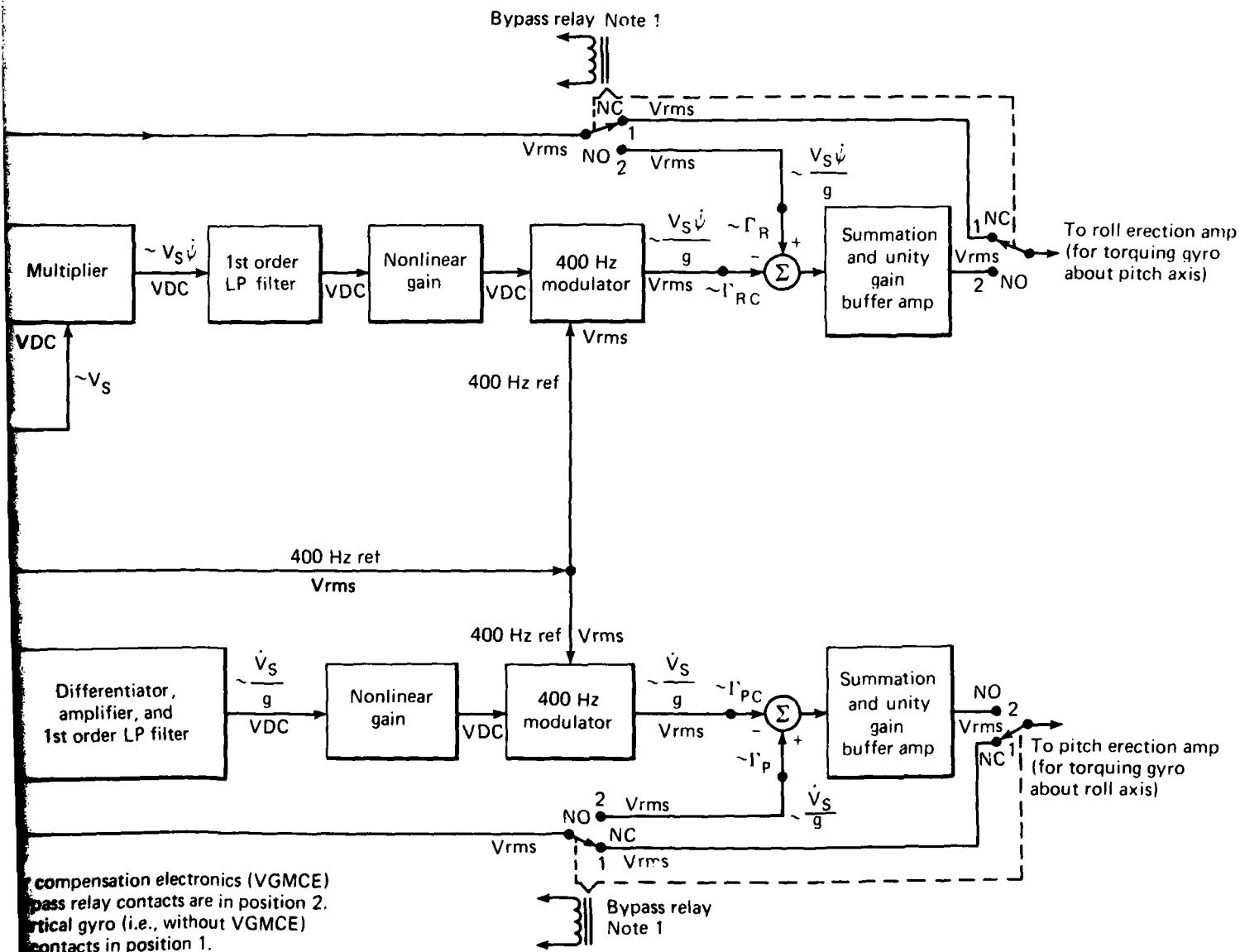
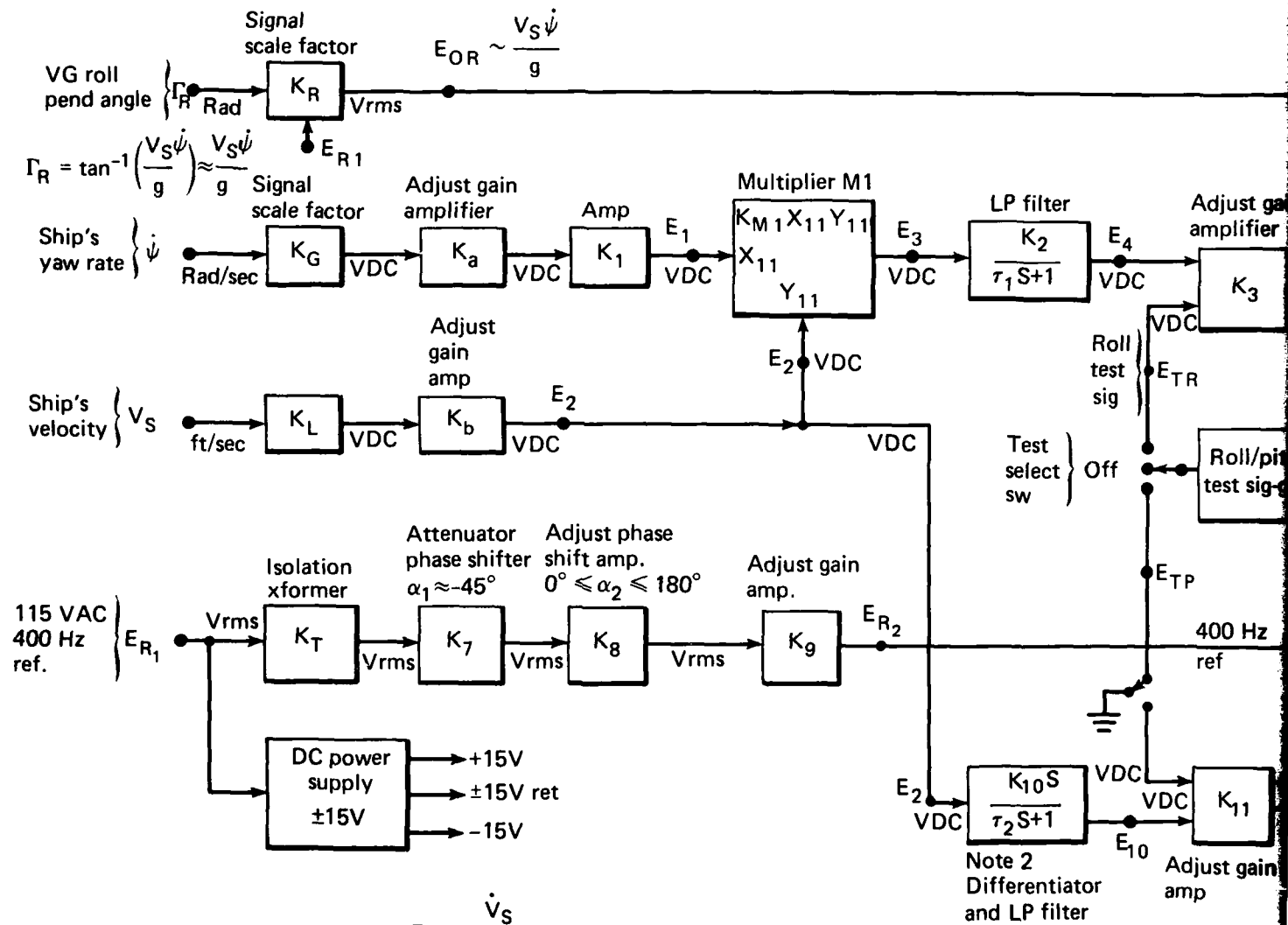


Fig. 18 Simplified block diagram of vertical gyro maneuver compensation electronics.



Notes:

1. VGMCE is in operation when bypass relay contacts are in position 2. Normal operation of VG (i.e., without VGMCE) occurs for bypass relay contacts in position 1.
2. Filter time constants τ_1, τ_2 depend on response time of VG being used. For VG's to be used, $\tau_1 = \tau_2 = 8$ sec or 27 sec.

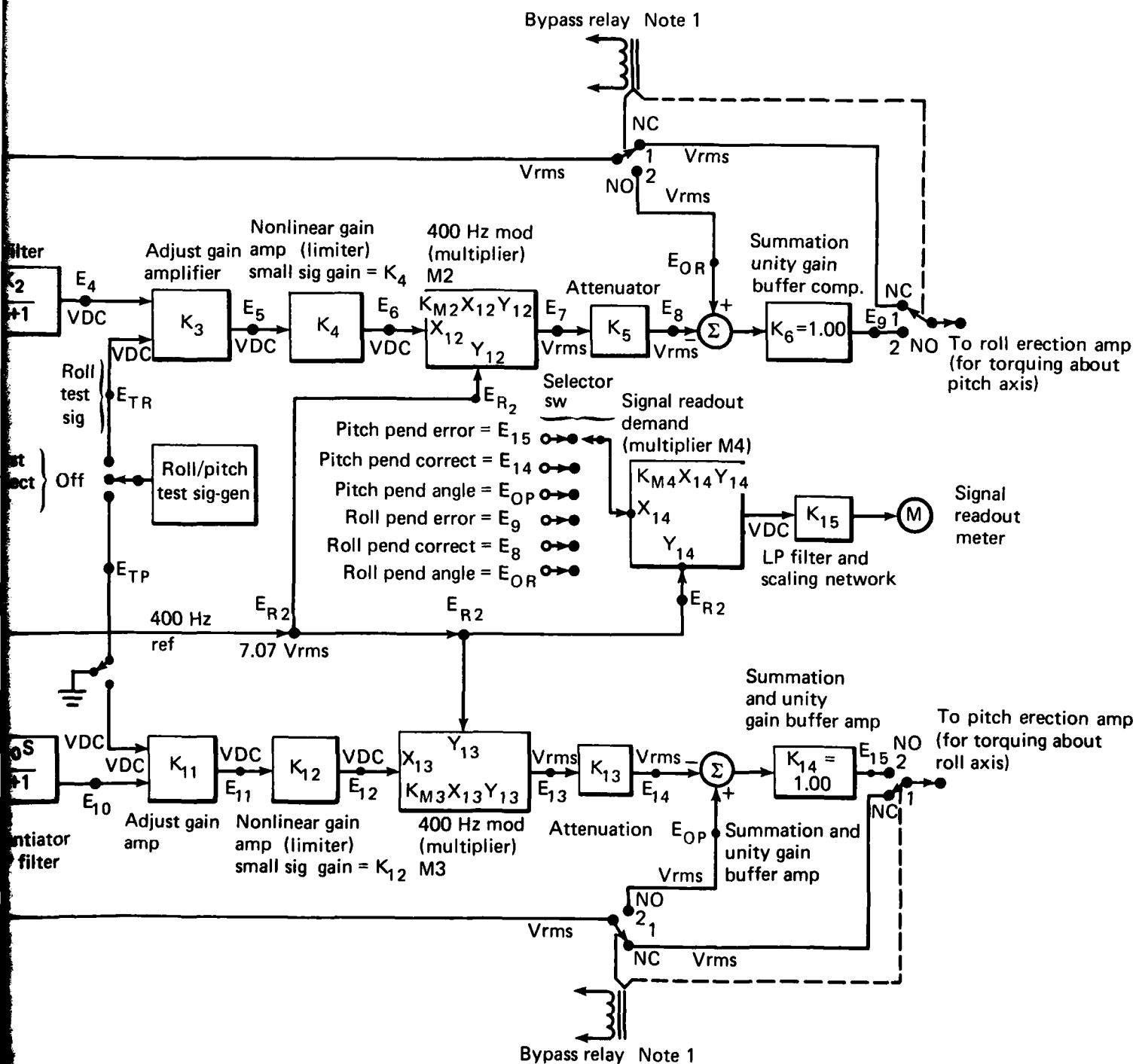


Fig. 19 Instrumentation diagram for vertical gyro maneuver compensation electronics.

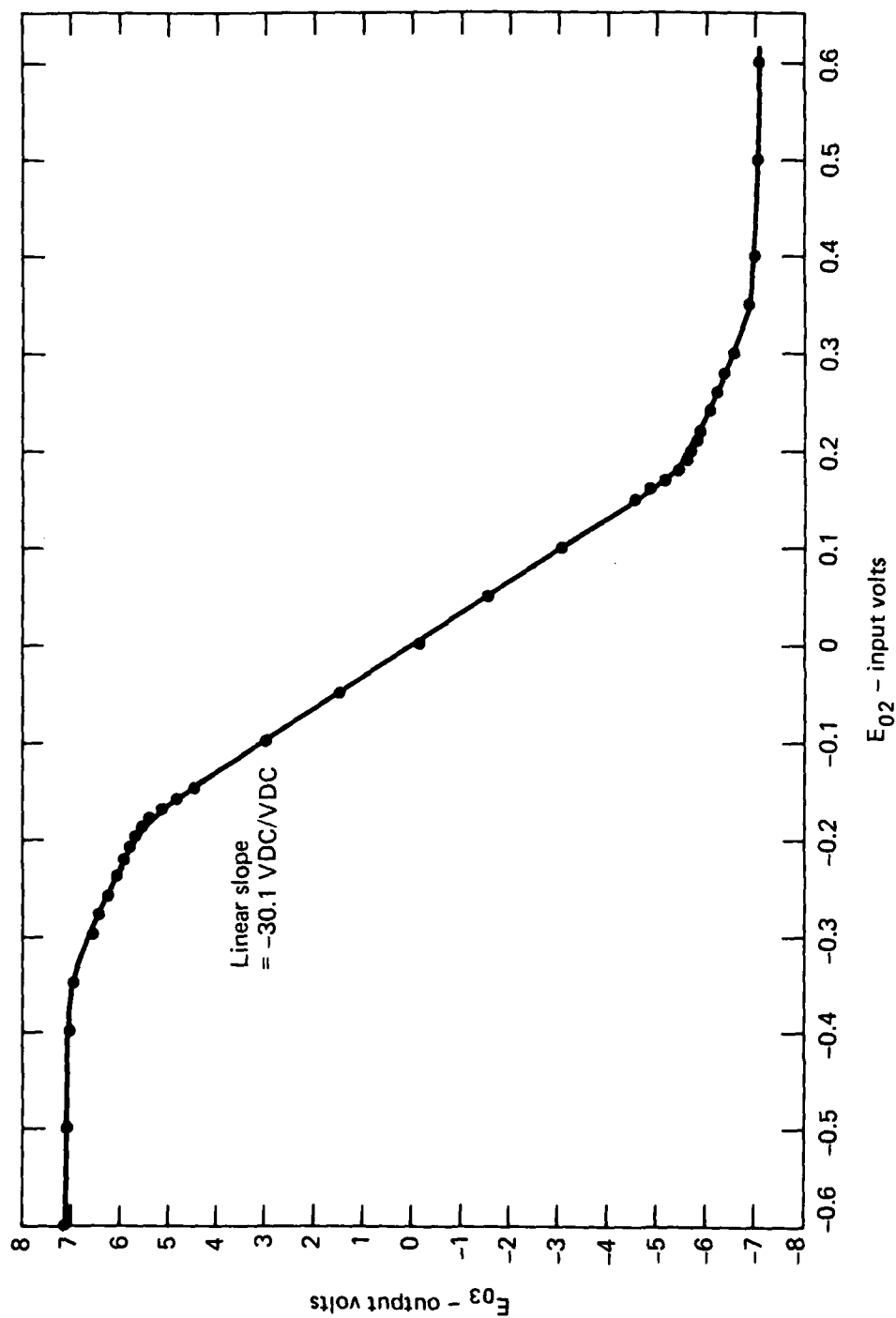


Fig. 20 Input-output characteristic for nonlinear gain amplifier K₄.

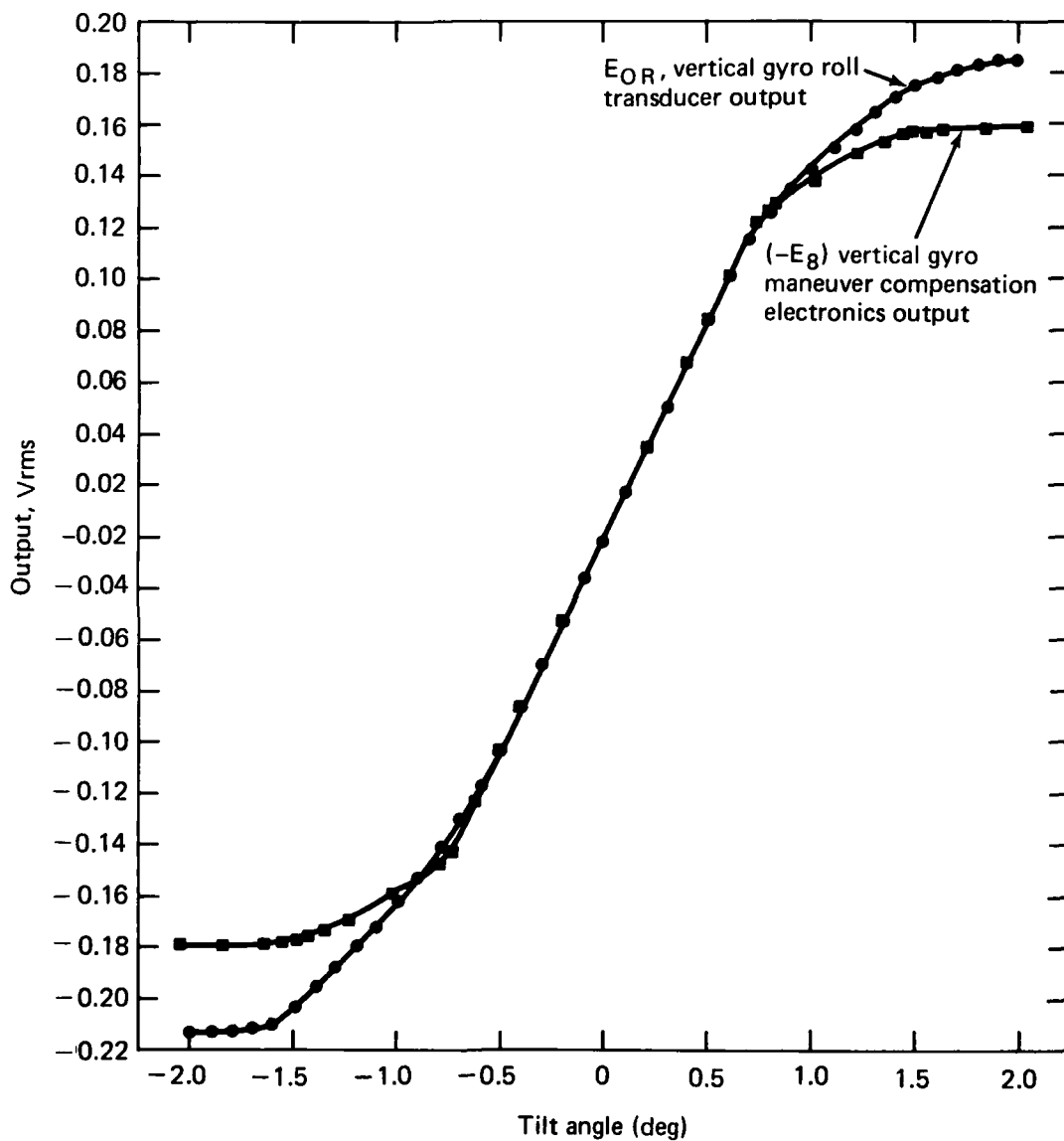


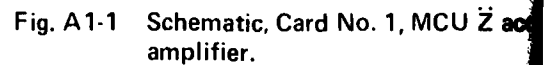
Fig. 21 Outputs of VGMCE $(-E_g)$ and SN193 vertical gyro roll pendulum transducer (E_{OR}) as functions of pendulum tilt angle.

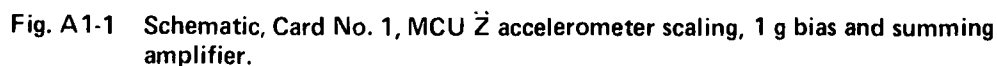
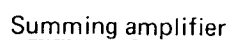
Appendix A
WAVE PROFILING SYSTEM ELECTRONICS SCHEMATICS,
ASSEMBLY DRAWINGS, AND PHOTOGRAPHS

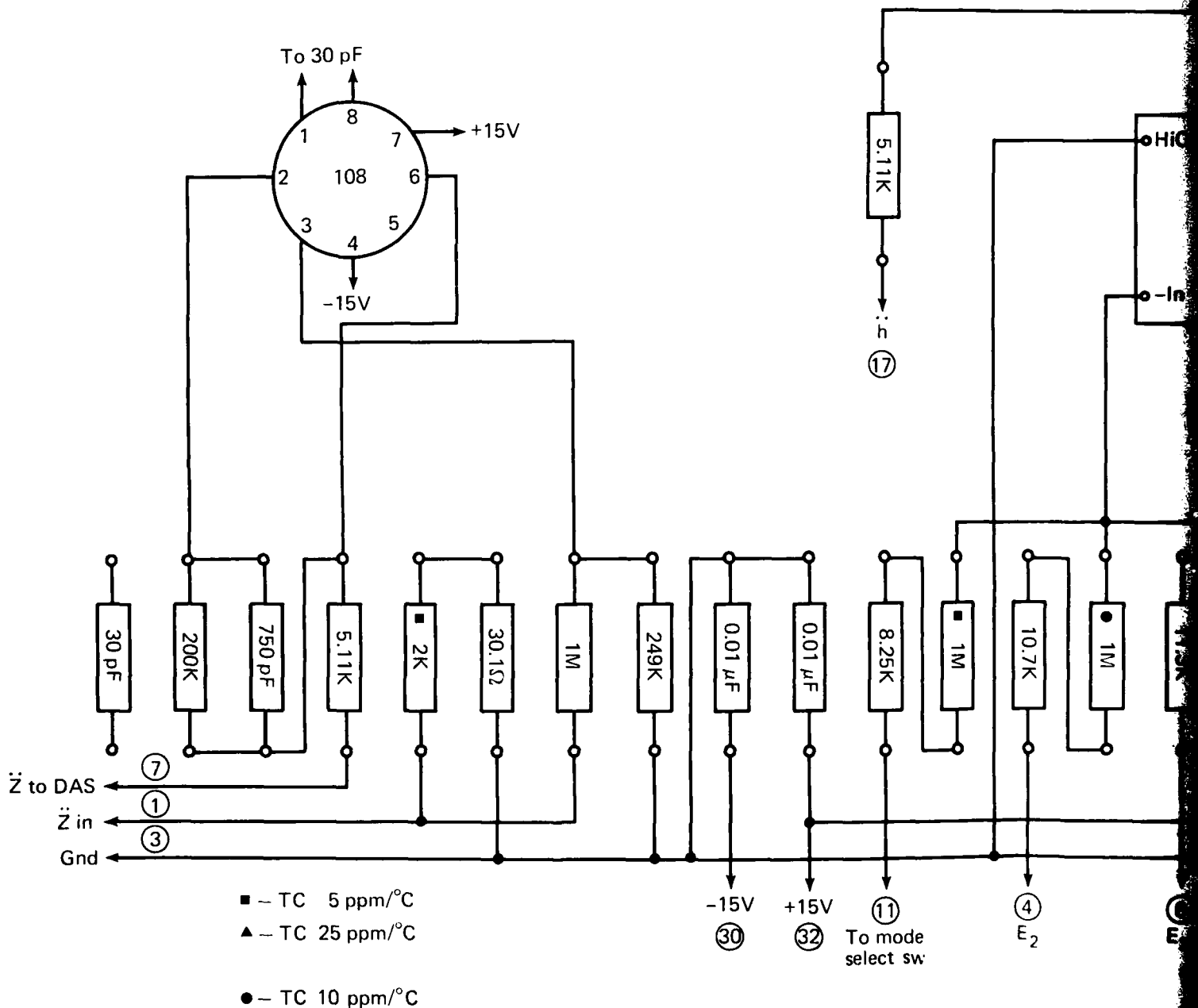
Board No. 1

Notes:

1. \bigcirc denotes pins on connector.
2. All resistors: MEA metal-film $\pm 1\%$, 100 ppm/ $^{\circ}\text{C}$ or equivalent unless otherwise noted.
3. All capacitors: Mica $\pm 10\%$ or equivalent unless otherwise noted.
4. These resistors should have temperature coefficient of ± 5 ppm/ $^{\circ}\text{C}$ or better.
5. Select to yield scale factor of 2.500 V/g $\pm 0.2\%$ with all loads connected.
6. These resistors should have temperature coefficient of ± 25 ppm/ $^{\circ}\text{C}$ or better.
7. Select such that channel resistances R_d , R_e , R_f match within $\pm 0.2\%$ and that each channel resistance does not exceed $1.01 \text{ M}\Omega$.
8. Select R_c such that $R_c = 0.25 R_b \pm 0.2\%$.
9. Select R_g and adjust P_1 such that $E_g \leq \pm 0.5 \text{ MV}$ with accelerometer triad Z axis vertical, corresponding to θ_p and θ_R set to 0° , and with P_1 set close to its midposition.
10. Measure E_{Z1} of 1N938B @ $I_z = 7.5 \text{ MA}$ and record value.
11. Measure E_{Z2} of 1N4579 @ $I_z = 2.0 \text{ MA}$ and record value.
12. Select R_t such that $R_t = \left(\frac{15 - E_{Z1}}{10} \right) \text{ K } \Omega$.
13. Select R_v such that $R_v = \left(\frac{E_{Z1} - E_{Z2}}{2.5} \right) \text{ K } \Omega$.
14. Pins 1 and 11, 8 and 9 are connected to the mode select switch on front panel and shown in operate position.
15. This resistor should have a temperature coefficient of ± 10 ppm/ $^{\circ}\text{C}$ or better.
16. DAS load impedance assumed to be $\geq 1 \text{ M}\Omega$.







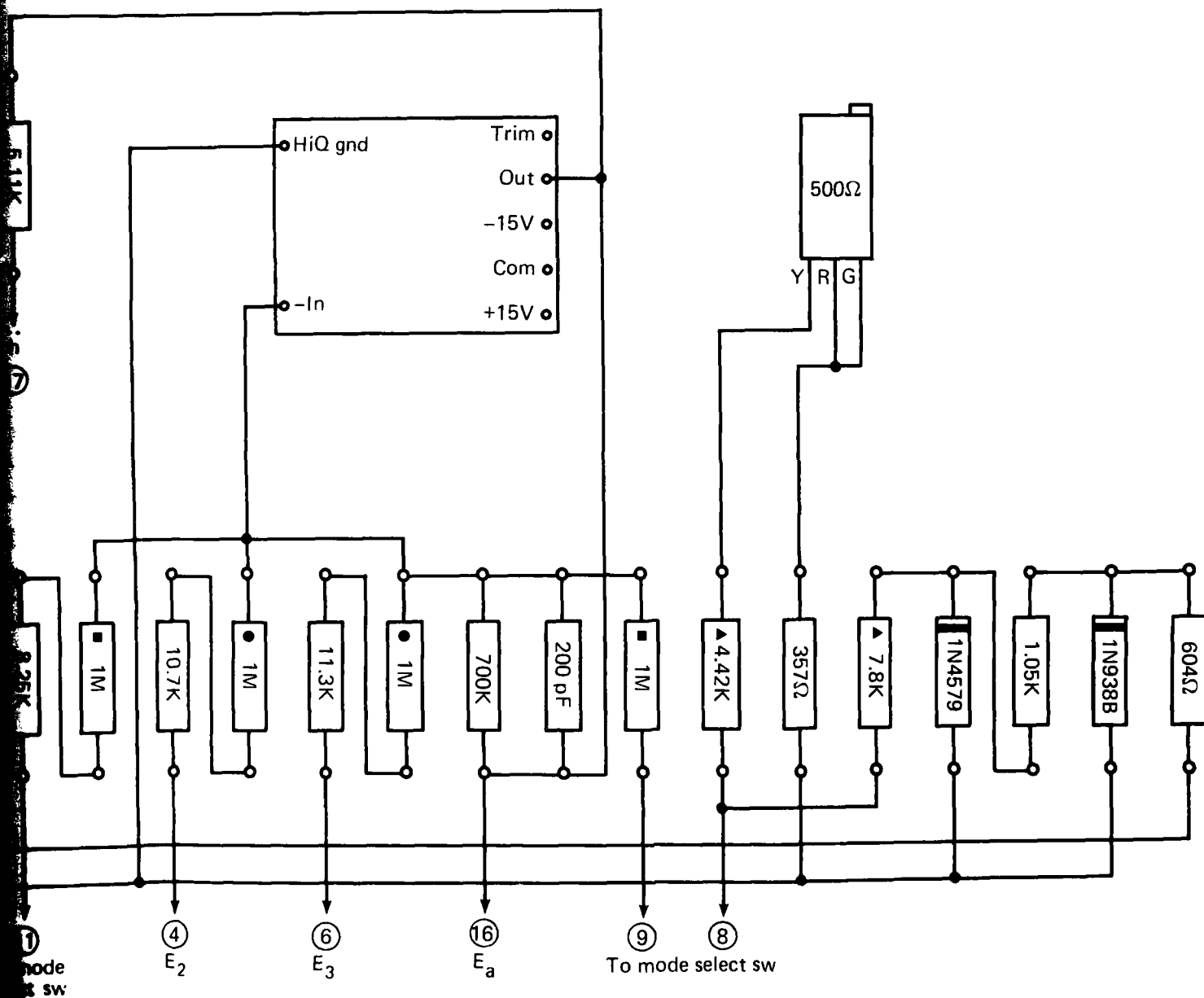
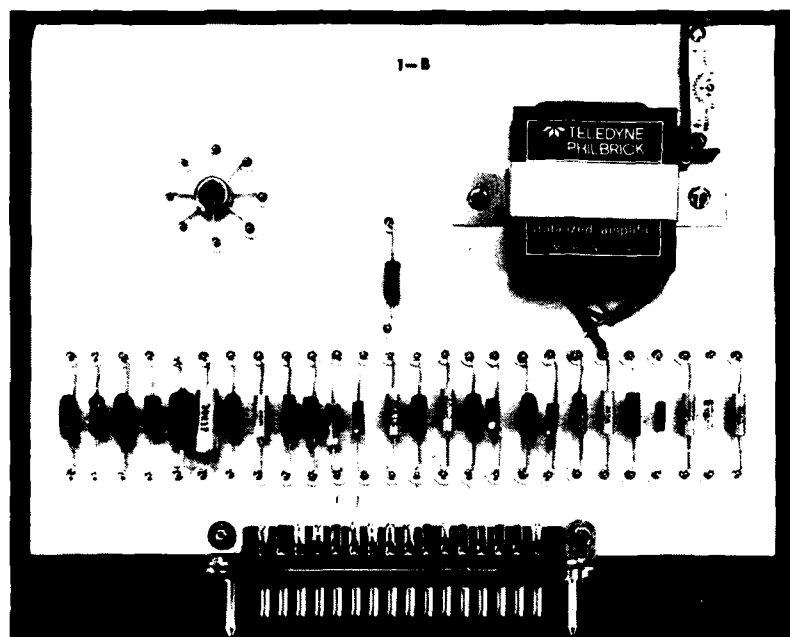
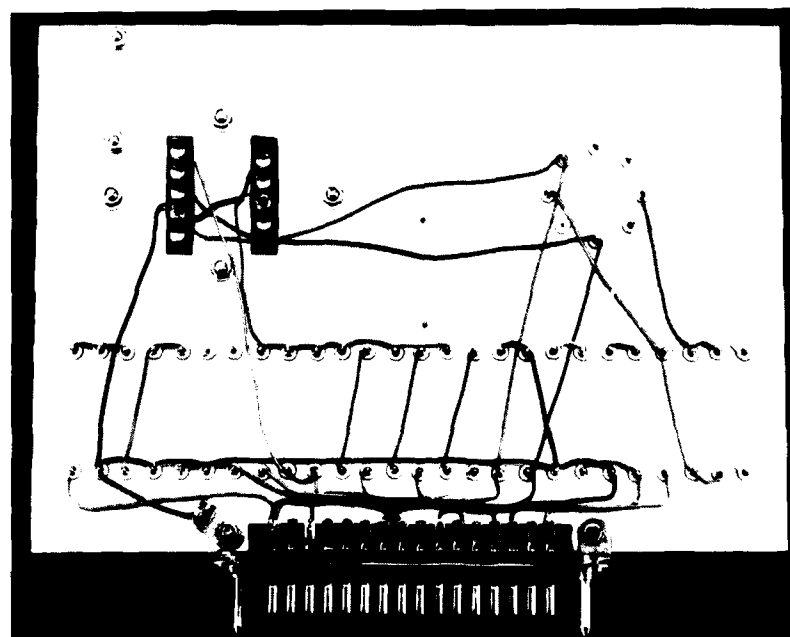


Fig. A1-2 Component layout, Card No.1, MCU \ddot{Z} accelerometer scaling, 1 g bias summing amplifier.



(a)



(b)

Fig. A1-3 MCU \ddot{z} accelerometer scaling, 1g bias and summing amplifier.

Board No. 17

Notes:

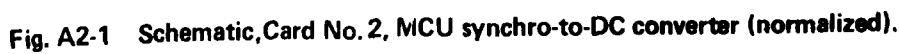
1. denotes pins on connector.
2. All resistors: MEA metal film $\pm 1\%$, 100 ppm $^{\circ}\text{C}$ or equivalent unless otherwise noted.
3. All capacitors: Mica $\pm 10\%$ or equivalent unless otherwise noted.
4. Adjust P_1 such that E_{02} is in phase or 180° out of phase with 400 Hz reference $E_{R2} \times 3$.
5. Adjust P_2 such that $E_{05} = 0 \text{ MV} \pm 10 \text{ MV}$ with $E_1 = 0.0 \text{ Vrms}$ and $E_{R1} = 8.00 \text{ VDC}$.
6. Adjust P_3 to yield overall gain of 10.0 V/rad with $S_1 - S_3$ within 5° of null.

To H-I
Pin 6

To H-I
Pin 8

$$\begin{aligned}\tau_1^2 &= R_1 R_2 C_1 C_2 \\ 2\zeta_1 \tau_1 &= (R_1 + R_2) C_2 \\ \tau_1 &= 1.988(10^{-3}) \text{ sec} \\ \zeta_1 &= 0.500 \\ f_1 &= \frac{1}{2\pi\tau_1} = 80.0 \text{ Hz}\end{aligned}$$

To 14.7
in series
Y input
multiplier



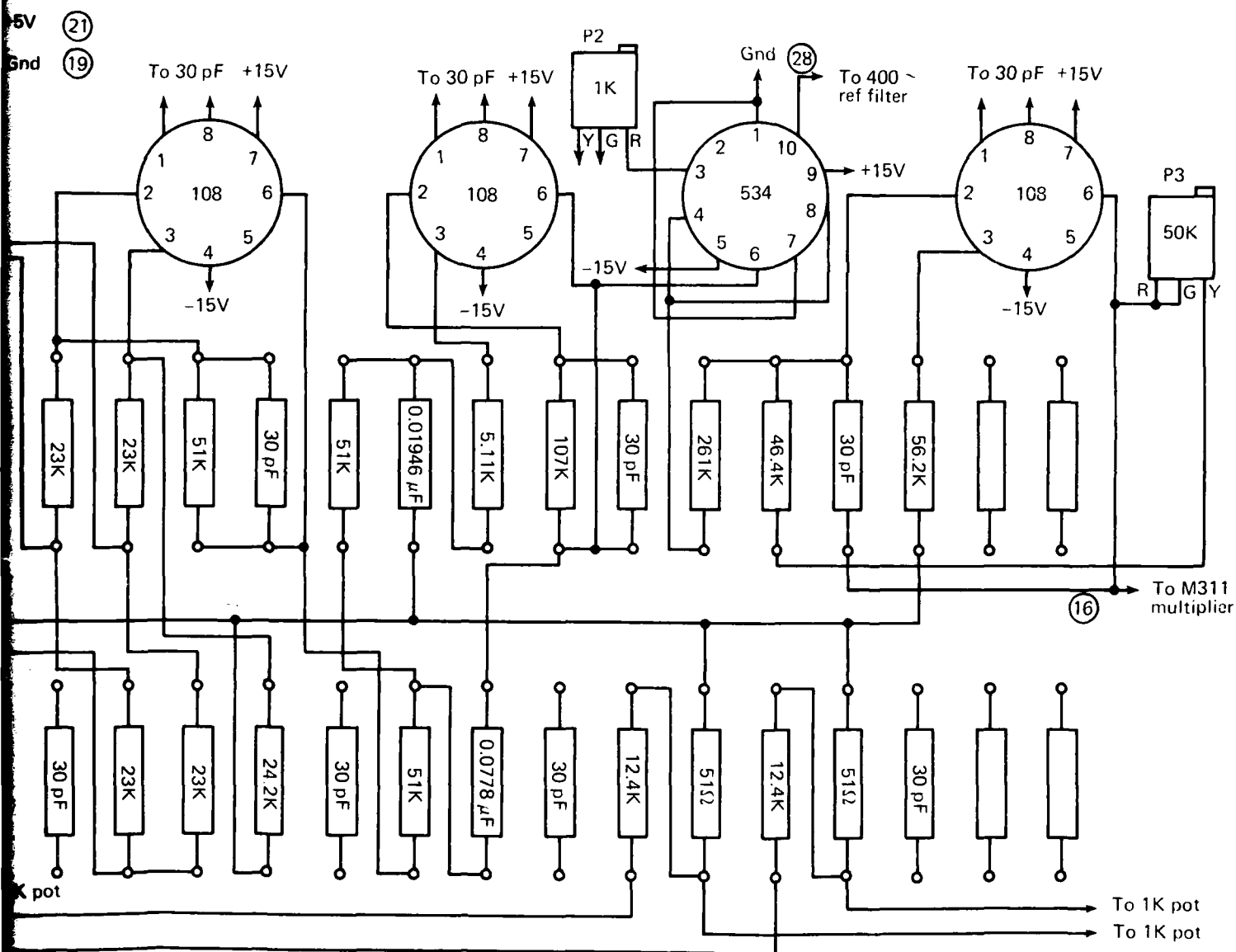
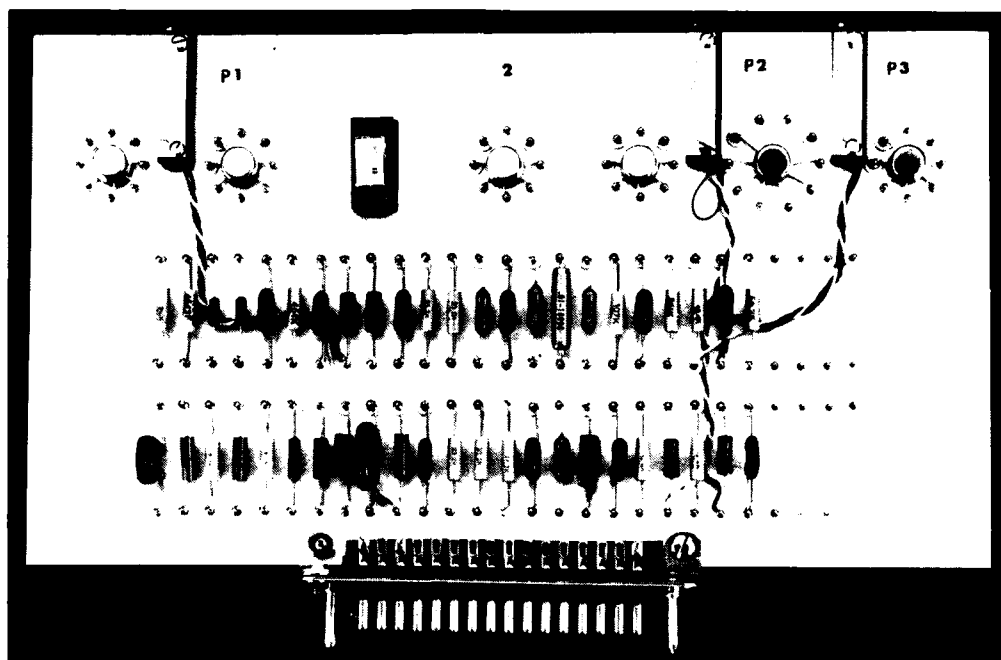
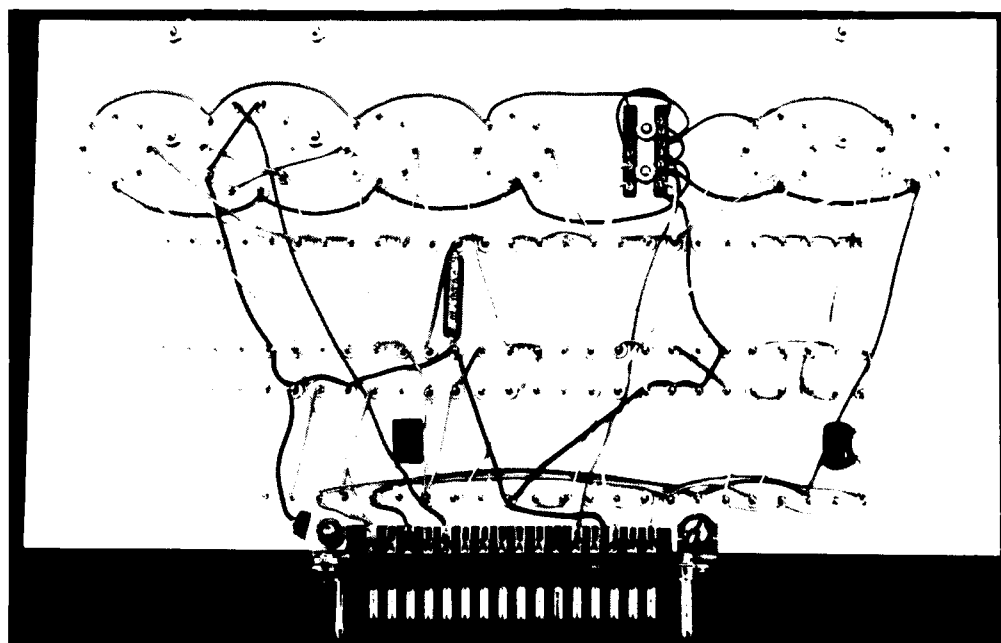


Fig. A2-2 Component layout, Card No. 2, MCU synchro-to-DC converter (normalized).



(a)



(b)

Fig. A2-3 MCU synchro-to-DC converter (normalized).

Board no. 3

Notes:

1. \bigcirc denotes pins on connector.
2. All resistors: MEA metal film $\pm 1\%$ 100 ppm/ $^{\circ}\text{C}$ or equivalent unless otherwise noted.
3. All capacitors: Mica $\pm 10\%$ or equivalent unless otherwise noted.
4. E_{R1} is signal proportional to average rectified value of 115 Vrms 400 Hz line.
5. Adjust P_1 to yield $E_{R1} = +8.00 \text{ VDC} \pm 0.080 \text{ VDC}$ when line voltage is exactly 115 Vrms.
6. E_{R1} is signal proportional to average rectified value of 115 Vrms 400 Hz line ($\approx E_R$)

To 400 Hz
ref XFMR
(UTC H-5)

Adjust P_1 to
yield $E_{R1} = 8.00 \text{ V}$
with E_R line
volt set at 115 Vrms
(Note 5)

Notes:

1. E_R
ave
115

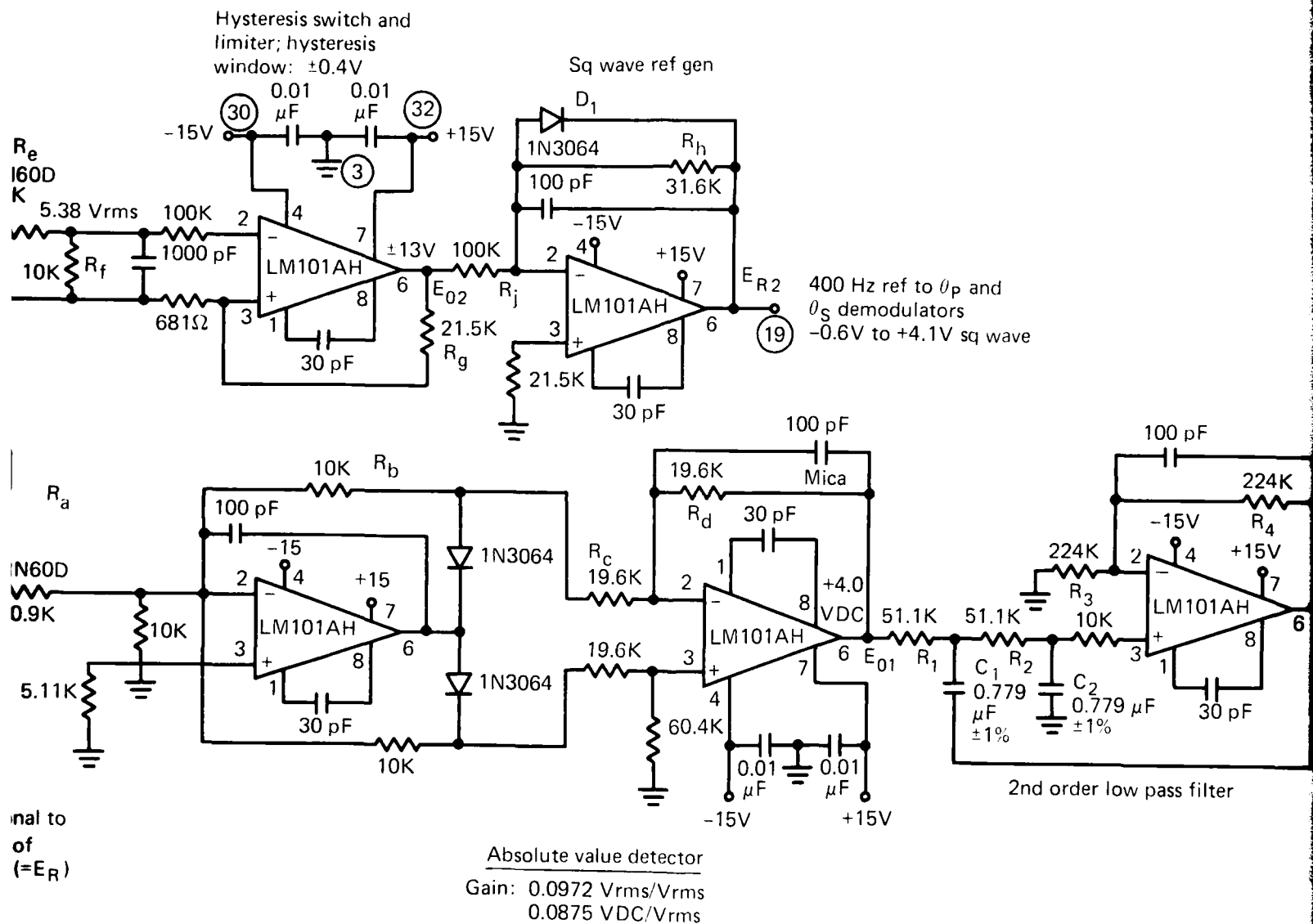
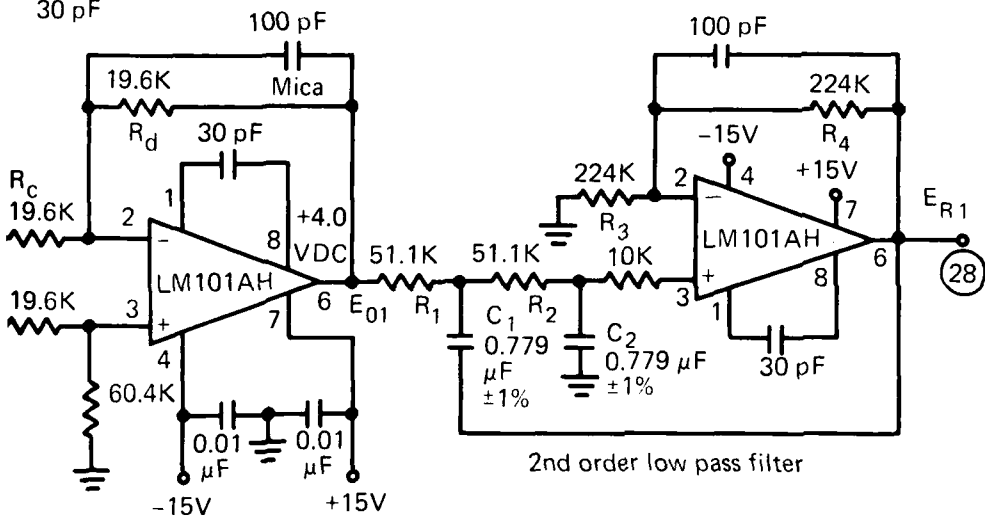
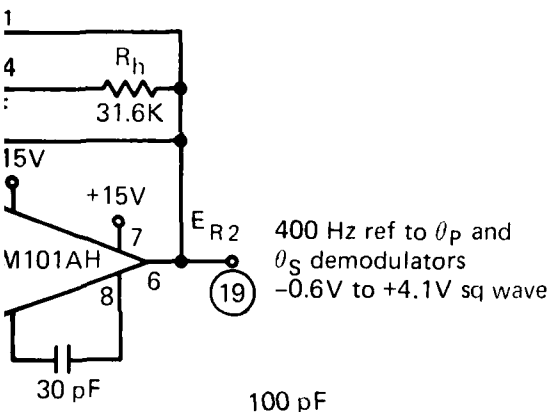


Fig. A3-1 Schematic Card No. 3, MC
 normalizing DC reference

wave ref gen



blue detector

2 Vrms/Vrms
5 VDC/Vrms

+8.00 VDC to dividers
in θ_P and θ_S channels
Note 5
Note 6

$$\frac{E_{R1}}{E_{01}} = \frac{K_2}{\tau_2^2 S^2 + 2\xi_2 \tau_2 S + 1}$$

$$\tau_2^2 = R_1 R_2 C_1 C_2$$

$$2\xi_2 \tau_2 = R_2 C_2 + R_1 (C_1 + C_2 - K_2 C_1)$$

$$K_2 = 1 + \frac{R_4}{R_3}$$

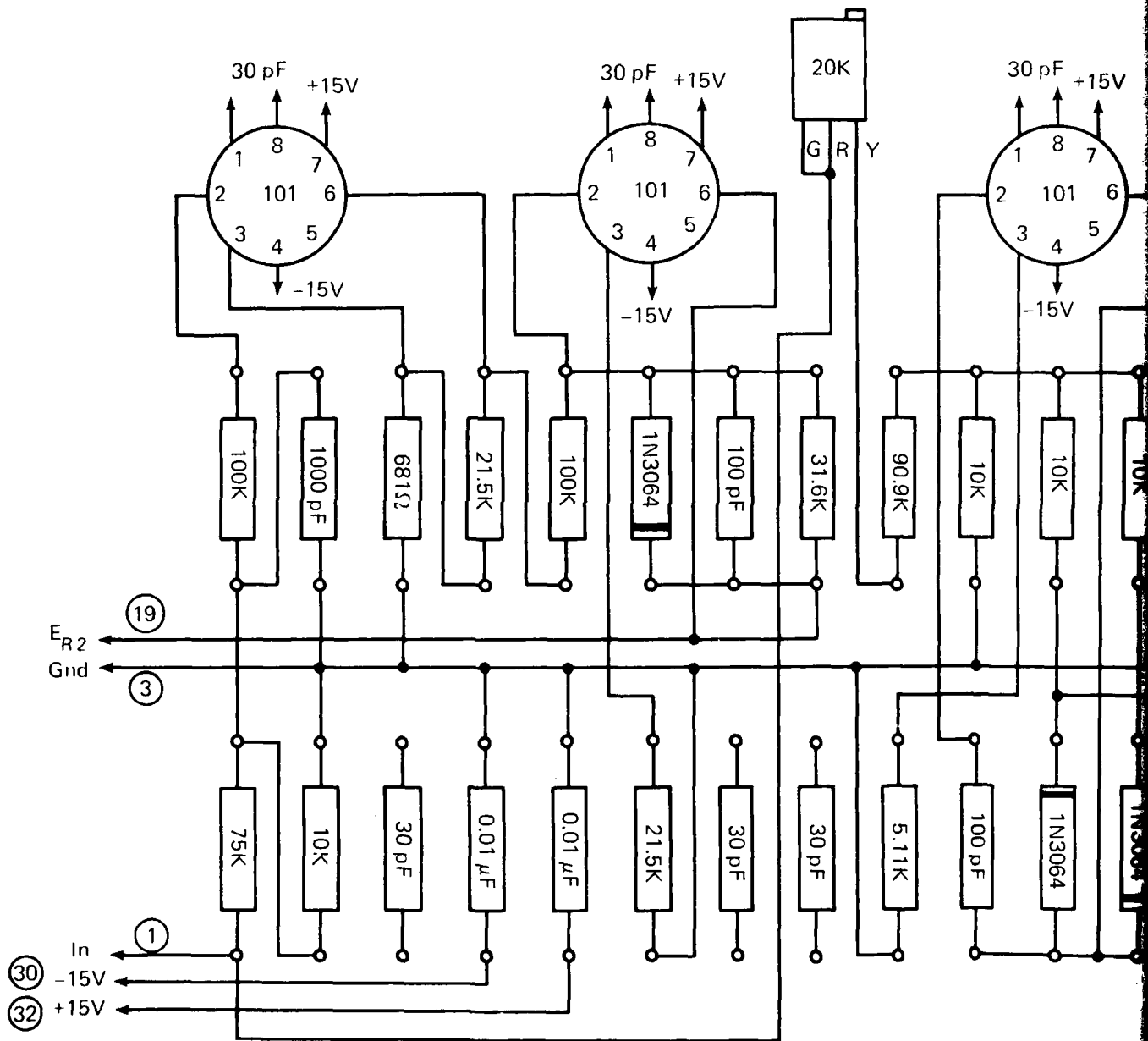
$$\tau_2 = 3.981(10^{-2}) \text{ sec}$$

$$\xi_2 = 0.500$$

$$K_2 = 2.00$$

$$f_2 = \frac{1}{2\pi\tau_2} = 4.00 \text{ Hz}$$

Fig. A3-1 Schematic Card No. 3, MCU 400 Hz square wave reference generator and normalizing DC reference signal.



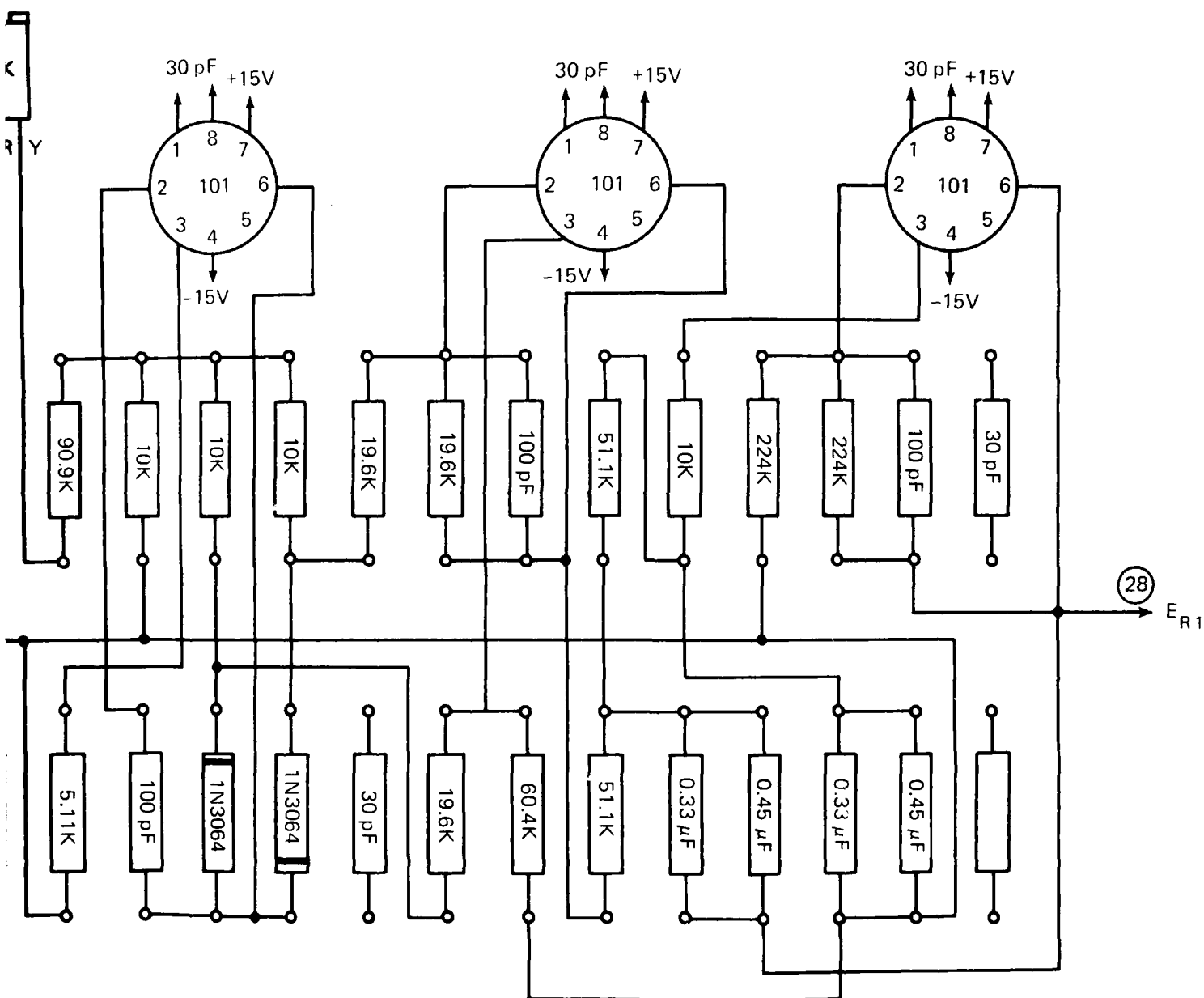
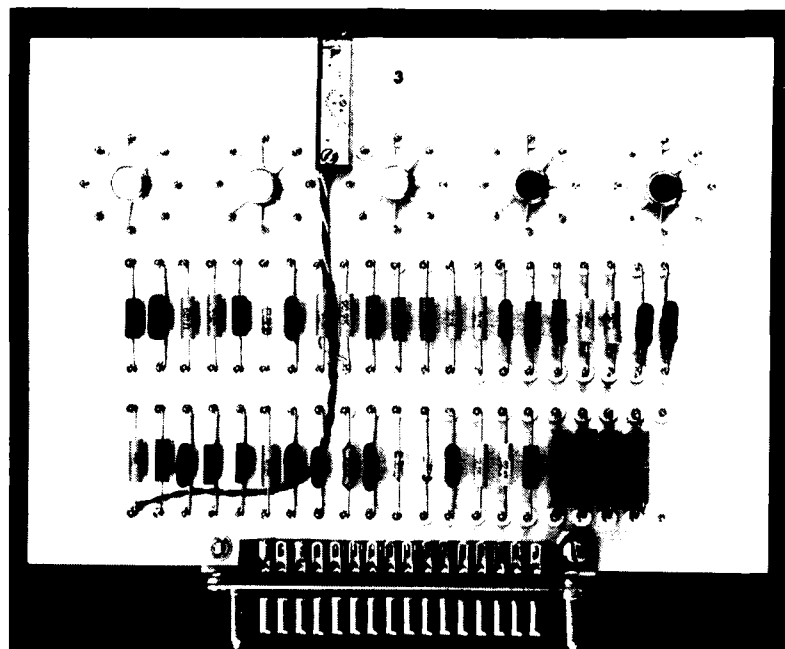
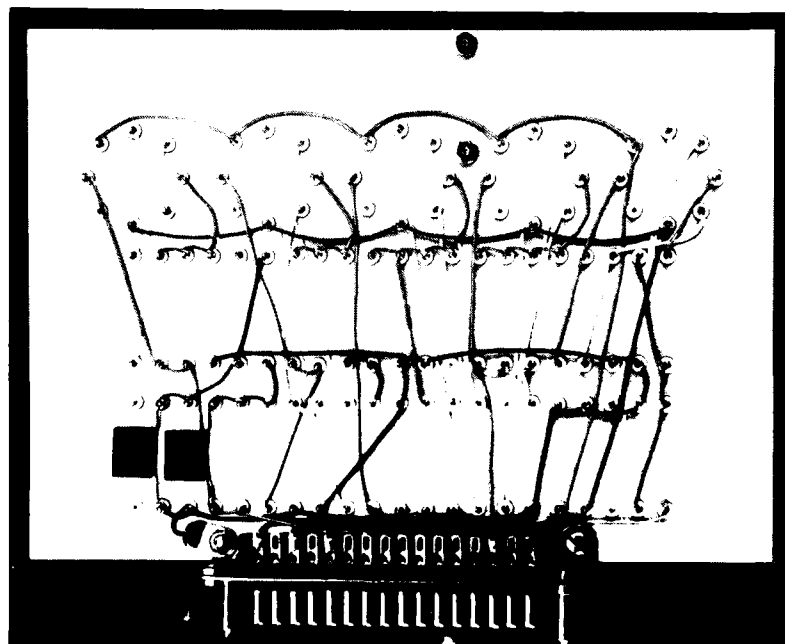


Fig. A3-2 Component layout, Card No. 3, MCU square wave reference generator 400 Hz.



(a)



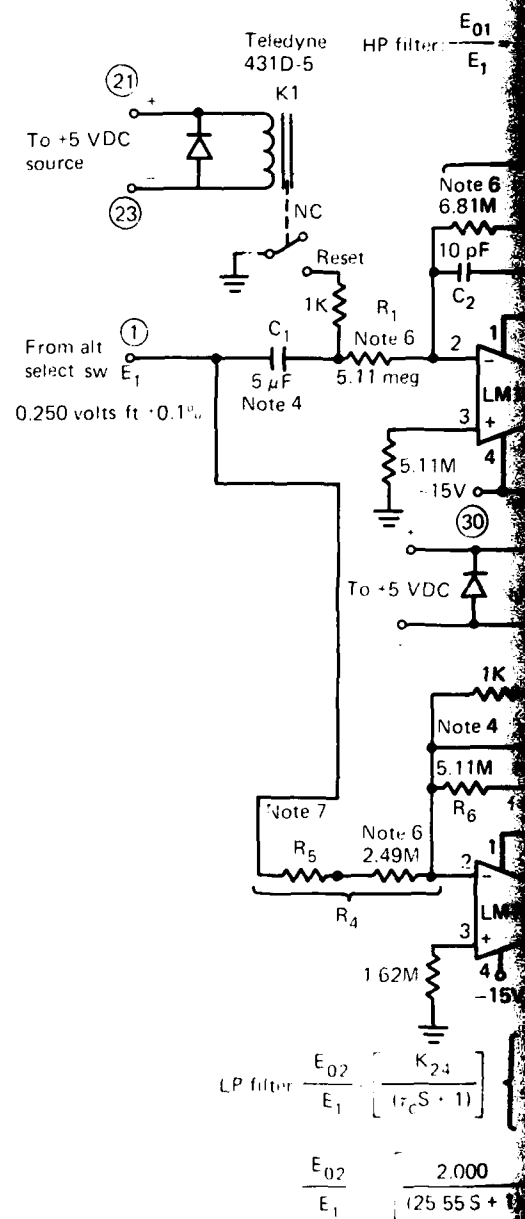
(b)

Fig. A3-3 MCU 400 Hz reference.

Board No. 4

Notes

- denotes pins on connector.
- All resistors: MEA metal film $\pm 1\%$, 100 ppm/°C or equivalent unless otherwise noted.
- All capacitors: Mica $\pm 10\%$ or equivalent unless otherwise noted.
- Wesco Electronics: Type 41 MPC, $\pm 5\%$, 50 VDC metallized, hermetically sealed polycarbonate capacitor. Connect case to signal ground.
- Choose R_3 such that gain @ 20 Hz = $\frac{E_{01}}{E_1} = -1.359 \pm 0.002$. Actual value (169K) required is shown on schematic. Nominal value = 134K Ω .
- Choose R_5 such that DC gain = $\frac{E_{02}}{E_1} = -2.000 \pm 0.002$. Nominal value of $R_5 = 65K \Omega$.



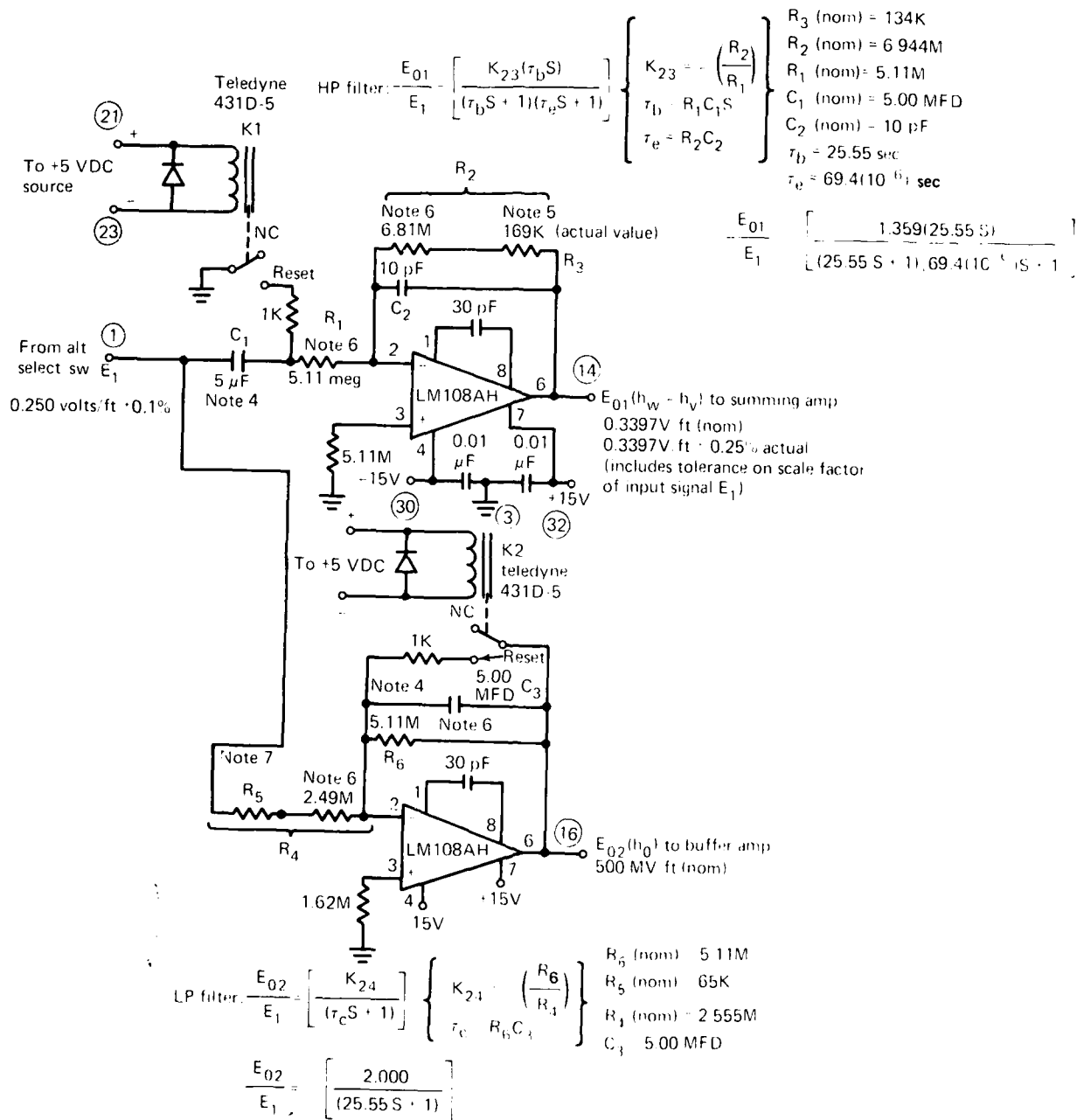


Fig. A4-1 Schematic, Card No. 4, MCU altimeter filter circuits.

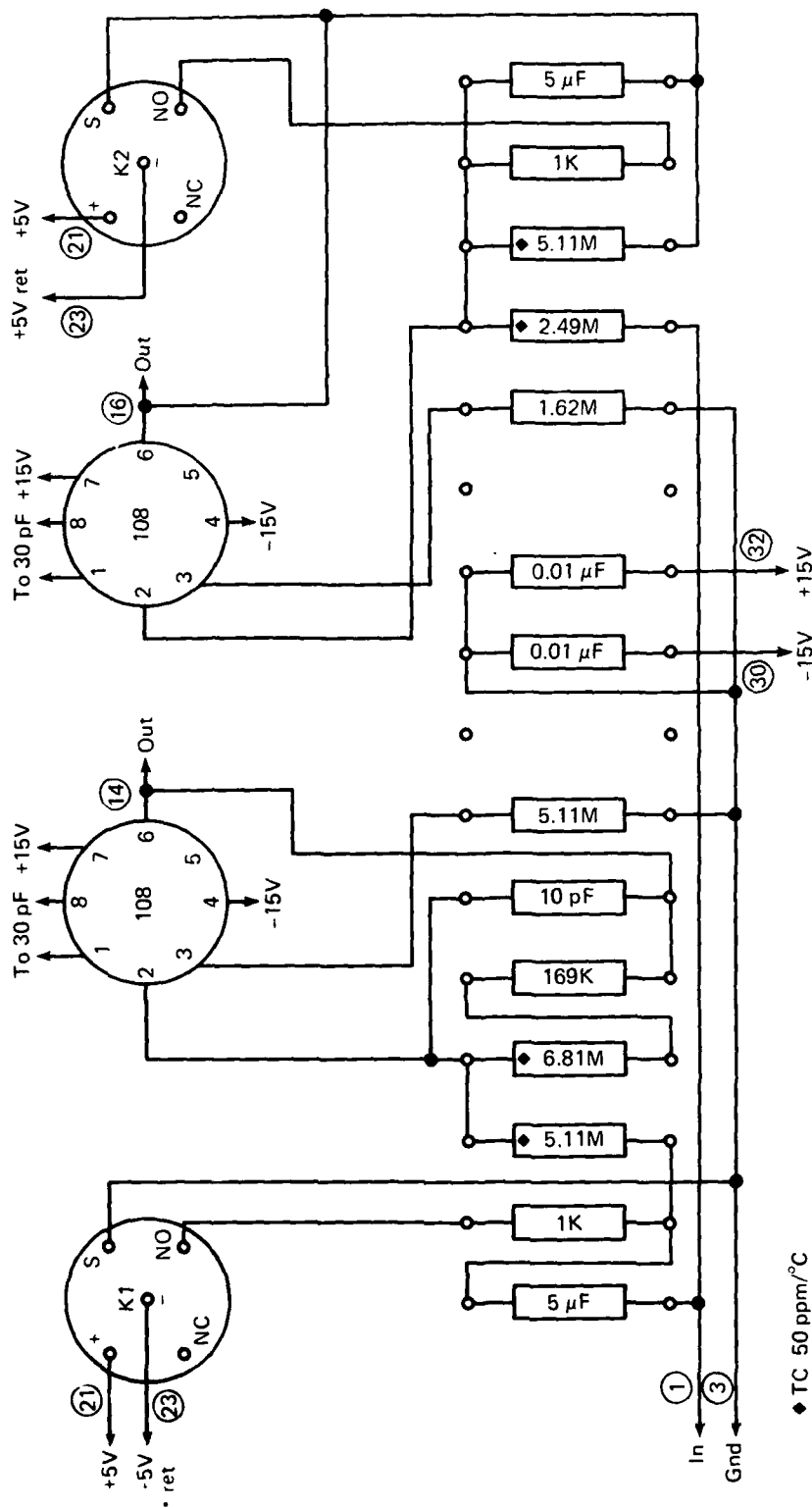
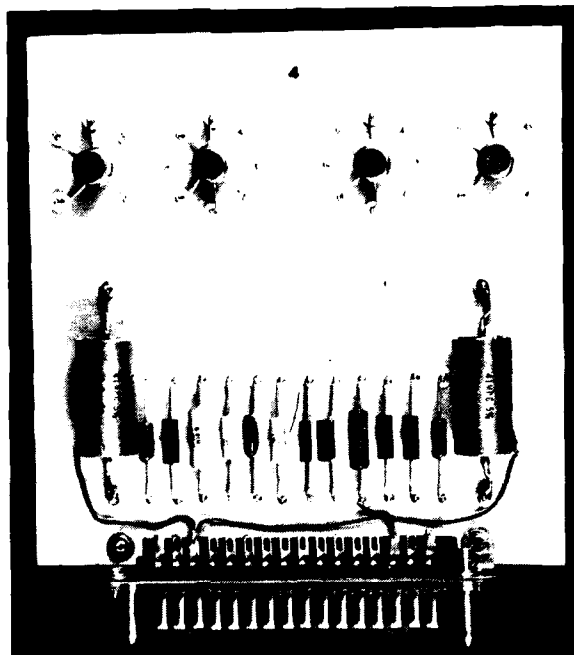
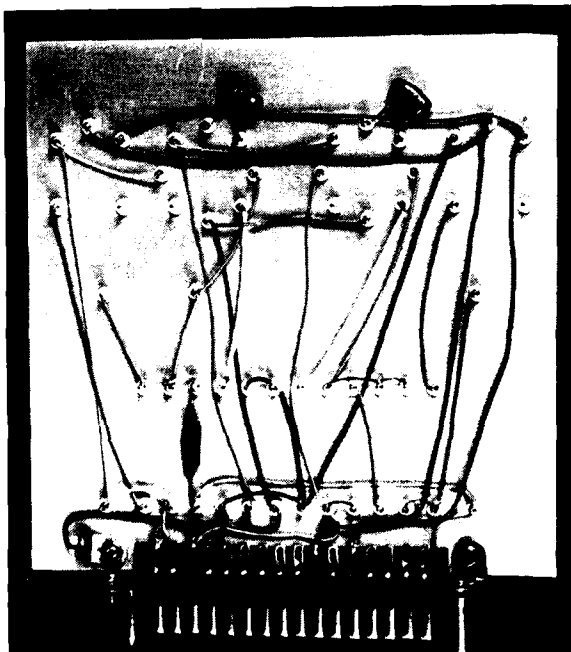


Fig. A4-2 Component layout, Card No. 4, MCU altimeter filter circuits.

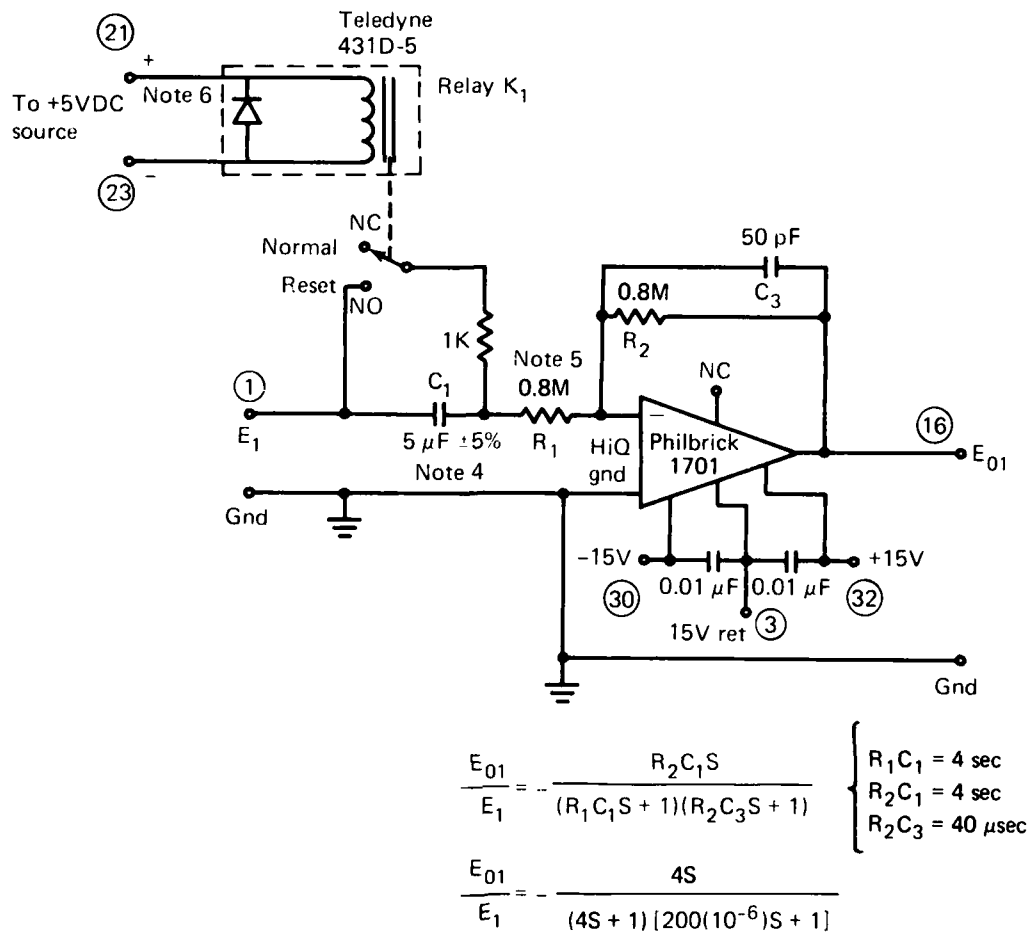


(a)



(b)

Fig. A4-3 MCU altimeter filter circuits.



Board no. 5

Notes:

- 1 ○ denotes pins on connector.
2. All resistors: MEA metal film $\pm 1\%$, 100 ppm/ $^{\circ}\text{C}$ or equivalent unless otherwise noted.
3. All capacitors: Mica $\pm 10\%$ or equivalent unless otherwise noted.
4. Wesco Electronics: Type 41 MPC, $\pm 5\%$ tolerance, 50 VDC metallized, hermetically sealed polycarbonate capacitor. Case should be connected to signal ground.
5. $R_1 C_1$ product should be $4 \text{ s} \pm 1.2 \text{ s}$, assuming R_1 and C_1 have a $\pm 1\%$ and $\pm 5\%$ tolerance, respectively.
6. 5 V return is to be connected to power ground. Power and signal grounds should be connected at one point only.

Fig. A5-1 Schematic, Card No.5, MCU high-pass filter.

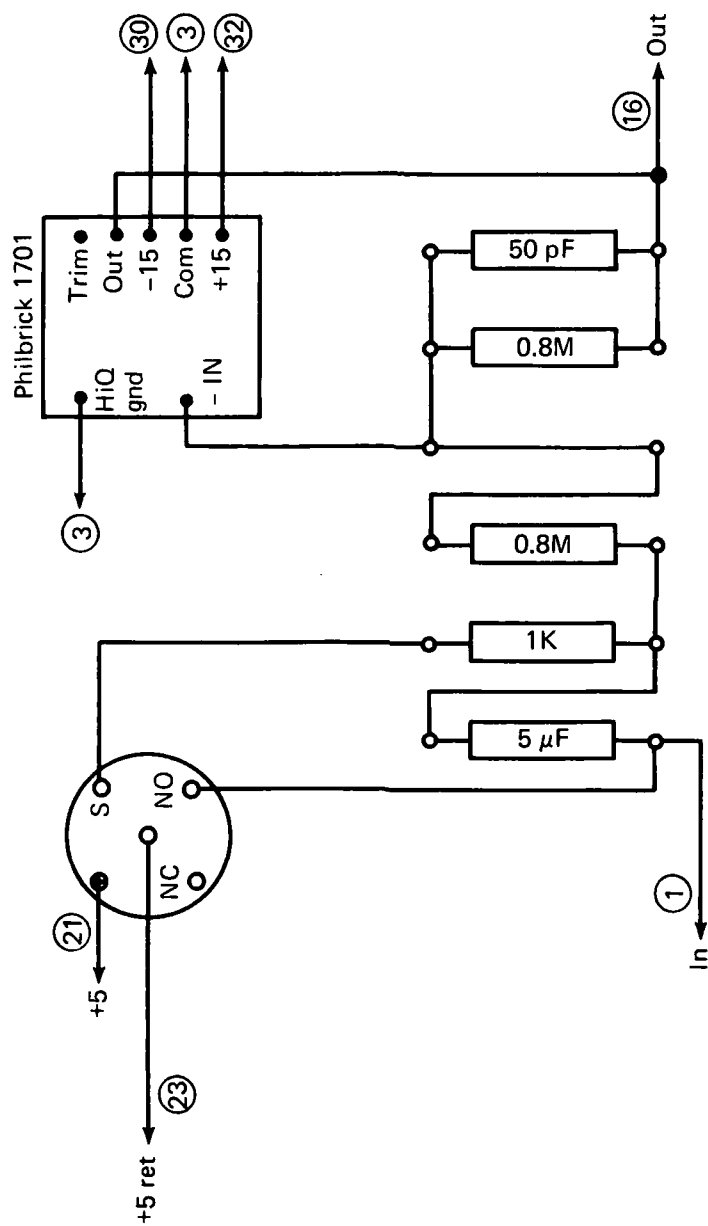
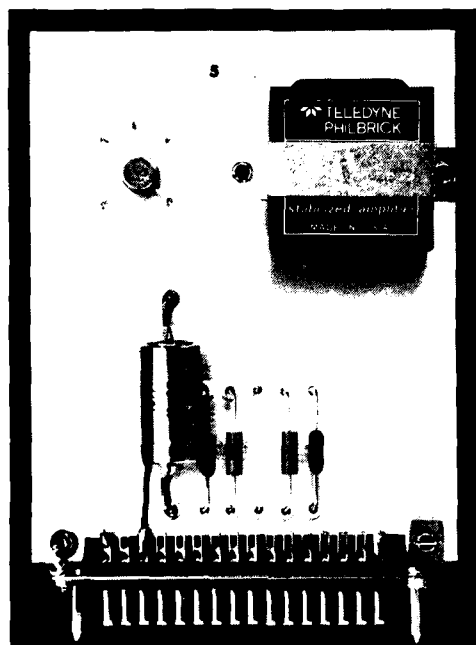
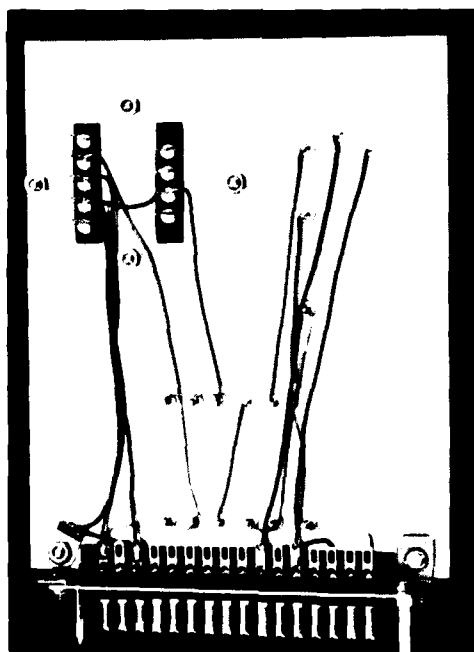


Fig. A5-2 Component layout, Card No.5, MCU high-pass filter.



(a)



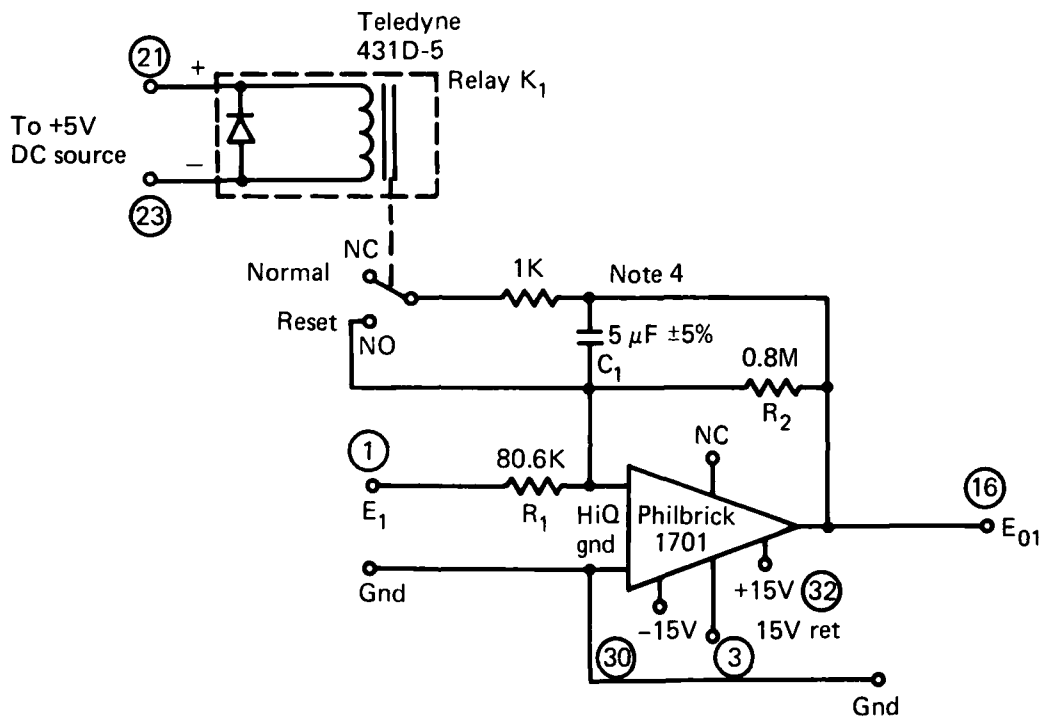
(b)

Fig. A5-3 MCU high-pass filter.

Board No. 6

Notes:

1. ○ denotes pins on connector.
2. All resistors: MEA metal film $\pm 1\%$, 100 ppm/ $^{\circ}\text{C}$ or equivalent, unless otherwise noted.
3. All capacitors: Mica $\pm 10\%$ or equivalent unless otherwise noted.
4. Wesco Electronics: Type 41 MPC, $\pm 5\%$ tolerance, 50 VDC metallized, hermetically sealed polycarbonate capacitor. Case should be connected to signal ground.
5. $R_2 C_1$ product should be $4 \text{ s} \pm 1.2\text{S}$, assuming R_2 and C_1 have a $\pm 1\%$ and $\pm 5\%$ tolerance, respectively.
6. 5 V return is to be connected to power ground. Power and signal grounds should be connected at one point only.



$$\frac{E_{01}}{E_1} = - \left(\frac{R_2}{R_1} \right) \left[\frac{1}{R_2 C_1 S + 1} \right] \left\{ \begin{array}{l} R_2 C_1 = 4 \text{ sec} \\ \frac{R_2}{R_1} = 9.92 \end{array} \right.$$

$$\frac{E_{01}}{E_1} = -9.92 \left[\frac{1}{4S + 1} \right]$$

Fig. A6-1 Schematic, Card No. 6, MCU low-pass filter.

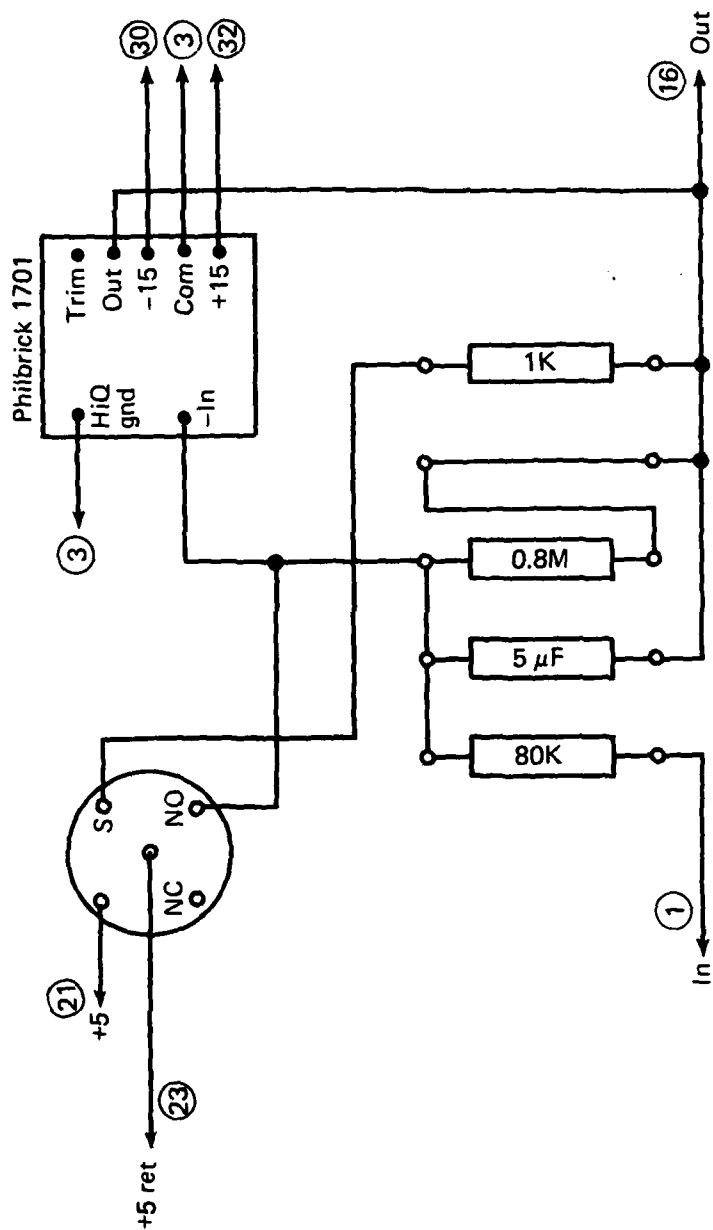
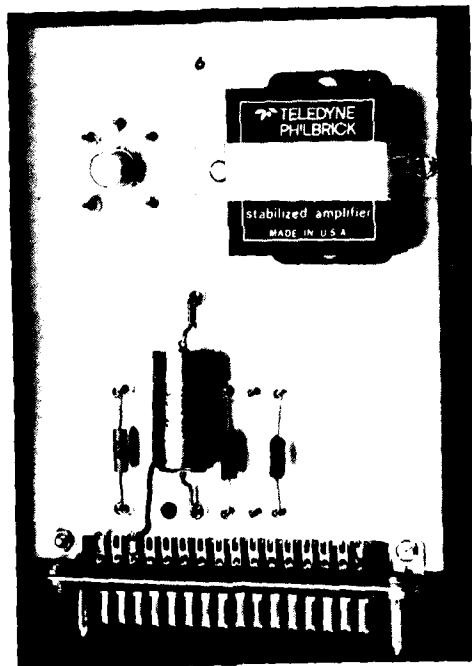
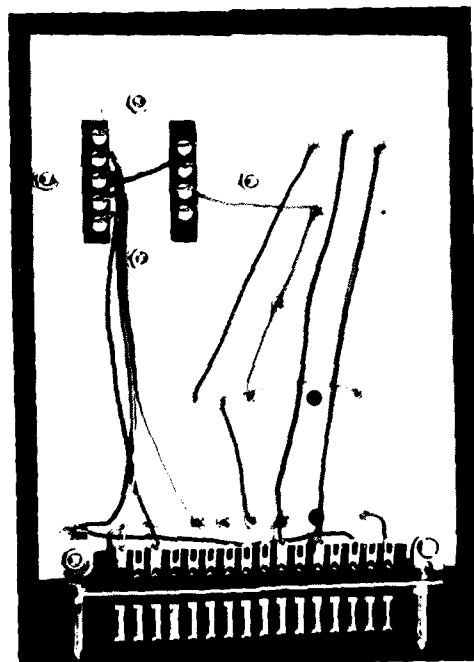


Fig. A6-2 Component layout, Card No. 6, MCU low-pass filter.



(a)



(b)

Fig. A6-3 MCU low-pass filter.

Board No. 7

Notes:

1. \bigcirc denotes pins on connector.
2. All resistors: MEA metal film $\pm 1\%$, 100 ppm/ $^{\circ}\text{C}$ or equivalent unless otherwise noted.
3. All capacitors: Mica $\pm 10\%$ or equivalent unless otherwise noted.
4. Bourns 10 turn trimpot. WW
5. Adjust P_2 so that E_{01} becomes $1.000 \sin [2\pi(1.000)t]$ V within $\pm 0.5\%$ when altimeter measures wave $h_w = 1.000 \sin [2\pi(1.000)t]$ ft with no vehicle motion. It is assumed pot P_1 is adjusted properly before this adjustment is made.
6. Adjust P_3 so that E_{02} becomes $1.00 \sin [2\pi(1.0)t]$ V within $\pm 0.5\%$ when input acceleration to \vec{Z} is $\vec{Z} = -1.226 \sin [2\pi(1.0)t]$ g with vehicle at 0° roll and pitch angles.
7. Adjust P_1 to null output E_{01} when vehicle motion alone in steady state is h_v where $h_v = 1.00 \sin [2\pi(1.0)t]$ when vehicle is at 0° for roll and pitch angles. This assumes altimeter responds to vehicle motion and that wave motion is eliminated.

To output of
5 stage filter in
accelerometer path

To output of single stage
HP filter in altimeter
path

Adjustable gain summing amplifier

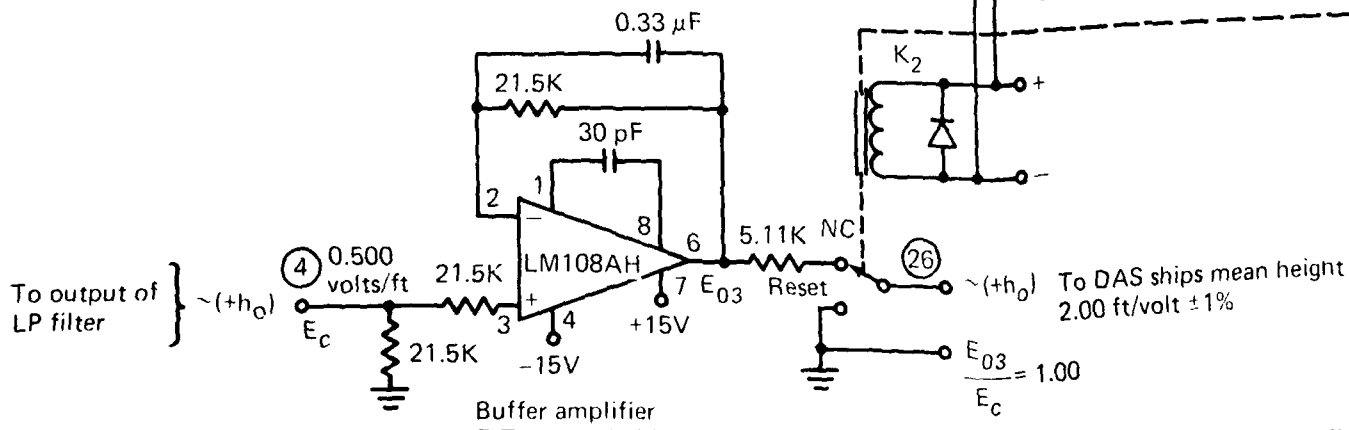
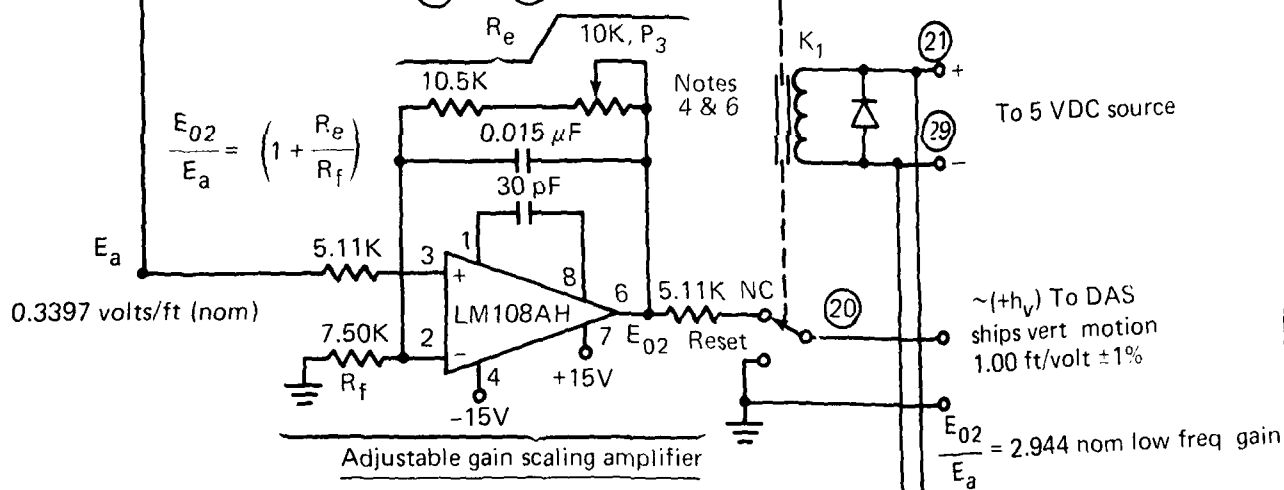
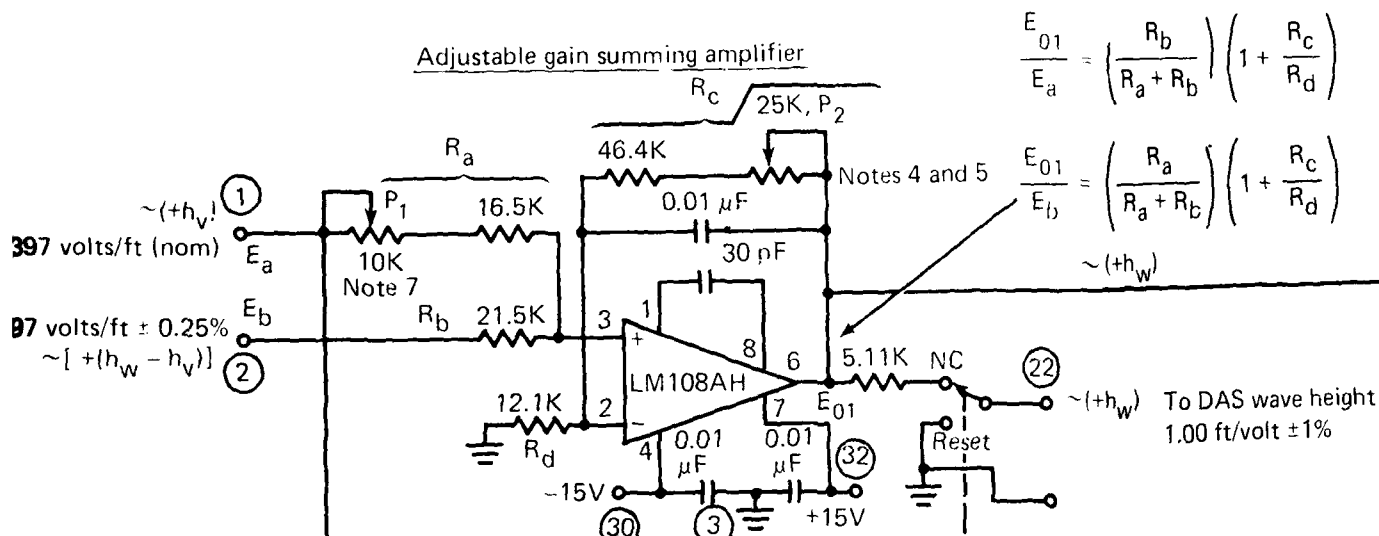


Fig. A7-1 Sc

$$\frac{E_{01}}{E_a} = \left(\frac{R_b}{R_a + R_b} \right) \left(1 + \frac{R_c}{R_d} \right)$$

4 and 5 $\frac{E_{01}}{E_b} = \left(\frac{R_a}{R_a + R_b} \right) \left(1 + \frac{R_c}{R_d} \right)$

$\sim (+h_w)$

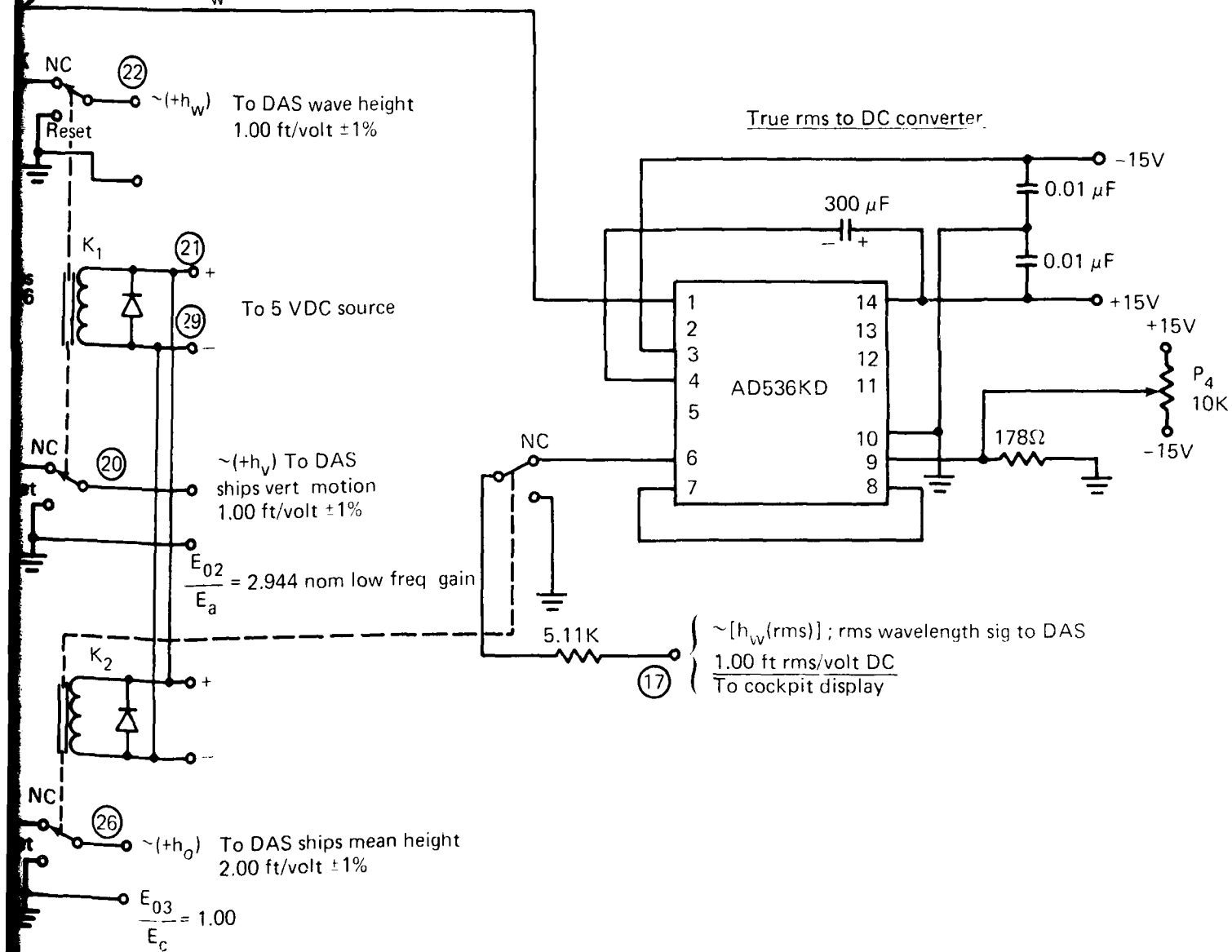
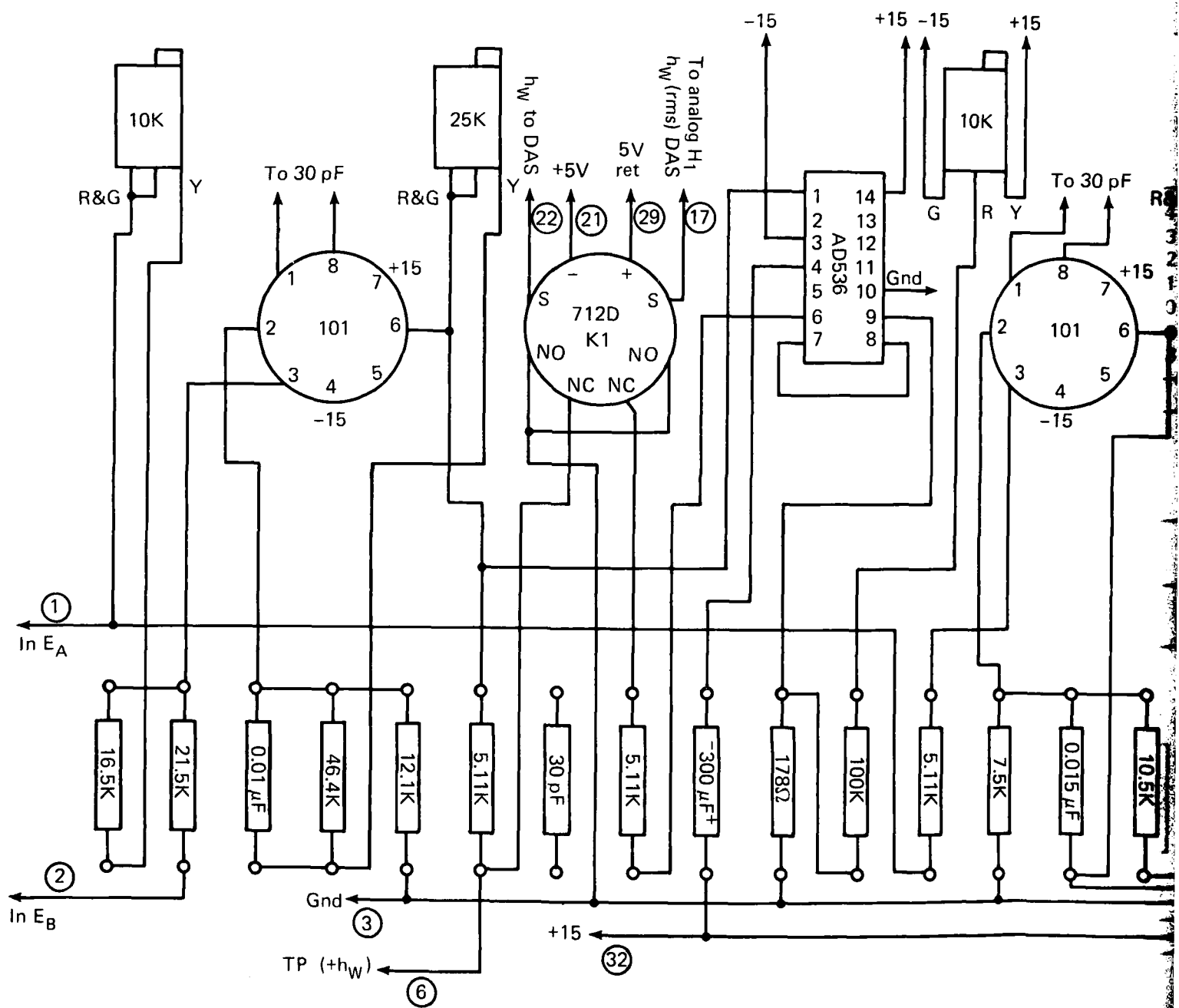


Fig. A7-1 Schematic, Card No. 7, MCU system output signal conditioning.



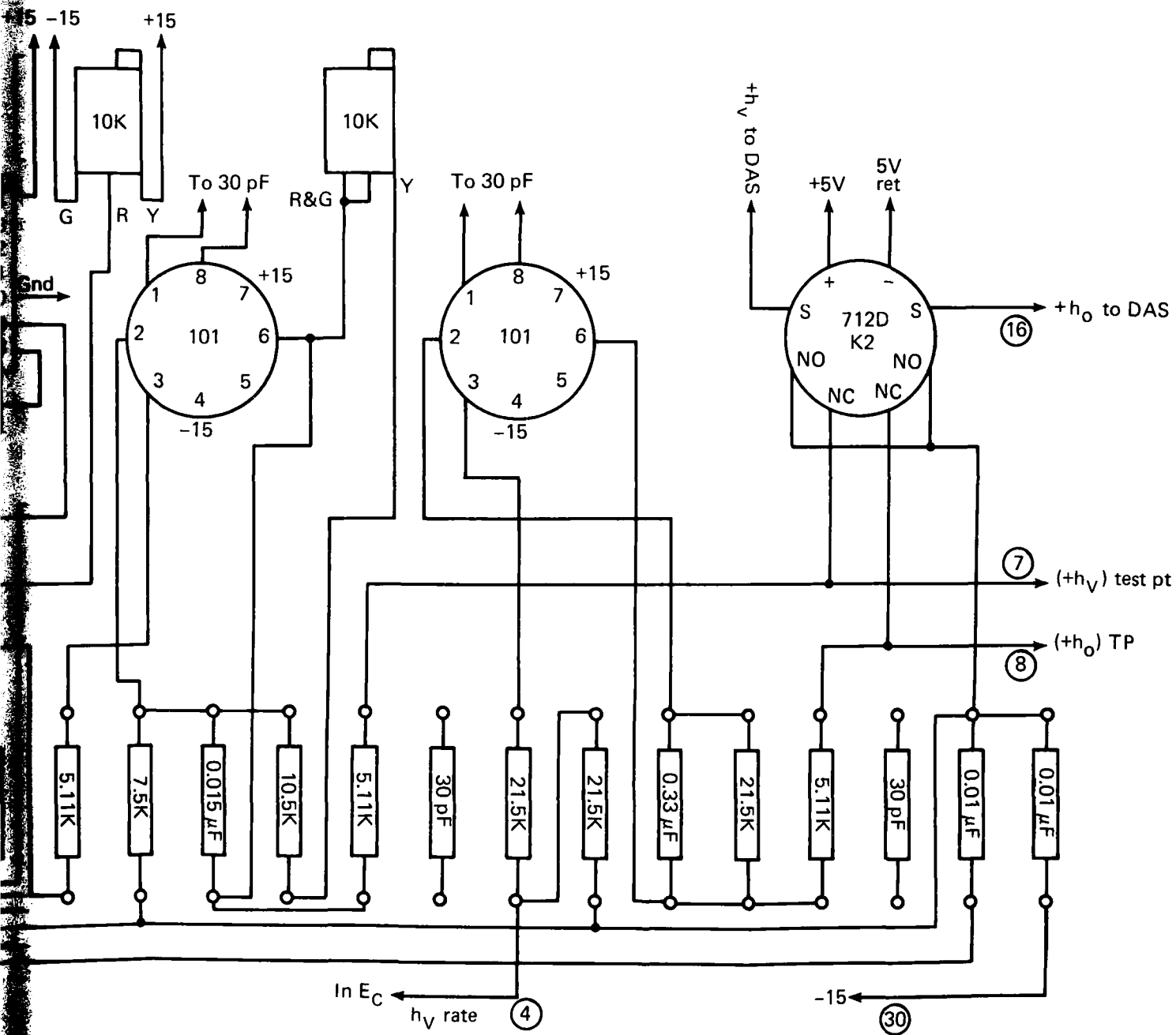
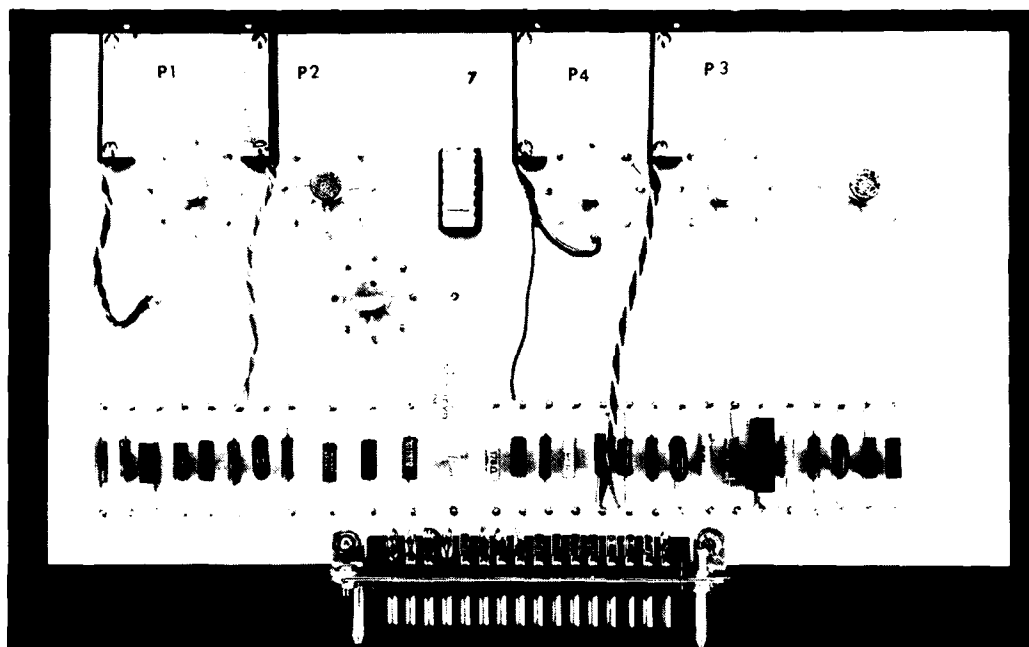
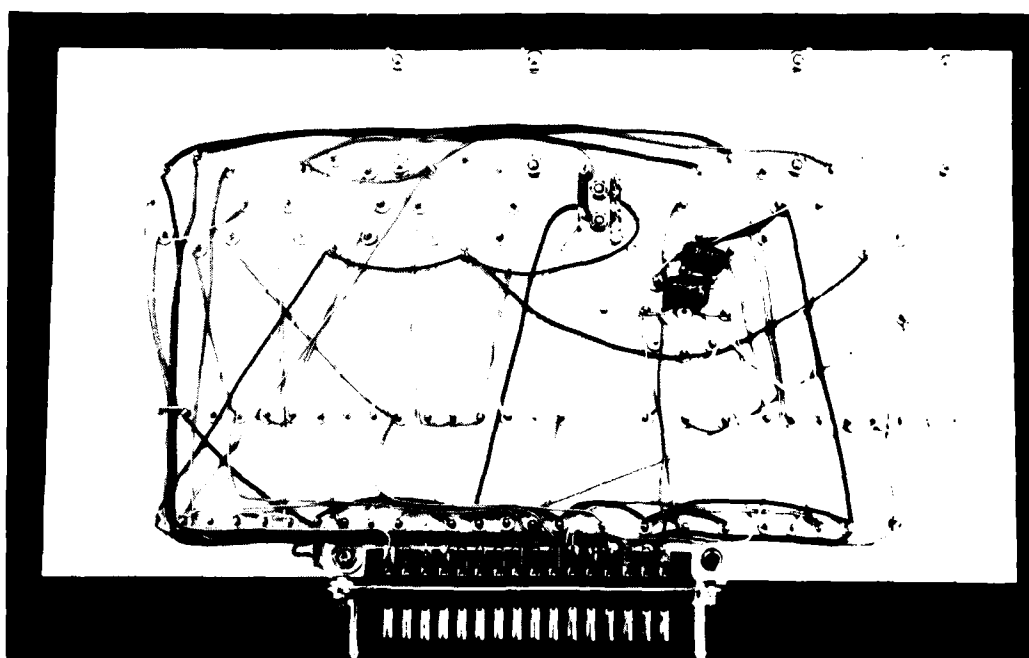


Fig. A7-2 Component layout, Card No. 7, MCU system output signal conditioning and rms converter.



(a)



(b)

Fig. A7-3 MCU system output conditioner and rms converter.

Board No. 8

Notes:

1. \bigcirc denotes pins on connector.
2. All resistors: MEA metal film $\pm 1\%$, ± 100 ppm/ $^{\circ}\text{C}$ or equivalent unless otherwise noted.
3. All capacitors: Mica $\pm 10\%$ or equivalent unless otherwise noted.
4. Select R_e such that $R_e = (7R_c - R_d) \pm 5\%$.
5. Pins 6 and 7 are connected to mode select switch on front panel and shown in operate position.
6. Pin 5 input is obtained from either the φ (roll) or θ (pitch) channels, corresponding to the \ddot{Y} or \ddot{X} accelerometer channels, respectively.
7. DAS load impedance assumed to be $\geq 1 \text{ M}\Omega$.

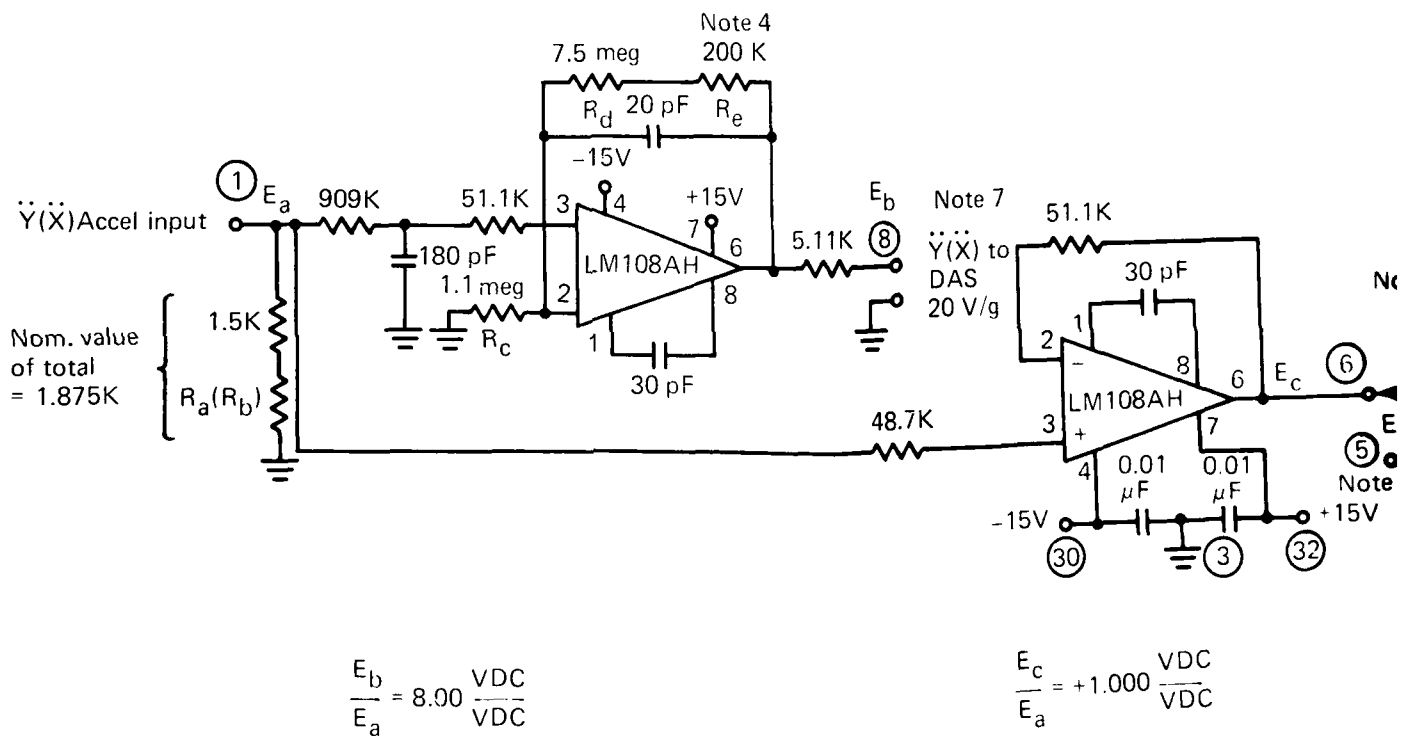


Fig. A8-1 Schenck converter

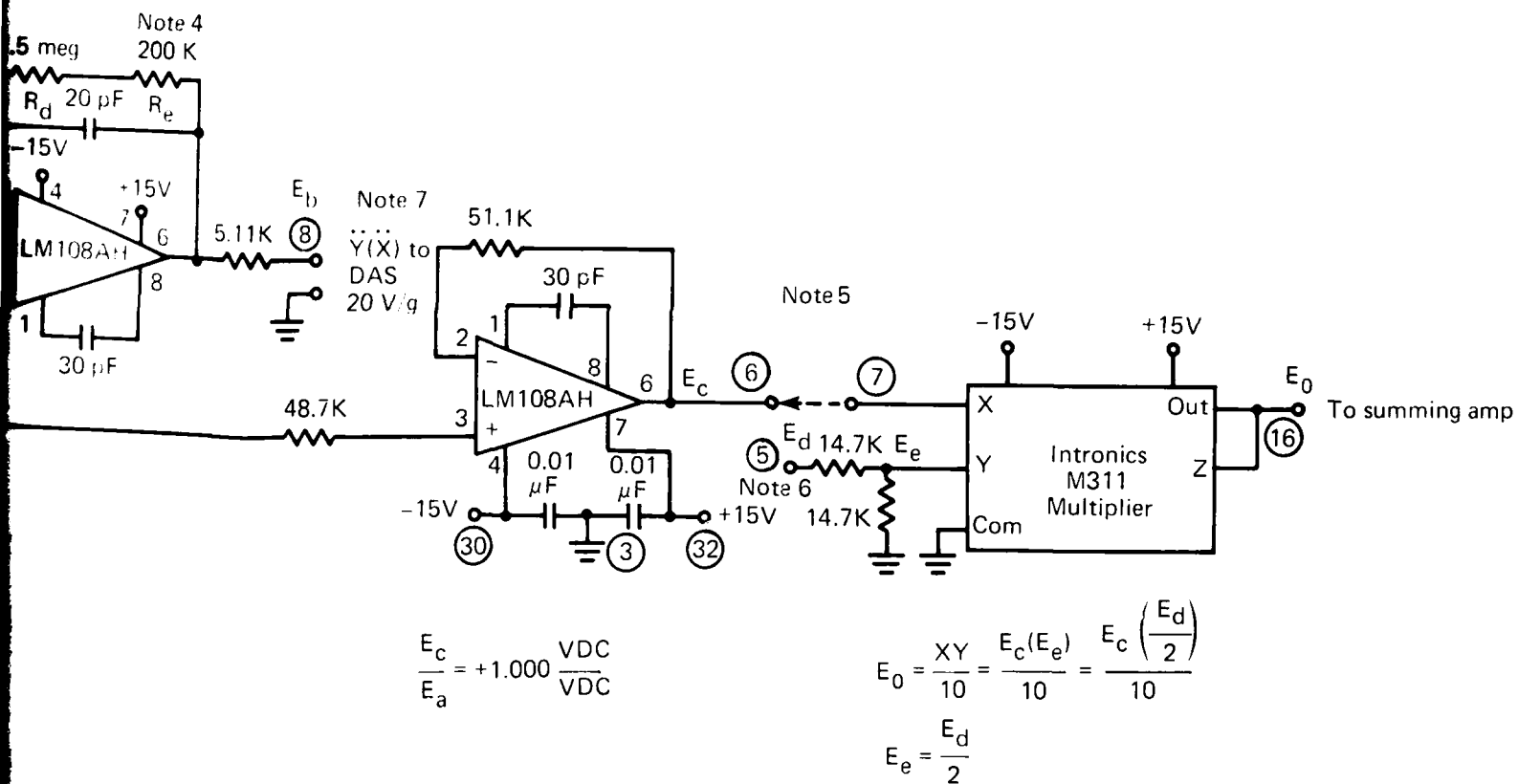


Fig. A8-1 Schematic, Card No. 8, \ddot{X}, \ddot{Y} accelerometer scaling coordinate conversion and DAS buffer.

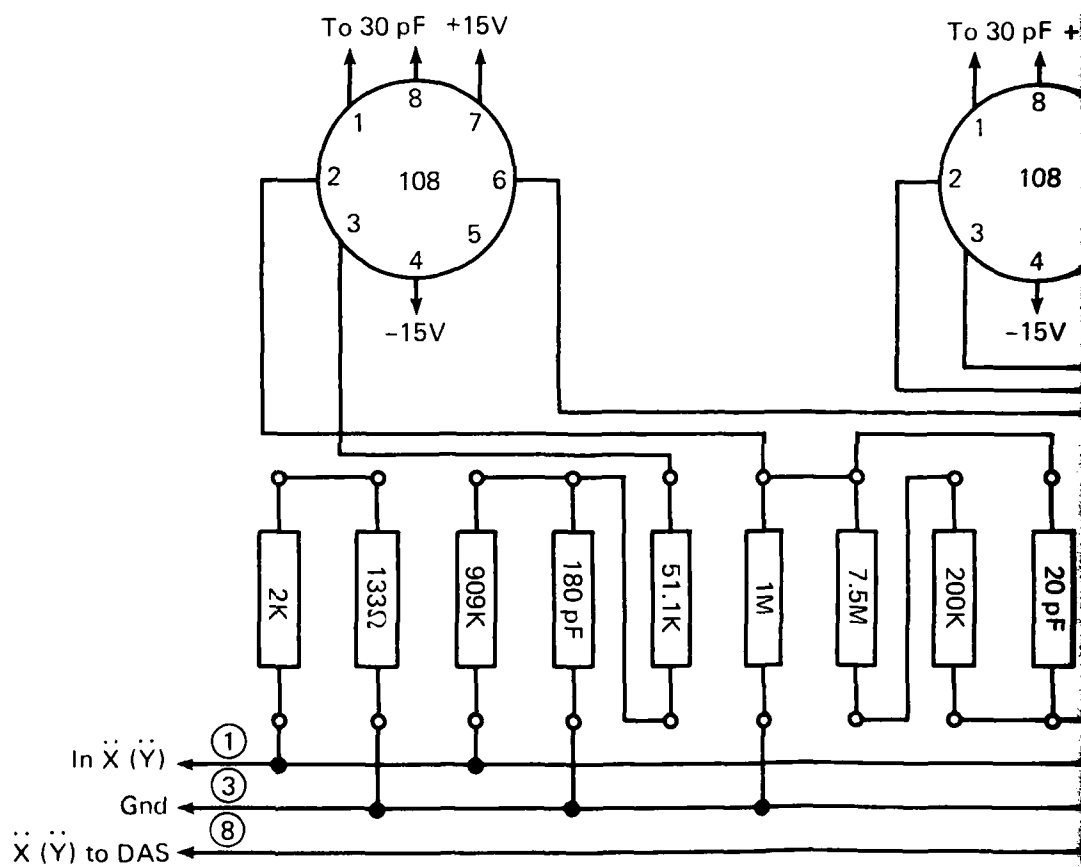


Fig. A8-2

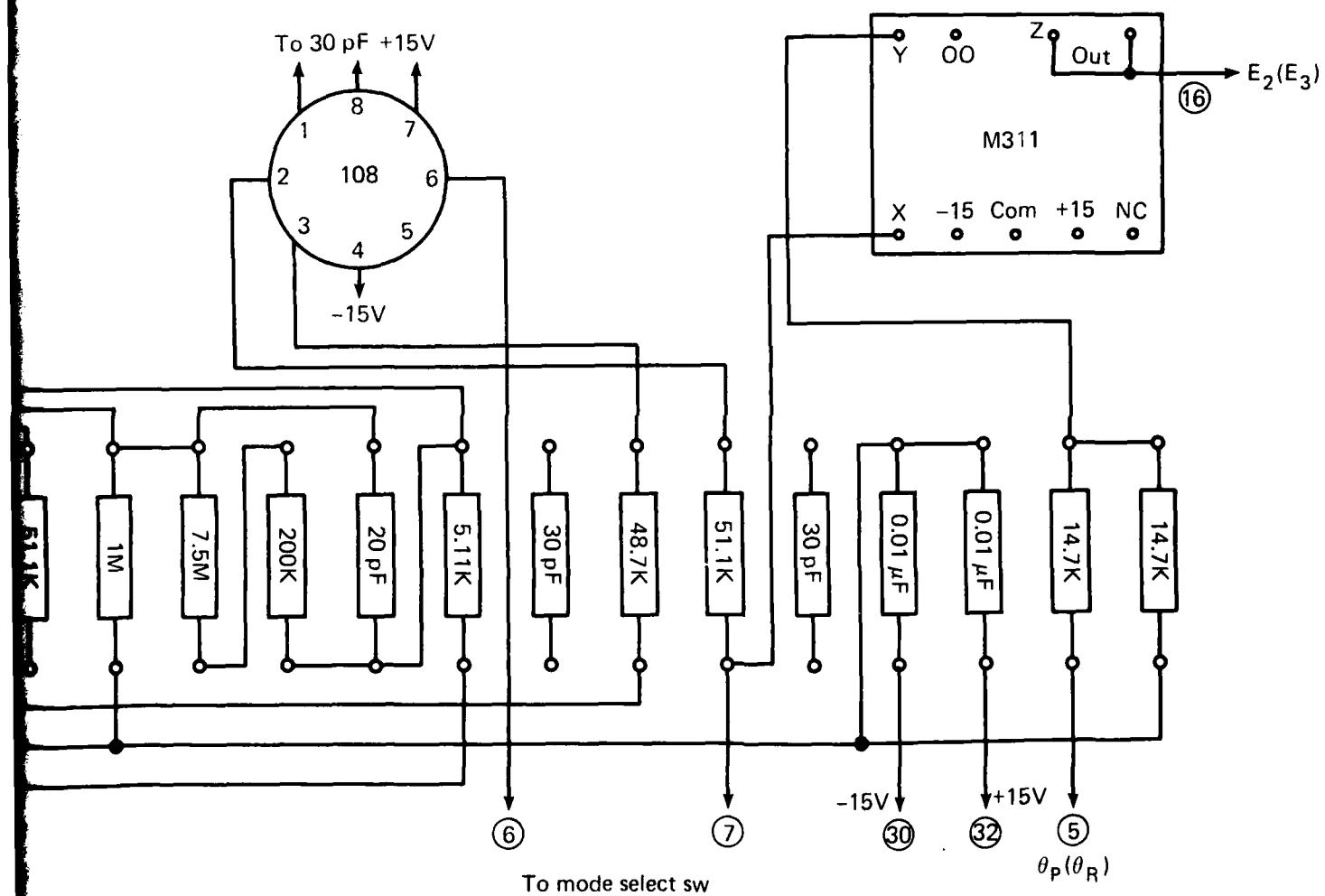
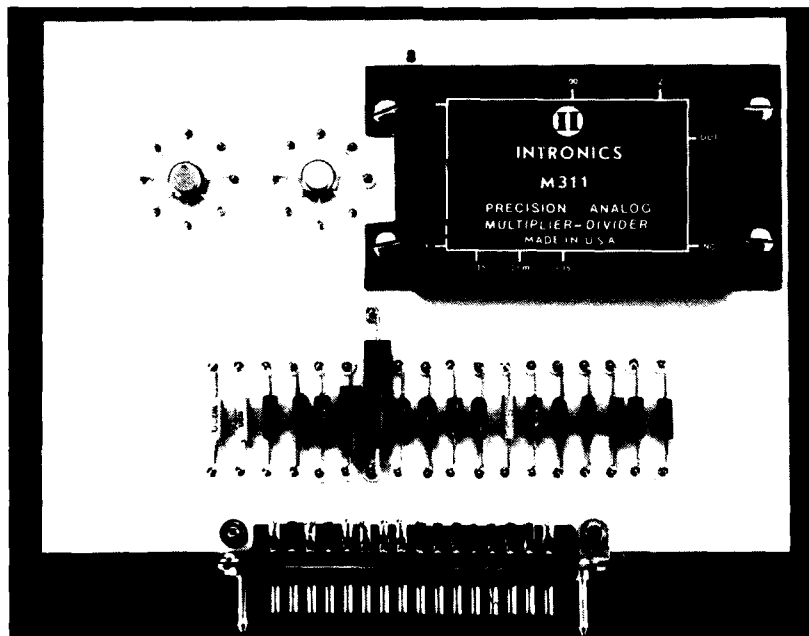
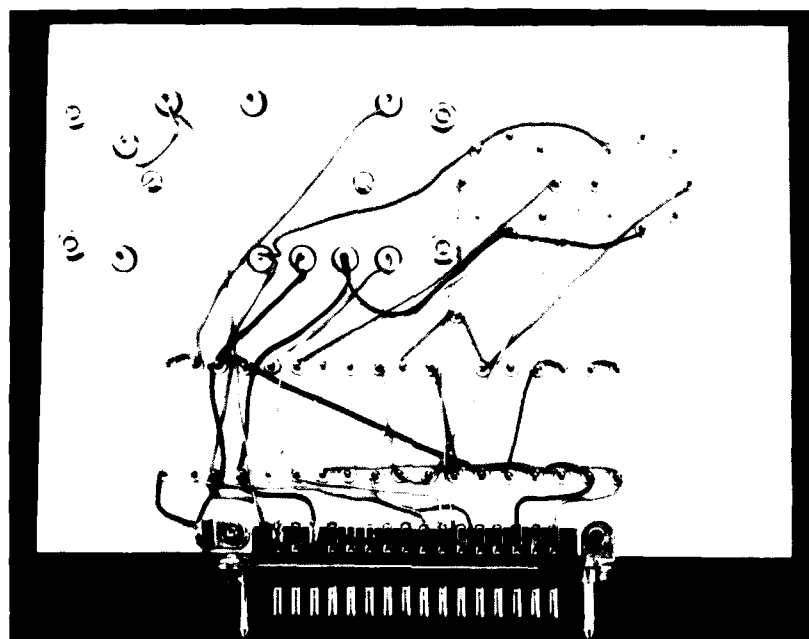


Fig. A8-2 Component layout, Card No. 8, MCU \ddot{X} , \ddot{Y} accelerometer scaling, coordinate conversion and DAS buffer.



(a)



(b)

Fig. A8-3 MCU \ddot{x} , \ddot{y} , accelerometer scaling, coordinate conversion, and DAS buffer.

Board No. 9

Notes:

1. denotes pins on connector.
2. All resistors: MEA metal film $\pm 1\%$, 100 ppm/°C or equivalent unless otherwise noted.
3. All capacitors: Mica $\pm 10\%$ or equivalent unless otherwise noted.
4. All 1M Ω resistors: Metal film $\pm 1\%$, 50 ppm/°C.
5. R_1 and R_1' , metal film $\pm 1\%$, 50 ppm/°C. Choose R_1 (R_1') such that a change in altitude of 10 ft causes E_{03} (E_{03}') to change by 2.45 V \pm 50 MV with P_1 (P_1') shorted. Then for a 10 ft change in altitude, set P_1 (P_1') for E_{03} (E_{03}') change of 2.5 V \pm 2.5 MV. Value shown for R_1 (R_1') is based on altimeter scale factor of 200 MV/ft.
6. Bias for "0" altitude should be \pm 25 ft.
7. 50K resistor: $\pm 1\%$ WW, 50 ppm/°C temperature coefficient.
8. Choose R_2 (R_2') such that the voltage at 25 ft position of front panel switch is 6.25 V \pm 50 MV. R_2 (R_2'): WW, $\pm 1\%$, 50 ppm/°C temperature coefficient.
9. Bourns 20 turn WW trimpot or equivalent.

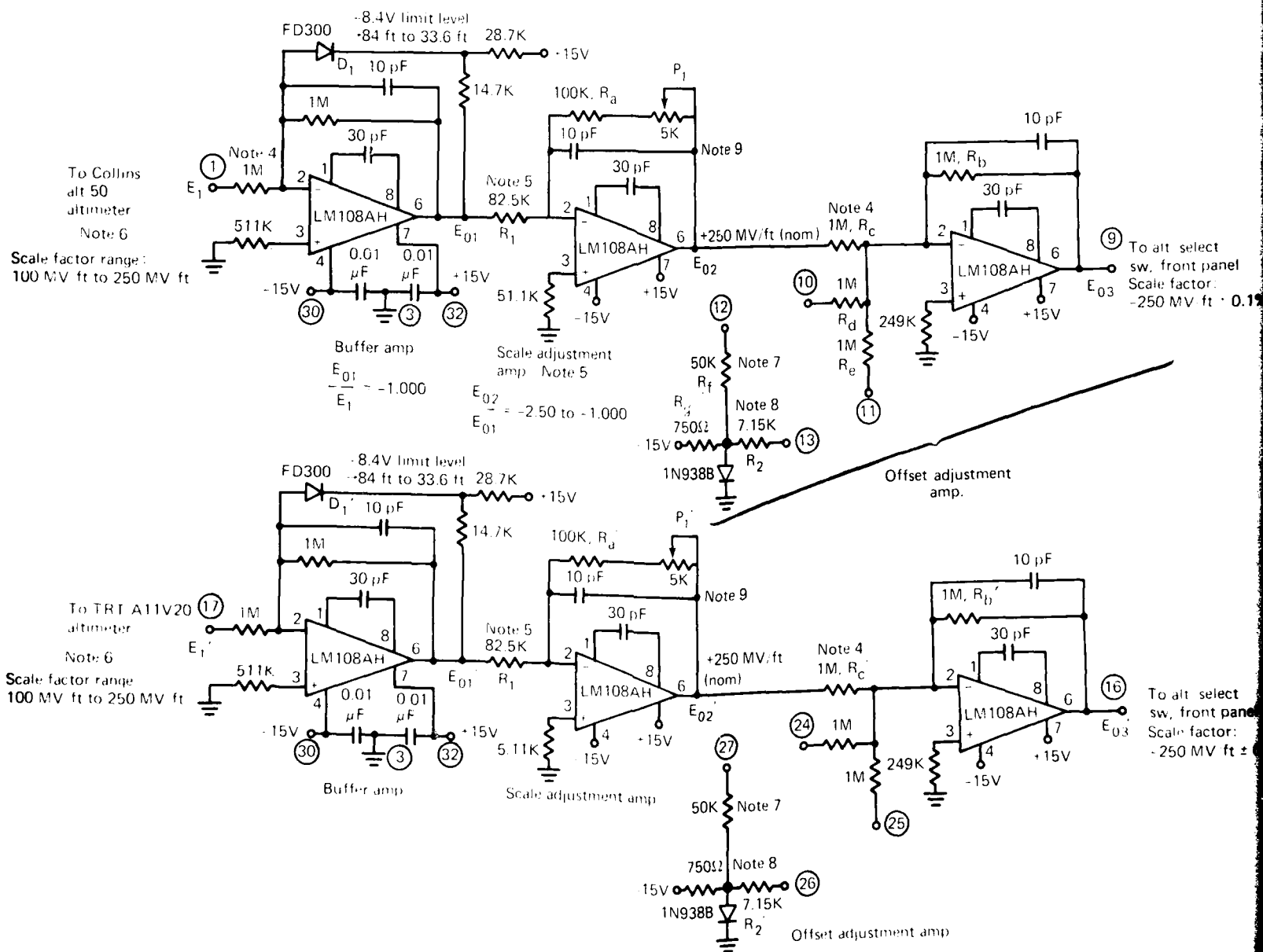
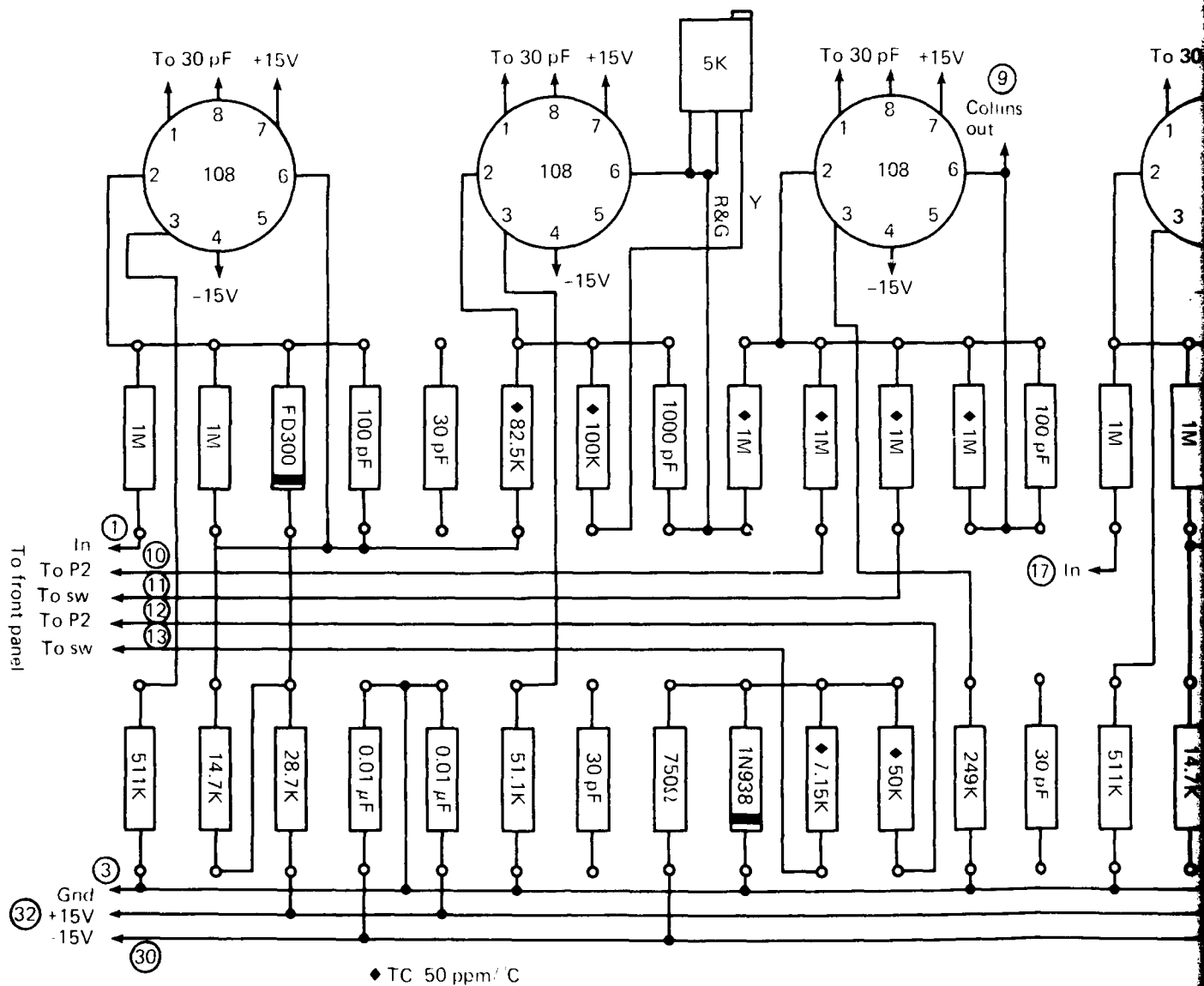


Fig. A9-1 Schematic, Card No. 9, MCU altimeter signal converter





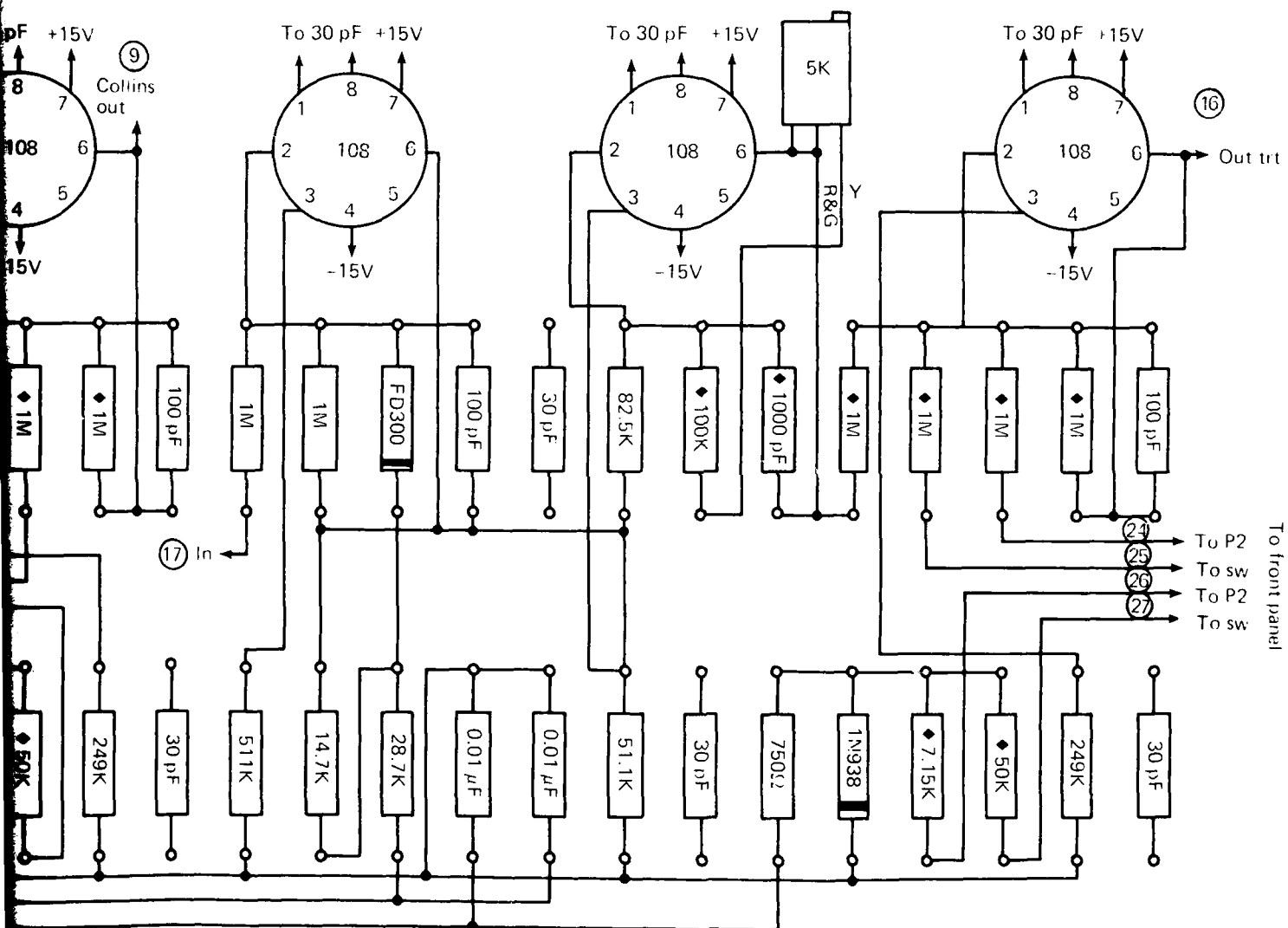
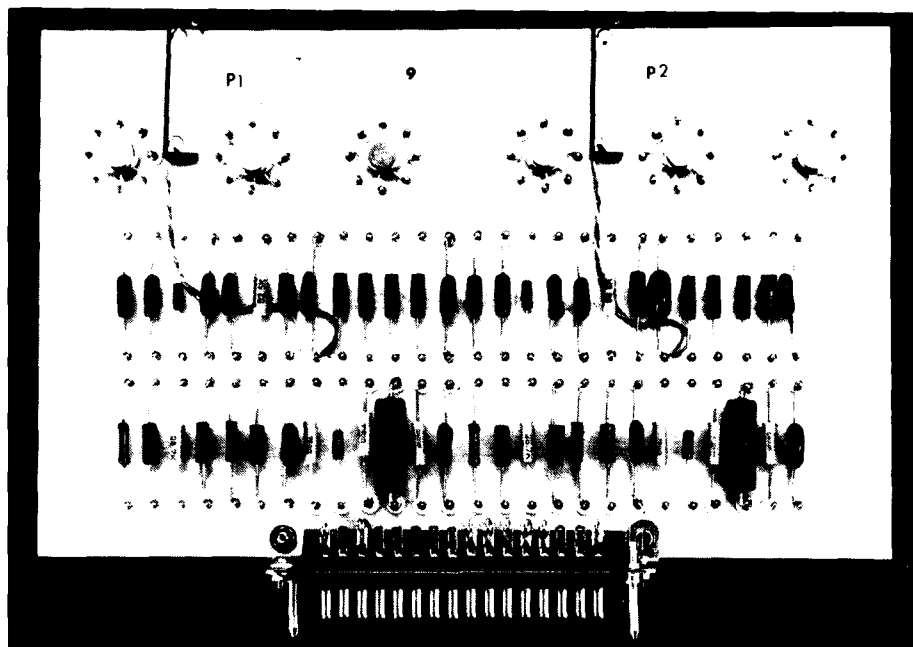
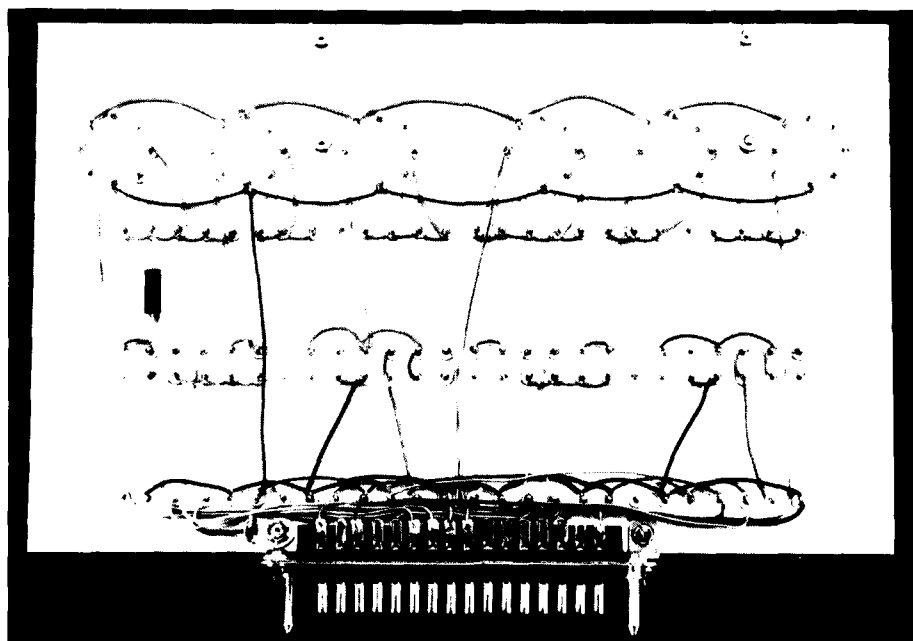


Fig. A9-2 Component layout, Card No.9, MCU altimeter signal conditioning.



(a)



(b)

Fig. A9-3 MCU altimeter signal conditioning.

Board No. 10

Notes:

1. \bigcirc denotes pins on connector.
2. All resistors: Metal film $\pm 1\%$, RN60D 100 ppm/ $^{\circ}$ C or equivalent unless otherwise noted.
3. All capacitors: Mica $\pm 10\%$ or equivalent unless otherwise noted.
4. Tantalum capacitors: 15 or 20 VDC rating.
5. Includes relays on following schematics: K_1 and K_2 on Fig. A4-1; K_1 on Fig. A5-1; K_1 on Fig. A6-1.
6. Includes relay on following schematics: K_1 and K_2 on Fig. A7-1.
7. Metal film $\pm 1\%$ RN65D, $\frac{1}{4}$ W rating, 100 ppm/ $^{\circ}$ C.

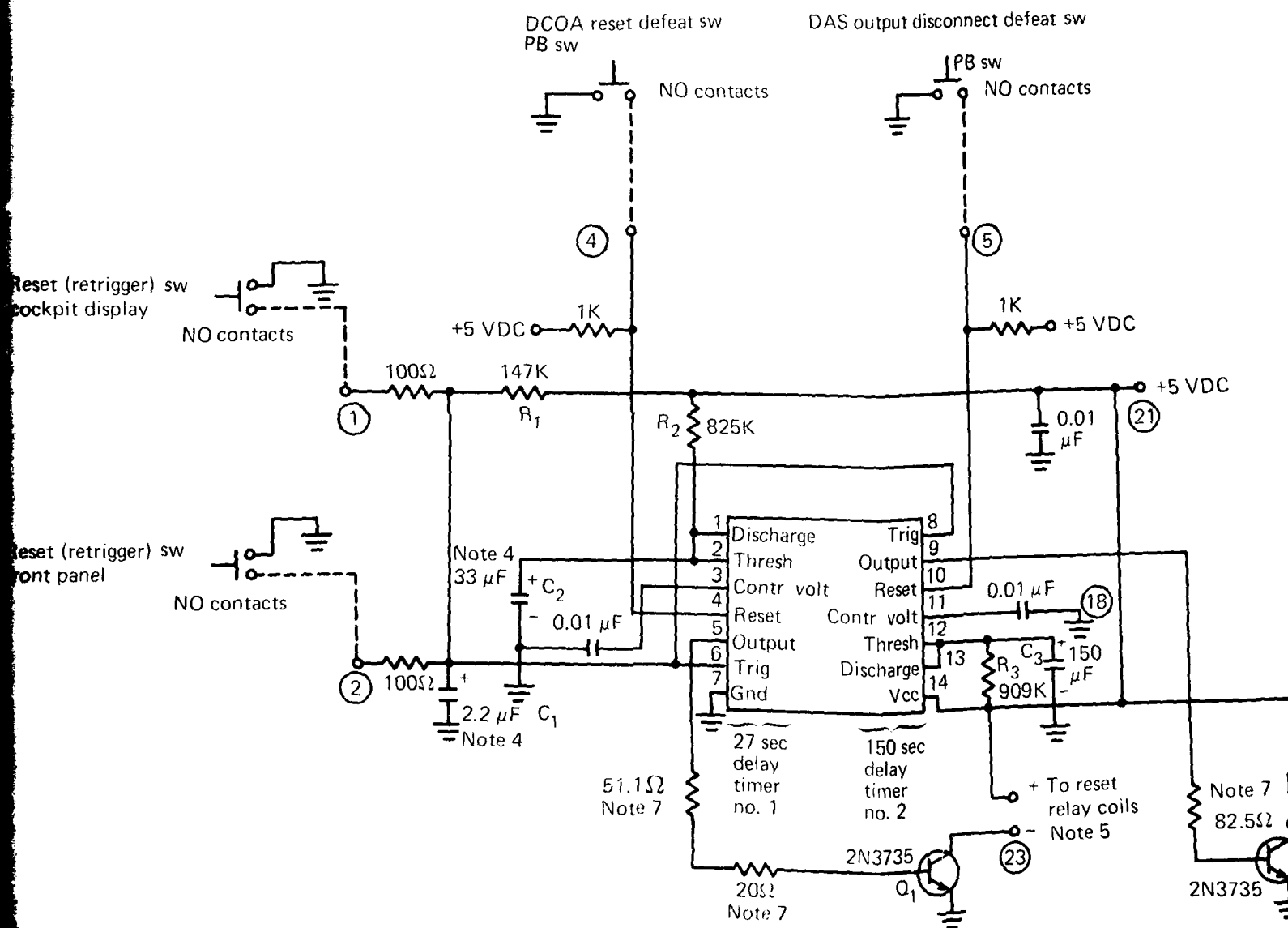


Fig. A10-

DAS output disconnect defeat sw

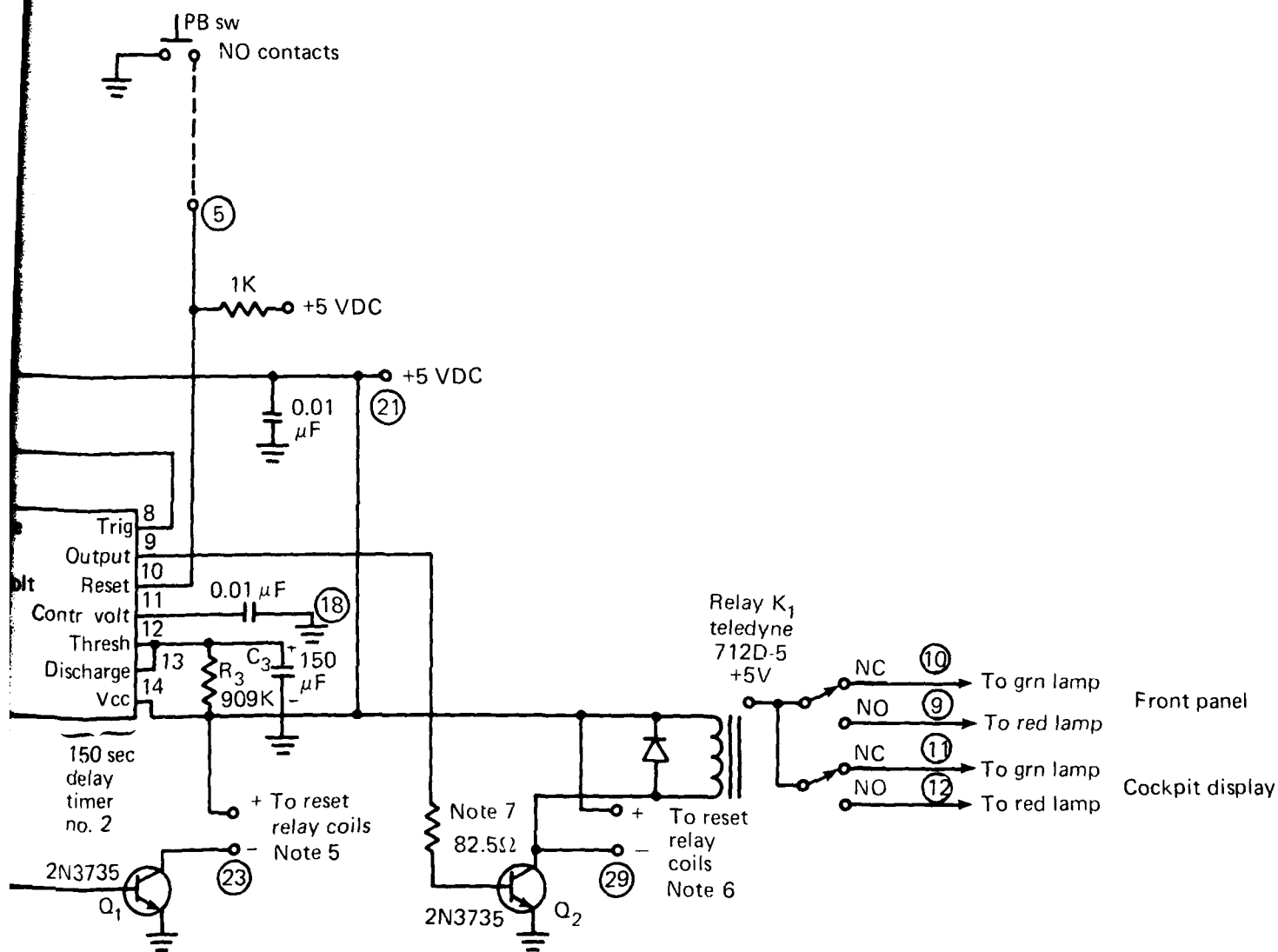
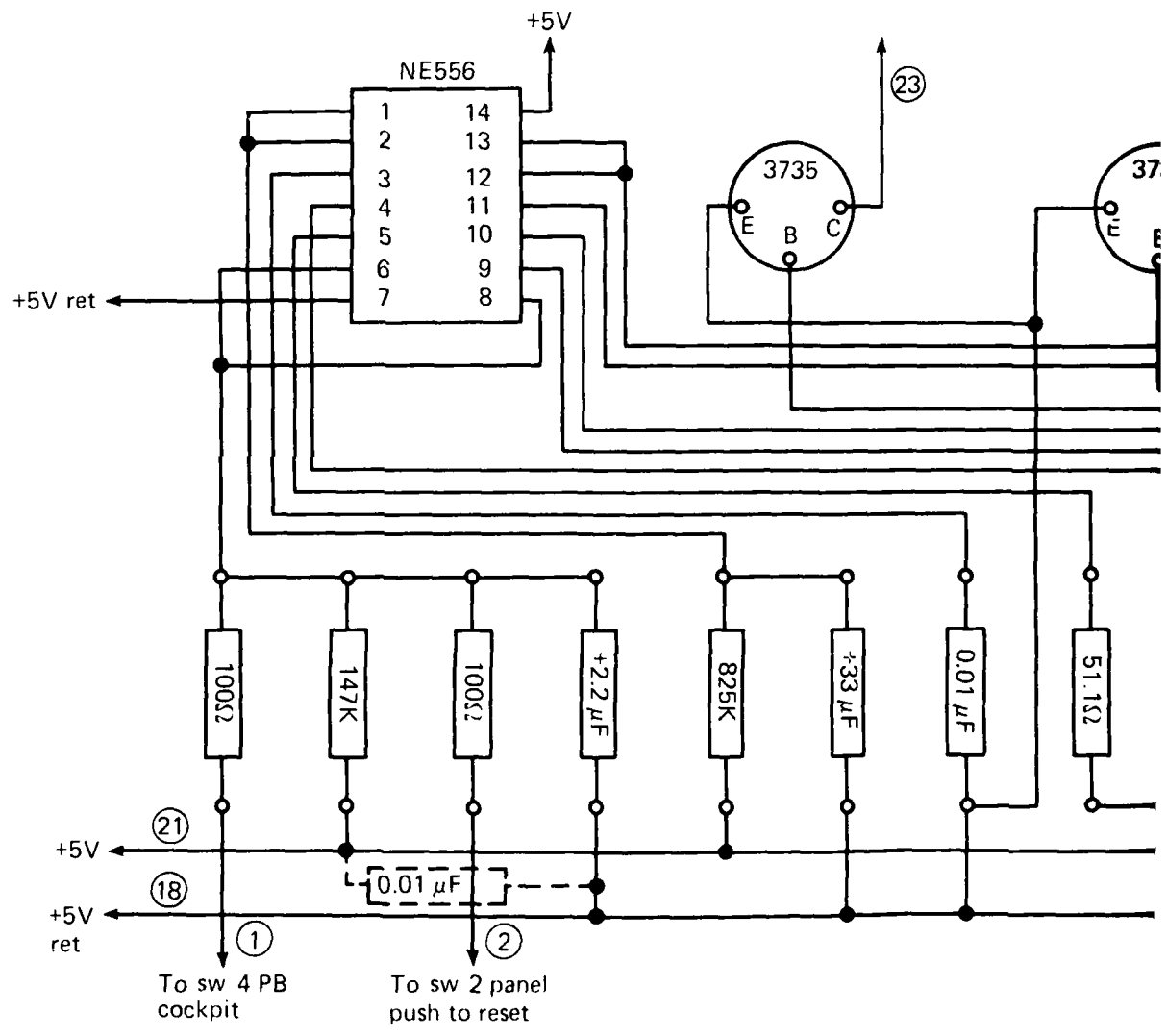


Fig. A 10-1 Schematic, Card No.10, MCU reset timing and control.



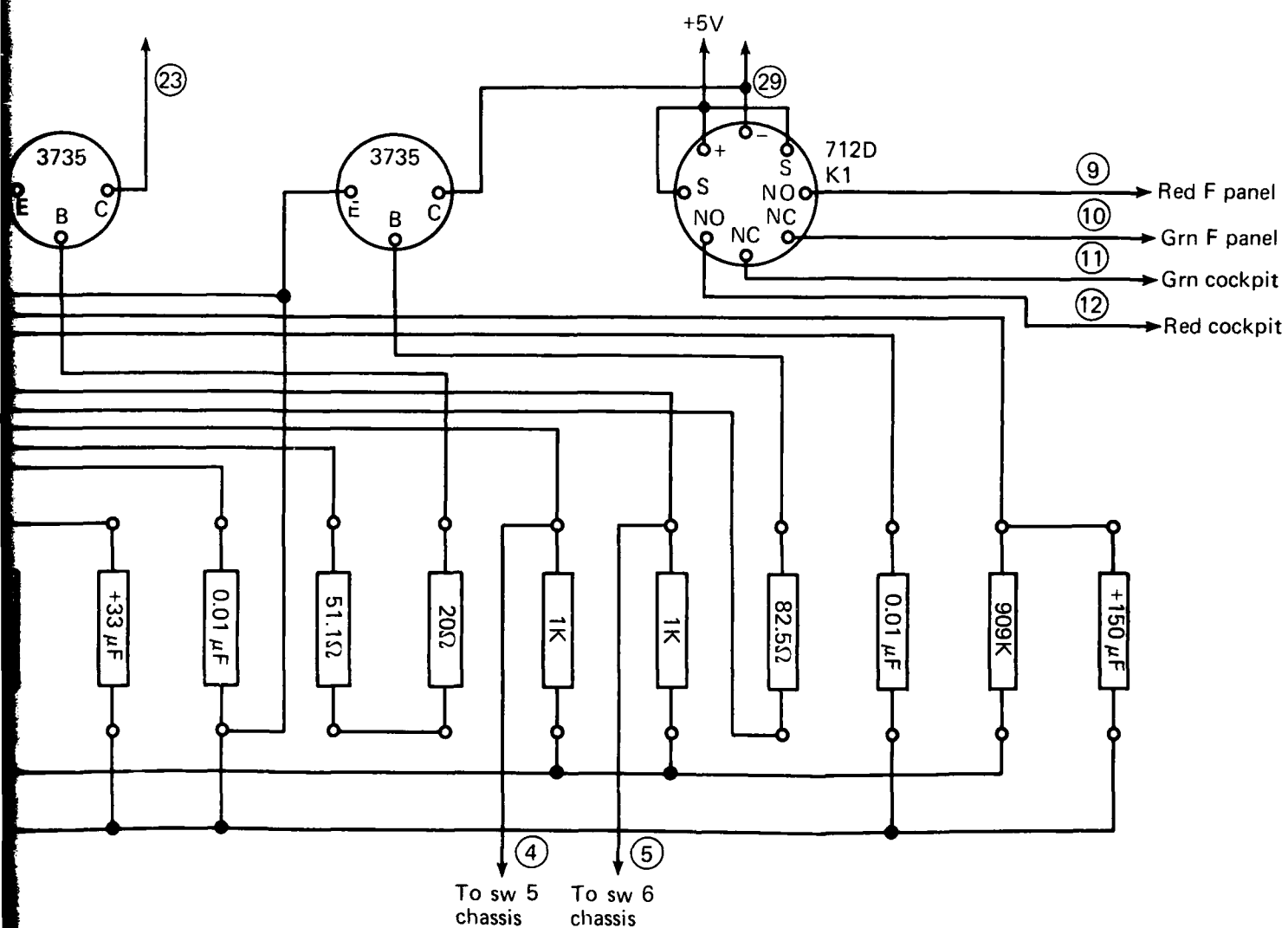
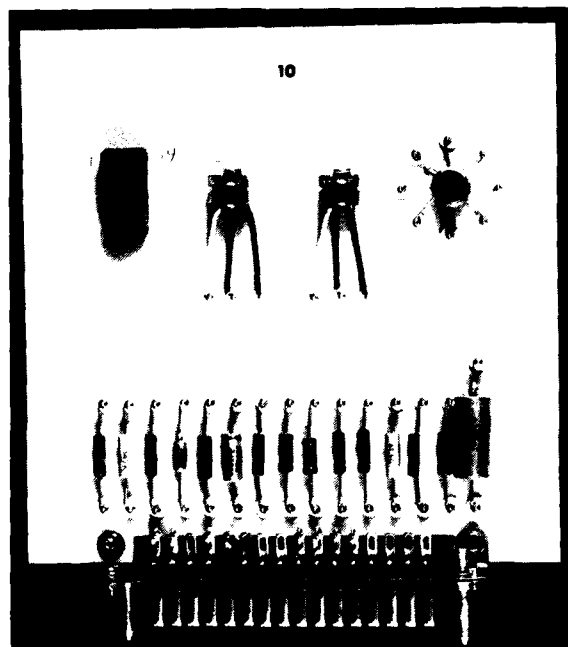
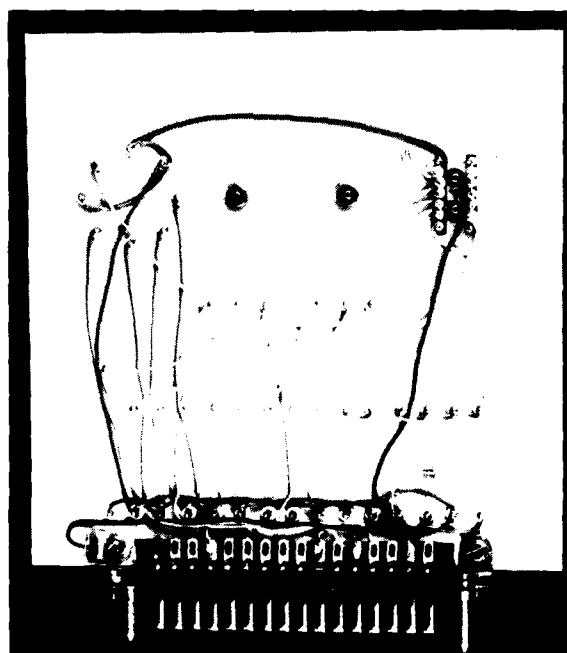


Fig.A10-2 Component layout, Card No.10, MCU reset timing and control.



(a)



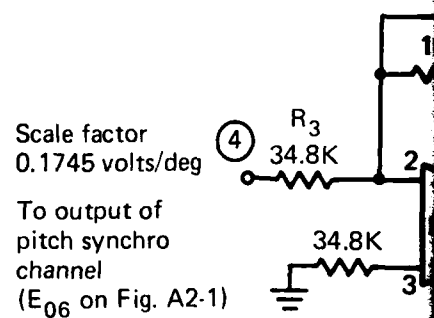
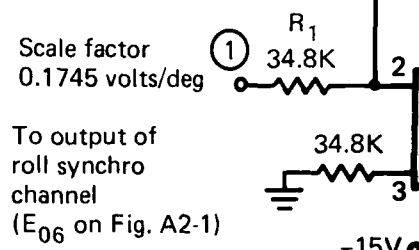
(b)

Fig. A10-3 MCU reset timing and control.

Board No. 11

Notes:

1. ○ denotes pins on connector.
2. All resistors: MEA metal film $\pm 1\%$, 100 ppm/ $^{\circ}\text{C}$ or equivalent unless otherwise noted.
3. All capacitors: Mica $\pm 10\%$ or equivalent unless otherwise noted.
4. Bourns 10 turn trimpot or equivalent.
5. Calibrate meter scales to read $(-2^{\circ}) - 0 - (+2^{\circ})$ full scale, with synchro angle set at 2° adjust P_1 and P_2 , respectively, to yield a reading of 2° on corresponding meters.



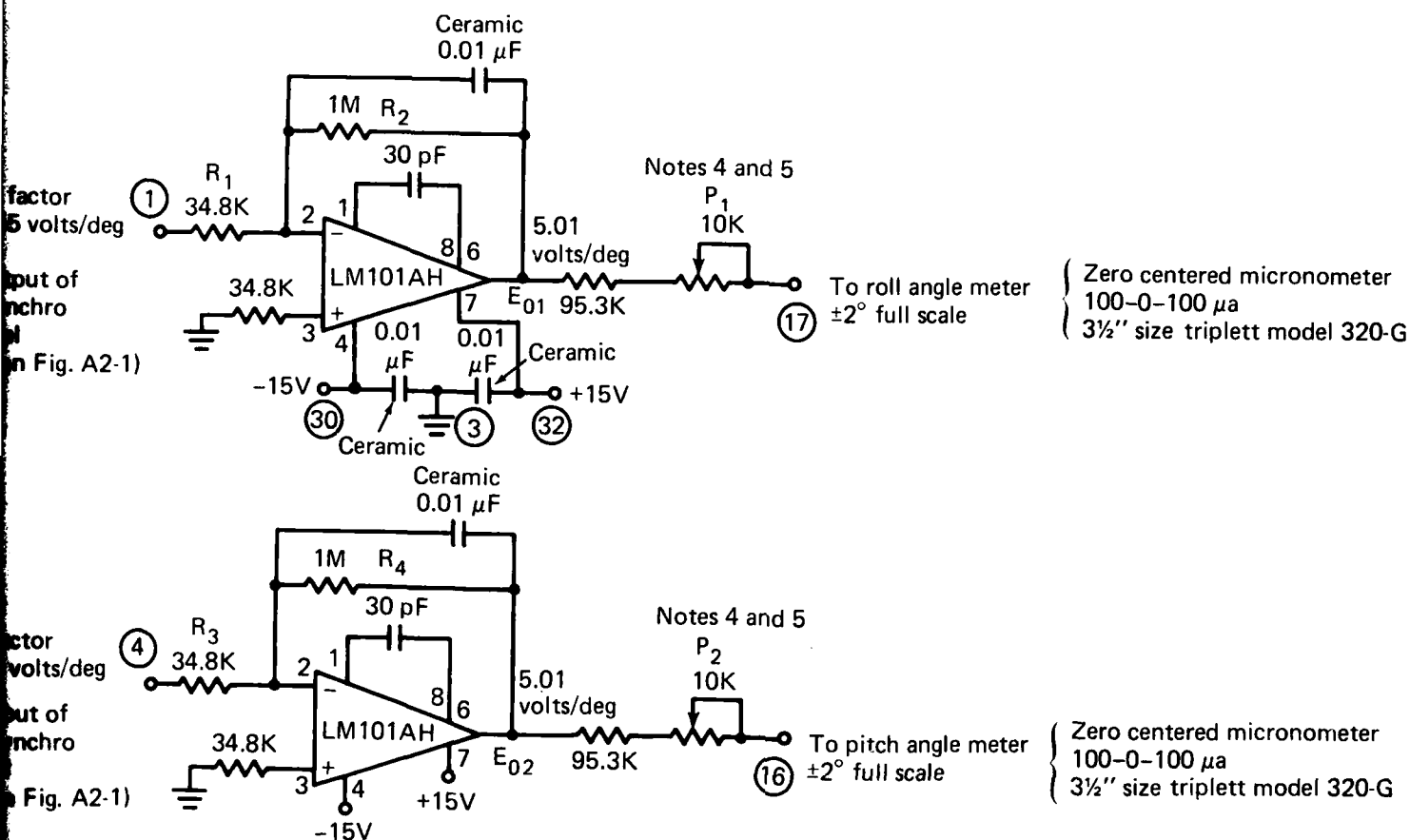


Fig. A11-1 Schematic, Card No.11, MCU ship's angular motion meter drive.

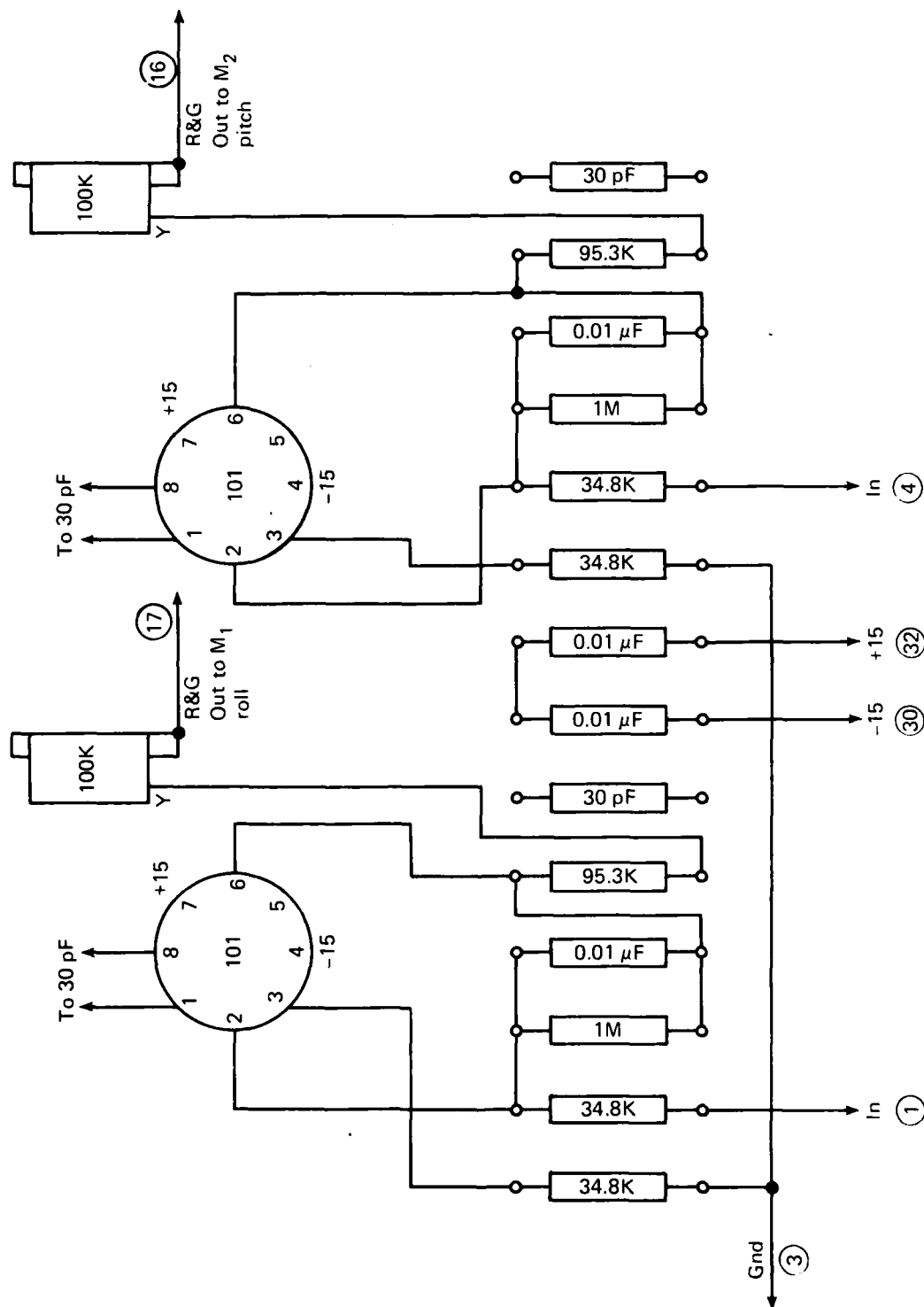
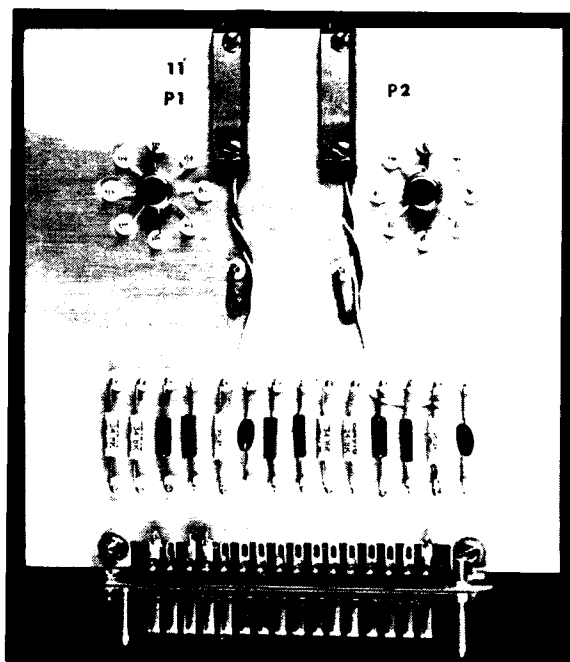
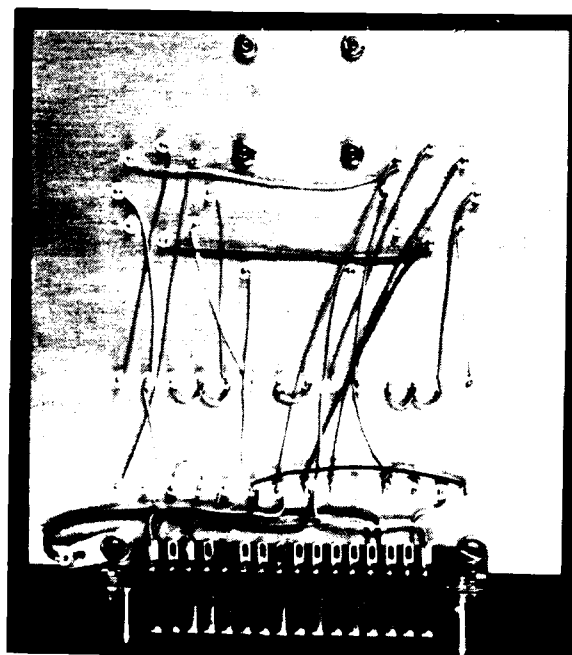


Fig. A11-2 Component layout, Card No. 11, MCU ship's angular motion meter drive.



(a)



(b)

Fig. A11-3 MCU angular motion meter drive.

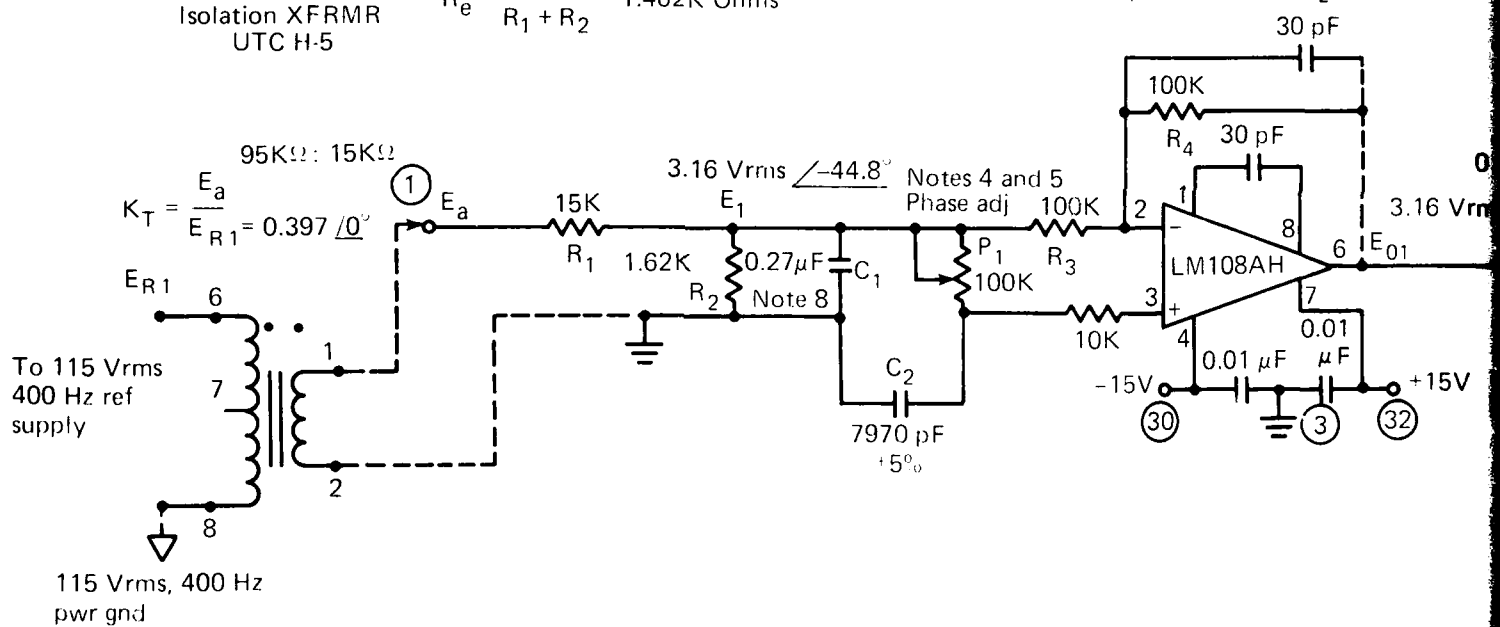
Board No. 12

Notes:

1. \bigcirc denotes pins on connector.
2. All resistors: RN60D metal film, $\pm 1\%$, ± 100 ppm/ $^{\circ}\text{C}$, or equivalent, unless otherwise noted.
3. All capacitors: Mica $\pm 10\%$, or equivalent, unless otherwise noted.
4. Bourns 10 turn cermet trimpot or equivalent.
5. Adjust P_1 to yield phase of E_{R2} such that roll and pitch pendulum signals are 180° out of phase with respective correction signals being summed with roll and pitch pendulum signals.
6. Adjust P_2 such that $E_{R2} = 7.07 \text{ Vrms} \pm 1\%$ with reference voltage E_{R1} at 115 Vrms.
7. Transformer shown for reference only. Transformer is not mounted on this card and is shown on "Chassis Wiring Diagram, Gyro Compensation Unit," Fig B 2-1.
8. Use GB Microflat Mylar 65F15AA234 0.22 MFD, 50 VDC in parallel with 65F12AA473 0.047 MFD, 50 VDC.

$$K_7 = \frac{E_1}{E_a} = \frac{0.0957}{R_e C_1 S + 1} = 0.0692 \angle -44.8^\circ @ 400 \text{ Hz}$$
$$K_T = \frac{E_a}{E_{R1}} = 0.397 \underline{0}$$
$$K_8 = \frac{E_{01}}{E_1} = \frac{1 - P_1 C_2 s}{1 + P_1 C_2 s} = 1.00 / -2 \tan^{-1}(\omega)$$

@ 400 Hz: $K_8 = 1.00 / \alpha_2, \alpha_2 = -2 \tan^{-1} [$
 For $0 \leq P_1 \leq 100K, 0^\circ \leq \alpha_2 \leq -127^\circ$



Adjustable phase shift amplifier

$$K_8 = \frac{E_{01}}{E_1} = \frac{1 - P_1 C_2 s}{1 + P_1 C_2 s} = 1.00 \angle -2 \tan^{-1} (\omega P_1 C_2) \text{ Vrms/Vrms}$$

$$\text{@ 400 Hz: } K_8 = 1.00 \angle \alpha_2, \alpha_2 = -2 \tan^{-1} [2.003(10^{-5})P_1]$$

$$\text{For } 0 \leq P_1 \leq 100\text{K}, 0^\circ \leq \alpha_2 \leq -127^\circ$$

Adjustable gain amp.

$$K_9 = \frac{E_{R2}}{E_{01}} = \left[1 + \left(\frac{R_6}{R_7 + P_2} \right) \right] \frac{0}{0}$$

$$\text{For } K_9 = 2.24, P_2 = 25.9\text{K Ohms}$$

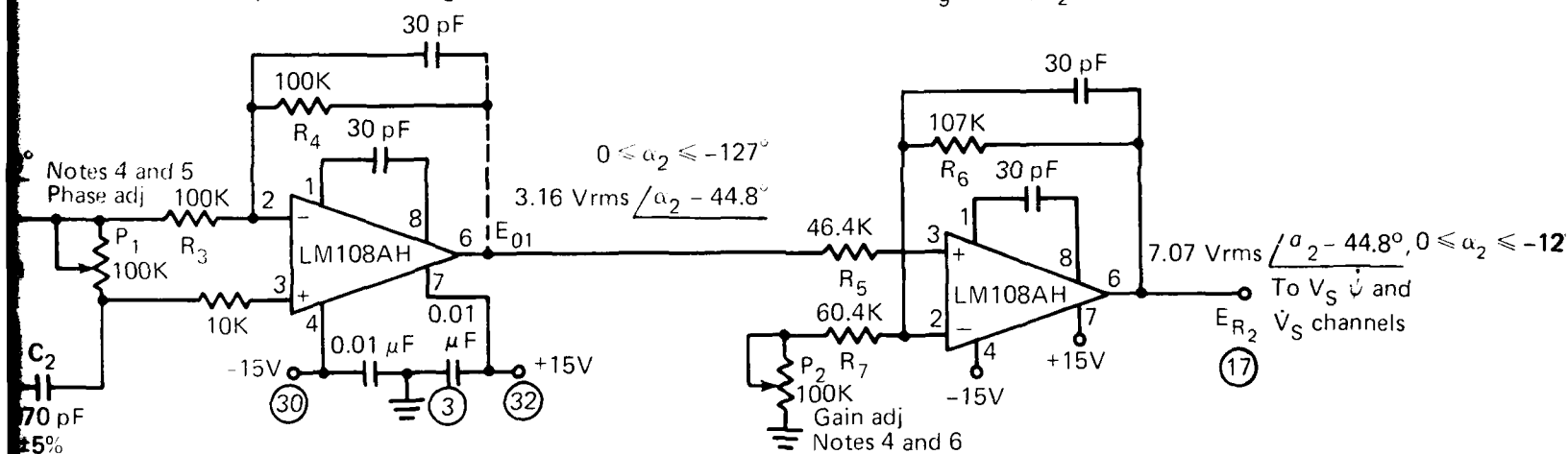


Fig. A12-1 Schematic, Card No. 12, GCU 400 Hz reference.

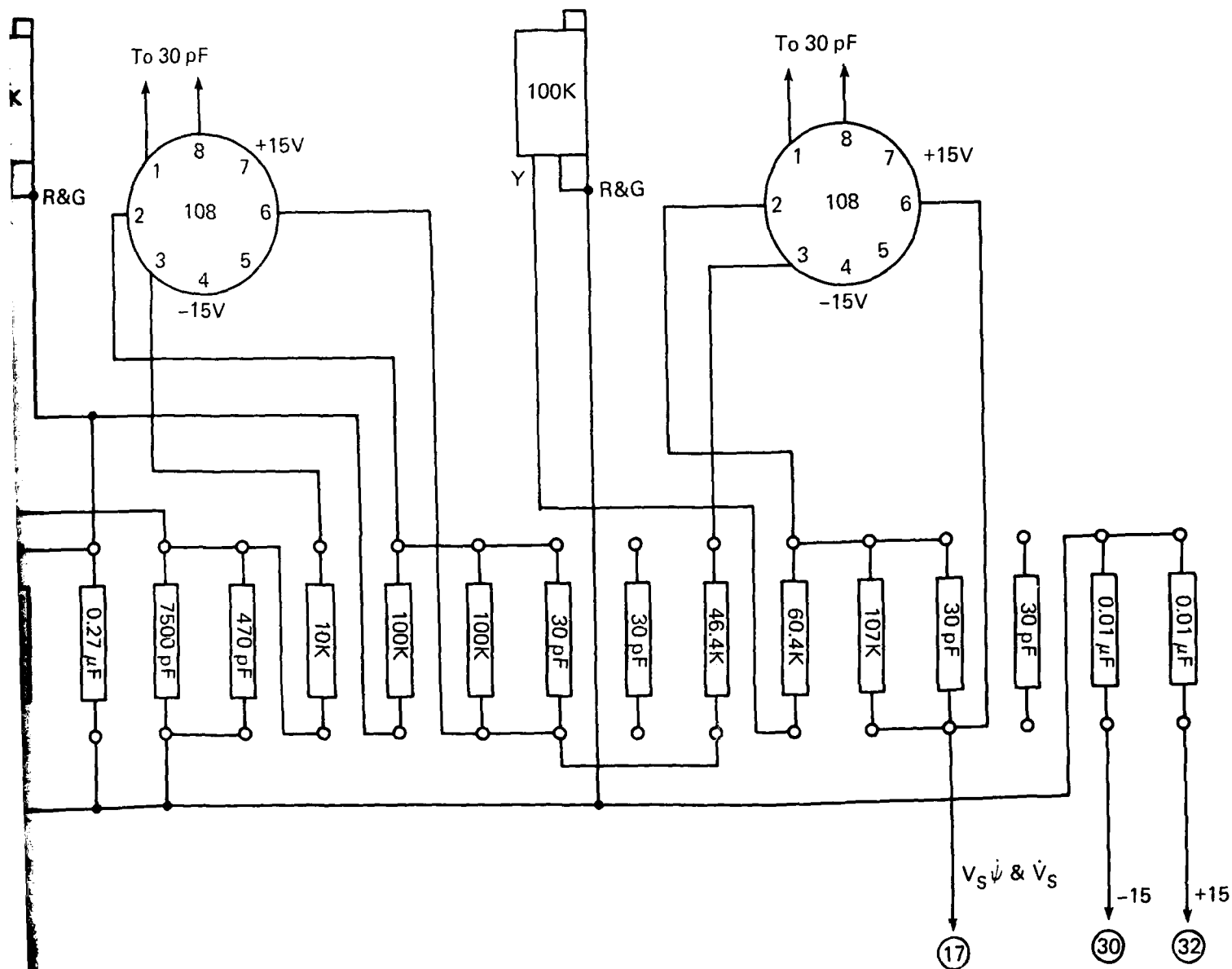
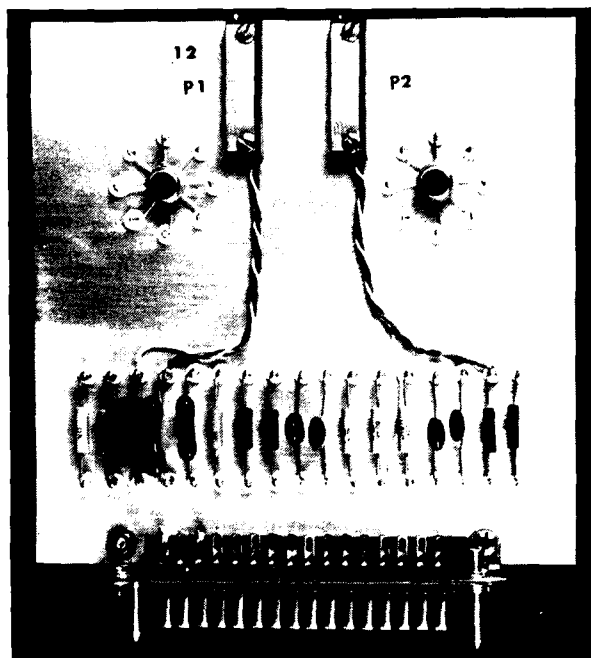
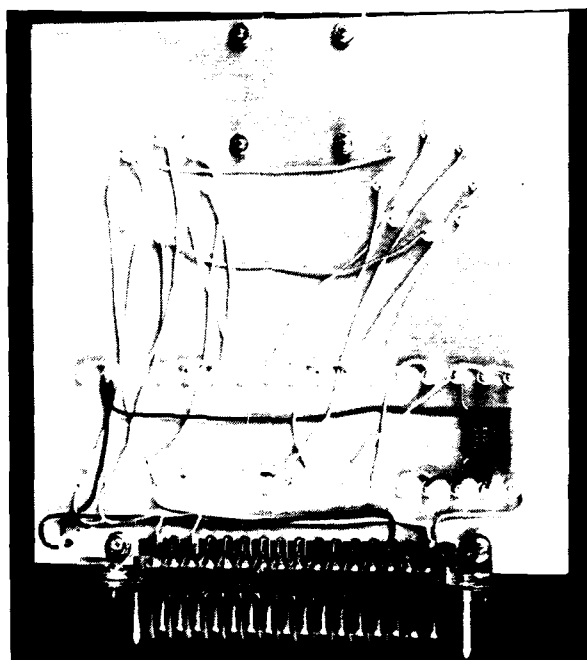


Fig. A12-2 Component layout, Card No.12, GCU 400 Hz reference.



(a)



(b)

Fig. A12-3 GCU 400 Hz reference.

Board No. 13

Notes:

1. ○ denotes pins on connector.
2. All resistors: RN60D metal film $\pm 1\%$, ± 100 ppm/°C or equivalent unless otherwise noted.
3. All capacitors: Mica $\pm 10\%$ or equivalent unless noted.
4. Bourns 10 turn WW trimpot or equivalent.
5. After offset adjustment of Note 9, set $\dot{\psi} = 0.0$ deg/sec, $V_S = 100$ knots, and adjust P_1 to yield change in $E_{04} = 0.000 \pm 0.005$ VDC.
6. With $\dot{\psi} = +1.00$ deg/sec, $V_S = 16.1$ ft/sec, set P_2 to yield change in DC output of LP filter block (following multiplier M1) = $+0.123$ VDC, after P_4 has been set per Note 8. DC gain adjustment on $K_a = (E_{01}/E_1) = 0.84$ to 1.53 .
7. After offset adjustment of Note 9, set $V_S = 0.0$ knots, $\dot{\psi} = 10$ deg/sec and adjust P_3 to yield change in $E_{04} = 0.000 \pm 0.005$ VDC; repeat for $\dot{\psi} = -10$ deg/sec. Pot P_3 should be set to value which yields equal and opposite changes in E_{04} when $\dot{\psi}$ is changed from 10 deg/sec to -10 deg/sec.
8. With $V_S = 100$ knots, set P_4 for change in $E_{03} = 10.00 \pm 0.02$ VDC. DC gain adjust on $K_b = \frac{E_{03}}{E_2} = 0.75$ to 1.25 .
9. With E_{02} and E_{03} at 0.00 V adjust P_5 to yield $E_{04} = 0.000$ V ± 5 MV. If DC offset at output of $[K_2/(\tau_1 S + 1)]$ LP filter is significant, P_5 should be adjusted to null its output within ± 2.5 MV.
10. GE flat mylar, 50 VDC or equivalent, $\pm 10\%$.
11. Ceramic, 50 VDC, $\pm 20\%$.
12. CP05A1KB474K3, 100 VDC, MIL-C-25C paper capacitor in metal case, or equivalent.
13. Bourns 10 turn trimpot, cermet, or equivalent.

$$K_a = \frac{E_{01}}{E_1} = \left(\frac{R_2}{R_1 + R_2} \right)$$

$$\tau_a = \left(\frac{R_3 + P_2}{R_3 + P_2 + R_4} \right) \tau_b$$

(note
7.32)
+15V

51

Scale factor:
 $K_G = 1.00$ VDC/(deg/sec)
 $= 57.3$ VDC/(rad/sec)
 $|\dot{\psi}(\max)| = 10$ deg/sec

(notes 6, 8) E_1

P_2
500K
(note 6)
DC offset
3.48V
+15V

51

Scale factor:
 $K_L = 0.0592$ VDC/(ft/sec)
 $= 0.100$ VDC/knot
 $|V_S(\max)| = 100$ knots
 $= 168.8$ ft/sec

(notes 6, 8) E_2

$$K_b = \frac{E_{03}}{E_2} = \left(\frac{R_7}{R_7 + P_4} \right)$$

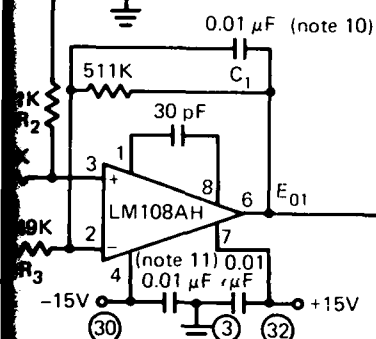
$$\tau_d = \left(\frac{R_9 + P_4}{R_9 + P_4 + R_{10}} \right)$$

stable gain amplifier

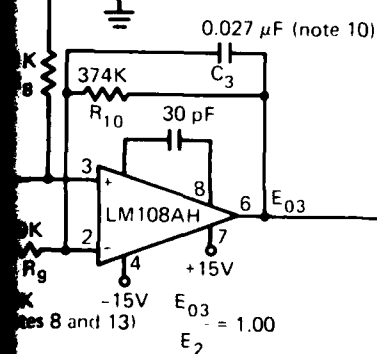
$$\frac{1}{P_2} \left[\frac{\tau_a S + 1}{\tau_b S + 1} \right] = \frac{1}{2} \left[1 + \frac{511K}{249K + P_2} \right] \left[\frac{\tau_d S + 1}{\tau_b S + 1} \right]$$

$$C_1; K_a(\text{nom}) = 1.00 \left[\frac{0.00256 S + 1}{0.00511 S + 1} \right]$$

P₁ DC offset adjust
1K -0.50V 7.32K -15V
511Ω



P₃ (notes 4 and 7)
1K -1.0V 3.48K -15V
511Ω



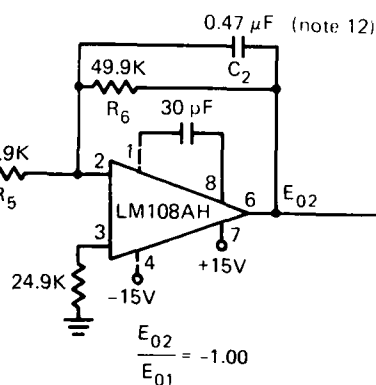
$$\frac{R_{10}}{R_9 + P_4} \left[\frac{\tau_d S + 1}{\tau_e S + 1} \right] = \frac{1}{2} \left[1 + \frac{374K}{249K + P_4} \right] \left[\frac{\tau_d S + 1}{\tau_e S + 1} \right]$$

$$= R_{10} C_3; K_b(\text{nom}) = 1.00 \left[\frac{0.00505 S + 1}{0.0101 S + 1} \right]$$

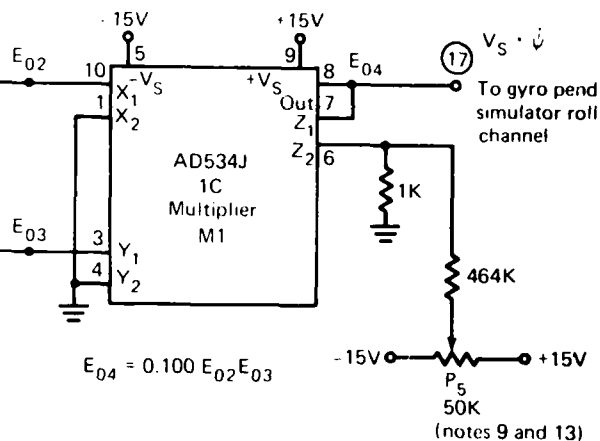
Amplifier

$$K_1 = \frac{E_{02}}{E_{01}} = - \left(\frac{R_6}{R_5} \right) \frac{1}{(\tau_c S + 1)} = - \left[\frac{1.00}{0.0235 S + 1} \right]$$

$$\tau_c = R_6 C_2 = 0.0235 \text{ sec}$$



$$\frac{E_{02}}{E_{01}} = -1.00$$



$$E_{04} = 0.100 E_{02} E_{03}$$

To gyro pend simulator pitch channel

To gyro pend simulator roll channel

Fig. A13-1 Schematic, Card No. 13, GCU V_s and $\dot{\psi}$ signal conditioner.

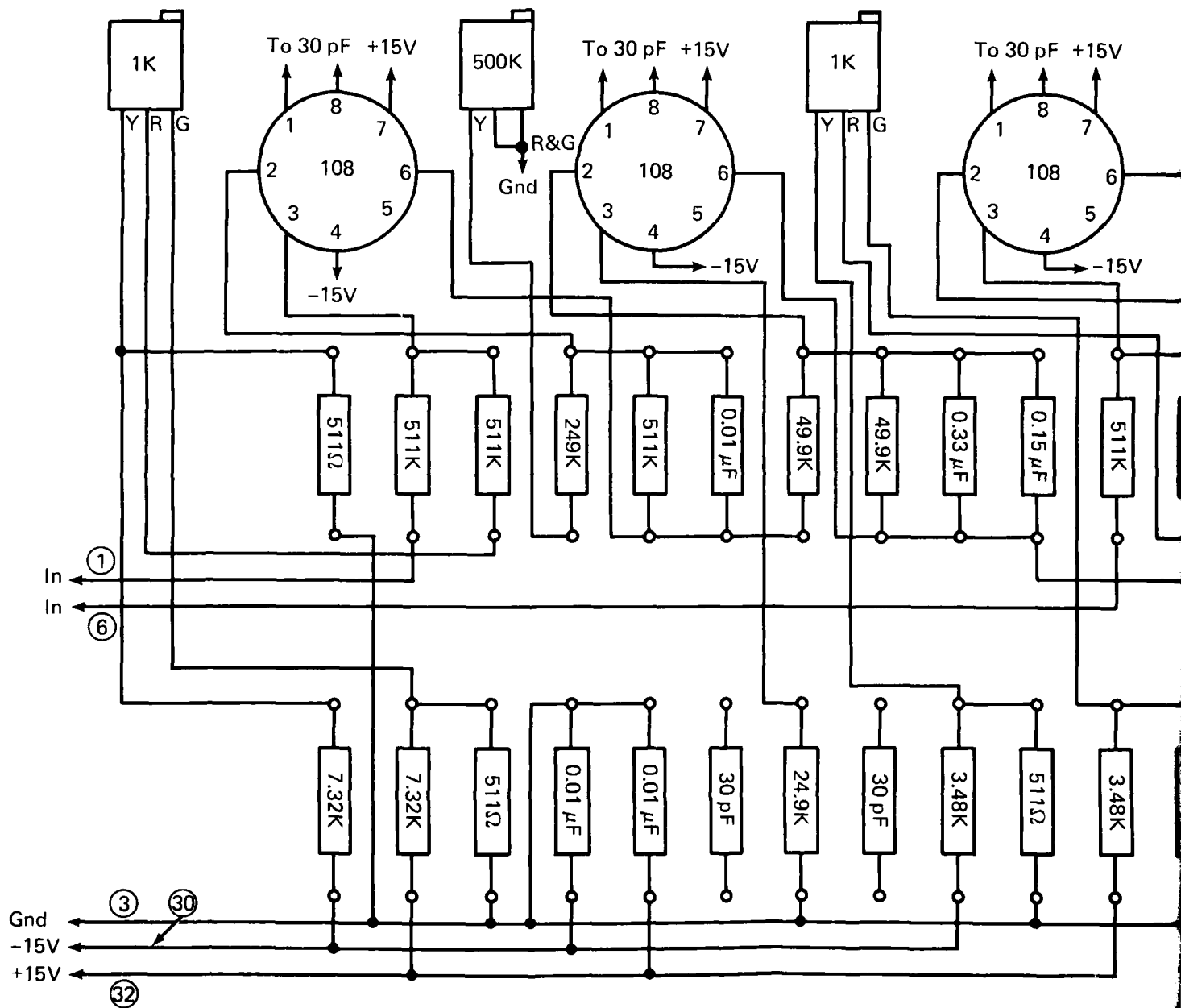


Fig. A13-2 Comp

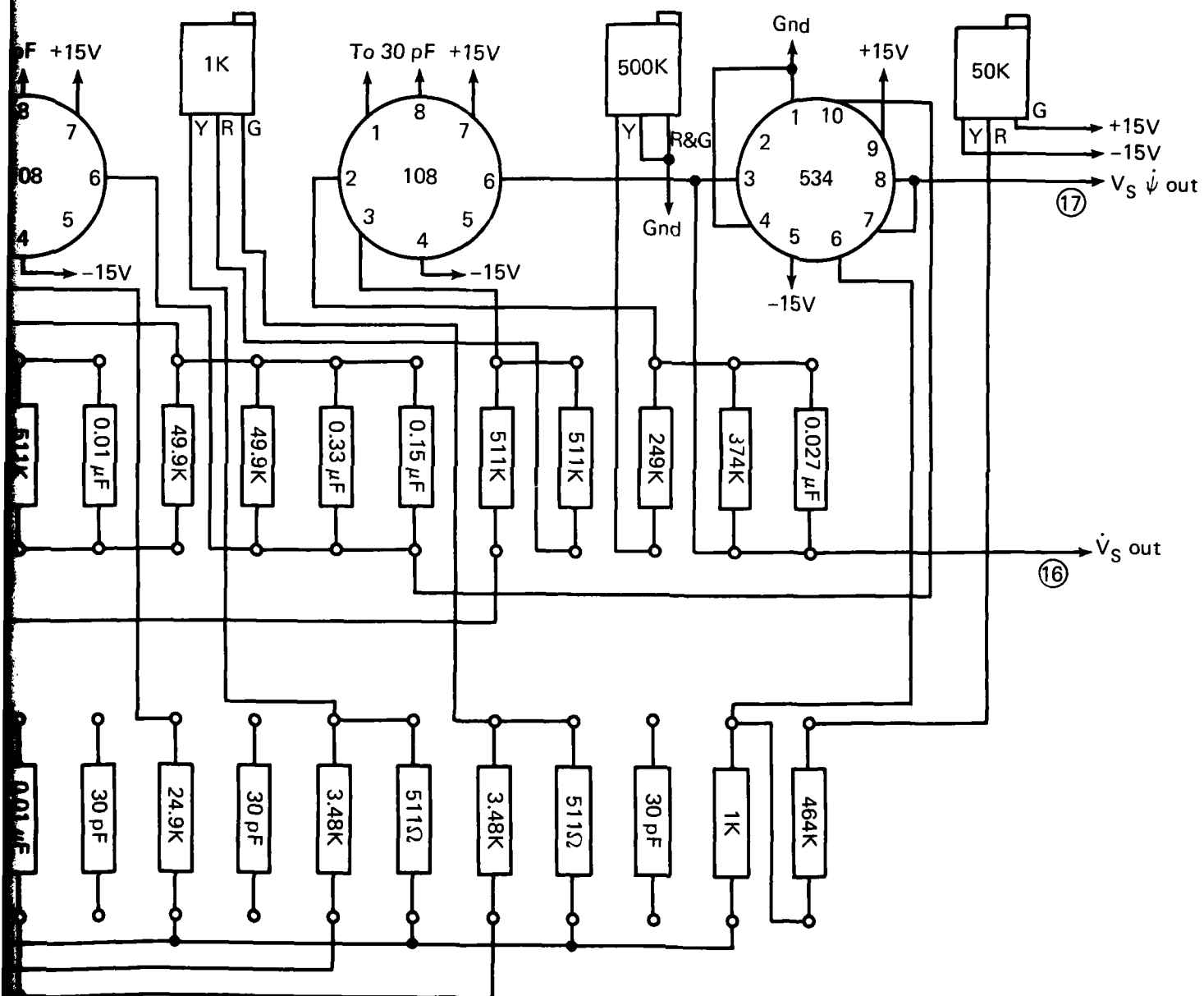
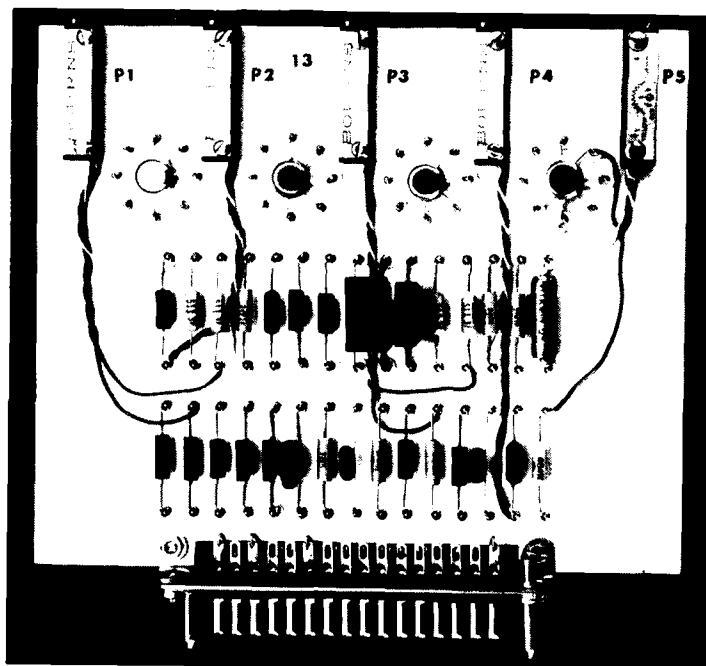
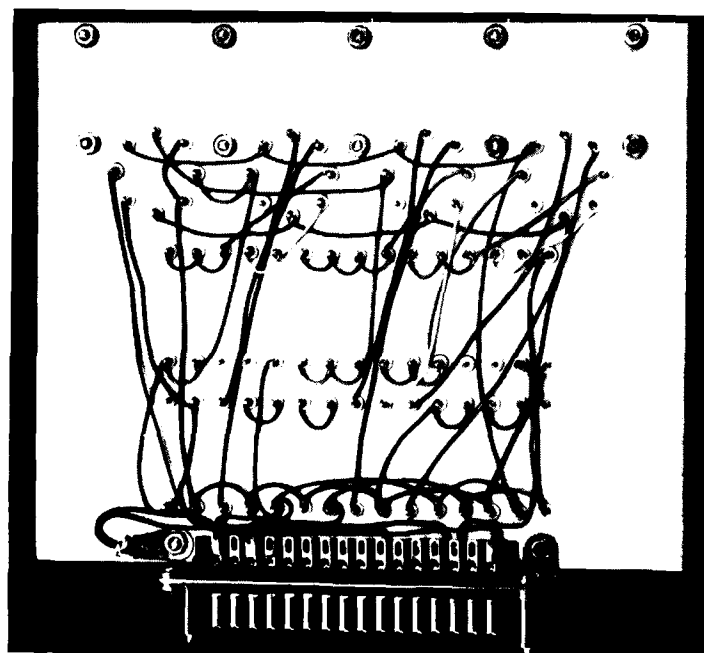


Fig. A13-2 Component layout, Card No.13, GCU V_S and ψ signal conditioner.



(a)



(b)

Fig. A13-3 GCU V_S and ψ signal conditioner.

Board No. 14

Notes:

1. ○ denotes pins on connector.
2. All resistors: RN60D metal film $\pm 1\%$, ± 100 ppm/ $^{\circ}$ C or equivalent unless otherwise noted.
3. All capacitors: Mica $\pm 10\%$ or equivalent unless otherwise noted.
4. Bourns 10 turn cermet trimpot. Pot setting should be such that output of amplifier that sums roll-pendulum signal with V_S $\dot{\psi}$ channel signal goes to null for tilt angles less than 0.5° in magnitude.
5. Trim valve to yield -123 MV between node (A) and gnd, nominal value = 665Ω .
6. Trim valve to yield $+123$ MV between node (B) and gnd, nominal value = 665Ω .
7. Make up value using GE Microflat Mylar 65F15AA and 65F16AA $\pm 10\%$ capacitors, 50 VDC. Parallel (2) 0.33 MFD and (1) 0.15 MFD and trim to 0.80 MFD $\pm 1\%$.
8. Make up value using Sprague 121D capacitors. Parallel 2.0 MFD and 0.68 MFD and trim to 2.70 MFD $\pm 1\%$.
9. Caddock ML181, $\pm 1\%$, ± 100 ppm/ $^{\circ}$ C.
10. Caddock MM215, $\pm 1\%$, ± 100 ppm/ $^{\circ}$ C.
11. Ceramic, 50 VDC.
12. RN65D metal film, $\pm 1\%$, ± 100 ppm/ $^{\circ}$ C or equivalent.
13. GE Microflat Mylar, 50 VDC, $\pm 10\%$.

$$\left(\frac{K_2}{\tau_1 S + 1} \right) = \frac{E_{01}}{E_1}$$

$$\tau_1 = R_2 C_1; C_1 = 0.8 \text{ MFD}, \tau_1 = 2.7 \text{ MFD}; \tau_1$$

From $V_S \dot{\psi}$ sig conditioner

Card no. 13

LP filter

$$\left(\frac{R_2}{R_1}\right) \frac{1}{(\tau_1 S + 1)} = - \left(\frac{1.296}{\tau_1 S + 1}\right)$$

ed via switch

0.0 sec
27 sec

(note 12) (note 9)
909K 6.81M

$$\frac{E_{01}}{E_1} = \frac{1.296}{T_2 S + 1} = T_2 \begin{cases} 8 \text{ sec} \\ \text{or} \\ 27 \text{ sec} \end{cases}$$

Not mounted
on card no. 14.
shown for
ref. only

Adjustable gain amplifier

$$K_3 = \frac{E_{02}}{E_{01}} = - \frac{R_4}{R_{3a}} \left(\frac{1}{\tau_a S + 1} \right) = - \left(\frac{1.00}{0.010 S + 1} \right) (\text{nom})$$

$$\tau_a = R_4 C_2 = 0.010 \text{ sec (nom)}$$

Sw shown here for ref only

To time select sw
on chassis

Non-linear gain amplifier (limiter)

$$K_4 = \frac{E_{03}}{E_{01}} = - \left(\frac{R_6}{R_5} \right) \left(\frac{1}{\tau_b S + 1} \right) = - \frac{30.}{0.010}$$

$$\tau_b = R_6 C_3 = 0.010 \text{ sec (nom)}$$

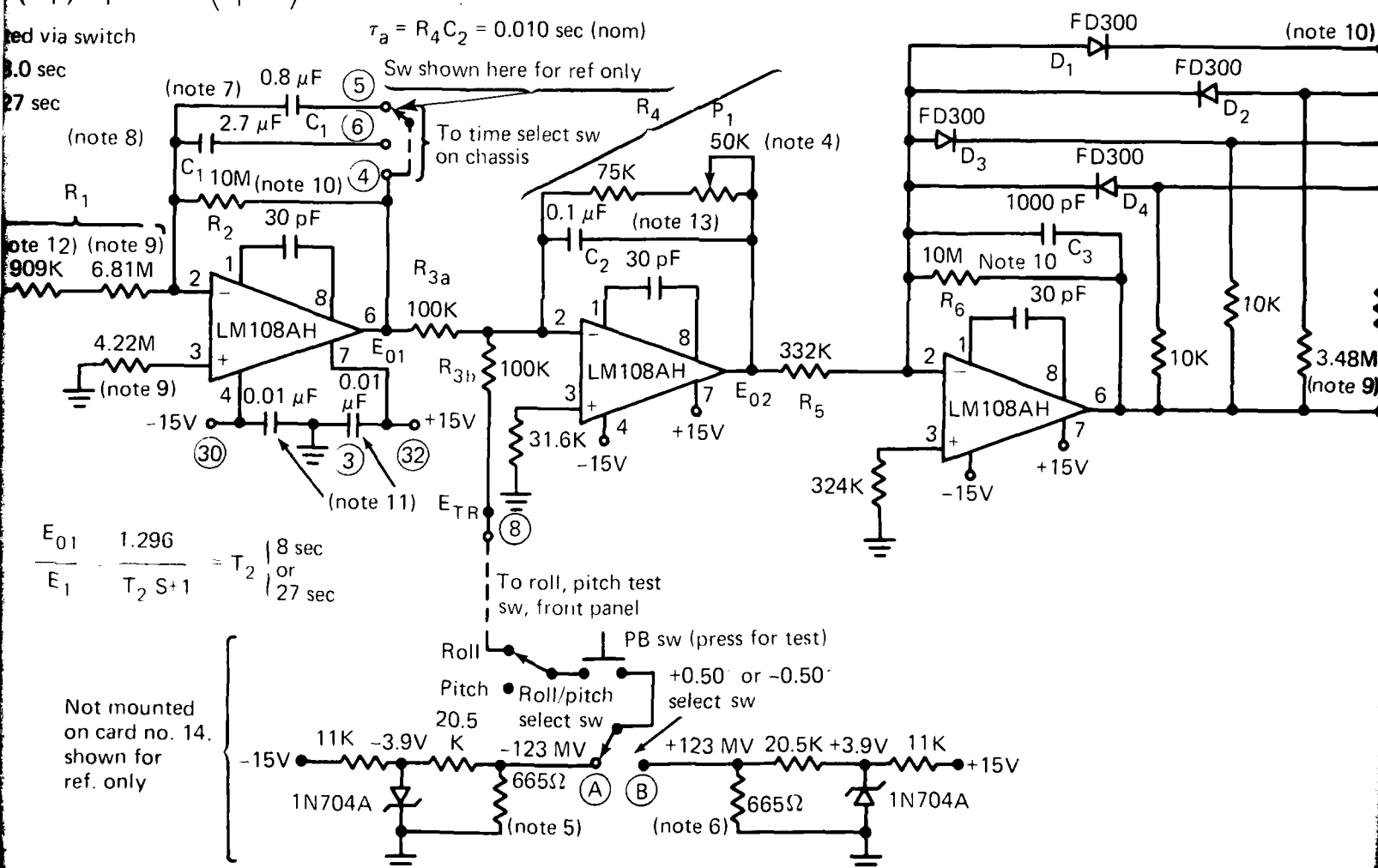


Fig. A14-1 Schematic, Card No.14, GCU gyro pendulum

$$\frac{R_4}{R_{3a}} \left(\frac{1}{\tau_a S + 1} \right) = - \left(\frac{1.00}{0.010 S + 1} \right) (\text{nom})$$

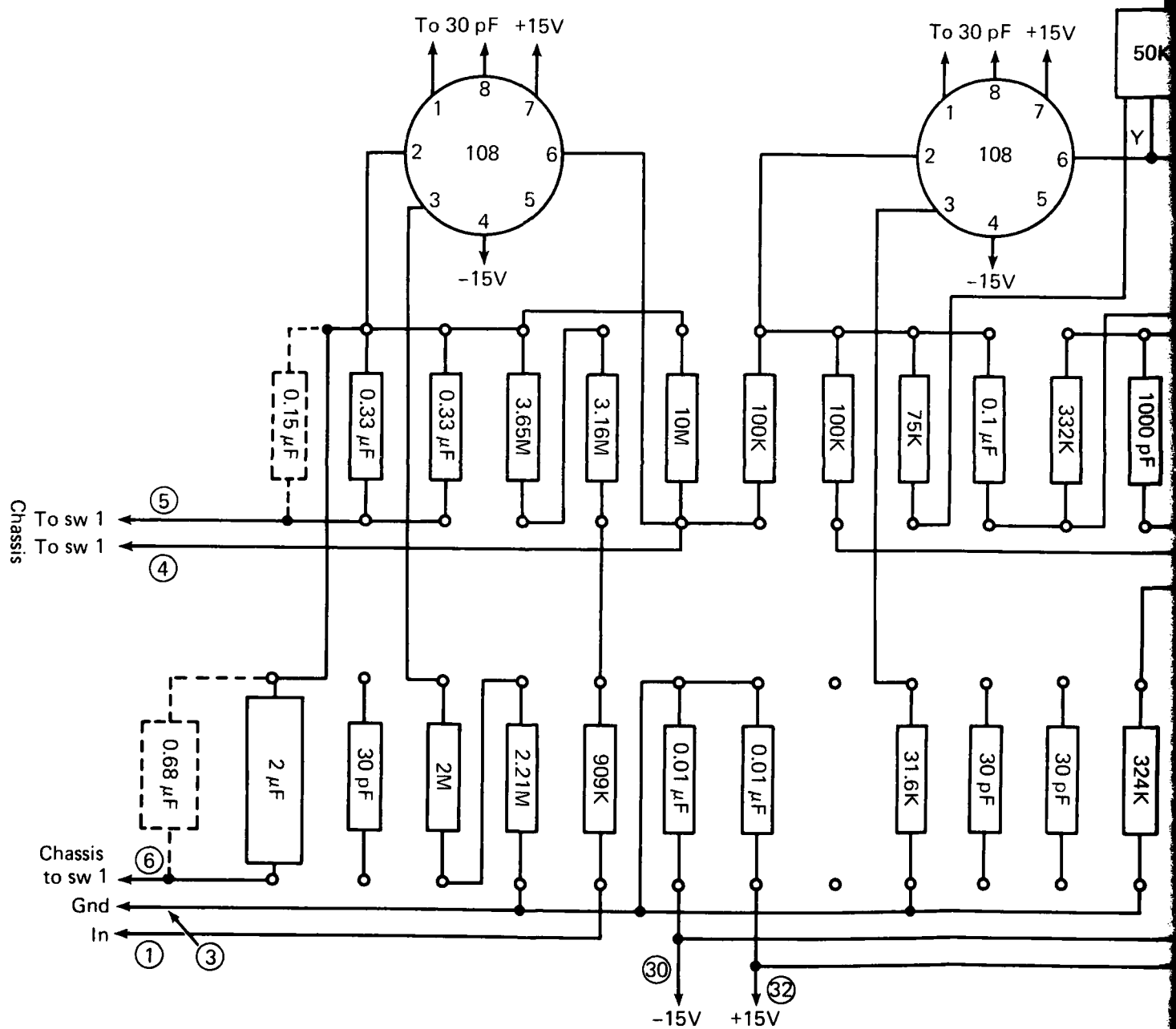
$$K_4 = \frac{E_{03}}{E_{01}} = - \left(\frac{R_6}{R_5} \right) \left(\frac{1}{\tau_b S + 1} \right) = - \frac{30.1}{0.010 S + 1}$$

$$\tau_h = R_6 C_3 = 0.010 \text{ sec (nom)}$$

in here for ref only

time select sw
chassis





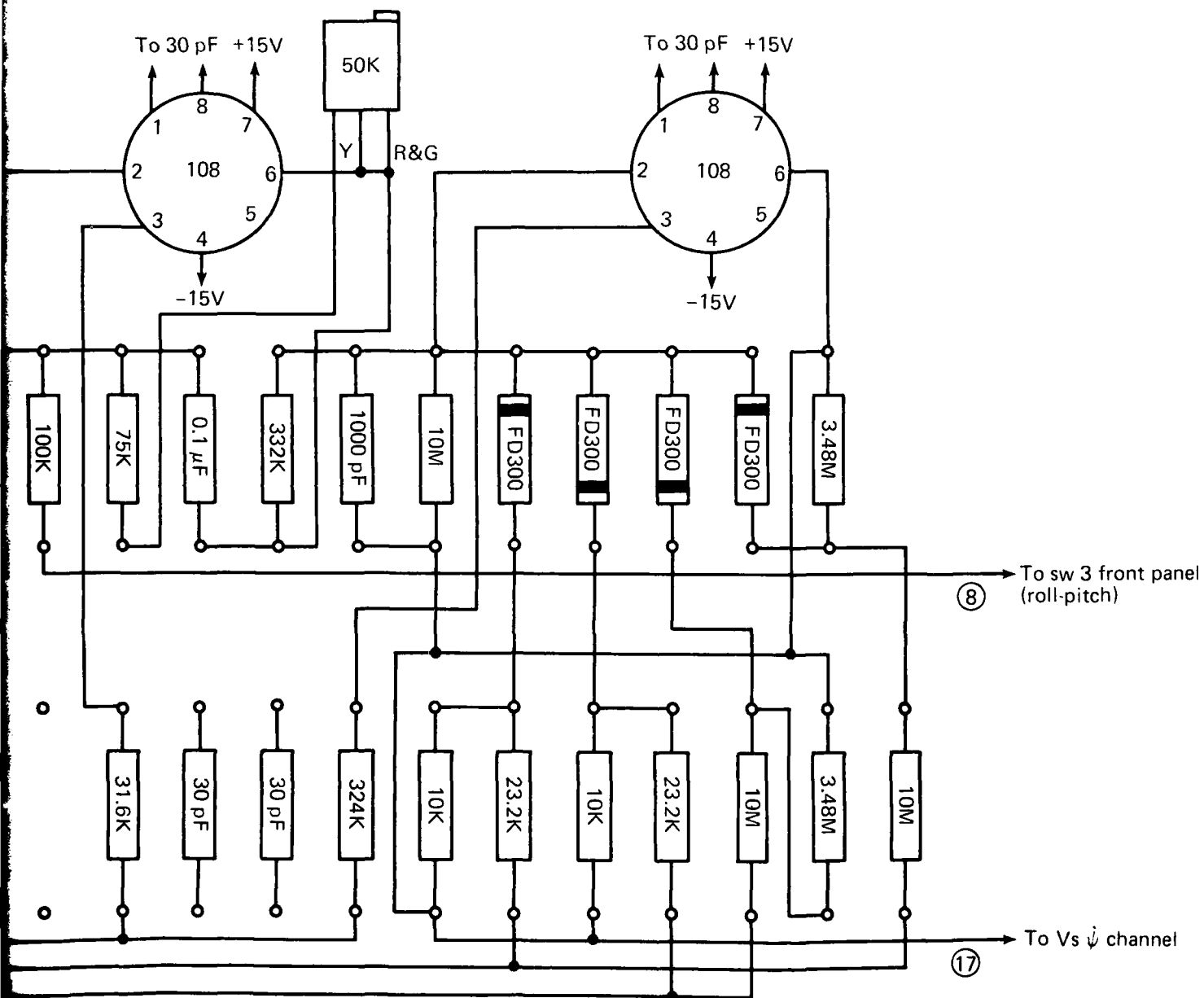
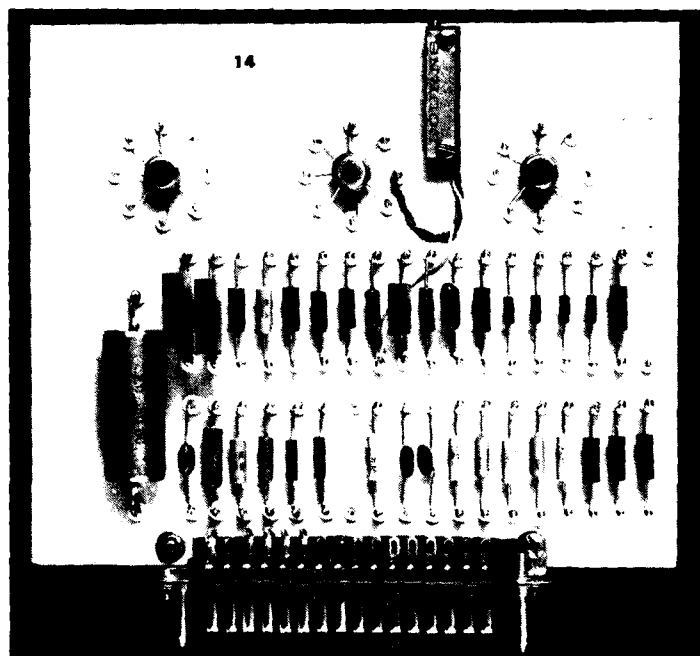
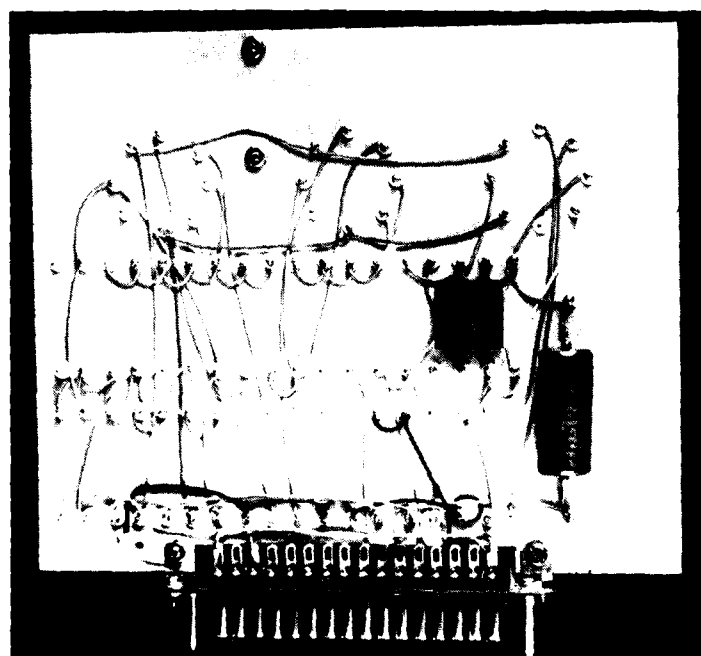


Fig. A14-2 Component layout, Card No.14, GCU gyro pendulum simulator roll channel.



(a)



(b)

Fig. A14-3 GCU gyro pendulum simulator roll channel.

AD-A088 593 JOHNS HOPKINS UNIV LAUREL MD APPLIED PHYSICS LAB

THE --ETC(U)

JUN 80 T M RANKIN; R L KONIGSBERG

N00024-78-C-5384

JHU/APL/SES-025

NL

AD A
08593

—

Board No. 15

Notes:

1. ○ denotes pins on connector.
2. All resistors: RN60D metal film $\pm 1\%$, ± 100 ppm/ $^{\circ}\text{C}$ or equivalent unless otherwise noted.
3. All capacitors: Mica $\pm 10\%$ or equivalent unless otherwise noted.
4. Bourns 10 turn trimpot. Pot setting should be such that output of amplifier that sums pitch-pendulum signal with V_S channel signal goes to null for tilt angle less than 0.5° in magnitude.
5. Nominal values of R_{2a} and R_{2b} shown. Trim R_{2b} such that $R_{2b} = R_{2a} \frac{C_{1a}}{C_{1b}}$ within $\pm 0.5\%$.
6. Make up value using GE Microflat Mylar 65F15AA and 65F16AA $\pm 10\%$ capacitors, 50 VDC. Parallel (2) 0.33 MFD and (1) 0.15 MFD capacitors and trim to 0.80 MFD $\pm 1\%$.
7. Make up value using Sprague 121D capacitors. Parallel 2.0 MFD and 0.68 MFD and trim to 2.70 MFD $\pm 1\%$.
8. GE Microflat Mylar 65F16AA $\pm 10\%$ capacitor, 50 VDC, or equivalent.
9. Trim value to yield -123 MV between Node (A) and gnd. Nominal value = 665Ω .
10. Trim value to yield +123 MV between Node (B) and gnd. Nominal value = 665Ω .
11. Caddock MM215, $\pm 1\%$, ± 100 ppm/ $^{\circ}\text{C}$.
12. Caddock ML181, $\pm 1\%$, ± 100 ppm/ $^{\circ}\text{C}$.

$$\frac{E_{01}}{E_1} =$$

$$K_a = -R$$

sw
for

To V_S
condi

$$\frac{K_a S}{S+1)(\tau_b S+1)} \approx \frac{K_a S}{(\tau_a S+1)} = -\left[\frac{7.41 S}{(8.0 S+1)}\right] \text{ or: } -\left[\frac{7.41 S}{(27.0 S+1)}\right]$$

$$\frac{K_a S}{S+1)(\tau_b S+1)} \approx \frac{K_a S}{(\tau_a S+1)} = -\left[\frac{7.41 S}{(8.0 S+1)}\right] \text{ or: } -\left[\frac{7.41 S}{(27.0 S+1)}\right]$$

$$2C_1 \left\{ \begin{array}{l} R_2 = R_{2a} \text{ or } R_{2b} \\ C_1 = C_{1a} \text{ or } C_{1b} \end{array} \right\}, \quad \begin{array}{l} \tau_a = R_1 C_1 = 8 \text{ sec or } 27 \text{ sec} \\ \tau_b = \left\{ \begin{array}{l} R_{2a} C_2 = 0.00927 \text{ sec} \\ R_{2b} C_2 = 0.00275 \text{ sec} \end{array} \right.$$

$$K_{11} = \frac{E_{02}}{E_{01}} = -\frac{R_4}{R_{3a}} \left(\frac{1}{\tau_c S + 1} \right) = -1.00 \left(\frac{1}{0.010S + 1} \right) \text{ (nom)}$$

$$\tau_c = R_4 C_3 = 0.010 \text{ sec (nom)}$$

$$K_{11} = \frac{E_{02}}{E_{01}} = -\frac{R_4}{R_{3a}} \left(\frac{1}{\tau_c S + 1} \right) = -1.00 \left(\frac{1}{0.010S + 1} \right) \text{ (nom)}$$

$$\tau_c = R_4 C_3 = 0.010 \text{ sec (nom)}$$

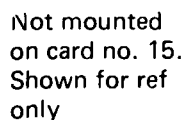


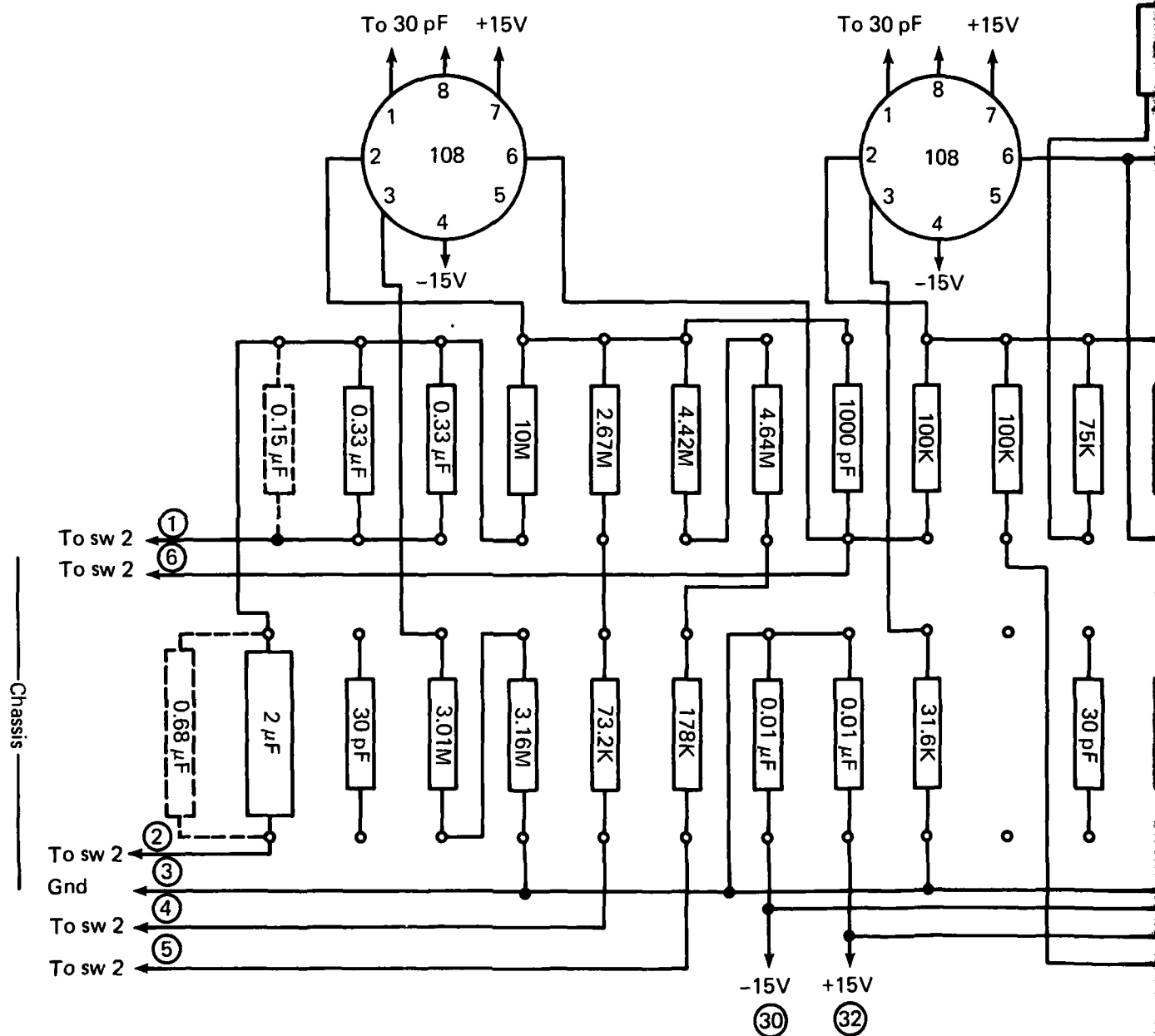
Fig. A15-1 Schematic

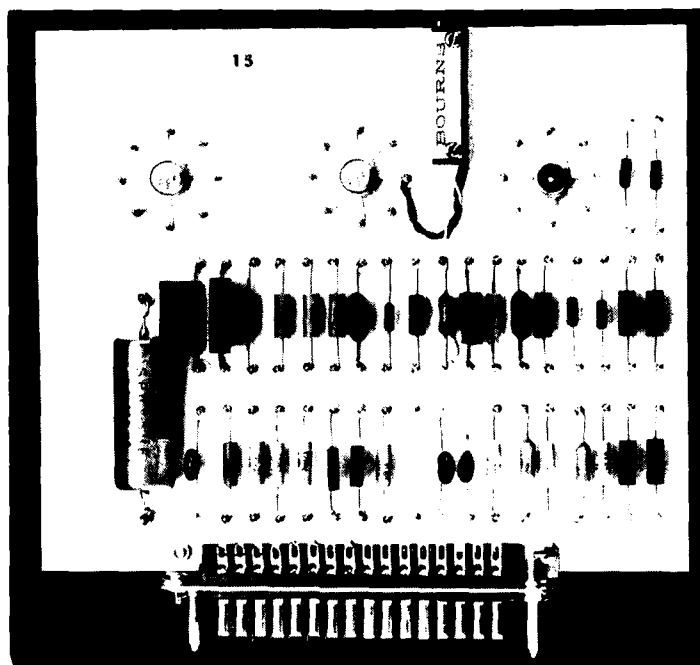
Adjustable gain amplifier

$$\tau_d = R_6 C_4 = 0.010 \text{ sec (nom)}$$

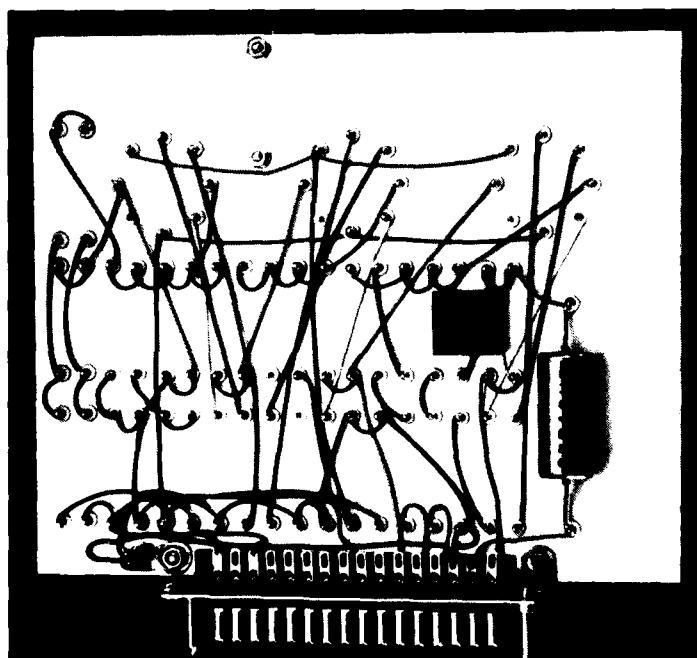
$$\tau_4 = R_4 C_3 = 0.010 \text{ sec (nom)}$$







(a)



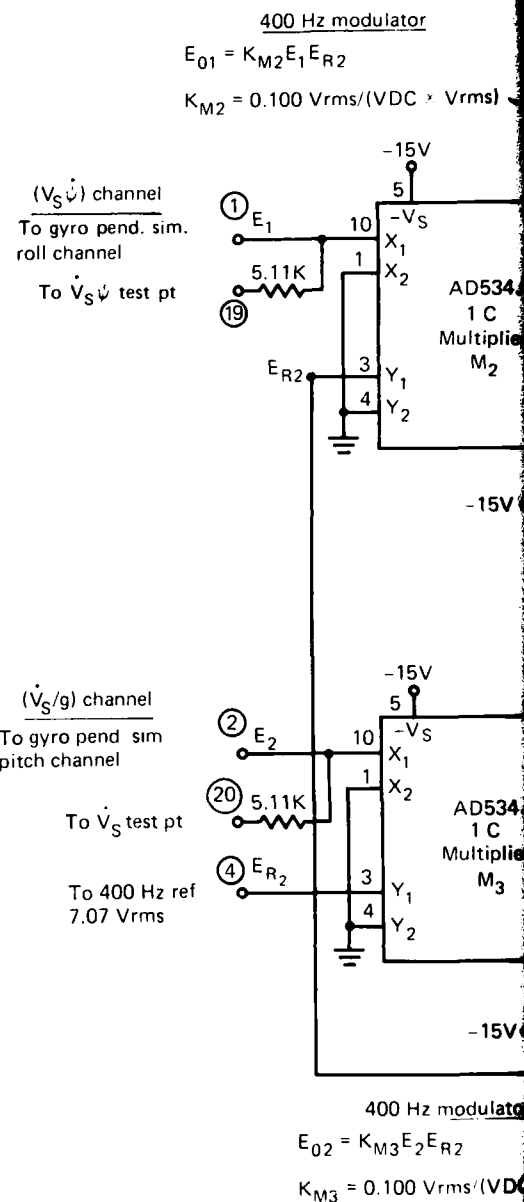
(b)

Fig. A15-3 GCU gyro pendulum simulator pitch channel.

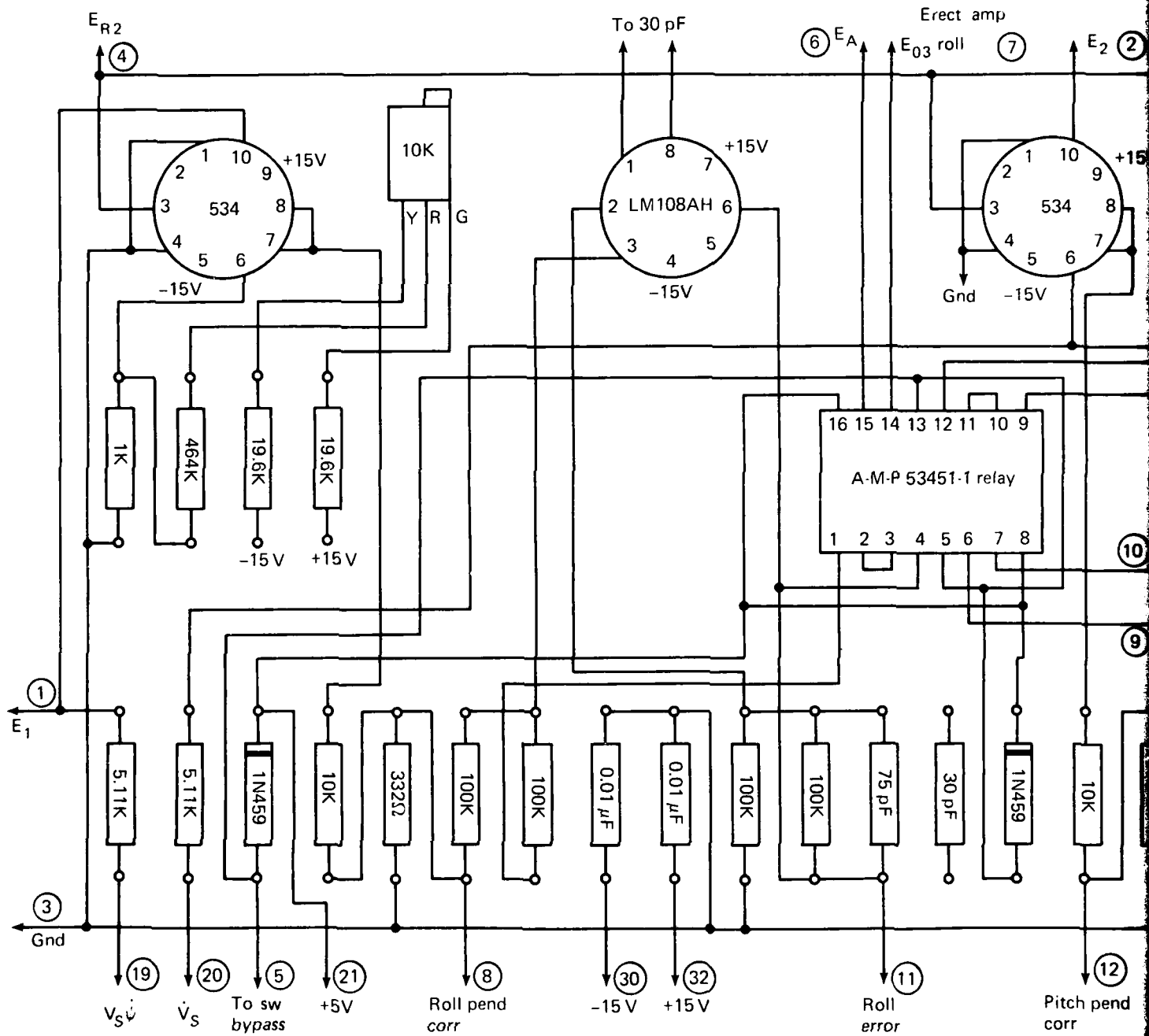
Board No. 16

Notes:

1. ○ denotes pins on connector.
2. All resistors: RN60D metal film $\pm 1\%$, ± 100 ppm/ $^{\circ}\text{C}$ or equivalent unless otherwise noted.
3. All capacitors: Mica $\pm 10\%$ or equivalent unless otherwise noted.
4. Calibrate tilt angle meter to read $(-2^{\circ}) - 0 - (+2^{\circ})$ full scale. With roll or pitch pendulum angle set to 0.5° , adjust P_1 for meter reading of $0.5^{\circ} \pm 0.01^{\circ}$. Nominal setting of P_1 is $\approx 10\text{K}$ ohms corresponding to roll and pitch pendulum output scale factors of $10.0 \text{ Vrms/rad} = (0.175 \text{ Vrms/deg} = 0.2475 \text{ V pk/deg})$.
5. With E_1 at 0.0 V adjust P_3 such that E_{01} yields $0.0 \text{ MV} \pm 10 \text{ MV}$.
6. With E_2 at 0.0 V adjust P_2 such that E_{02} yields $0.0 \text{ MV} \pm 10 \text{ MV}$.
7. Bourns 10 turn trimpot or equivalent. For nulling DC output at nodes E_{01} and E_{02} .
8. Wesco 10 MFD, 50 VDC type 32 MPC, $\pm 10\%$. Polycarbonate capacitor or equivalent.
9. Amp model 53451-1 dual DPDT relay in DIP package.







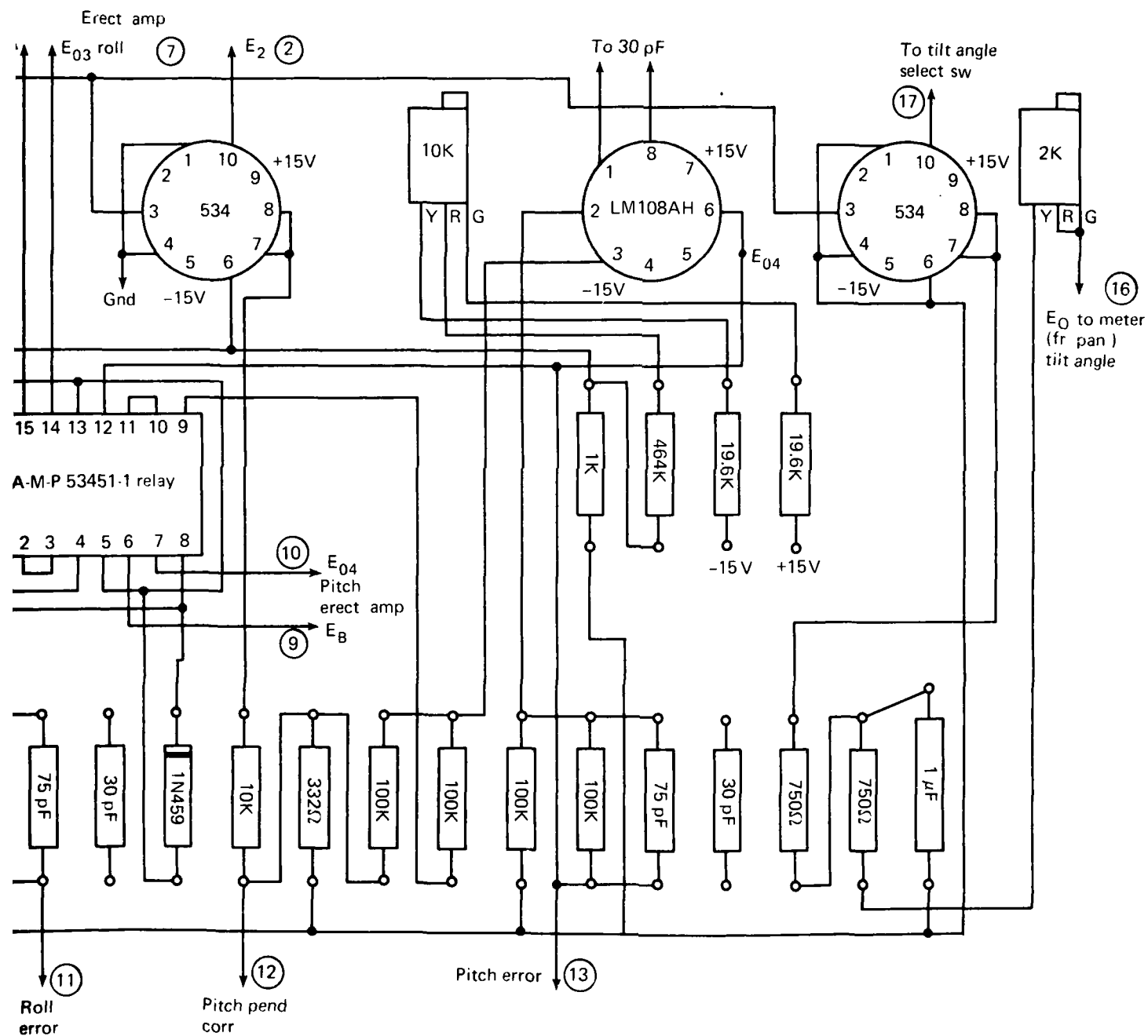
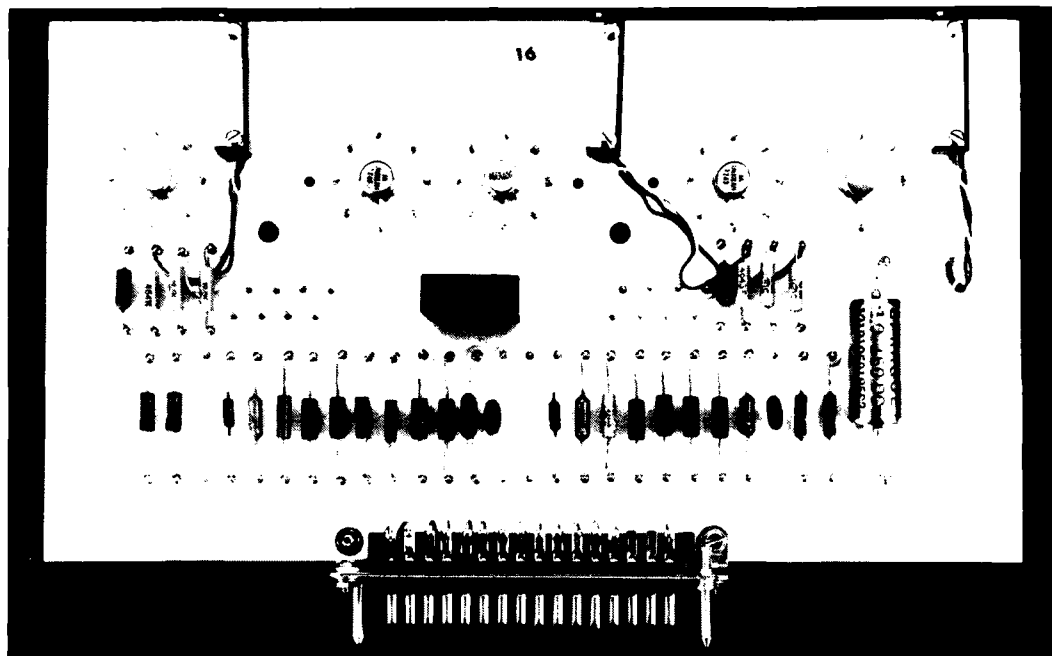
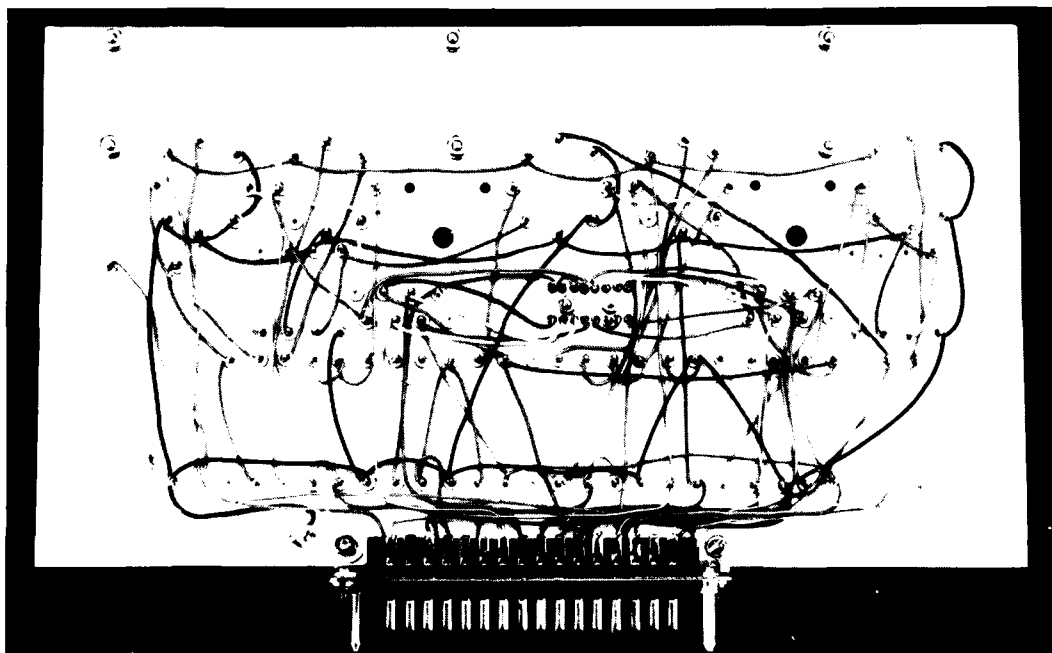


Fig. A16-2 Component layout, Card No.16, GCU simulator pendulum-400 Hz modulator maneuver compensation amplifier.



(a)



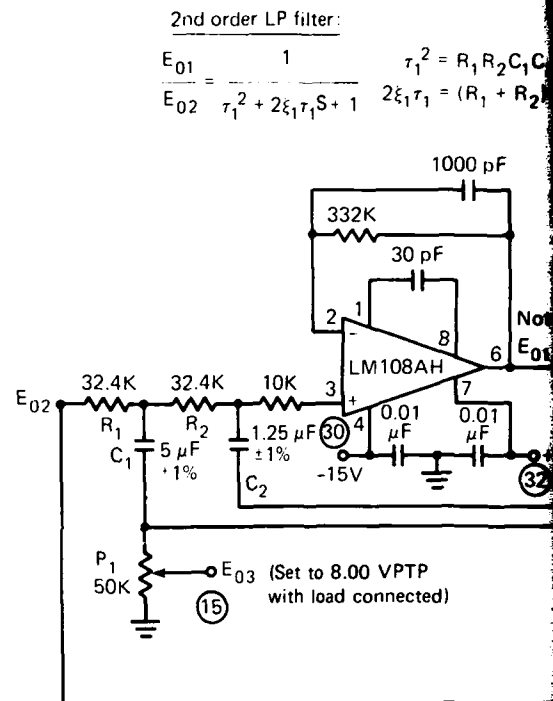
(b)

Fig. A16-3 GCU simulated pendulum, 400 Hz modulator maneuver compensation amplifier.

Board No. 17

Notes

- 1 denotes pins on connector.
- 2 All resistors - MEA metal film $\pm 1\%$, 100 ppm/°C or equivalent unless otherwise noted.
- 3 All capacitors - Mica $\pm 10\%$ or equivalent unless otherwise noted.
- 4 Trim R_3 to yield $E_{01} = 8$ V P-P at test frequency f_0 (≈ 2.00 Hz). Value of R_3 shown was that actually used in circuit.
- 5 This was actual value measured with load attached.



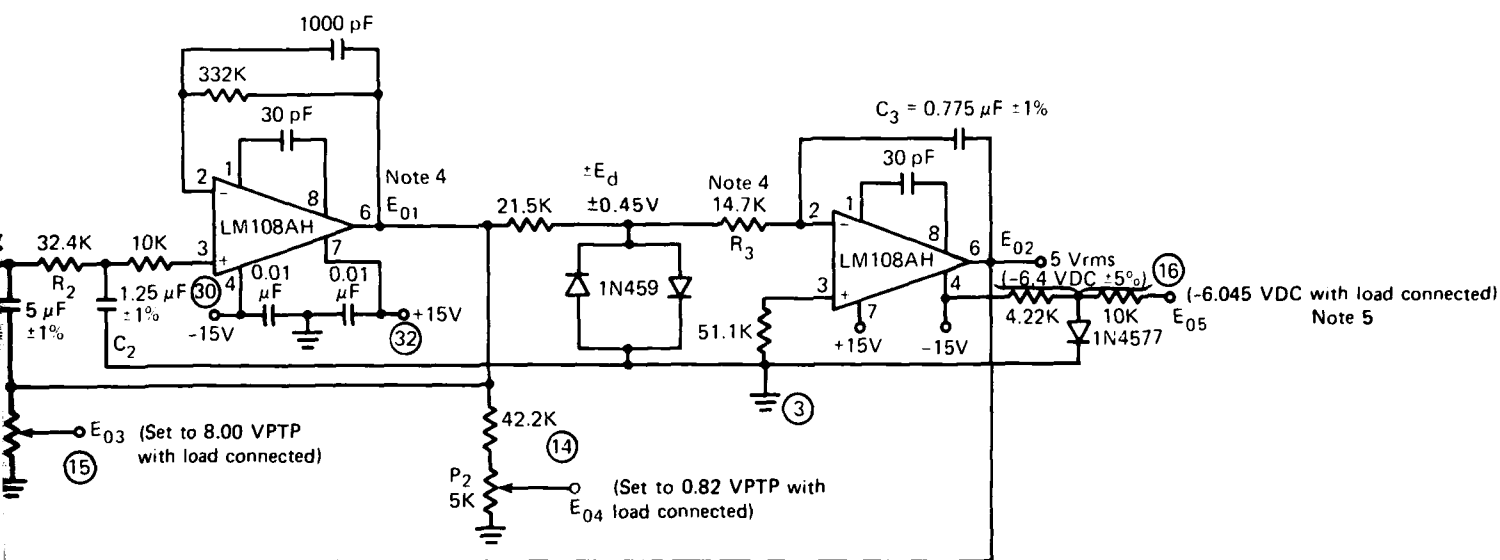
2nd order LP filter:

$$\frac{E_{01}}{E_{02}} = \frac{1}{\tau_1^2 + 2\xi_1\tau_1 S + 1} \quad \tau_1^2 = R_1 R_2 C_1 C_2$$

$$2\xi_1\tau_1 = (R_1 + R_2)C_2$$

Integrator:

$$\frac{E_{02}}{E_{01}} = -\frac{1}{R_3 C_3 S}$$



ation frequency, f_0 :

$$s^2 + 1 = 0, \text{ or } f_0 = \frac{1}{2\pi\tau_1}$$

= 0.0810 sec, $f_0 = 1.965$ Hz } for nominal component values

= 0.500

Fig. A17-1 Schematic, Card No.17, MCU system test reference generator.

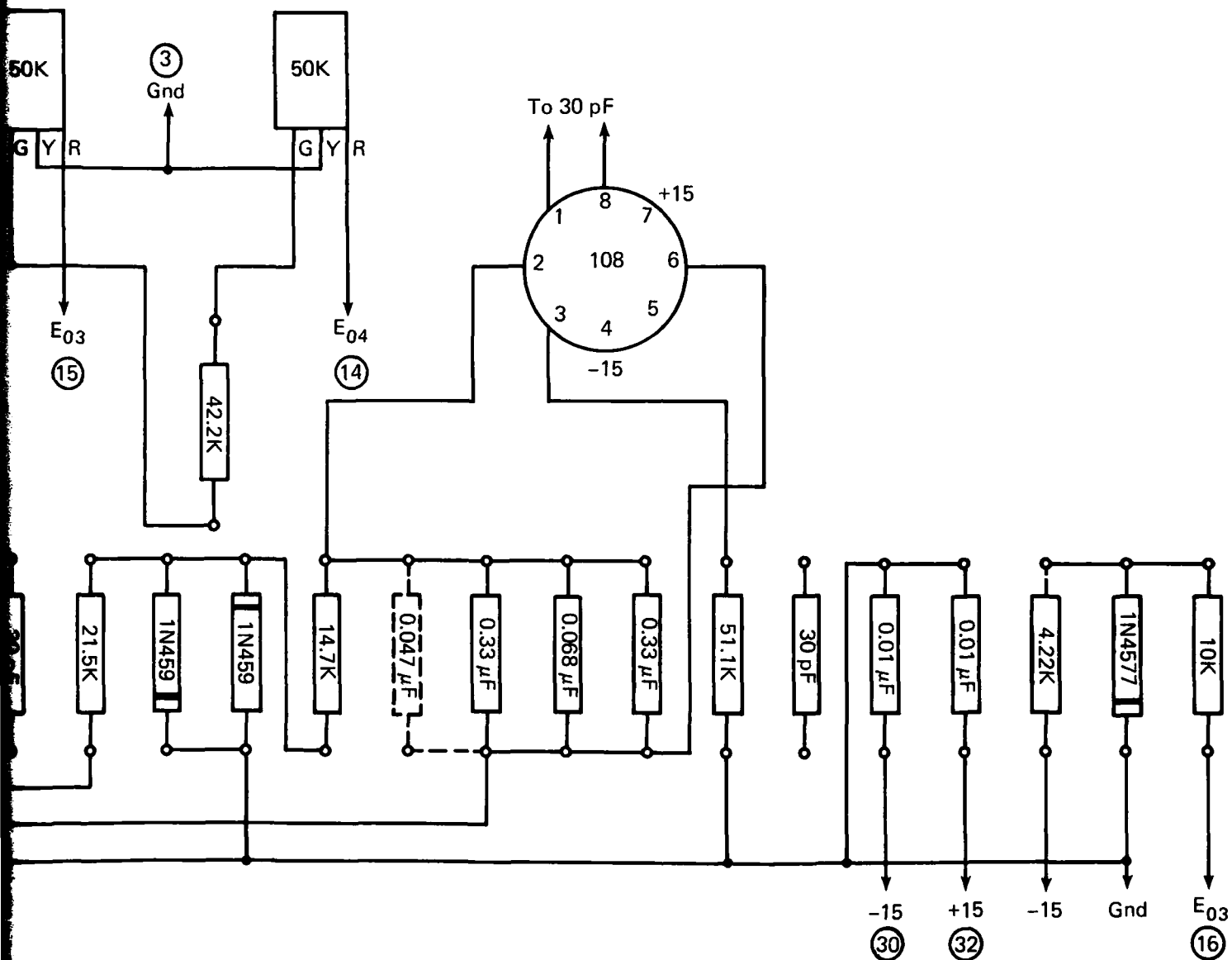
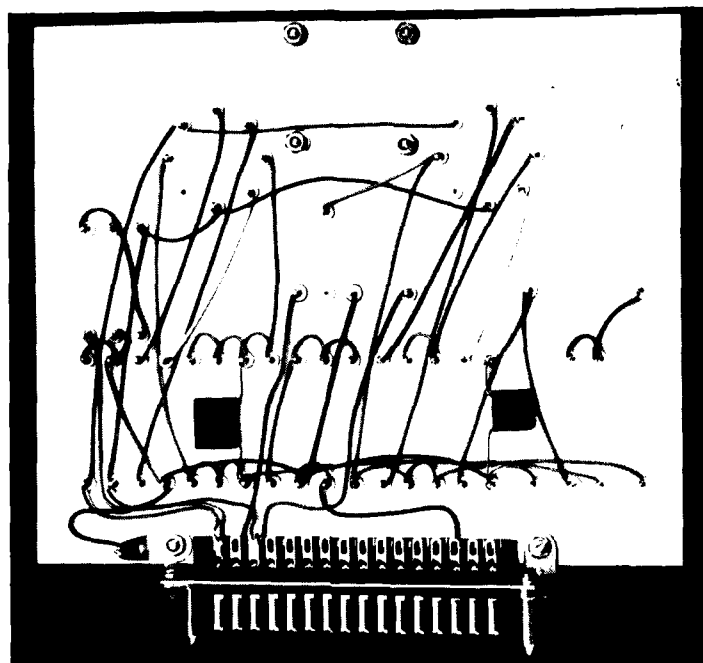
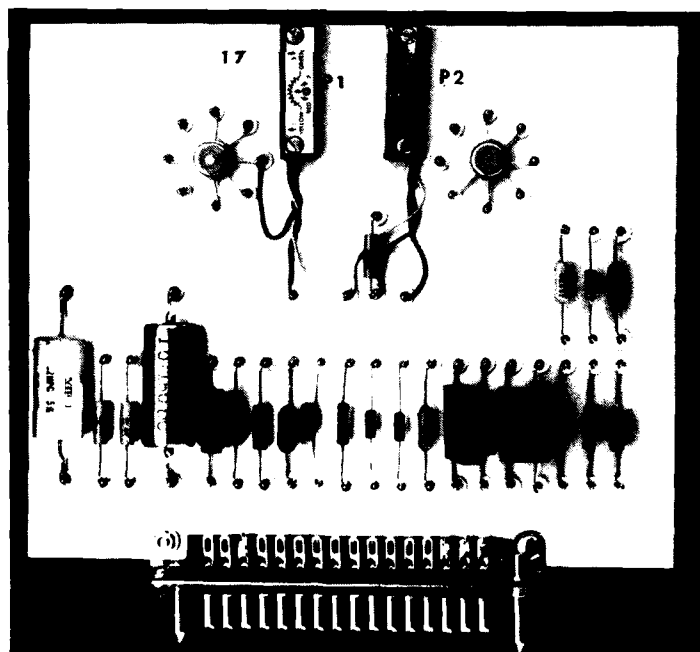


Fig. A17-2 Component layout, Card No.17, GCU MCU system test reference generator.



(a)



(b)

Fig. A17-3 GCU MCU system test reference generator.

THE JOHNS HOPKINS UNIVERSITY
APPLIED PHYSICS LABORATORY
LAUREL, MARYLAND

Appendix B
WAVE PROFILING SYSTEM ELECTRONIC
UNIT CHASSIS WIRING DIAGRAMS
AND PHOTOGRAPHS

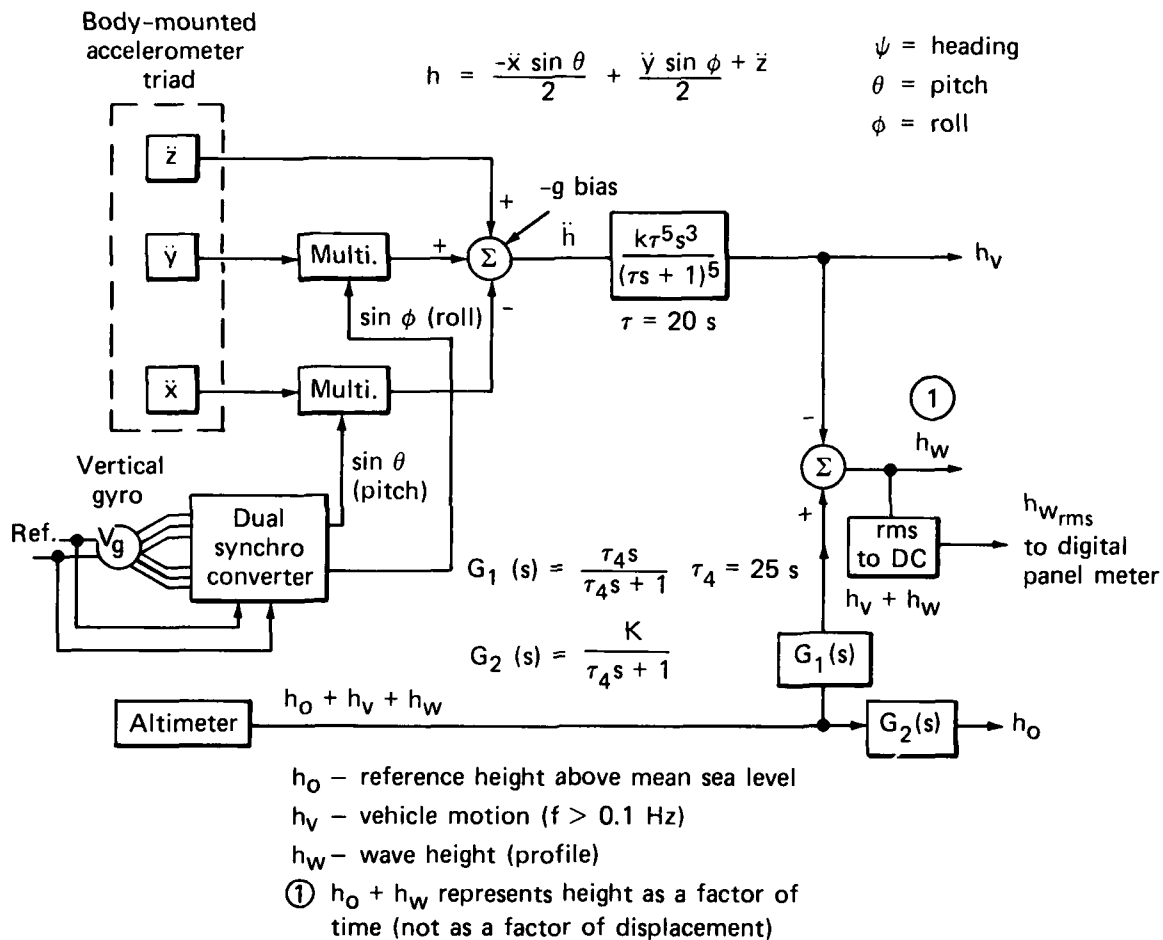


Fig. B1-1 Block diagram of wave profiling system.

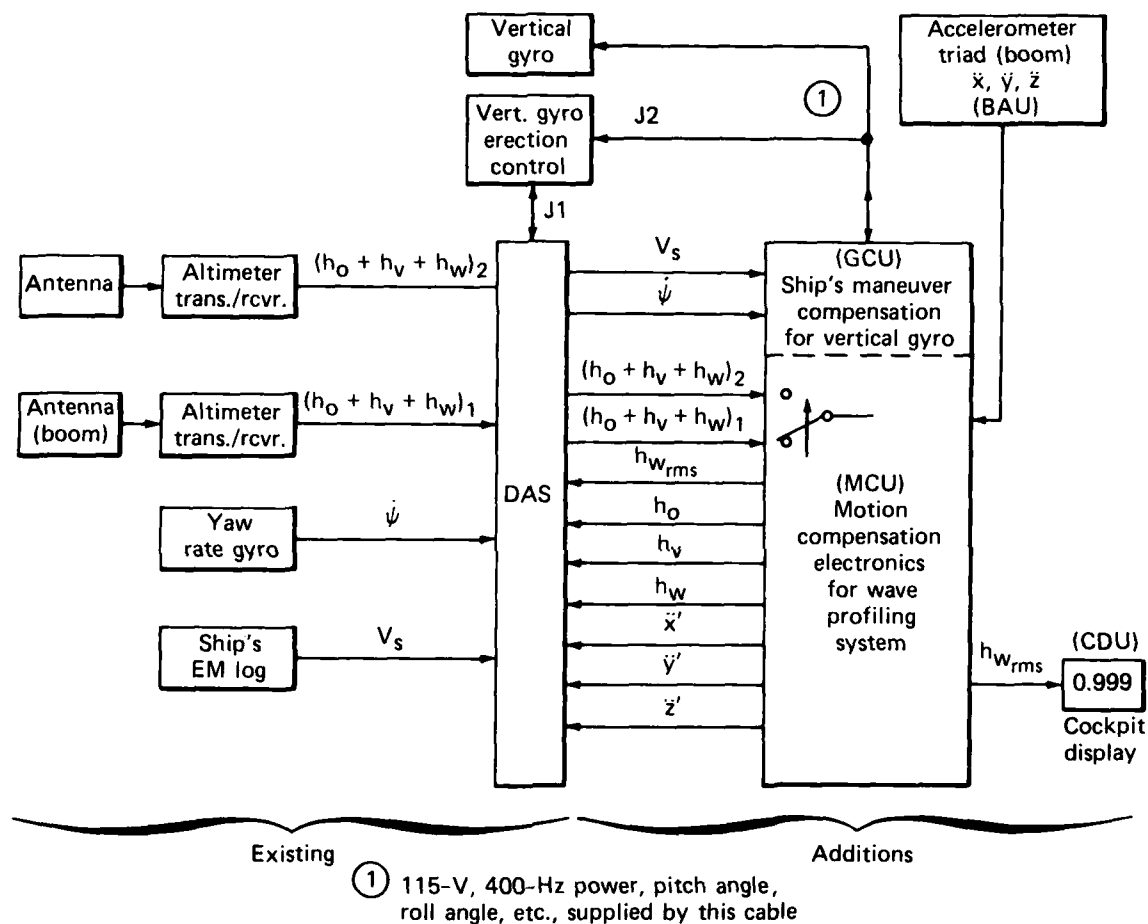


Fig. B1-2 Interface diagram of motion compensated wave profiling system for the SES-100A.

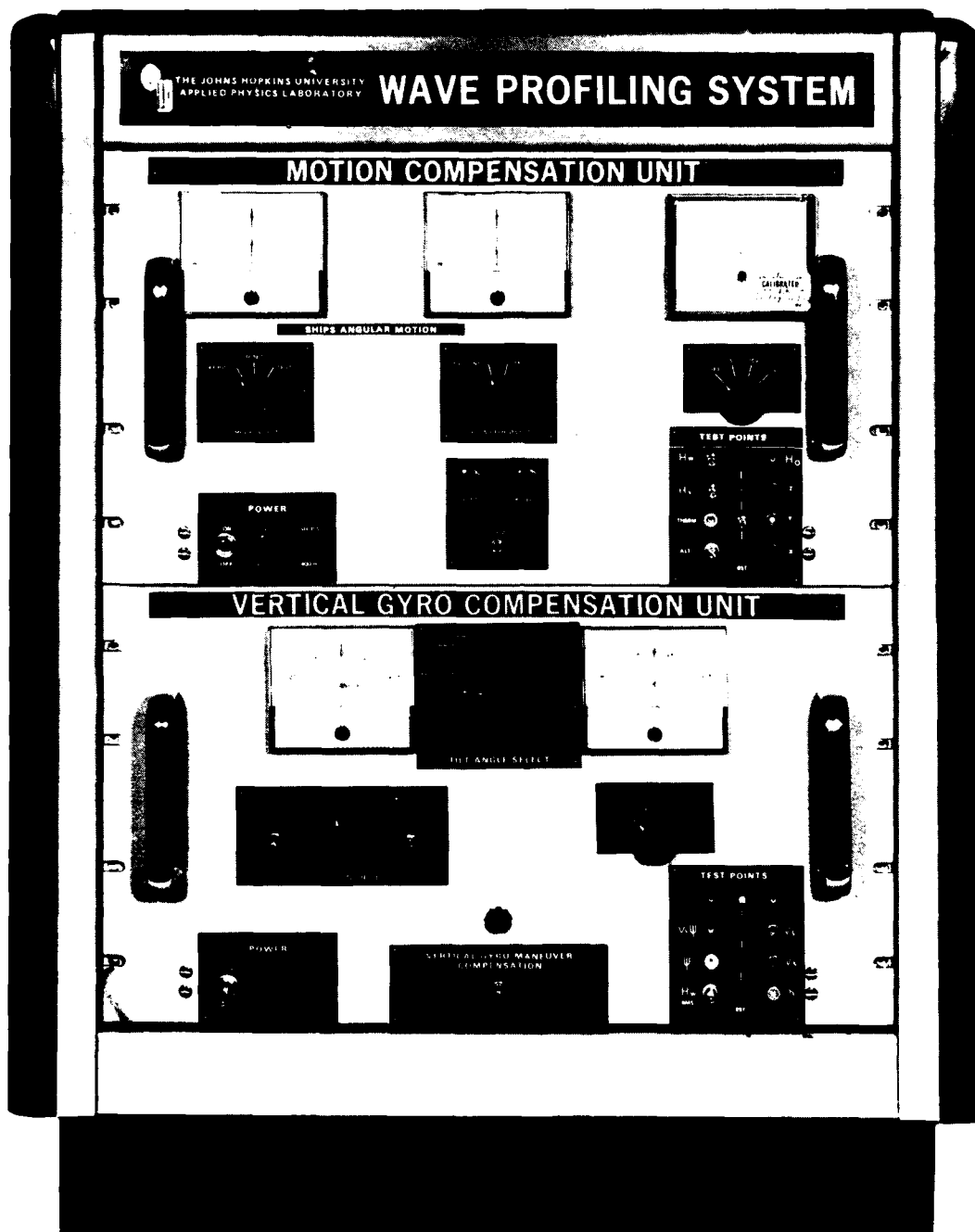


Fig. B1-3 Wave profiling system.

Wave profiler
motion compensation
electronics rack

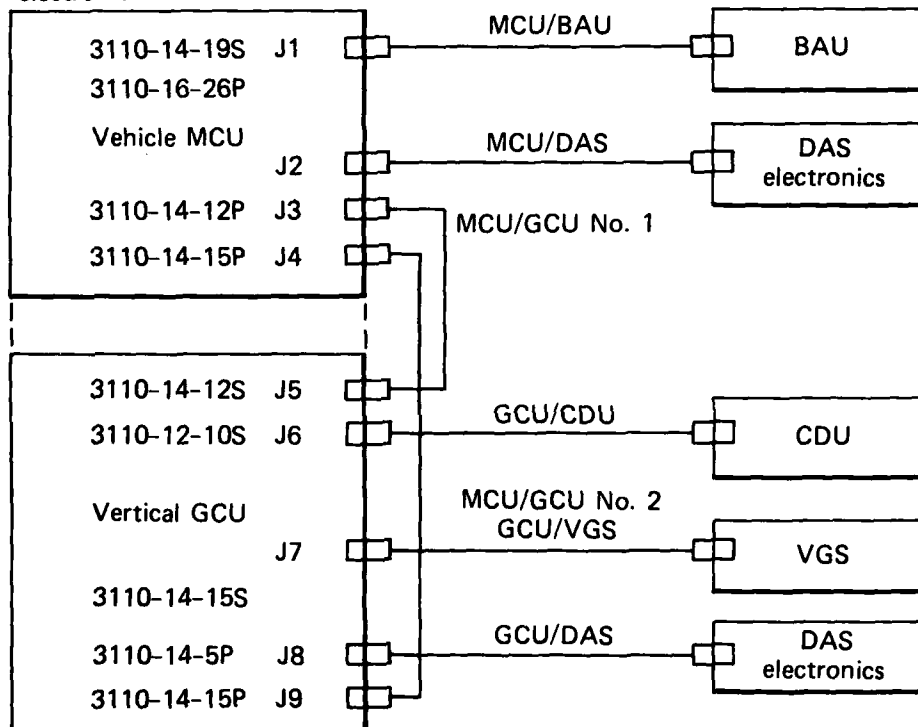
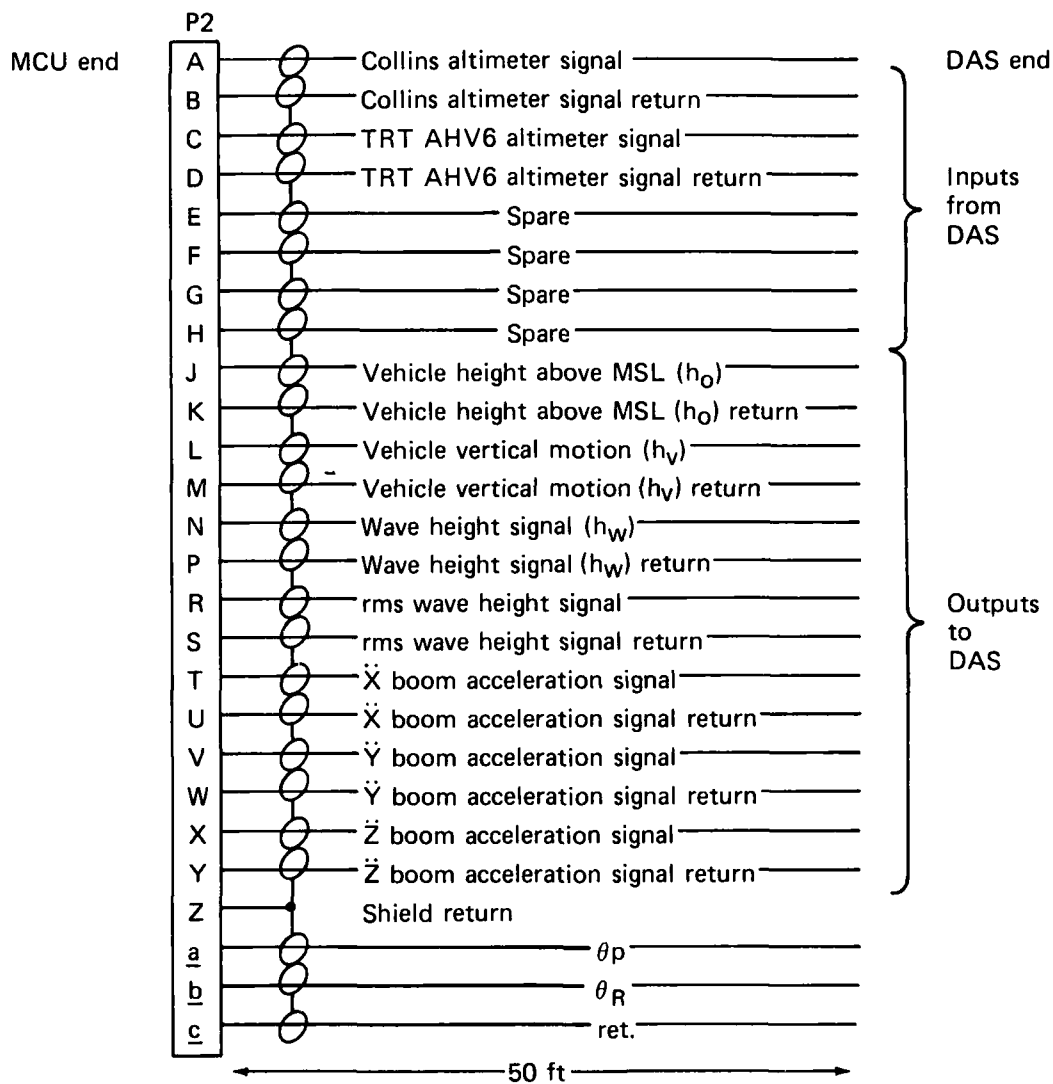


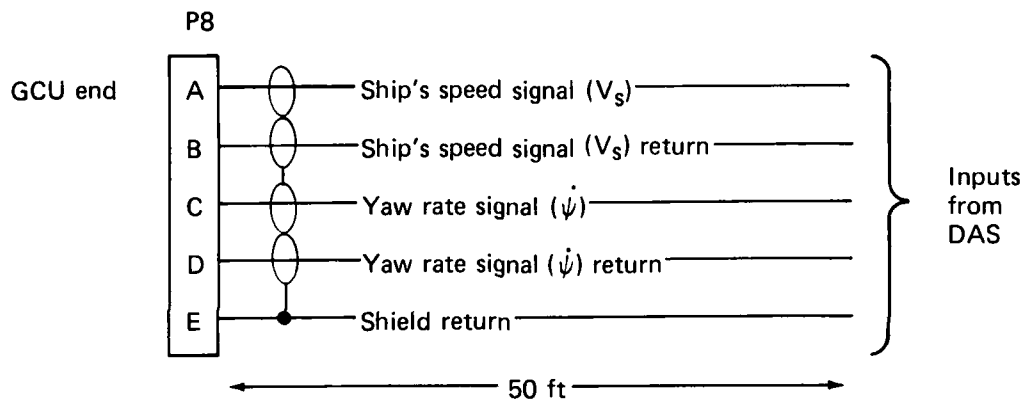
Fig. B1-4 Cabling diagram for SES-100A motion compensation rack.



MS-3116F-16-26S

All conductors #22 with Teflon insulation (twisted shielded pairs)
All shields tied down at MCU end of cable only

Fig. B1-5 MCU/DAS cable diagram.



MS-3116F-14-5S

All conductors No. 22 twisted shielded pairs
All shields tied at GCU end of cable only

Fig. B1-6 GCU/DAS cable diagram.

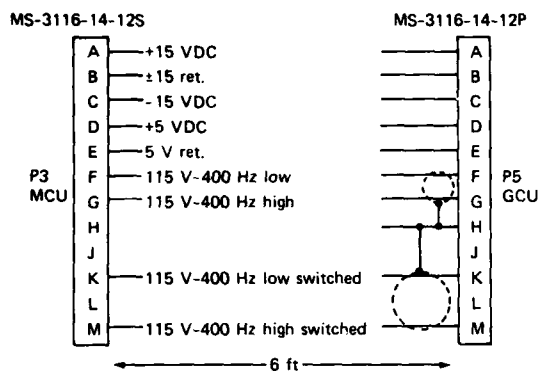


Fig. B1-7 MCU/GCU cable diagram.

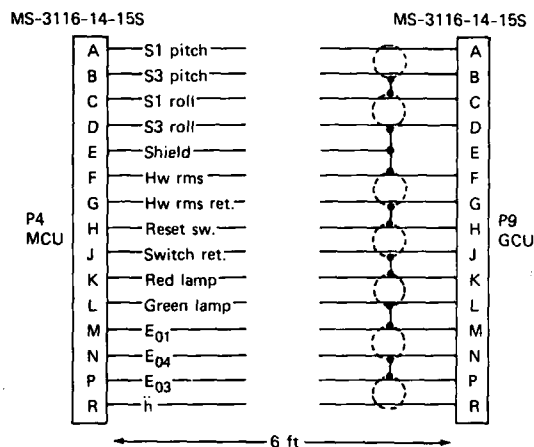


Fig. B1-8 MCU/GCU cable diagram.

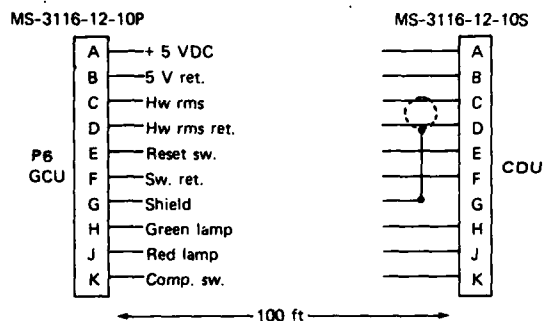


Fig. B1-9 GCU/CDU cable wiring diagram.

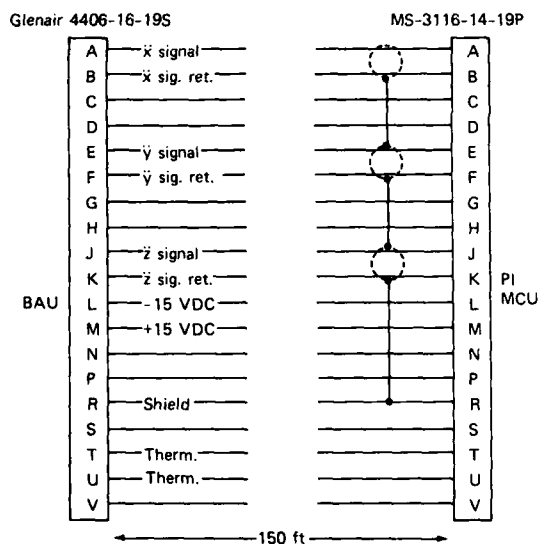


Fig. B1-10 MCU/BAU cable wiring diagram.

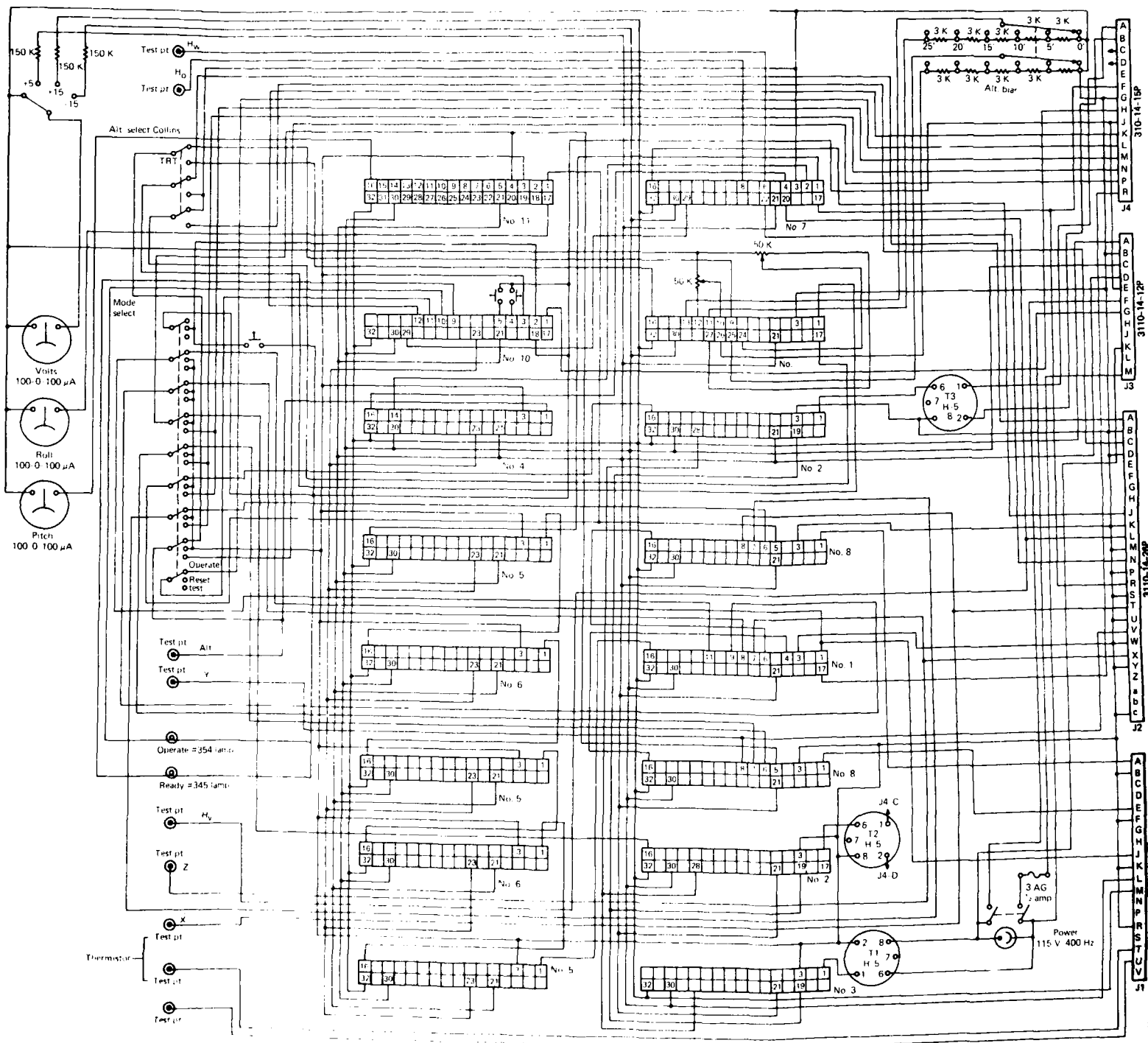


Fig. B2-1 Wiring diagram, MW

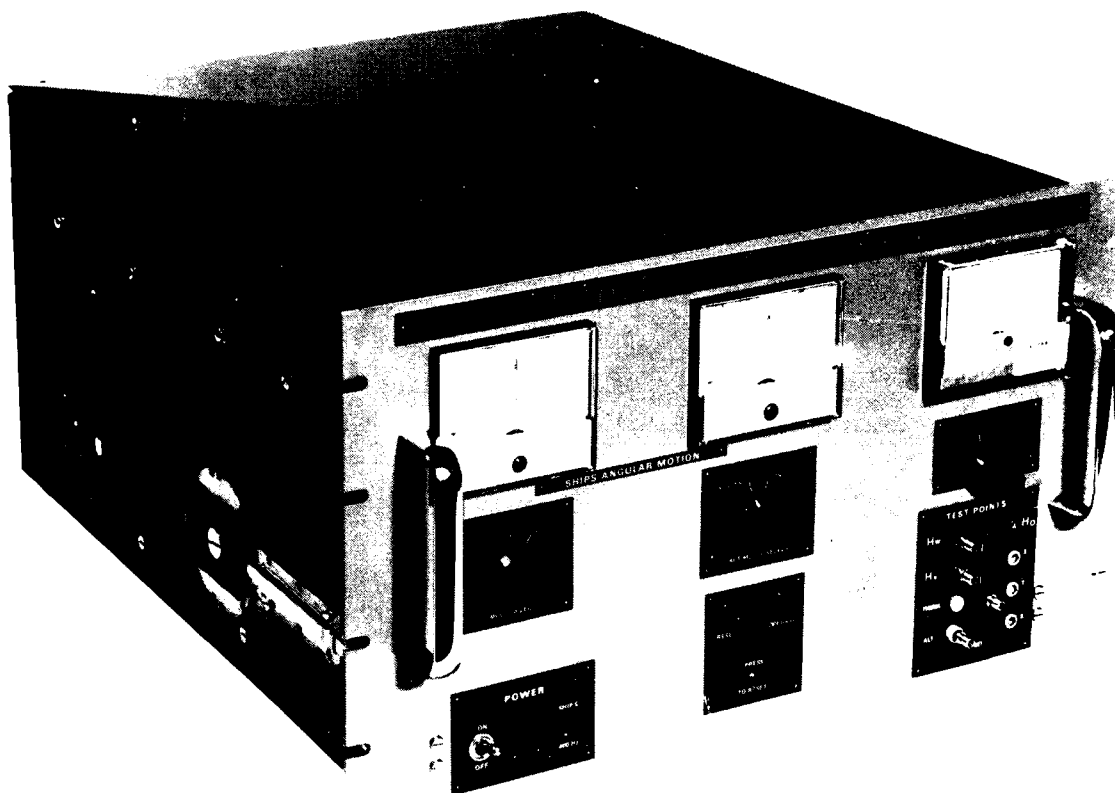


Fig. B2-2 Front panel of MCU.

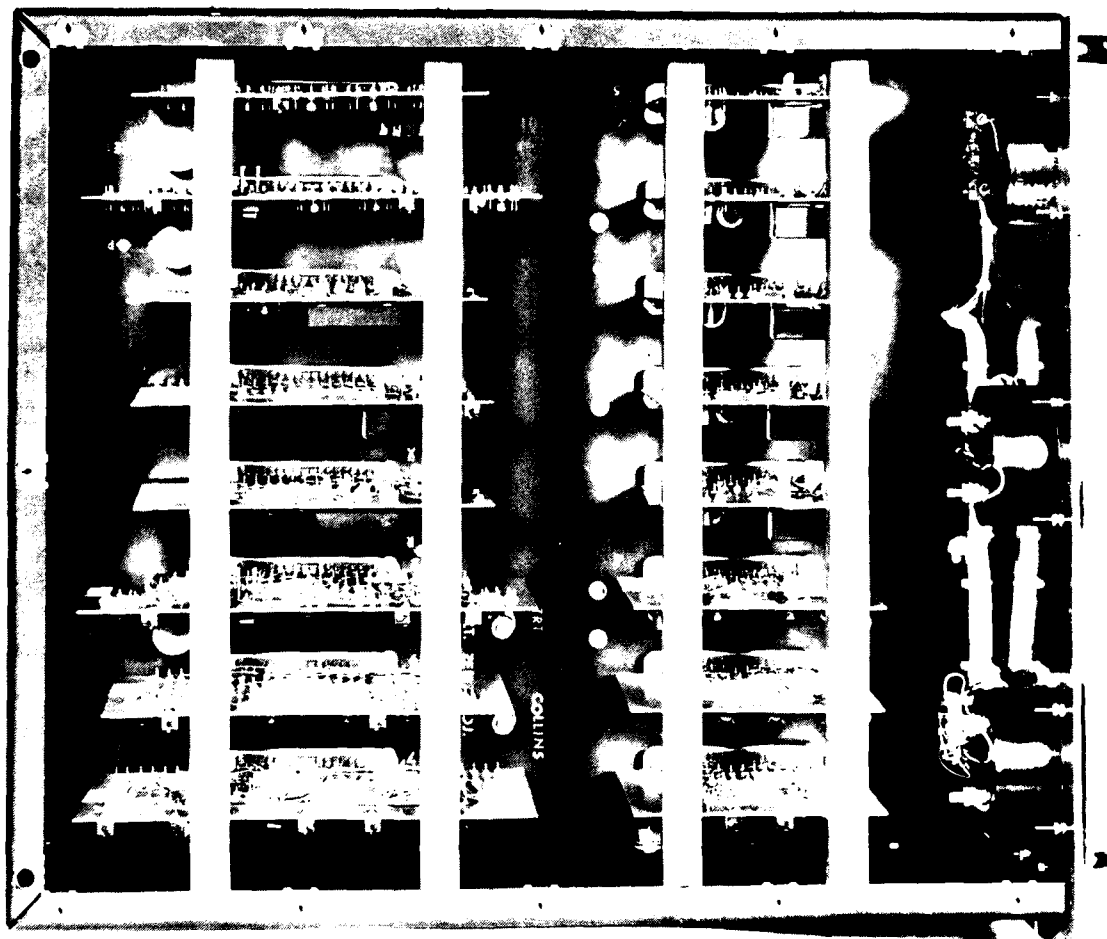


Fig. B2-3 Top view of MCU, cover removed.

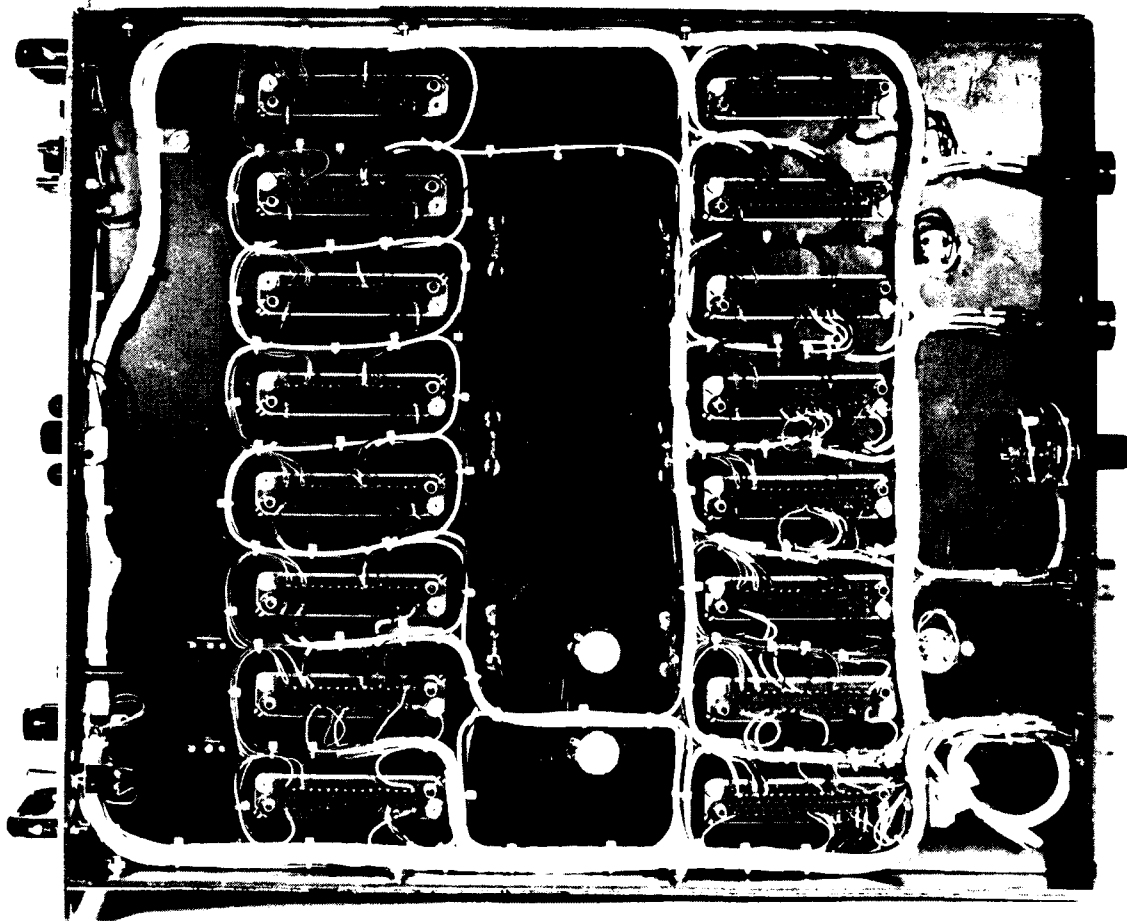


Fig. B2-4 Bottom view of MCU.

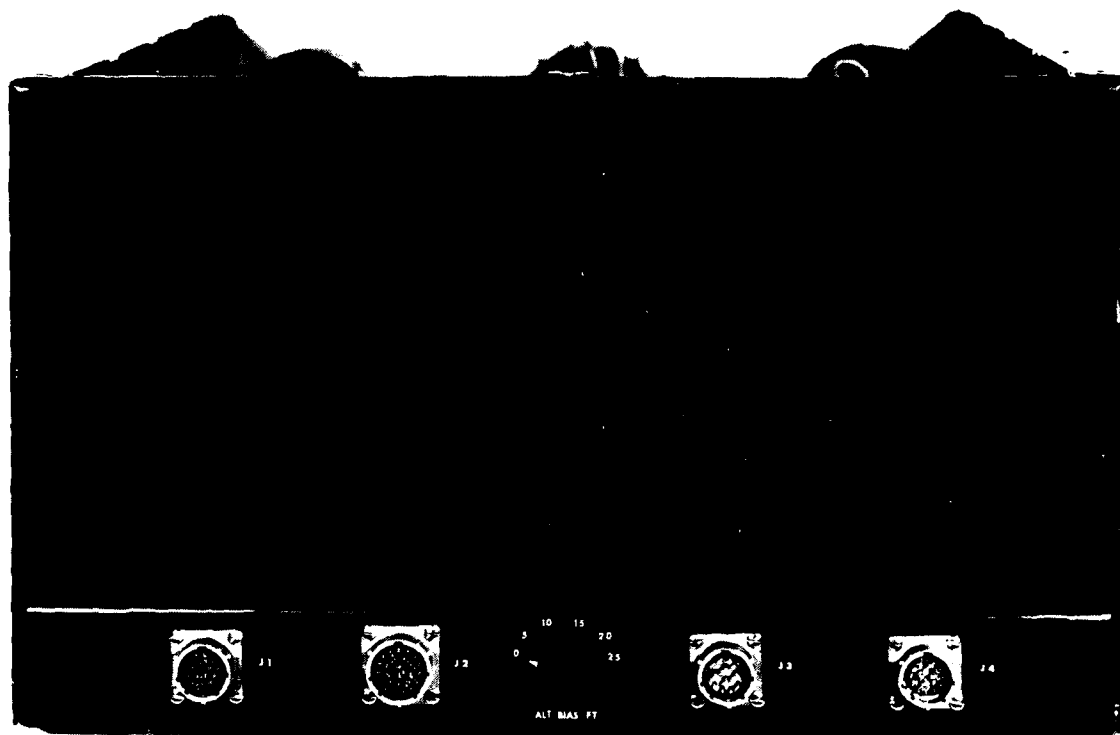


Fig. B2-5 Rear view of MCU showing connectors.

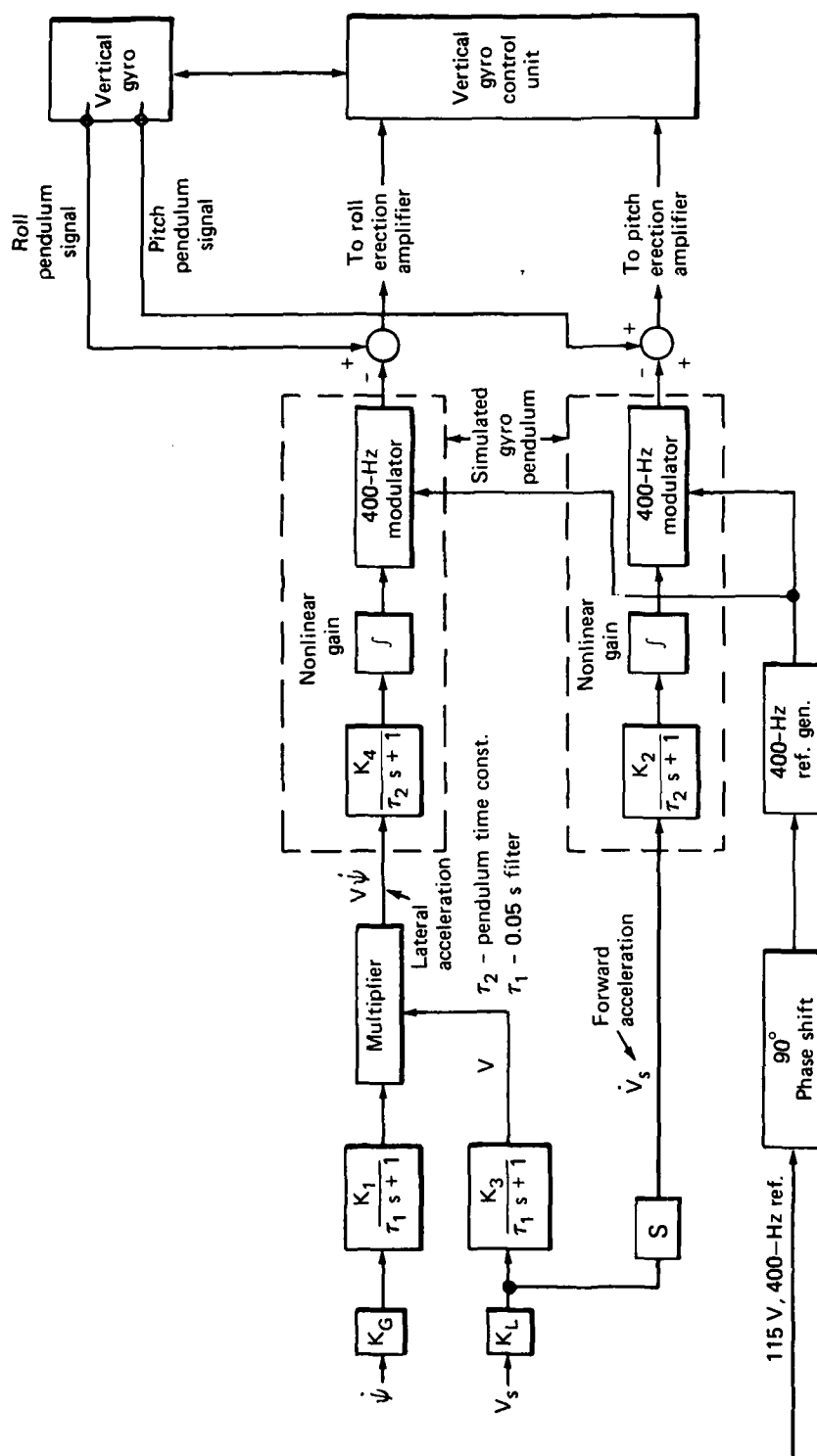


Fig. B3-1 Vertical gyro maneuver compensation, block diagram.

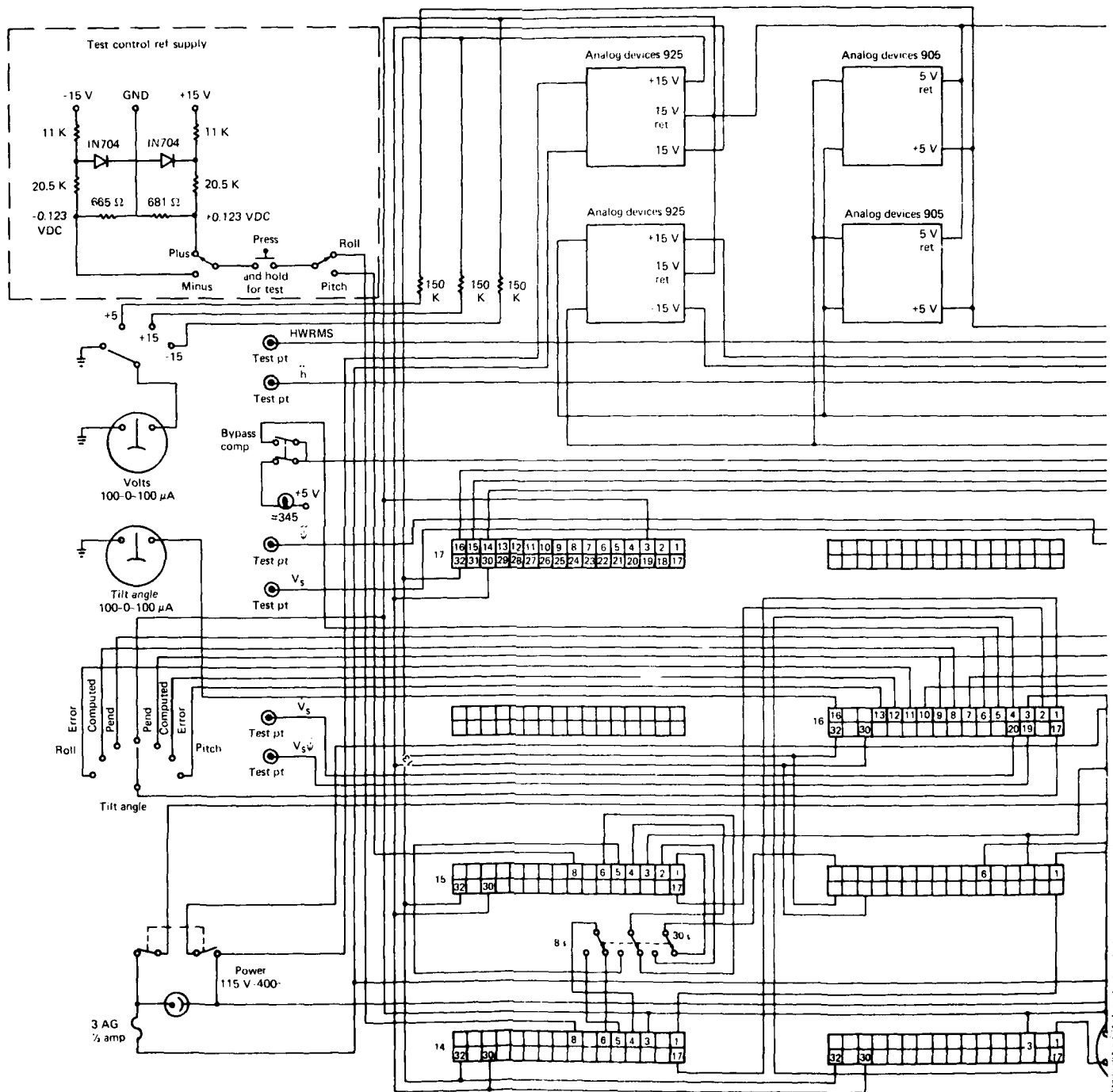


Fig. B3-2

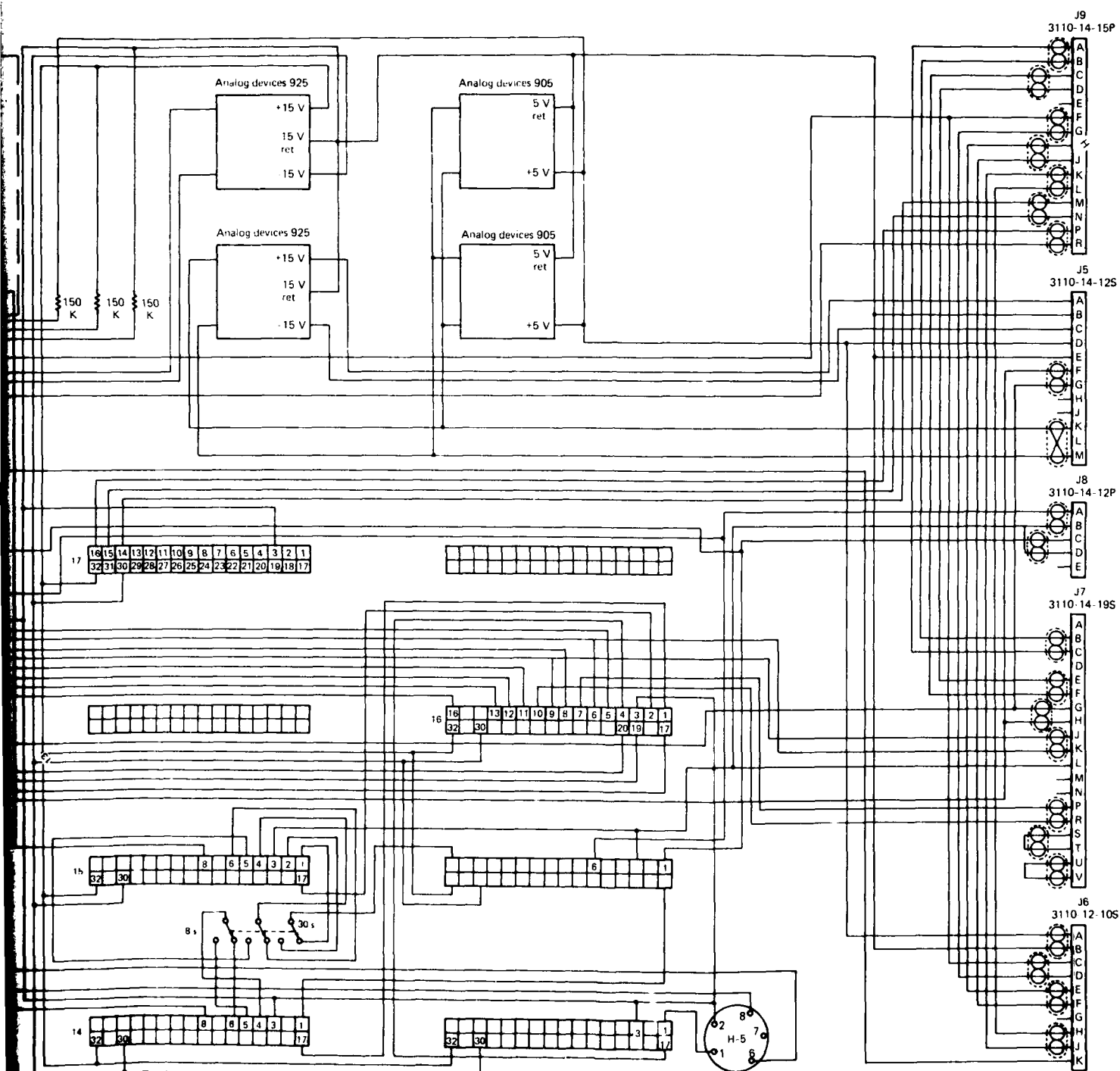


Fig. B3-2 Chassis wiring diagram, gyro compensation unit.

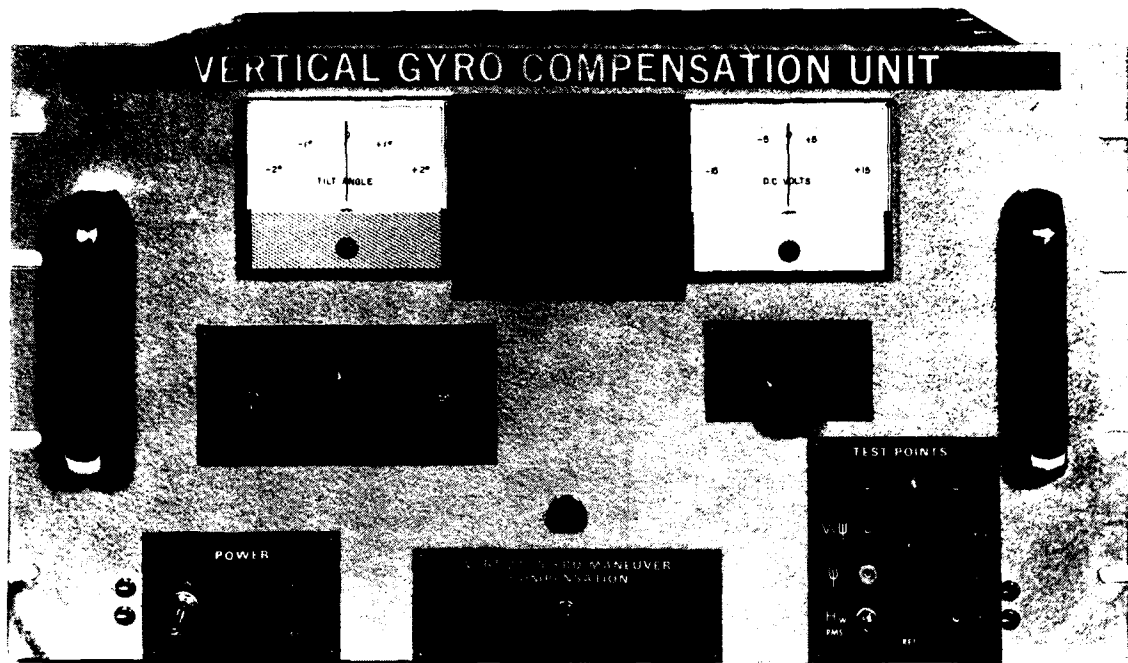


Fig. B3-3 Front panel of GCU.

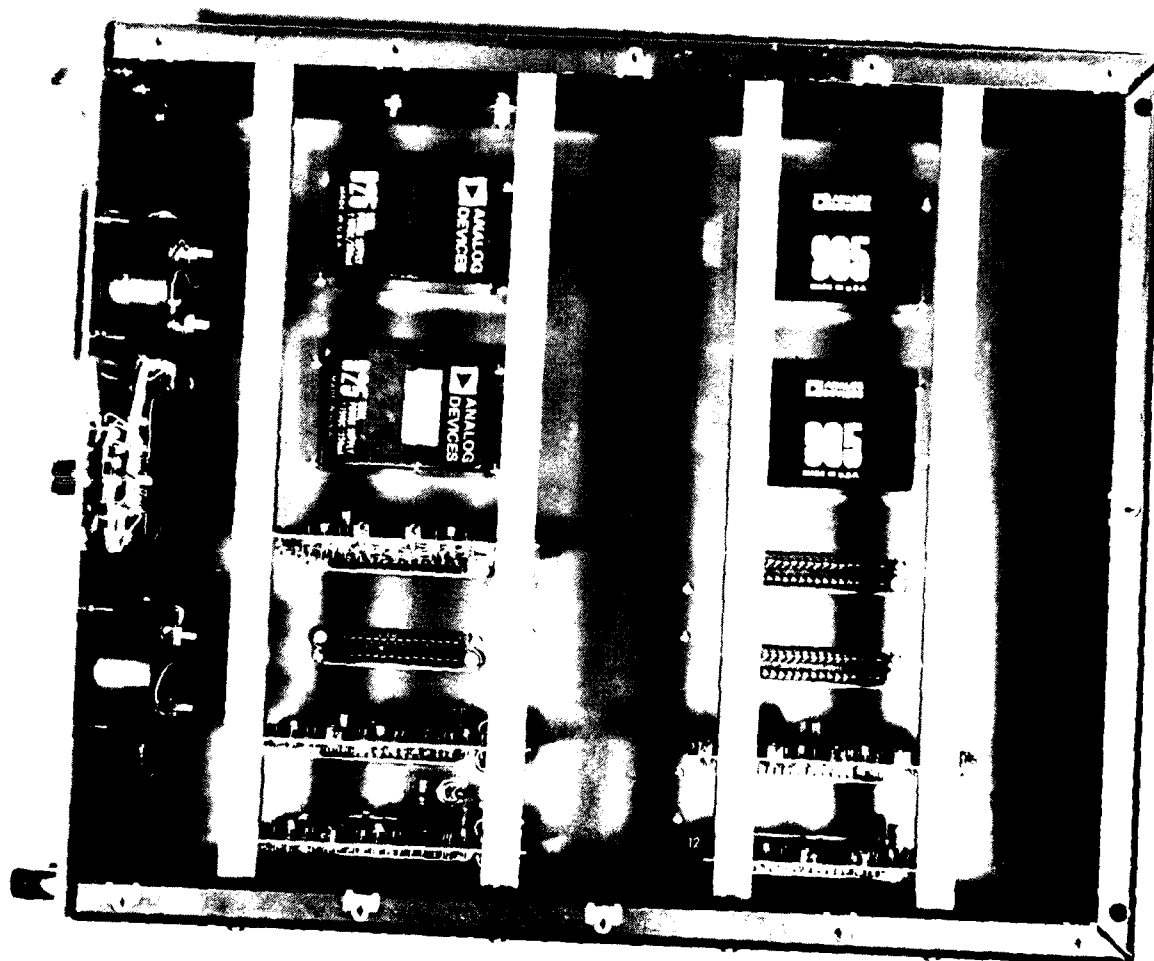


Fig. B3-4 Top view of GCU, cover removed.

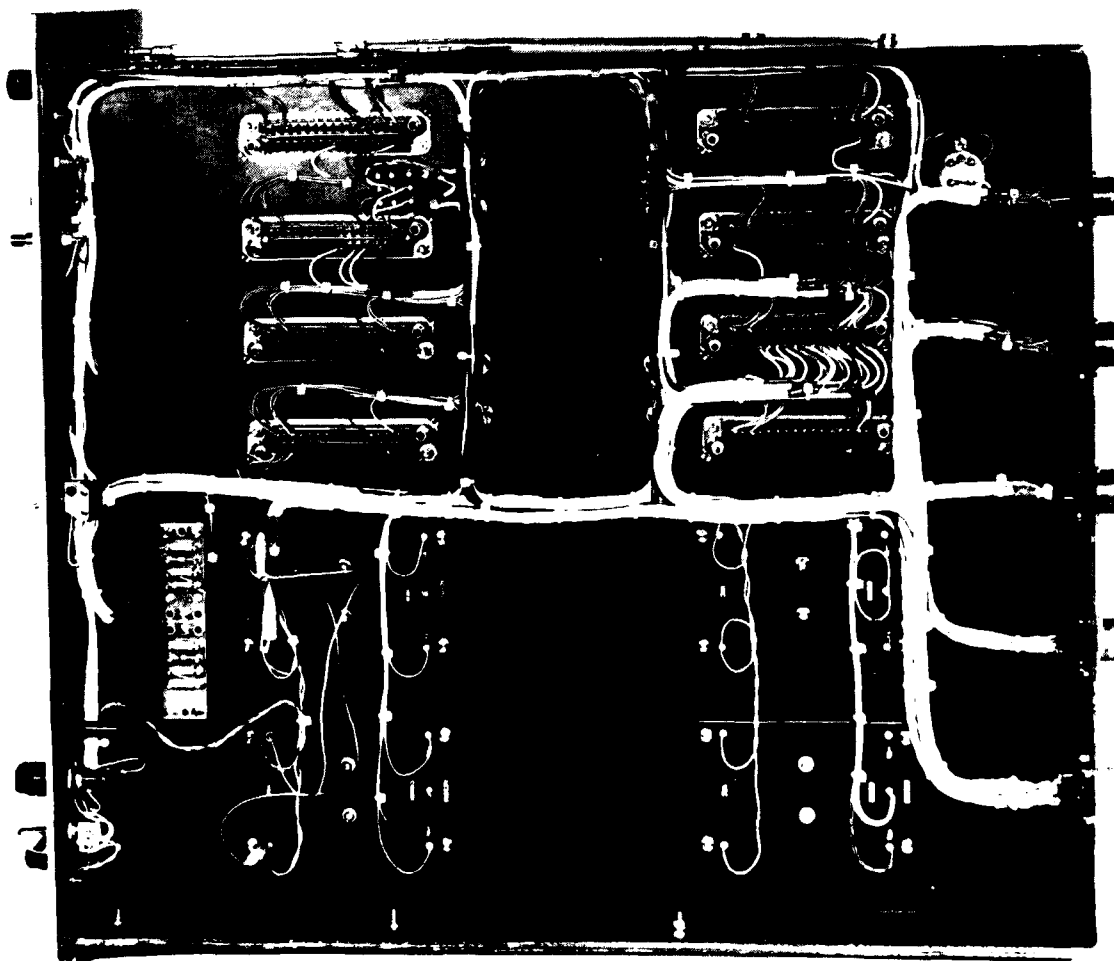


Fig. B35 Bottom view of GCU.

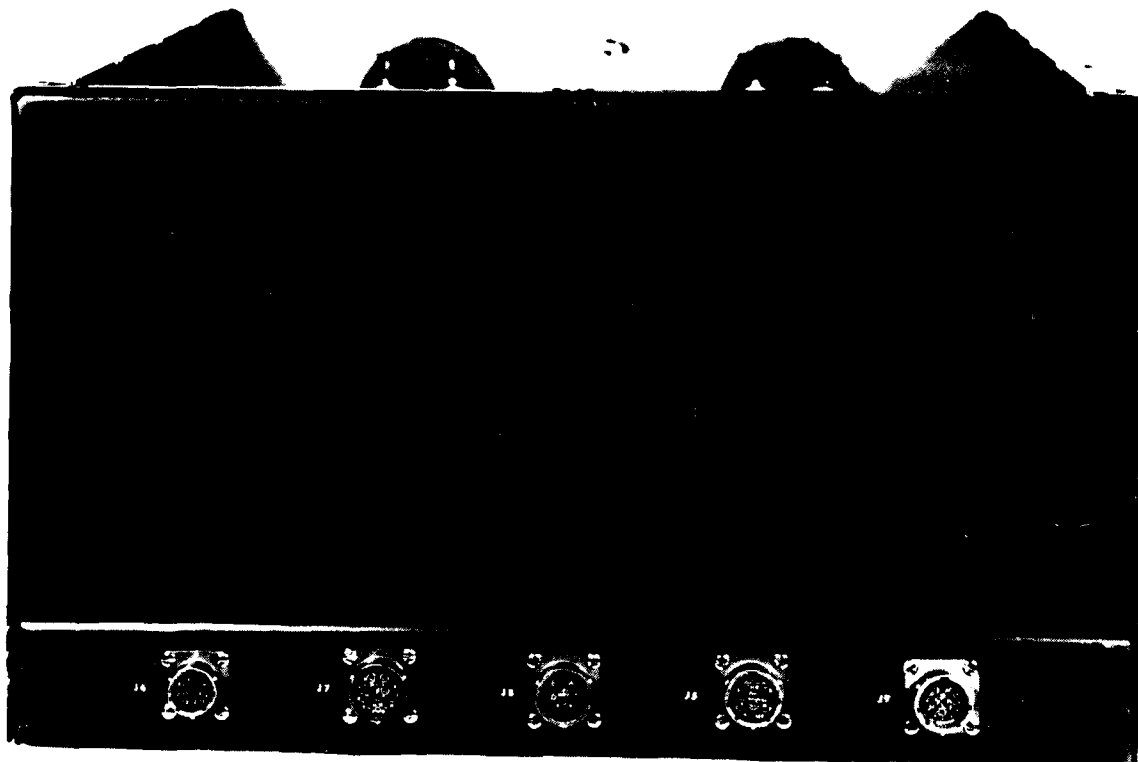


Fig. B3-6 Rear view of GCU.



Fig. B4-1 Wave profiling system mounted on Ling shaker for vertical axis vibration qualification testing.

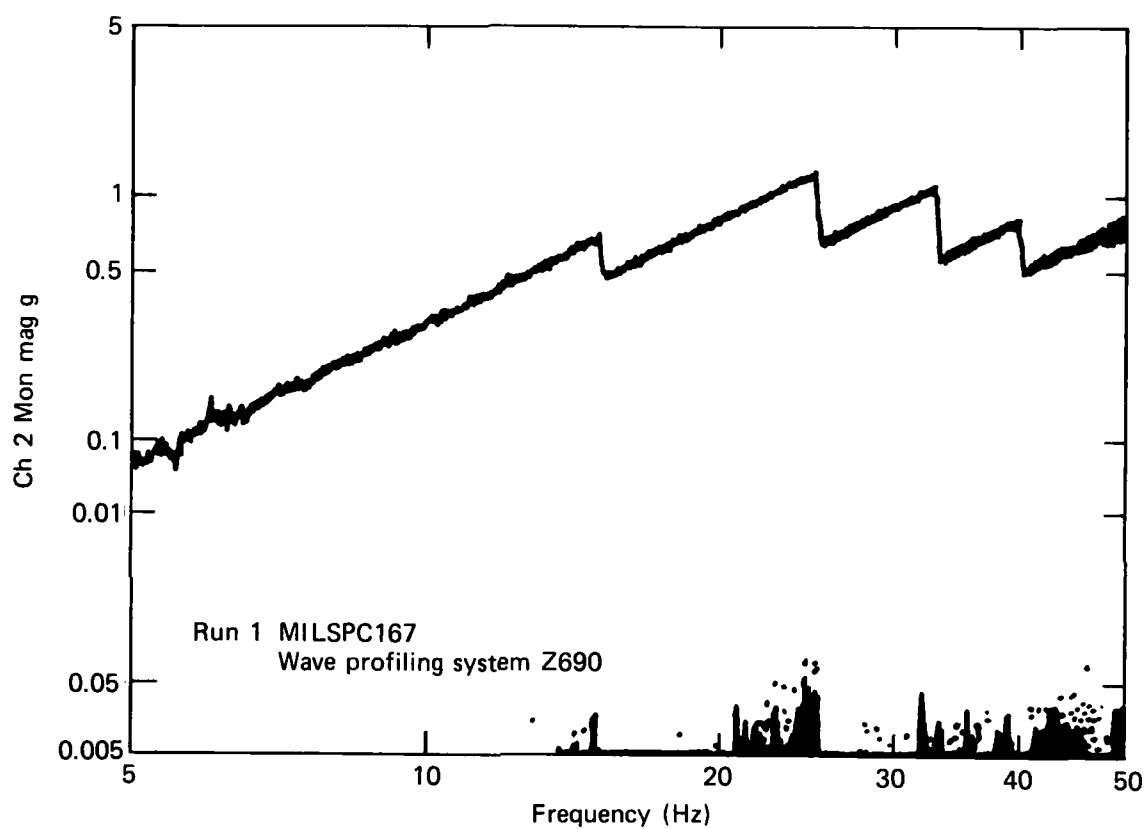
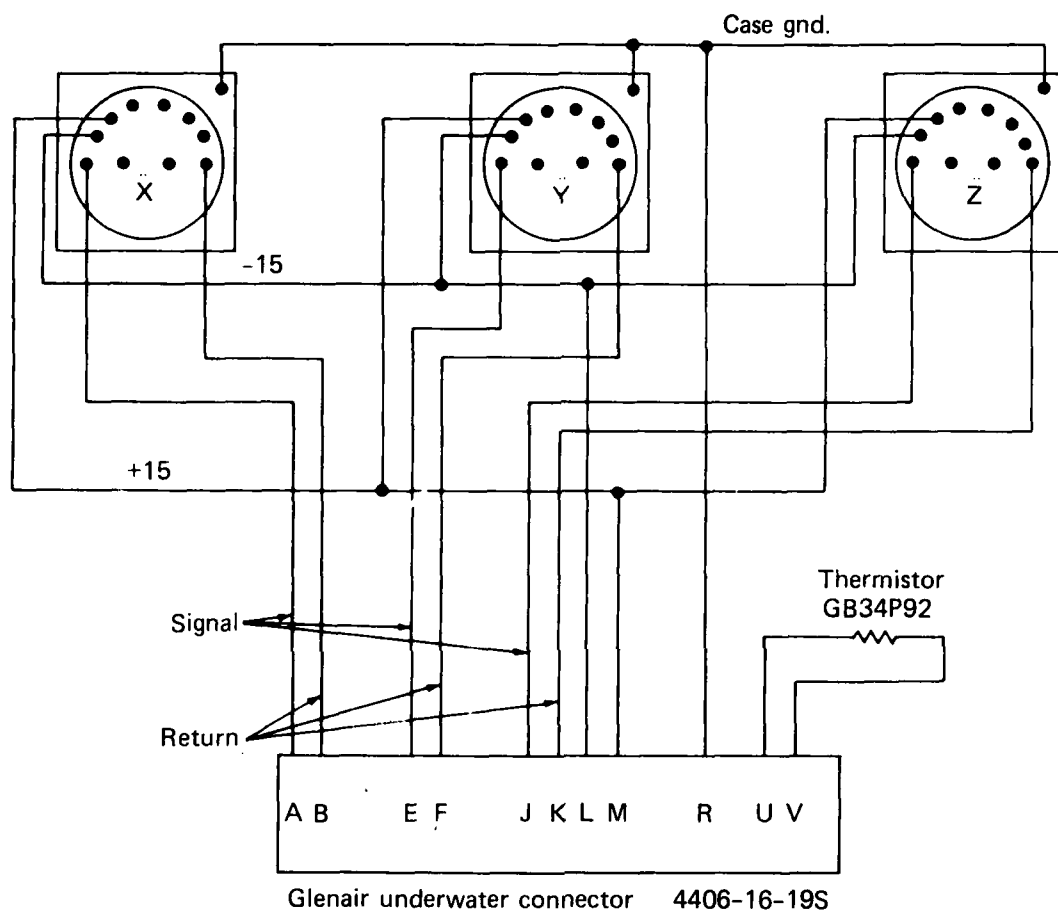


Fig. B4-2 Input vibration spectrum as per Mil Spec 167.

THE JOHNS HOPKINS UNIVERSITY
APPLIED PHYSICS LABORATORY
LAUREL MARYLAND

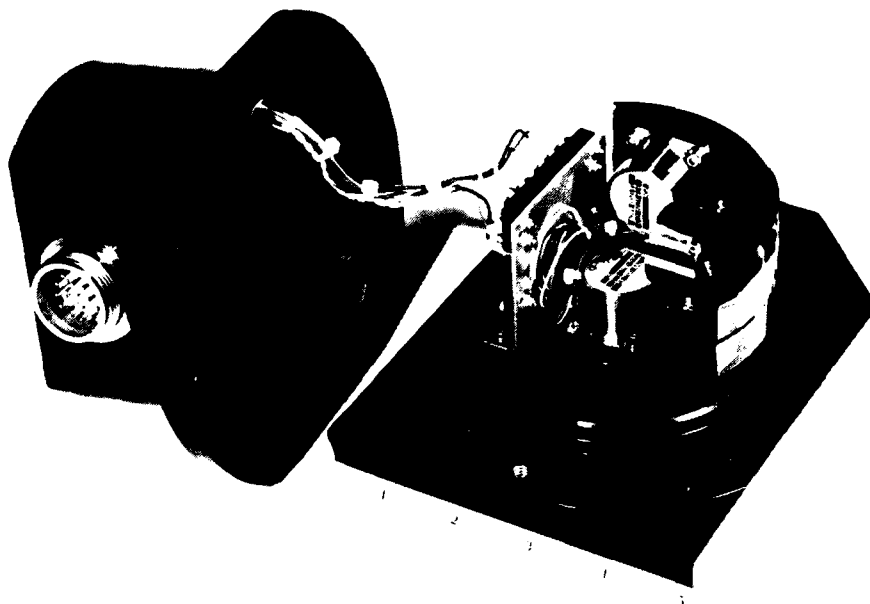
Appendix C
BOW ACCELEROMETER UNIT WIRING
DIAGRAM, PHOTOGRAPHS, AND
MECHANICAL DESIGN DRAWINGS



Note:

1. BAU chassis floating.
2. Accelerometer cases isolated from BAU chassis and connected to ± 15 V ret. in MCU.
3. Sundstrand Data Control Accelerometers. Model QA 1200 AA08

Fig. C1-1 BAU wiring diagram.



(a)



(b)

Fig. C1-2 BAU (a) with cover removed; (b) unit with cover.

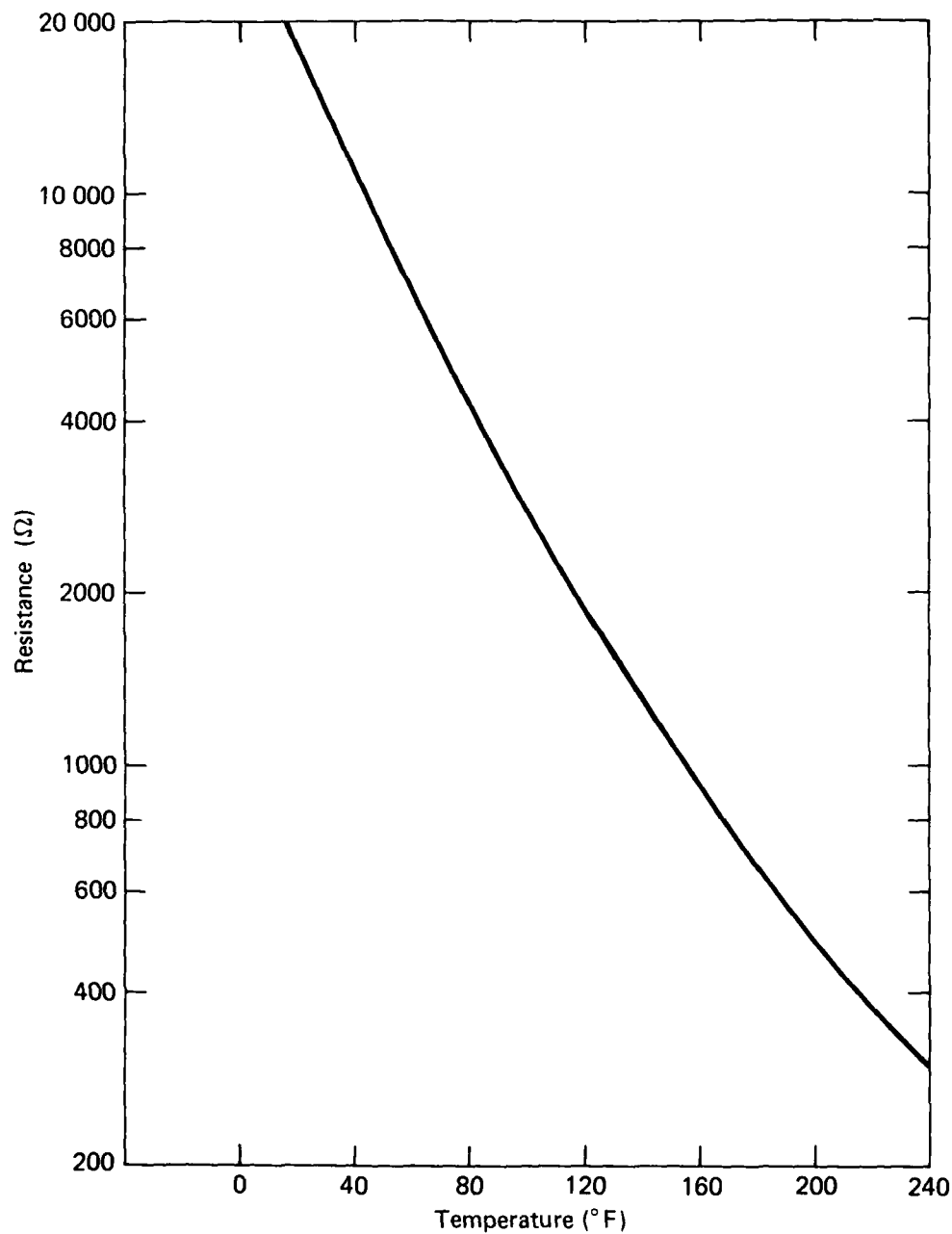
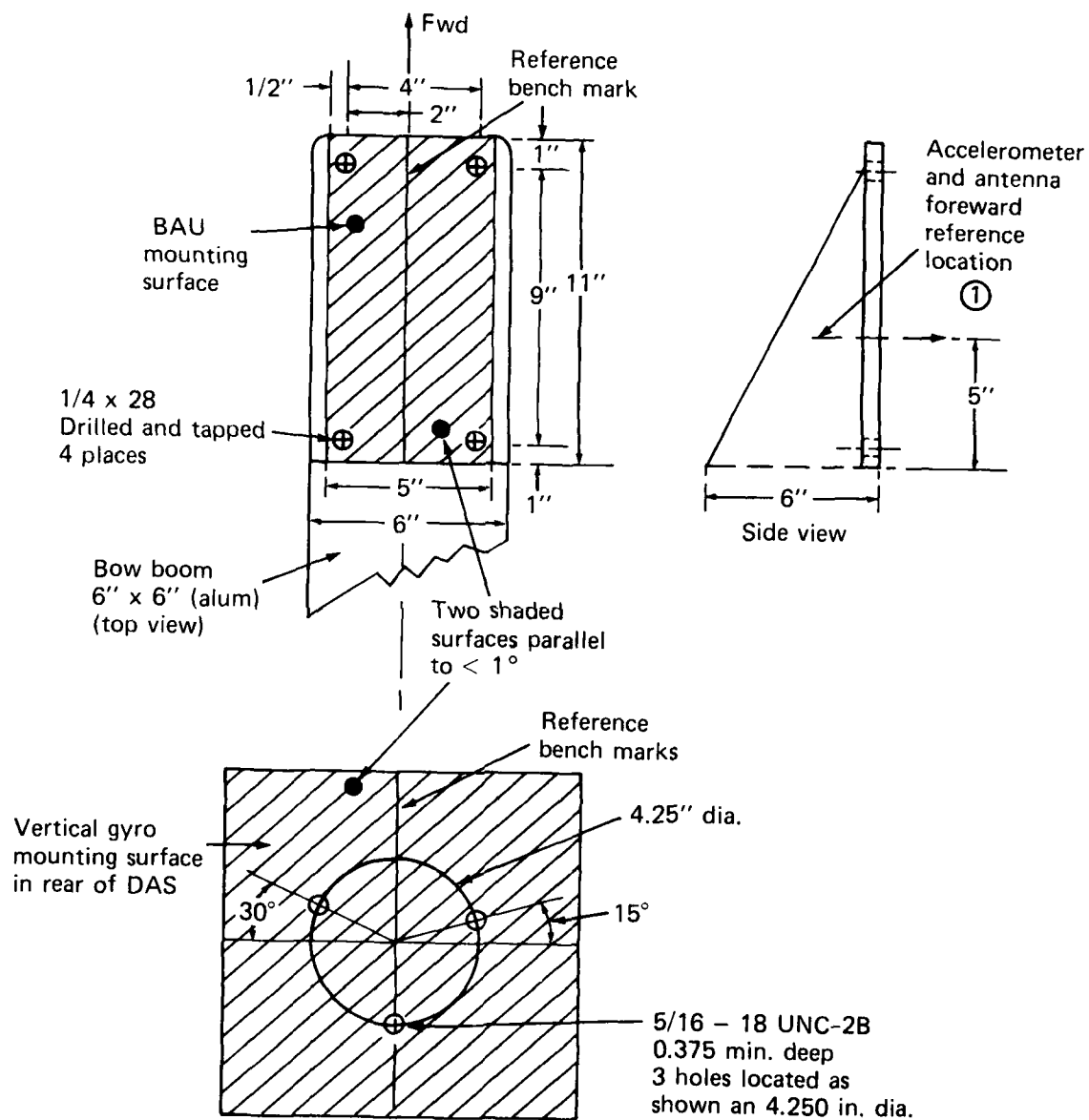


Fig. C1-3 Resistance-temperature curve for BAU temperature sensor.



① Note: Fore-aft center of the two altimeter antennas (T_x and rcvr) should be located at the reference distance.

Fig. C1-4 BAU installation details.

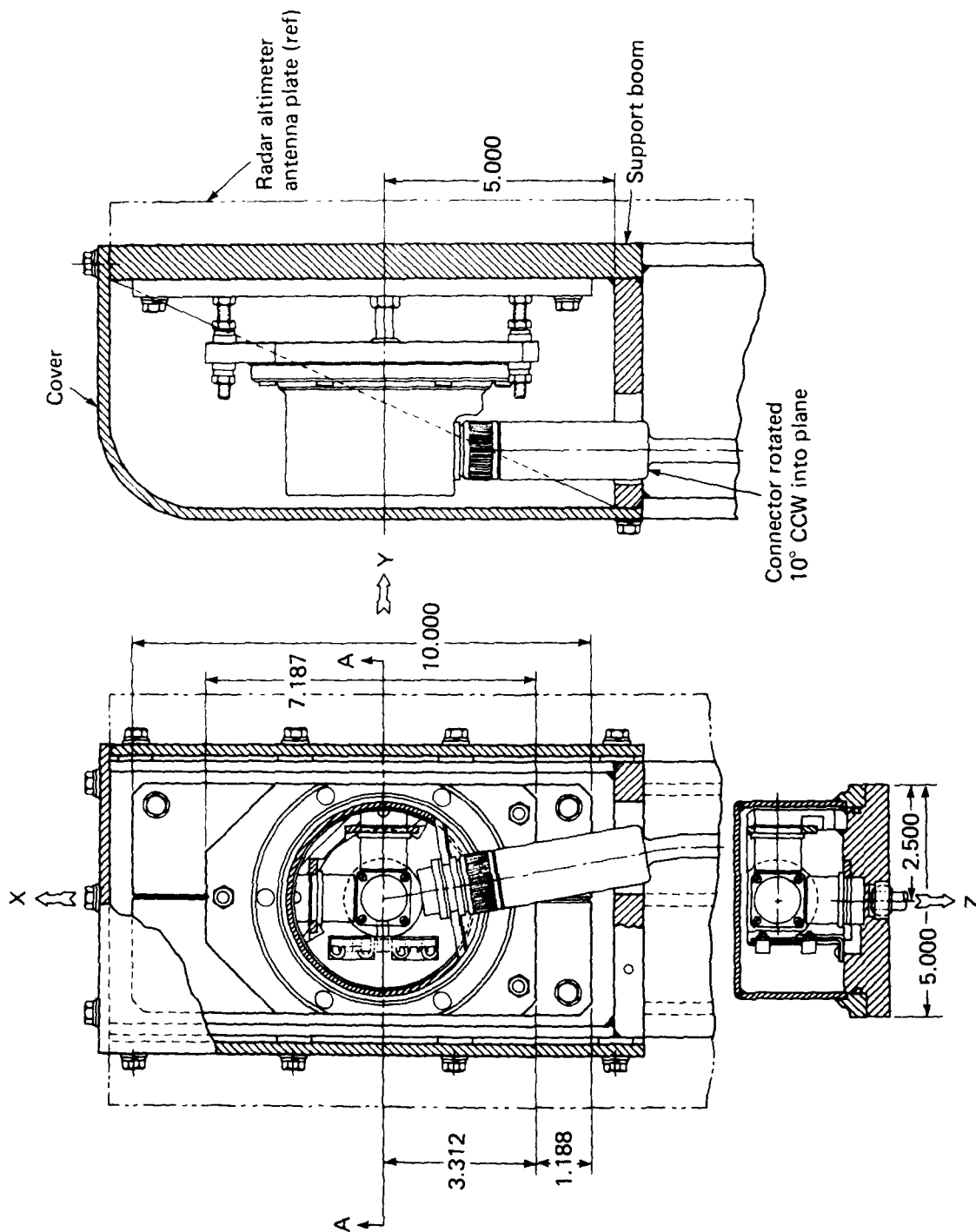


Fig. C1-5 Bow boom accelerometer unit.

THE JOHNS HOPKINS UNIVERSITY
APPLIED PHYSICS LABORATORY
LAUREL MARYLAND

EXCERPTS FROM SUNDSTRAND
DATA CONTROL ON THE
QA-1200-AA08



Section I

DESCRIPTION

1.1 INTRODUCTION

This manual contains information concerning the QA-1200 series Q-FLEX Accelerometers which are manufactured by Sundstrand Data Control Incorporated, Redmond, Washington 98052. These accelerometers are a unique design combining the state-of-the-art electronics, using hybrid circuits manufactured at Sundstrand with quality features of the quartz flexure: No pivot and jewels to wear out, no preload error (stiction), very little hysteresis, no metal flexure to bend and give bias shifts due to non-operational shock, a dither voltage is not required for measurements around 0-g acceleration. These accelerometers are environmentally sealed, lightweight, compact servo devices, designed to perform low-g, low frequency applications such as: platform leveling, platform inclination, drill steering, oil well down-hole measurements, horizontal mining operations, or on equipment such as: manned spacecraft, aircraft, missiles, and undersea vehicles.

The accelerometers will operate from 4 wires, however, each have additional features that might be utilized. Model QA-1000 accelerometers employ a 6 pin integral connector, while the QA-1100 accelerometers have a 6 pin header, the QA-1200 and QA-1300 have a 10 pin header. The electronics are power isolated from case ground.

The Q-FLEX series part number is a characteristic description of the capabilities (refer to the "How to Order" section of the Q-FLEX product brochure). Several models do not have an internal load resistor and are intended for current operation. An external load resistor R_L must be provided for these models. (Refer to the product brochure for model numbers.) The schematic references for the QA-1000 and QA-1100 show only the internal load resistor, the -02 or -12 models must have an external load resistor, as with QA-1200 and QA-1300.

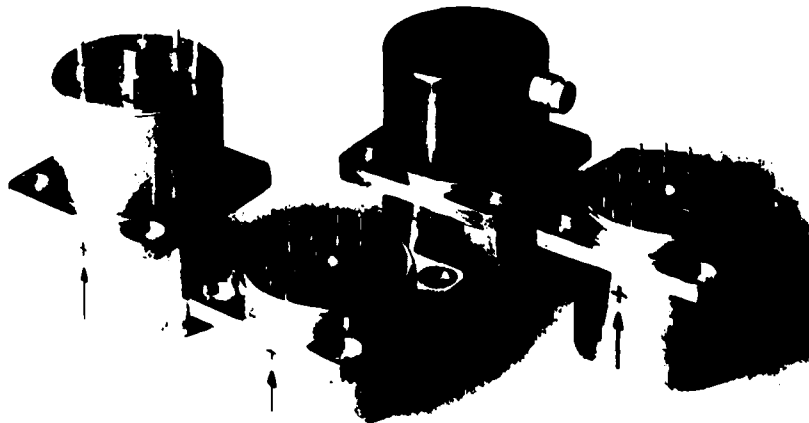


Figure 1-1. Model QA-1000, QA-1100, QA-1200 and QA-1300 Q-FLEX Accelerometers



1.2 SPECIFICATIONS AND CHARACTERISTICS

Specifications, physical characteristics and ordering information are contained in the data sheet located in the back of this manual. All dimensions in this manual are in the English standard system, inches, followed by International units (mm) in parenthesis.

1.3 DEFINITIONS

- A. PICKOFF. A device which produces a signal output, generally a voltage, as a function of the relative linear or angular displacement between two elements.
- B. PROOF MASS (SEISMIC MASS). The effective mass whose inertia transforms an acceleration along or about an input axis into a force or torque. The effective mass takes into consideration the contributing parts of the suspension.
- C. ZERO UNBALANCE. An accelerometer output, other than zero, when no acceleration is applied.
- D. SENSOR. A device that receives and responds to a signal or stimulus.
- E. MICRO-ELECTRONIC RESTORER. An electronic circuit made of minute electronic parts and used to restore the accelerometer proof mass to the quiescent position during acceleration measurement.
- F. INERTIAL REACTIVE FORCES. Movement of the proof mass in response to accelerated movement. (Actual displacement is minute due to the torque coil rebalance current).

1.4 GENERAL FUNCTIONAL DESCRIPTION

The basic electro-mechanical operation, depicted in Figure 1-2 is a linear single axis electro-mechanical device for measuring acceleration. The operation is based on movement of the proof mass during acceleration, the pick-off sensing the displacement of the mass, and the servo amplifier developing a rebalance current through the torque coil. The rebalance current then becomes a factor of acceleration proportional to acceleration. As more acceleration is applied to the accelerometer the assembly will maintain the proof mass position and the rebalance current will increase with increased acceleration until the acceleration limit is reached.

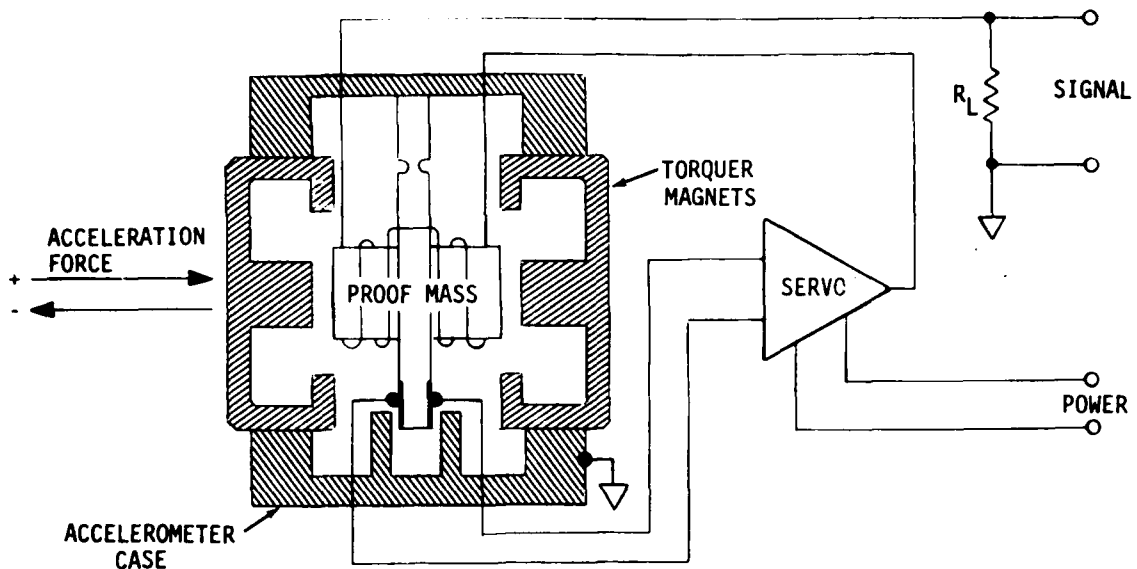


Figure 1-2 Eyestone-Wilson Sensor

The sensor consists of the following key elements:

- A. A proof mass, pendulously supported and ideally constrained so as to allow only one degree of freedom about a well-defined axis fixed within the sensor.
- B. A pickoff that can sense extremely small displacements of the proof mass.
- C. A torquer, which is a coil positioned within a permanent magnetic field and attached to the proof mass, allowing force to be applied to the proof mass in response to a current passed through the coil.
- D. A restorer circuit, or servo, that causes an electrical current to flow through the torquer coil in response to a pickoff signal. The resulting electromagnetic force balances the inertial reactive forces. In this manner the current passing through the torquer becomes an extremely accurate measure of the acceleration.

1.4.1 Sensor Construction. In the Q-FLEX design the proof mass is highly compliant in only one direction and at the same time it is free of the friction effects associated with jewel pivots and bearings. Yet it is without the hysteresis, instability, and fatigue associated with metal flexures. This is because the flexure and proof mass are formed from a single blank of specially-processed quartz, as shown in Figure 1-3. A slot is cut in the blank in such a manner as to form an annular



section and central disc connected by a narrow bridge. The central disc serves as part of the proof mass, the bridge as a flexure, and the annular section as the flexure support. The bridge section is chemically milled in order to form the flexure. A portion of the central disc is made conductive by vacuum vapor-depositing metallic films to provide electrical surfaces, as required for the capacitance pickoff. Conducting leads for the pickoff signals and the torquer coil drive current are formed across the flexure by similarly vacuum-vapor-depositing metallic films. Finally, attaching the torquer coils onto the central disc completes the proof mass, flexure, and flexure support sub-assembly. This sub-assembly is then clamped between the magnet structures. The magnet structures hold the magnets in proper position and keep the proof mass assembly from moving.

The balanced capacitance bridge pickoff is formed by the small gaps between the metallized portion of the quartz proof mass and the fixed reference plates in the magnet structure.

The small, precise gap between the magnet housings and the proof mass assembly also provides damping through gauss motion. A high level of damping is achieved without the use of liquids.

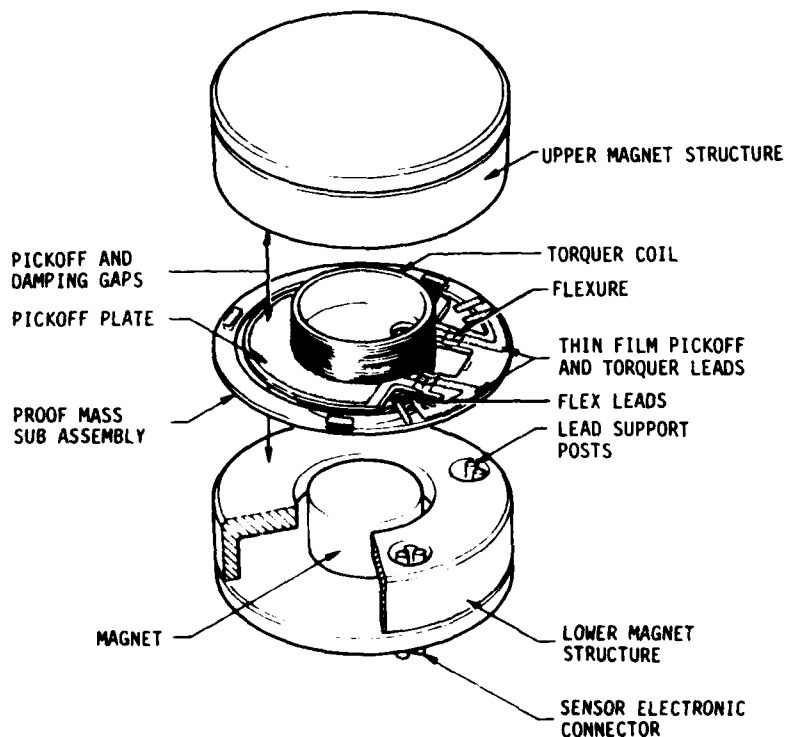


Figure 1-3. Q-FLEX Sensor Assembly, Exploded View.

Sundstrand Data Control, Inc.

REDMOND, WASHINGTON 98052
unit of Sundstrand Corporation



1.4.2 Restorer Electronics. Figure 1-4 is a block diagram of the accelerometer servo system.

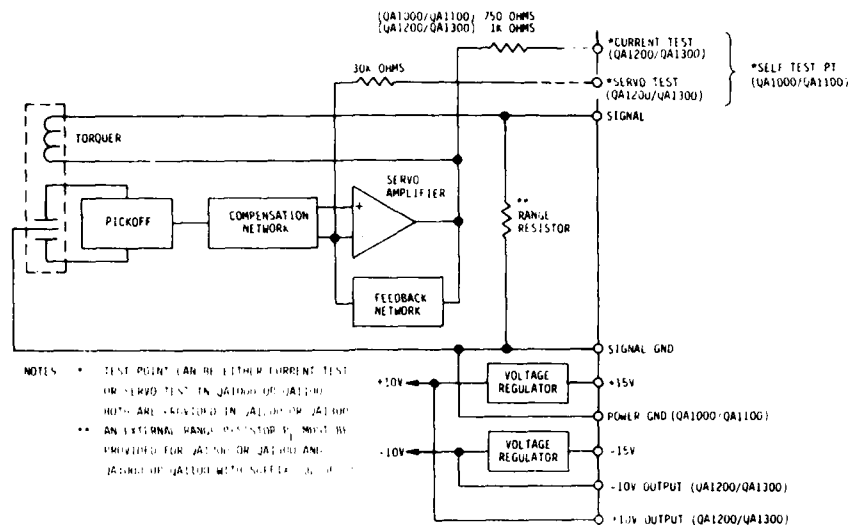


Figure 1-4. Q-FLEX Accelerometer, Block Diagram.

- The Pickoff develops a voltage proportional to the proof mass displacement.
- The Compensation network circuit shapes the servo frequency response for optimum stiffness and stability.
- The Servo Amplifier drives the restoring current through the torquer. This current is sensed across range resistor R_L and in turn this voltage is the accelerometer output.
- The Feedback Network sets the gain of the servo amplifier and provides negative feedback to the compensation network.
- R_L may be either internal or external and depending upon model number is typically 250 to 3.8K ohms, internal value. The external R_L used with QA-1200 or QA-1300 can be 0 to 20 megohms. R_L used with QA-1000 or QA-1100 external R_L models, can be 150 to 15K ohms. The output sensitivity is proportional to the R_L value, selection is discussed in paragraph 3.5.
- ± 10 VDC Regulated Output power is available as an output from the QA-1200 or QA-1300 for supplying power to an operational amplifier or biasing circuit (5mA maximum) (See paragraph 3.6).



1.5 AVAILABLE FEATURES

1.5.3 QA-1200 and QA-1300

- 10 Pin Header
- Environmental Seal (not welded)
- Servo Self-Test
- and - Current Torque Self-Test
- ± 10 VDC Output
- ± 13 VDC to ± 28 VDC Operation
- No Internal Load Resistor
- Output Short Circuit Protected (will operate even on a short circuit)



Section II

INSTALLATION

2.1 MOUNTING, PROVISIONS AND PRECAUTIONS

- 2.1.1 Standard Mounting. The accelerometer should be mounted directly to the mounting surface, flatness 0.0001 in/in (0.001 mm/cm), using the central flange, with 4-40 socket head screws. Torque the screws to 3.0 in/lb (3500 gm/cm) per screw in 1.0 in/lb (1200 gm/cm) increments using sequence as indicated by Δ in figure 2-1. The sensitive axis will be normal to the mounting surface within six minutes of arc.

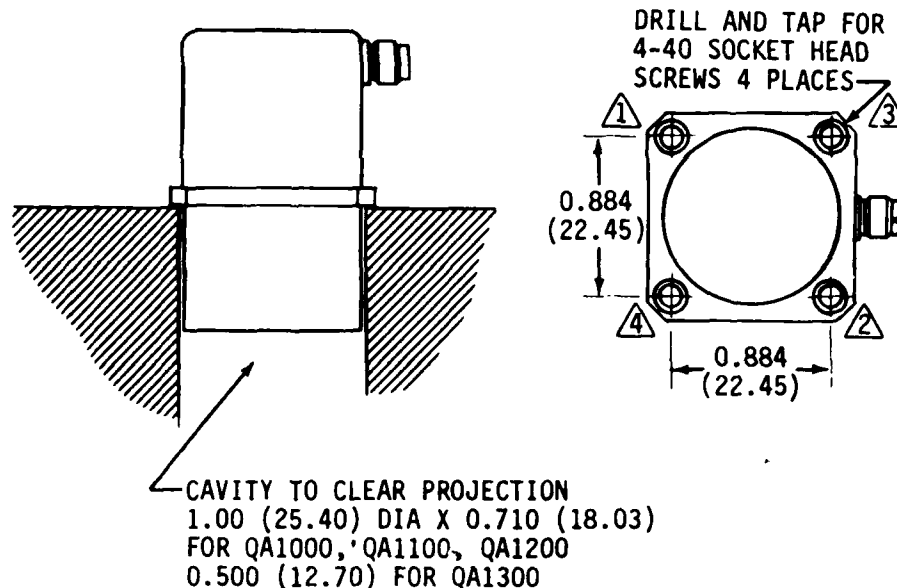


Figure 2-1. Model QA-1000 Accelerometer, Mounting Diagram.
(Also applies to QA-1100, QA-1200 and QA-1300)

CAUTION: USE CARE NOT TO IMPACT INSTALLATION TOOLS ON THE ACCELEROMETER. SHOCKS OF SEVERAL THOUSAND g 'S CAN BE IMPARTED TO THE ACCELEROMETER FROM THE IMPACT OF A METAL WRENCH ON THE CASE.



- 2.1.2 Mounting Adaptors. Mounting adapters, shown in the product brochure at the back of this manual, allow alternate mounting configurations. These mounting adapters can be used to mount the Q-FLEX accelerometers. The triax accelerometer mounting bracket is made such that three (3) accelerometers can be mounted with the sensitive axes 90° apart horizontal and vertical.
- 2.1.3 Mounting Precautions. Clamping the accelerometer to a surface which is not flat within 0.0001 in/in (0.001 mm/cm) will cause misalignment of the accelerometer and can permanently deform the flange.

Mount the accelerometer by screwing or clamping the flange of the accelerometer.

DO NOT CLAMP AROUND THE CYLINDRICAL CASE.

Electrical cables to the accelerometer should be carefully supported to prevent any strain on connections.

2.2 ELECTRICAL

- 2.2.1 Generally the QA-1000, QA-1100, QA-1200 and QA-1300 accelerometers are designed to operate within $\pm 13V$ to ± 28 VDC power source. When operating the accelerometer at ± 21 VDC derate the operating temperature range to $100^\circ C$. When operating the accelerometer at $\pm 28VDC$ derate the operating temperature to $75^\circ C$. The quiescent current required is approximately 12 ma. An additional $1.33 \pm 10\%$ ma per g of acceleration input ($3.33 \pm 10\%$ for the QA-1300) is required. The wiring configuration is shown in Figure 2-2. Note the difference in pin usage by model number. The output signal is developed across load resistor R_L . Signal return and power return are connected internally. Ground loop interference can result when a single wire is used for power return and signal return in a long wire system. This is most prominent when using the internal load resistor models QA-1000 or QA-1100. A solution is to provide separate wires for power and signal return. When using the external load resistor models the single wire power and signal return does not cause as much interference when the load resistor is at the end of the wire away from the accelerometer since the torquer current also flows through R_L . If an external load resistor is connected at the accelerometer, the same two wire precautions should be used as with the internal load resistor models.

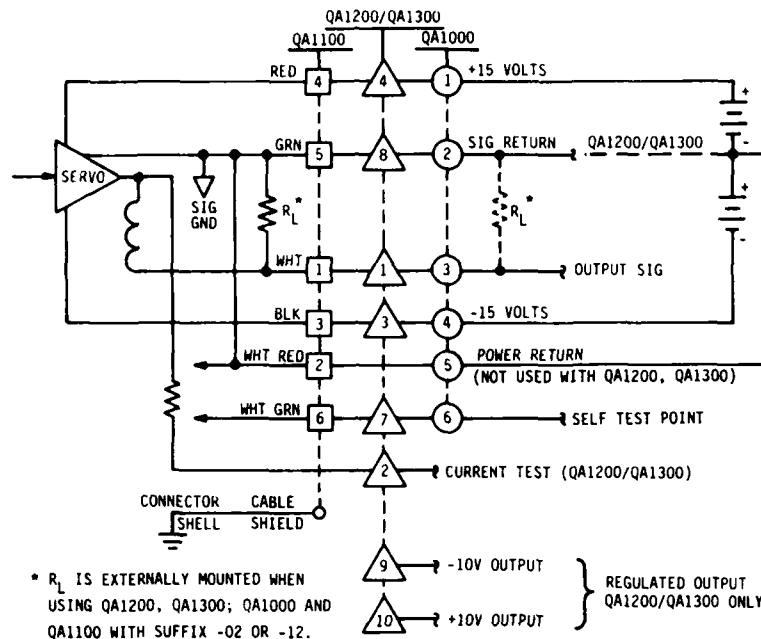


Figure 2-2. Electrical Connections, Models QA-1000, QA-1100, QA-1200 and QA-1300.

2.3 CONNECTORS AND CABLES

- 2.3.1 Connectors. Model QA-1000 is equipped with an integral miniature 6 pin connector; it is supplied with the Model CA116-15-30; a 6 conductor, 30 inch, shielded cable with a mating connector. Longer cables are available to order. See Figure 2-2 for color code.
- 2.3.2 Cables. Multiconductor cable can be used to connect Model QA-1100, QA-1200, or QA-1300. Refer to the "Cables and Adapters Product Brochure" at the back of this manual.

SECTION IV

CALIBRATION AND SERVICE

4.1 CALIBRATION

4.1.1 Factory Calibration

Every unit is tested, at various stages of assembly and as part of Sundstrand's QA procedure. The specific calibration sheet is included with each accelerometer. Replacement calibration sheets can be obtained from the permanent factory files.

Factory recalibration, performed against standards traceable to the National Bureau of Standards, is available at nominal charge. This recalibration service is the ideal solution to the user's need for routine periodic certified calibration.

4.1.2 User Testing and Calibration

The user may perform simple tests to assure that an accelerometer has not sustained damage in shipment or in subsequent use. Such tests also serve to isolate and identify faults, expediting factory repairs. The user may perform relative calibration by using the Earth's nominal one-g field.

4.1.2.1 Electrical faults most frequently are revealed by:

- a. Drastic change in current supplied to accelerometer;
- b. Full scale output;
- c. Increased noise at oscillator frequencies ($\approx 500K$ Hz);
- d. Change in voltage sensitivity of output (without current sensitivity change);
- e. Drastic change in frequency response.

Accordingly, current supplied to the accelerometer should be monitored during any tests and conditions causing any change should be evaluated.

4.1.2.2 Mechanical faults are usually indicated by:

- a. Change in zero-g output of the unit;
- b. Loss of output;
- c. Constant output despite change in acceleration input;
- d. Nonrepeatable zero-g output;
- e. Limiting of range (always accompanies change in zero-g output);
- f. Change in current sensitivity (always appears as a change in voltage sensitivity);
- g. Drastic change in frequency response.



4.1.2.3 The calibration/tests recommended are:

- a. Static calibration (para. 4.1.3);
- b. Scale Factor measurement (para. 4.1.6);
- c. Bias Calculation (para. 4.1.7);
- d. Repeatability tests (para. 4.1.8);
- e. Elevated temperature test (para. 4.1.9);
- f. Lowered-temperature test (para. 4.1.10);
- g. Transverse-sensitivity tests (para. 4.1.11);
- h. Frequency-response test (para. 4.1.12);
- i. Noise test (para. 4.1.13)

4.1.3 Static Calibration

Static calibration is accomplished by using the Earth's gravity vector as the input and aligning the accelerometer's sensitive axis with this field.

NOTE: This relative calibration is accurate for subsequent work at the site where the calibration is performed, but high-trajectory or long-distance work will require correction factors: consult Sundstrand Engineering in each such specific case.

This procedure requires a precision voltmeter with accuracy of 0.01 percent, a mounting surface that can be leveled to 1/4 degree, and an accurate mounting bracket that can be inverted. Refer to Figure 4-1 and proceed as follows:

- a. Set up the accelerometer as shown in Figure 4-1 and connect as described by Figure 2-2. Connect the output signal to the voltmeter.
- b. Mount the accelerometer with the sensitive axis vertical in the +lg position. Test mounting orientation by rocking the mounting back and forth approximately 1/2 degree: the output signal is maximum when the instrument is properly aligned. Record the +lg output signal after the instrument has had sufficient warm-up time.
- c. Invert the accelerometer by 180 degrees \pm 1/4 degree. The output will now be of opposite polarity. Test the 180 degree inversion by rocking the instrument as in step b above. Again, proper alignment is achieved when the magnitude of the output signal is maximum. Record the -lg output signal.
- d. Compute sensitivity by numerically subtracting the +g and -g voltages and dividing by two.
- e. Compute zero output by numerically adding the -g reading from the +g reading and then dividing by two.

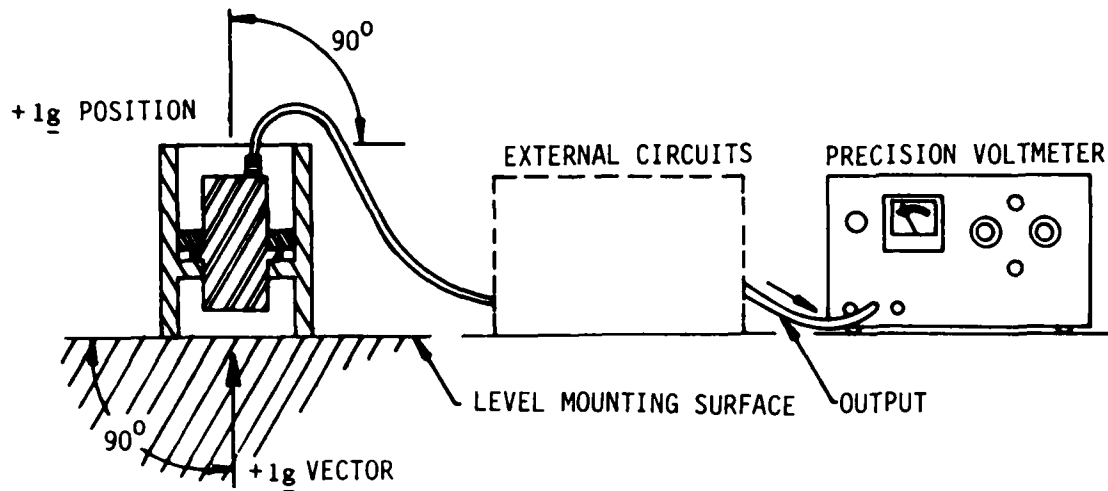
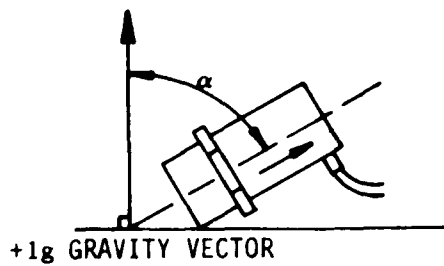


Figure 4-1. Setup for Static Calibration

4.1.4 Static Angular Calibration. Earth's gravity field also supplies the force for accurately-controllable inputs between $+1g$ and $-1g$ (see Figure 4-2). The static force is equal to the cosine of the angle alpha shown in Figure 4-2, and this principle can be applied to tilted surfaces, tilted accelerometers, and vector motions.

4.1.5 Higher-Level Calibrations. Calibration procedures at higher static levels require the use of centrifuges. Dynamic calibration usually is accomplished using vibration exciters or shake tables.



Angle Alpha	Applied g's
0°	1.0g
30°	0.866g
36° 52' 12"	0.800g
45°	0.707g
53° 07' 48"	0.600g
60°	0.5g
66° 25' 19"	0.400g
75°	0.259g
78° 27' 47"	0.200g
90°	0g
180°	(-) 1g
(COS-1g)	(COS Alpha)

Figure 4-1. Angle Calibration Factors



4.1.6 Scale Factor Measurement. Obtain scale factor as follows:

- a. Set up the accelerometer as shown in Figure 4-1 and connect per Figure 2-1. Connect the output signal to the voltmeter.
- b. Follow procedure of paragraph 4.1.3b and c.
- c. Algebraically subtract (numerically add) the $-g$ reading from the $+g$ reading, then divide by 2. The result is the scale factor expressed in Volts per g .

NOTE: The actual accelerometer current sensitivity is not normally provided for the voltage output models of the QA-1000 and QA-1100 (internal load resistor). For current torque self-test models the current sensitivity can be determined by supplying current torque to the accelerometer and reversing the polarity of the input to simulate a positive and negative input (refer to Paragraph 3.3). The accelerometer must not be moved or rotated and care must be taken to remain within the linear output range of the accelerometer.

$$CSF = \frac{I_{test}}{(+V_{out}) - (-V_{out})} \quad X \quad \text{Scale Factor}$$

CSF is Current Scale Factor

Scale Factor is found on the Accelerometer Data Sheet.



NOTE: For voltage self-test accelerometers the current scale factor and internal load resistor may be determined by shunting the internal load resistor with an external resistor (R_S) of known value and measuring the output in $+1g$ and $-1g$.

$$SF_2 = \frac{(+V_{out}) - (-V_{out})}{2} \quad \text{with shunt resistor}$$

$$R_L = \left(\frac{SF_1}{SF_2} - 1 \right)$$

SF_1 is from the accelerometer data sheet.

$$CFS = \frac{SF_1}{R_L}$$

4.1.7 Bias Calculation. Algebraically subtract the scale factor (para 4.1.6c) from $+1g$ reading (para 4.1.3b); the result is the bias voltage. Divide this bias voltage by the scale factor to obtain bias in g 's.

4.1.8 Repeatability Tests. Place the accelerometer in a $+1g$ field (para 4.1.3) and record the output voltage. Remove power for 2 seconds, then turn power on and record output voltage reading at turn-on; the difference in readings (if any) is the nonrepeatability of the instrument.

4.1.9 Elevated-Temperature Test

- a. Install the fixturing of 4.1.3 in a chamber. Measure the (ambient) temperature at the mounting surface of the instrument. Perform the static $\pm 1g$ measurements and calculate scale factor and bias (paragraph 4.1.6 and 4.1.7).
- b. Increase the temperature of the chamber as desired ($<200^\circ F$). The instrument's temperature has stabilized, again, determine the scale factor and bias.
- c. The shift in data can now be calculated as well as the temperature coefficient of shift.

4.1.10 Lowered-Temperature Test

Repeat paragraph 4.1.10 procedure using a lower temperature (not lower than $-65^\circ F$).

Sundstrand Data Control, Inc.

REDMOND, WASHINGTON 98052
unit of Sundstrand Corporation



4.1.11 Transverse Sensitivity Test

- a. The static and low frequency transverse sensitivity of the Q-FLEX is due mainly to manufacturing tolerances in the orientation of the accelerometer mechanism relative to the mounting surface of the accelerometer case. In a nominally transverse field g , the mechanism responds to g (Figure 4-2); (small and in radians). The total output is the Bias + g + Transverse Sensitivity times g .
- b. First the instrument is mounted in a "perfect" cylinder with the instrument mounting surface perpendicular to the axis of the cylinder. The cylinder is laid in a precision V block on a stable surface such that the instrument sees a $1g$ transverse field.
- c. Now the cylinder is rotated about its axis. A position will be found where the instrument output will be a maximum. 180° around the output will be a minimum.
- d. The instrument bias and g are constant in this test. The transverse sensitivity is;

$$\frac{V_{\max} - V_{\min}}{2g \times \text{Voltage Scale Factor}} \leq 0.002 \text{ } g/g$$

4.1.12 Frequency Response Test

- a. Mount the Q-FLEX and a vibration standard close together on a stiff fixture. Mount the fixture to a shaker. Drive the shaker with a sine wave.
- b. Shake at a g level below half the rating of the instrument to avoid clipping at the natural frequency.
- c. Compute the response by dividing the Q-FLEX output by the reference standard output at the frequencies of interest.

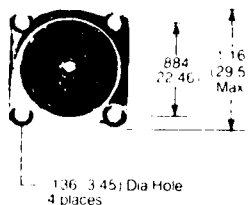
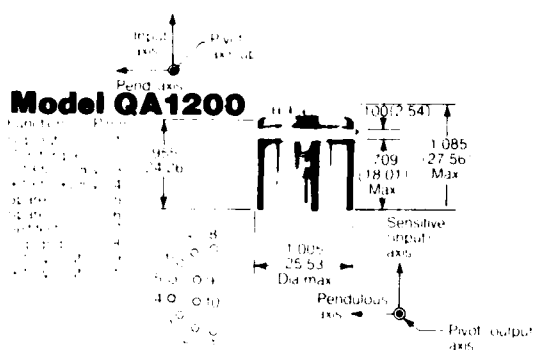
4.1.13 Noise Test. Use an RMS voltmeter or oscilloscope to look at the noise output of the accelerometer. For measurements in the audio range, a very quiet environment is required.

4.2 SERVICE

The accelerometers are completely encapsulated units. Except for cable connections, field service is precluded.

If an accelerometer appears to have sustained internal damage, it should be returned intact to the factory for repair, recalibration, or replacement. Include a report referring to the instrument by serial number and describing the installation and the trouble.

Refer to the Warranty located in the back of this manual.



Weight less than 65 g
Features low profile design with state-of-the-art servo electronics. Unit can be externally scaled and compensated without affecting the dynamics of the internal servo loop.

Accessories

Supplied

Instruction manual
calibration card
carrying case
mounting screws
wrench
Cable No. CA116-15-30, Supplied with QA1000

Optional

Model MB-116-15A mounting bracket (base)
Model MB-116-15B mounting bracket (side)
Model MB-116-15C mounting bracket (stud)
Model MB-116-15D mounting bracket (screw)
Model MB-116-15T mounting bracket (triaxial)
Model 517 servo amplifier

How to order

When you order a Sundstrand Q-flex accelerometer, your ordering code is also your part number.

QA 1 2 00-AA05-14

Standard prefix for
Quartz Accelerometer.

Fixed for 1000 series.

Style and basic geometry.

See dimension in "Features" section.

Scale factor & self test features.
See Table 3 below.

Special performance requirements.
See Table 2 below.

Special accessories or
characteristics. See Table 1.

Table 1

Special Accessories or Characteristics*

Digits	Description	Comments
00	As Shown	
01	Welded Environmental Seal	QA 1100 only
02	Power Splitter +28 VDC or \pm V Operation	QA 1000 only

* Other options available on request

Table 2

Performance Requirements

4 Digit Number	Bias Temperature Coefficient (μ g/ $^{\circ}$ C)						
• •	135	90	45	30	20	10	
KA00	**						
AA01 KA01	**						
AA03 KA03		**					
AA05 KA05			**				
AA06				*			
AA08					*		

* Environmental shock 250 g 11 millsec Half sine all axes

* Heavy duty 1000 g 0.5 millsec Half sine all axes

Note: Other improved performance characteristics available

- Initial bias
- Bias stability (aging)
- Bias repeatability (environmental)
- Axis misalignment
- Vibration rectification coefficient
- Scale factor linearity
- Scale factor temperature coefficient
- Scale factor repeatability (environmental)
- Scale factor calibration

Table 3

Scale Factor and Self Test Features

Unit number (with servo self test)	Units	01	02	03	04	05	06	07	08
Unit number (with current torque self test)		11	12	13	14	15	16	17	18
Scale Factor	V/g	33	*	25	50	100	250	500	350
Output Impedance	K ohms	25	*	19	38	76	190	380	270
Range (full scale)*									
with \pm 15 VDC	\pm g	20	*	25	15	10	5	2.5	3.5
with \pm 28 VDC†		38	*	44	30	19	9	5	7
Output Voltage (max)*									
with \pm 15 VDC	Volts	6.6	*	6.3	7.5	10	12.5	12.5	12.5
with \pm 28 VDC†		12.5	*	11	15	19	22.5	25.0	25.0

QA 1200 and QA 1300 models supplied only in -02 and -12 versions

* Unit may be operated from \pm 13 VDC to \pm 28 VDC. Range and output voltage will vary accordingly

† At voltages higher than \pm 21 VDC maximum operating temperature should be reduced to 100°C

* Unit supplied with current output (no internal load) and calibrated at 25 V/g for \pm 5% frequency response to 300 Hz

QA 1000 1100 and QA 1200 current scale factor 1.33 m/g \pm 10%

QA 1300 Current scale factor 3.0 m/g \pm 10%

Range and output voltage reduced by approximately 25% for QA 1300 series

Sundstrand Data Control, Inc.

Unit of Sundstrand Corporation



Overlake Industrial Park, Redmond, WA 98052 206/885-3711 TWX 910/449-2860 Telex 32-0313

Specifications

Performance

Range	See Table III
Scale Factor/Sensitivity	See Table III
Output Resistance	See Table III
Frequency Response ($\pm 5\%$)	300 Hz
Natural Frequency	Greater than 800 Hz
Damping Ratio	0.3 to 0.7
Noise	
0-10 Hz	< 10 picoamps RMS
0-50 Hz	< 100 picoamps RMS
500-10 K Hz	< 1 microamp RMS
Excitation/Power supply voltage	See Table III
Excitation/Power Supply quiescent current	15 ma per supply
Scale Factor/Sensitivity shift with supply voltage	.002%/V
Bias/Zero shift with supply voltage	10 micro-g/V
Resolution (DC)	0.000001 g
Threshold (DC)	0.000001 g
Linearity (DC)	
QA 1000, 1100, 1200	20 μ g/g ²
QA 1300	30 μ g/g ²
Hysteresis	0.001% of full scale
Repeatability	0.003% of full scale
Bias/Zero unbalance	± 3 milli-g typical ± 10 milli-g max
Bias Temperature coefficient/Thermal zero shift	See Table II
Scale Factor Temperature coefficient/Thermal sensitivity shift	180 ppm/ $^{\circ}$ C (maximum)
Axis Alignment/Transverse sensitivity	0.002 g/g
Vibration rectification coefficient (discrete point)	75 μ g/g ² RMS uncompensated. Can be trimmed on QA1200 and QA1300.
Constant G random spectrum 50 to 2 K Hz	40 μ g/g ² RMS

Electrical

Connection	See Outlines
Grounding	Electronics are isolated from case 50 Megohms of 50 VDC. Shield is common to case.

Physical

Sensing Element	Q-Flex
Weight	See "Features"
Mounting Configuration	Flange per "Features"
Case Material	Stainless Steel

Environmental

Temperature:	
Operating Range	-55 $^{\circ}$ C to 115 $^{\circ}$ C
Specified Performance Range	-18 $^{\circ}$ C to 100 $^{\circ}$ C
Storage Range	-65 $^{\circ}$ C to 125 $^{\circ}$ C
Static Overload	100 g
Shock	See Table II
Vibration	50 g pk. sine all axes
Humidity	Epoxy sealed (weld seal on QA 1100 if required)

THE JOHNS HOPKINS UNIVERSITY
APPLIED PHYSICS LABORATORY
LAUREL MARYLAND

Appendix D
COCKPIT DISPLAY UNIT



..... leadership in
data conversion
technology

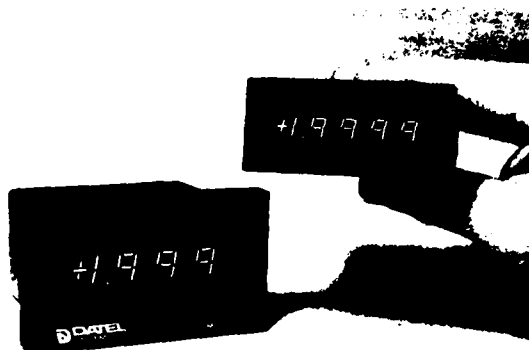
NEW PRODUCT TECHNICAL DATA

LOW-COST, DISPLAY-ONLY
DIGITAL PANEL METERS
MODEL DM-3100 & DM-4100 SERIES

PRELIMINARY INFORMATION 9/1/77

FEATURES

- . Balanced Differential Inputs on $3\frac{1}{2}$ digit models
- . Choice of $3\frac{1}{2}$ or $4\frac{1}{2}$ Digits
- . Choice of LED or LCD Digits
- . LCD Model for Portable Instruments:
+9V Power @ 3 mA
- . Low Profile, Minimum Area Case
Fits Other Manufacturers' Cutouts
- . Short-Depth Case Interchangeable
with Other Datedel DPM's
- . Ultra-Low Prices
 $3\frac{1}{2}$ Digit LED: \$29 (100's), \$35 (1-9)
 $4\frac{1}{2}$ Digit LED: \$59 (100's), \$69 (1-9)



DESCRIPTION

Model DM-3100 and DM-4100 series digital panel meters (DPM's) offer high performance at the very lowest cost for display-only applications. $3\frac{1}{2}$ digit models feature balanced differential inputs. Both models include automatic zero correction. These features are normally found only on much more expensive instruments. The DM-3100 and DM-4100 use an LSI MOS integrated circuit to perform A/D conversion for very high reliability and low parts count.

Digital Panel Meters find wide application as replacements for 1% and finer mechanical meter movements used in analytical instruments, process controllers, vehicle panels, portable instruments and automatic test equipment. External circuits supplied by the user allow DPM's to measure AC voltages, current, resistance, frequency, period, RPM, temperatures, pressure, flow rate and practically all other physical variables. These DPM's accept a dc or slowly-varying input voltage between -2

Volts and +2 Volts. This input is converted and displayed on solid-state decimal digits. A polarity sign is automatically displayed for bipolar inputs. The input impedance is very high - 100 megohms minimum. This reduces errors which would normally be caused by excessive loading of an input source with series resistance (such as measurement bridges). The balanced differential inputs reduce common mode errors, typically from AC power lines with long input leads. The differential configuration adapts readily to most bridge-type transducers and sensors.

Four models in this series use red self-illuminated, solid-state light-emitting diode (LED) displays. Model DM-3100X uses a field effect liquid crystal display (LCD) requiring room light to view readings.



1020 TURNPIKE STREET, CANTON, MASS. 02021
TELEX: 924461 PRINTED IN U.S.A.

TEL. (617) 828-8000 TWX: 710-348-0135
DATEDEL SYSTEMS

The LCD DPM forms black digits against a light background and features ultra-low power consumption of 15 mW typical. The DM-3100X may be operated for many hours on a single small 9 V battery. The LCD model is available only in 3½ digit resolution and packaged in the short-depth case.

The LSI MOS control chip inside the DPM's offers low-drift readings over the 0 to +50°C operating temperature range. The chip also includes auto-zeroing to practically eliminate temperature drift of the zero setting.

Two case styles are offered for the DM-3100's and DM-4100's. Datel's standard poly carbonate plastic case offers the shortest panel depth (2.2 inches) and mechanical mounting which is identical to other Datel DPM's. A low-profile case is also offered which measures only 1.31 inches high and uses less than 4 square inches of panel space. This low-profile case will fit in many other manufacturer's panel cutouts.

LED models require regulated +5 Vdc power supplies and LCD models may be powered from +4 V or +14 Vdc. All models include selectable decimal points for convenient scale factoring.

INPUT/OUTPUT CONNECTIONS DM-3100L

BOTTOM TOP

	A	B	
ANALOG RETURN	1	1	NO CONNECTION
ANALOG LO INPUT	2	2	NO CONNECTION
NO CONNECTION	3	3	NO CONNECTION
ANALOG HI INPUT	4	4	NO CONNECTION
NO CONNECTION	5	5	NO CONNECTION
REFERENCE OUT	6	6	REFERENCE IN
NO CONNECTION	7	7	NO CONNECTION
NO CONNECTION	8	8	NO CONNECTION
NO CONNECTION	9	9	NO CONNECTION
DEC PT 1999	10	10	NO CONNECTION
DEC PT 19.99	11	11	NO CONNECTION
DEC PT 199.9	12	12	NO CONNECTION
DEC PT 1999	13	13	NO CONNECTION
NO CONNECTION	14	14	DISPLAY TEST
NO CONNECTION	15	15	DEC PT COMMON
POWER COMMON	16	16	POLARITY ENABLE
+5V POWER OUT	17	17	NO CONNECTION
+5VDC PWR IN	18	18	DISPLAY ENABLE

INPUT/OUTPUT CONNECTIONS DM-3100X

BOTTOM TOP

	A	B	
ANALOG RETURN	1	1	NO CONNECTION
ANALOG LO INPUT	2	2	NO CONNECTION
NO CONNECTION	3	3	NO CONNECTION
ANALOG HI INPUT	4	4	NO CONNECTION
NO CONNECTION	5	5	NO CONNECTION
REFERENCE OUT	6	6	REFERENCE IN
NO CONNECTION	7	7	NO CONNECTION
NO CONNECTION	8	8	NO CONNECTION
NO CONNECTION	9	9	HORIZ POL OUT
DEC PT 199.9	10	10	NO CONNECTION
DEC PT 19.99	11	11	NO CONNECTION
DEC PT 1999	12	12	NO CONNECTION
NO CONNECTION	13	13	DEC PT COM
NO CONNECTION	14	14	DISPLAY TEST
NO CONNECTION	15	15	HORIZ POL IN
SV PWR COM	16	16	SV PWR COM
A/D PWR IN	17	17	VERT POL IN
SVDC/DC PWR IN	18	18	VERT POL OUT

DM-4100L

INPUT/OUTPUT

CONNECTIONS

BOTTOM TOP

	A	B	
REFERENCE IN	1	1	REFERENCE OUT
ANALOG LO INPUT	2	2	NO CONNECTION
ANALOG LO INPUT	3	3	ANALOG HI INPUT
DEC. PT. COMMON	4	4	NO CONNECTION
DEC. PT. 1.9999	5	5	
DEC. PT. 19.999	6	6	
DEC. PT. 199.99	7	7	
DEC. PT. 1999.9	8	8	
DEC. PT. 19999.	9	9	NO CONNECTION
NO CONNECTION	10	10	BUSY/DONE OUT
	11	11	RUN/HOLD IN
	12	12	UNDER SCALE OUT
	13	13	OVER SCALE OUT
	14	14	NO CONNECTION
NO CONNECTION	15	15	DISPLAY TEST
POWER COMMON	16	16	NO CONNECTION
POWER COMMON	17	17	+5VDC PWR. IN
POLARITY ENABLE	18	18	DISPLAY ENABLE

INPUT/OUTPUT CONNECTIONS DM-4100N

BOTTOM TOP

	A	B	
DEC PT 1999.9	1	1	DEC PT COM
DEC PT 199.99	2	2	BUSY/DONE OUT
DEC PT 19.999	3	3	RUN/HOLD IN
DEC PT 1.9999	4	4	NO CONNECTION
NO CONNECTION	5	5	ANALOG LO INPUT
NO CONNECTION	6	6	OVERSCALE OUT
ANALOG HI INPUT	7	7	UNDERSCALE OUT
DISPLAY TEST	8	8	DISPLAY ENABLE
NO CONNECTION	9	9	+5VDC PWR IN
POWER COMMON	10	10	POLARITY ENABLE

SPECIFICATIONS (Typical at +25°C unless noted)

ANALOG INPUT

Configuration	True balanced differential bipolar (3½ digits) or single-ended (4½ digits).
Full Scale Input Range	-1.999 Vdc to +1.999 Vdc (3½ digit models). -1.9999 Vdc to +1.9999 Vdc (4½ digit models). Input pad area will accept user-installed range change and current or ohmeter connection.
Input Bias Current	2 pA typical, 50 pA maximum
Displayed Accuracy @ +25°C	Within ±0.02% of Reading, ±1 count (4½ digit models) Within ±0.1% of Reading, ±1 count (3½ digit models)
Resolution	1 mV (3½ digit models) 100 µV (4½ digit models)
Temperature Drift of Gain	Within ±50 ppm of Reading/°C typ. Within ±100 ppm of Reading/°C max.
Temperature Drift of Zero	Autozeroed, ±1 count over 0 to +50°C
Input Impedance	100 Megohms, minimum
Input Overvoltage	±250 Volts dc, 155 VRMS continuous max. ±300 Volts intermittent max. (Resistor and diode clamp protected)
Com-on Mode Rejection	80 dB, DC to 60 Hz, 1 Kilohm unbalance
Common Mode Voltage Range	±2 Vdc referenced to POWER COMMON
Warm-up Time	Stable readings within 15 seconds from power turn-on
Reference	Internal, referred to +5 V POWER INPUT. External Reference optional for ratiometric operation.
External Ref. Range	Must be within the range of the positive and negative supply voltages.

DISPLAY

Number of Digits	3 decimal digits and most significant "1" digit (3½ digit models). 4 decimal digits and most significant "1" digit (4½ digit models).
------------------	--

Decimal Points

Selectable decimal points are included for scale multipliers

Display Type

Red, light-emitting diode (LED) self-illuminated. (Models DM-3100L, -3100N, -4100L, -4100N) field effect, sealed liquid crystal displays (LCD) requiring external illumination. Black digits against a light background. (Model DM-3100X)

Display Height

0.5 inches (12,7 mm) All models except:
0.3 inches (7,6 mm): DM-4100N models only.

Overscale

Inputs exceeding the full scale range cause the display to blink.

Autopolarity

A polarity sign is automatically displayed for bipolar inputs.

Sampling Rate

Factory set at 3 conversions per second. May be rewired up to 20 conversions/second.

<u>I/O Connections</u>	<u>Models</u>	<u>Pins</u>	<u>Function</u>
Analog HI Input	DM-3100L DM-3100N DM-3100X	A4 6 A4	Differential input voltages are connected between these inputs. A bias current path to POWER COMMON from both these inputs must be externally provided. External circuits must constrain Analog LO In to be within ± 2 V of POWER COMMON. (See application drawings and discussion.)
Analog LO Input	DM-3100L DM-3100N DM-3100X	A2 H A2	
	DM-4100L DM-4100N	A2, A3 5	
Analog Return	DM-3100L DM-3100X DM-3100N	A1 A1 F	On DM-3100X only, this point may be used as a bias current return path or input circuit reference point for the 9 V powered circuit only. This point is elevated from POWER GROUND approximately +3.2 V and may be used as bias current return for limited common mode voltages less than +1 Volt. ANALOG RETURN should <u>never</u> be connected to POWER COMMON.

<u>I/O Connections</u>	<u>Models</u>	<u>Pins</u>	<u>Function</u>
Reference IN	DM-3100L DM-3100X DM-4100L	B6 B6 A1	Normally, REF IN should be jumpered to REF OUT. An external reference may be substituted for ratiometric operation. See application note.
Reference Out	DM-3100L DM-3100X DM-4100L	A6 A6 B1	
Busy/ <u>Done</u> Out	DM-4100L DM-4100N	B10 2	
OVERSCALE OUT } UNDERSCALE OUT }	DM-4100L DM-4100N		This output is logic "HI" during A/D conversion and logic "LO" when conversion is complete. It may be used in automatic equipment to prevent changing the input voltage during conversion. A logic "HI" on either output indicates an out of range input for autoranging applications.
<u>Power Connections</u>	<u>Models</u>	<u>Pin</u>	<u>Function</u>
A/D POWER IN	DM-3100X	A17	This pin is connected to the internal positive supply rail. External positive supply voltages should be connected to it.
5 V DC/DC POWER IN	DM-3100X	A18	This pin should be externally connected to pin A17 only for +5 V power input requiring the DC/DC converter. Do not connect for 9 V power configuration.
5 V POWER COMMON	DM-3100X	A16	Use only for 5 V power configuration. Do not use for 9 V power configuration. This pin may be used as a bias current return path for input signals.
9 V POWER COMMON	DM-3100X	B16	This pin is connected to the internal negative supply rail and to the output of the DC/DC Converter. Use only as the negative voltage for 9 V supplies.
+5 V POWER OUT	DM-3100L	A17	This pin is internally connected to pin A18 and is used to reference an external, isolated voltage reference source. This pin is connected to the DC/DC converter input common and to digital common.

<u>I/O Connections</u>	<u>Models</u>	<u>Pins</u>	<u>Function</u>
DECIMAL POINTS	DM-3100N DM-4100N		Connect selected pin to decimal point common <u>only</u> with a 270 ohm resistor in series.
DECIMAL PT. COMMON	DM-3100L DM-3100X DM-4100L	B15 B13 A4	On these models <u>only</u> , connect this pin to the selected decimal point pin to illuminate the corresponding decimal point.
Display Enable	DM-3100L DM-3100N DM-4100N DM-4100L	B18 K 8 B18	Connect to +5 Vdc power to illuminate display. Disconnect to blank display, but keep A/D converter cycling.
Run/Hold In	DM-4100L DM-4100N	B11 3	A TTL "HI" or open pin enables continuous sampling. TTL "LO" or ground will hold and display the last sample for temporary single sample storage or to copy down a reading.
Display Test	DM-3100L DM-3100N DM-3100X DM-4100N	B14 3 B14 J	Connect this input to +5 Vdc to light all display segments
Polarity Enable	DM-3100L DM-3100N DM-4100N DM-4100L	B16 10 10 A18	Ground this input to automatically display a minus sign for negative inputs.
Horiz. Polarity In Horiz Polarity Out	DM-3100X	B15 B9	Normally these inputs are jumpered together to continuously illuminate the horizontal portion of the polarity sign. Omit the B15-B9 jumper for applications not requiring sign display.
Vert. Polarity In Vert. Polarity Out	DM-3100X	B17 B18	Jumper these inputs when B15-B9 is jumpered for automatic sign display with bipolar inputs. For reverse sensing applications, B18 may be jumpered to B15 only (no other connections). This will display a minus sign with positive inputs and no sign with negative inputs.
Reference In/Out	DM-3100N	2	Normally there is no connection on this pin. Users may install internal jumpers to make the internal reference available at the connector pins or to use an external reference for ratio-metric operation.

POWER REQUIREMENTS

LED Models

External +5 \pm 0.25 Vdc regulated required at 190 mA typical, 250 mA max. (3½ digits) or 350 mA typical, 400 mA max. (4½ digits). Logic spikes must not exceed 50 mV. Power current varies rapidly so that unregulated supplies cannot be used.

LCD Models

Accepts either +5 Vdc, or +9 Vdc power. +5 V power uses an internal DC/DC Converter to generate negative supply voltage. Operating ranges: +5 V: +4 V to +8 V

+9 V: +8 V to +14 V

Power current @ +5 V is 6 mA typ., 10 mA max.

Current @ +9 V is 3 mA typ., 6 mA max.

A multiturn screwdriver pot accessible by removing the case adjusts the full scale reading (gain).

Zero is automatic (autozeroing). Suggested recalibration in stable conditions is 90 days.

PHYSICAL-ENVIRONMENTAL

Outline Dimensions

2.53"W x 3.25"D x 0.94"H
(64,3 x 82,5 x 23,8 mm)

Cutout Dimensions

2.53"W x 0.97"H min.
(64,3 x 24,6 mm)

Mounting Method

Through a front panel cutout secured by a rear flange plate and two removable side case screws. Panel thickness up to 0.62" (15,9 mm). See mounting diagram.

Short-Depth Case

(Interchangeable with other Datel cases)

Outline Dimensions

3.00"W x 2.15"D x 1.76"H
(76,2 x 54,6 x 44,7 mm)

Cutout Dimensions

1.812"H x 3.062"W
(46,0 x 77,8 mm)

Mounting Method

Through a front panel cutout secured by (4) 4-40 front access screws which are concealed by the bezel. See mounting diagram.

Weight

Approx. 5 ounces (142 g)

Connector	Double-sided, edgeboard PC type, solder tab, gold-plated fingers.
Mounting Position	Any
Operating Temperature Range	0 to +50°C
Storage Temperature Range	-25°C to +85°C
Altitude	0 to 15,000 feet (4900 m)
Relative Humidity	20% to 80%, non-condensing

MODEL NUMBERS AND PRICES

DISPLAY	3½ Digit Resolution Differential	4½ Digit Resolution Single-ended	CASE TYPE
LED DISPLAY	DM-3100N \$35 (1-9) \$29 (100+)	DM-4100N \$69 (1-9) \$59 (100+)	LOW PROFILE CASE
	DM-3100L \$35 (1-9) \$29 (100+)	DM-4100L \$69 (1-9) \$59 (100+)	
LIQUID CRYSTAL DISPLAY LOW POWER	DM-3100X \$49 (1-9) \$41 (100+)	NOT AVAILABLE	SHORT DEPTH CASE

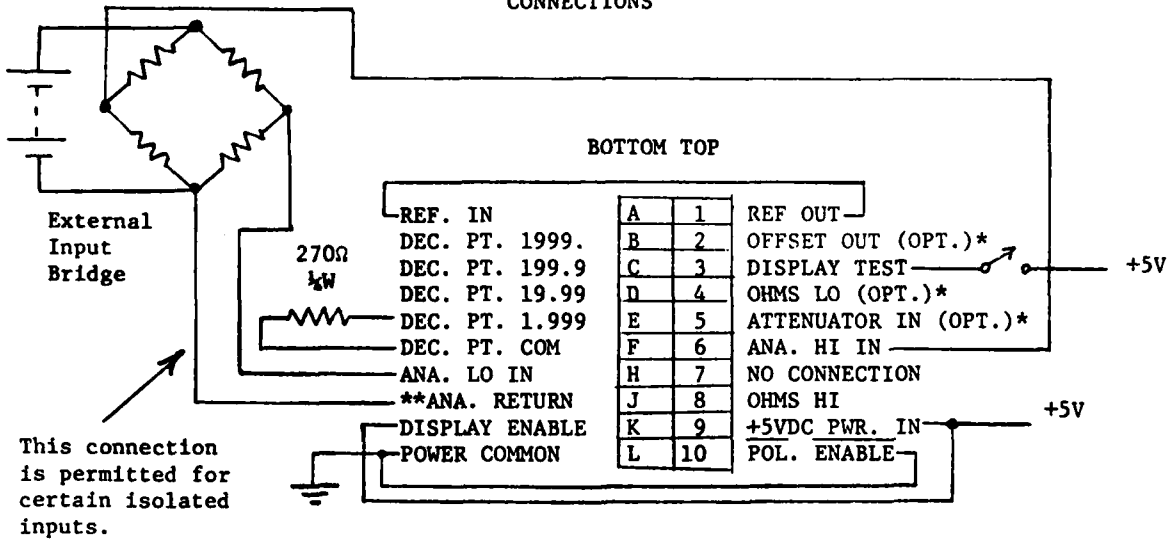
Prices do not include PC Board connectors. Please include with you DPM order.

Connector Model	DPM Case	Description	Viking Equiv.	Price (1-9)
58-2075010	Short-Depth	Dual 18-pin, 0.1" ctrs	3VH18/1JN5	\$2.95
58-2073082	Low-Profile	Dual 10-pin, 0.156" ctrs	2VH10/1AN5	\$1.95

9/9/77

DM-3100N

INPUT/OUTPUT Typical CONNECTIONS



*These connections are optional extra features and require PC board installation of additional components by the user. See application notes in full brochure.

**DO NOT connect Analog Return to Power Common. Power Common may be used as Analog Common. Analog Return is approximately -2.8VDC below plus Vs and may be used as bias current return in some applications. See full brochure. Connecting to Analog Return rather than Power Common will produce lower noise although Analog Return cannot source or sink more than 1mA. Connect long, noisy cable shields to Power Common.

PM-35A

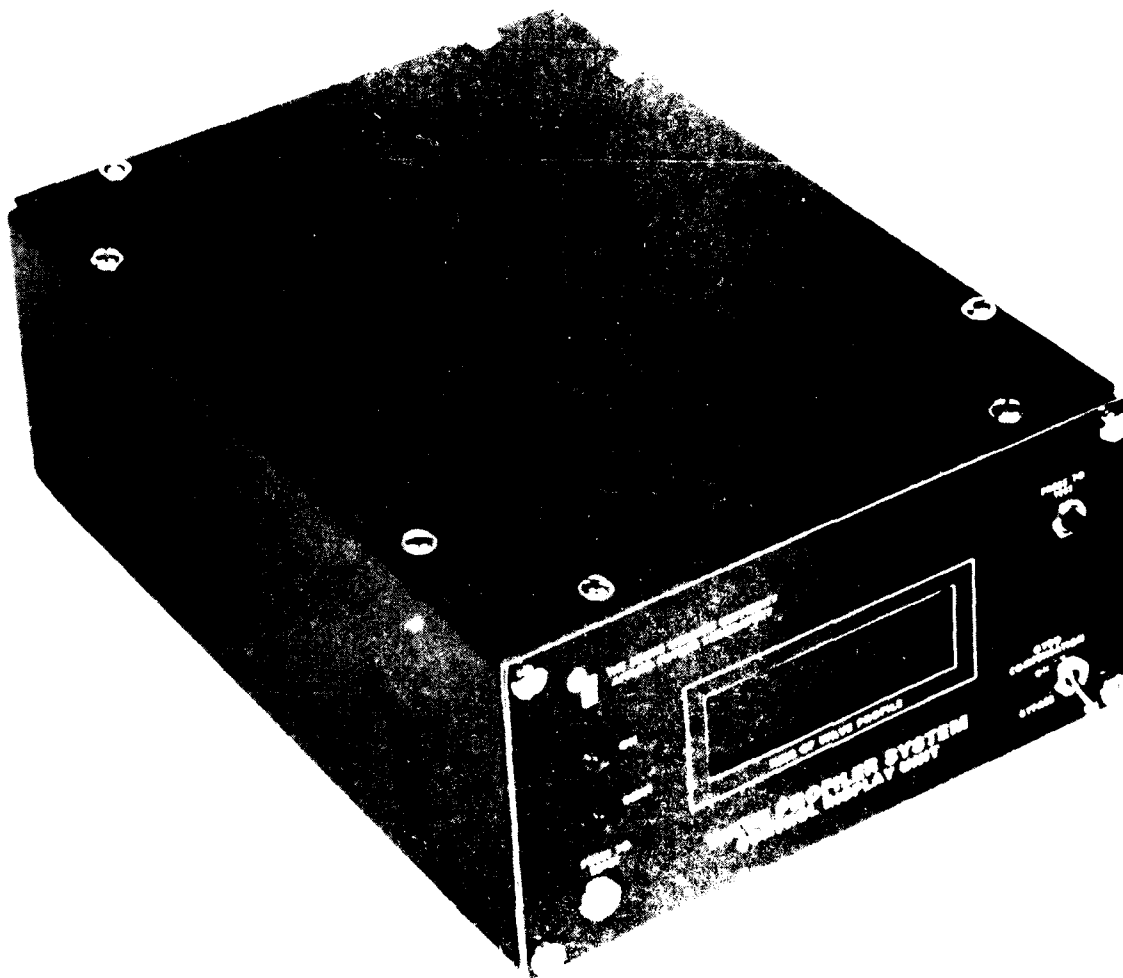


Fig. D1.1 Cockpit control and display unit (CDU).

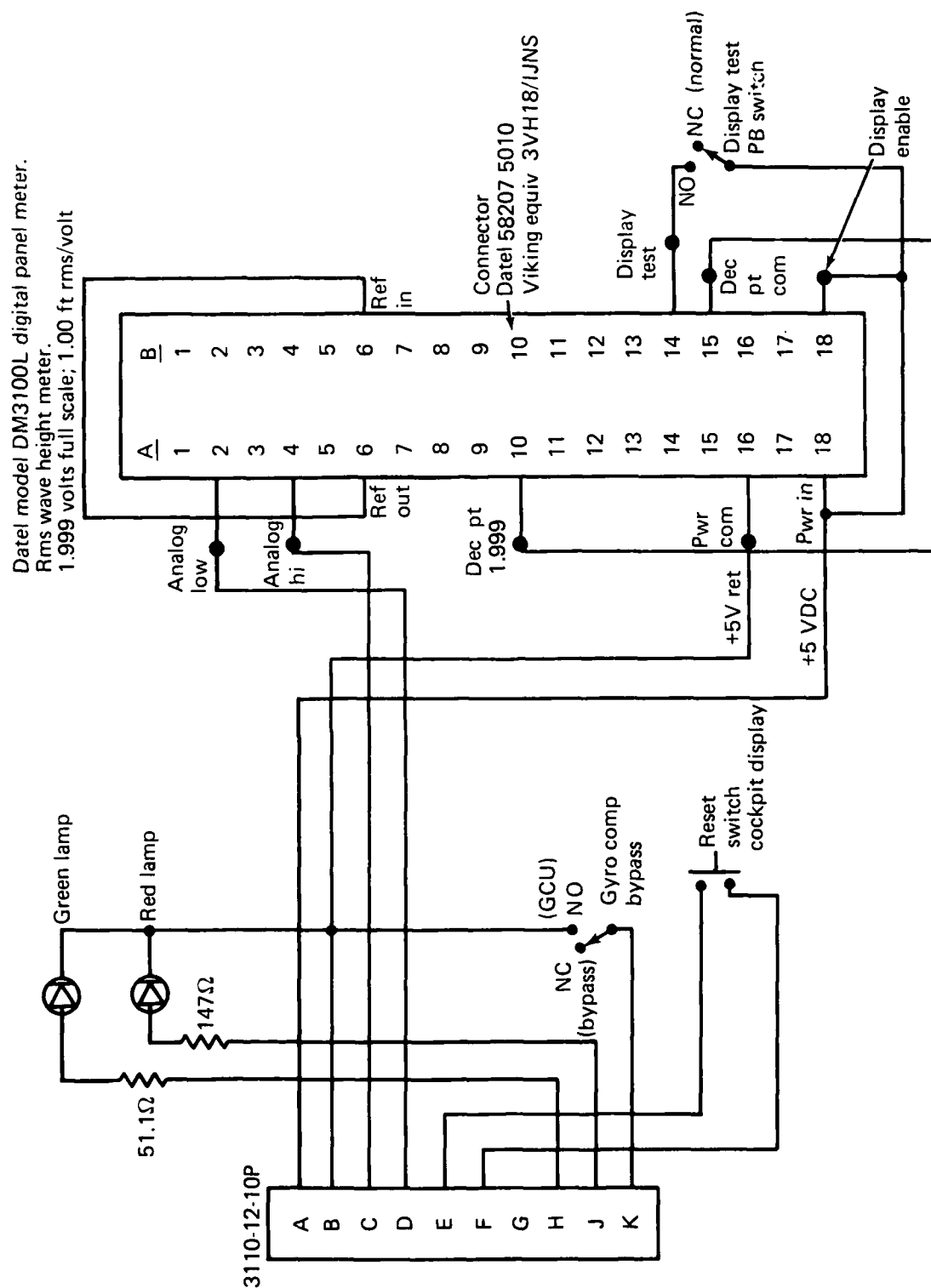


Fig. D1-2 Cockpit control display unit, wiring diagram.

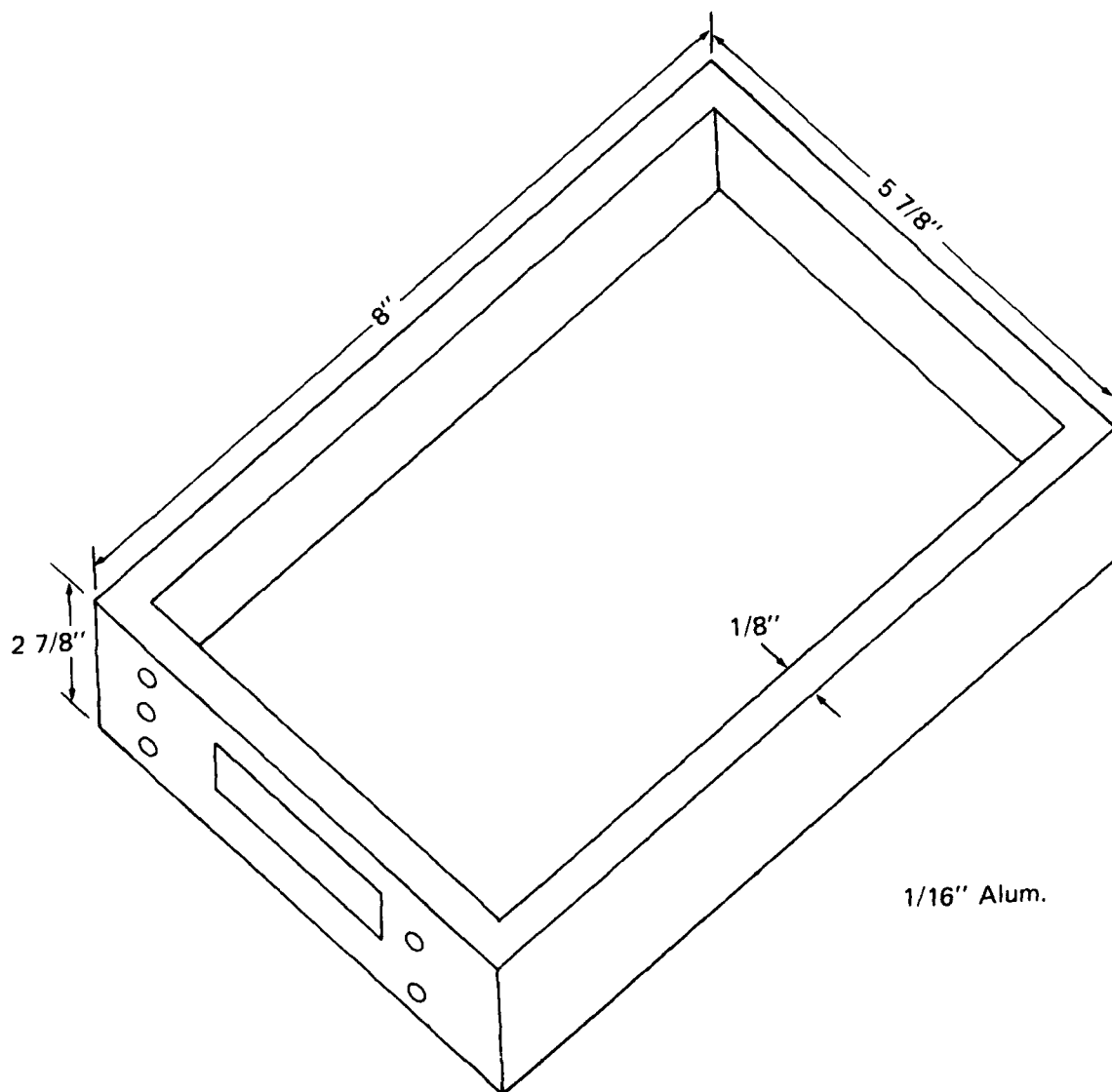


Fig. D1-3 Cockpit display unit, mechanical design.

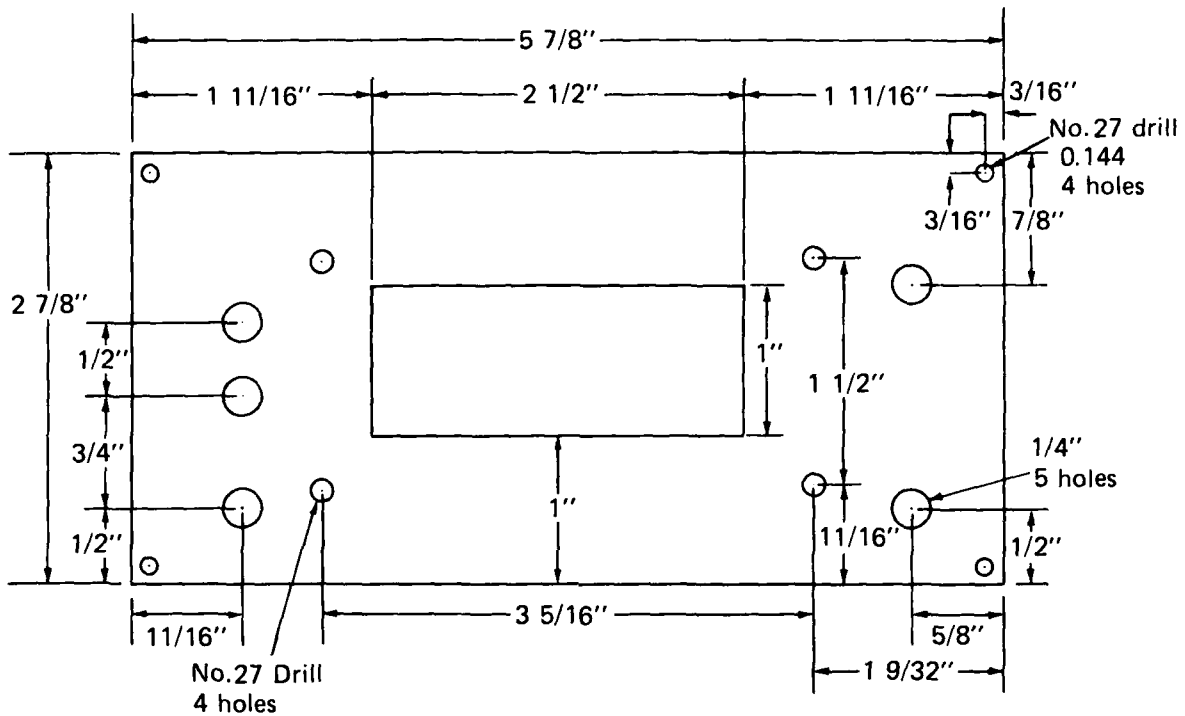


Fig. D1-4 Cockpit display unit, front panel details.

Appendix E

RESULTS OF COMPUTER SIMULATION STUDY RELATING TO THE FIFTH-ORDER FILTER RESPONSE TO VEHICLE HEIGHT CHANGES

A computer simulation of the fifth-order filter was constructed using a Runge-Kutta integration routine to evaluate the system time response to vehicle height changes for various filter time constants. The fifth-order filter has inputs of acceleration and its output is ideally considered as vehicle height. Ideally, the filter is to remove constant changes in height, such as those due to bow and stern seal height settings, etc.

Four different acceleration profiles, each of which simulates a particular transient condition of the vehicles as shown in Figs. E1-1 through E1-4 were input to the filter for each of three filter time constants ($\tau = 20, 30, \text{ and } 40 \text{ s}$). The first input, input (a), represents a vehicle responding to 1 g of acceleration for 0.01 s, which builds up a vertical velocity of 0.3 ft/s. This is sustained for 15 s, then the acceleration of -1 g is input to stop the vertical motion at a 5 ft height change. Acceleration input (b) represents a 1 g input for 0.03 s to yield a vertical velocity of 1 ft/s. This motion is stopped by a -1 g for 0.03 s at 0.5 s to yield an overall height change of 0.5 ft. Input (c) is a 0.04 g acceleration for 0.25 s to yield a velocity of 0.33 ft/s, which is halted at 15 s by a -0.04 g acceleration input for 0.25 s, for an overall vehicle height change of 5 feet. The fourth simulated input is a 1 g for 0.25 s, followed immediately by a -1 g for 0.25 s. The peak velocity buildup was 8 ft/s. The overall height change was 2 ft.

Figure E1-5 is a block diagram of the fifth-order filter showing the gains used for each filter time constant considered. The gain was computed based on the following:

$$\text{Accelerometer gain} = 2.5 \text{ V/g}$$

$$\text{Filter output} = 2 \text{ ft/V}$$

At high frequency, the filter reduces to the desired second-order integration K_1/s^2 .

Typically the filter response for $\tau_a = 20$ s to input (a) is shown in Figs. E2-1 through -5, when E2-1 is the first-stage output, E2-2 is the second-stage output, etc., and E2-5 is the final filter output as a function of time after initiation of the input. The actual filter stages saturate at ± 12 V. One must avoid saturation due to loss of information, and, secondly, if the OA's used saturate, they require an excessive time to recover. Saturation of the fifth-stage OA would occur at an equivalent output of ± 24 ft. Of the four cases considered, no saturation of any of the stages of the filter occurred.

Table E2-1 is a summary of the system response to the four different acceleration inputs showing maximum excursions for the fourth and fifth stages for each of the time constants considered and the maximum derivation (error) after a reset delay of 150 s. Cases (b) and (d) are most likely to occur during an operational test run of the craft. There is a 0.5 ft height change in a 5 s time or a 2 ft height change in a 0.5 s time, each of which is affected by a seal height change. As shown in Table E2-1, the maximum error in system output in feet for case (b) is ≈ 0.3 ft occurring at 0.5 s after excitation and for case (d) is 1.3 ft at 0.5 s independent of the filter time constant. However, this error reduces very rapidly for the 20 s filter compared to the 40 s filter. The 20 s filter error is less than 0.05 ft in 25 s, while the 40 s system response error is still greater than 0.5 ft at 25 s. For this reason the filter time constant τ_a was reduced from 40 s to 20 s to achieve a better operational use of the equipment. Figures E2-6 through -10 are the filter responses for each stage ($\tau_a = 20$ s) with input (b). Figures E2-11 through -15 are the filter responses for each stage ($\tau_a = 20$ s) with input (c). Figures E2-16 through -20 are the filter responses for each stage ($\tau_a = 20$ s) with input (d). Figures E2-21 through -24 are the responses of the fifth-stage filter ($\tau_a = 30$ s) output for each input (a) through (d), respectively. Figures E2-25 through -28 are the responses of the fifth-stage filter ($\tau_a = 40$ s) output for each input (a) through (d), respectively.

After operating the system at sea, the filter time constant (τ_a) was further reduced to 4 s to minimize the transient errors. Figures E2-29 through E2-32 are the fifth-order filter responses for the four different simulated inputs. The maximum transient errors are all less than 0.15 ft after 5.0 s.

Table E2-1
Fifth-order filter, summary of response data.

System Input (g)	Filter Input (V)	$E_{00}(\text{max})$			$E_{05}(\text{max})$ ($V = 2$ ft)			$E_{05}(\text{max})$ (equivalent E_{05} max after 25 ft decay)		
		$\tau = 0.0$ (s) (V)	$\tau = 30$ (s) (V)	$\tau = 60$ (s) (V)	$\tau = 40$ (s) (V)	$\tau = 30$ (s) (V)	$\tau = 20$ (s) (V)	$\tau = 40$ (s) (V)	$\tau = 30$ (s) (V)	$\tau = 20$ (s) (V)
(a) 1 g 10 ms -1 g at 15 s for 10 ms 5 ft steep (1.5 s)	1 g = 1.75	0.729 (15 s)	0.53125 (12.5 s)	0.3675 (8.3 s)	0.579 (12.9 s)	0.434 (9.7 s) (31 s)	0.368 (26 s)	1.16 ft max at 15 s -1.225 ft after 150 s	1.07 ft at 15 s -1.07 ft after 150 s	1.07 ft max at 15 s -1.07 ft after 150 s
(b) 1 g 30 ms at 5 s -1 g 30 ms 0.5 ft steep (1.5 s)	1 g = 1.75	0.15 (0.5 s)	0.145 (0.5 s)	0.145 (0.5 s)	0.15 (0.5 s)	0.148 (0.5 s)	0.145 (0.5 s)	0.145 ft max at 15 s -0.145 ft after 150 s	0.145 ft max at 15 s -0.145 ft after 150 s	0.145 ft max at 15 s -0.145 ft after 150 s
(c) 0.04 g for 0.25 s -0.04 g at 15 s for 0.25 s 5 ft steep (1.5 s)	0.04 g = 0.07	0.728 (14.76 s)	0.5516 (12.6 s)	0.3675 (8.4 s)	0.58 (13 s)	0.44 (9.9 s) (31 s)	0.41 (27 s)	1.16 ft max at 15 s -1.225 ft after 150 s	1.07 ft at 15 s -1.07 ft after 150 s	1.07 ft max at 15 s -1.07 ft after 150 s
(d) 1 g for 0.25 s -1 g for 0.25 s 2 ft steep (0.5 s)	1 g = 1.75	0.0665 (0.49 s)	0.6615 (0.49 s)	0.4475 (0.49 s)	0.6615 (0.49 s)	0.656 (0.49 s)	0.6615 (0.49 s)	1.16 ft max at 15 s -1.225 ft after 150 s	1.07 ft at 15 s -1.07 ft after 150 s	1.07 ft max at 15 s -1.07 ft after 150 s

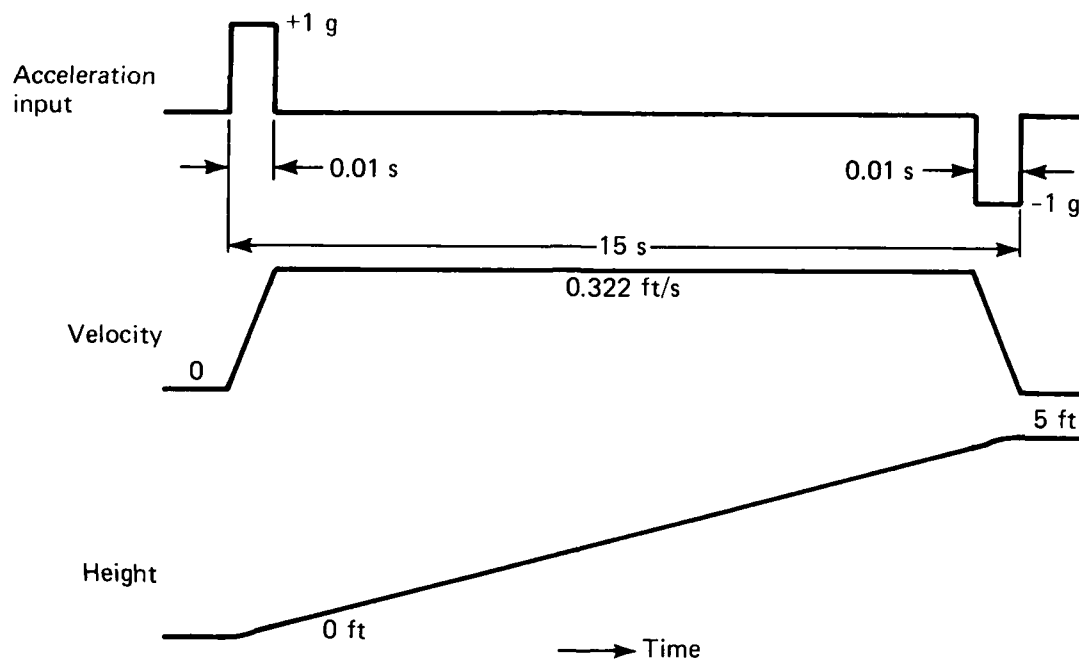


Fig. E1-1 Acceleration input (a).

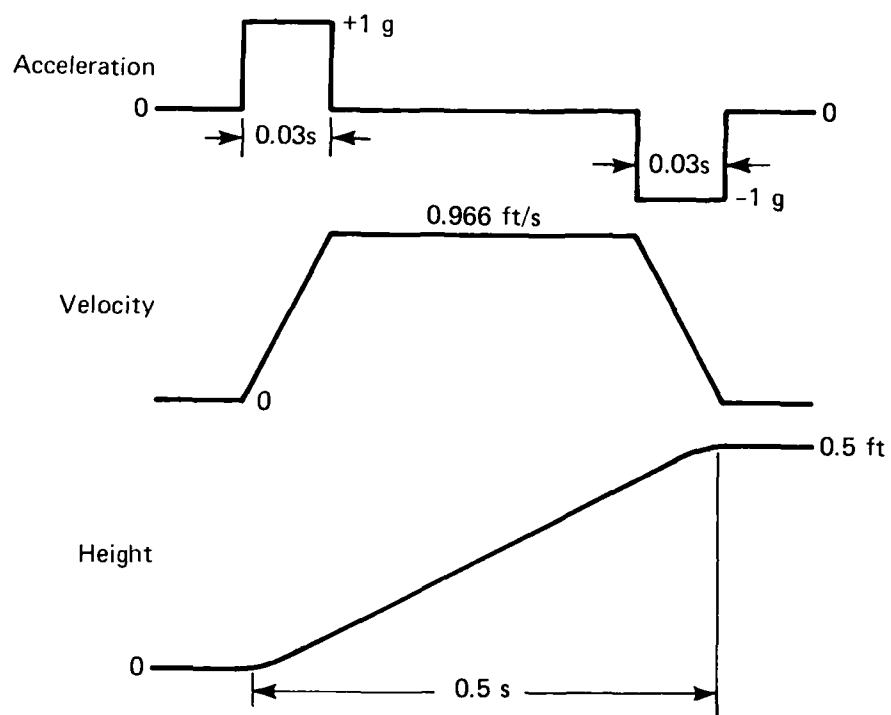


Fig. E1-2 Acceleration input (b).

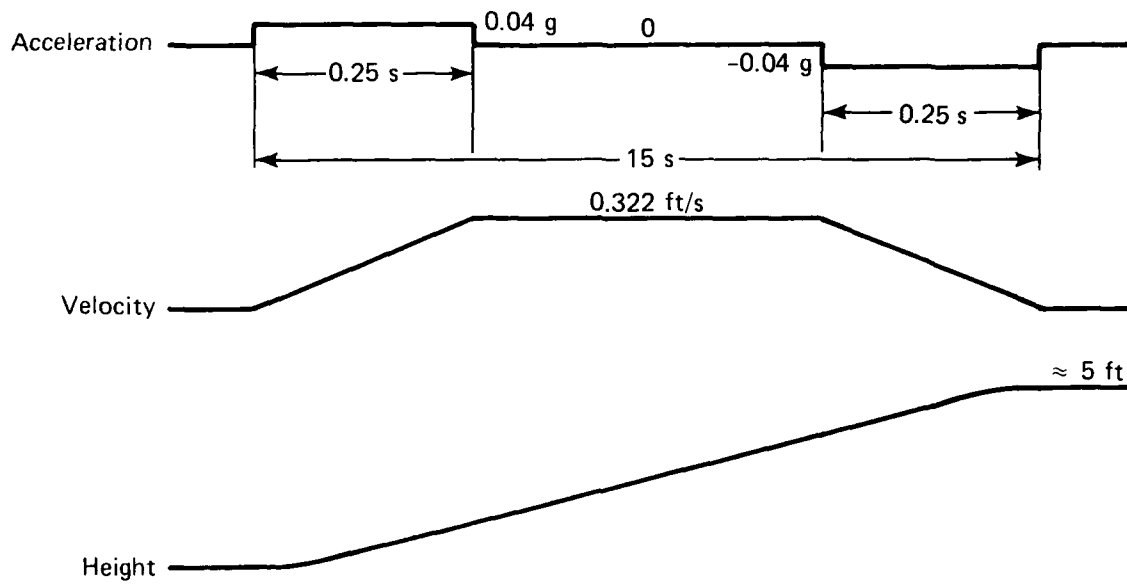


Fig. E1-3 Acceleration input (c).

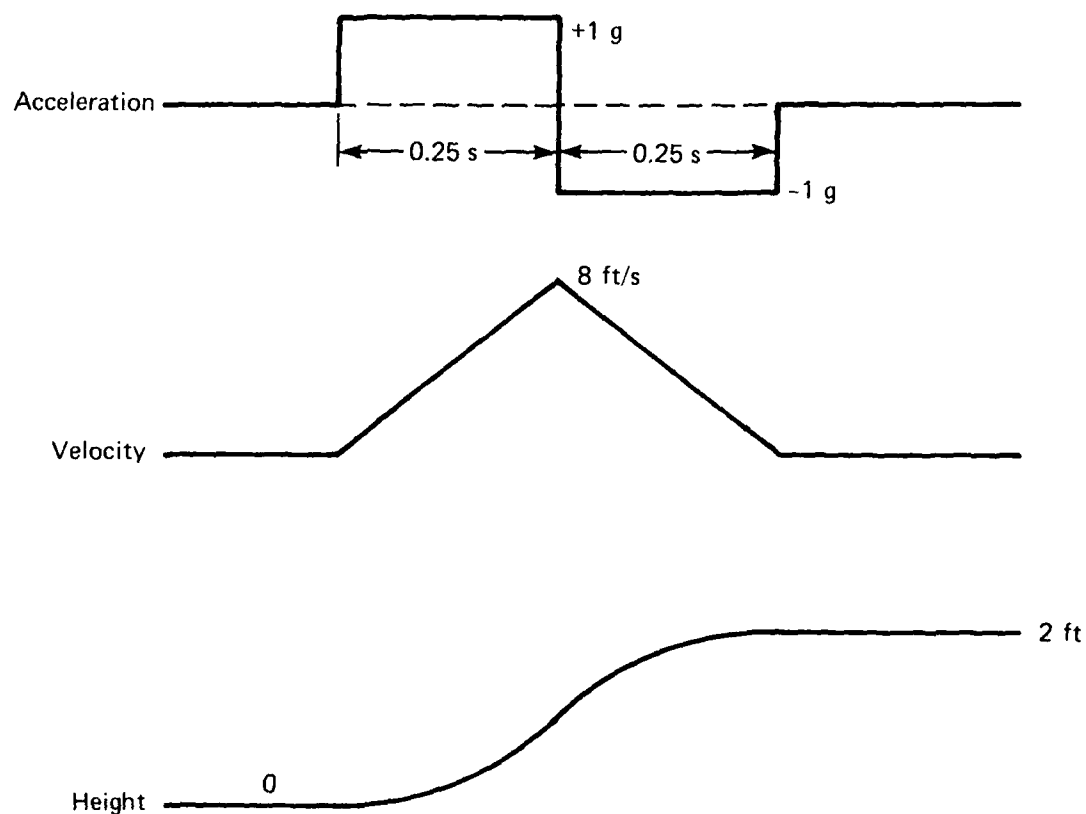
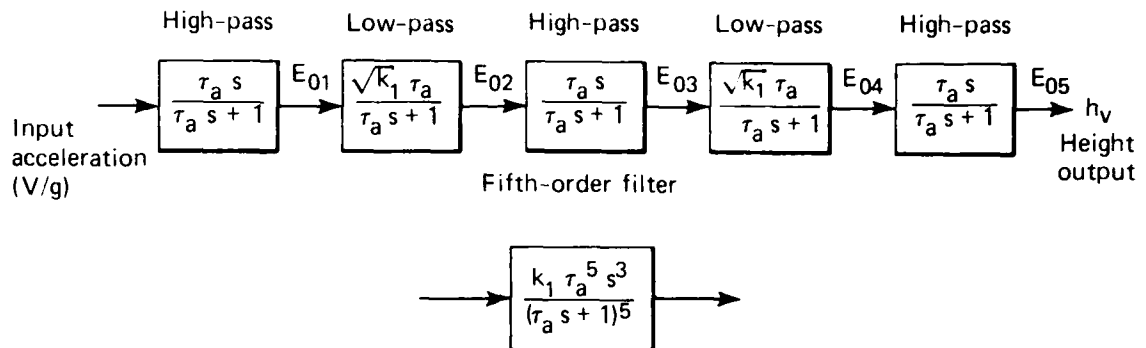


Fig. E1-4 Acceleration input (d).



Where $\sqrt{k_1} = 2.5 \text{ rad/s}$
 $\sqrt{k_1} \tau_a = 10$ for $\tau_a = 4 \text{ s}$
 $\sqrt{k_1} \tau_a = 50$ for $\tau_a = 20 \text{ s}$
 $\sqrt{k_1} \tau_a = 75$ for $\tau_a = 30 \text{ s}$
 $\sqrt{k_1} \tau_a = 100$ for $\tau_a = 40 \text{ s}$

Fig. E1-5 Block diagram of the fifth-order filter.

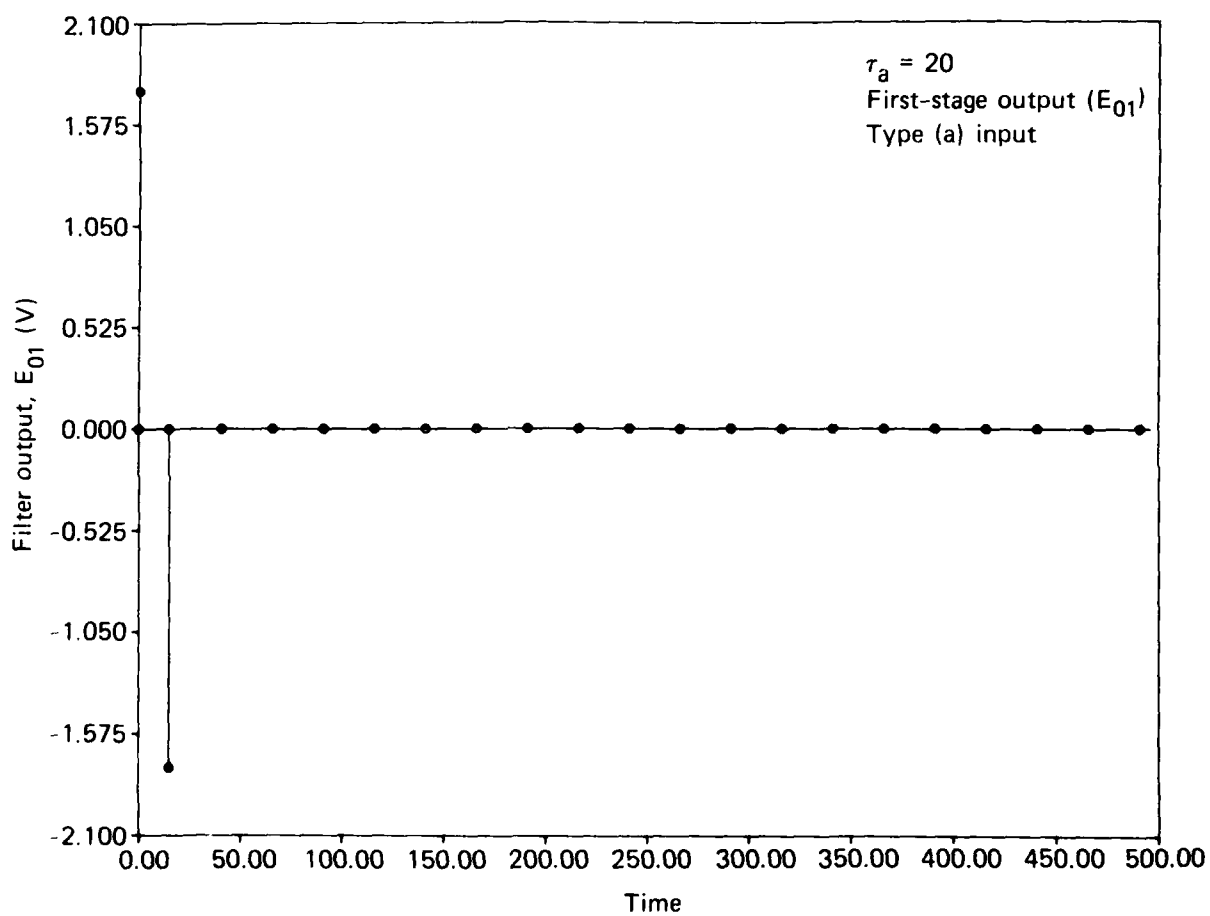


Fig. E2-1 First-stage filter output in response to a 5 ft vehicle height change in a 15 s period for $\tau_a = 20$.

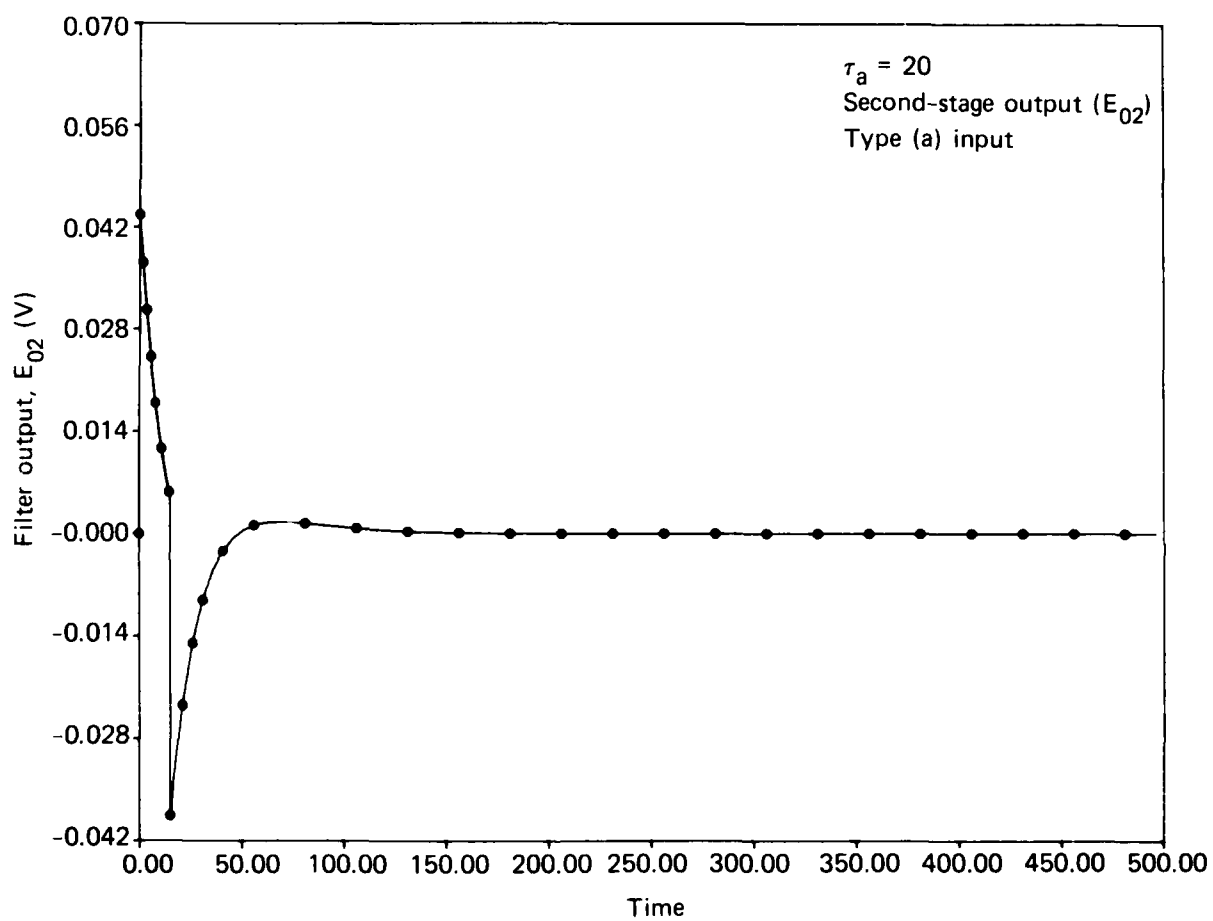


Fig. E2-2 Second-stage filter output in response to a 5 ft vehicle height change in a 15 s period for $\tau_a = 20$.

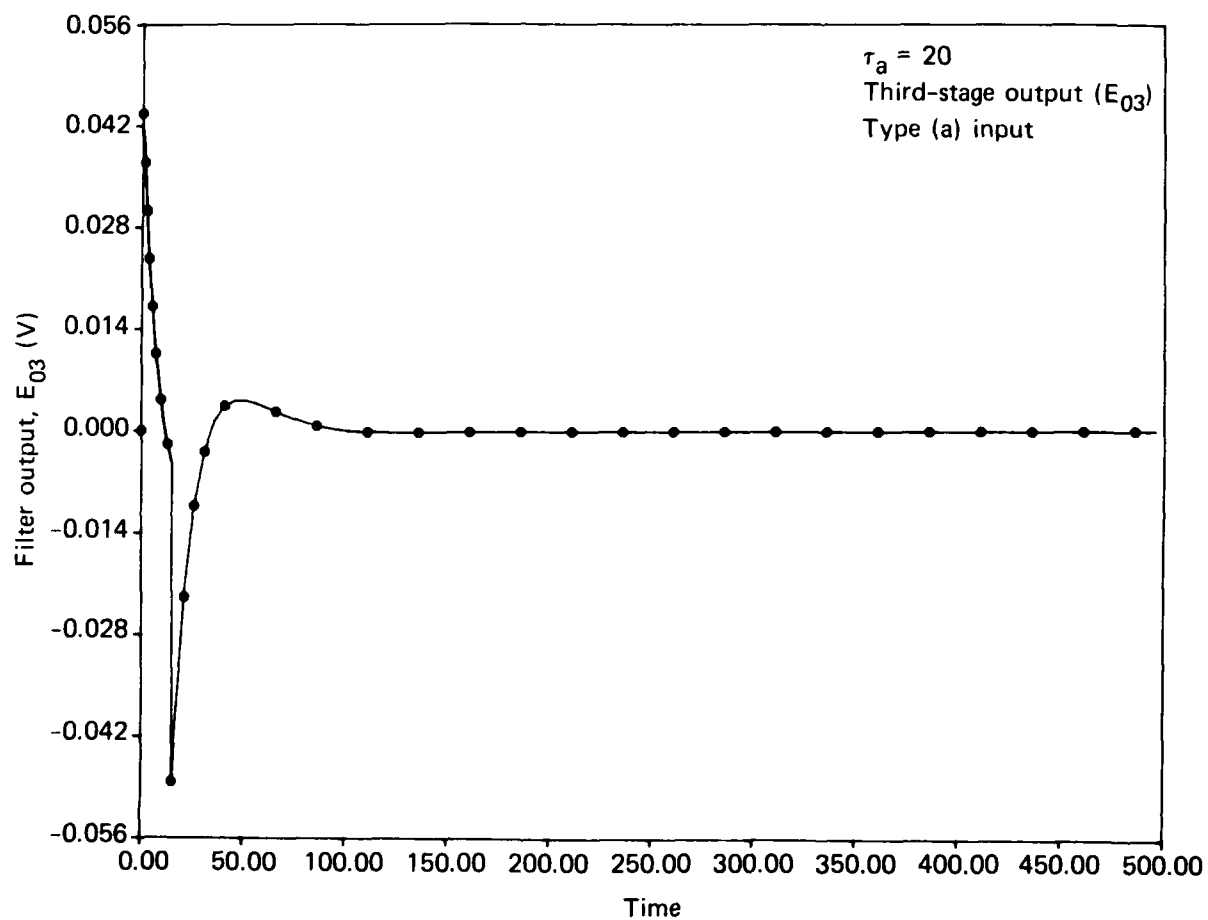


Fig. E2-3 Third-stage filter output in response to a 5 ft vehicle height change in a 15 s period for $\tau_a = 20$.

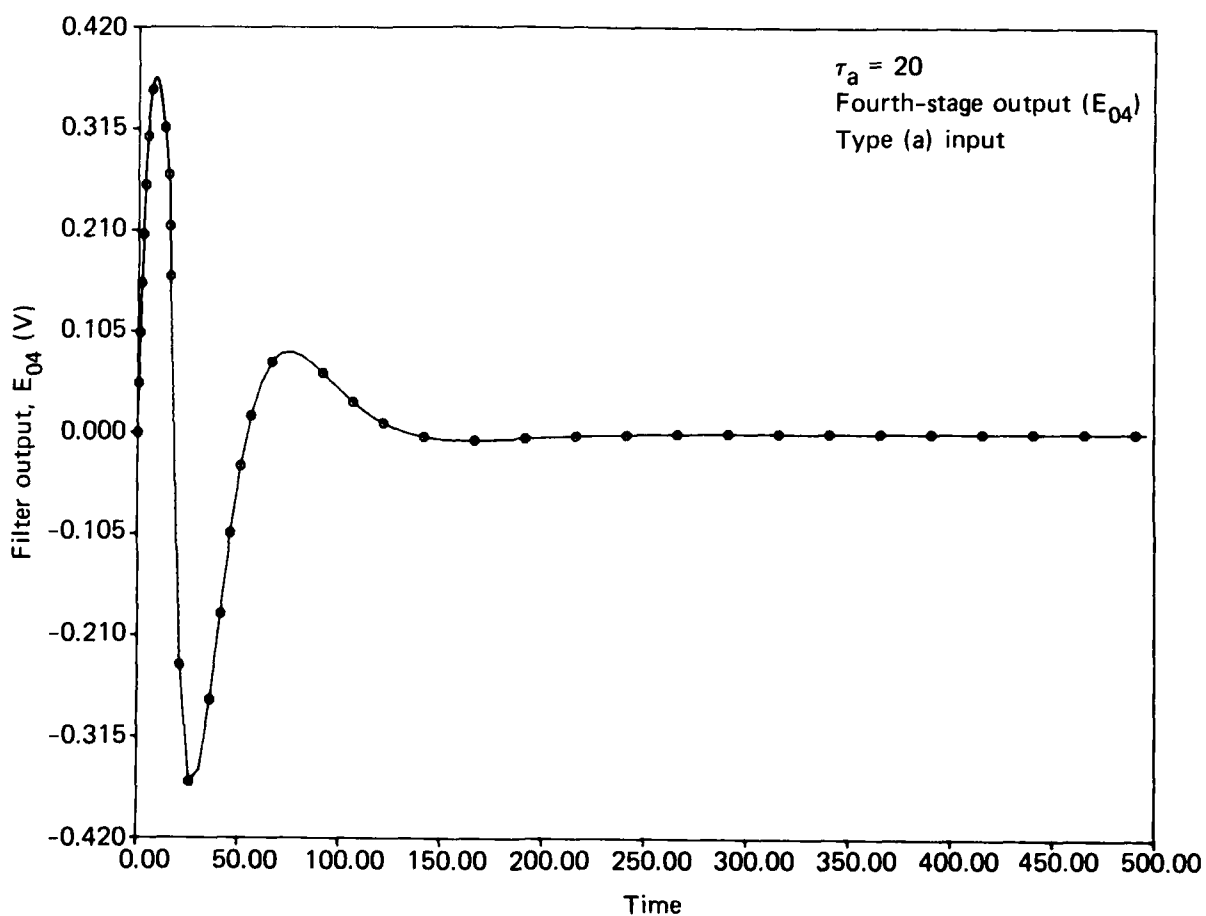


Fig. E2-4 Fourth-stage filter output in response to a 5 ft vehicle height change in a 15 s period for $\tau_a = 20$.

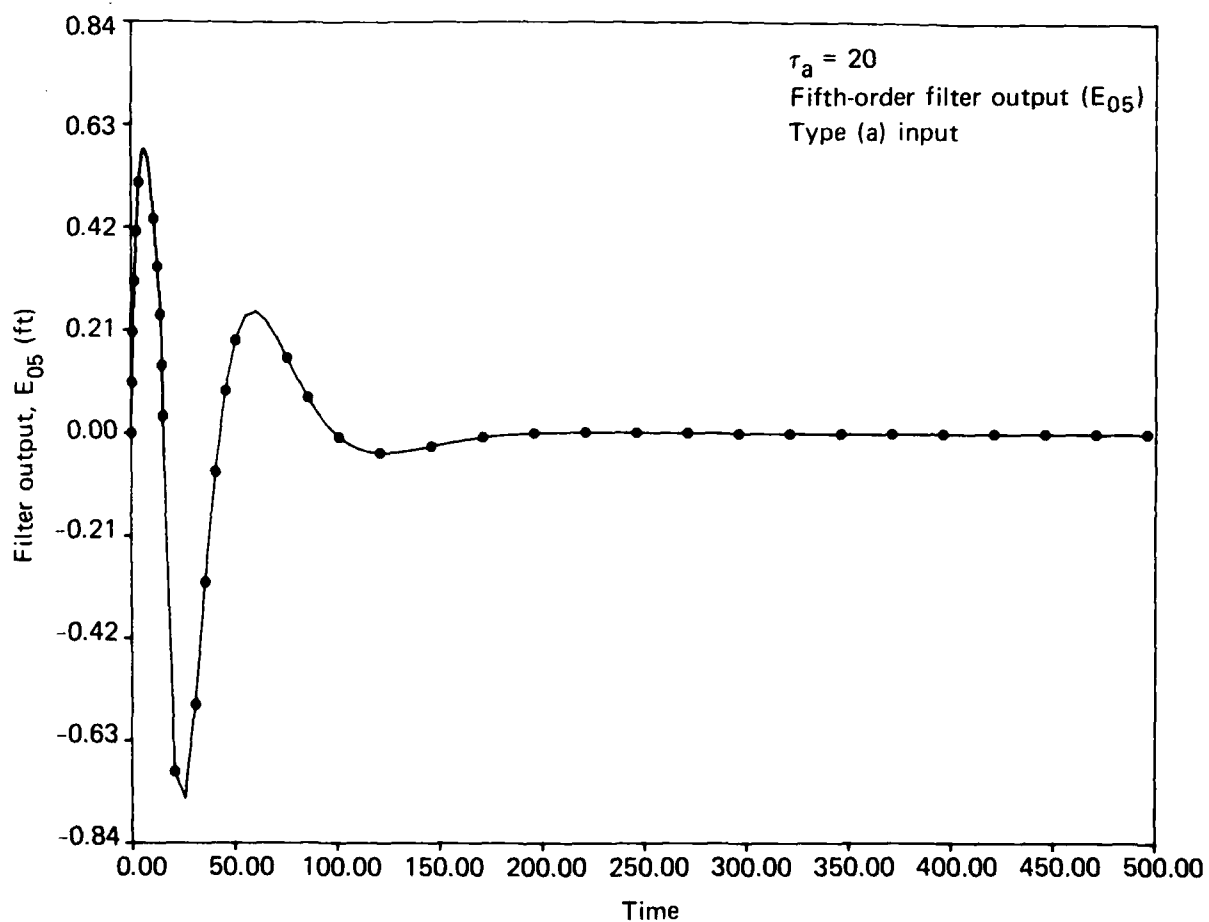


Fig. E2-5 Fifth-order filter output in response to a 5 ft vehicle height change in a 15 s period for $\tau_a = 20$.

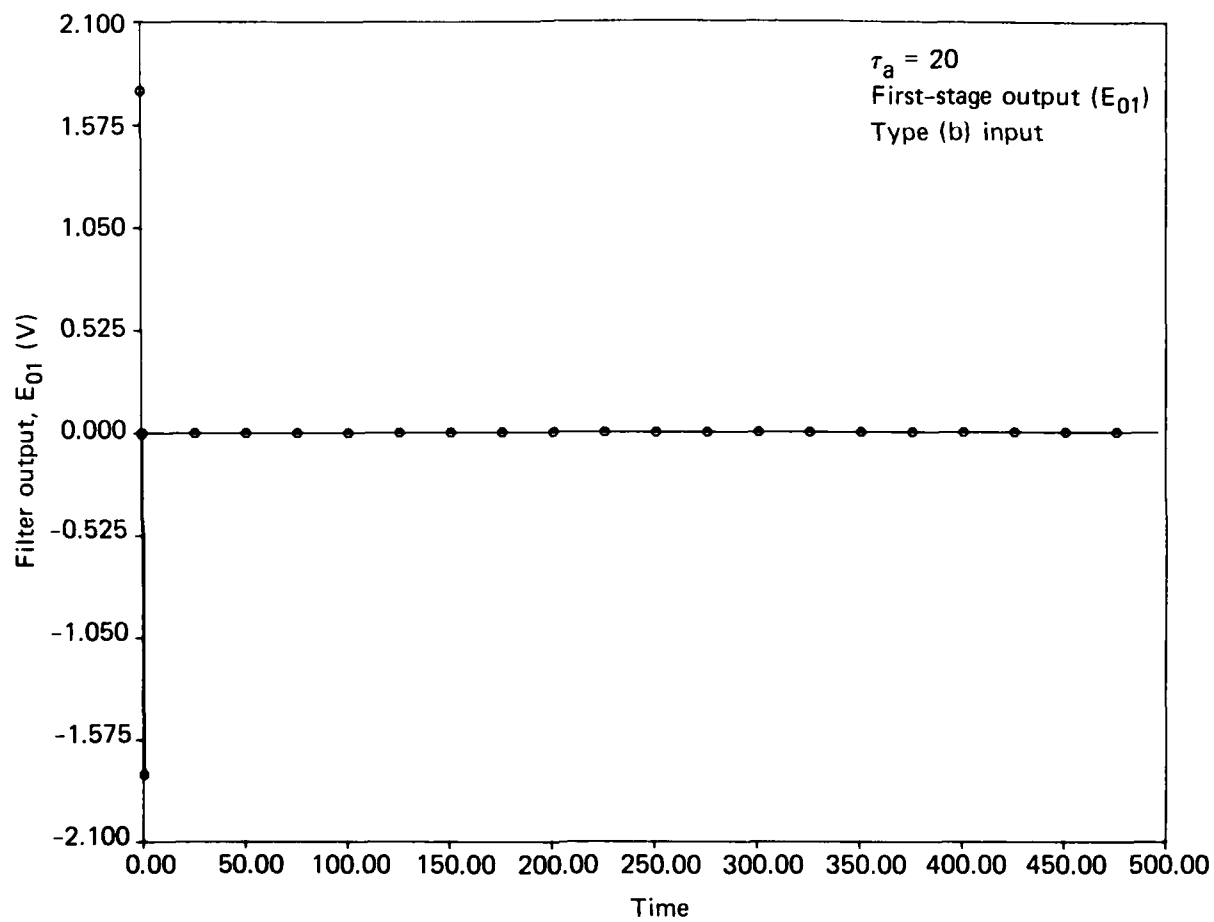


Fig. E2-6 First-stage filter output in response to a 0.5 ft vehicle height change in a 0.5 s period for $\tau_a = 20$.

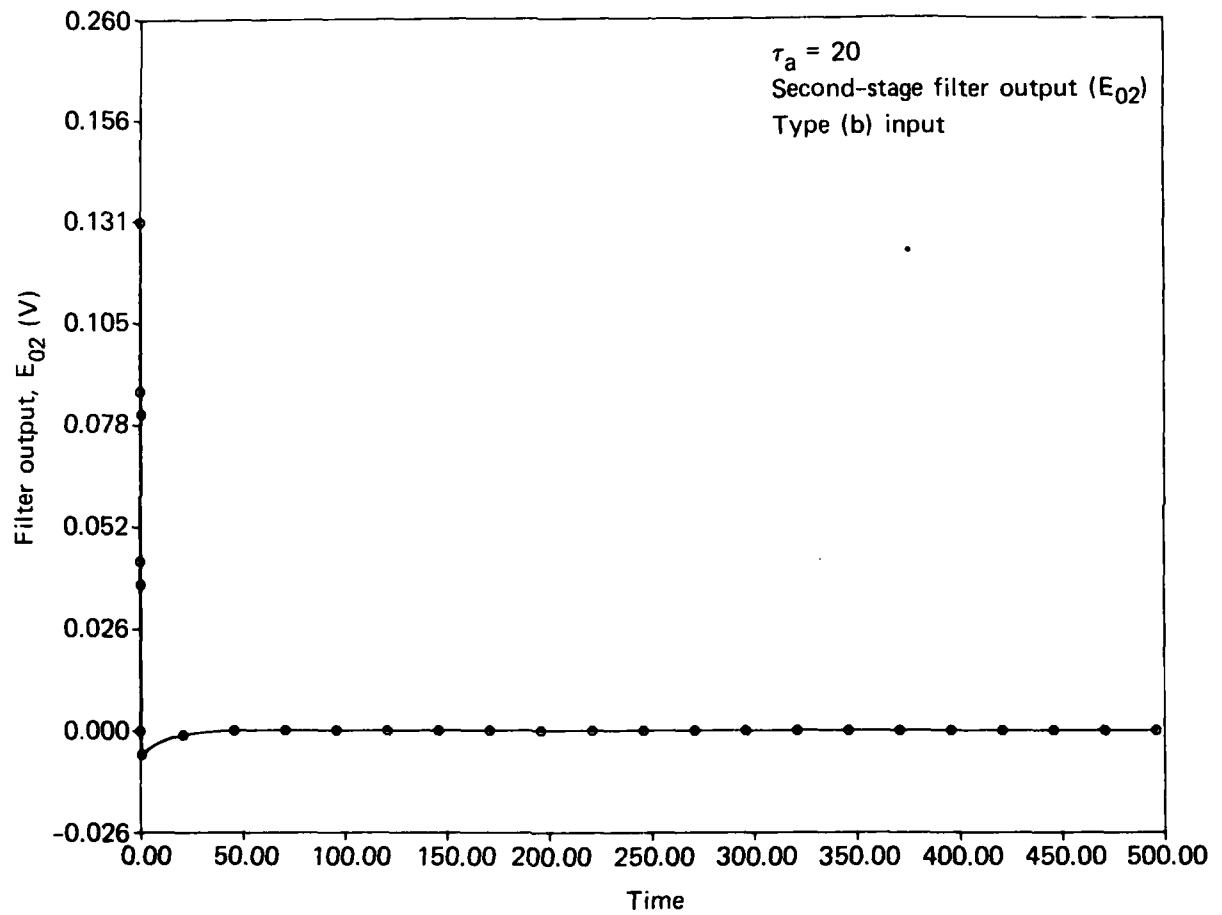


Fig. E2-7 Second-stage filter output in response to a 0.5 ft vehicle height change in a 0.5 s period for $\tau_a = 20$.

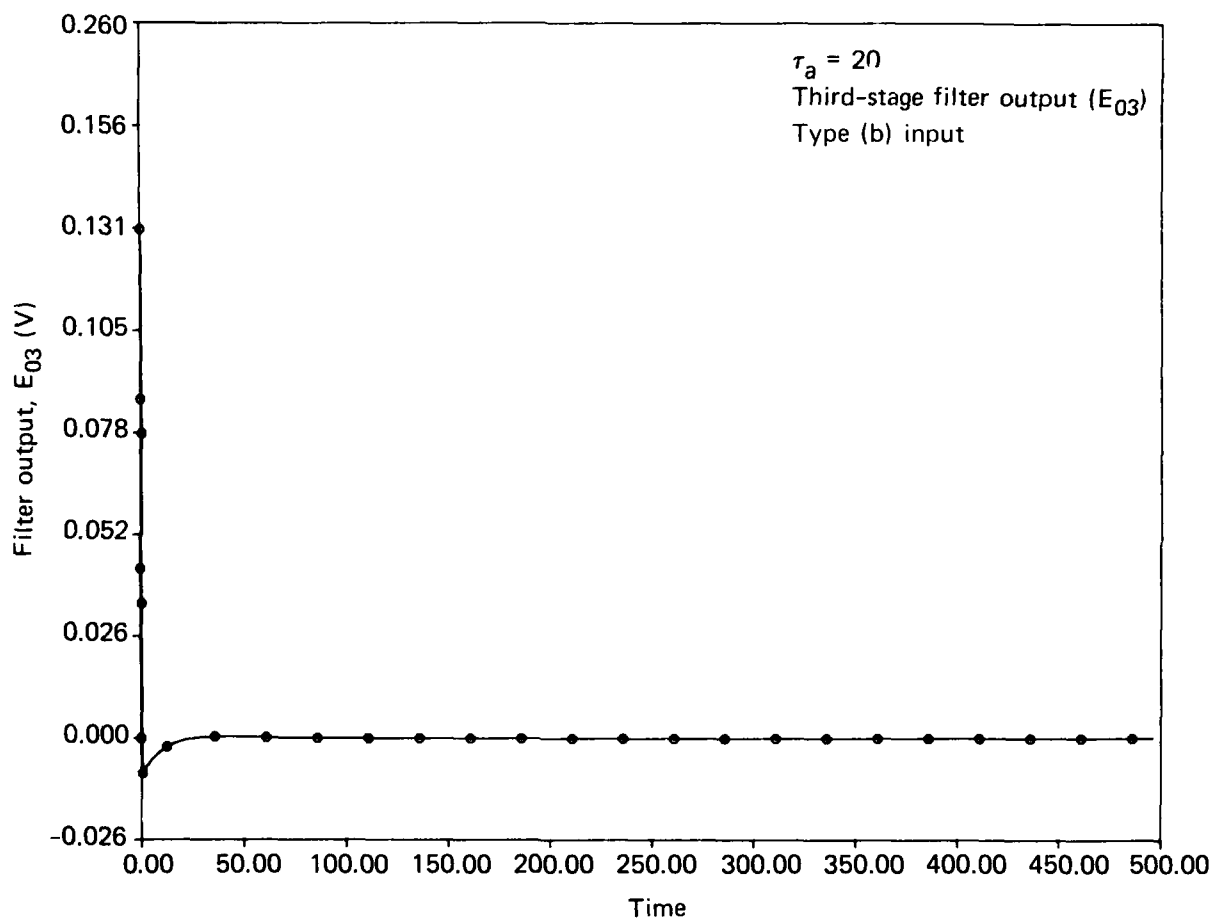


Fig. E2-8 Third-stage filter output in response to a 0.5 ft vehicle height change in a 0.5 s period for $\tau_a = 20$.

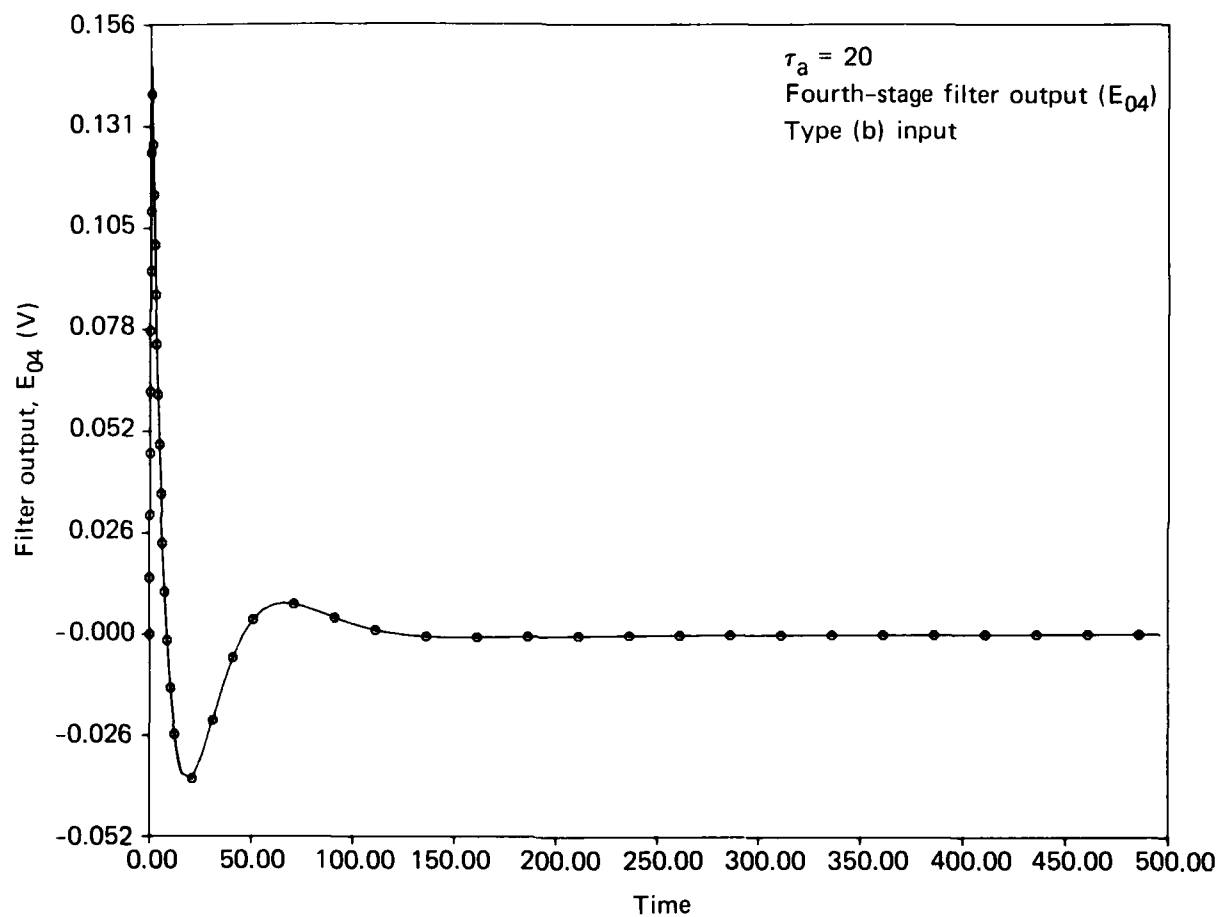


Fig. E2-9 Fourth-stage filter output in response to a 0.5 ft vehicle height change in a 0.5 s period for $\tau_a \approx 20$.

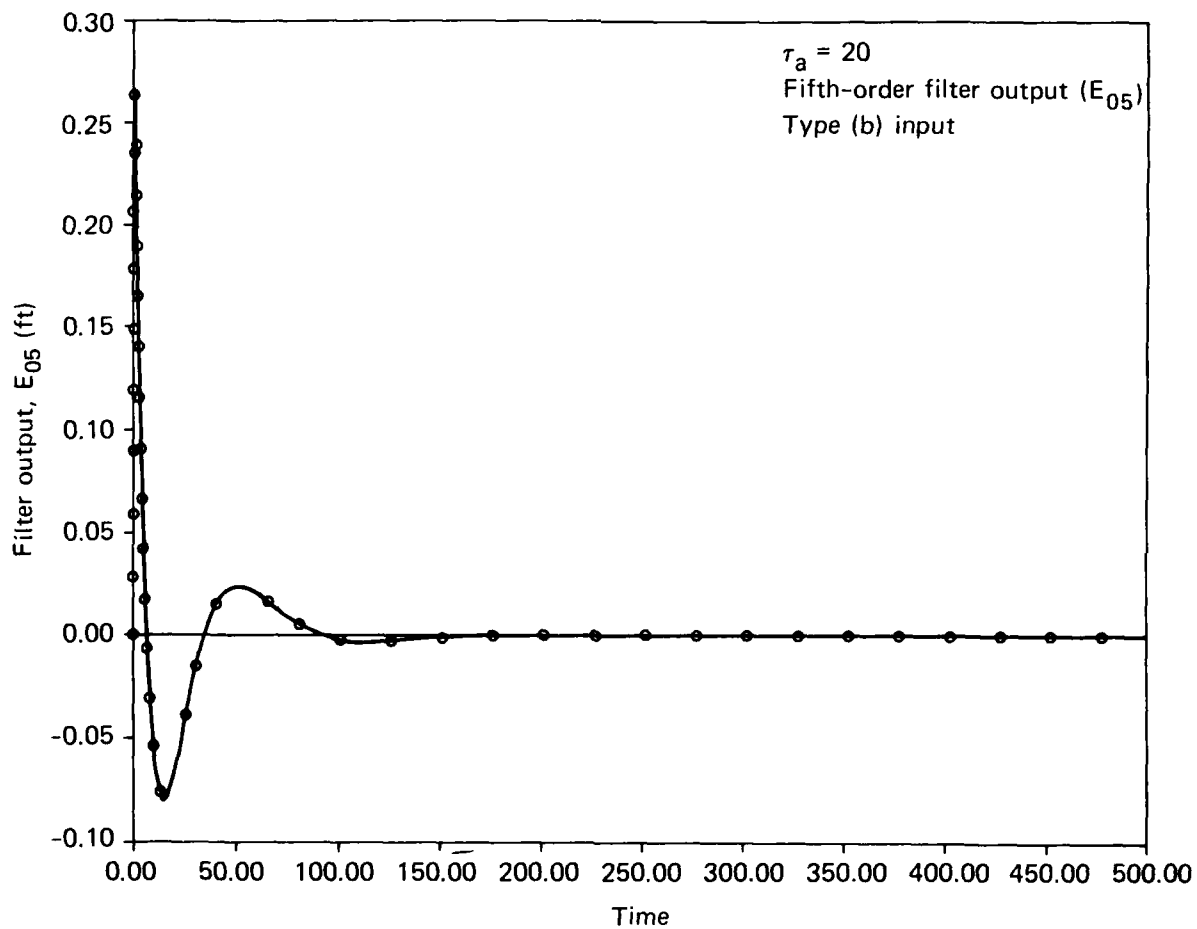


Fig. E2-10 Fifth-order filter output in response to a 0.5 ft vehicle height change in a 0.5 s period for $\tau_a = 20$.

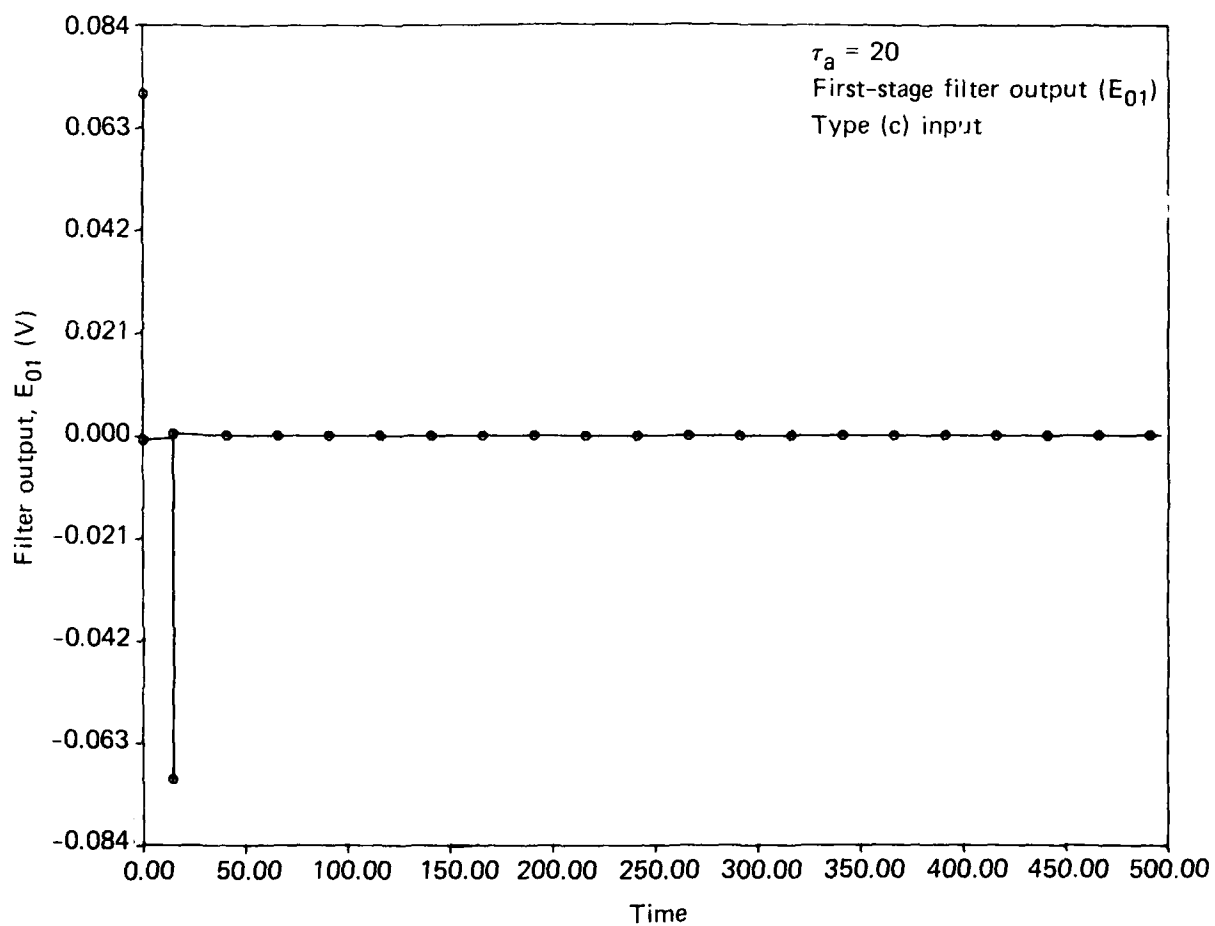


Fig. E2-11 First-stage filter output in response to a 5 ft vehicle height change in a 15 s period for $\tau_a = 20$.

AD-A088 593

JOHNS HOPKINS UNIV LAUREL MD APPLIED PHYSICS LAB F/6 13/10
DOCUMENTATION OF DESIGN, PERFORMANCE, AND QUALIFICATION OF THE --ETC(U)
JUN 80 T M RANKIN, R L KONIGSBERG N00024-78-C-538*

UNCLASSIFIED

JHU/APL/SES-025

NL

5 OF 5

00000000



END

DATE

FILED

10-80

DTIC

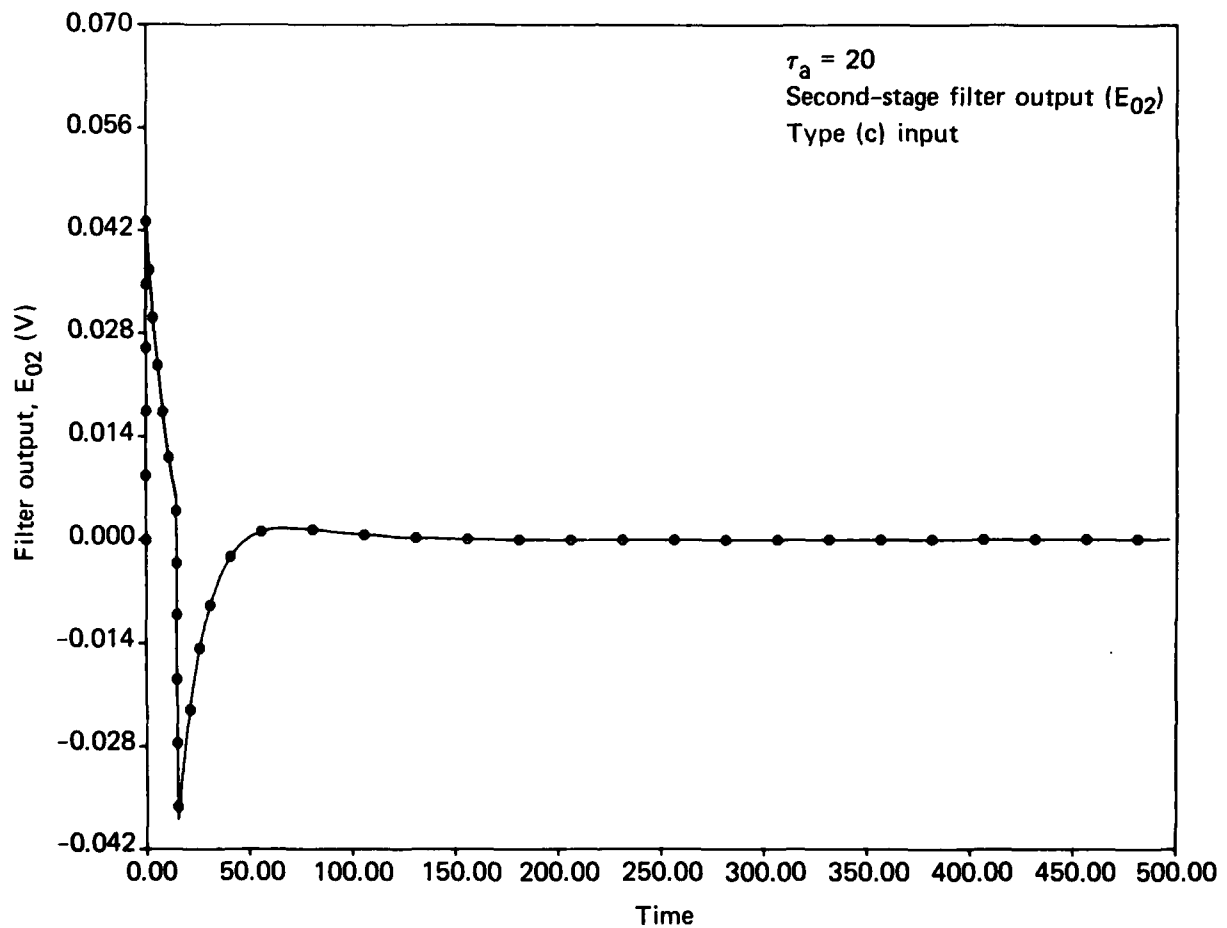


Fig. E2-12 Second-stage filter output in response to a 5 ft vehicle height change in a 15 s period for $\tau_a = 20$.

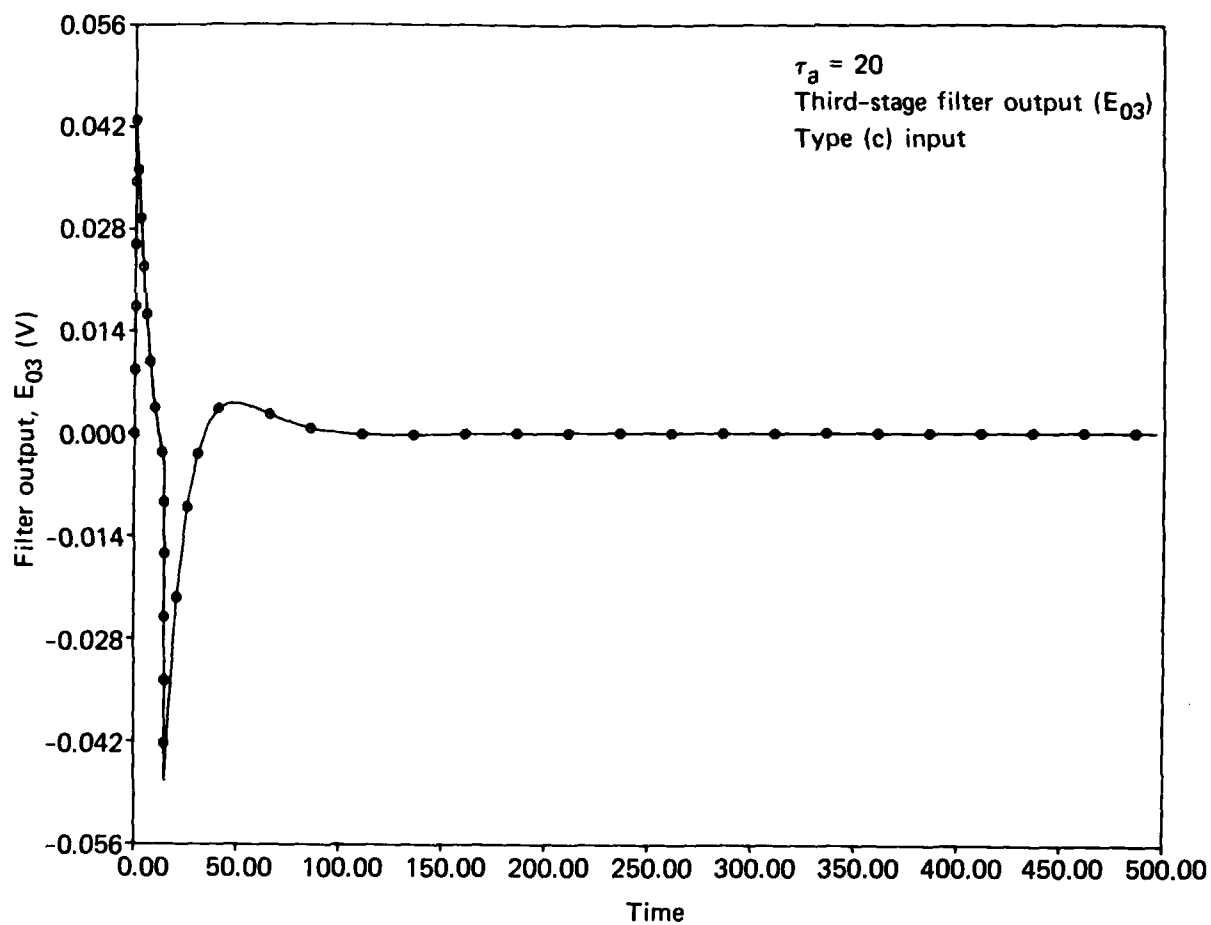


Fig. E2-13 Second-stage filter output in response to a 5 ft vehicle height change in a 15 s period for $\tau_a = 20$.

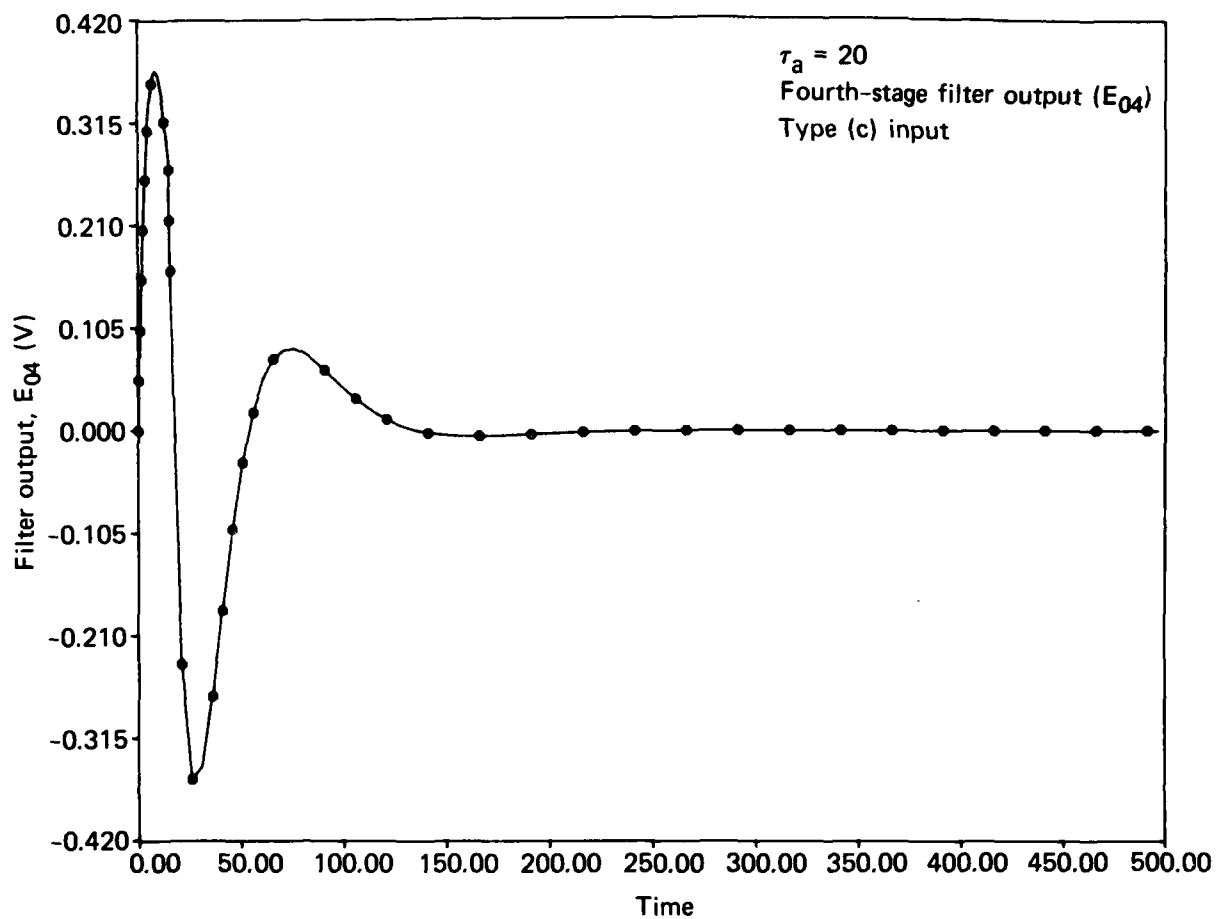


Fig. E2-14 Fourth-stage filter output in response to a 5 ft vehicle height change in a 15 s period for $\tau_a = 20$.

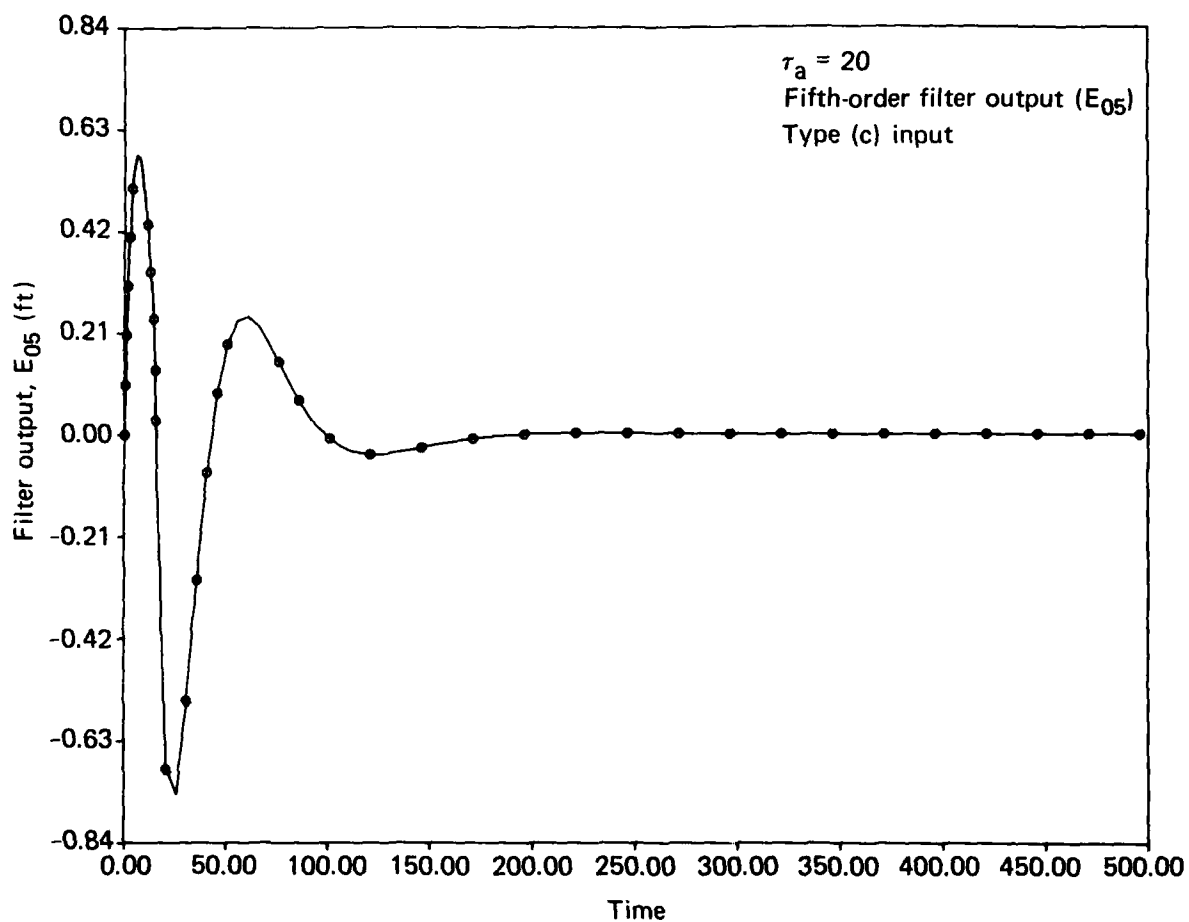


Fig. E2-15 Fifth-order filter output in response to a 5 ft vehicle height change in a 15 s period for $\tau_a = 20$.

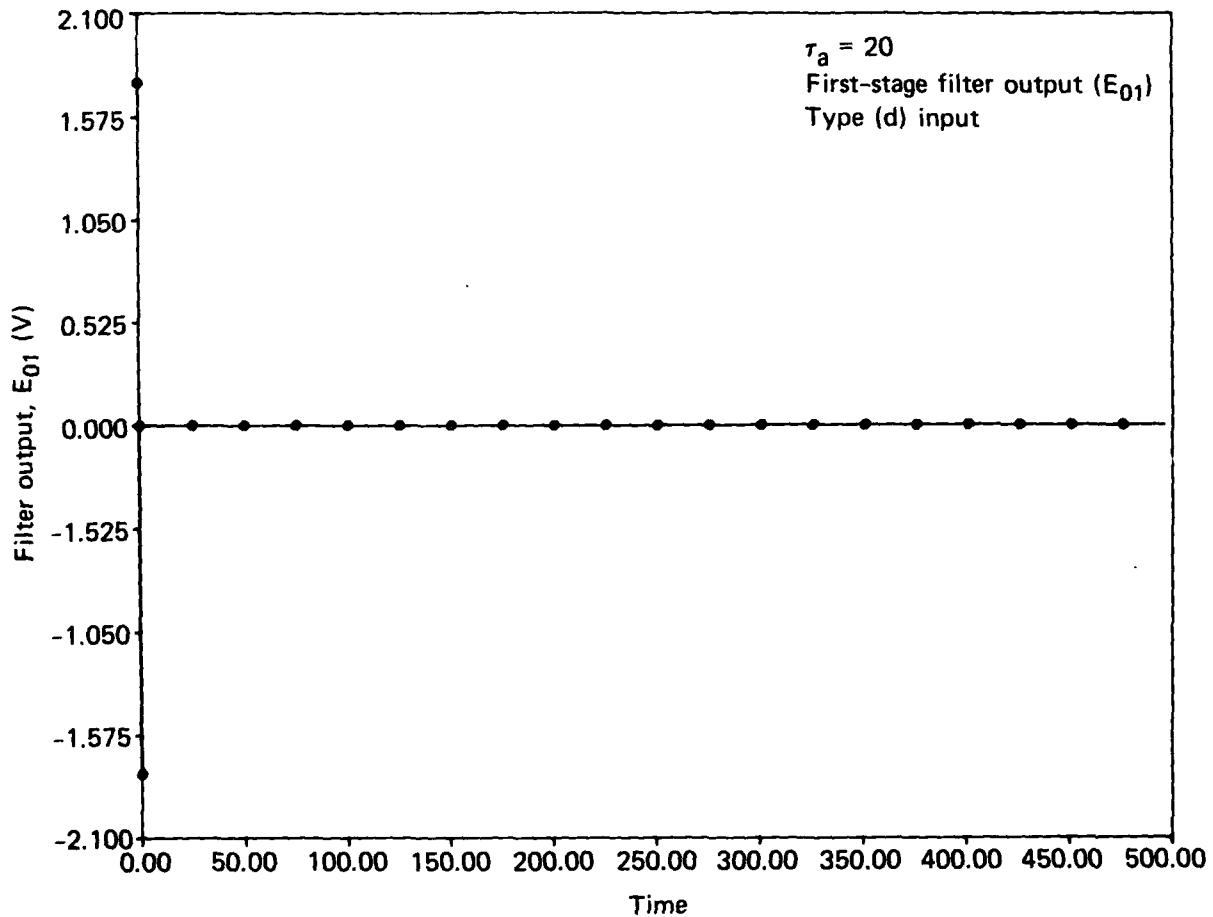


Fig. E2-16 First-stage filter output in response to a 2 ft vehicle height change in a 0.5 s period for $\tau_a = 20$.

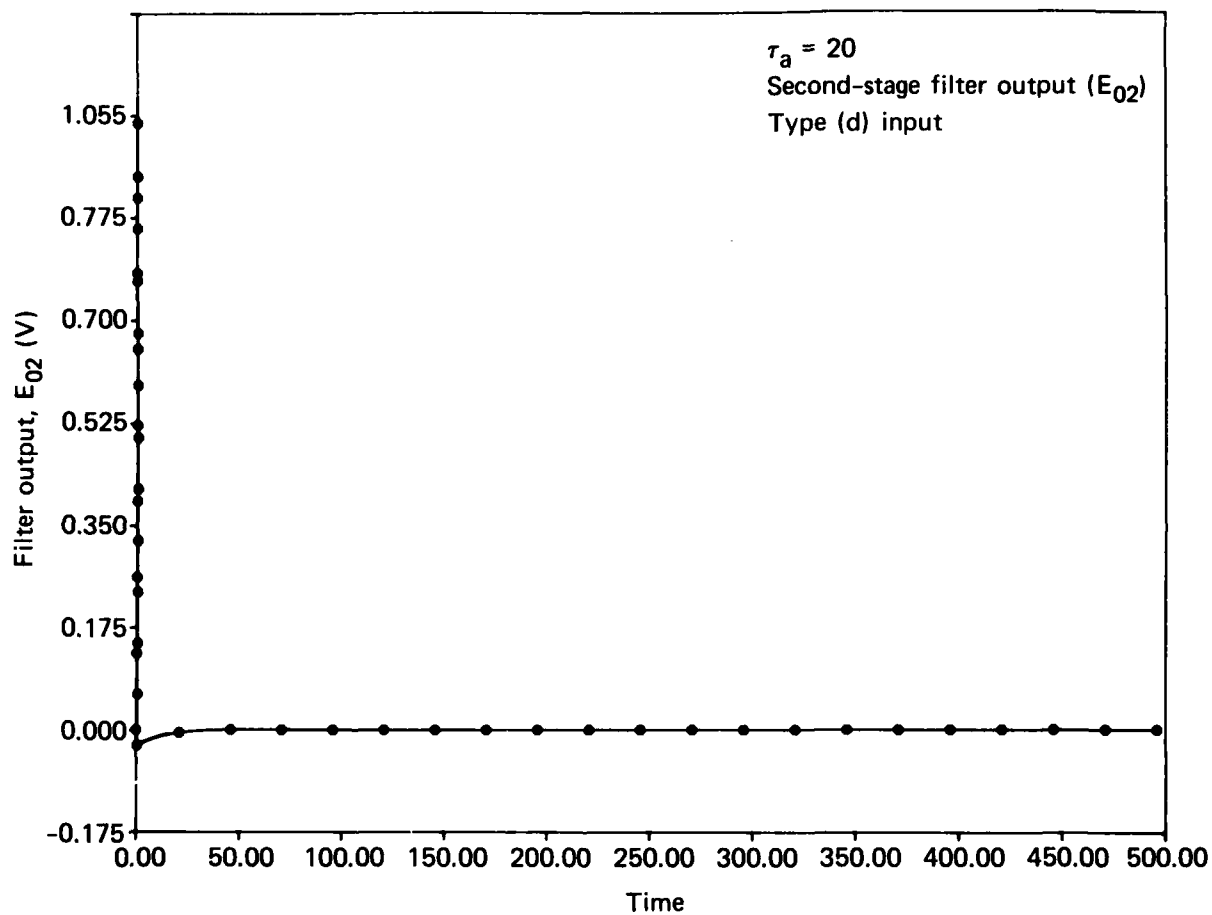


Fig. E2-17 Second-stage filter output in response to a 2 ft vehicle height change in a 0.5 s period for $\tau_a = 20$.

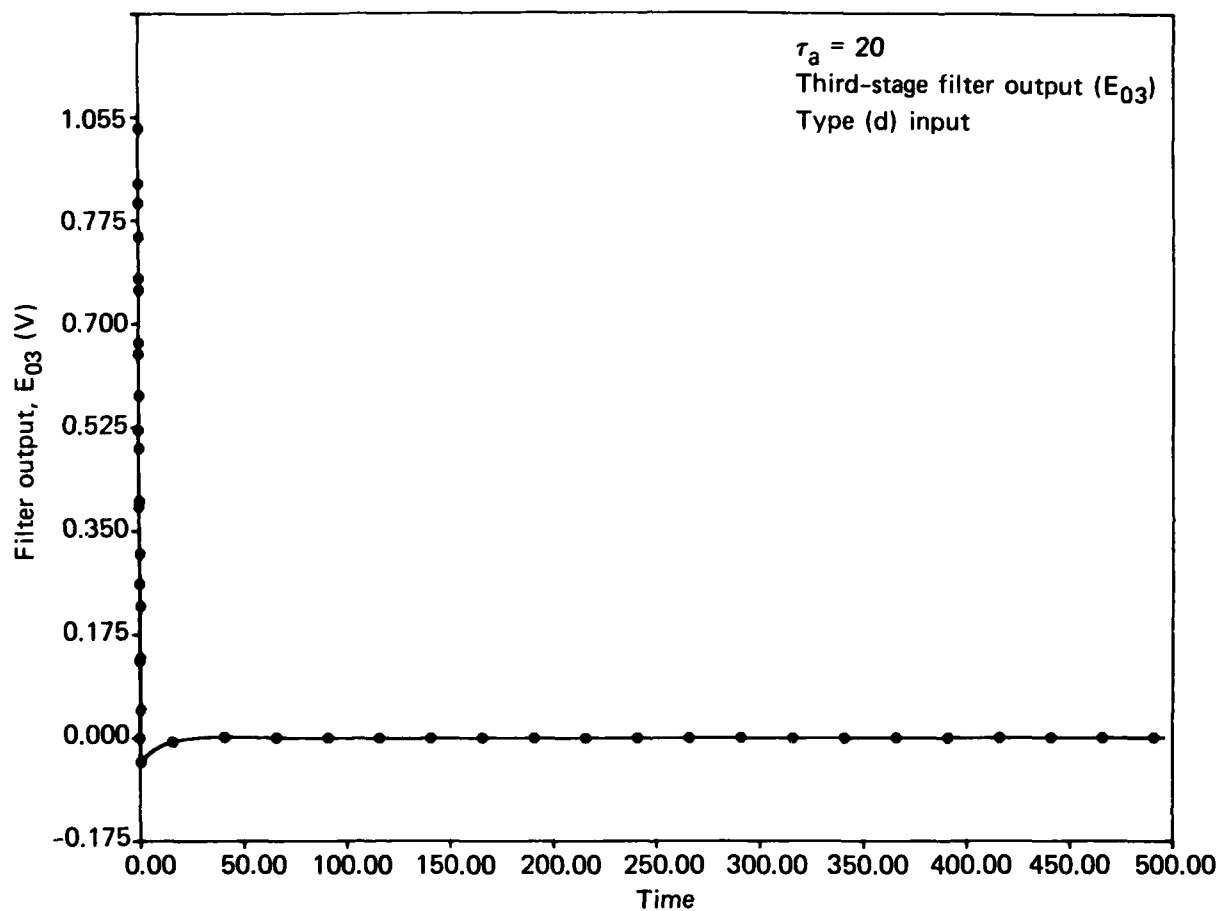


Fig. E2-18 Third-stage filter output in response to a 2 ft vehicle height change in a 0.5 s period for $\tau_a = 20$.

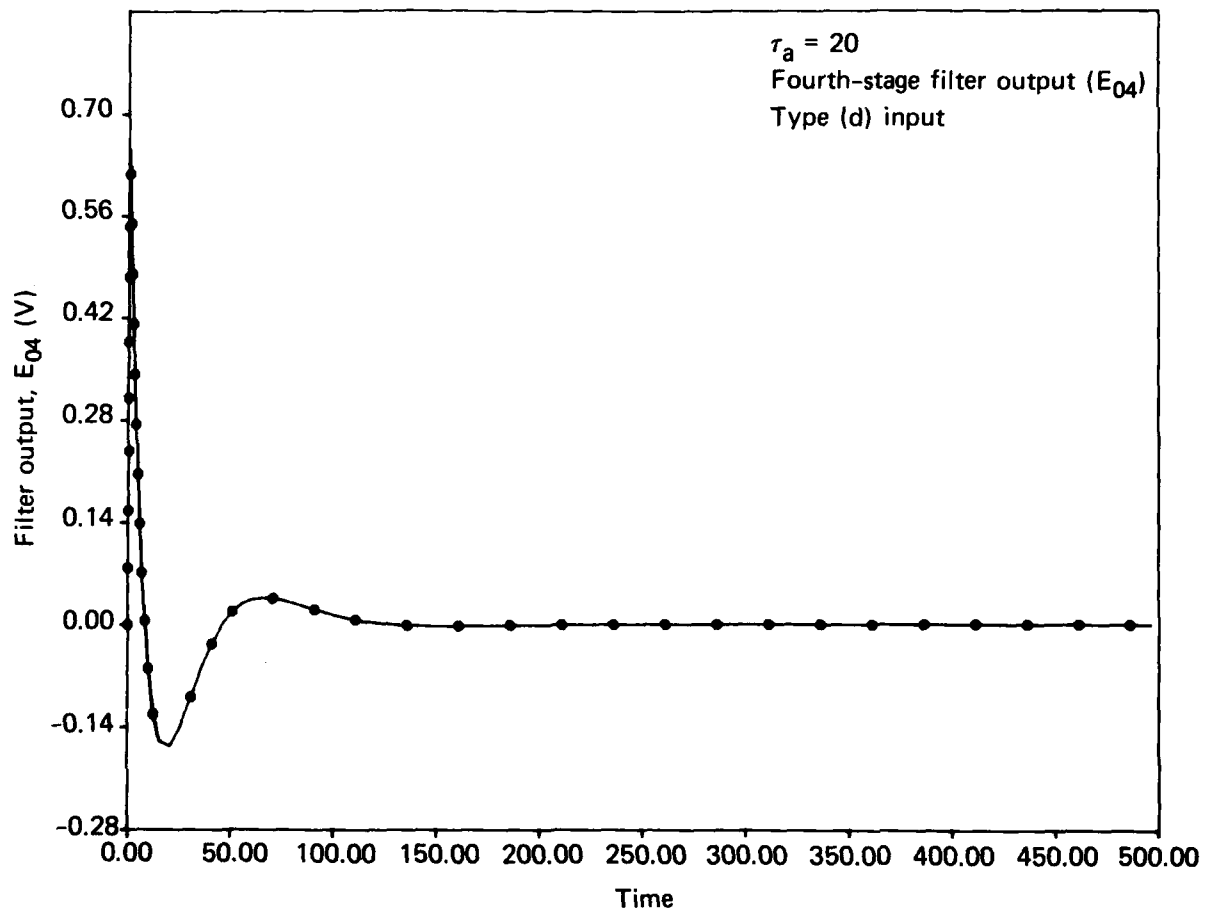


Fig. E2-19 Fourth-stage filter output in response to a 2 ft vehicle height change in a 0.5 s period for $\tau_a = 20$.

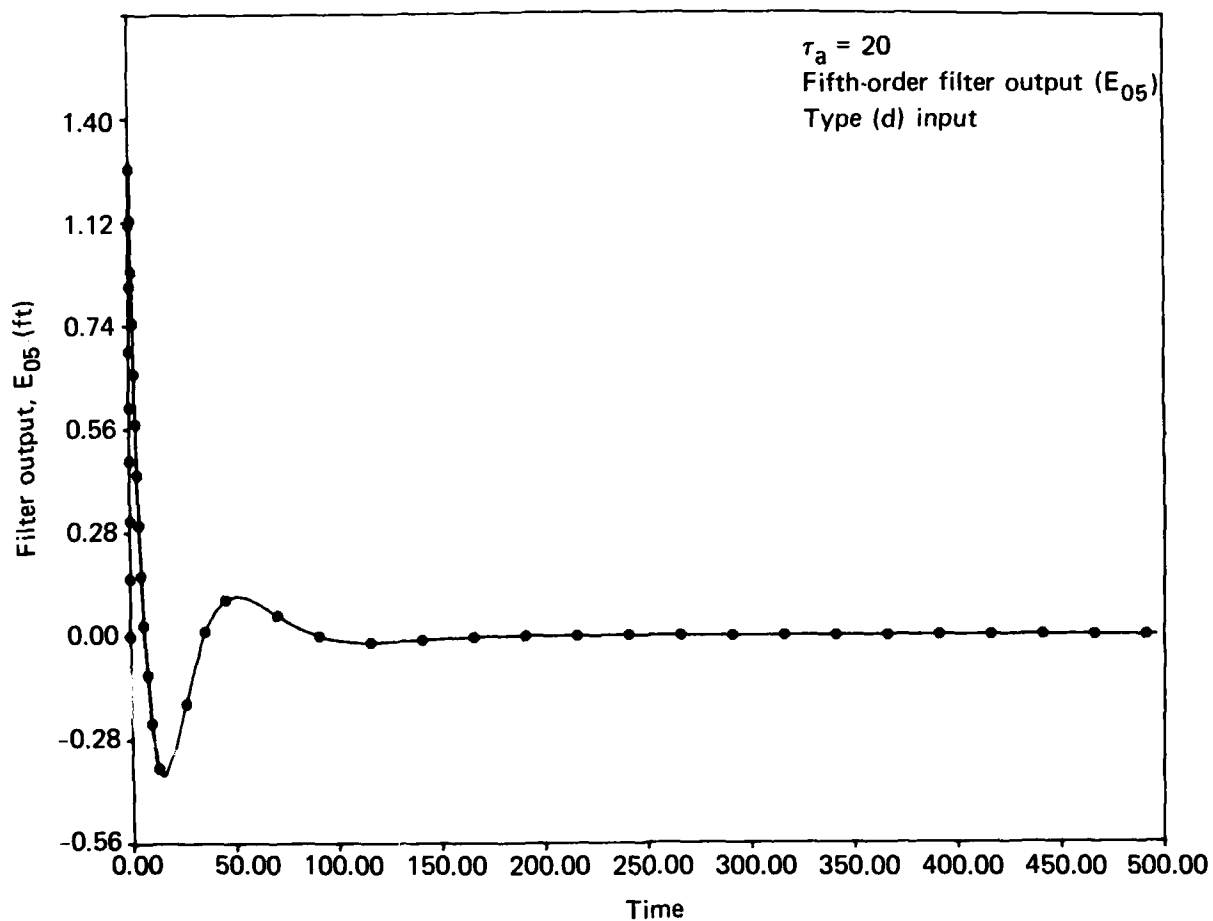


Fig. E2-20 Fifth-order filter output in response to a 2 ft vehicle height change in a 0.5 s period for $\tau_a = 20$.

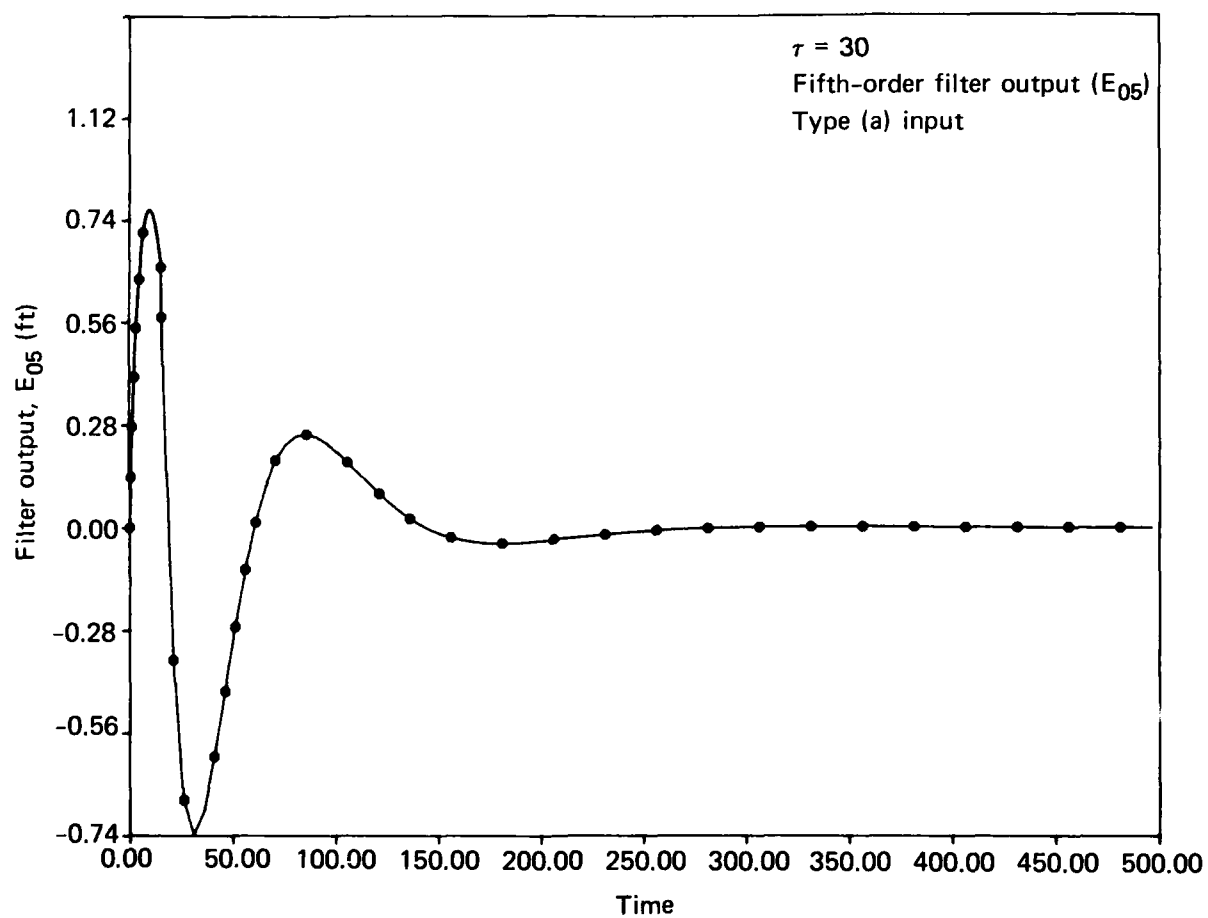


Fig. E2-21 Fifth-order filter output in response to a 5 ft vehicle height change in a 15 s period for $\tau_a = 30$.

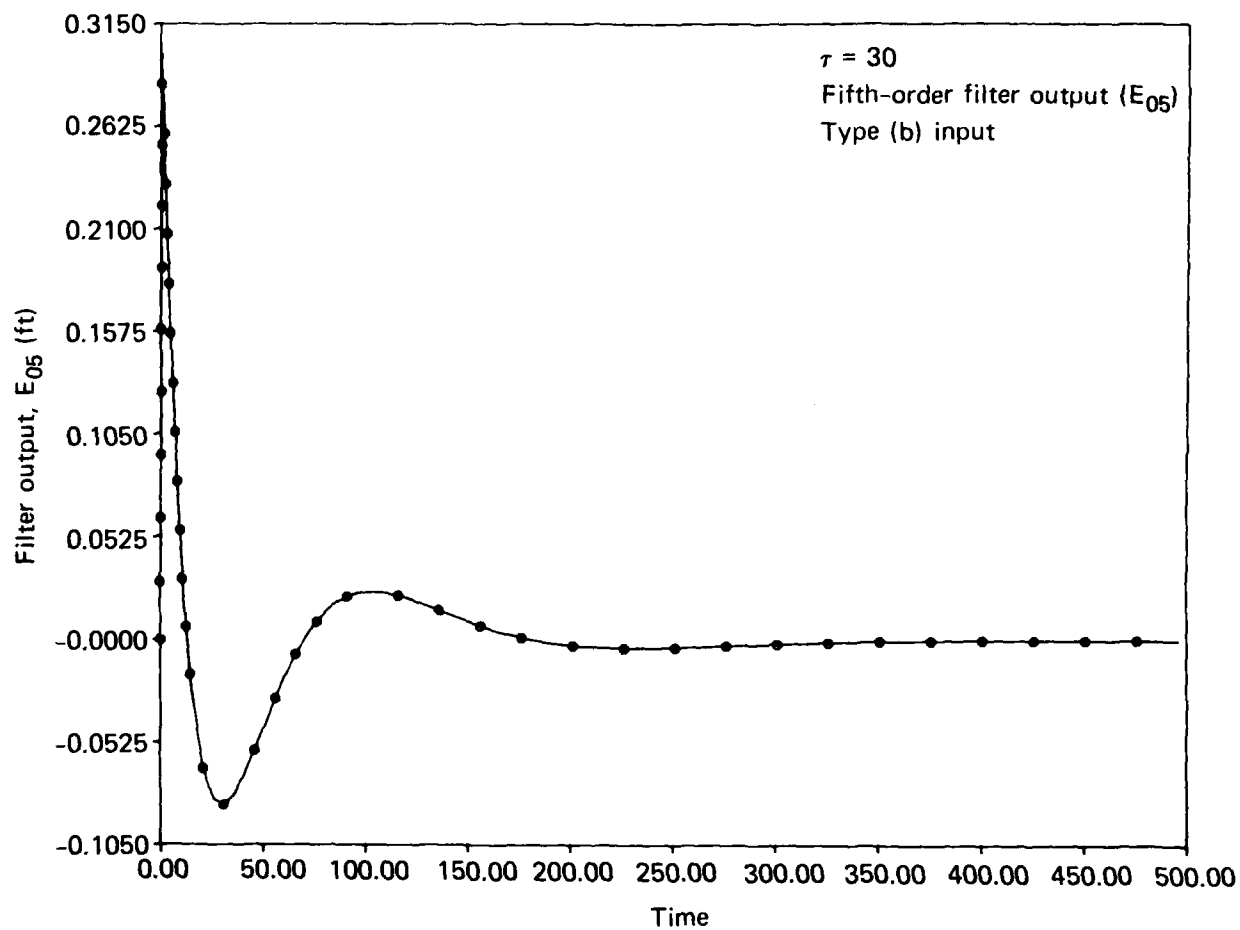


Fig. E2-22 Fifth-order filter output in response to a 0.5 ft vehicle height change in a 0.5 s period for $\tau_a = 30$.

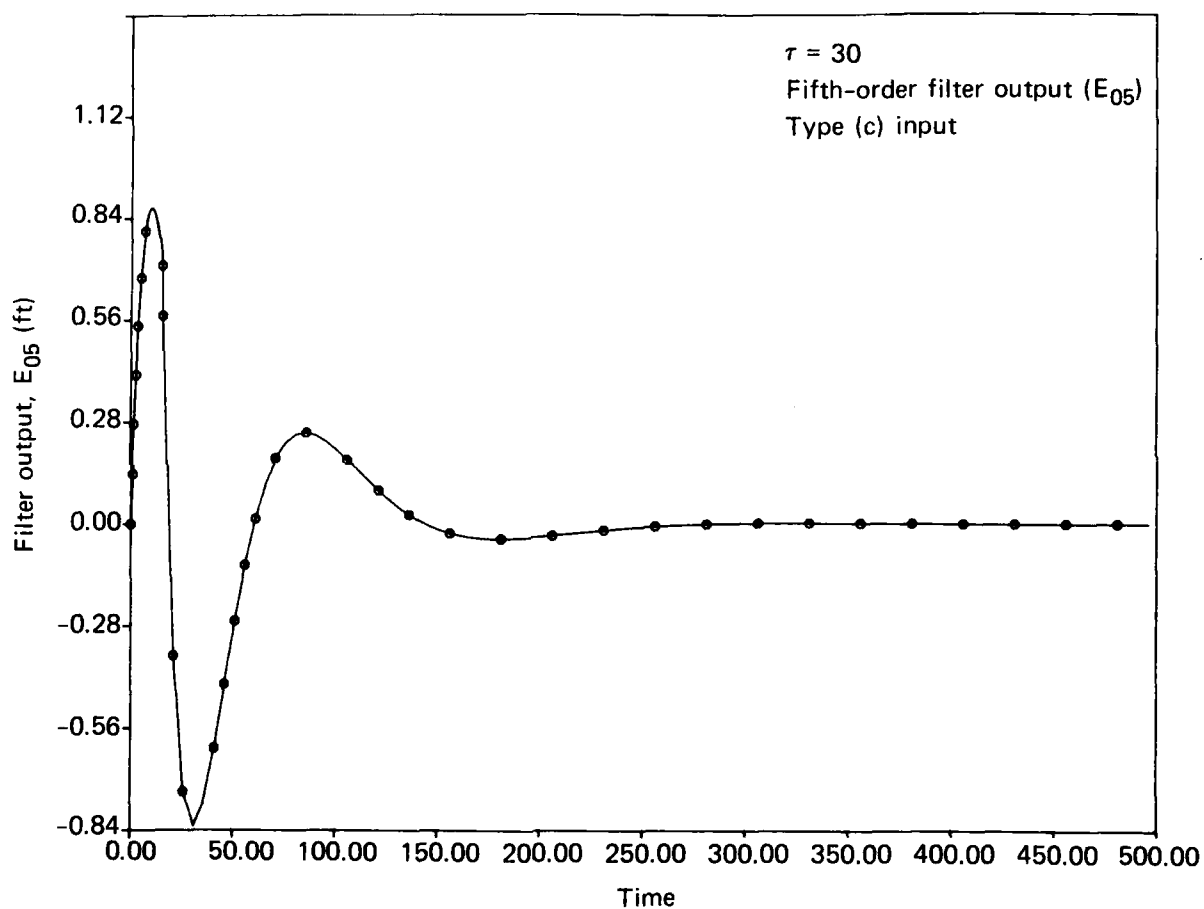


Fig. E2-23 Fifth-order filter output in response to a 5 ft vehicle height change in a 15 s period for $\tau_a = 30$.

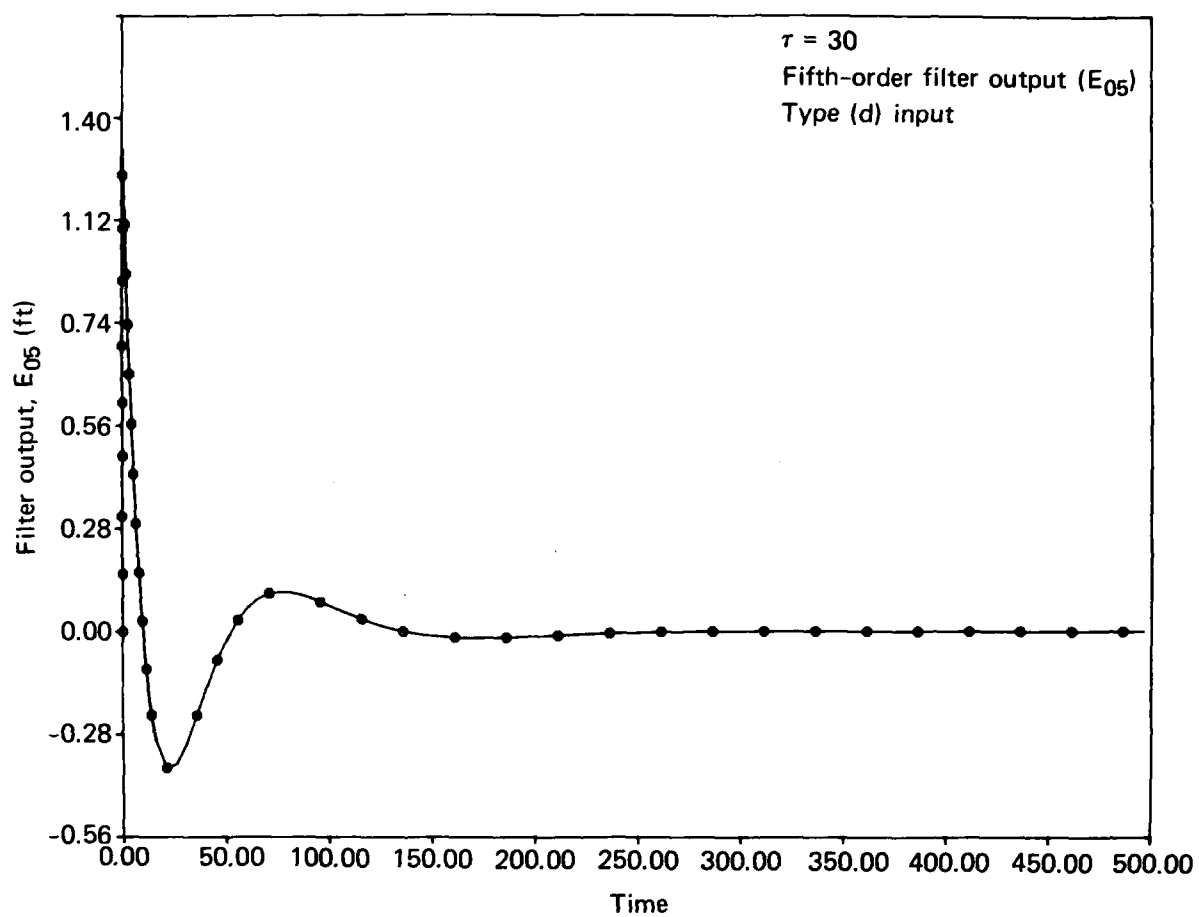


Fig. E2-24 Fifth-order filter output in response to a 2 ft vehicle height change in a 0.5 s period for $\tau_a = 30$.

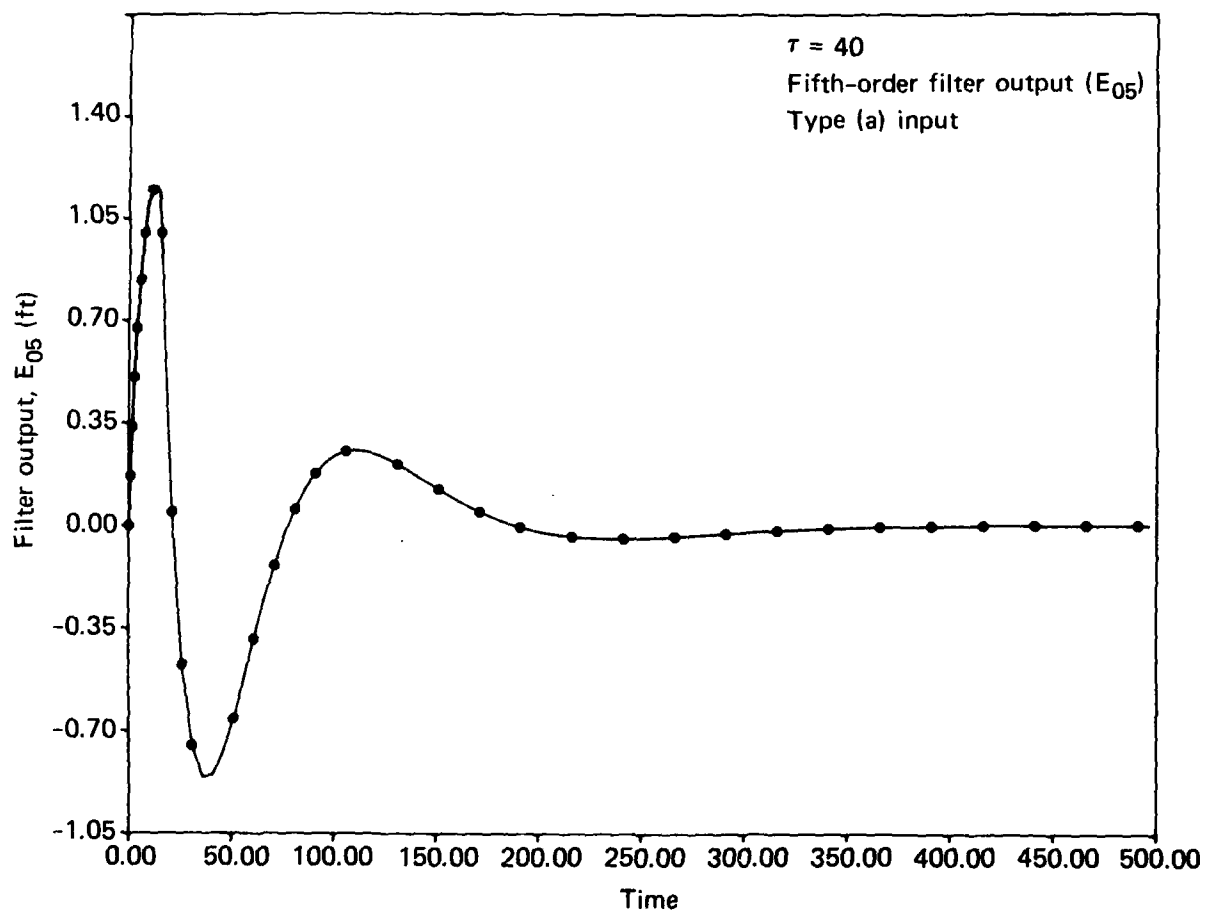


Fig. E2-25 Fifth-order filter output in response to a 5 ft vehicle height change in a 15 s period for $\tau_a = 40$.

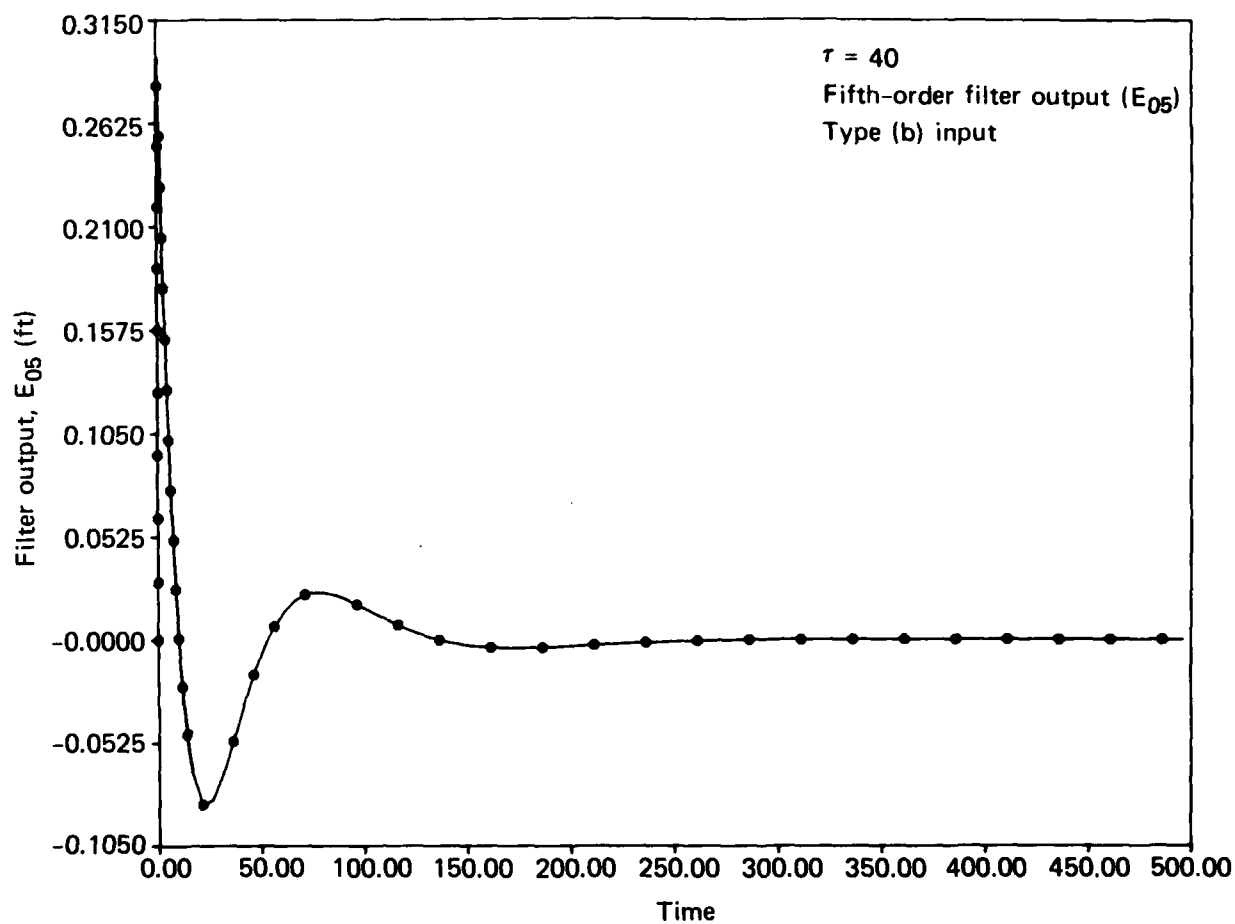


Fig. E2-26 Fifth-order filter output in response to a 0.5 ft vehicle height change in a 0.5 s period for $\tau_a = 40$.

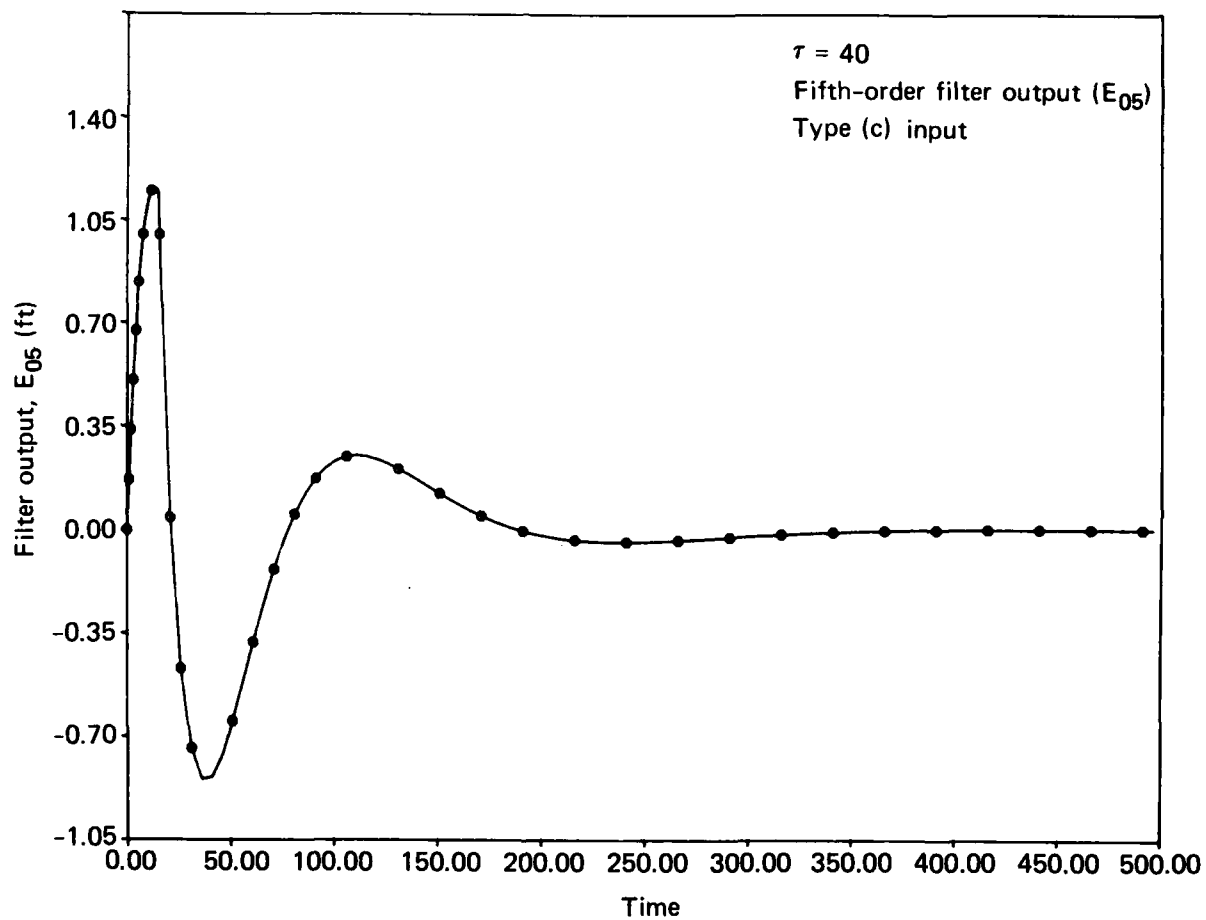


Fig. E2-27 Fifth-order filter output in response to a 5 ft vehicle height change in a 15 s period for $\tau_a = 40$.

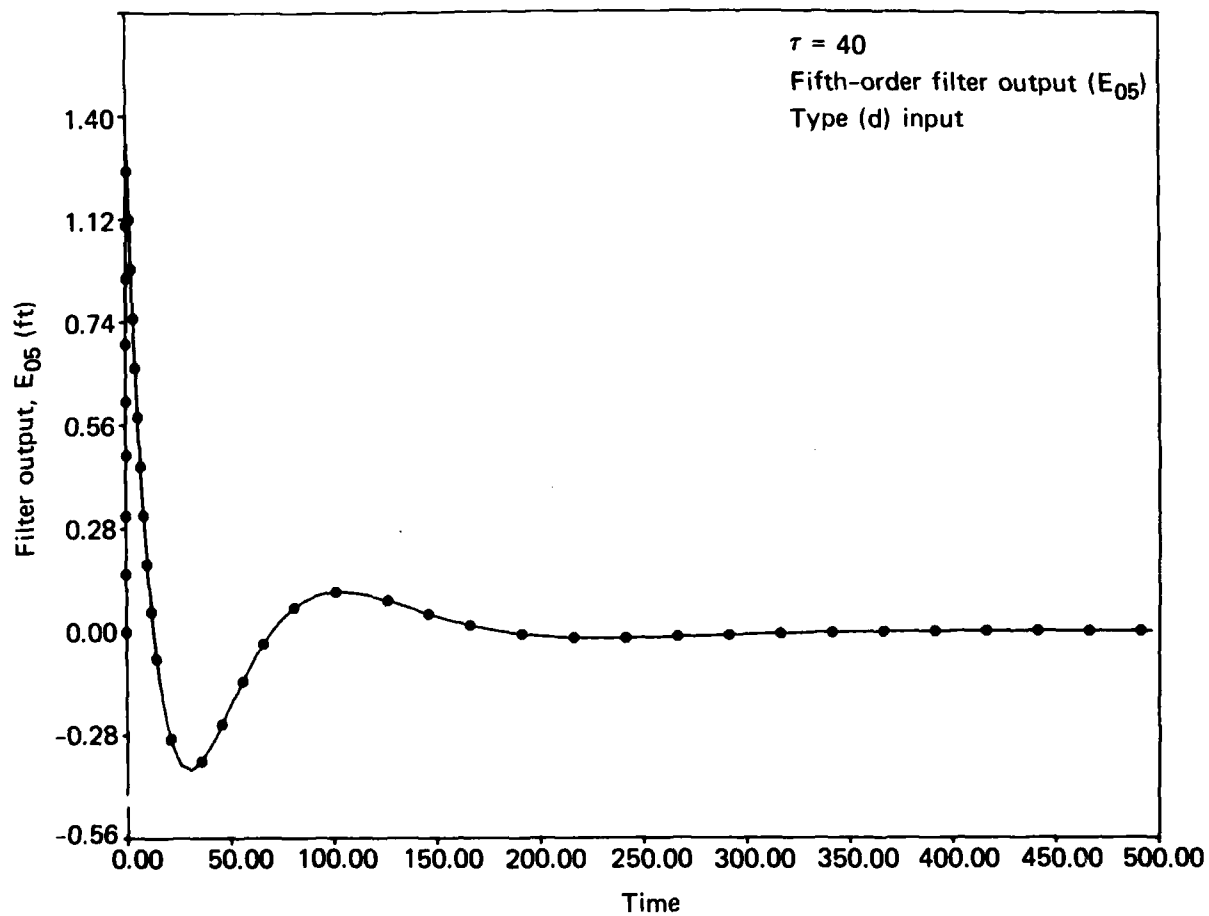


Fig. E2-28 Fifth-order filter output in response to a 2 ft vehicle height change in a 0.5 s period for $\tau_a = 40$.

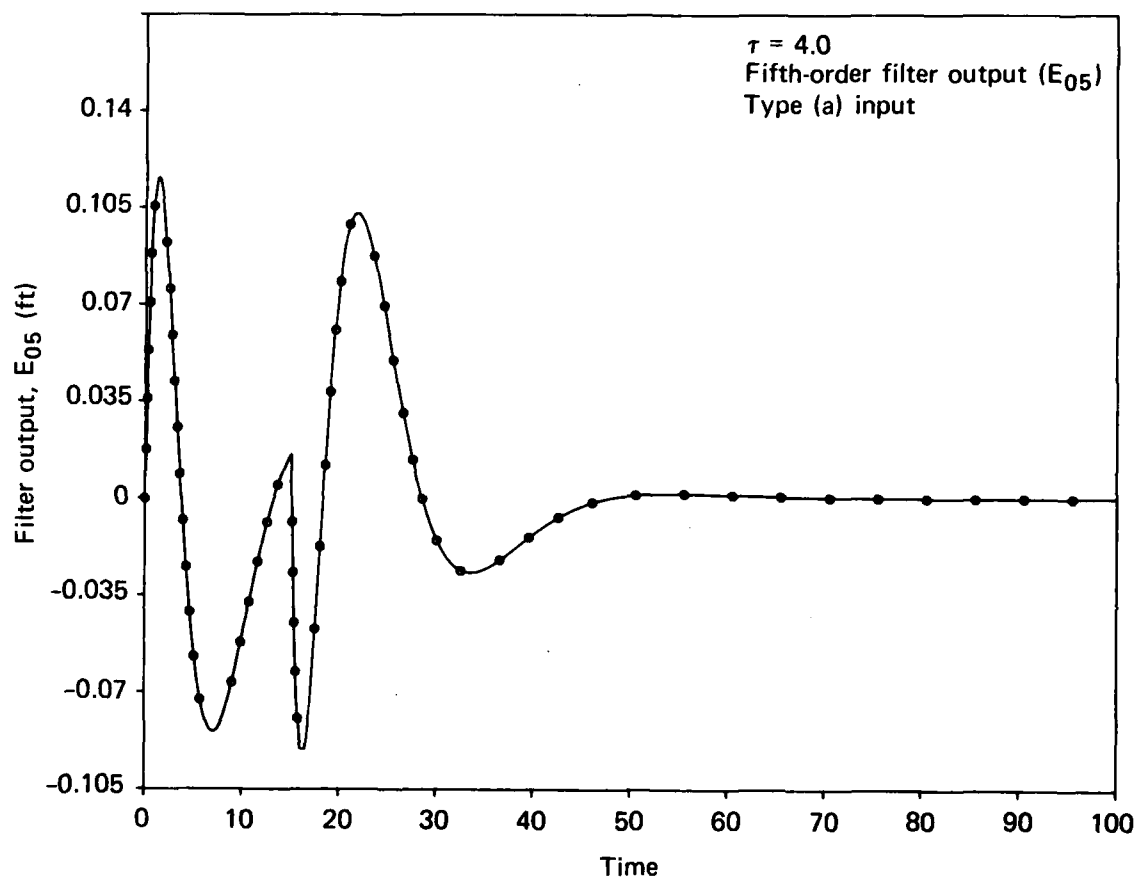


Fig. E2-29 Fifth-order filter output in response to a 5 ft vehicle height change in a 15 s period for $\tau_a = 4.0$.

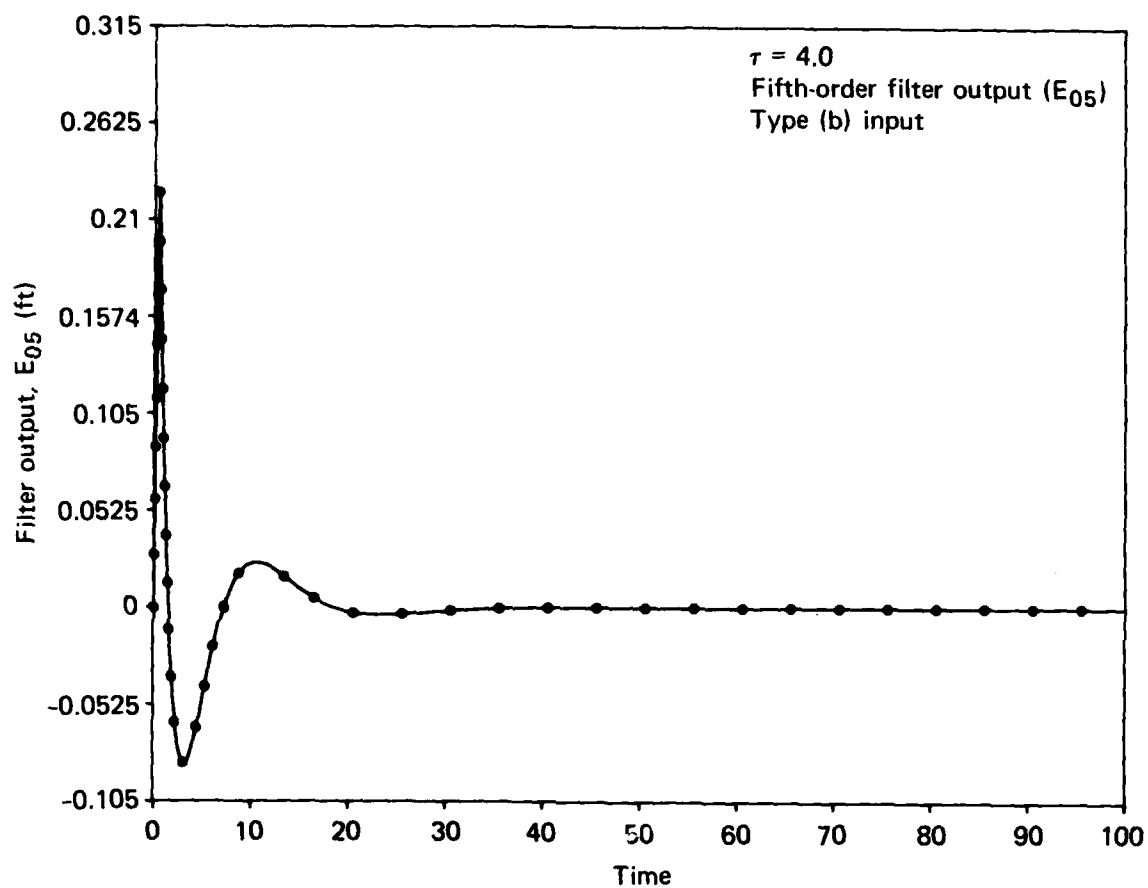


Fig. E2-30 Fifth-order filter output in response to a 0.5 ft vehicle height change in a 0.5 s period for $\tau_a = 4.0$.

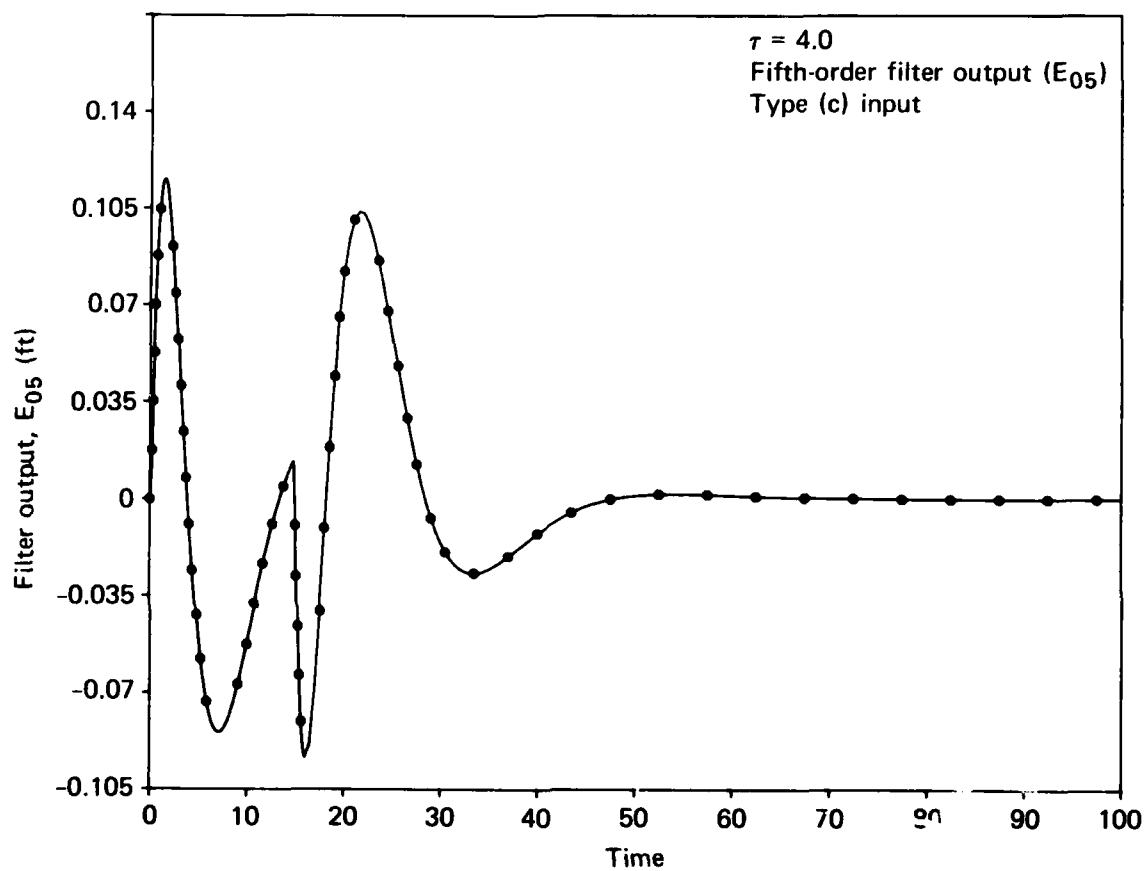


Fig. E2-31 Fifth-order filter output in response to a 5 ft vehicle height change in a 15 s period for $\tau_a = 4.0$.

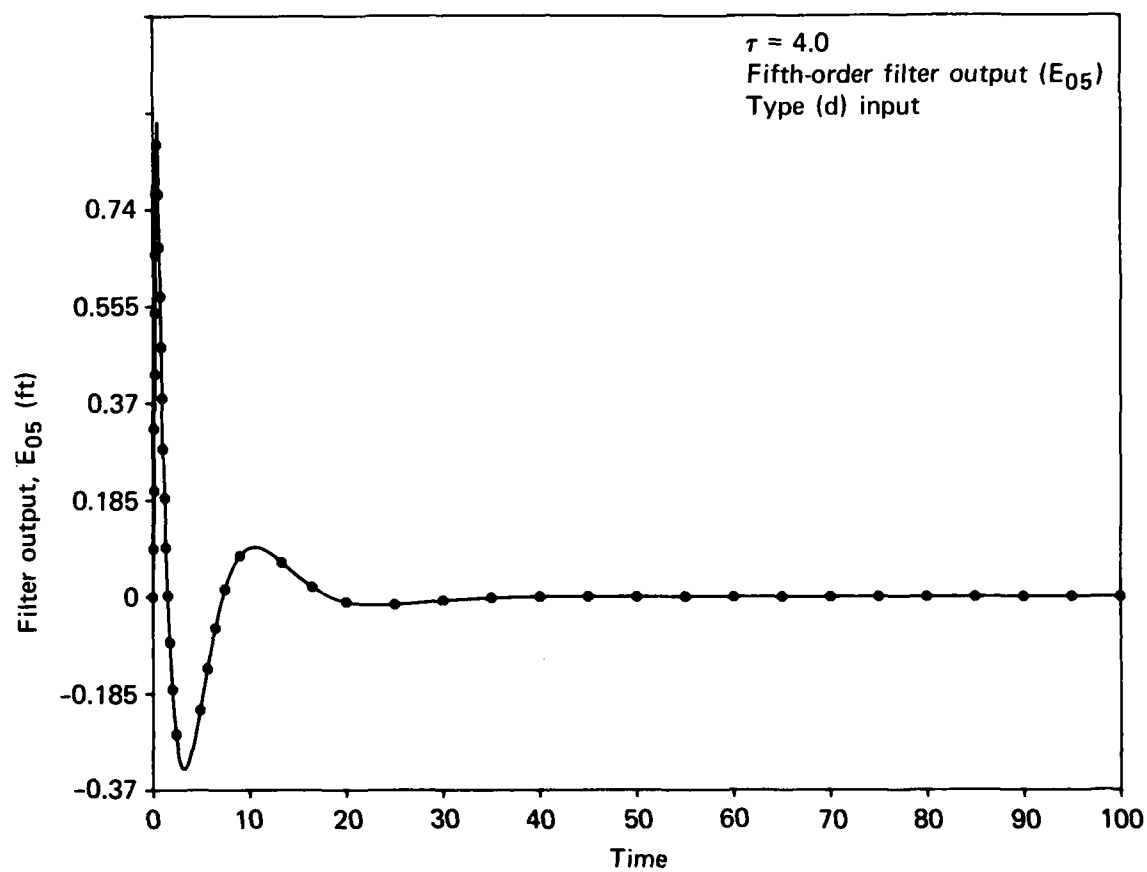


Fig. E2-32 Fifth-order filter output in response to a 2 ft vehicle height change in a 0.5 s period for $\tau_a = 4.0$.

INITIAL DISTRIBUTION EXTERNAL TO THE APPLIED PHYSICS LABORATORY*

The work reported in SES 025 was done under Navy Contract N00024-78-C-5384.
This work is related to Task Z69D, which is supported by Naval Sea Systems Command (PMS-304-24).

ORGANIZATION	LOCATION	ATTENTION	No. of Copies
DEPARTMENT OF DEFENSE			
DDC	Alexandria, VA		12
<u>Department of the Navy</u>			
CNM	Washington, DC	MAT-03	1
NAVSEASYS COM	Washington, DC	SEA-03	1
		SEA-032	1
		SEA-09G3	2
		PMS-304-20	2
		PMS-304-21 (S. Davis)	10
		PMS-304-24 (W. Malone)	10
NSRDC	Washington, DC	Code 2960 (R. Stillwell)	10
NAS	Patuxent River, MD	PMS-304-50 (SES Test Facility, J. Paradis)	5
NAVPRO	Laurel, MD		1
Requests for copies of this report from DoD activities and contractors should be directed to DDC, Cameron Station, Alexandria, Virginia 22314 using DDC Form 1 and, if necessary, DDC Form 55.			

*Initial distribution of this document within the Applied Physics Laboratory has been made in accordance with a list on file in the APL Technical Publications Group.